1996 Annual water column monitoring report

Massachusetts Water Resources Authority

Environmental Quality Department
Report ENQUAD 98-11

1996 Annual Water Column Monitoring Report

submitted to

MASSACHUSETTS WATER RESOURCES AUTHORITY
Environmental Quality Department
100 First Avenue
Charlestown Navy Yard
Boston, MA 02129
(617) 242-6000

prepared by

Stephen J. Cibik
Kristyn B. Lemieux

ENSR
35 Nagog Park
Acton, MA 01720
(978) 635-9500

and
Brian L. Howes
CMAST
New Bedford, MA 02744
and

Craig D. Taylor
Cabell Davis
Woods Hole Oceanographic Institution
Woods Hole, MA 02543

and

Theodore C. Loder, III
Robert D. Boudrow
University of New Hampshire
Durham, NH 03824

December 1998

Citation:

Cibik SJ, Lemieux KB, Howes BL, Taylor CD, Davis CS, Loder TC, III, Boudrow RD. 1998. 1996 Annual water column monitoring report. Boston: Massachusetts Water Resources Authority. Report ENQUAD 98-11. 416 p.

CONTENTS

CONTENTS (Cont'd)

CONTENTS (Cont'd)

LIST OF TABLES

LIST OF FIGURES

Acknowledgements

The authors wish to acknowledge the innumerable people who contributed to the monitoring studies presented in this annual report. First and foremost, we recognize the scientific teams fielded by the many organizations who participated in the MWRA's monitoring program, both at sea and in the laboratory. It was their expertise and dedication which produced the high-quality data reported herein, despite working frequently under exceedingly difficult conditions. Special recognition is given to Mr. Steven Wolf, ENSR Operations Manager, and Mr. Don Boyé, ENSR Chief Scientist, for their logistical abilities that made it all happen. Recognition is also given to ENSR's "Data Champions", including Ms. Joan Tracey and Ms. Stephanie Kelly, who "shepherded" the data from their former home in Massachusetts Bay to their new home in the MWRA database and in this report. We also thank Mr. Mel Higgins and Dr. Joshua Lieberman for their database expertise.

We additionally recognize Ms. Dale Goehringer of WHOI, Mr. Rob Boudrow of UNH, and Mr. Richard Lacouture of the Academy of Natural Sciences' Estuarine Research Center for coordinating the various laboratory efforts. We also thank the masters and crews of the vessels *Isabel S* and *Christopher Andrew*, with special thanks to Mr. Frank Mirarchi and Mr. Chip Rhyther of CR Environmental for their capable support of our sea operations.

The authors also received generous technical support and information from numerous agencies outside of the program. We thank in particular Ms. Fran Hotchkiss, Mr. Bill Strahle, and Dr. Rich Signell of the USGS Woods Hole office for providing data and information on mooring deployments. We thank Mr. Tom Shepard, Mr. Russell Gadoury, and Ms. Jessica Stock-Alvarez of the USGS Marlborough, Massachusetts, Office for providing river discharge data. Thanks also to Douglas Hankins of WETLabs for providing timely data for continuous chlorophyll monitoring, and to Kathy Vreeland of the Northeast Regional Climate Center for meteorological data.

Thanks are also extended to Dr. Don Anderson of WHOI for additional data on the occurrence and distribution of *Alexandrium tamarense* in Massachusetts Bay during the monitoring period, Dr. Steve Bates of the Bedford Institute of Oceanography, Marine Environmental Sciences Division for consultations on domoic acid and *Pseudo-nitzschia*, and to Dr. David Taylor of the MWRA Central Laboratory for chlorophyll data from Boston Harbor. Thanks also to Dr. Bernie Gardner of UMass Boston for his input on the interpretation of physical oceanography data.

Finally, we acknowledge that there are certainly several people we have overlooked who deserve specific mention, to whom we extend our thanks and our apologies for our momentary lapse in memory.

1996 ANNUAL WATER COLUMN REPORT
EXECUTIVE SUMMARY

The Massachusetts Water Resources Authority (MWRA) Harbor and Outfall Monitoring (HOM) Program has collected water quality data in Massachusetts and Cape Cod Bays since 1992. This monitoring is in support of the HOM Program mission to assess the potential environmental effects of effluent discharge relocation from Boston Harbor into Massachusetts Bay. The data are being collected to establish baseline water quality conditions and ultimately to provide the means to detect significant departure from that baseline. The data include physical water properties, nutrients, biological production and respiration, and plankton measurements. Two types of surveys are performed: nearfield surveys with stations located in the area around the future outfall site, and more comprehensive combined nearfield/farfield surveys that include stations in Boston Harbor, Massachusetts Bay, and Cape Cod Bay.

This report presents the results of the fifth continuous year of water column monitoring. The data presented in this report were collected throughout 1996 (February to December) in the Massachusetts Bay system. The scope of this annual report is to provide a comprehensive review of the 1996 data, to provide an integrative synthesis of results across the various technical disciplines, and to provide a comparison of results with data collected during previous monitoring years.

The Massachusetts Bay system undergoes strong seasonal stratification of the water column, and the timing of the onset and breakdown of vertical stratification influences seasonal nutrient cycling and its effect on critical issues such as dissolved oxygen depletion in stratified bottom water. The interpretation of monitoring data is thus intricately associated with the physical characteristics of the Massachusetts Bay environment. This summary first presents an overview of events that occurred during 1996, and then provides a comparison with monitoring data collected in previous years.

1996 Monitoring Results

During early February the water column was well-mixed and replete with nutrients. A localized phytoplankton bloom in eastern Cape Cod Bay was the only area showing evidence of surface water nutrient depletion, indicating strong algal productivity. By the second regional survey in late February, a system-wide bloom was evidenced by high chlorophyll concentrations (ranging from 5-12 μgL^{-1}) measured in Cape Cod Bay, Massachusetts Bay, and in the nearfield. Cape Cod Bay had the highest regional phytoplankton densities, dominated by centric diatoms (*Chaetoceros*, *Thalassiosira*). Boston Harbor was the only region sampled that had relatively low chlorophyll concentrations (<2 μgL^{-1}). Peak late winter production in the outer nearfield reached around 3,000 $mgCm^{-2}d^{-1}$.

By the third (nearfield only) survey conducted in March, nutrients were largely scavenged from surface water, ending the late winter bloom in Massachusetts Bay. The bulk of chlorophyll and carbon from the bloom was found in the lower water column, resulting in high bottom water respiration. Horizontally, chlorophyll was highest inshore, although mid-depth samples from the more seaward stations of the nearfield also showed

elevated concentrations. Supported by data collected for the MWRA Boston Harbor Water Quality Monitoring Program, the coastal chlorophyll component appeared associated with a continuation of the early season bloom within the harbor and coastal regions that lasted into May. Regional data collected during the combined nearfield/farfield survey in April documented the continued dominance of centric diatoms at harbor and coastal stations, with the centric diatom *Chaetoceros* comprising 60% of the total phytoplankton abundance at station N10. This bloom produced the peak annual productivity rates at station N10 (around 5,000 $mgCm^{-2}d^{-1}$). Chlorophyll and phytoplankton densities remained low at more offshore stations in Mass Bay and at Cape Cod Bay stations throughout the spring.

The onset of vertical stratification was occurring in the inner nearfield by mid-April, but setup was not complete until mid-May in the outer nearfield. Stratification was augmented by an intrusion of low salinity surface water to the outer nearfield during May, resulting from a Gulf of Maine spring freshet. This intrusion apparently resupplied nutrients to the impoverished surface water, with evidence of between-survey phytoplankton production found in productivity, particulate carbon, and respiration results. However, chlorophyll concentrations in the water column remained low during the surveys, potentially a result of grazing as total zooplankton abundances peaked at outer nearfield stations N04 and N16 during the June survey. A localized surface bloom of the centric diatom *Rhizosolenia fragilissima* did occur at nearfield station N04 in early July, yielding productivity rates around 2,000 $mgCm^{-2}d^{-1}$. Based on continuous monitoring results from the USGS mooring, this bloom may have developed throughout the nearfield in the ensuing week after the survey.

Maximum annual productivity measurements were made at Harbor station F23 in June (5,200 $mgCm^{-2}d^{-1}$). The plankton assemblage was still dominated by centric diatoms, but the dominant at this time was *Skeletonema costatum*. Productivity rates at station N10 were similarly high, reaching 4,500 $mgCm^{-2}d^{-1}$.

The water column was vertically stratified throughout August, primarily due to the strong temperature differential between surface and bottom water. Nutrient concentrations in the surface mixed layer of all regions were low except for in Boston Harbor, which remained relatively well mixed. However, concentrations in Boston Harbor were low during August compared with subsequent results from harbor surveys during October and December. This was attributed to the combined effects of high algal productivity in the harbor during August which apparently reduced nutrient concentrations, and to nutrient loading from runoff caused by heavy rainfall during October and December.

Outside of Boston Harbor and adjacent coastal stations, nutrient and chlorophyll concentrations were low until nutrients trapped in the stratified bottom layer began to be released by the storm activity during September. The first of two weekly hurricane events during early September (Eduoard and Fran), caused a partial release of bottom water nutrients to the surface. Continuous chlorophyll sensor readings showed a constant increase in nearfield chlorophyll concentrations from around September 10th. The passage of the former Pacific Hurricane Fausto in mid-September also resulted in vertical mixing in the water column. This mixing resulted in a more substantial release of nutrients which appeared to initiate the fall bloom, as evidenced by a marked increase in continuous chlorophyll sensor data. Survey results indicated that algal activity in shallower regions of

Massachusetts Bay peaked during early October, but more offshore stations continued to bloom through the end of the month.

Dissolved oxygen concentrations in bottom water declined throughout the stratified period, with minimum concentrations in the nearfield recorded in early October. It appeared that the storm activity during September mitigated the severity of the seasonal decline in Massachusetts Bay due to ventilation of the bottom layer. Minimum DO concentrations in the nearfield only fell from 7.9 mgL^{-1} in August to 7.2 mgL^{-1} in early October, and actually increased at coastal stations. However, minimum DO concentrations in Cape Cod Bay during this same period fell from 7.1 mgL^{-1} to 5.5 mgL^{-1}. DO concentrations in all other regions remained above 7.4 mgL^{-1} for seasonal minima.

Biological activity during the latter part of the year focused around two events: the August bloom in the harbor and adjacent coastal water, and the fall bloom in Massachusetts Bay in late September and early October. The Harbor bloom in August was dominated by the centric diatoms *Rhizosolenia fragilissima* and *Leptocylindrus minimus*. The fall bloom in Massachusetts Bay appeared to initiated during September by cryptophytes, followed by a consortium of centric diatom whose composition changes with distance from shore. *Skeletonema costatum*, *Chaetoceros* spp., *R. fragilissima*, and *Cyclotella* sp. were the dominant centrics inshore, while an unidentified centric diatom (probably of the genus *Thalassiosira*) dominated the offshore assemblage along with the pennate diatom *Thalassionema nitzschoides*. While the inshore bloom diminished quickly, the offshore bloom appeared to persist into November with an apparent dominance by from *R. fragilissima*.

Measured rates for primary production and respiration during the August inshore bloom were the highest of the second half of the year (around 2,400 $mgCm^{-2}d^{-1}$ at N10). The fall bloom in offshore waters produced lower production rates, however, cloudy conditions were prevalent during these latter surveys. High-resolution production calculations, which incorporate daily irradiance to estimate production between surveys, indicated that productivity during the fall bloom was often two to three times higher than that for the specific survey dates, and that a second peak in production at station N04 occurred during November. Overall, estimates of seasonal production based on survey data alone were about 60 percent lower than the estimates from the high-resolution calculations. Carbon-specific respiration within the nearfield, coupled with chlorophyll and productivity data, suggested that *in situ* carbon fixation, rather than import of detrital carbon, is the major source of organic matter throughout the nearfield.

Zooplankton densities peaked in the harbor and inshore stations concurrently with the August bloom, followed by a general decline thereafter. More seaward stations showed a general increase from early September through the end of October, apparently in response to the fall bloom in Massachusetts Bay. The numerical dominant was *Oithona similis*, while biomass was dominated by *Centropages typicus*. Substantial abundances of bivalve larvae were also observed during early October.

1992-1996 Interannual Comparisons

The key parameters for assessing potential eutrophic impacts to the water column from the outfall relocation are chlorophyll and dissolved oxygen. This summary therefore focuses on the interannual variability seen during the baseline monitoring for these two parameters. Ongoing baseline monitoring has continued to document the substantial degree of variability inherent in the Massachusetts Bay system. The spring bloom during 1996 was the largest documented during the baseline monitoring period. It yielded a seasonal average (February through April) of 2.43 μgL^{-1}, which well exceeded previous maxima (1.97 and 1.94 μgL^{-1} in 1992 and 1994, respectively). Alternatively, 1996 ranked fifth in the baseline period for summertime average chlorophyll concentrations (May through August average of only 0.78 μgL^{-1}), and lowest for the fall average (September through December average of 1.47 μgL^{-1}).

With respect to bottom water dissolved oxygen minima, 1996 ranked fourth in the baseline record for severity of low seasonal DO concentration in the nearfield (with 1993 being the least severe). However, 1996 produced the second lowest individual measurement of the baseline period (5.48 mgL^{-1} at Cape Cod Bay station F01), exceeded in magnitude only by the 4.82 mgL^{-1} measured at nearfield station N01 during 1994. It was similar in magnitude to the 1995 minimum of 5.60 mgL^{-1} recorded at Cape Cod Bay station F02. It ranked third in the rate of seasonal oxygen decline during the stratified period (tied with 1993 at 0.025 $mgL^{-1}d^{-1}$), with 1994 and 1995 yielding rates of 0.031 $mgL^{-1}d^{-1}$ and 0.027 $mgL^{-1}d^{-1}$, respectively.

These results further emphasize the scales of variability inherent to the Massachusetts Bay system. Seasonal blooms vary in magnitude and duration, and are controlled by a variety of physical, chemical and biological factors. DO concentration in bottom water is subject to influence by water temperature, carbon inputs from photosynthetic activity and other sources, respiration rates, duration and intensity of stratification, resuspension from storm activity, and the frequency and magnitude of reaeration through advection and atmospheric exchange. This inherent variability severely constrains our predictive capability, and requires that post-relocation impact assessments incorporate detailed, integrated investigations of potential causality.

1.0 INTRODUCTION

The Massachusetts Water Resources Authority (MWRA) has implemented a long term monitoring plan for the proposed MWRA wastewater outfall in Massachusetts Bay. The purpose of the Harbor and Outfall Monitoring (HOM) Program is to verify compliance with the discharge permit and to assess the potential effects of the relocated discharge of treated effluent into Massachusetts Bay. To help establish the present conditions, ENSR conducted the baseline water quality monitoring in 1996. This report represents the fifth continuous year of monitoring results since the program was established in February, 1992.

The objective of this report is to describe the 1996 seasonal baseline conditions of the water column in Boston Harbor and Massachusetts and Cape Cod Bays. Vertical profiles of the water column, along with discrete water samples obtained at predetermined depths, provide the basis to identify the predominant spatial scales of variability, the sources of the variability, and the general features of circulation and mixing at the time of the measurements. Analysis of seasonal fluctuations is performed to assess the temporal variability of each of the water properties, as well as the primary mechanisms responsible for the variability. Comparison to data collected in previous years is made to help establish interannual variability and to distinguish any trends.

The water quality data presented herein include the physical characteristics of temperature, salinity and density, annual nutrient cycling, chlorophyll, dissolved oxygen, productivity and respiration, and phytoplankton and zooplankton. Each are discussed in separate sections. A concluding section summarizes the principal events/observations noted within each section, and synthesizes results with a discussion of carbon cycling under existing and future discharge conditions.

2.0 DATA SOURCES AND 1996 PROGRAM OVERVIEW

This section identifies the various sources of information and data integrated in this annual report. The MWRA has a comprehensive bibliography of technical reports generated by the HOM Program. A general description of the documents associated with the 1996 water column monitoring tasks is provided below, along with an overview of the sampling program.

2.1 Data Sources

Full details of technical procedures, equipment, and quality controls are presented in the Combined Work/Quality Assurance Project Plan (CW/QAPP) for Water Quality Monitoring: 1995-1997 (Bowen *et al.*, 1997). This includes descriptions of standard survey methods, instrument specifications, laboratory support, and quality control procedures. Individual survey locations and descriptions, sampling methodologies, sequences of events, navigational and vessel information, and scientific crew are documented in individual survey plans prior to each survey and confirmed in survey reports. These reports also describe deviations in standard methods, detail any marine mammal observations, and present raw sensor data after each survey is completed.

Detailed summaries of water column survey data are available in three data reports (nutrient, plankton, and productivity/respiration) that are issued five times a year. Nutrient reports include sensor and chemistry data and plankton reports cover whole-water phytoplankton, screened phytoplankton, and zooplankton results. Finally, semiannual reports integrate results and provide initial interpretation of data. All quantitative data generated by the program are available in MWRA's HOM Program Database.

2.2 1996 Monitoring Program Overview

There were 17 water quality monitoring surveys conducted in Boston Harbor and Massachusetts and Cape Cod Bays during 1996. They were divided into two main types of surveys: nearfield/farfield combined surveys, which comprehensively samples all stations in the monitoring program (Figures 2-1 and 2-2) over several days, and nearfield surveys to sample the stations in the nearfield grid (Figure 2-2). Additional components were included within this framework to meet specific objectives. These included a Stellwagen Basin survey which was conducted in late fall to monitor dissolved oxygen levels at station F12 (located in Stellwagen Basin, see Figure 2-1), and a winter nutrients survey to determine the winter nutrient levels in the Massachusetts Bay area after the fall mixing event. Note however that inclement weather during the winter nutrients survey restricted data collection to the nearfield only.

The nearfield stations are located in a grid pattern over the future outfall site to provide a detailed picture of conditions in the water column in the vicinity of the discharge (Figure 2-2). The farfield stations are located throughout Boston Harbor, Cape Cod Bay and Massachusetts Bay in a strategic pattern that is intended to provide an overall characterization of the area. Stations are grouped into six regions in the Farfield area according to their location (Figure 2-1). These regions include Boston Harbor (stations F23, F30 and F31), the coastal region (stations F18, F24, F25, F14, F13, and F05), an offshore region (stations F22, F19, F16, F15, F10, F06 and F07,

and F17), a boundary region (stations F26, F27, F28, F12, and F29), and Cape Cod Bay (stations F01, F02, and F03).

The nearfield/farfield combined surveys were conducted six times during the course of the year, intended to capture periods of peak activity in the Massachusetts coastal waters. Two surveys during February, and one each in April and June, encompass the potential range of the spring bloom and the onset of stratification. One took place in August during peak stratification of the water column, and the last survey was in October during the late summer dissolved oxygen minima and prior the onset of the fall water column turnover. The nearfield-only surveys were performed an additional eleven times throughout the year at intervals of every two to three weeks (Table 2-1), from February through early December.

Altogether there are 42 stations located in the nearfield and farfield survey areas, 17 in the nearfield and 25 in the farfield. N16 is sampled as both a nearfield and farfield station. Stations are assigned categories which signify the types of analyses conducted at that station, with each category represented by a letter (A, D, E, F, G, R, and P) (Table 2-2). These station categories are also depicted in the station maps (Figures 2-1 and 2-2).

At each station, five depths are typically sampled (surface, mid-surface, middle, mid-bottom, and bottom, designated A, B, C, D and E, respectively). Shallower inshore stations were only sampled at three depths (surface, middle, and bottom). Detailed descriptions of station coverages and individual analyses performed are available in each of the survey plans and in the CW/QAPP.

TABLE 2-1

1996 Schedule of Survey Events

Event Number	Type of Survey	Date
W9601	Nearfield/Farfield	February 5-10
W9602	Nearfield/Farfield	February 23-March 28
W9603	Nearfield	March 18-20
W9604	Nearfield/Farfield	April 1-6
W9605	Nearfield	April 22-26
W9606	Nearfield	May 13-14
W9607	Nearfield/Farfield	June 17-20
W9608	Nearfield	July 1-2
W9609	Nearfield	July 23-24
W9610	Nearfield	August 5-6
W9611	Nearfield/Farfield	August 18-23
W9612	Nearfield	September 3-4
W9613	Nearfield	September 23-24
W9614	Nearfield/Farfield	October 6-11
W9615	Nearfield	October 29-30
W9616	Nearfield/Stellwagen Bank	November 17 - 19
W9617	Nearfield/Winter Nutrients	December 16-17

TABLE 2-2

Station Types and Analyses
(& Number of Depths Sampled)

Analysis	A	D	E	F	G	P	R
Dissolved Inorganic Nutrients (NH_4, NO_3, NO_2, PO_4, SiO_4)	5	5	5	5	3		
Other Nutrients (DOC, TDN, TDP, PC, PN, PP, Biogenic Si)	2	3			2		
Chlorophyll	5	5			3		
Total Suspended Solids	3	3			3		
Dissolved Oxygen	4	4		4	3		
Phytoplankton and Urea		2			2		
Zooplankton		1			1		
Respiration							3
Productivity						5	

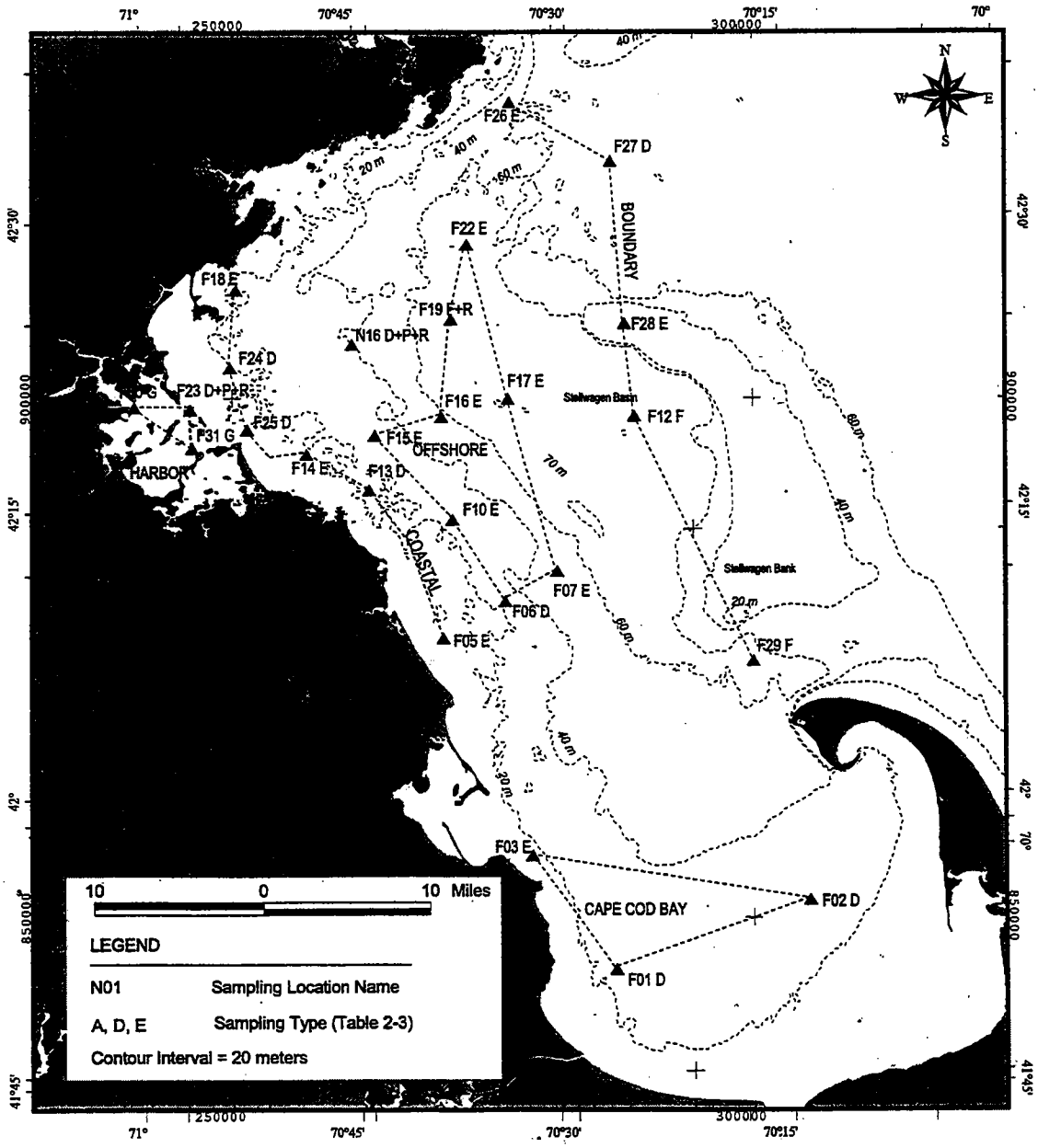

FIGURE 2-1
Location of Farfield Stations Showing Regional Geographic Classifications

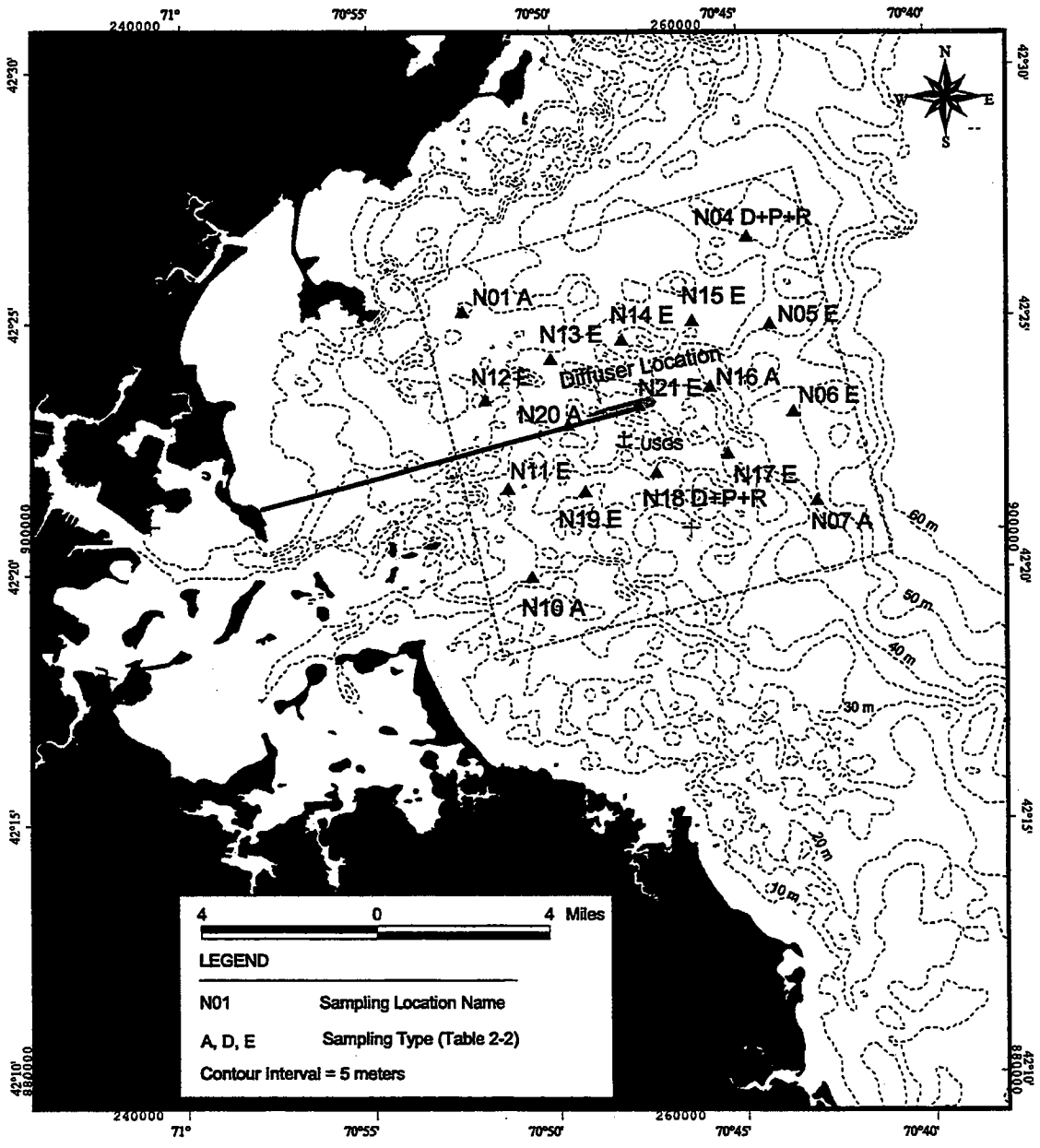

FIGURE 2-2
Location of Nearfield Stations and USGS Mooring

3.0 PHYSICAL CHARACTERIZATION OF SYSTEM

This section provides a basic overview of the physical structure of the water column in the Massachusetts Bay system. Data from the 1996 monitoring period are illustrated to contrast conditions in the various regions of the monitoring area, and to provide the context in later sections for presentations of chemical and biological processes also sampled by the HOM program. For easy reference and to facilitate integration of results from the various sections, significant events throughout the year are summarized in Table 9-1. The 1996 record is also compared with 1992-1995 baseline monitoring data to support interannual comparisons of monitoring results.

3.1 Meteorological Summary

This section presents an overview of weather conditions in Massachusetts during 1996. An effort was made to focus on information that occurred in coastal Massachusetts during the 1996 calendar year, including precipitation, temperature, and major storm events. This meteorological summary was obtained from the Northeast Regional Climate Center (NRCC, 1997). Precipitation's effects on stream flows are qualitatively summarized in this section as well, while quantitative discharge data for the Merrimack and Charles Rivers are included in Section 3.3.3. The meteorological information is used in later sections to evaluate the influence that specific meteorological events may have had on the physical, biological, or chemical structure of the water column of Massachusetts Bay, and is also summarized in Table 9-1 (beginning with February, the first month of monitoring).

3.1.1 January

January temperature's in the Northeast were unseasonably cold during the first half of the month (5°F below normal), followed by unseasonably warm temperatures during the latter half (15°F above normal). Precipitation was 191% of normal in Massachusetts. Both rain and snow contributed to this departure from average, producing above normal stream flows for January.

January 1996 was an active month for major storm events. The first storm was on the 2nd with slightly more than a foot of snow. Back to back storms occurred from the 7th to the 13th, beginning with the "blizzard of '96", followed by an Alberta Clipper, and ending with an East Coast storm, producing more than two feet of snow above normal. Wind maxima between 40mph to 51mph accompanied these storms. Winds in excess of 67mph were recorded for a rain storm on the 27th in Boston, Massachusetts.

3.1.2 February

As with January, February was unseasonably cold for the first half of the month, and unseasonably warm for the second half in the Northeast. Precipitation fell slightly below the monthly average for February (92%). Two storms occurred during February, the first storm between the 1st and 2nd produced 5-11 inches of snow in eastern Massachusetts, the second storm on the 16th and 17th accumulated 7 inches of snowfall in Boston. A northeaster

produced sustained winds of 50-80 mph on the 24th and 25th of the month to the southern coast of Massachusetts.

3.1.3 March

March temperatures in Massachusetts were 2.6°F below average for the month. March precipitation was below average (81%), but exceeded the monthly average for snow (16.8 inches in Boston, Massachusetts). Stream flows were reported as being normal. There were two significant storms in March, one on the 2nd and the other from the 5th-8th.

3.1.4 April

Temperatures matched historical averages for the month of April. April precipitation was 171% of normal due both to snow and rain in Massachusetts, although stream flow remained normal for April. April began with a snow storm on the 9th, which remained mostly to the central portions of Massachusetts, followed by heavy winds between the 16th-19th.

3.1.5 May

The average temperature for May was approximately one degree cooler than historical averages for Massachusetts. The colder than usual temperatures were interrupted by a small heat wave between the 18th and the 24th in the Northeast, with temperatures in excess of 80° to 90°F. Statewide, Massachusetts experienced a dry month in May, accompanied by average stream flows.

May was a calm month in terms of significant storm events in coastal Massachusetts. The severe weather remained to the west and southwest, except for one intense thunderstorm which occurred on the 21st of May which had winds in excess of 70mph.

3.1.6 June

June was 1.4°F degrees warmer than average for Massachusetts. June's precipitation increased from 74% of the normal precipitation in 1995 to 112% of the norm in 1996 in the Northeast. However, precipitation for Massachusetts remained slightly below average during the month (80% of norm). Stream flows remained average during the month. June was also relatively calm with respect to significant storm events.

3.1.7 July

The average temperature for July was approximately one degree cooler than historical averages in Massachusetts. July 1996 was the wettest July in 58 years, attaining 181% of the monthly normal precipitation statewide. Thunderstorms accompanied by high winds dominated July between the 14th-16th. Rainfall on July 12th and 13th (associated with Tropical Storm Bertha) exceeded four inches, resulting in above-average stream flows and

generating flash floods and swollen rivers. Peak wind gusts of 33mph were reported in Boston on the 13th and 14th.

3.1.8 August

August fell within the long term average for temperature. Massachusetts underwent an unusually dry month in August, with only 61% of the normal precipitation for Massachusetts. Stream flow was average for August. Rain and thunderstorms associated with high winds were recorded on the 16th, 23rd, and 27th, but remained mostly in western areas of the state.

3.1.9 September

Temperatures for the Northeast were warmer than normal for the month of September. Precipitation was 227% above normal, making it the third wettest September on record and producing above average stream flows in Massachusetts.

Hurricanes Edouard, Fran, and Fausto contributed to September's high precipitation total. Hurricane Edouard generated a one to two foot storm surge, wind gusts up to 75 mph, and 6 inches of rainfall on the 2nd. Hurricane Fran brought flooding, high winds, and heavy rainfall between the 6th and 9th. The Pacific Hurricane Fausto reached the southern New England coast on the 17th, bringing high winds and 4.71 inches of rainfall, recorded at Blue Hills Observatory in Massachusetts.

3.1.10 October

Temperatures in October were slightly under the average. Precipitation was more than double (225%) the normal rainfall average, making it the wettest October in 98 years for Massachusetts. The heaviest rains fell between October 18th and 21st. Monthly stream flow averages were also above normal.

On October 8th, Hurricane Josephine predominately affected the Mid-Atlantic region, but did produce significant rainfall in Massachusetts Bay. The remnants of Hurricane Lili affected coastal Massachusetts with high winds and flooding on October 20th and 21st, producing 8-12 inches of rain over a 24-hr period in Northeastern Massachusetts.

3.1.11 November

Temperatures in November were colder than normal, averaging 4.3°F below average in Massachusetts. Precipitation levels were 75% of the average statewide, but above-normal stream flows continued. One significant storm dominated November on the 8th and 9th, with 2-4 inches of rain and high winds (peak velocity at Blue Hill Observatory was 67 mph).

3.1.12 December

Temperatures for the Northeast were warmer than normal for the month of December. December precipitation was 147% of the long-term average (165% of the norm in Massachusetts), and contributed to making 1996 the wettest calendar year on record. Stream flows were above normal for the month. The major storm event of December was a snowstorm on the 6th which produced eight inches of snow in Massachusetts.

3.2 Annual Temperature Cycle

3.2.1 Nearfield

The 21 monitoring stations in the nearfield were sampled with the greatest frequency (n=17), providing the best resolution for the annual temperature cycle in Massachusetts Bay based on shipboard measurements. Additional continuously-recorded temperature data were available from USGS arrays moored within the nearfield (USGS, 1997b). During the 1996 period, these sensors were located 5m below the surface, and 22 m below the surface.

Nearfield temperature data from the 1996 HOM sampling program are presented for three regions: inner nearfield stations which are influenced by the Harbor's strong tides (Stations N10 and N11; refer to Figure 2-2); Broad Sound (off of Winthrop and Nahant) as represented by Station N01; and outer nearfield as represented by offshore stations N04, N07, N16, and N20 (Figure 3-1a, b, and c).

February data indicated that water temperatures in the inner nearfield area were colder than was observed in the more offshore stations, which appeared to still be cooling during February. By mid-February, average water temperatures were uniform both horizontally and vertically across the nearfield (ca. 2°C), after which surface warming began. Maximum surface (typically <2.5m depth) temperatures had been reached by the end of July in the inshore waters and mid-August in the offshore waters. Offshore water averages were somewhat warmer (ca. 19°C) than inshore waters (< 19°C). With surface waters beginning to cool after early August, bottom waters (typically >80 percent water column depth) continued toward their maxima. Inshore waters reached their maxima around the beginning of September while offshore area reached theirs towards the end of September. Inshore bottom averages were somewhat warmer (ca. 14°C) than offshore waters (12°C). The water column appeared to be vertically homogenous by early October in the inshore waters and late October in the offshore waters (Table 9-1).

Continuous data collected in 1996 from the USGS mooring located near the center of the nearfield (Figure 2-2) were plotted along with data from station N16 (Figure 3-2). These continuous measurements at the surface and bottom confirmed that the nearfield stations reached their annual temperature minima during mid- to late-February. Moored sensor and shipboard measurements were quite similar except for a few surface measurements during the summer, which are attributable to the difference in depth (5m for mooring, typically <2.5 m for shipboard measurements).

Notable features evident in the moored temperature data include a slight reduction in bottom water temperature in late April, possibly indicative of advective movement of water into the nearfield. The rapid warming of surface

waters associated with the weeklong heat wave in May (Sect. 3.1.5) is also evident in the mooring data, followed by fluctuation surface temperature in late May and early June. Tropical storm Bertha appeared to reduce surface temperatures in mid-July, also seen in shipboard measurements from survey W9609 (Figure 3-1). Two reductions in bottom water temperature in late July and again in mid-August were suggestive of advection or upwelling.

The moored temperature sensors indicated that hurricane activity during early September caused substantial mixing in the water column, with the 5m and 22m sensors showing temperature convergence twice during the month (between surveys W9612 and W9613). Although the thermocline appeared to be somewhat restored in late September, isothermal temperatures were recorded shortly after survey W9614 in early October. The temperature data therefore suggest that the water column mixing occurred during early September, with the annual turnover complete by mid-October.

3.2.2 Regional Comparisons

Regional comparisons were made using farfield survey data. Average surface and bottom temperature data were calculated from farfield survey data (n=6) for the regions defined in Section 2.

In late winter, regionally averaged survey temperatures revealed colder waters inshore throughout the water column (Figure 3-3a through e). After April, surface temperatures increased and were for the most part similar throughout the regions for the rest of the year. Bottom waters reflected the differences in regional depths, with harbor waters reaching maximum temperatures around 15°C in August, while bottom waters in deeper offshore and boundary regions warmed more slowly and reached maxima of only around 10°C in October. Cape Cod Bay was similar to the coastal stations.

3.2.3 1992-1996 Interannual Comparisons

The annual cycle for average nearfield surface and bottom water temperatures for the period 1992 to 1996 was plotted to examine interannual differences (Figure 3-4, top). Surface temperatures were similar for each year, although 1995 peaked approximately 2°C higher than that seen in previous years and 1994 had maxima approximately 2°C lower than that seen in other years. The most pronounced feature of the five-year record is the relatively high bottom temperatures evident in the latter parts of 1994, 1995 and 1996. While bottom temperatures did not exceed 9°C during either 1992 or 1993, the maximum temperature during 1994 was around 12°C, and was just slightly higher during 1995 and 1996.

More importantly, the bottom temperature in the nearfield during 1994 and 1996 exceeded the 9°C 1992-1993 maxima for a duration of almost five months. Although peak bottom temperatures were slightly higher in 1995 than in 1994, the duration of temperatures above 9°C was only around two months. The potential for high metabolic activity and respiration was therefore greatest during 1994 and 1996. This potential is discussed in greater detail in Sections 6 and 7.

A similar scenario was evident in Stellwagen Basin (Figure 3-4, bottom). Surface temperatures were similar in each of the five years except for the August 1994 survey which yielded cooler than usual temperatures (16°C) and the August 1995 survey which yielded slightly higher than usual temperatures. Average maximum bottom temperatures in Stellwagen Basin during 1992-1993 were only around 7°C. However, the maximum bottom temperature in 1994 and 1996 was around 10°C, while maximum temperatures in 1995 were around 9°C. The infrequency of farfield measurements did not permit a precise determination of how long temperatures in 1994, 1995 and 1996 remained above 1992-1993 maxima, but it appeared that this may have lasted for a minimum of two months.

3.3 Salinity

3.3.1 Nearfield

As with the temperature data, surface and bottom salinity profiles were plotted for the three regions of the nearfield (Figure 3-5). General trends showed surface salinity decreasing through June, with a large drop in salinity evident in late May apparently due to advection from the Gulf of Maine. Bottom salinity ceased its seasonal decline in mid-April, and remained fairly stable through August. Surface salinity increased through June and July, but showed a sharp decrease in August, again apparently due to advection. Salinity data indicated mixing during early September from Hurricanes Eduoard and Fran, and again in October from Hurricane Josephine.

Continuously-recorded data from the USGS mooring documented similar surface and bottom salinities in the nearfield during February and March (Figure 3-6). Reductions in salinity at the surface at the end of May are especially evident in the continuous mooring data. Bottom water measurements remained stable, providing further evidence that the May event was the result of surface advection of fresher waters into the nearfield (Table 9-1). A similar but less conspicuous event occurred in late August (Figure 3-6). The effects of hurricanes in early September and October are clearly evident in the USGS data. Partial stratification mixing occurred in early September and again in late September. Complete water column mixing occurred by mid-October.

3.3.2 Regional Comparisons

Harbor and coastal stations had the lowest regional salinity averages (Figure 3-7). In general, surface waters were consistently lower in salinity than bottom waters throughout the year. Coastal and Cape Cod Bay stations did exhibit convergence of surface and bottom salinity during the winter surveys. Surface and bottom water salinity at the coastal stations converged again in early October.

Offshore and boundary stations were fairly homogenous through the April survey. The June and August surveys documented more than a 1.0 PSU difference between surface and bottom, while subsequent surveys indicated much less vertical difference. Cape Cod Bay averages indicated that any vertical salinity differences were quite modest, and overall were quite similar to the coastal stations.

3.3.3 Influence of Precipitation and River Discharge on Salinity

Precipitation data from Logan Airport obtained from the Northeast Regional Climate Center (NRCC, 1997) documented nine large precipitation events (> 1" rainfall) throughout 1996, making 1996 the wettest calendar year on record (Figure 3-8a). The first large precipitation event occurred in April when 1.5 inches of rain fell. This rainfall combined with the meltdown of winter snow resulted in peak spring discharges in the Merrimack River (greater than 50,000 cfs)[1] and the Charles River (ca. 1,200 cfs)[2] (Figure 3-8c). Additional periods of heavy rain in July resulted in a second pulse of riverine discharge, with the Merrimack peaking over 20,000 cfs and the Charles discharging approximately 500 cfs for slightly less than one month. Peaks in September and October were followed the maximum precipitation which occurred at the end of October. Precipitation was double the normal rainfall average (211%) in October with a peak of 6 inches in late October. The large amount of rainfall resulted in peak fall discharges in the Merrimack River (ca. 45,000 cfs) and the Charles River (greater than 2,500 cfs).

The periods of heavy discharge from the two rivers during April and May coincide with the large decline in salinity seen in the moored data during these periods (Figure 3-8b). Precipitation events in July and September also coincided with modest surface salinity drops. Rainfall and river discharge was also high in late November and early December during which there was a concurrent drop in salinity visible in both the nearfield survey data and moored sensor data.

3.3.4 1992-1996 Interannual Comparisons

Interannual plots of surface and bottom salinities in the nearfield and Stellwagen Basin indicated that the highest salinities occurred in 1994 and 1995 (Figure 3-9). Lowest salinities for the baseline period occurred in 1996, reflecting its status as the wettest year on record. 1996 also had a large degree of variability in the surface water salinity due to the frequent occurrence of major storm events. The GOM intrusion in May of 1996 discussed previously is reminiscent of an even larger one in 1993.

3.4 Water Column Stratification

Massachusetts Bay is typically characterized by a seasonal cycle from cold, well-mixed waters during winter months to strong stratification during summer. Early stratification during spring is salinity-driven due to freshwater runoff from the major rivers to the north and from coastal runoff, while temperature dominates the density structure during summer and fall (Geyer *et al.*, 1992). In the following sections, the water column

[1] Merrimack R. data from gage 01100000 in Lowell, MA., multiplied by 1.08 to estimate discharge at mouth of river (USGS, 1997b)

[2] Charles R. data from gage 01104500 at Waltham, MA., multiplied by 1.27 to estimate discharge at mouth of river (USGS, 1997b)

structure in the nearfield during 1996 is compared with other regions within the system, as well as with previous baseline monitoring years.

3.4.1 1996 Nearfield Stratification

The density data for the both the Inner Nearfield and Broad Sound stations indicated that stratification developed before the May survey W9606 (Figure 3-10). Afterwards, water column stratification was strong until early September. Stratification in the Outer Nearfield developed slightly later and remained stratified until early October.

Perturbations in the water column were most evident at the shallower Inner Nearfield and Broad Sound stations, which are subject to breakdown of stratification from upwelling and downwelling events and to tidal influences from Boston Harbor. However, each of the nearfield regions showed evidence of partial mixing during July. In the Inner Nearfield in early August, surface density dropped substantially from the previous survey's measurements, illustrating the advective event previously discussed. The decrease in bottom density during the next survey was due to the mixing from the hurricanes in early September.

In early September the waters at the Inner and Broad Sound stations appeared to converge somewhat earlier than the outer nearfield stations, primarily due to greater mixing in shallower waters from the hurricanes. More complete mixing in deeper waters occurred in October due to Hurricane Josephine (Table 9-1), effectively ending stratification for the year.

3.4.2 Regional Comparisons

The winter months were characterized by a well mixed water column throughout the survey area (Figure 3-11). Harbor stations exhibited little seasonal vertical structure. Offshore and Boundary stations were most similar to outer nearfield stations, primarily due to their comparatively deep depths.

The seasonal progression of stratification was plotted for several stations representing a transect from inshore to offshore (Figures 3-12 to 3-17). The stations selected for this illustration included the five productivity and respiration stations (F23, N16, N04, N07, and F19), providing reference for the discussions of these results in Section 7. Station N10 was included in this transect in order to demonstrate the tidal influence from the harbor on water column structure in the inner nearfield.

Harbor station F23 showed slight vertical stratification during the early winter (W9601), early spring (W9604) and fall (W9614). Stratification was more defined during the summer (W9607 and W9611) (Figure 3-12). Nearfield station N10 showed indications of stratification beginning during the third survey and becoming completely stratified during survey W9605. (Figures 3-13). Station N16 showed similar but more pronounced patterns of stratification. Salinity-driven stratification was evident during survey W9601 (Figure 3-14). The salinity-driven stratification was also evident in results from N04 along with more pronounced patterns of stratification (Figure 3-15). Station N07 also became stratified during survey W9605 with slight stratification evident during survey W9601. (Figure 3-16). Station F19 in Stellwagen Basin appeared to be similar to N04 with

the exception of an early onset of stratification during survey W9604. (Figure 3-17, note reduced frequency of survey coverage).

Beyond this early season influence from salinity, the water column remained fairly homogenous until the onset of thermally-driven stratification by survey W9605. The stratified period lasted from late April until October when the water column began to turn over (survey W9614). However, the extent of the July mixing event described in earlier sections is well-documented in the nearfield station results. Mixing to a depth of approximately 10m was evident in profiles from survey W9610, particularly at the more inshore station N10. By survey W9614, the water column had mixed almost to the bottom at each station.

3.4.3 1992-1996 Interannual Comparisons

A comparison of the surface and bottom densities for the 1992-1996 data record indicated that the structure of the water column in the nearfield was most stable during 1994 (Figure 3-18a). Although surface densities showed similar patterns, bottom densities were highest and had the least amount of variability. Results from 1996 were more similar to 1995 than previous years, with the greatest departure associated with the drop in density in August and the variability in measurements during the fall surveys. Results for the Stellwagen basin stations were much more comparable between the years, with the main difference being the more dense surface waters during 1994 (Figure 3-18b).

3.5 Currents

The U.S. Geological Survey (USGS) collected current meter data at the mooring deployed in Massachusetts Bay (Figure 2-2), within the nearfield grid (USGS, 1997a). Current data were available at three depths in the water column (approximately 5, 22 and 30 meters). The availability of oceanographic mooring data coincident with the nearfield sampling surveys is represented in Table 1 in Appendix A.

In order to visualize the large volume of data collected by the current meters, and to help conceptualize the potential movement of water within the nearfield around the time of each survey, progressive vector plots were developed (Appendix A). These plots project the progressive movement of a hypothetical particle within the water column at the depth of each sensor based on measurements taken at the mooring. As the particle travels further away from the mooring, however, the projection becomes less reliable as it assumes that the water movement at locations increasingly distant from the mooring remains the same. In order to minimize this potential error, the plots use the survey date as time zero, and project particle movement both backward and forward in time. Another way to illustrate current data is through the use of stick plots (see USGS, 1997b).

Table 3-1 summarizes the net movement of water around the time of each survey during 1996, and estimates the residence time of a water particle in the nearfield at each depth. Current meter data from the surface water and bottom water were available only for surveys W9602 through W9617, while data from the mid-depth were obtained for all surveys. In general, surface water was the fastest moving layer, with the bottom water layer being the slowest. Also evident from the plots in Appendix A and Table 3-1 is that the currents at the different depths often move in opposing directions (e.g., survey W9610 in Appendix A).

Residence times (i.e. time to traverse a 10km box) in surface water were typically less than 3 days, and ranged from less than one day to >11 days (Table 3-1). Large estimated residence times at the surface were often due to reversing current direction (e.g., survey W9602 in Appendix A). Residence times at the mid-depth were typically on the order of one week, while bottom water was often greater than two weeks. It is noteworthy that the estimated residence time in bottom water decreased during surveys W9609 and W9610, a critical period with respect to oxygen depletion during the stratified period (Section 6).

The progressive vector plots for periods of time associated with the advection or mixing discussed previously were examined to discern if the current data could provide further insight into these events. For example, the data from W9605 clearly indicate an onshore movement of water at both the bottom and mid-depths. This observation, coupled with a net easterly flow at the surface, decreasing bottom water temperature (Figure 3-2), and increasing bottom salinity (Figure 3-6), is consistent with coastal upwelling. Unfortunately, the large Gulf of Maine intrusion in late May evident in the salinity data is not readily apparent in the progressive vector plot for W9606 as it largely occurred after this survey. USGS (1997b) stick plots confirm advection into the nearfield during the period, although the surface data are highly variable. Potential periods of advection of water into the nearfield suggested by temperature and salinity data during mid-July and early August again fall between surveys, and thus are also better depicted in the USGS stick plots.

The results from the various physical data are used in the following sections to help interpret the chemical and biological results, and provide a better understanding of the processes and events that occur in Massachusetts Bay.

SURVEY	DEPTH					
	Surface		Mid-depth		Bottom	
	Direction	R.T.	Direction	R.T.	Direction	R.T.
W9601	X	X	SE - NW	9	X	X
W9602	S - NW	7	NW	9	W	7
W9603	S	7	SE - NW	>14	W	>14
W9604	SW	3	NULL	>10	NW - E	>11
W9605	SE - NE	2	NW	5	SW	5
W9606	S - N	3	NULL	>10	SW	>10
W9607	NE	3	SW - NE	>9	NULL	>14
W9608	E	1	SE	6	W	>14
W9609	W	4	SE	7	SW	10
W9610	W	1	SE - NW	4	SE - SW	8
W9611	NW	>11	SE	7	SW	>14
W9612	SE	1	SE - N W	6	E - W	7
W9613	SW - E	3	NW	7	W	6
W9614	N - S	3	E - N	8	SW	10
W9615	SW - NE	2	N	5	SW - W	>10
W9616	NE - SW	2	SE - NW	>10	S - W	>12
W9617	S	<1	SE - NW	4	SE - SW	5

Notes:
NULL = no distinguishable movement
R.T. = Residence time (reported in days)
X - surface and bottom water current velocity not recorded

TABLE 3-1
Net Movement and Residence Time within the Nearfield

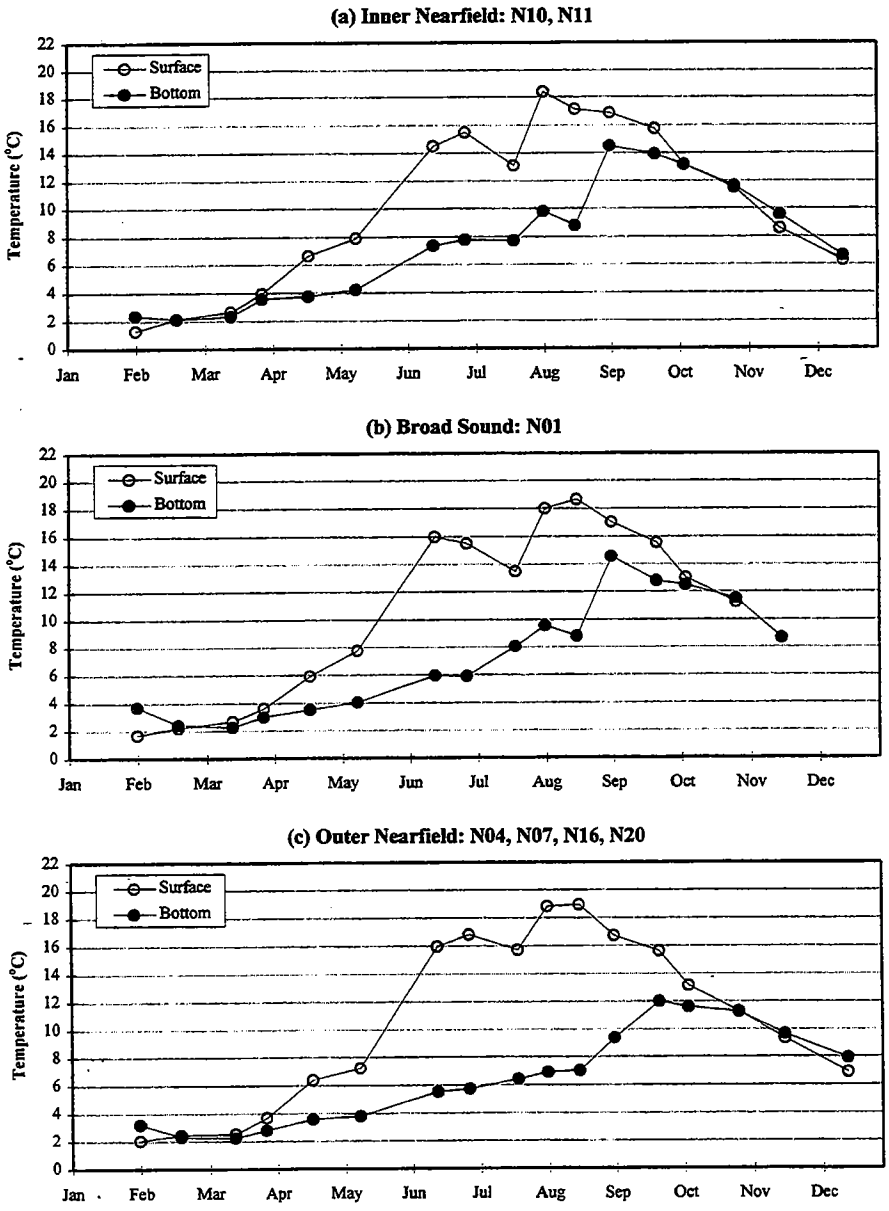

FIGURE 3-1

1996 Nearfield Temperature Cycle

Surface, Bottom, and Delta (Surface - Bottom) Survey Averages

3-1TEMP.XLS

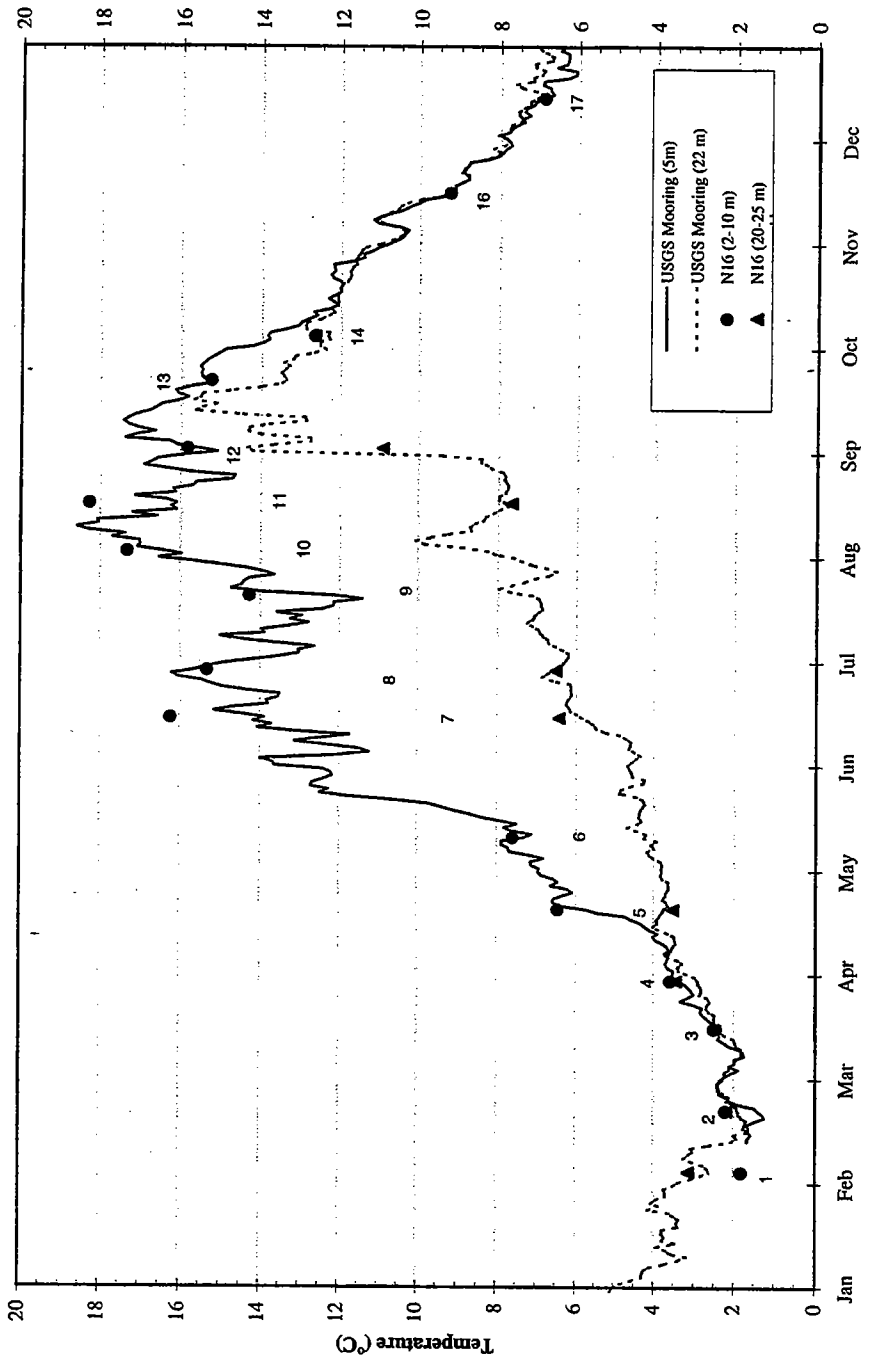

FIGURE 3-2
1996 Water Column Temperature at the USGS Buoy Mooring and Nearfield Station N16

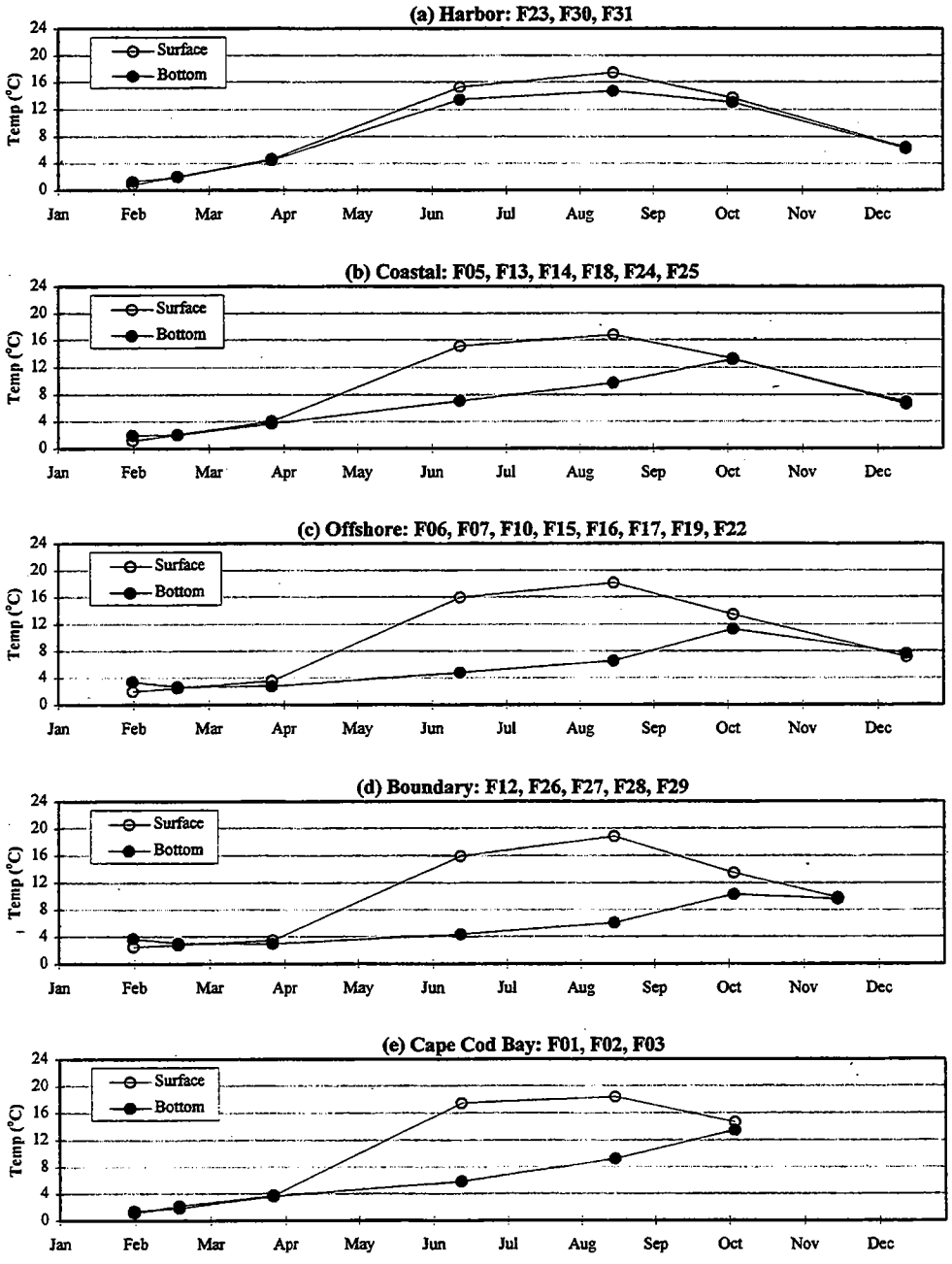

FIGURE 3-3
1996 Regional Temperature Averages
Surface, Bottom, and Delta (Surface - Bottom) Survey Averages

3-3TEMP.XLS

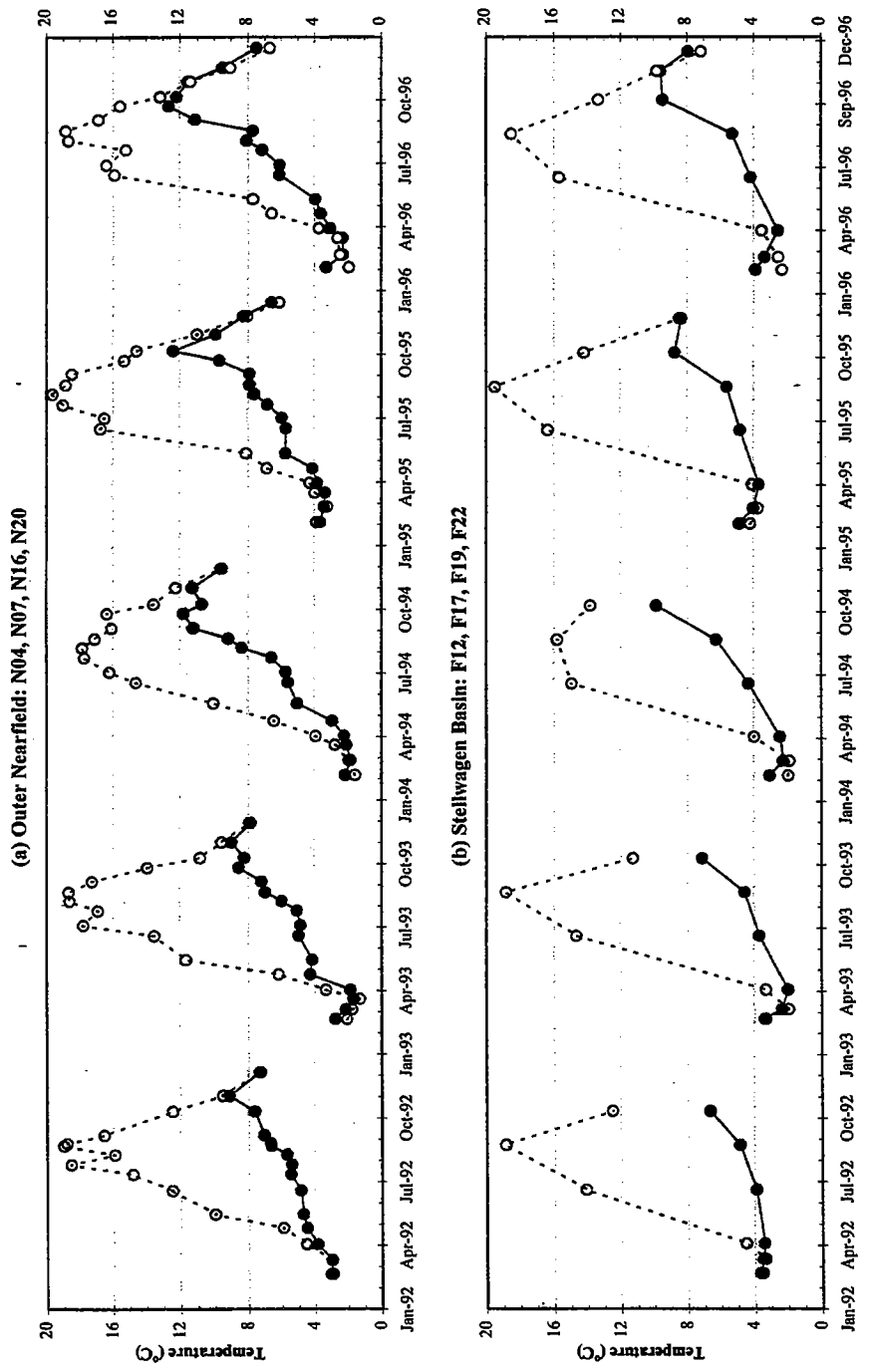

FIGURE 3-4

Interannual Comparison of Temperature in the Nearfield and Stellwagen Basin Regions

Surface (A, open symbols) and Bottom (E, solid symbols) depths averaged over stations as indicated.

3-4TEMP.XLS

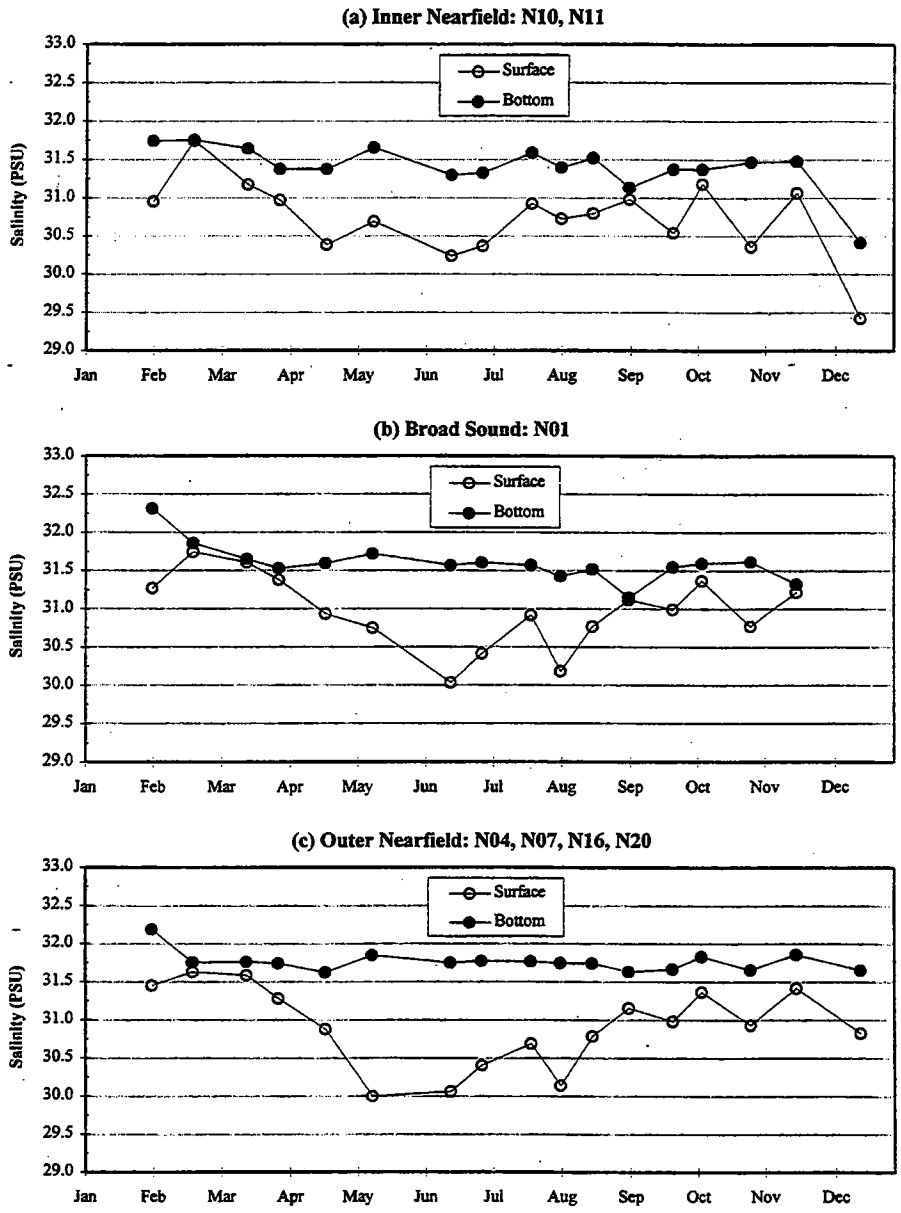

FIGURE 3-5

1996 Nearfield Salinity Cycle

Surface, Bottom, and Delta (Surface - Bottom) Survey Averages

3-5SAL_XLS

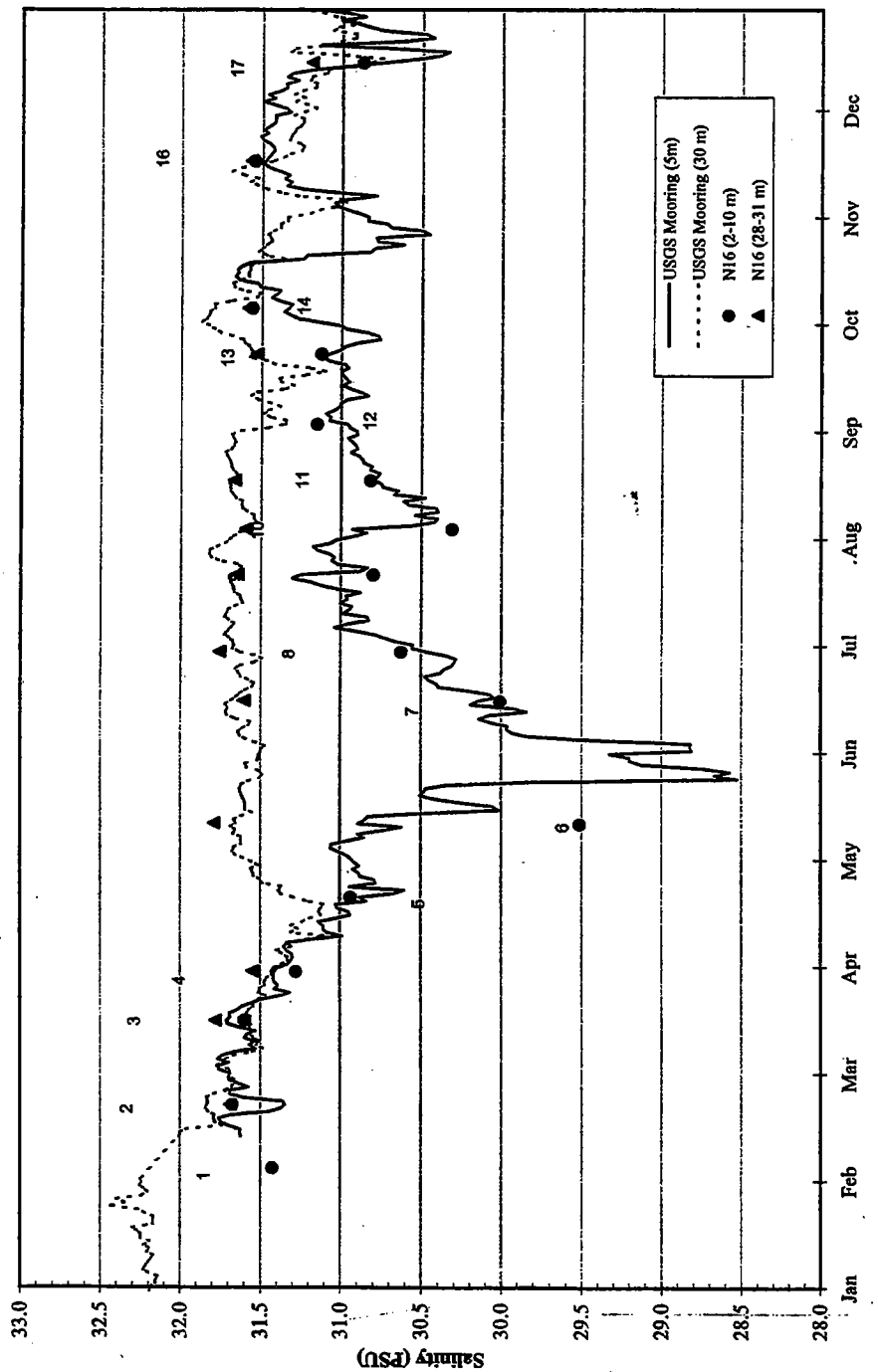

FIGURE 3-6
1996 Water Column Salinity for the USGS Buoy and Nearfield Station N16

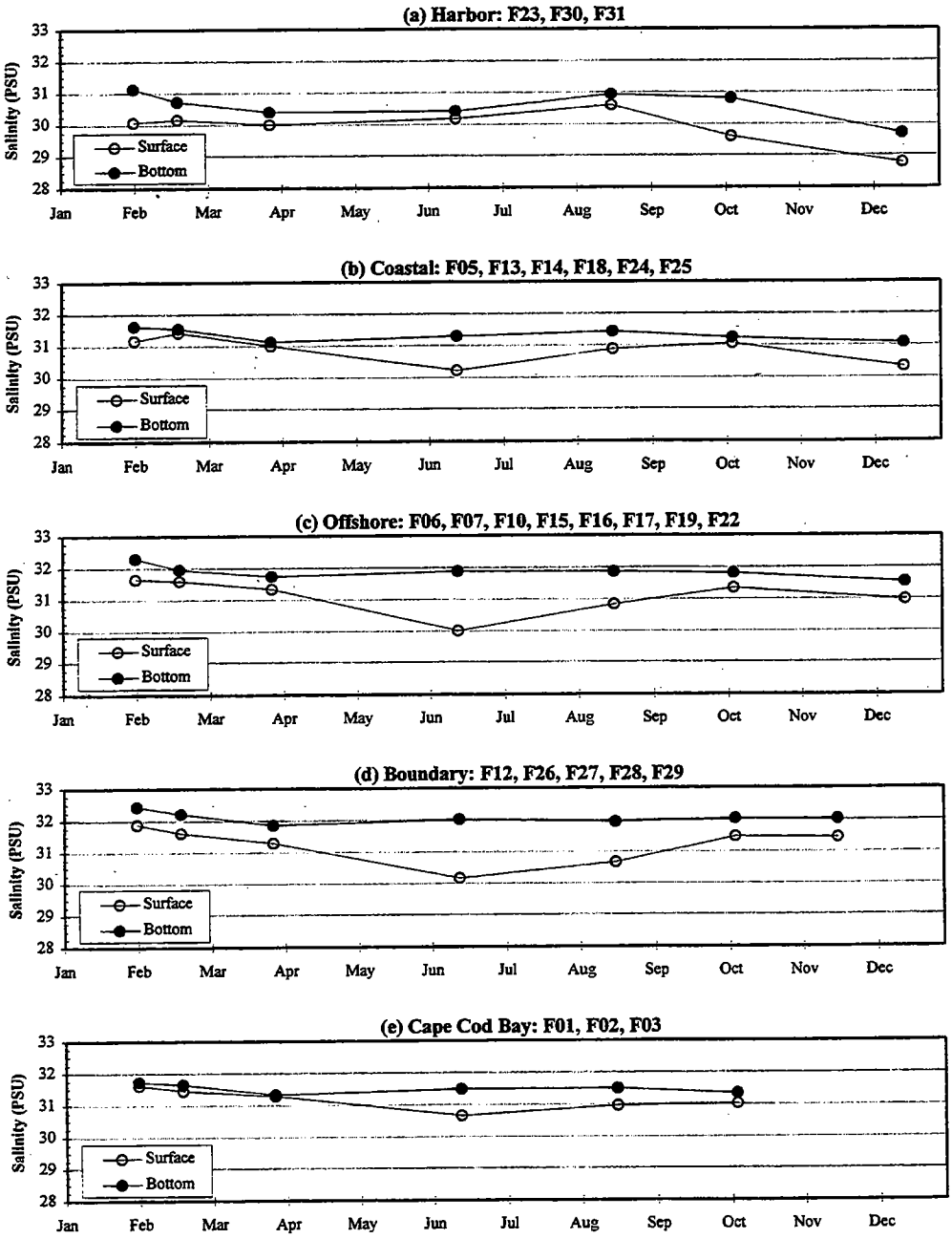

FIGURE 3-7
1996 Regional Salinity Averages
Surface, Bottom, and Delta (Surface - Bottom) Survey Averages

3-7SAL_XLS

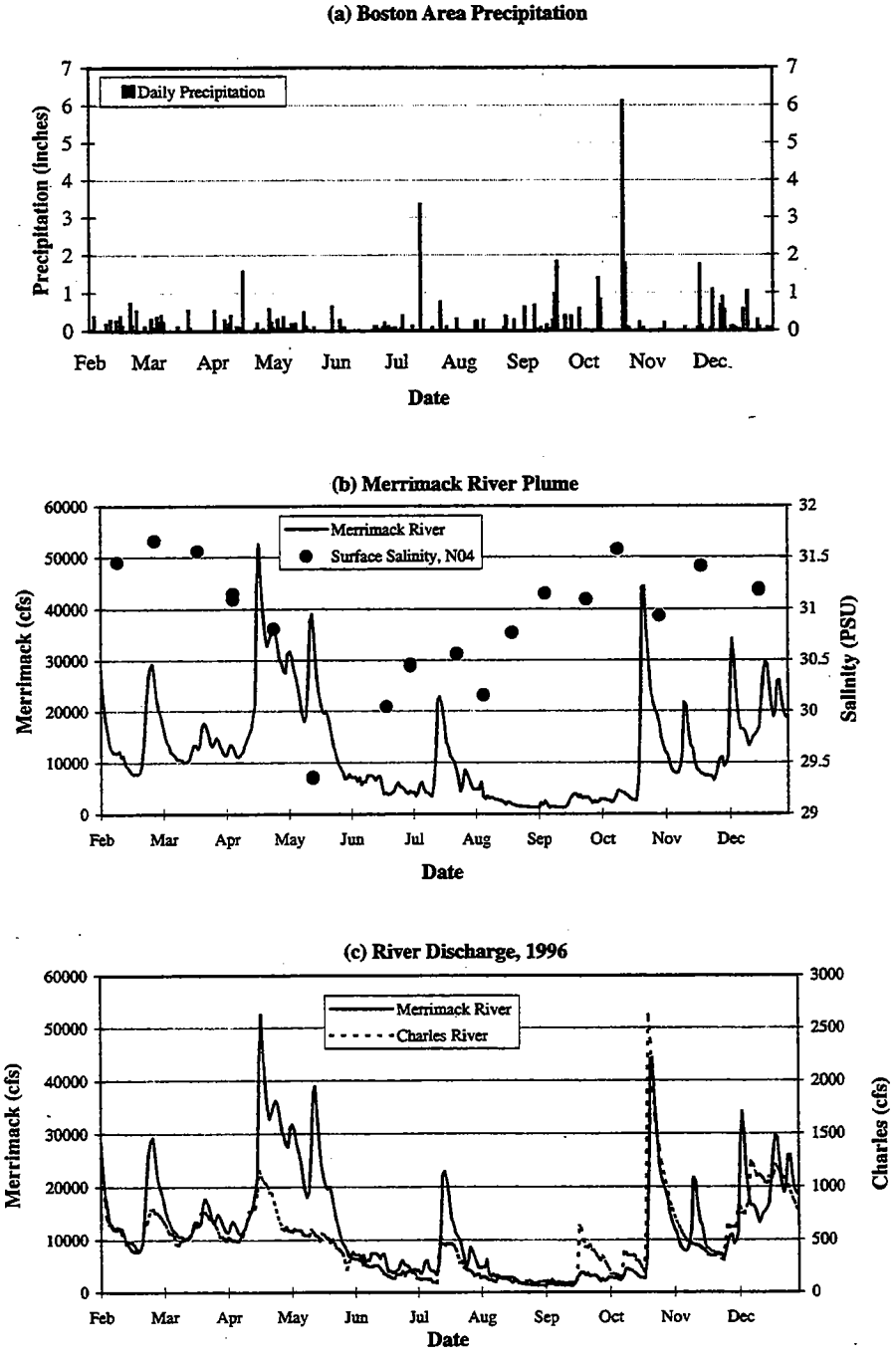

FIGURE 3-8

1996 Daily Precipitation (Logan International Airport) and River Discharge Data
Merrimack and Charles Rivers

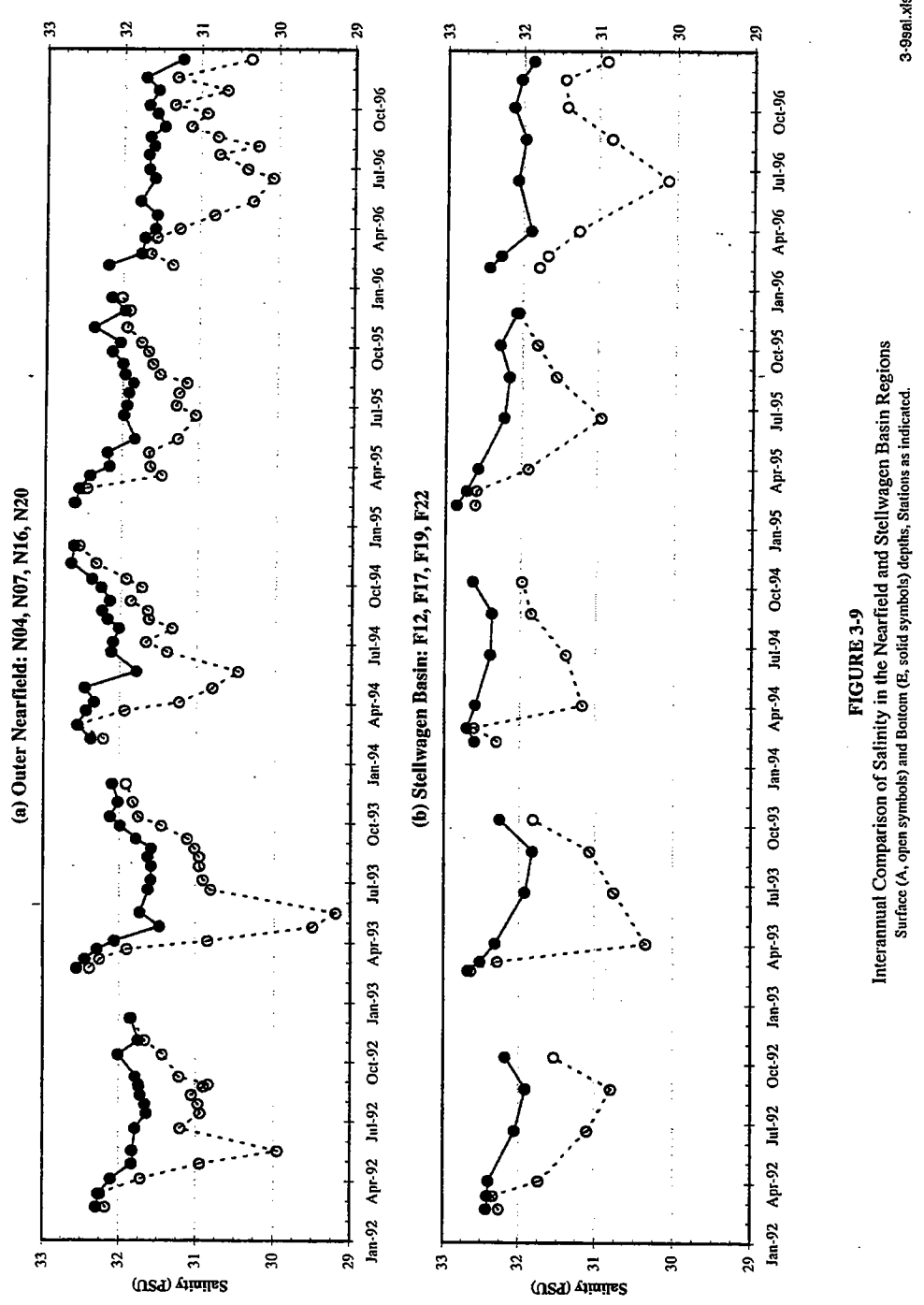

FIGURE 3-9
Interannual Comparison of Salinity in the Nearfield and Stellwagen Basin Regions
Surface (A, open symbols) and Bottom (E, solid symbols) depths, Stations as indicated.

3-9sal.xls

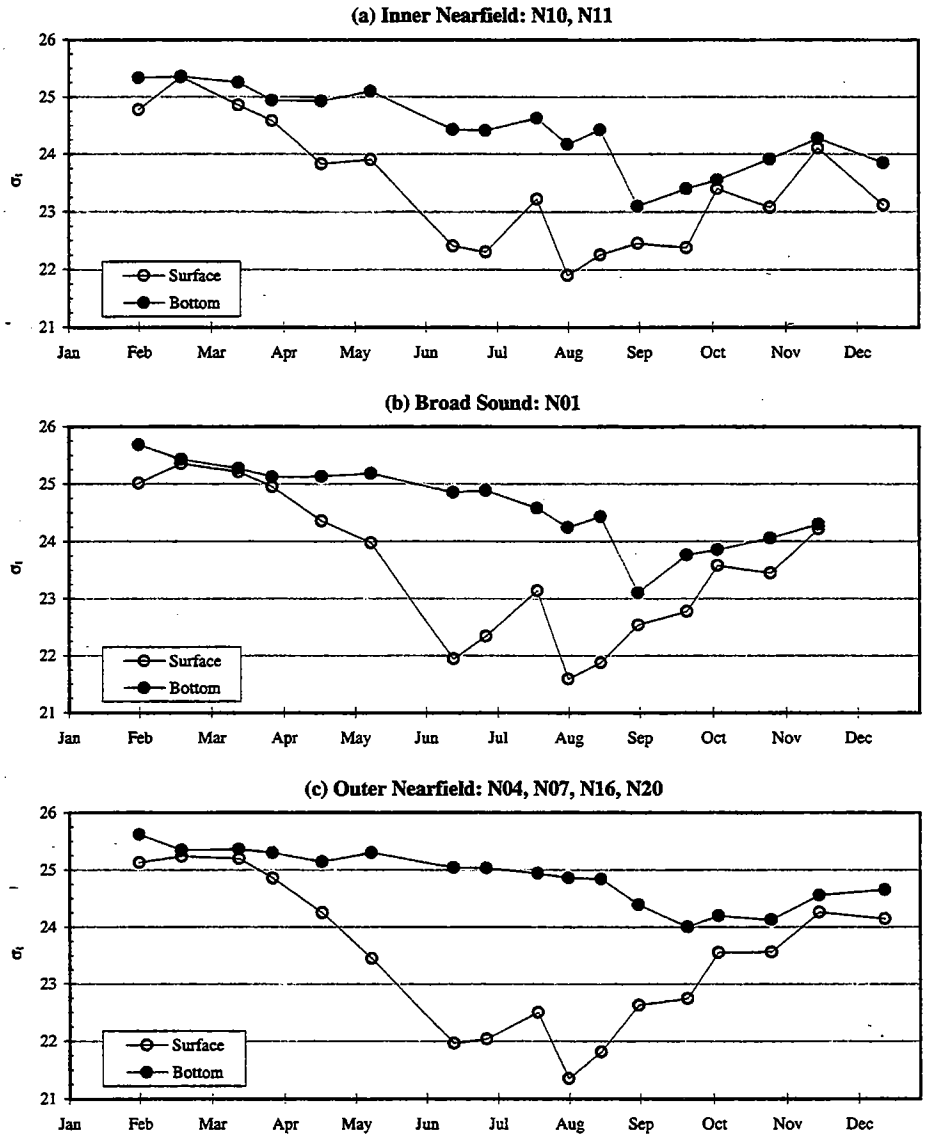

FIGURE 3-10
1996 Nearfield Density (σ_t) Cycle
Surface, Bottom, and Delta (Surface - Bottom) Survey Averages

3-10sig.xls

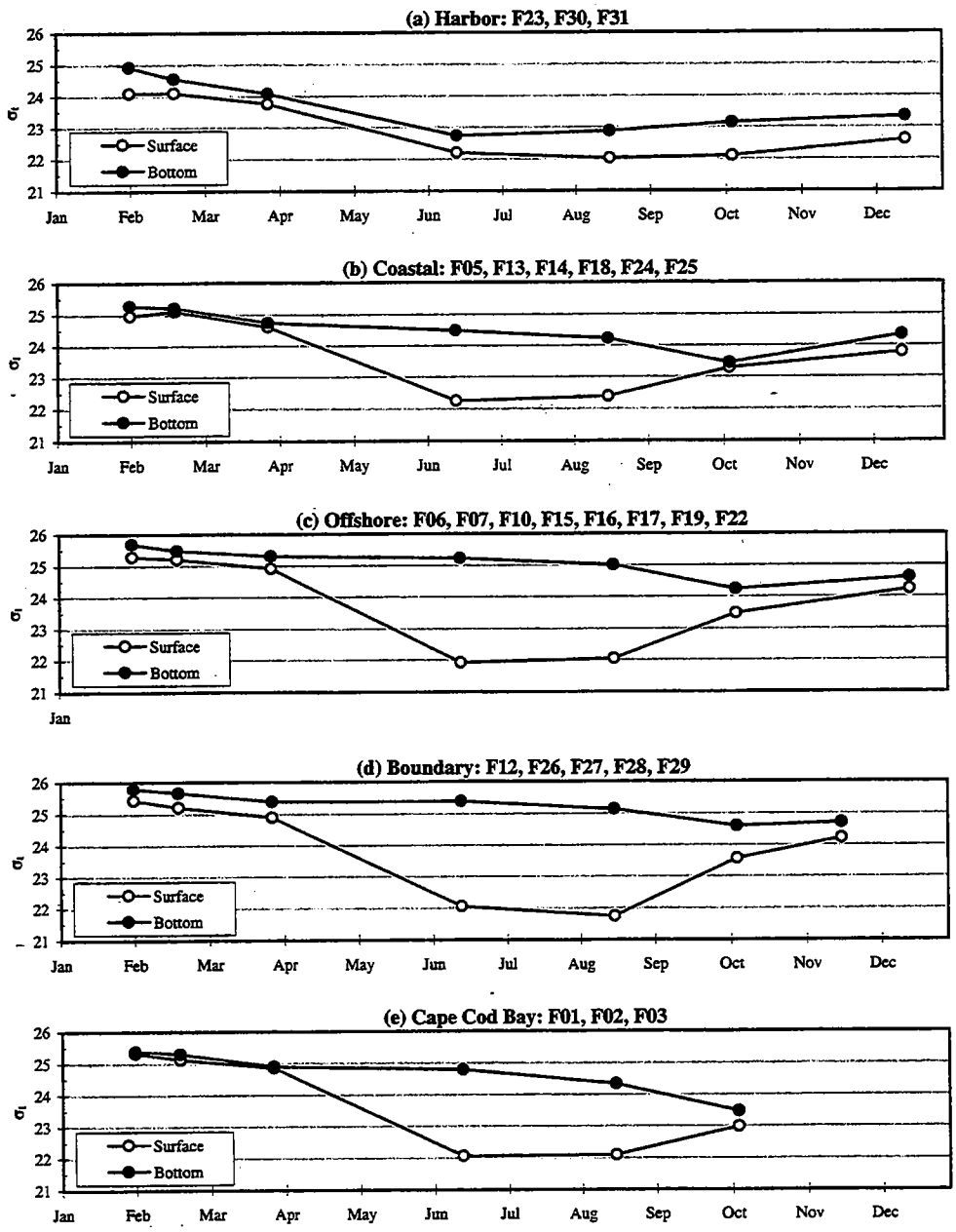

FIGURE 3-11

1996 Regional Density (σ_t) Averages

Surface, Bottom, and Delta (Surface - Bottom) Survey Averages

3-11sig.XLS

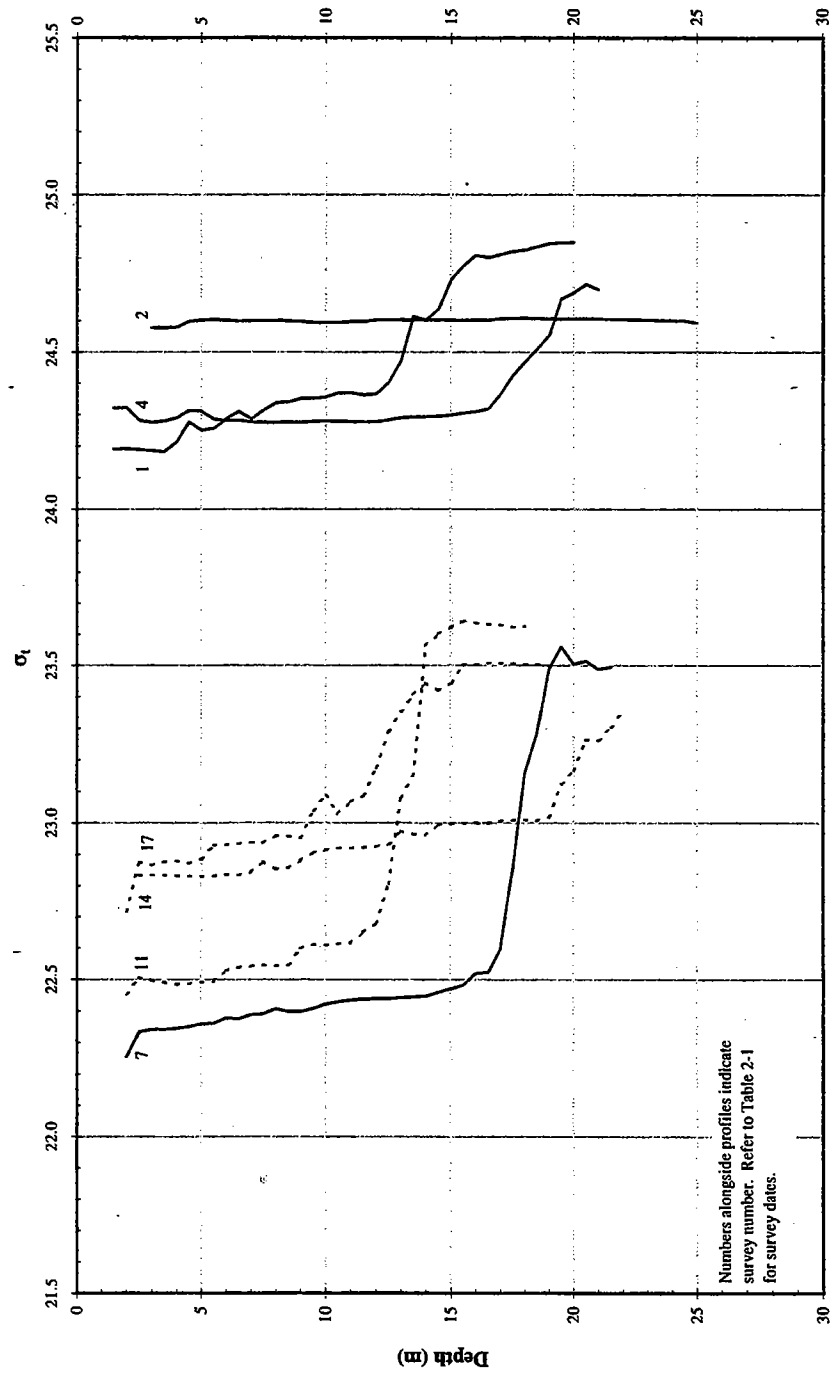

FIGURE 3-12
1996 Seasonal Density (σ_t) Cycle at Productivity/Respiration Station F23

3-12slg.xls

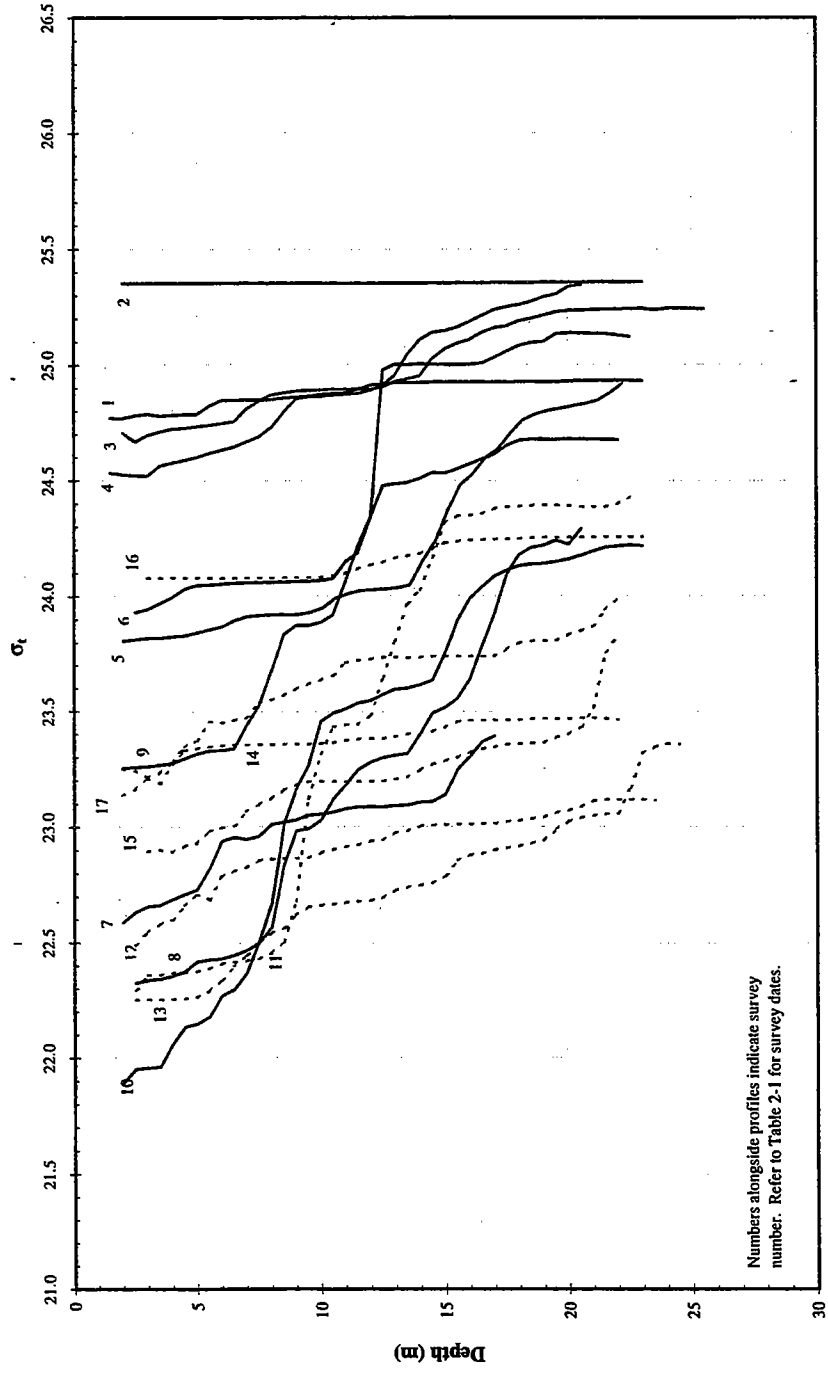

FIGURE 3-13
1996 Seasonal Density (σ_t) Cycle at Station N10

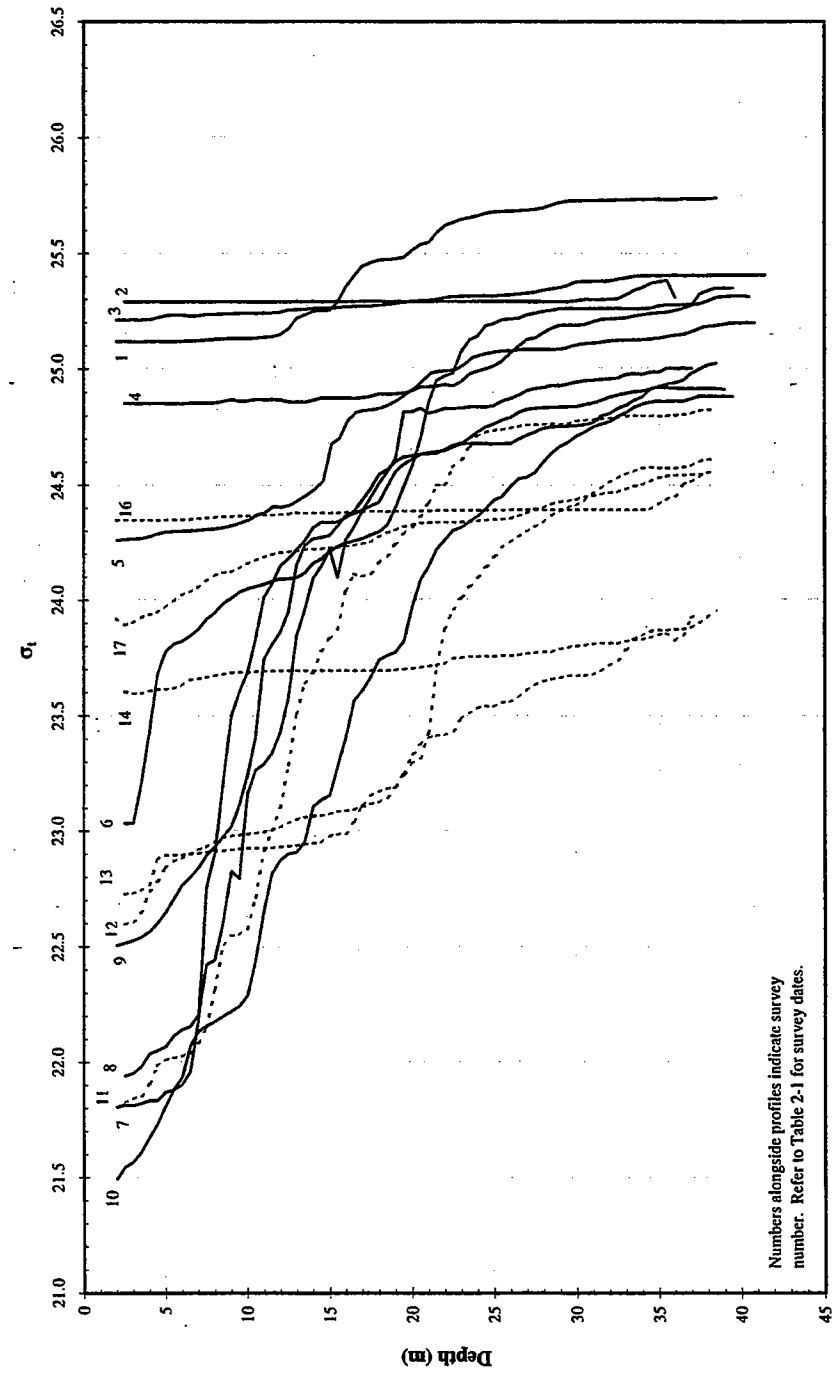

FIGURE 3-14
1996 Seasonal Density (σ_t) Cycle at Productivity/Respiration Station N16

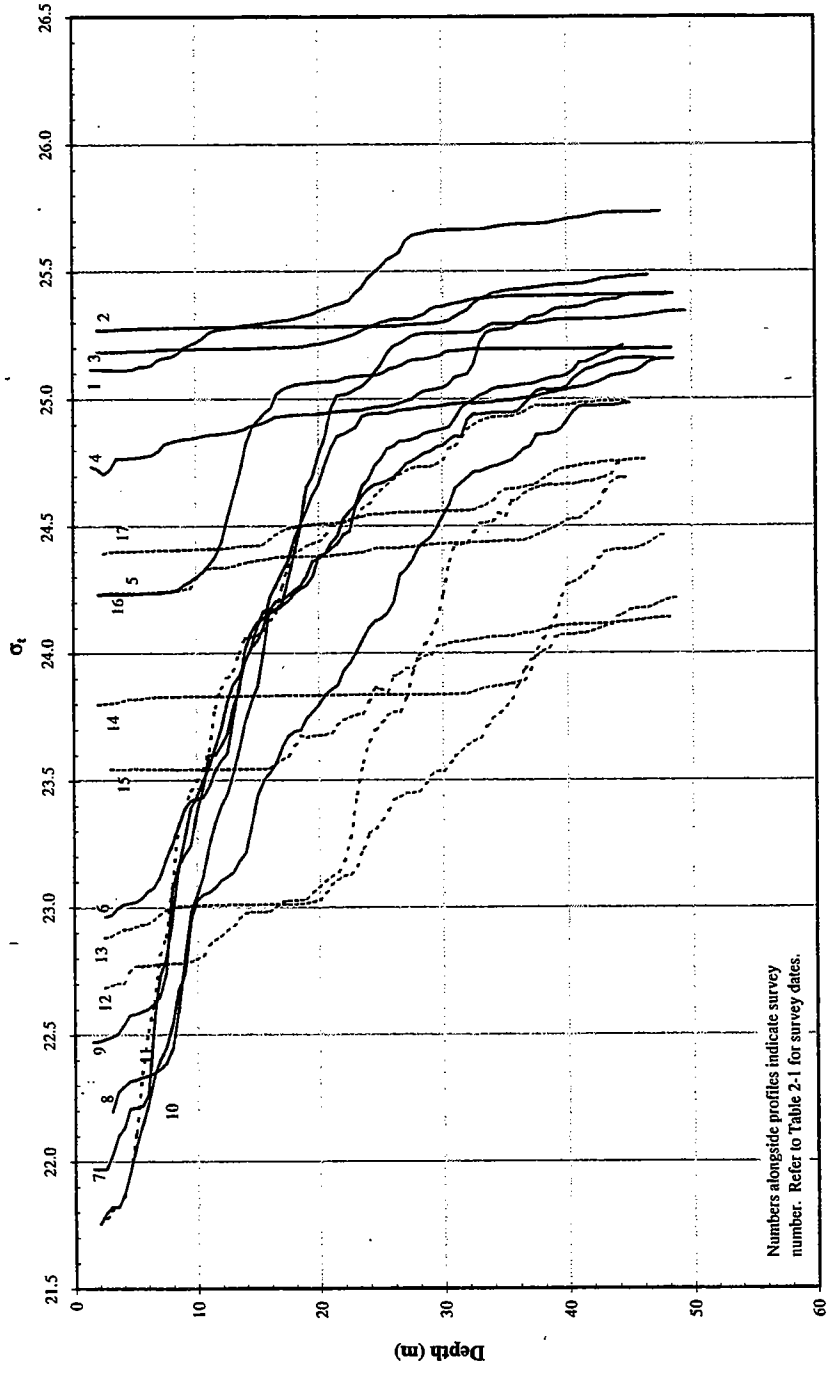

FIGURE 3-15
1996 Seasonal Density (σ_t) Cycle at Productivity/Respiration Station N04

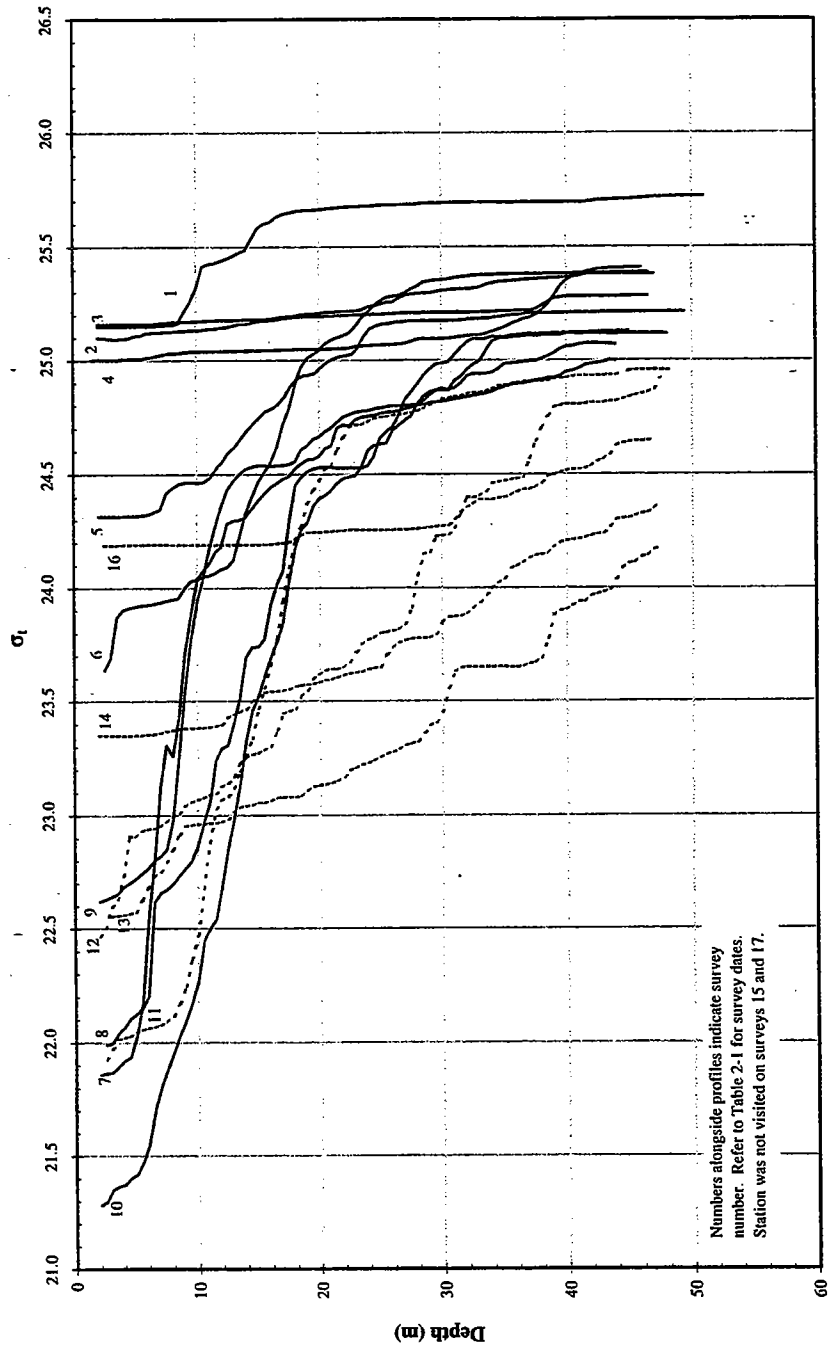

3-16SIG.xls

FIGURE 3-16
1996 Seasonal Density (σ_t) Cycle at Productivity/Respiration Station N07

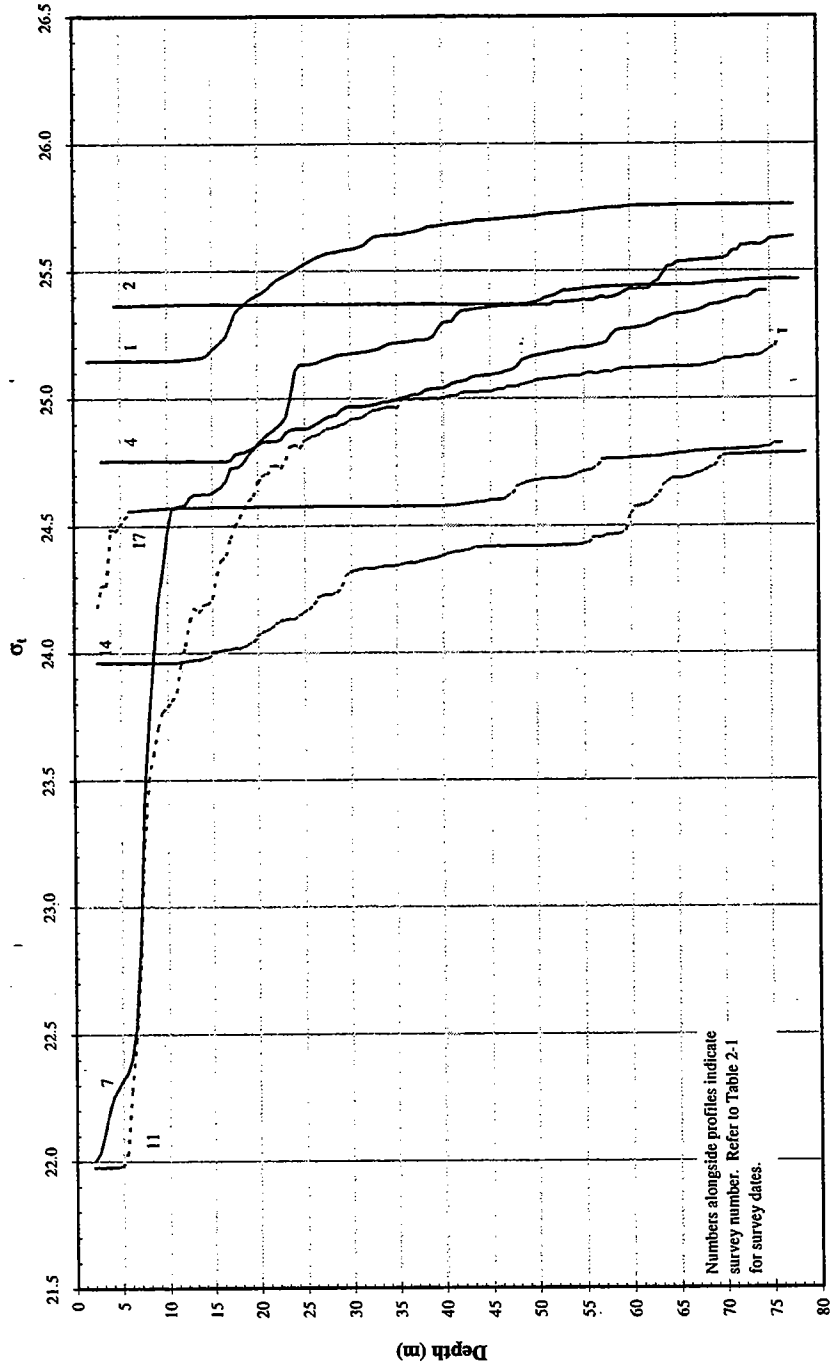

FIGURE 3-17
1996 Seasonal Density (σ_t) Cycle at Respiration Station F19

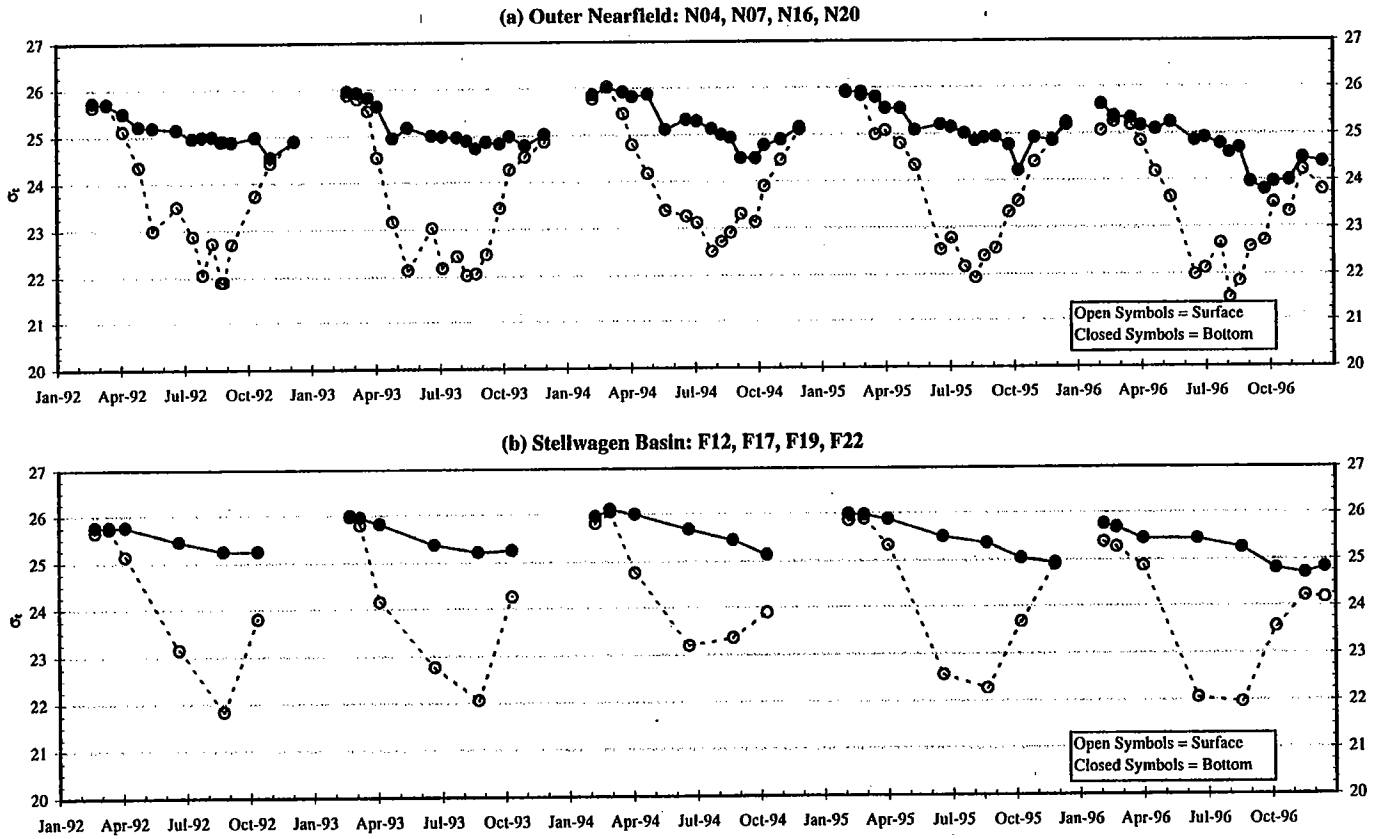

FIGURE 3-18

Interannual Comparison of Density (σ_t) in the Nearfield and Stellwagen Basin Regions

A and E depths, Stations as indicated

3-18SIG.xls

4.0 NUTRIENTS

This section provides an overview of the distribution of dissolved nutrients in the water column of the Massachusetts Bay system from February to December for the nearfield area and for February to October for the farfield regions. Selected data from the 1996 sampling period are presented and discussed both with regard to seasonal changes in the nearfield region and to spatial changes in various regions of the Bays. The 1996 nutrient record for the new outfall site in the nearfield is compared with similar data from the 1992-1995 sampling periods to illustrate interannual variability at this location. The main nutrient data presented here include water column concentrations for nitrate + nitrite, ammonium, phosphate, and silicate, some combined data such as DIN (nitrate + nitrite + ammonium), and DIN:phosphate and DIN:silicate ratios.

Included are plots and discussion of certain dissolved parameters such as dissolved organic carbon (DOC), dissolved organic nitrogen (DON), dissolved organic phosphorus (DOP), total dissolved nitrogen (TDN), and total dissolved phosphorus (TDP). Also included are plots of some particulate parameters such as particulate organic carbon (POC), particulate organic nitrogen (PON), particulate phosphorus (PP), biogenic silica (BioSi) and total suspended solids (TSS). Although discussed elsewhere in detail, dissolved oxygen and fluorescence have been included to aid in data interpretation.

4.1 Annual Nutrient Cycle in the Nearfield

Several key nearfield stations were sampled for nutrients more consistently throughout this study than others, either due to planned sampling schedules or unplanned weather problems. Thus subsets of the station data, representing the most consistent sampling during the year, were chosen to provide insights on temporal and spatial changes that occurred in this region during 1996. Some of these trends are summarized in Table 9-1, where they can be compared to other parameters. In the following sections, the nearfield nutrient and nutrient parameter data are plotted in several different ways to help interpret changes throughout the year and include both temporal vertical and horizon distributions as well as comparisons to the previous years' studies (1992-1995). The stations chosen and their rationale are presented in each subsection below.

4.1.1 Vertical Distribution of Nutrients in Nearfield

In order to show nutrient trends in the surface and bottom water of the entire nearfield region, nutrient concentrations were plotted vs. time (Figures 4-1 to 4-3). In addition, fluorescence and dissolved oxygen concentrations were also plotted the same way to allow direct comparisons with these parameters (Figure 4-4a and b). All nearfield stations were included to show variability within the nearfield region. All of the averaged concentration data for each station (described below) were plotted in order to show scatter better than would be shown by simple standard deviation brackets. In addition, total average lines were also plotted to indicate average seasonal trends.

Individual surface data from the A and B depths of the water column are represented by the symbol "o". The averages of the data are shown as a thin line labeled "Ave. Surface". Both of these depths are typically above the

thermocline in the mixed surface layer. Individual bottom data from the D and E depths of the water column are represented by the symbol "Δ". The averages of the data are shown as a bolder line labeled "Ave. Bottom". Both of these depths are typically below the thermocline and at or near the bottom. Only the average line is shown for the mid-depth (C depth, which was typically centered on the thermocline).

The average data lines show the seasonal differences and trends between the surface and bottom water concentrations. These differences reflect the effects of vertical mixing, stratification, and the different rates of phytoplankton uptake and nutrient regeneration in the surface and bottom layers. The vertical distribution of nutrients in the nearfield can also be observed on the concentration/depth/time contour plots (Figures 4-6 to 4-9), though these contain only a subset of the nearfield data.

Between February to late-March (surveys W9601 through W9604), when the water column was well mixed (as indicated by near uniform top to bottom salinity and temperature, Figures 3-2 and 3-6), nutrients were removed from the water column due to a strong spring diatom bloom (Section 8.1). This removal occurred for all the nutrients except for ammonium, whose bottom concentrations actually increased slightly during this period (Figure 4-1b). Surface concentrations for nitrate + nitrite, phosphate and silicate were on average a little lower than the bottom concentrations, probably due to slightly earlier uptake and removal (Figures 4-1a; 4-3). However, removal rates appear to have been largely similar throughout the water column since the slopes of surface and deep water concentration vs. time were nearly parallel for these three nutrient types (phosphate seemed to deviate the most). Table 4-1 summarizes the removal rates (uptake rates) and calculated carbon fixation rates (primary production) based on estimated nutrient ratios of C:N:P:Si of 106:16:1:16. The C:N:P ratios are the traditional Redfield ratios, while the N:Si of 1:1 is based on the previous observation that the distribution of DIN and silicate concentrations fall on a 1:1 ratio line (see Figure 4-22a in Murray *et al.* 1998; Cibik *et al.* 1998).

Although the removal rates were similar in both the surface and bottom layers, there were sufficient differences to warrant that separate surface and bottom layer rates be used to calculate the water column integrated averages for production (mg $C/m^2/d$) listed in Table 4-1. This was accomplished by multiplying the estimated primary production rates (mg $C/m^3/d$) times the average water layer thickness (m) and adding the surface and bottom values. The resultant values represent estimated primary production rates averaged over 18-21 day periods. The higher estimates based on silicate instead of DIN probably result from the use of an assumed N:Si ratio of 1:1 in the calculation, whereas the observed water column ratios were closer to 0.7:1. The parallel removal of nitrate + nitrite and silicate is typical of a diatom-dominated spring bloom in these water., During this period, ammonium was initially higher in the surface water due to the influence of the present outfall and other coastal sources. By mid- to late-March, ammonium was higher in the bottom water, probably due to initial ammonification of the organic matter produced during the spring bloom.

By survey W9603 in mid-March, nitrate + nitrite and silicate concentrations were well below 1.0 μM at the surface and mid-depths and bottom concentrations were only slightly higher. Phosphate concentrations had reached their average summertime surface water minima (about 0.2 μM) by this time as well. Since DIN concentrations were typically dominated by the concentration of nitrate + nitrite, DIN distributions (Figure 4-2) were similar to those of nitrate + nitrite, tempered by ammonium. This nutrient removal pattern is typical of a

year in which there is an early strong diatom bloom such that the nutrients are nearly stripped from the water column by late March prior to significant water column stratification.

Once the water column had stabilized in late spring and summer, nitrate + nitrite, phosphate, and ammonium all remained low in the surface water throughout the summer, although there were short-lived increases in early May (W9606) and late August (W9611). These observations indicate that the water masses advecting into the region (Table 9-1) were relatively rich in nutrients. Over the course of the spring and summer, silicate slowly increased in the surface water to 2-3 μM, but decreases in June (W9607) and August (W9611) indicated surface diatom activity (Figure 4-3b). In the bottom water, concentrations of nitrate + nitrite, phosphate, and silicate all increased during the summer months, with a sharp increase evident in mid-August (W9611). Ammonium reached its bottom water maximum during April as ammonification of the spring-bloom organic matter occurred. Then as late summer nitrification continued, ammonium reached its bottom minimum concentration by mid-August. The mid-depth concentrations of all the nutrients typically fell between the surface and bottom concentrations, though often closer in concentration to surface averages then the bottom averages.

Although there was strong mixing in early September from Hurricanes Eduoard and Fran, the water column did not completely mix. The effect on nutrient concentrations was to slightly decrease the bottom and mid-depth concentrations, with slight increases in surface concentrations. Continued mixing (as evidenced in Figures 3-2 and 3-6) during September and October caused nitrate + nitrite, ammonium, and phosphate concentrations to slowly increase in the surface layer. Silicate was removed in the surface layer in October during the strong fall bloom (Figure 4-4a).

The increased scatter in elevated surface layer ammonium concentrations during this period (Figure 4-1b) was partly attributable to the high concentrations of ammonium in the outfall and other coastal sources which typically influence the surface water of the inner nearfield. This same combined influence had an observable but lesser effect on the surface phosphate concentrations (Figure 4-3a). By the end of October (W9615), following the fall bloom (Figure 4-4a), concentrations of all nutrients increased through the remainder of the year.

Dissolved inorganic nitrogen (DIN = nitrate + nitrite + ammonium) to phosphorus ratios (DIN:P) in both surface and bottom water were typically much lower than the Redfield ratio of 16:1, ranging on average from ~9-12:1 during the winter months throughout the water column. During the summer months these ratios fell to ~5-6:1 in the bottom water, while surface and mid-depth values were even lower (ranging from ~1-3:1). These values slowly increased during the fall in the bottom water as a result of regeneration. Overall, these water are depleted in nitrogen relative to phosphorus throughout the whole year, especially in the surface water during the summer months. A few of the surface samples in September (W9613) did exhibit higher ratios of DIN:P (Figure 4-5a), apparently due to the increases in surface ammonium concentrations in coastal water (Figure 4-1b).

DIN to silicate ratios (DIN:Si) remained well below 1:1 throughout almost the entire year, with the exception of the spring bloom period of March and April when average values were from ~1-2.5:1 (Figure 4-5b). The ratios slowly increased during the late summer and early fall to about 1:1 due to the slow return of DIN to the water column. It is interesting to note that the ratios remained relatively constant in the bottom water (0.5 to 0.8:1 from May to October) even though the actual concentrations increased dramatically during this time period. This same

range of ratios was observed in 1995 and suggests that nitrogen and silicate were being remineralized at similar rates in the bottom water.

4.1.2 Vertical Distribution of Nutrient Related Parameters in Nearfield

Figures 4-6 through 4-9 contour 1996 results for concentration, depth, and time period. Annual changes for concentration were determined by averaging each depth for a given survey from stations N04, N07, N16 and N20. Data from W9615 (October 30, 1996) were not included on the plots since only station (N04) was sampled due to bad weather. The stations were chosen to represent the area of the future outfall site. In addition to dissolved inorganic nutrients (Figure 4-6), which are discussed above, a number of other related parameters are presented, including DIN:PO4 and DIN:SiO4 ratios, fluorescence, dissolved oxygen and temperature (Figure 4-7). Figure 4-8 compares particulate parameters, including particulate organic carbon (POC), particulate organic nitrogen (PON), particulate phosphorus (PP), biogenic silica (BioSi), and total suspended solids TSS). Finally, Figure 4-9 compares various dissolved parameters, including dissolved organic carbon (DOC), dissolved organic nitrogen (DON), dissolved organic phosphorus (DOP), total dissolved nitrogen (TDN = DIN + DON), and total dissolved phosphorus (TDP = PO4 + DOP).

The general seasonal trends of all the nutrients (Figure 4-6) and for DIN:PO4 and DIN:SiO4 ratios (Figure 4-7) were discussed above in section 4.1.1 and will not be further discussed here. Note, however, the water column properties during the advection events during late April/early May and August (described above). In each case, fluorescence results indicated some degree of response from the phytoplankton, although not nearly of the magnitude of the spring and fall blooms (Figure 4-7). Note also distribution of chlorophyll concentrations in the water column, with the spring bloom (W9602 and W9603) distributed throughout the water column, and the remaining events, including the fall bloom in October (W9614) largely restricted to the surface water. Dissolved oxygen and temperature are plotted for reference at this set of stations and are discussed elsewhere in this report.

All of the particulate parameters shown in Figure 4-8 show somewhat similar trends during the year since these parameters are largely controlled by the influence of plankton blooms and the amount of plankton in the water column. Hence the patterns for POC, PON and PP are all very similar, showing the highest relative concentrations during the spring and fall blooms. There were also relatively high concentrations during a late summer bloom in mid-August and in late June. PON concentrations of 3-5 μM (during maximum bloom periods) indicated that 20-30% of the total nitrogen in the water column was in the particulate form, whereas in other periods (e.g., early summer), only about 10% of total nitrogen is in the PON form. Finally, during the winter months, only about 5% of the total nitrogen is PON. POC concentrations showed similar percentages of the totals. Although the highest concentrations of POC and PON occurred during the fall bloom, the highest PP concentrations were found near the bottom during the end of the spring bloom. The concentrations of PP during these blooms was about 30% of the total phosphorus, while during the summer months it reached about 40%. The details of these nitrogen and phosphorus forms are beyond the scope of this present report and are investigated by Wang (UNH Master's thesis, in preparation).

The concentration of BioSi, which mainly represents diatom silica, was highest near the bottom in November, probably due to settling and concentration of the diatoms comprising the fall bloom (Figure 4-8). Concentrations

were also high during the spring bloom. The concentrations of BioSi during the summer blooms were relatively low, reflecting lower biomass and perhaps dominance by non-diatom species (see Section 8.1).

TSS concentrations were typical for this area of Massachusetts Bay, ranging from about 0.5 to 3 mg/L (Figure 4-8). In addition to phytoplankton biomass, TSS concentrations are also affected by resuspension of bottom material during storms, and transformations due to zooplankton grazing. Hence, concentrations are typically higher during the winter months and during periods of high production (spring and fall blooms). Concentrations tend to be lower during the summer months when there is little storm activity, the water column is stratified, and zooplankton grazing rates keep pace with primary production. The lowest concentrations were found during the August-September period in the surface water.

Dissolved organic carbon (DOC) concentrations (Figure 4-9) were relatively constant during most of the year and fell between 60-100 μM, except during the spring bloom when values of well over 120 μM were observed at mid-depth. Dissolved organic nitrogen (DON) concentrations (Figure 4-9) were also relatively constant during most of the year with values falling between 6-10 μM. DON values were above 10 μM only in a few surface samples during the summer and in November after the fall bloom. DON is often the predominant form of nitrogen in the water column, and can range from about 50% of the total nitrogen during blooms to nearly 80% during summer months. By contrast, the dissolved organic phosphorus (DOP) usually represents only about 15-30% of the total phosphorus in the water column (Figure 4-9). Both the total dissolved nitrogen (TDN) and total dissolved phosphorus (TDP) plots (Figure 4-9) show that the highest concentrations were found in the bottom water during the late summer months and throughout the water column during the winter months. This is due mainly to the additional influence of the dissolved inorganic forms (Figure 4-6).

There is evidence that while the buildup of DIN and silicate in the bottom water occurred at similar rates, the regeneration of these nutrients varies with location. Measured rates of sediment regeneration from the soft sediments of the Nearfield and Stellwagen Basin show flux of silicate to the overlying water column to be greater than five times as high as that as DIN. The average DIN:Si ratio of the fluxes in July and August was 0.17 (s.e.=0.03) and 0.11 (s.e.=0.01) in 1995 and 1996 respectively (Howes 1997, 1998). This suggests the likelihood of preferential remineralization of DIN over silicate as particles fall through the watercolumn and that particles settling to the bottom are enriched in silicate (frustules). Degradation of these N "depleted" particles (relative to Si) results in the silicate "enriched" nutrient regeneration from the sediments. These processes are consistent with the significantly lower DIN:Si ratio during stratification, when the effect of the sediments on bottom water nutrient pools is greatest (Figure 4-7).

4.1.3 Inner/Outer Nearfield Nutrient Gradients

In order to characterize the differences between nearfield stations located close to Boston Harbor and the existing outfall, and those representing the future receiving water, station data for both the western (two areas) and eastern portions of the nearfield were averaged and plotted (Figures 4-10 to 4-14). Stations N10 and N11, from the southwestern corner of the nearfield (Figure 2-2) were chosen to represent the inner nearfield, since a preliminary examination of the data suggested that these two stations often showed elevated concentrations of nutrients

associated with the present outfall plume and other harbor sources. Station N01 in Broad Sound (labeled "Upwelling") was chosen to represent a nearshore station where upwelling has often been reported, yet exhibits less influence from the harbor. Stations N04, N05, N06, and N07 on the eastern edge of the nearfield station grid were chosen to represent the outer nearfield. In order to make plots, data from each of the 5 depths (A-E) were separately averaged across the chosen stations and then plotted at the average depth for each of the depths and each of the 17 (16 for N01) sampling periods. The average depth of the inner stations was about 20-25 m, while the average depth for the outer stations was nearly 50 m.

In general, concentrations of nitrate + nitrite, phosphate and silicate were nearly vertically uniform for the first four surveys, especially at the shallow inner and upwelling stations (Figures 4-10, 4-13, and 4-14). Overall concentrations decreased during this time period as the spring bloom progressed, from the high winter values to below 1 μM for nitrate + nitrite and silicate and below 0.3 μM for phosphate. Although the outer stations showed the nearly vertical distribution in the upper part of the water column during that time period, the deeper water maintained higher concentrations. Ammonium concentrations were higher near the surface than in deep water at both the inner and upwelling stations during the first two surveys due to the input from Boston Harbor (Figure 4-11). Phosphate did not show a surface concentration increase inshore during the spring as was seen in ammonium, although it did during the 1995 spring period.

During the summer months, all nutrients except ammonium slowly increased in the bottom water, reaching a late summer maximum concentration by late August (W9612; see Section 4.1.1). The concentrations in the bottom water were higher at the outer stations because of the greater depths. Ammonium reached its maximum summer concentration (>1.5 μM) at all locations in April and then again at the inner station in July. Summer surface concentrations at the inner station were typically higher than at either of the other two locations. Although summer surface nitrate + nitrite concentrations were low (< 1.0 μM) at all stations, phosphate, ammonium and silicate had a period of increased concentrations during July (W9608 and W9609) at both the inner and upwelling stations. Both April and July increases may be attributed to riverine discharge associated with large precipitation events (Figure 3-8) and easterly surface currents (Table 3-1). The increase during July was barely detectable at the outer stations.

The greatest differences in nutrient concentrations between the three locations were observed during the fall/early winter period, with the inner station having the highest concentrations. All nutrients showed increased surface concentrations at the inner stations starting in September with mixing from the two hurricanes (Table 9-1), followed by continued increases in concentration until the mid-December survey (W9617). Silicate surface concentrations did decrease somewhat during the fall bloom in October, but then resumed their increase.

Nutrients in the bottom water also increased during the fall period as regeneration occurred so that by December, concentrations in the bottom water were nearly the same as the surface. However, surface enrichment of ammonium and phosphate was observed for the fall and early winter surveys when the highest concentrations for the year were observed. This is similar to observations made in 1995. At the upwelling station, there was only a slight increase in surface concentrations of nitrate + nitrite and ammonium, while silicate and phosphate initially increased in the bottom water, indicating minimal influence from Boston Harbor. There was no obvious indication of a nutrient influence at the outer stations, since the nutrient concentrations for nitrate + nitrite,

phosphate and silicate all increased from the bottom to the surface water as the fall progressed into early winter. Only ammonium values decreased during this period, dropping to less than 0.5 μM by November (W9616).

4.1.4 Interannual Nutrient Variability in the Nearfield

Inter-annual variability in the area of the future discharge in the nearfield was illustrated by using four stations that had the most complete data coverage during the five years of monitoring. These stations (N16, N04, N07, and N20) form a triangle with station N16 in the center (Figure 2-2). Data from these stations (including nutrients and fluorescence) for the five discrete sampling depths (A-E) were averaged over stations for each depth and then plotted at each average depth for the 17 sampling surveys. The average depth of the bottom samples at these stations was about 38-42 m. These data are presented in the concentration/depth/time contour plots for the years 1992-1996 (Figures 4-15 to 4-20). Fluorescence data were plotted in addition to the nutrient data to help in interpretation, and are discussed in greater detail in Section 5. When examining these plots, note that the sampling season was longer (started earlier and ended later) in 1995 and 1996 than in the previous years, especially 1993. For example, it appears that there were much higher winter DIN concentrations in the water column during 1995 and 1996 compared with 1992 (Figure 4-17), which is attributable to the earlier sampling in later years.

Plots for each nutrient show there were substantial differences in the concentration patterns over the five years presented. Data from 1995 departed most from the baseline norm, attributable to the bi-modal winter-spring bloom (Figure 4-20). While the other years appear more similar with respect to nitrate + nitrite and phosphate (Figure 4-15 and 4-18, respectively), silicate patterns were substantially different from year to year (Figure 4-19). The timing of the development for the late winter bloom also heavily influenced the initial concentrations in the water column from year to year.

The spring bloom in 1996 yielded the highest fluorescence values over the five-year data period (Figure 4-20). Loder and Boudrow (1997) noted that the early spring bloom, which typically results in N+N concentrations below 1 μM by the end of March (Figure 4-15), occurred in varying degrees five out of eight years for which data were available from 1988 and 1996. During the other three years, similarly low levels of N+N were not reached until May. We do not yet understand the triggering processes for the spring bloom or what controls its intensity, but hypothesize that they are likely related to a combination of light and physical conditions in the water column, or perhaps chemical conditioning of the water column. These issues were discussed briefly by Loder and Boudrow (1997) and are presently under further investigation. The fall bloom appears to be a more persistent feature than the spring bloom in the nearfield area, though the timing shifts slightly from year to year (Figure 4-20).

4.2 Annual Nutrient Cycle in Massachusetts and Cape Cod Bays

The annual nutrient cycle in Massachusetts Bay was examined using both nutrient vs. depth plots and nutrient vs. nutrient plots for all nearfield and farfield stations. On each figure, the data were plotted using different symbols for each of the six areas of Massachusetts Bay, as shown in Figures 2-1 and 2-2, in order to distinguish regional

concentration differences and processes. The data were not averaged because of the large differences between stations within each of the areas.

4.2.1 Regional Nutrient Variability With Depth

In order to examine nutrient concentration differences throughout the Massachusetts Bay system, concentration vs. depth plots were made that included all data. However, only a few of the nutrient vs. depth plots (available comprehensively in Murray *et al.*, 1998; Cibik *et al.*, 1998) are presented here to make specific points about regional processes and differences (Figures 4-21 to 4-30). It is important to note that the sampling of the entire bay occurred only six times during the year and that these survey data are "snapshots" at these points in time. We have included the nearfield data on the plots as well to help in interpretation of the trends.

Within the Massachusetts Bays system, nutrient levels change over an annual cycle due to different biological regimes and different nutrient sources within various sub-areas. On the plots shown, we have separated the data by location (i.e., boundary, Cape Cod Bay, coastal, harbor, nearfield, and offshore, Figure 2-1) since these different regions often act as semi-independent or independent systems with regards to temporal and spatial variability of nutrient concentrations as well as other parameters.

During 1996, as in previous years, several trends become apparent. In early February (W9601), nutrient concentrations were relatively high in most regions of Massachusetts Bay (Figures 4-21 to 4-23). The exceptions to this were that concentrations of nitrate + nitrite, ammonium and silicate were much higher in the harbor area, while concentrations of all nutrients were very low at one Cape Cod Bay station (F02, where the spring diatom bloom had nearly run its course). The concentration of silicate in Cape Cod Bay had dropped to just over 1 μM (Figure 4-23b), while the concentration of BioSi was 10-11 μM (Figure 4-28). These results indicated that a late winter diatom bloom was already in progress. With the exception of Cape Cod Bay, regional BioSi values ranged between 1μM to 4μM. The elevated nutrient concentrations in the harbor area were associated with lower salinity water. The higher concentrations of ammonium and phosphate typically can be used as markers to track plumes of harbor water, although even nitrate + nitrite concentrations were higher in the harbor samples (Figure 4-22a).

For the farfield surveys W9602, W9604, W9607 and W9611, only the DIN vs. depth plots are shown. By late February (W9602), the spring bloom had started in much of Massachusetts Bays and nutrient concentrations had started to decrease nearly everywhere (Figure 4-24). There was also more scatter in the nutrient concentrations due to different timings of the spring bloom in the different areas. Thus DIN values were lowest in the Cape Cod Bay, offshore and boundary areas while concentrations were higher in the nearfield, harbor and coastal areas, mainly due to the continued influence of the harbor water. The relative distributions of phosphate and silicate were similar to DIN. BioSi values began to decrease in eastern Cape Cod Bay, while increasing in all the other areas of the region as the diatom bloom began to spread throughout the area (Figure 4-28).

By April (W9604), DIN values at depths down to 20-30 m were depleted to less than 3 μM, except for the harbor station where concentrations were only slightly higher (due to ammonium). In the deeper bottom layers, DIN concentrations were higher than at the surface, but still only about 20-60% of their winter concentrations

observed in February. Again, the relative distributions of phosphate and silicate were similar to DIN. BioSi values (Figure 4-29) had depleted to pre-diatom bloom levels everywhere except for the Harbor and Coastal areas, where concentrations remained elevated. The depleted concentrations of all nutrients and high BioSi concentrations during W9604 indicated a widespread diatom bloom.

In June (W9607), surface DIN concentrations were even lower than those in April, though a couple of harbor and coastal stations had slightly elevated concentrations (Figure 4-25). In the bottom water, the nearfield DIN values reached their yearly minimum, while the DIN in the boundary and offshore areas nearly doubled in concentration due to an increase in nitrate + nitrite. It appears that there was a delay in the bottom water regeneration of nutrients in the nearfield compared to deeper water in the rest of Massachusetts Bay. This is probably not a true delay, but reflects the continued uptake of nutrients in the bottom water of the nearfield into the early summer. Silicate and phosphate (not shown) also showed relatively large concentration increases in the boundary and offshore areas due to the deep-water regeneration of nutrients from the settled spring bloom phytoplankton material.

In August (W9611), surface DIN concentrations were still low and similar to the concentrations in June (Figure 4-25). However, the nearfield concentrations of DIN in the deeper water had increased and were now similar to deep water concentrations in the other areas of Massachusetts Bay, almost entirely due to the increase in nitrate + nitrite. This probably reflects decreased bottom water uptake or increased rates of regeneration, or perhaps a combination of both. Phosphate and silicate deep-water concentrations showed similar trends to the DIN, except that concentrations in the deeper water were the same or higher than those in the boundary and offshore areas (Figure 4-26). BioSi values remained relatively stable throughout the region during the summer ($<4\mu M$) with moderately higher concentrations observed for the Harbor (up to $6\mu M$; Figures 4-29 and 4-30).

By October (W9614), DIN concentrations in the surface water were still low at many of the nearfield stations, but some of the stations showed elevated DIN due to the increased influence of the harbor ammonium as well as nitrate + nitrite (Figure 4-27). DIN concentrations were relatively high at harbor and coastal stations, again possibly attributable to high precipitation and riverine discharge. Phosphate (not shown) was also high in the harbor and coastal surface water (1-1.2 μM), though it remained relatively low in most of the other areas. Silicate concentrations (not shown) were generally low and scattered in the surface water with the higher concentrations found at the harbor and coastal stations. The increase in BioSi values throughout the region in early October (W9614) indicate a fall bloom dominated by diatoms. The increase was most noticeable in the harbor and coastal areas (Figure 4-30).

Although a complete farfield survey was not done in December (W9617), a harbor, coastal and several offshore stations were sampled. DIN concentrations (mainly nitrate + nitrite) were in the 6-10 μM range, while near-surface water concentrations in the harbor and adjacent stations were quite elevated (Figure 4-27) due to increases in both ammonium and nitrate + nitrite. The distribution trends of phosphate and silicate (not shown) were similar to DIN.

Nutrients in Cape Cod Bay often showed similar trends with the rest of the stations, however, there were some notable exceptions. As mentioned above for February, all nutrients were depleted before the rest of

Massachusetts Bay due to the early onset of the spring bloom there. In June, August and October, ammonium and silicate concentrations were as high or higher than other stations throughout Massachusetts Bay at the bottom depths (about 30 m) for station F02. A "nutrient trap" has been reported by both Becker (1992) and Coniaris and Loder (unpublished data) in this vicinity, which may result in higher concentrations during these periods. However, the differences in results may also be due to differential uptake of nutrients in the various regions of the study area, a factor which must be closely examined in conjunction with these comparisons.

4.2.2 Nutrient vs. Nutrient Relationships

Nutrient relationships were investigated through the use of nutrient-nutrient plots (Figures 4-31 through 4-37). Nutrient ratios relating nitrogen to phosphorus (N:P) and nitrogen to silicate (N:Si) are useful in determining nutrient limitation of phytoplankton growth. Plots of these nutrient relationships can also be used to identify water masses with unique nutrient signatures and provide insights into nutrient sources and removal processes. Using these plots, three distinct systems, Boston Harbor-Coastal, Massachusetts Bays (Nearfield, Offshore, and Boundary), and Cape Cod Bay become evident during certain times of the year.

Early-February, late February, and early April (surveys W9601-W9604) all showed similar trends with respect to dissolved inorganic nitrogen (DIN) and phosphate, though the overall concentrations decreased during this period. In mid-February, DIN to phosphorus ratios (DIN:P) were ~10-14:1 for most of Massachusetts Bays, while the Harbor region exhibited values of around 14-18:1 due to enrichment from the harbor and coastal sources (Figure 4-31). Eastern Cape Cod Bay (station F02) data were slightly set off from the rest of Massachusetts Bays, indicating earlier uptake activity by the phytoplankton community.

In late February (W9602), the overall concentrations had decreased from the previous survey. The DIN:P ratios also decreased to around 10:1, while DIN:Si ratios began a subtle divergence, indicating the beginning of two separate water masses with different characteristics (Figure 4-32). During this period, the higher DIN:Si water of the harbor and harbor-influenced stations, and the lower DIN:Si water of the Boundary area mixed with the water in the nearfield region, creating the bifurcated distribution of these properties. Most of the harbor and harbor-influenced coastal and nearfield stations had DIN:Si ratios at or above 1:1, while most of the deeper offshore and boundary stations exhibited ratios below 1:1, with a trend slope approximately 1:2. Highest concentrations were observed in the Harbor-influenced stations. Cape Cod Bay concentrations were all much lower then the rest of the system due to the near completion of the late winter diatom bloom, with the DIN:Si removed at about a 1:1 ratio.

In early April (W9604), the DIN:P ratios conformed more to the 4:1 trend line (Figure 4-33). Mixing and regeneration narrowed the concentration ranges of data, and the bifurcation seen earlier in the DIN:Si ratios disappeared as DIN:Si centered on a ratio of about 2:1 throughout the region. The exception was in Cape Cod Bay, where a 1:2 ratio was observed.

During the summer months, the concentration data became more scattered, though still showing a 10:1 trend for DIN:P and around 1:1.2 for DIN:Si (i.e., late June, Figure 4-34). The actual DIN:P ratios in the nearfield were low since most of the DIN values in the surface water were below 2 μM. The trend line intercepts the zero DIN

value at a phosphate concentration of about 0.4 μM, indicating that as the nitrogen is used up there is still residual phosphate in the water column. This situation continued throughout the summer and into the fall.

During the August and October surveys (W9611 and W9614), the DIN and phosphate concentrations were tightly covariant, and fell on a trend line of 16:1 slope throughout all of Massachusetts Bay (Figure 4-35 and 4-36). The zero DIN intercept was about 0.2 μM phosphate. However, the DIN:Si plot shows divergent trends, with the harbor and coastal water exhibiting a DIN:Si of about 2:1 (enriched in nitrogen), while the ratio for the nearfield, boundary and offshore regions is about 1:2 (Figure 4-35). Although the DIN:P plot did not show this divergent trend, the divergence was seen in the NH4:P ratios (Figure 4-37a). The NH4:P trend line is about 8:1 for nearshore/offshore samples, and less than 4:1 for the harbor/coastal samples.

Survey #	Date	Δ Days	Aver. N+N (μM)	Δ N+N (μM)	Δ N+N per day (μM/d)	Est Prim Prod (mg C/m^3/d)	Avg Dep (M)	Est Prim Prod (mg C/m^2/d)	Total Water Col Prod(mg C/m^2/d)
Surf 1	2/9/96		8.90				15.9		
Surf 2	2/27/96	18	4.24	-4.67	-0.259	20.6	16.2	334	
Surf 3	3/19/96	21	0.14	-4.10	-0.195	15.5	17.2	267	
Bot 1	2/9/96		10.49				19.6		Surf + Bottom
Bot 2	2/27/96	18	5.60	-4.89	-0.272	21.6	19.3	419	753
Bot 3	3/19/96	21	1.32	-4.28	-0.204	16.2	18.1	294	561

Survey #	Date	Δ Days	Aver. DIN (μM)	Δ DIN (μM)	Δ DIN per day (μM/d)	Est Prim Prod (mg C/m^3/d)	Avg Dep (M)	Est Prim Prod (mg C/m^2/d)	Total Water Col Prod(mg C/m^2/d)
Surf 1	2/9/96		9.71				15.9		
Surf 2	2/27/96	18	4.85	-4.86	-0.270	21.5	16.2	348	
Surf 3	3/19/96	21	0.49	-4.36	-0.208	16.5	17.2	284	
Bot 1	2/9/96		11.02				19.6		Surf + Bottom
Bot 2	2/27/96	18	6.41	-4.61	-0.256	20.4	19.3	394	742
Bot 3	3/19/96	21	2.36	-4.05	-0.193	15.4	18.1	278	562

Survey #	Date	Δ Days	Aver. PO_4 (μM)	Δ PO_4 (μM)	Δ PO_4 per day (μM/d)	Est Prim Prod (mg C/m^3/d)	Avg Dep (M)	Est Prim Prod (mg C/m^2/d)	Total Water Col Prod(mg C/m^2/d)
Surf 1	2/9/96		0.85				15.9		
Surf 2	2/27/96	18	0.51	-0.34	-0.019	24.3	16.2	394	
Surf 3	3/19/96	21	0.23	-0.28	-0.013	17.0	17.2	293	
Bot 1	2/9/96		1.05				19.6		Surf + Bottom
Bot 2	2/27/96	18	0.61	-0.43	-0.024	30.7	19.3	594	988
Bot 3	3/19/96	21	0.42	-0.19	-0.009	11.5	18.1	209	502

Survey #	Date	Δ Days	Aver. SiO_4 (μM)	Δ SiO_4 (μM)	Δ SiO_4 per day (μM/d)	Est Prim Prod (mg C/m^3/d)	Avg Dep (M)	Est Prim Prod (mg C/m^2/d)	Total Water Col Prod(mg C/m^2/d)
Surf 1	2/9/96		13.67				15.9		
Surf 2	2/27/96	18	6.62	-7.05	-0.392	31.2	16.2	505	
Surf 3	3/19/96	21	0.22	-6.40	-0.305	24.3	17.2	417	
Bot 1	2/9/96		14.19				19.6		Surf + Bottom
Bot 2	2/27/96	18	8.01	-6.18	-0.343	27.3	19.3	529	1034
Bot 3	3/19/96	21	0.98	-7.03	-0.335	26.6	18.1	482	899

TABLE 4-1
Spring Bloom Primary Production Estimates Based on Different Nutrient Removal Rates During Surveys 1-3 for all Nearfield Stations, 1996. See text for calculation details.

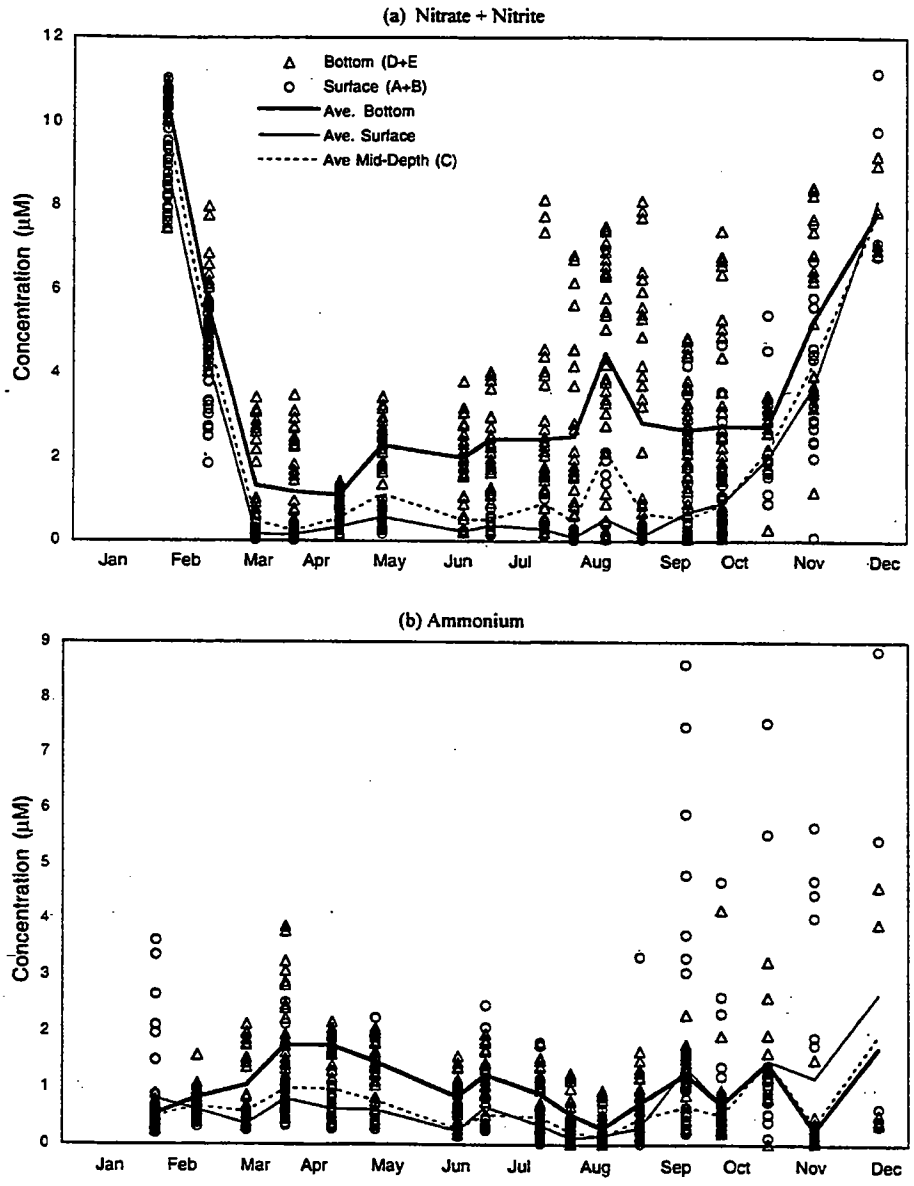

FIGURE 4-1

1996 Nearfield Nutrient Cycles

Surface, Bottom, Surface Averages, Mid-Depth Averages, and Bottom Averages

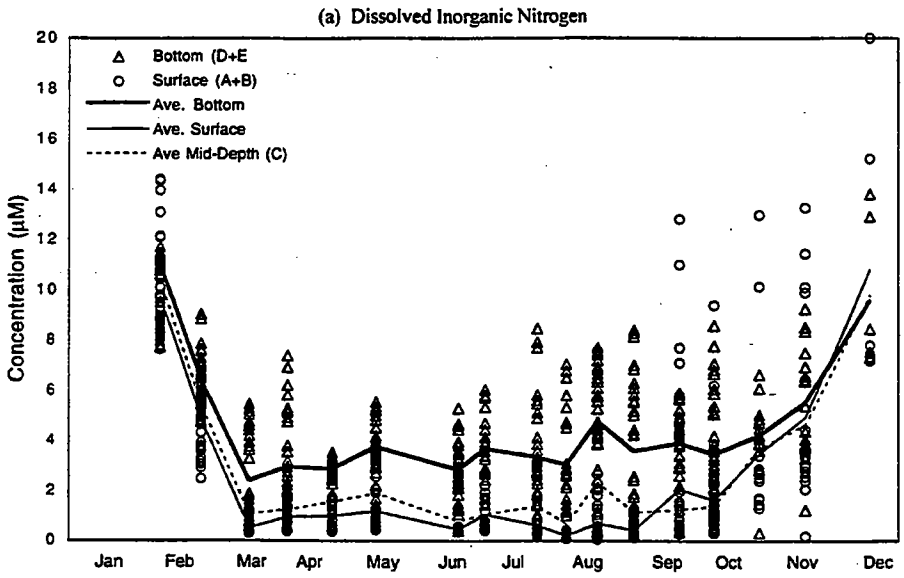

FIGURE 4-2
1996 Nearfield Nutrient Cycles
Surface, Bottom, Surface Averagse, Mid-Depth Averagse, and Bottom Averages

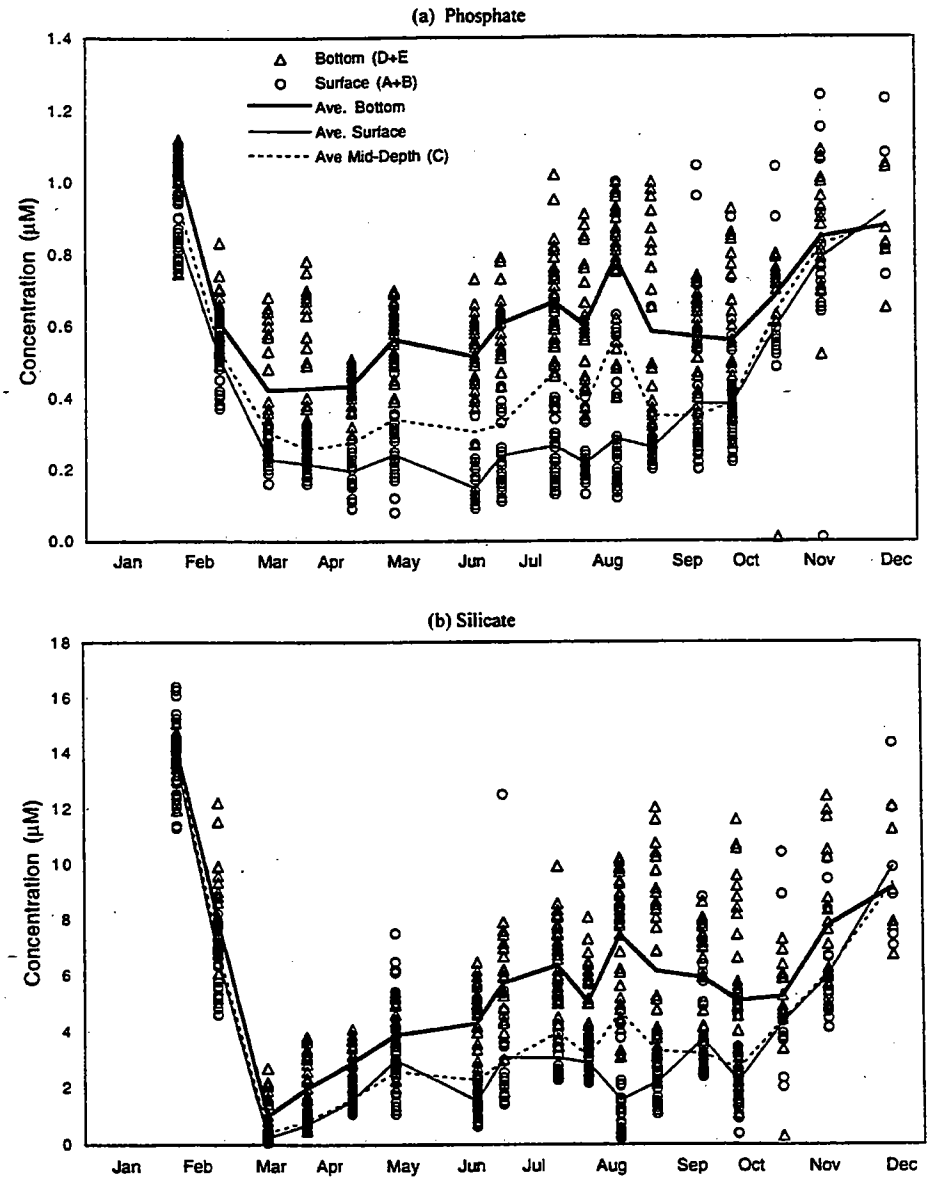

FIGURE 4-3
1996 Nearfield Nutrient Cycles
Surface, Bottom, Surface Averages, Mid-Depth Averages, and Bottom Averages

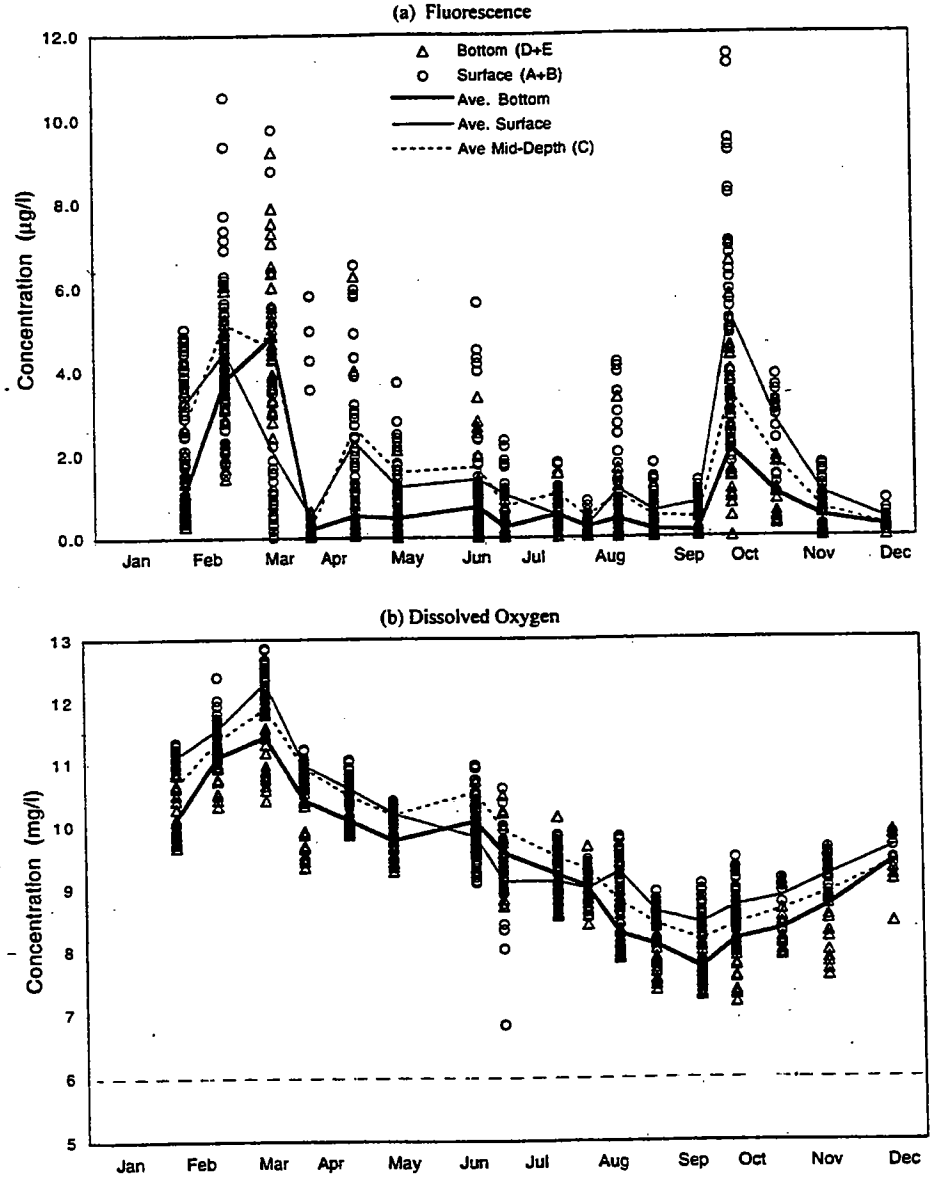

FIGURE 4-4

1996 Nearfield Nutrient Cycles

Surface, Bottom, Surface Averages, Mid-Depth Averages, and Bottom Averages

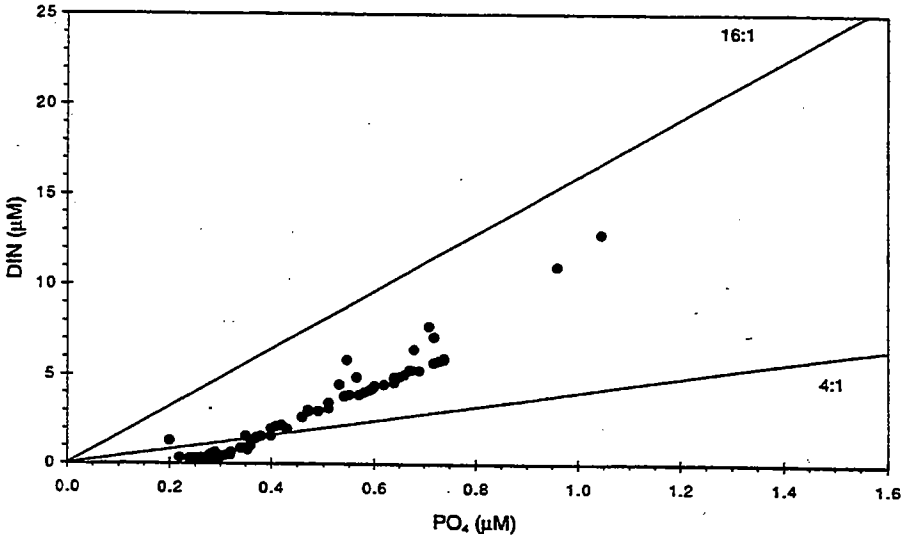

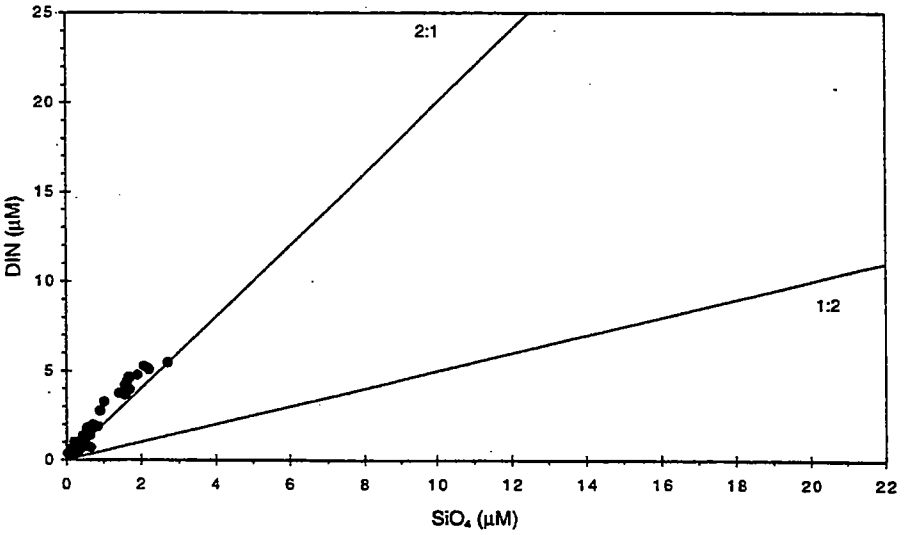

FIGURE 4-5
DIN vs phosphate concentrations for survey W9613 (September 1996) and DIN vs silicate concentrations for W9603 (March 1996)

1996 Nearfield (N04, N07, N16, N20)

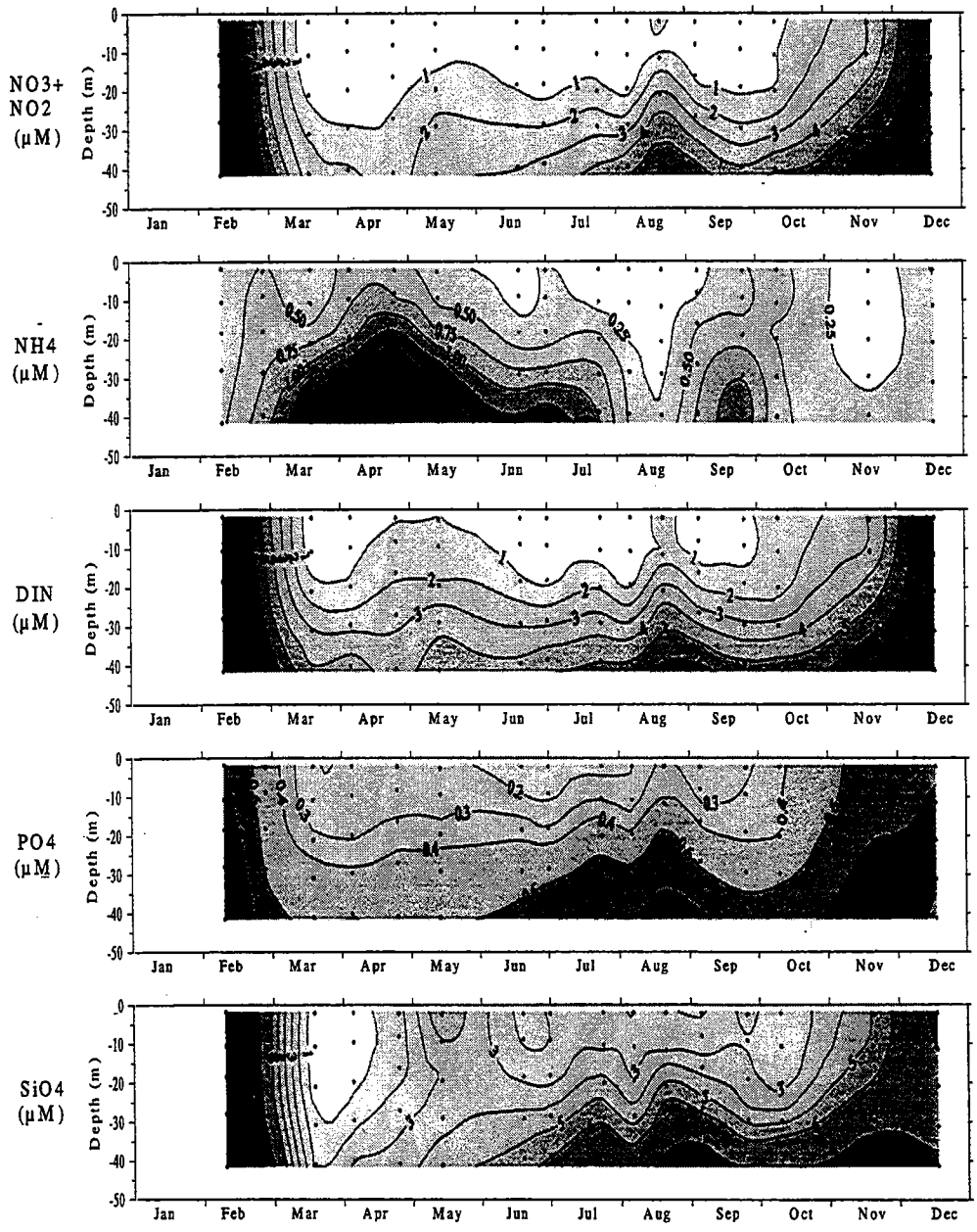

FIGURE 4-6

1996 Nearfield Averaged Nutrient Parameter Annual Distributions

Concentration/Depth/Time contours for NO3+NO2, NH4, DIN, PO4, and SiO4

1996 Nearfield (N04, N07, N16, N20)

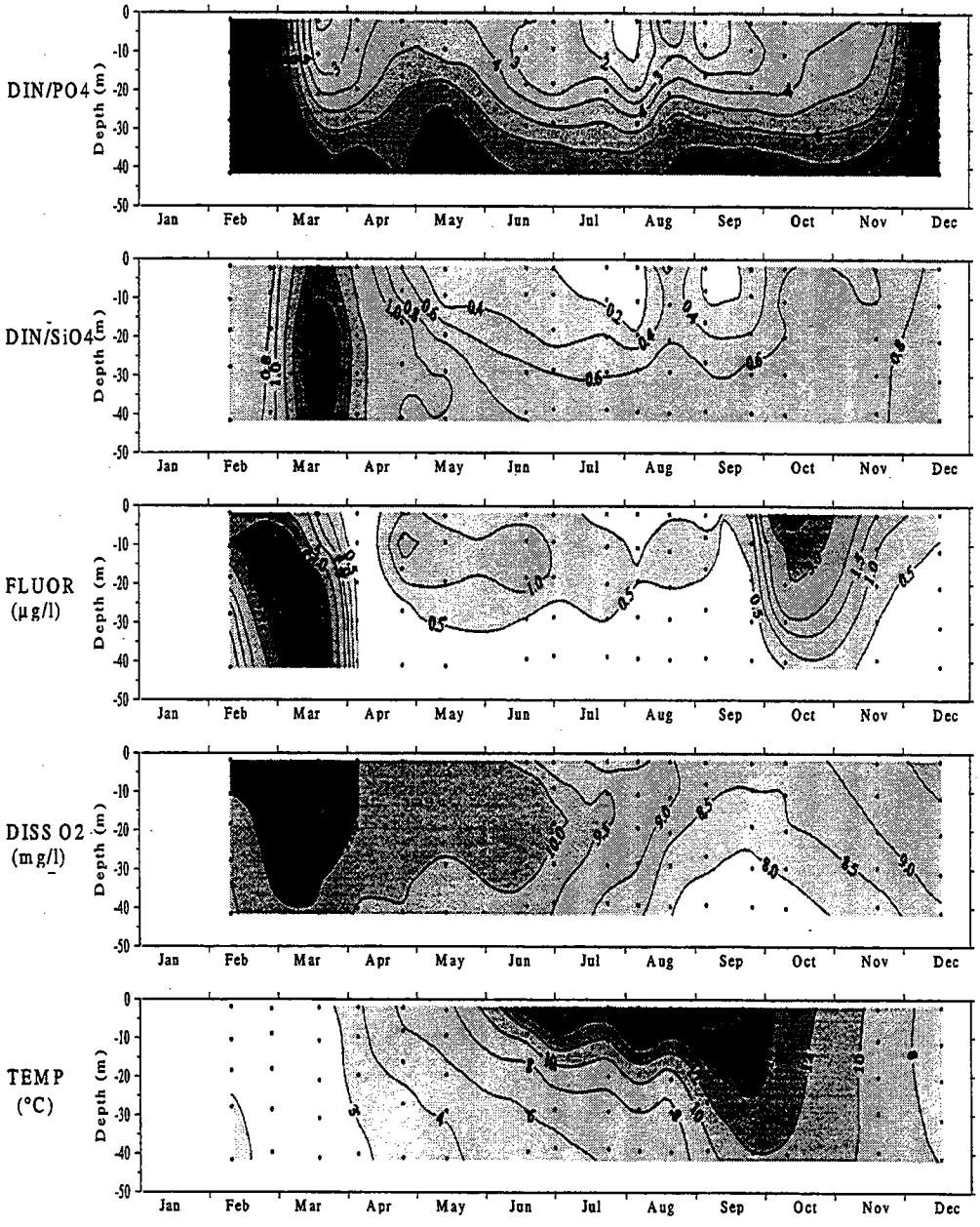

FIGURE 4-7

1996 Nearfield Averaged Nutrient Parameter Annual Distributions

Concentration/Depth/Time contours for DIN/PO4, DIN/SiO4, Fluorescence, Diss. Oxygen and Temperature

1996 Nearfield (N04, N07, N16, N20)

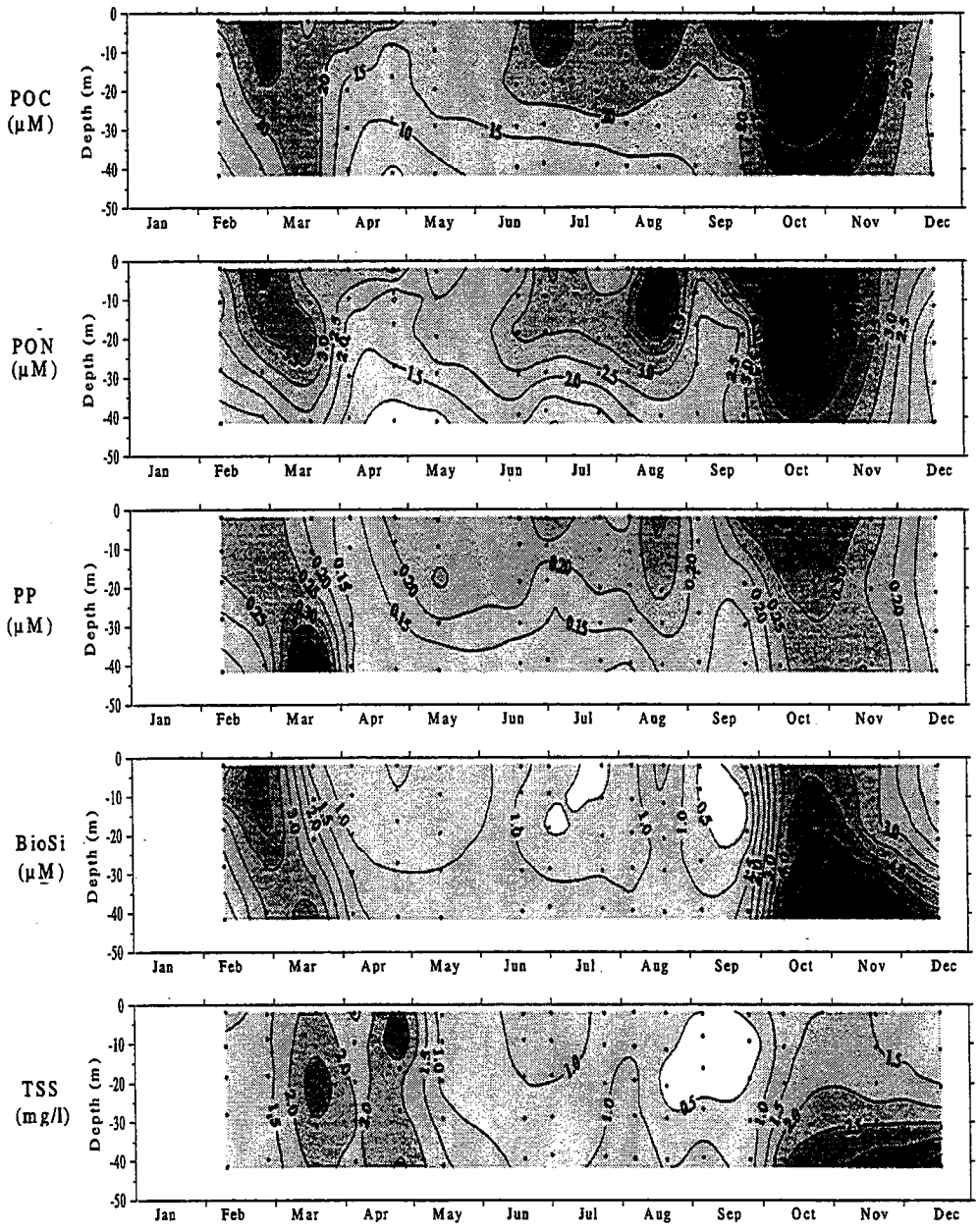

FIGURE 4-8

1996 Nearfield Averaged Particulate Nutrient Parameter Annual Distributions
Concentration/Depth/Time contours for POC, PON, PP, BioSi, and TSS

1996 Nearfield (N04, N07, N16, N20)

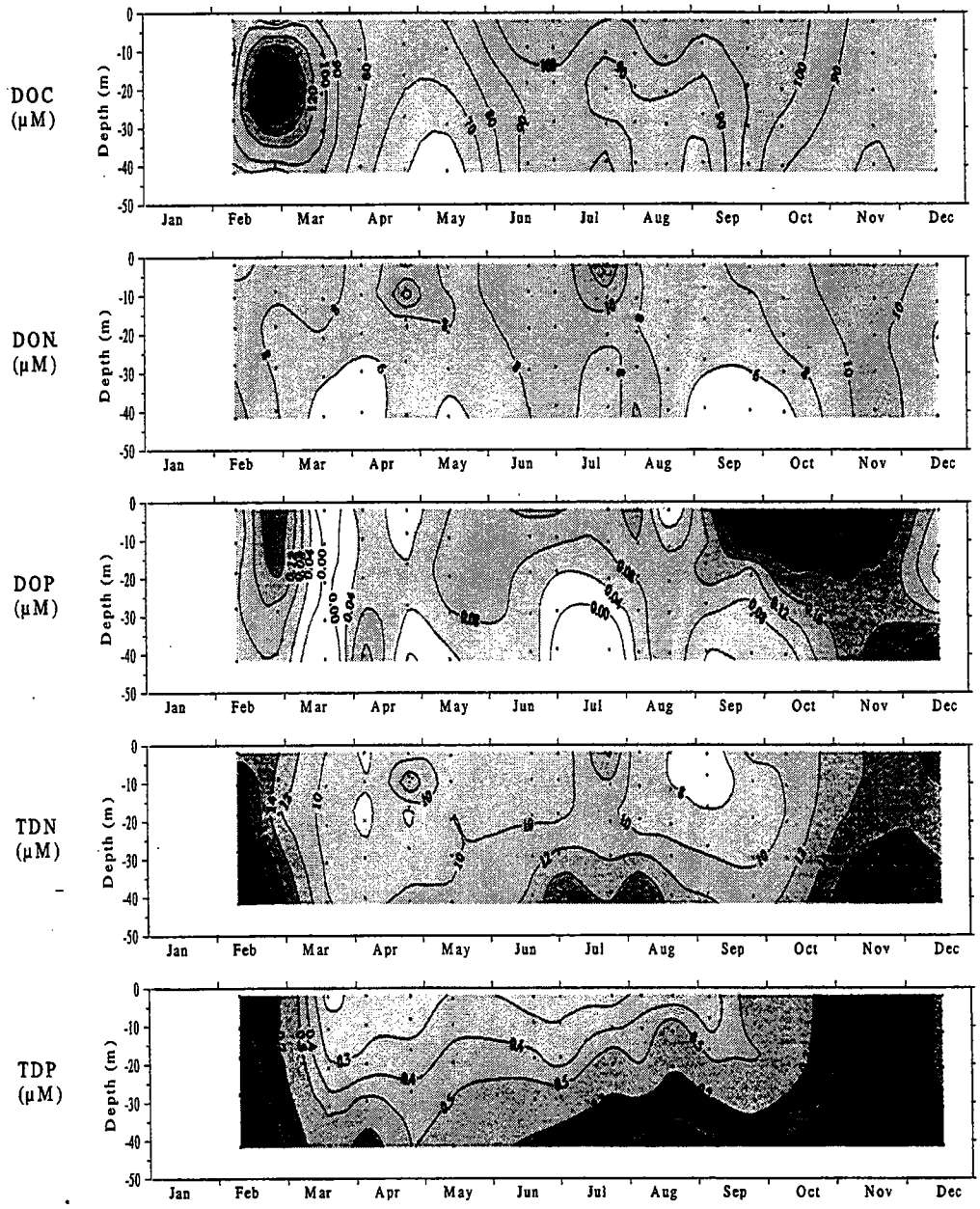

FIGURE 4-9
1996 Nearfield Averaged Dissolved Nutrient Parameter Annual Distributions
Concentration/Depth/Time contours for DOC, DON, DOP, TDN, and TDP

Nitrate + Nitrite (NO3+NO2 µM)

Upwelling (N01)

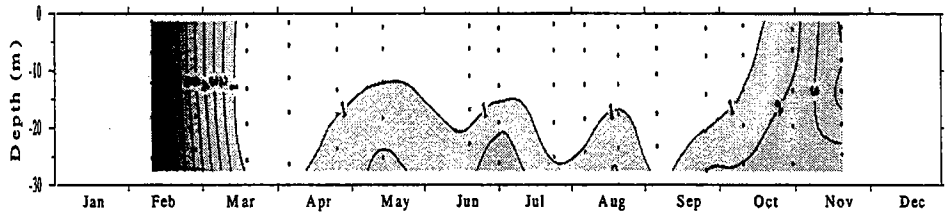

Inner (N10, N11)

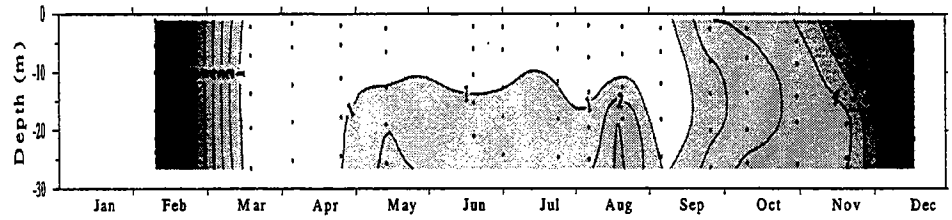

Outer (N04, N05, N06, N07)

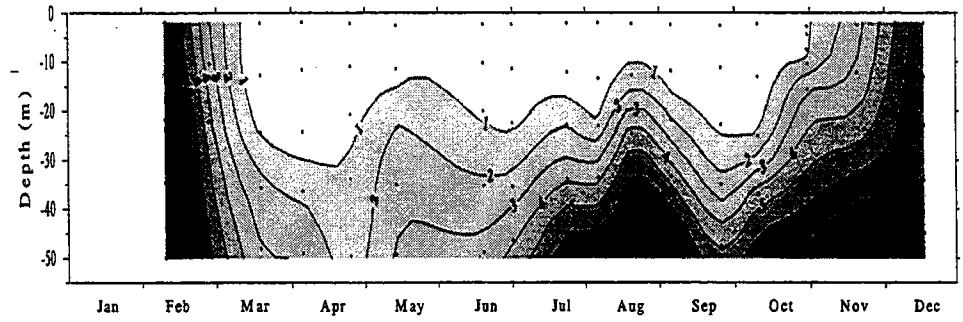

FIGURE 4-10

1996 Nearfield (3 Locations) Averaged Nutrient Annual Distributions

Concentration/Depth/Time contours for NO3+NO2 at Upwelling, Inner, and Outer Stations

Ammonium (NH4 µM)

Upwelling (N01)

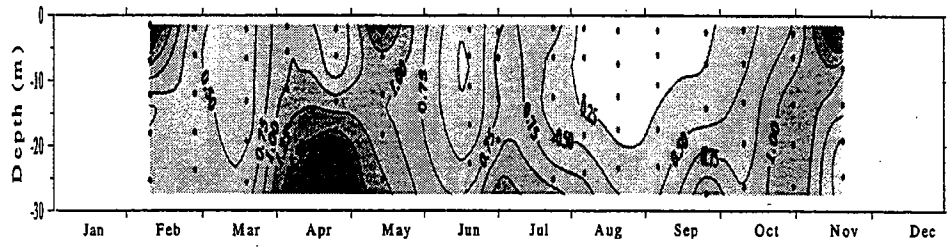

Inner (N10, N11)

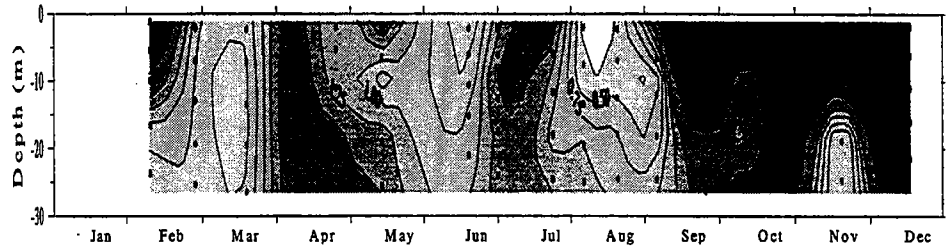

Outer (N04, N05, N06, N07)

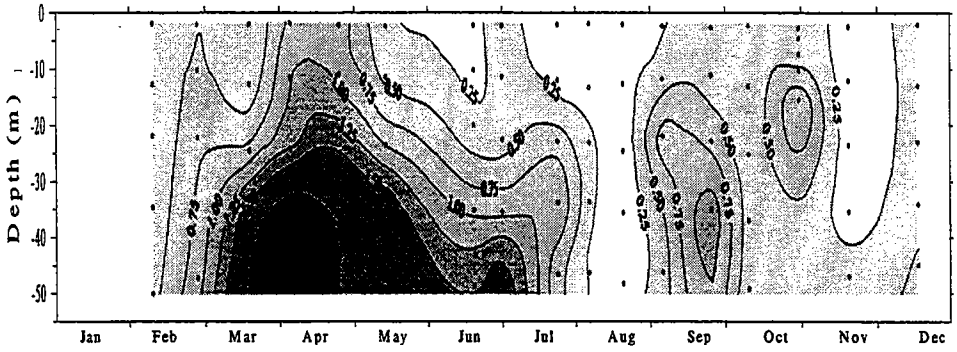

FIGURE 4-11

1996 Nearfield (3 Locations) Averaged Nutrient Annual Distributions
Concentration/Depth/Time contours for NH4 at Upwelling, Inner, and Outer stations

Dissolved Inorganic Nitrogen (DIN µM)

Upwelling (N01)

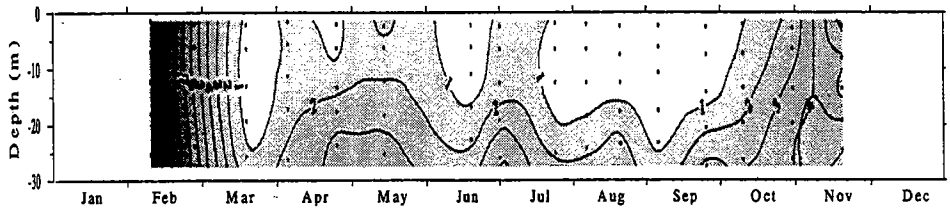

Inner (N10, N11)

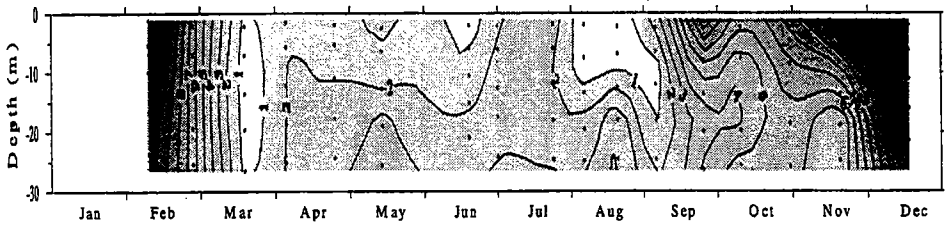

Outer (N04, N05, N06, N07)

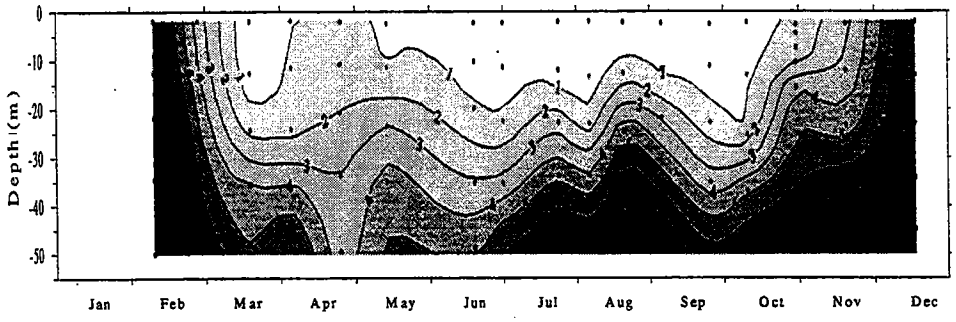

FIGURE 4-12

1996 Nearfield (3 Locations) Averaged Nutrient Annual Distributions
Concentration/Depth/Time contours for DIN at Upwelling, Inner, and Outer stations

Phosphate (PO4 µM)

Upwelling (N01)

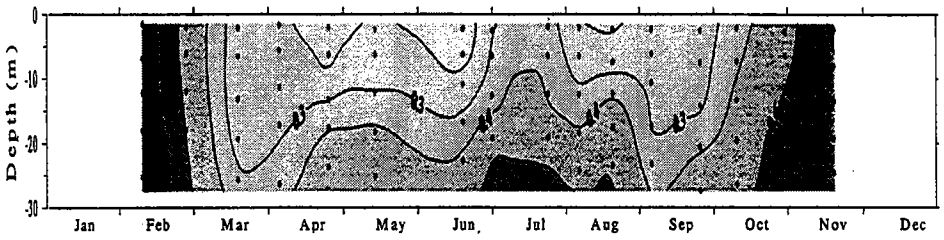

Inner (N10, N11)

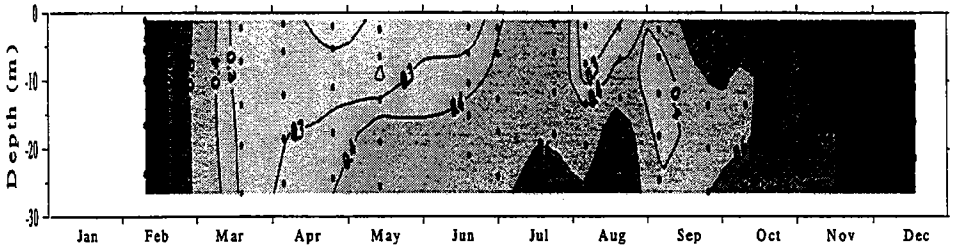

Outer (N04, N05, N06, N07)

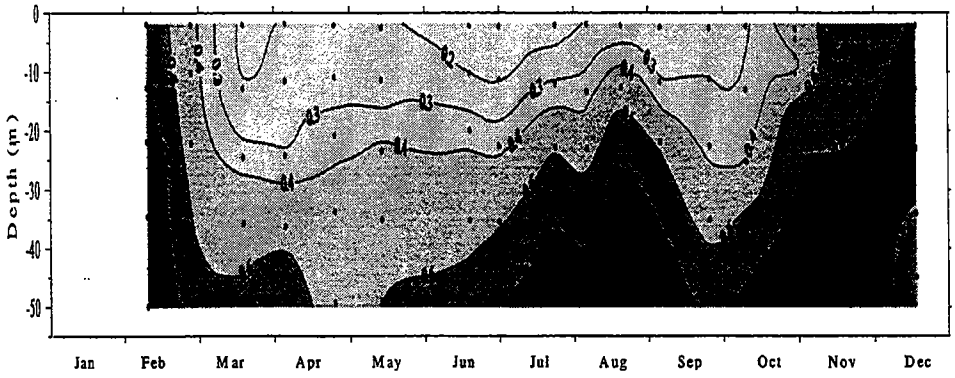

FIGURE 4-13

1996 Nearfield (3 Locations) Averaged Nutrient Annual Distributions

Concentration/Depth/Time contours for PO4 at Upwelling, Inner, and Outer stations

Silicate (SiO4 µM)

Upwelling (N01)

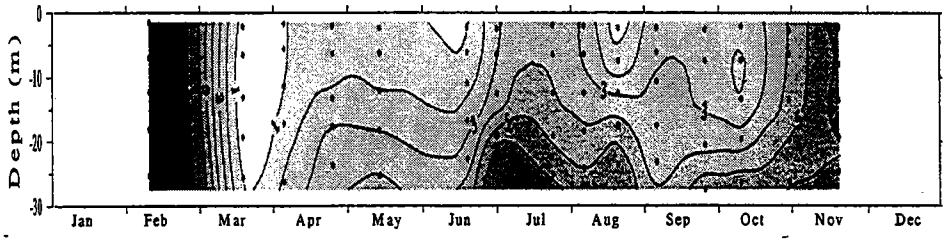

Inner (N10, N11)

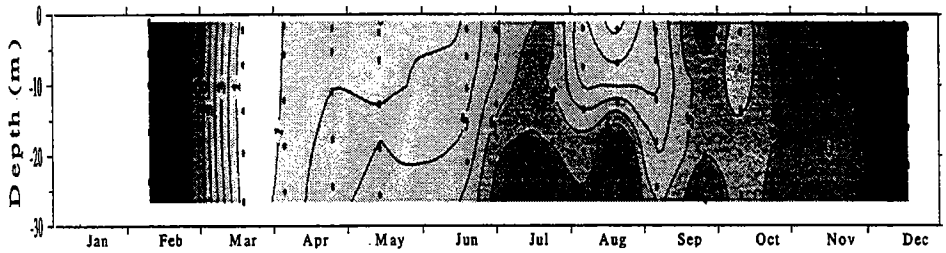

Outer (N04, N05, N06, N07)

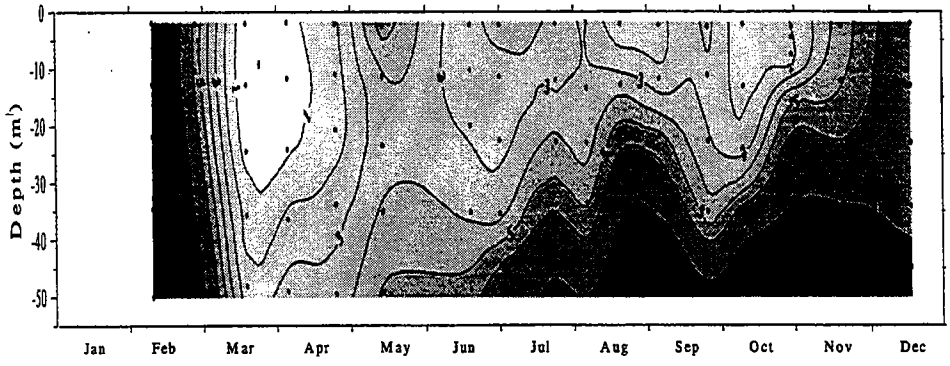

FIGURE 4-14

1996 Nearfield (3 Locations) Averaged Nutrient Annual Distributions

Concentration/Depth/Time contours for SiO4 at Upwelling, Inner, and Outer stations

Nearfield (N04, N07, N16, N20)
Nitrate + Nitrite (µM)

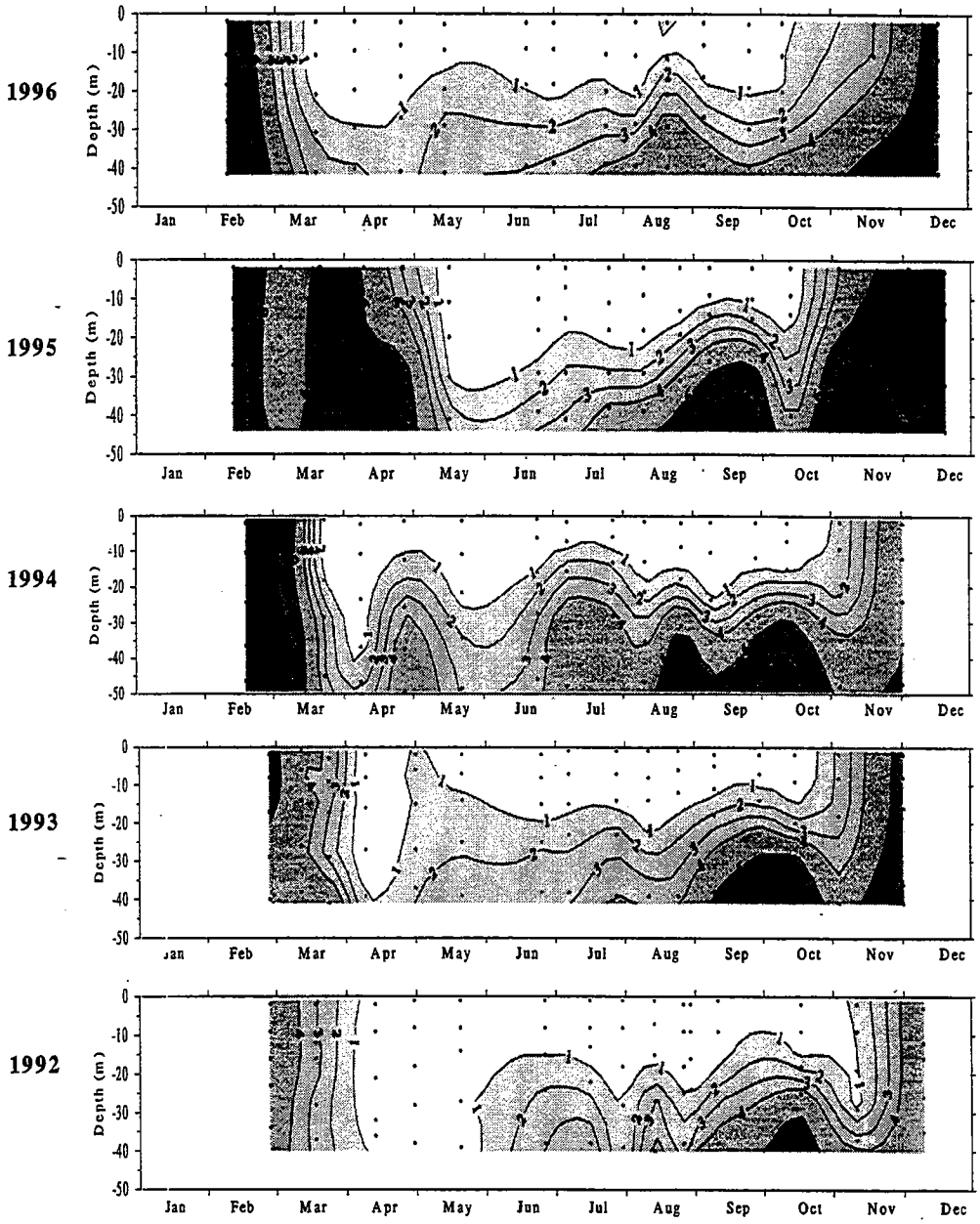

FIGURE 4-15
1992-1996 Nearfield Averaged Nutrient Annual Distributions
Concentration/Depth/Time contours for NO3+NO2

Nearfield (N04, N07, N16, N20)
Ammonium (µM)

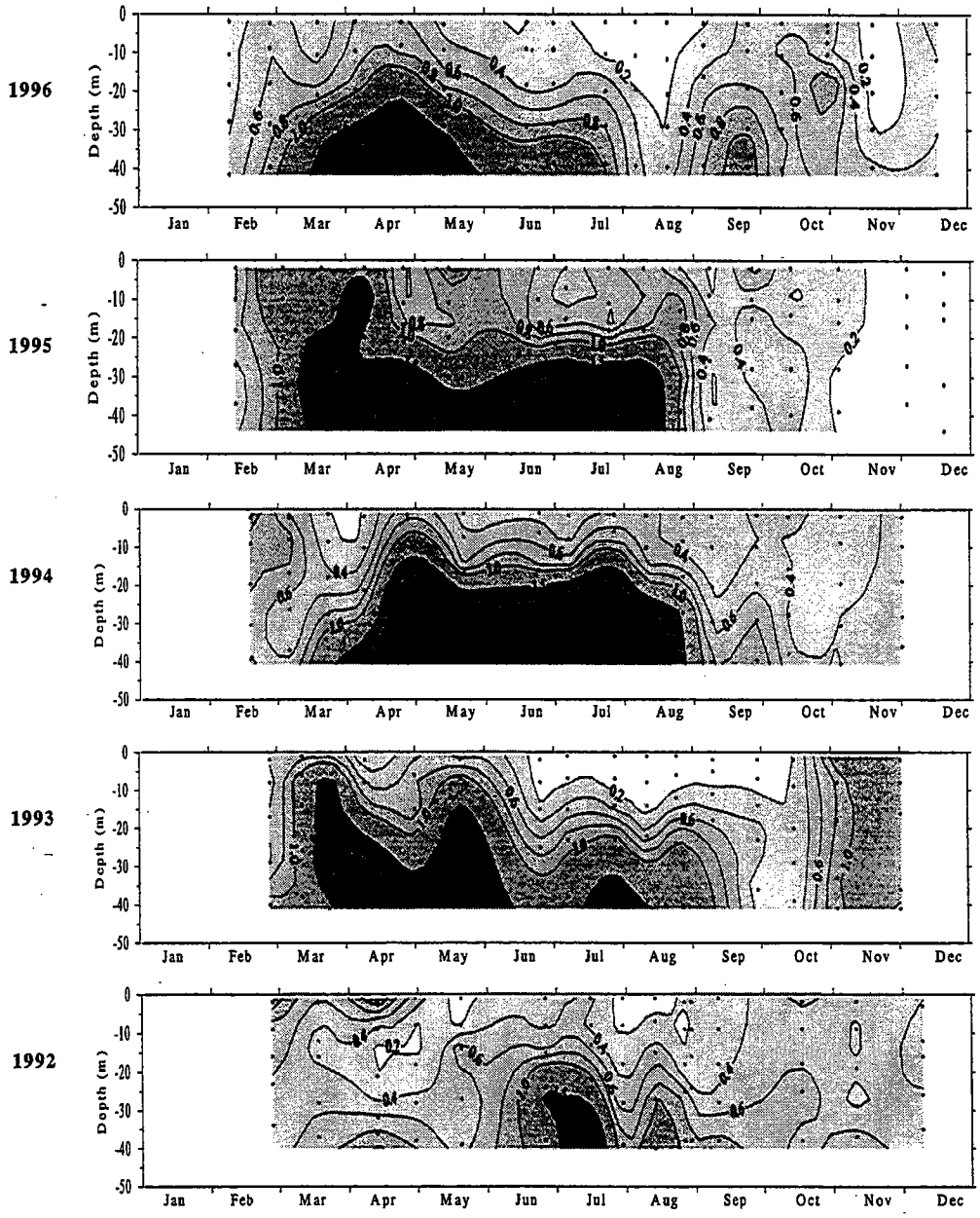

FIGURE 4-16

1992-1996 Nearfield Averaged Nutrient Annual Distributions
Concentration/Depth/Time contours for NH4

Nearfield (N04, N07, N16, N20)
DIN (Nitrate + Nitrite + Ammonium) (µM)

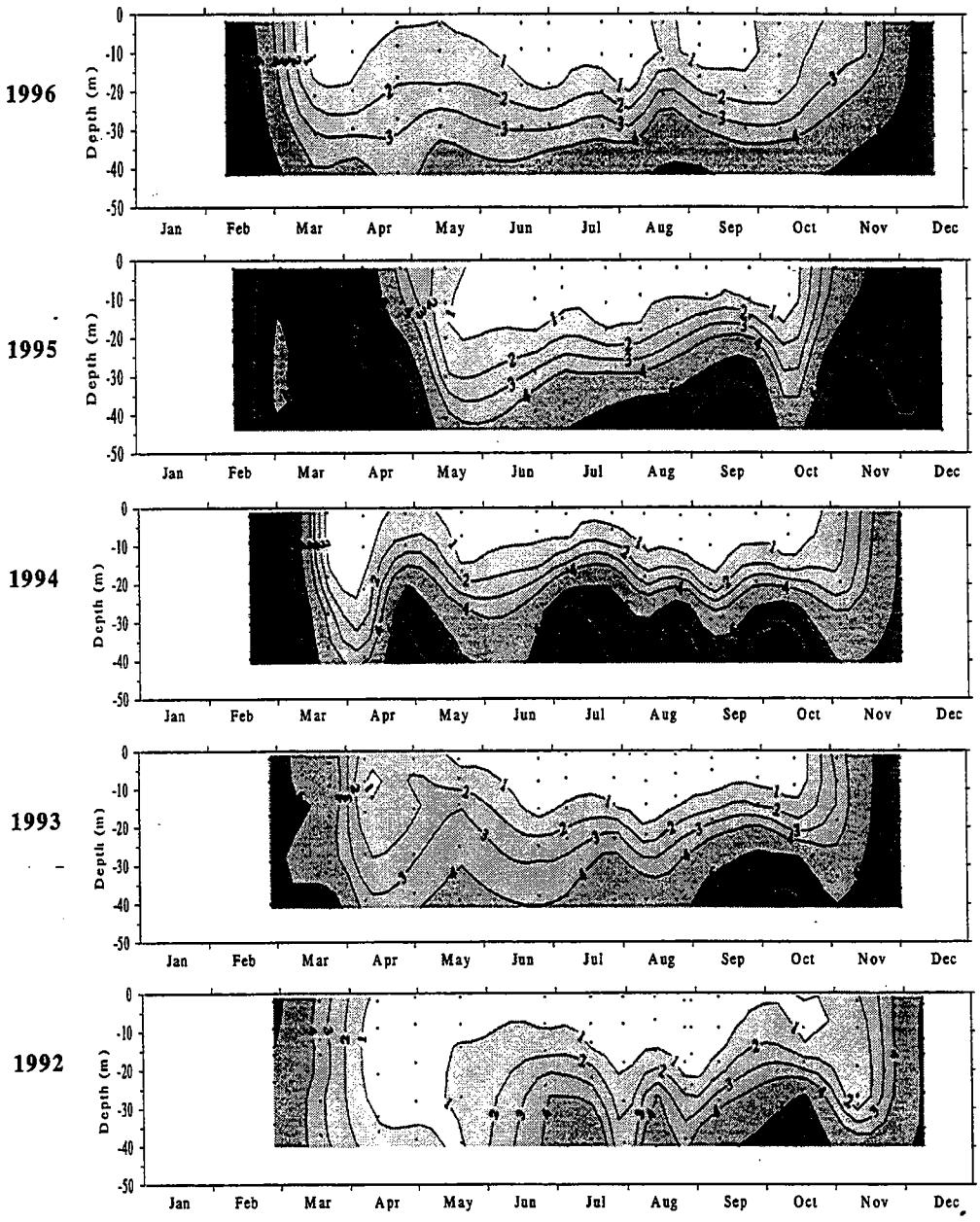

FIGURE 4-17

1992-1996 Nearfield Averaged Nutrient Annual Distributions

Concentration/Depth/Time contours for DIN

Nearfield (N04, N07, N16, N20)
Phosphate (µM)

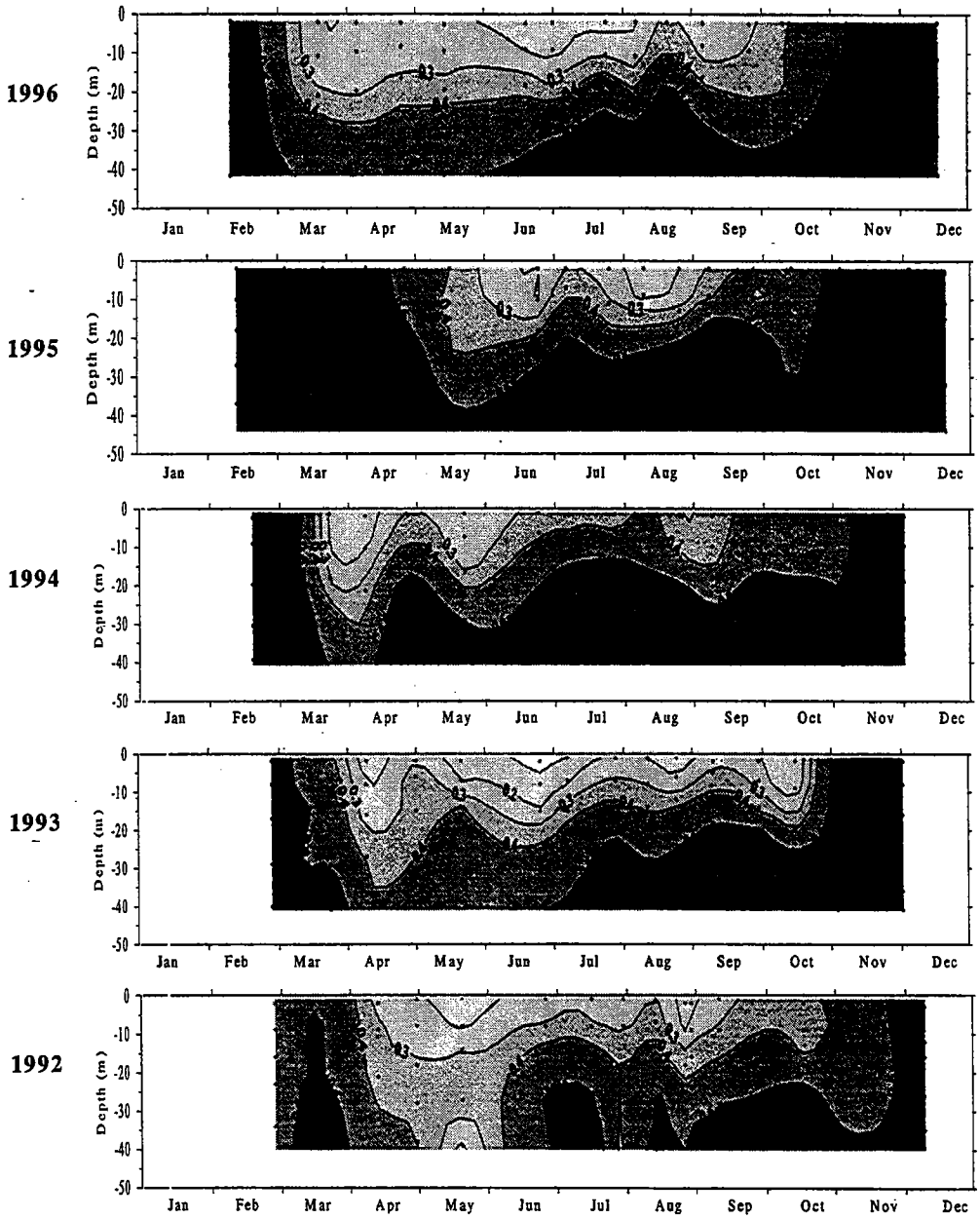

FIGURE 4-18

1992-1996 Nearfield Averaged Nutrient Annual Distributions
Concentration/Depth/Time contours for PO4

Nearfield (N04, N07, N16, N20)
Silicate (µM)

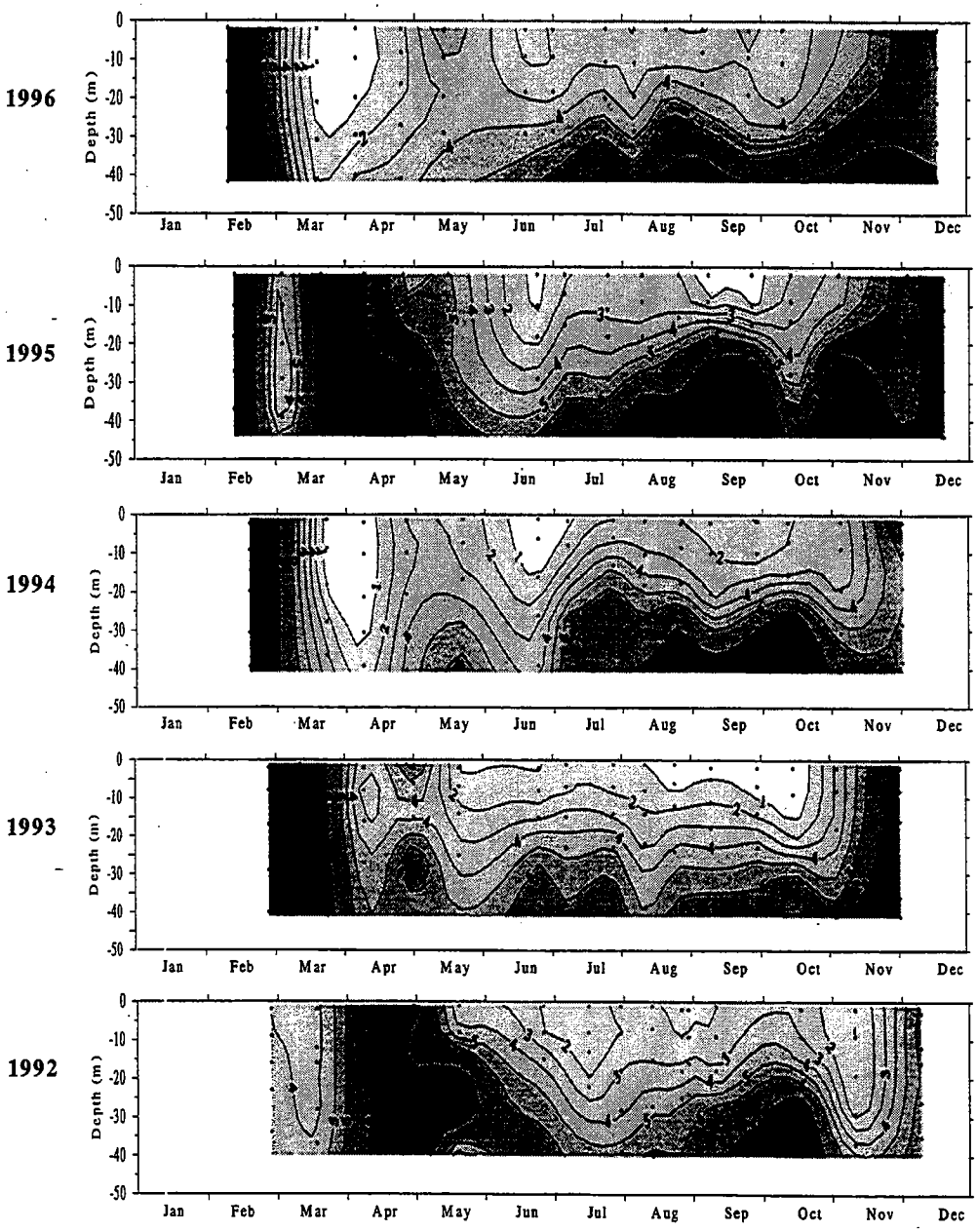

FIGURE 4-19
1992-1996 Nearfield Averaged Nutrient Annual Distributions
Concentration/Depth/Time Contours for SiO4

Nearfield (N04, N07, N16, N20)
Fluorescence (µg/l)

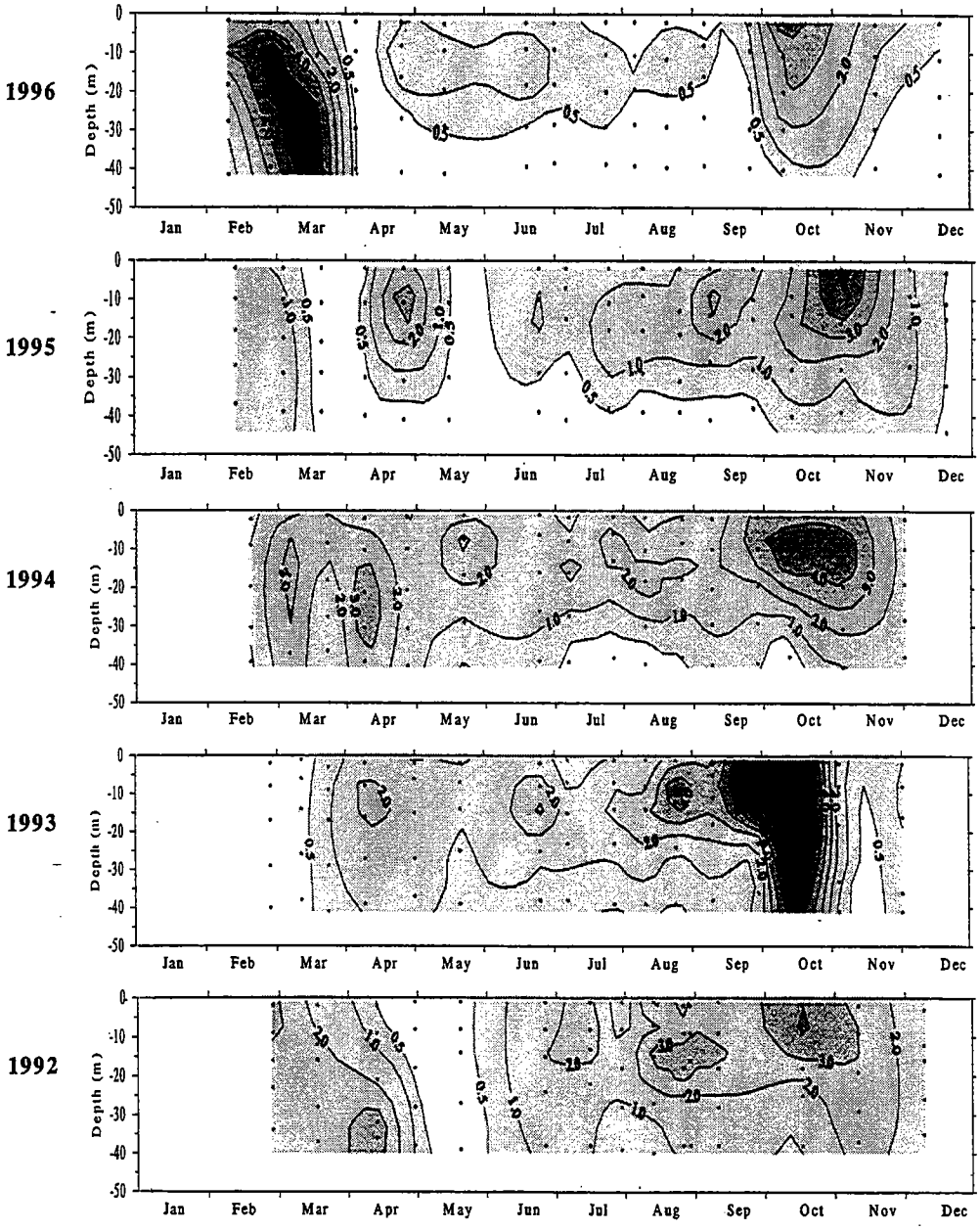

FIGURE 4-20
1992-1996 Nearfield Averaged Nutrient Annual Distributions
Concentration/Depth/Time contours for Fluorescence

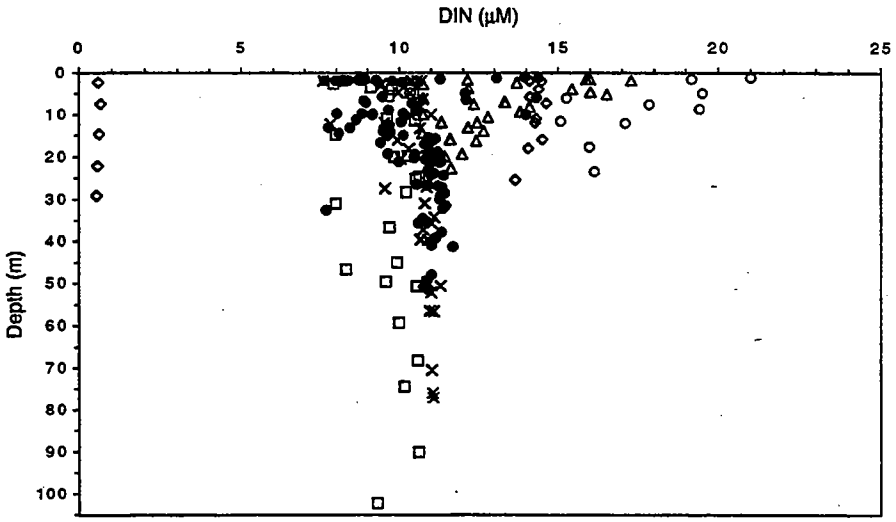

□ Boundary ◇ Cape Cod Bay △ Coastal ○ Harbor ● Nearfield × Offshore

FIGURE 4-21
Depth vs. DIN concentrations for farfield survey W9601 (February, 1996)

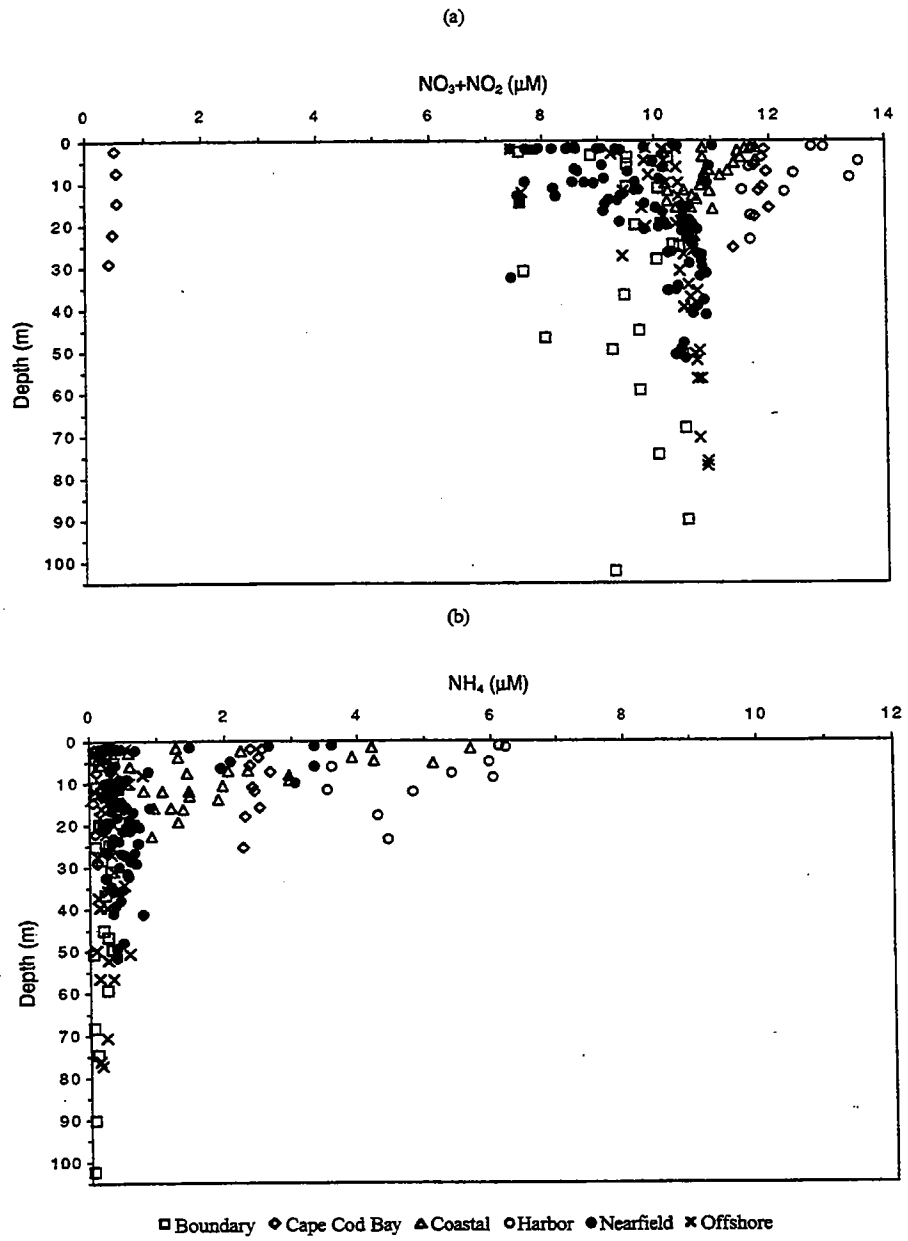

FIGURE 4-22
Depth vs. nitrate plus nitrite and ammonium concentrations for farfield survey W9601 (February, W9601)

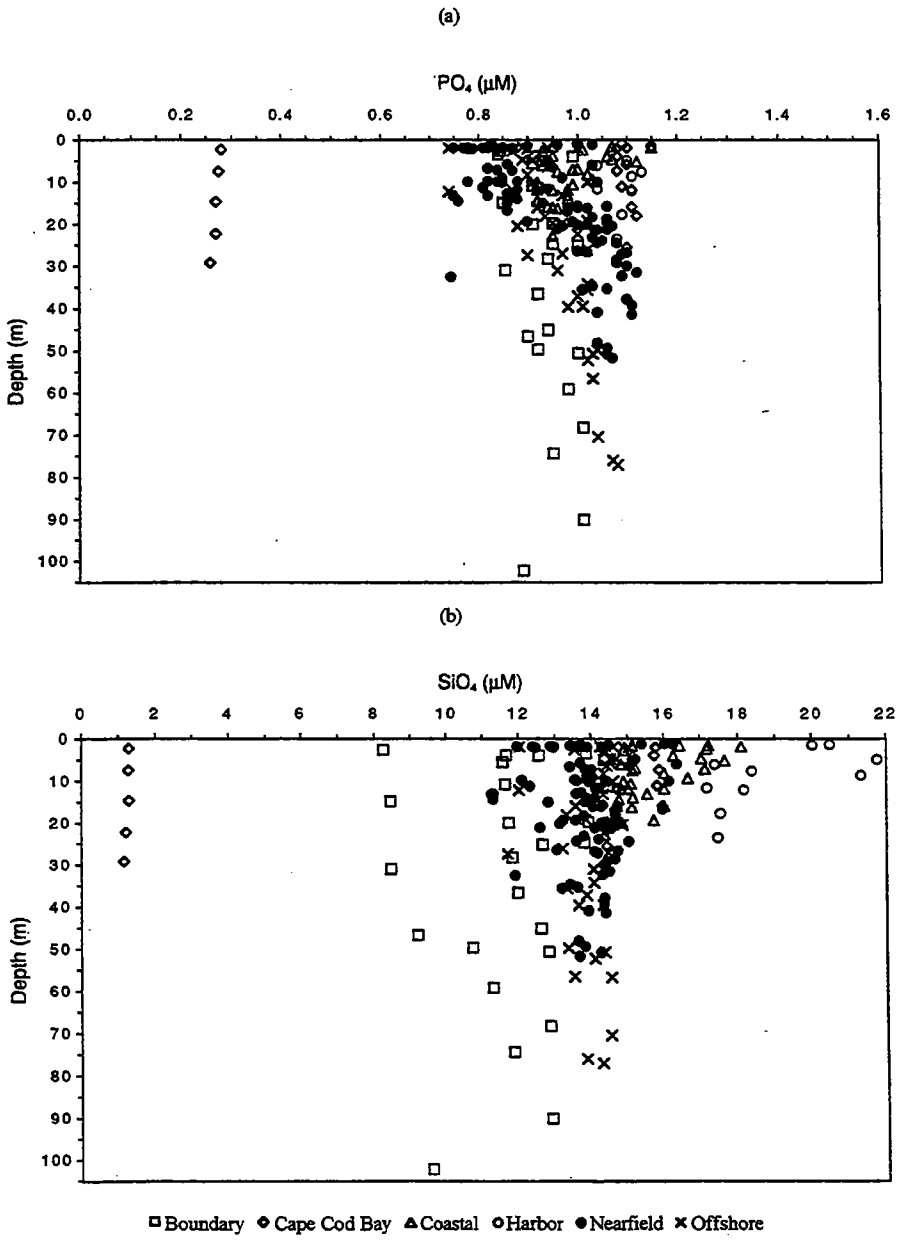

FIGURE 4-23
Depth vs. phosphate and silicate concentrations for farfield survey W9601 (February, W9601)

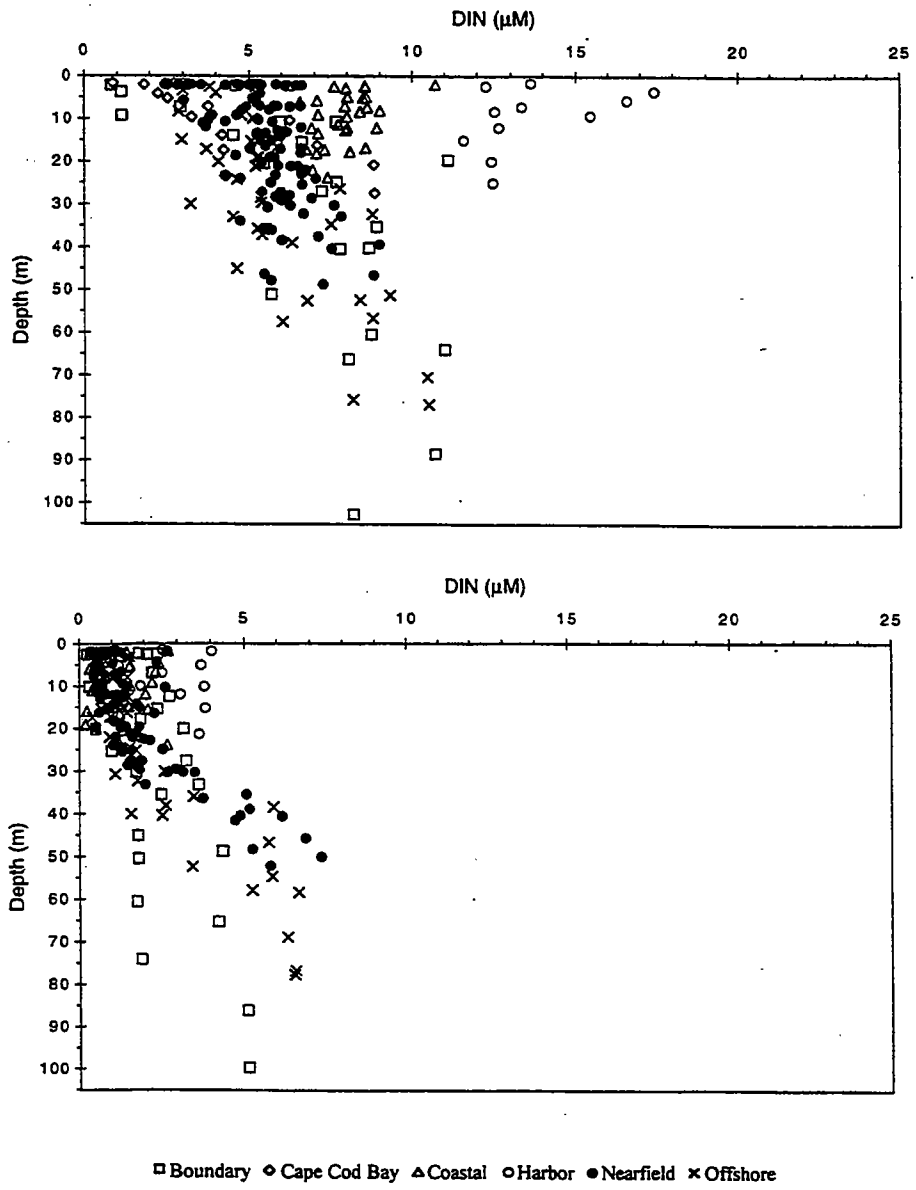

FIGURE 4-24
Depth vs. DIN concentrations for farfield surveys W9602 (February, 1996) and W9604 (April, 1996)

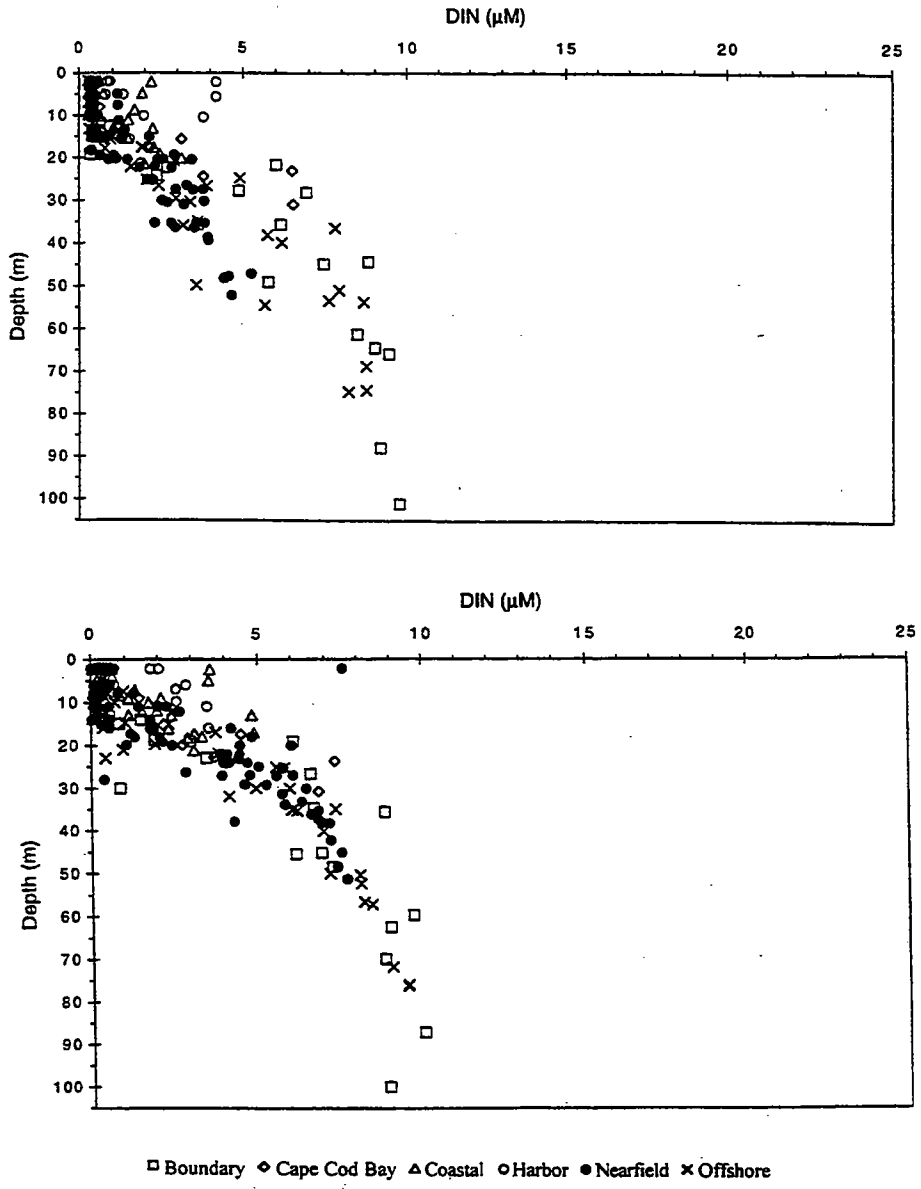

FIGURE 4-25
Depth vs. DIN concentrations for farfield surveys W9607 (June, 1996) and W9611 (August, 1996)

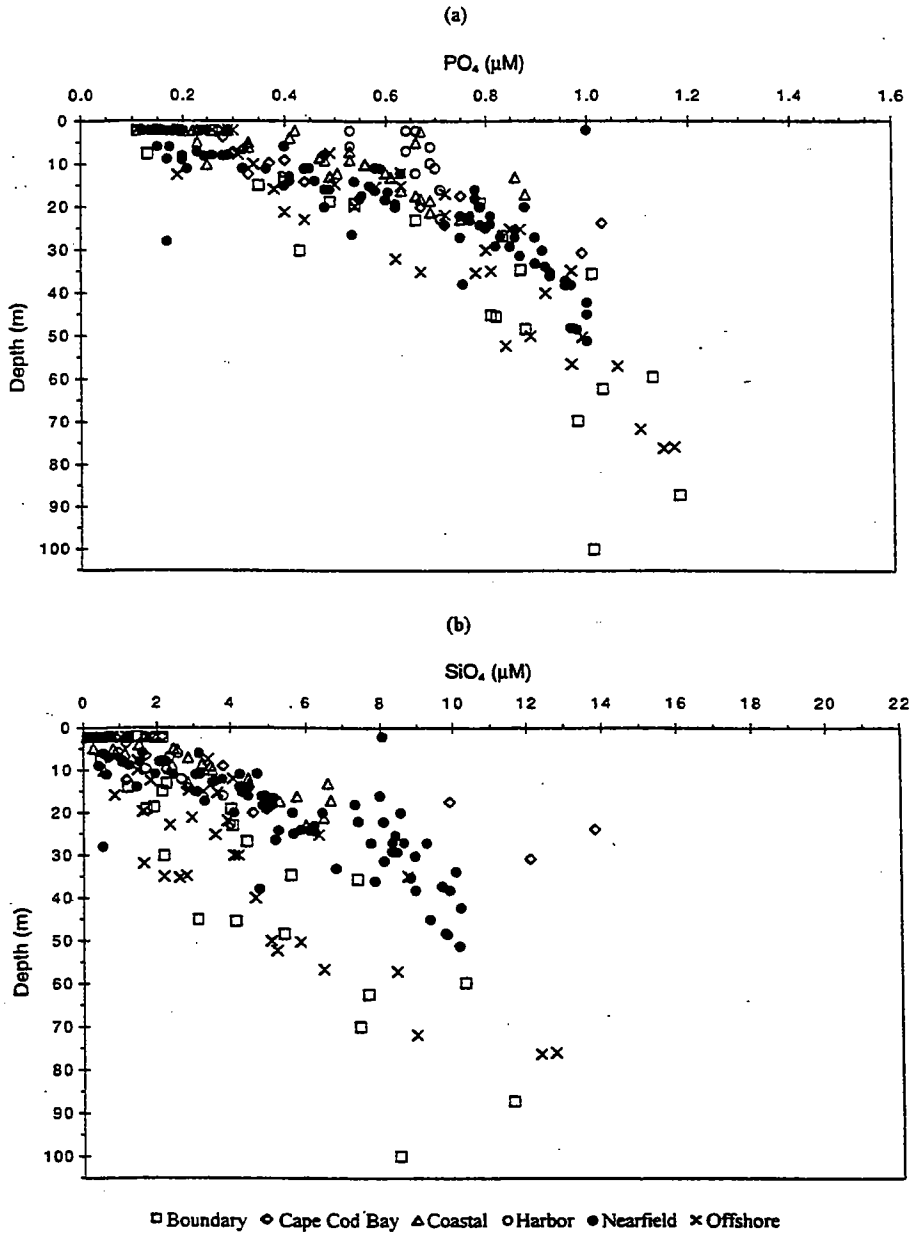

FIGURE 4-26
Depth vs. phosphate and silicate concentrations for farfield survey W9611 (August , 1996)

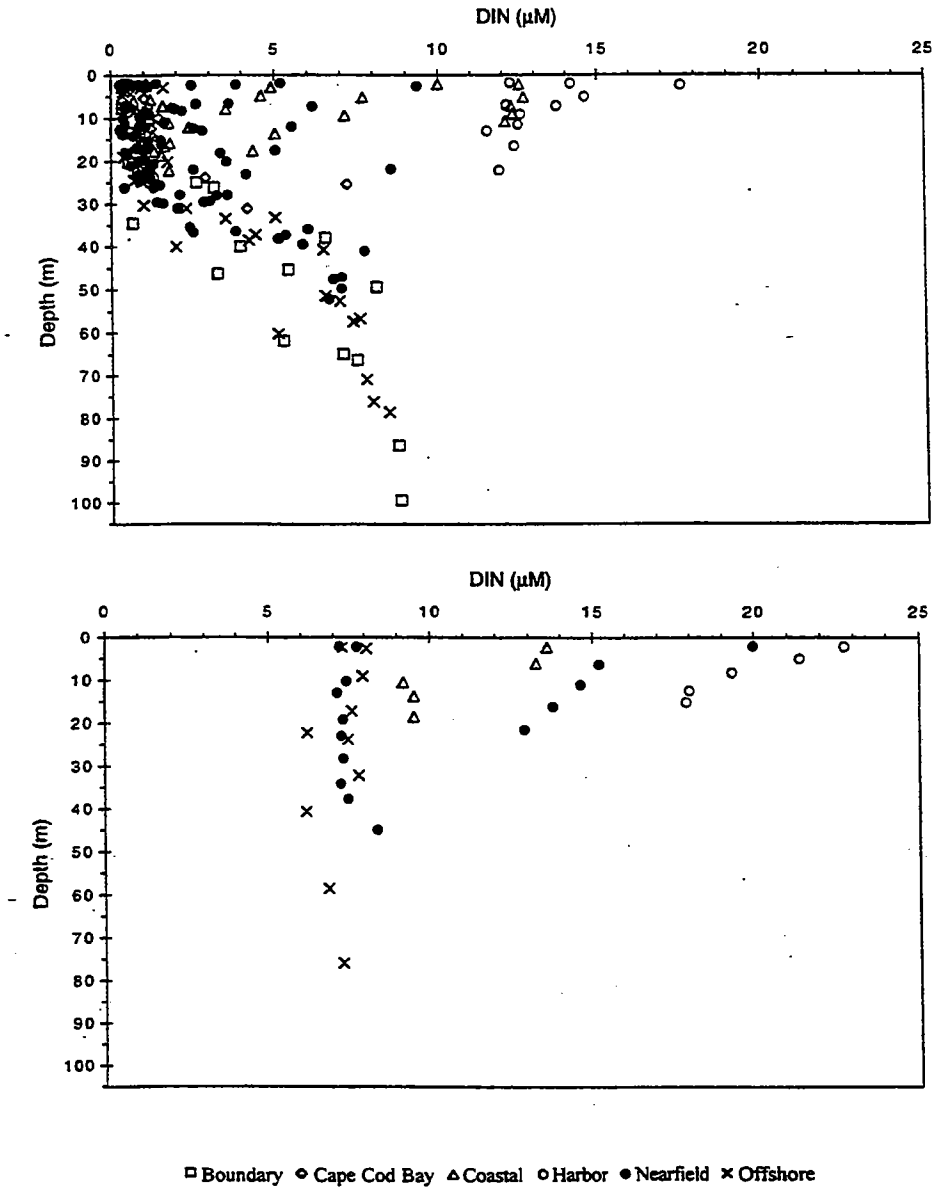

FIGURE 4-27
Depth vs. DIN concentrations for farfield surveys W9614 (October, 1996) and W9617 (December, 1996)

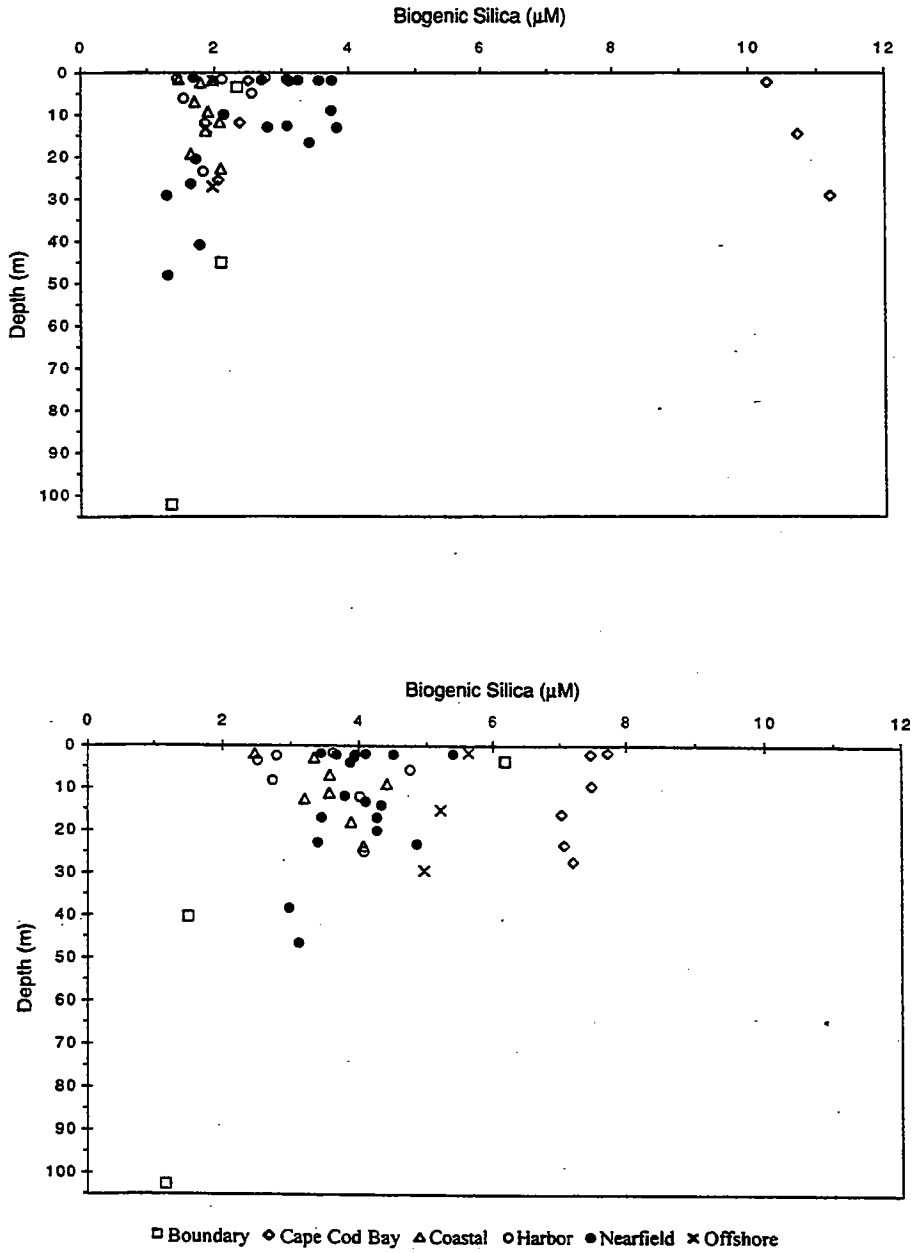

FIGURE 4-28
Depth vs. biogenic silica concentrations for farfield surveys W9601 and W9602 (February, 1996)

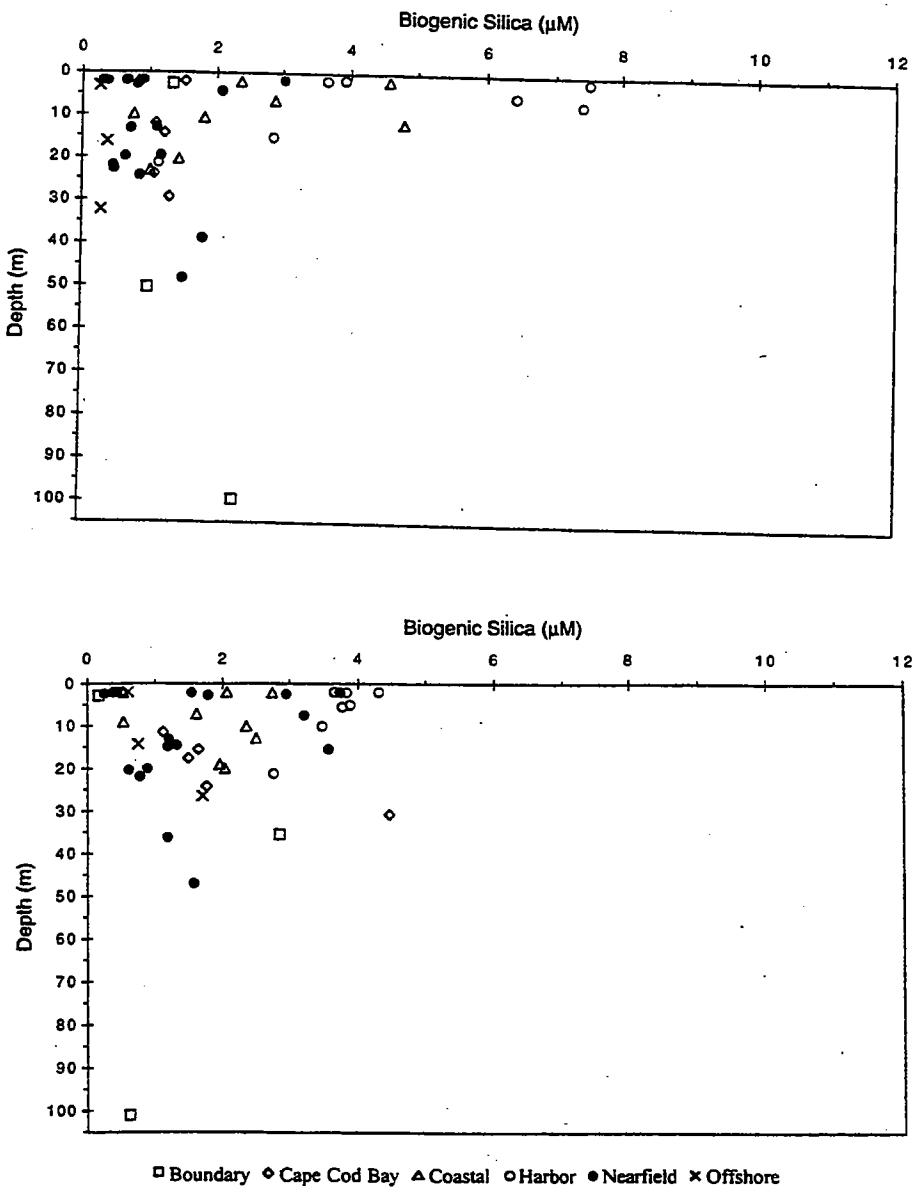

FIGURE 4-29
Depth vs. biogenic silica concentrations for farfield surveys W9604 (April, 1996) and W9607 (June, 1996)

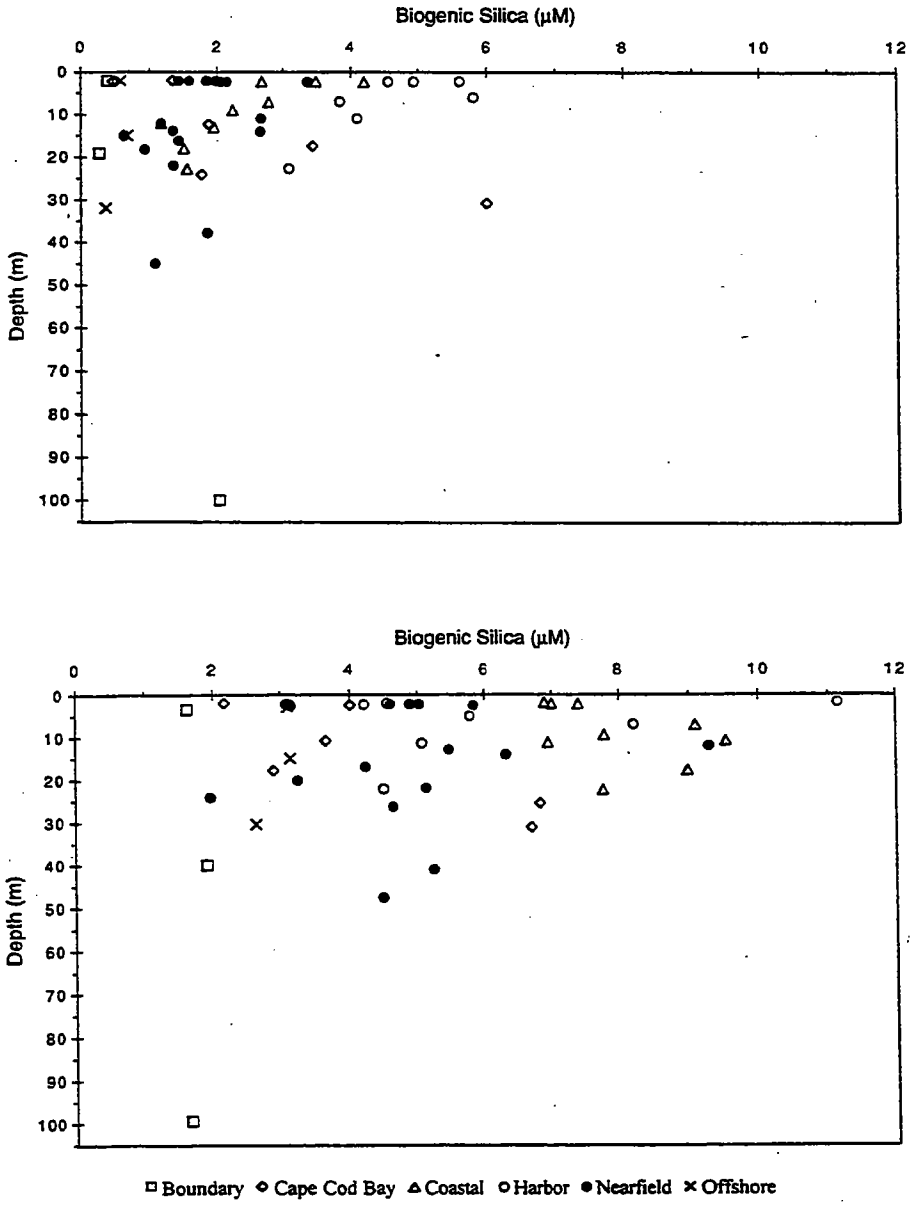

FIGURE 4-30
Depth vs. biogenic silica concentrations for farfield surveys W9611 (August, 1996) and W9614 (October, 1996)

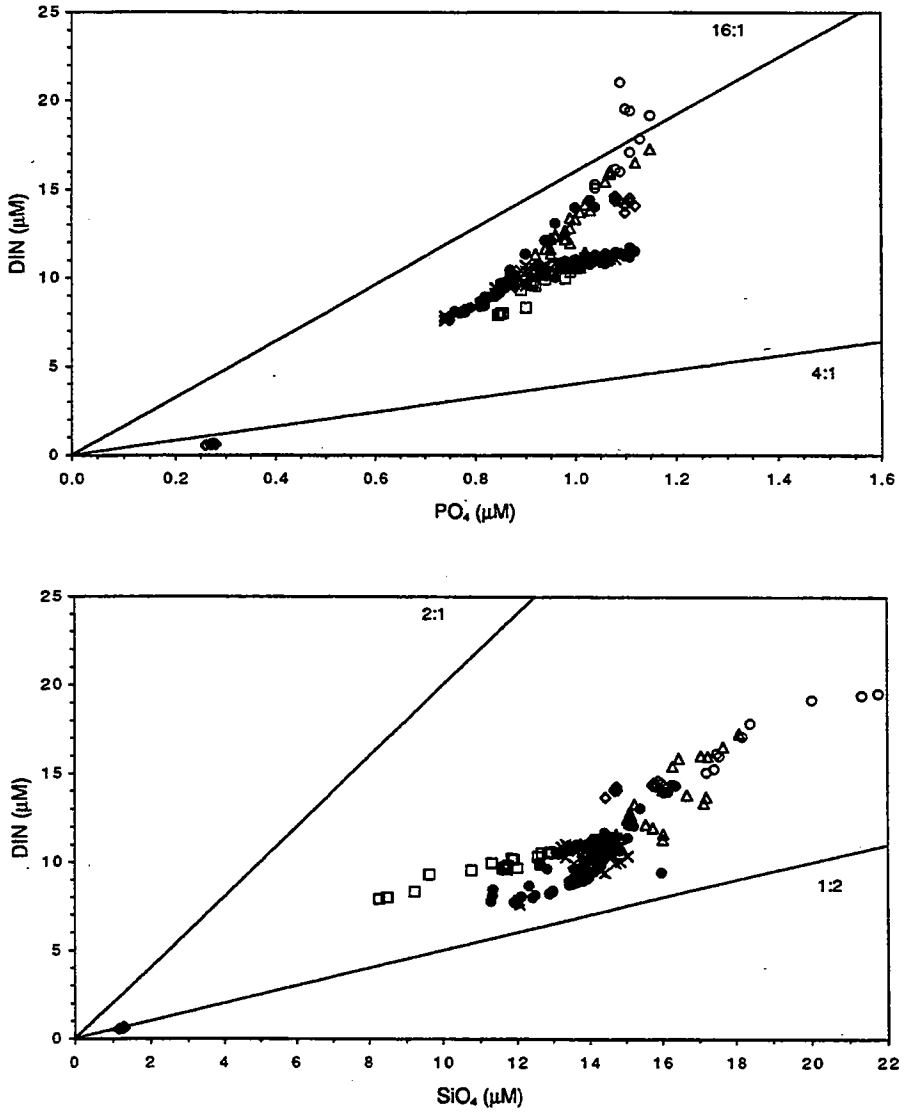

FIGURE 4-31
DIN vs. phosphate and silicate concentrations for farfield survey W9601 (February, 1996)

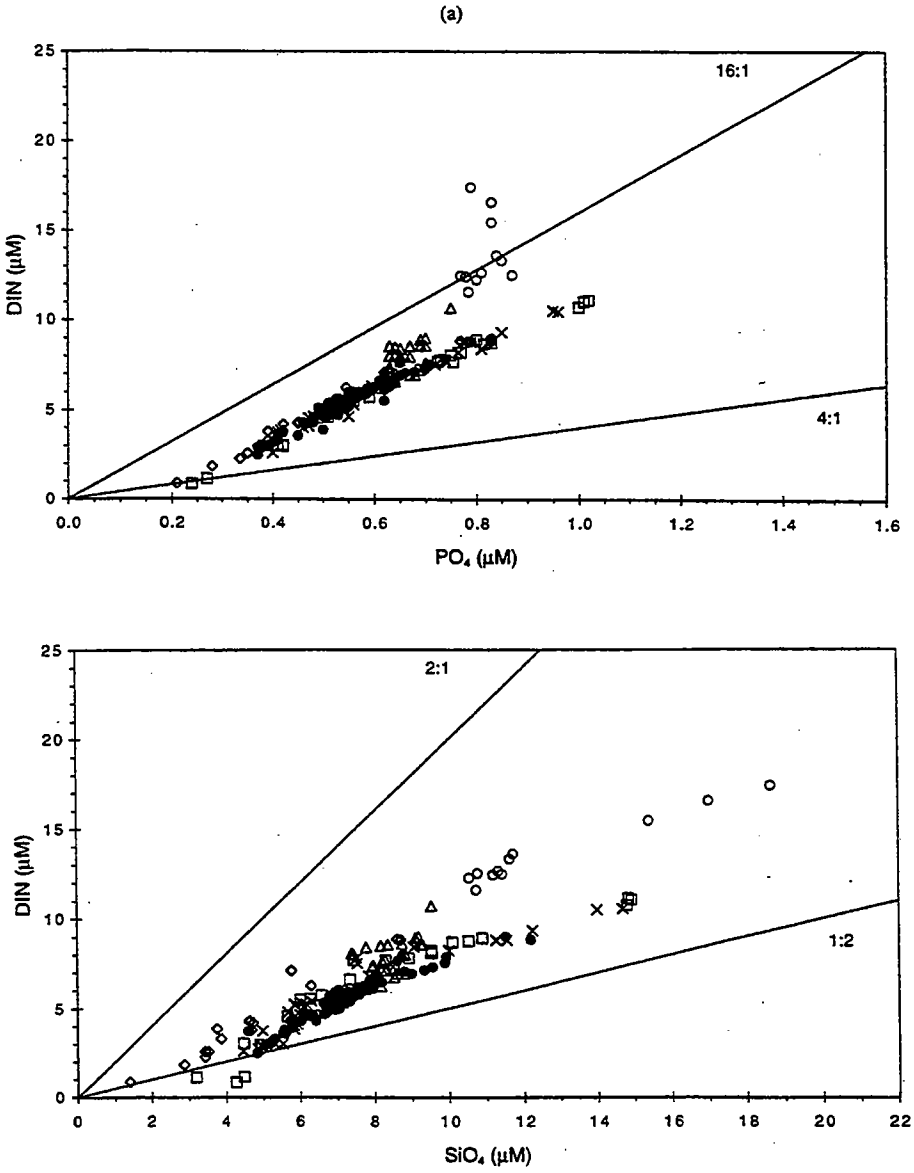

FIGURE 4-32
DIN vs. phosphate and silicate concentrations for farfield survey W9602 (February, 1996)

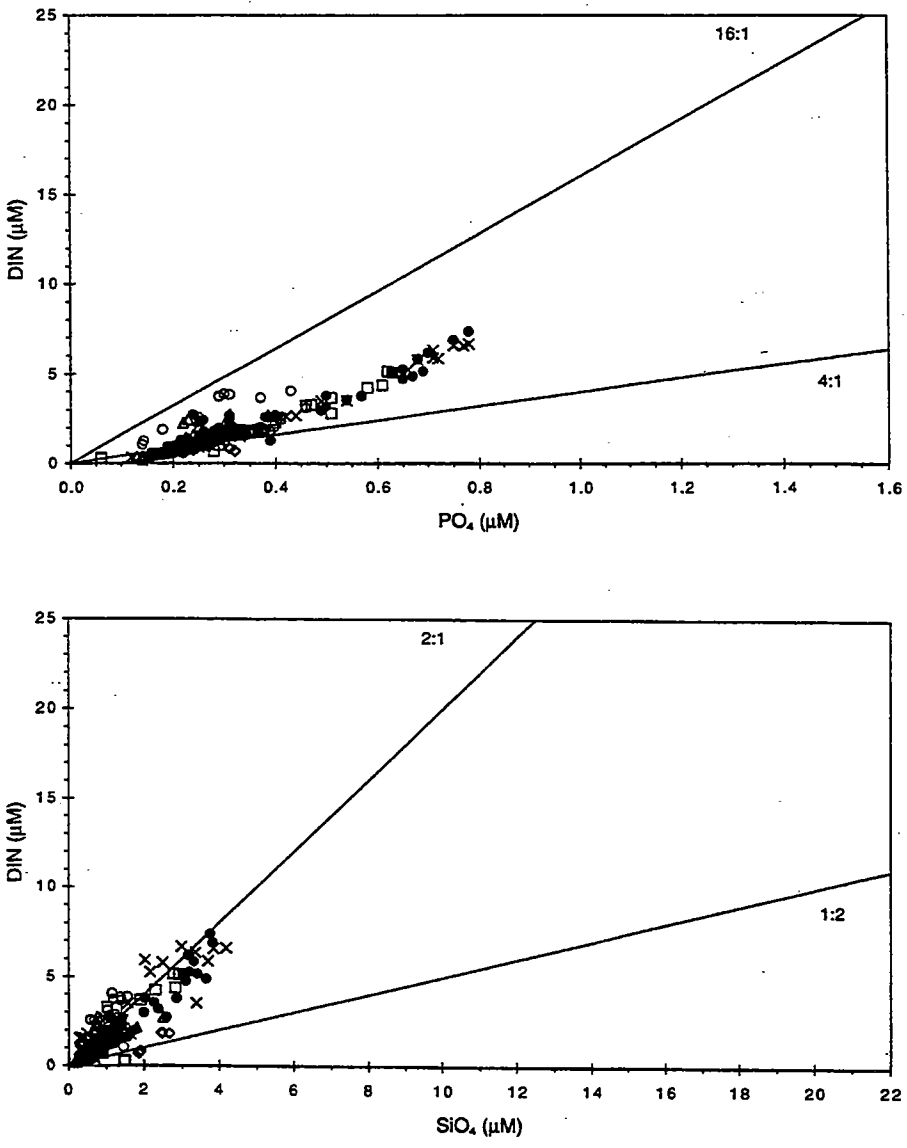

FIGURE 4-33
DIN vs. phosphate and silicate concentrations for farfield survey W9604 (April, 1996)

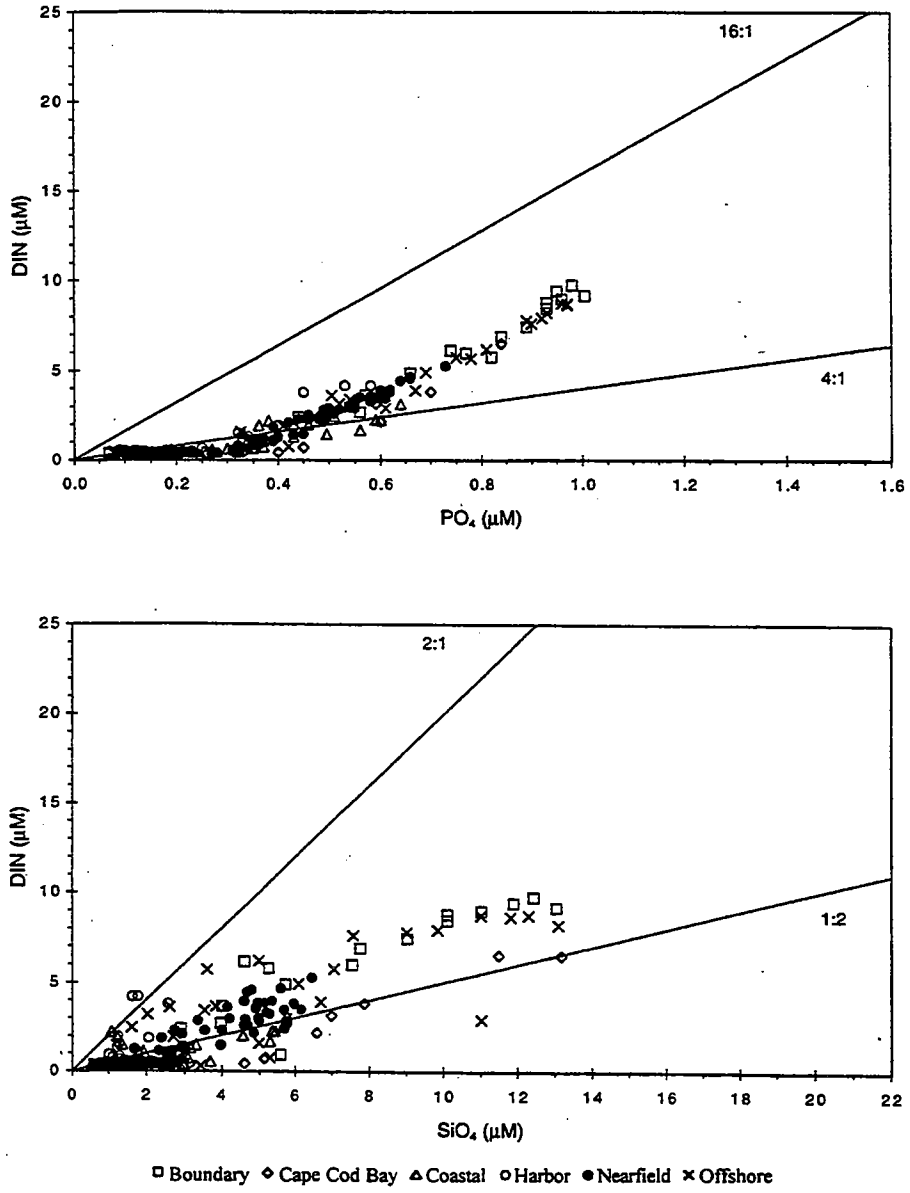

FIGURE 4-34
DIN vs. phosphate and silicate concentrations for farfield survey W9607 (June, 1996)

(a)

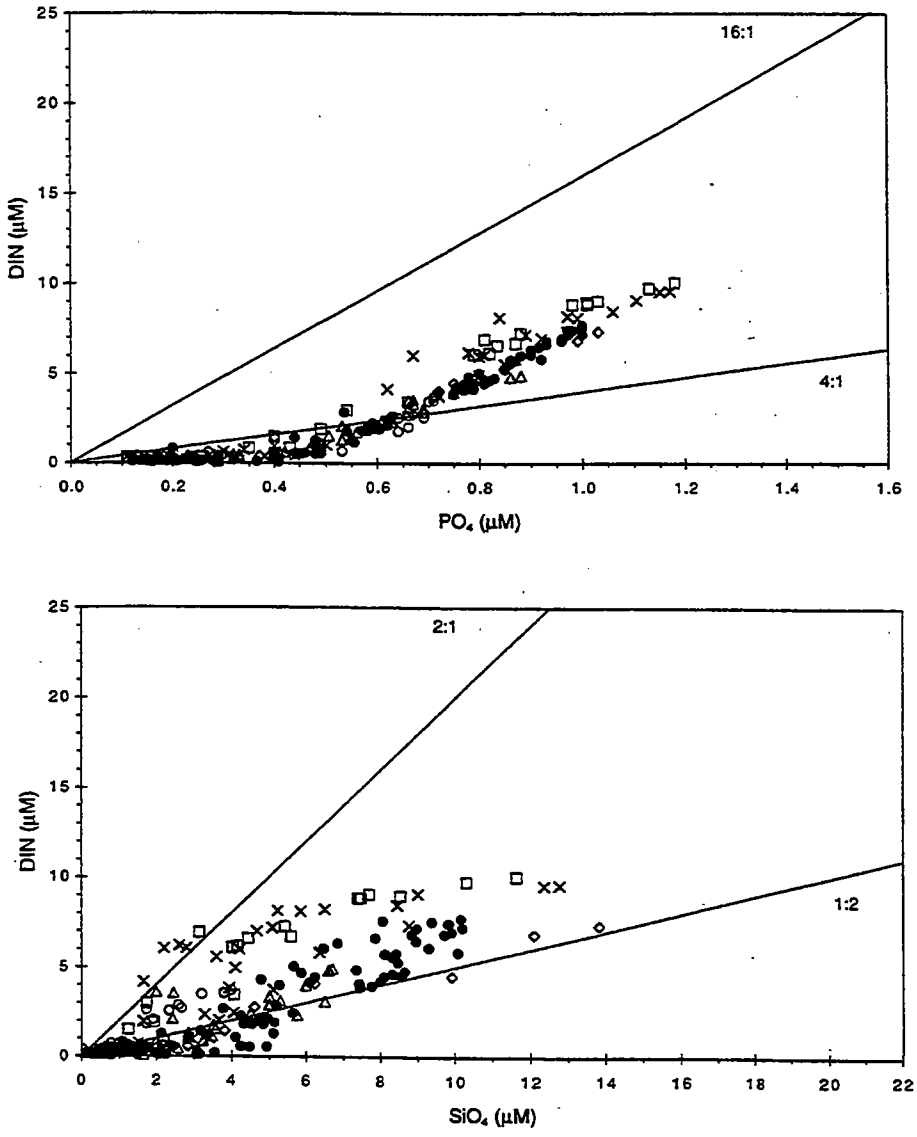

FIGURE 4-35
DIN vs. phosphate and silicate concentrations for farfield survey W9611 (August, 1996)

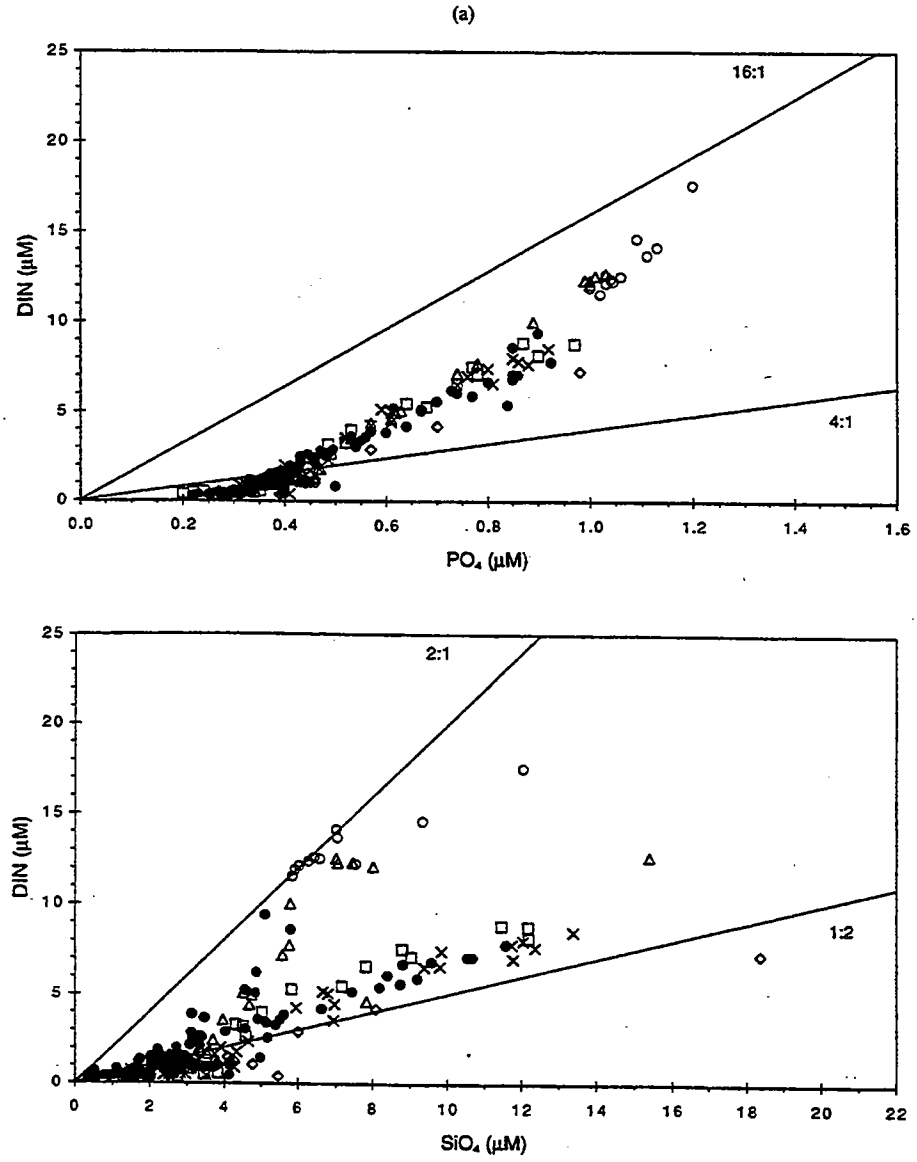

FIGURE 4-36
DIN vs. phosphate and silicate concentrations for farfield survey W9614 (October, 1996)

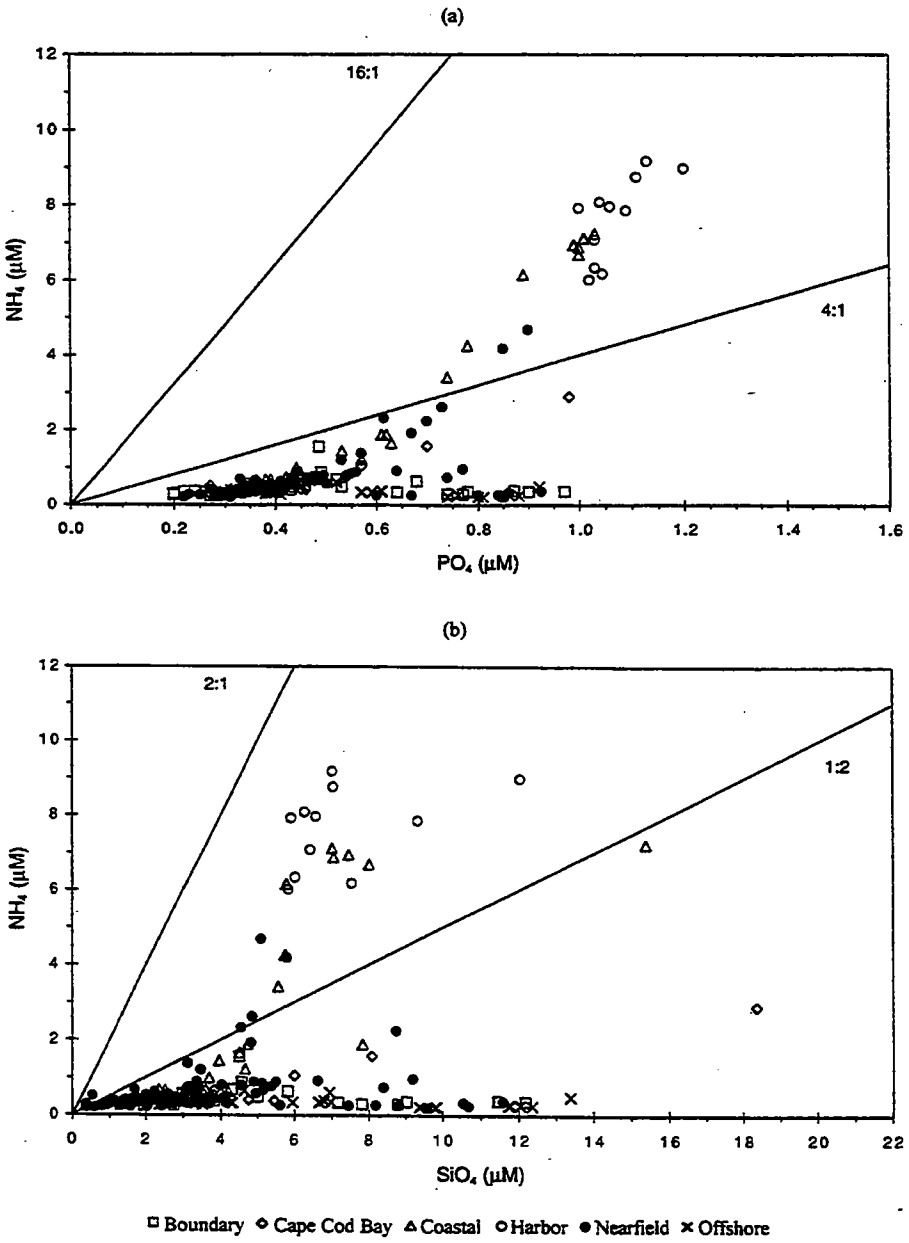

FIGURE 4-37
Ammonium vs. phosphate and silicate concentrations for farfield survey W9614 (October, 1996)

5.0 CHLOROPHYLL

Chlorophyll concentration is an indicator of phytoplankton biomass and thus used in the HOM Program as a surrogate for biomass and standing stock of phytoplankton, to normalize productivity measurements, and to ultimately assess the potential for eutrophic effects from the outfall relocation. Chlorophyll was measured on a comprehensive scale by *in-situ* fluorometry during continuous downcasts at each sampling station, and during upcasts when discrete Niskin bottle samples were taken in order to allow comparisons with nutrients, DO, and other parameters.

The *in-situ* fluorometric sensor was calibrated to analytical determinations of chlorophyll *a* from a subset of the discrete samples. Discrete chlorophyll analyses also included determination of the concentration of phaeopigments, which are degradation products of chlorophyll *a*. These results can be used to assess the physiological status of the phytoplankton community, and can be an indicator of zooplankton grazing when productivity is high (breakdown of chlorophyll *a* by digestion leading to proportionally high phaeopigment concentrations).

In this section, chlorophyll results from the 1996 monitoring activities are presented for the nearfield stations and on a regional basis, and are compared with the 1992-1995 data set. Unless otherwise stated, the results presented consist of calibrated *in situ* fluorescence readings taken at the upcast sampling depths. Included is an evaluation of results taken from the surface and at the mid-depth, which we operationally refer to in this report as the chlorophyll maximum (chl_{max}). Complete presentation of phytoplankton monitoring results is included in Section 8.1. Further detail on chlorophyll concentrations at individual stations within the nearfield grid is included with the discussion of primary productivity in Section 7.1. As with previous sections, significant events in the chlorophyll data are summarized in Table 9-1.

5.1 1996 Nearfield Results

The frequency distribution of chlorophyll results for all stations and all depths (Figure 5-1) indicated that the majority of samples had relatively low concentrations. Approximately 57 percent of results were less than 1 µg/L, and just over 92 percent were less than 5 µg/L. The average nearfield concentration for the year was 1.54 µg/L, and the maximum concentration was 11.5 µg/L (Table 5-1). Less than one percent of results exceeded 8 µg/L. Almost 7 percent of results were categorized as zero, which indicated that the fluorescence recorded by the sensor was predominantly due to the presence of phaeopigments.

The temporal and spatial distributions of chlorophyll within the nearfield were plotted for several stations within the nearfield grid to illustrate the response of phytoplankton to the horizontal inshore-offshore nutrient gradient (see Section 4). Surface, mid-depth, and bottom concentrations were plotted to evaluate vertical differences (Figures 5-2a & b). Additional plots were prepared for other selected stations in Massachusetts Bay and Cape Cod Bay for comparative purposes (Figure 5-2c).

The inshore station N10, which is influenced by tidal exchange with Boston Harbor and also exhibits a lesser degree of stratification (refer to Figure 3-5; also see Townsend *et al.*, 1991; Kelly and Turner, 1995) exhibited a different pattern from other nearfield areas after mid-March (Figure 5-2a & b). Chlorophyll *a* concentrations at N10 fluctuated from June through August, especially in surface water and at mid-depth. N10 also exhibited a late summer peak not seen in other nearfield stations, which was attributable to a large summertime harbor and near-coastal bloom (see plot for F23 in Figure 5-2c; Cibik *et al.*, 1998). Monitoring conducted by the Boston Harbor Studies Program documented chlorophyll concentrations during the period in excess of 20 µg/L (D. Taylor, pers. comm).

The fall bloom occurred in early October during the sixth combined nearfield/farfield survey (W9614). Highest chlorophyll concentrations (>9µg/L) were observed at stations N01 (off Nahant) and N20 (>7 µg/L). Chlorophyll concentrations at the outer nearfield stations (e.g., N04 and N07) during the fall bloom were slightly lower (3-5µg/L). Surface concentrations were typically at least 1 µg/L higher than the deeper samples, with the exception of station N07 where the mid-depth sample was higher. High seas and deteriorating weather conditions prevented sampling of several stations in late October (W9615), however, data from N04 indicated that surface chlorophyll concentrations diminished somewhat, whereas concentrations at the deeper depths increased. Results from November (W9616) documented continued, albeit somewhat diminished, phytoplankton growth, but data from the final survey in December showed the bloom to have ended.

Continuously recorded chlorophyll results (WETLabs ac-3) from the USGS mooring in the center of the nearfield were available for a four-month period during 1996 (June 10, 1996 through September 23, 1996) for comparison with the shipboard survey measurements. These results were plotted with the HOM survey dates (Figure 5-3). Beyond the daily variability associated with both physical and biological factors, these data indicated short-term maxima of varying intensity. The USGS mooring documented increases in chlorophyll concentrations during early July and mid-August, and indicated that the fall bloom was initiated around the middle of September.

To further evaluate the vertical distribution of chlorophyll in the nearfield, ratios were calculated to compare chlorophyll concentrations from the mid-depth (operationally referred to in this report as the chlorophyll maximum (chl_{max}) sample depth) (Figure 5-4). Harbor station F31 demonstrated virtually no difference between the two depths (Figure 5-4a), even during the stratified period (Figure 3-12a). Inshore station N10 illustrated the least variability for nearfield stations (Figure 5-4b), with subsurface peaks evident in early May and early August. The more offshore stations developed pronounced maxima at depth, reaching ratios of 8:1 between July and September (Figure 5-4c through 5-4e).

5.2 1996 Regional Comparisons

A frequency distribution for chlorophyll *a* results was calculated for all stations and all depths sampled in Massachusetts and Cape Cod Bays during the combined nearfield/farfield events (Figure 5-5). These results indicated that the distribution of chlorophyll concentrations were similar baywide as that seen in the nearfield (refer to Figure 5-1). Massachusetts Bay as a whole had a slightly higher average annual concentration (1.81 µg/L), and a maximum concentration of 13.4 µg/L (Table 5-1).

Regional plots of fluorescence data indicated highest chlorophyll concentrations during the summer in the harbor, represented by station F23 (Figure 5-6). These summer results showed highest concentrations in surface samples in the harbor, whereas at the more stratified Cape Cod Bay and offshore stations they were often highest in the mid-depth sample. While the harbor did not exhibit any notable late winter/spring event, both the offshore (station F06) and Cape Cod Bay (station F02) regions showed a substantial late winter bloom, followed by low chlorophyll concentrations throughout the summer. The offshore and Cape Cod Bay stations exhibited a modest increase in chlorophyll concentration during the October survey (W9614), indicating the fall bloom evident in the nearfield also occurred in these regions (but either not to the same degree or perhaps not concurrently).

5.3 Interannual Comparisons of Chlorophyll Concentration

5.3.1 Nearfield Comparisons

The annual seasonal cycles for chlorophyll (surface and bottom) in the nearfield for the period 1992 to 1996, along with the extent of spatial and temporal variability for nearfield stations as a whole, is depicted in Figure 5-7. The size of the error bars (standard deviations) indicates the degree of horizontal and vertical variability encountered during one survey. Large interannual differences can also be seen during both the spring and fall blooms. The largest spring seasonal average occurred during 1996 (2.43 µg/L), followed by 1992 and 1994. The largest fall seasonal average occurred during 1993 (4.42 µg/L), followed by 1995, 1994, and 1992. This graphical representation of the data also demonstrates that both the spring and fall events may reach peak densities over a period of a month or more, while the events themselves may shift by a month or more.

Despite the differences observed in the magnitude of bloom events from year to year, annual nearfield averages only differed by around 1 µg/L, ranging from 1.39 µg/L in 1995 to 2.36 µg/L in 1993 (Table 5-1). The overall average calculated for the 1992-1996 baseline period was 1.88 µg/L. Variability in chlorophyll *a* concentrations was more significant seasonally. Seasonal *in-situ* chlorophyll *a* concentrations were calculated for all years as part of the baseline evaluation (Table 5-2). Spring chlorophyll *a* concentrations ranged from 1.01 µg/L during 1993 to 2.43 µg/L during 1996, with a baseline average of 1.68 µg/L.

As might be expected from previous discussions, chlorophyll *a* concentrations were generally lowest during the summer, ranging from 0.73 µg/L in 1995 to 1.88 µg/L in 1992, and a baseline average of 1.35 µg/L. The exception occurred during the summer 1993, when the average summertime chlorophyll *a* concentration (1.81 µg/L) was almost double the average for the spring (1.01 µg/L). The fall produced the overall highest average for chlorophyll *a* (2.68 µg/L), with individual years ranging from a low in 1996 of 1.47 µg/L to a high of 4.42 µg/L in 1993.

5.3.2 Regional Comparisons

Table 5-1 also provides annual averages for results from the regional stations sampled during the six combined surveys (1992 through 1996). Average results ranged from 1.2 µg/L to 2.84 µg/L, with results from 1995 again the lowest of the five years. In order to examine these interannual differences on a regional and temporal basis, results from selected stations in each sampling region were plotted for 1992 through 1996 (Figure 5-8). Harbor

stations typically increased in concentrations through the summer, with no pronounced fall bloom evident (Figure 5-8a). Coastal stations (e.g. F13, Figure 5-8b) follow a similar pattern but do experience the fall bloom. The 1993 bloom was well documented throughout the regional stations, including Cape Cod Bay (F02), which typically shows only a modest increase in the fall, if any. Conversely, Cape Cod Bay typically yields the largest spring bloom, reaching 12 µg/L or more in 1994 and 1996.

Year	Mean (µg/L)	Standard Deviation	N	Maximum (µg/L)
Nearfield				
1992	2.08	1.69	1465	17
1993	2.36	3.11	1851	20.5
1994	1.96	1.48	1863	13.7
1995	1.39	2.32	1682	18.1
1996	1.54	1.89	1275	11.5
1992-1996 Baseline	**1.88**	**2.23**	**8136**	**20.5**
Massachusetts Bay				
1992	2.24	1.75	2200	
1993	2.84	3.85	1103	21.1
1994	2.27	2	1132	16.9
1995	1.20	1.74	1102	15.0
1996	1.81	2.18	1275	13.4

Notes:
Nearfield = all Nearfield stations, all depths
Massachusetts Bay = all Farfield stations + 6 Nearfield stations (N01, N04, N07, N10, N16, N20), all depths

TABLE 5-1
Comparison of Annual and Regional In-situ Chlorophyll a Characteristics

TABLE 5-2
Mean MWRA Baseline Seasonal Chlorophyll Data

17 Nearfield Stations, All Depths, In-situ Chlorophyll *a*

Year	Spring	Summer	Fall
1992	1.97	1.88	2.46
1993	1.01	1.81	4.42
1994	1.95	1.55	2.47
1995	1.02	0.73	2.58
1996	2.43	0.78	1.47
1992-1996			
Mean	1.68	1.35	2.68
Standard Deviation	0.63	0.56	1.07
N	5	5	5

T5-2flu.XLS

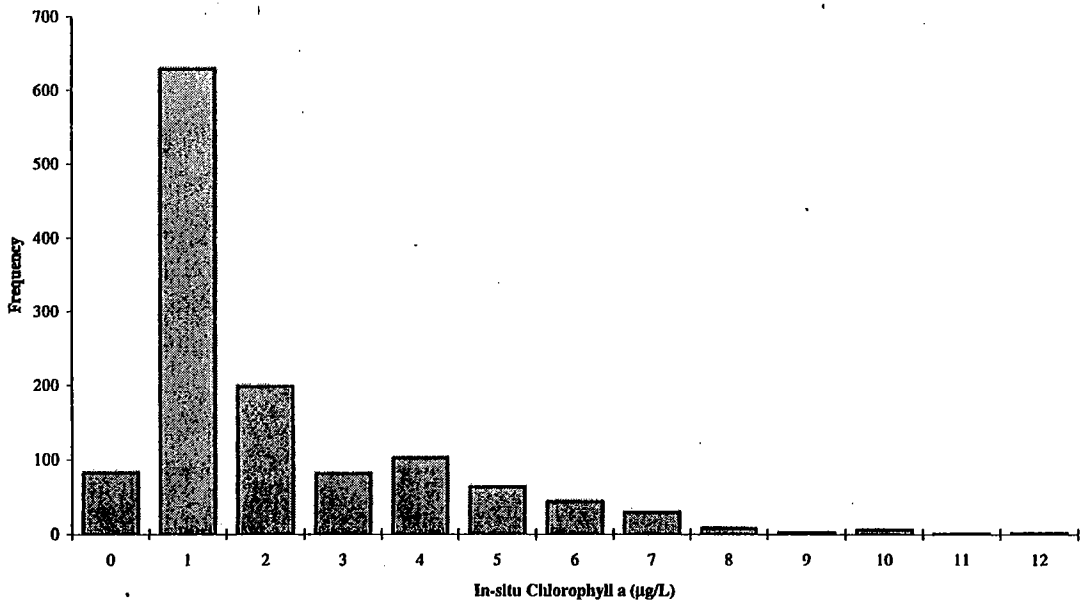

Nearfield	83	629	198	81	102	63	43	29	8	3	6	1	2	1248
Total Number	83	629	198	81	102	63	43	29	8	3	6	1	2	1248
Percent	6.7%	50.4%	15.9%	6.5%	8.2%	5.0%	3.4%	2.3%	0.6%	0.2%	0.5%	0.1%	0.2%	100.0%
Cumulative Number	83	712	910	991	1093	1156	1199	1228	1236	1239	1245	1246	1248	
Cumulative Percent	6.7%	57.1%	72.9%	79.4%	87.6%	92.6%	96.1%	98.4%	99.0%	99.3%	99.8%	99.8%	100.0%	

Note: Bin number denotes upper limit of bin.

Figure 5-1
Frequency Distribution of 1996 Nearfield In-situ Chlorophyll *a* Results
All depths at all nearfield stations on all nearfield surveys.

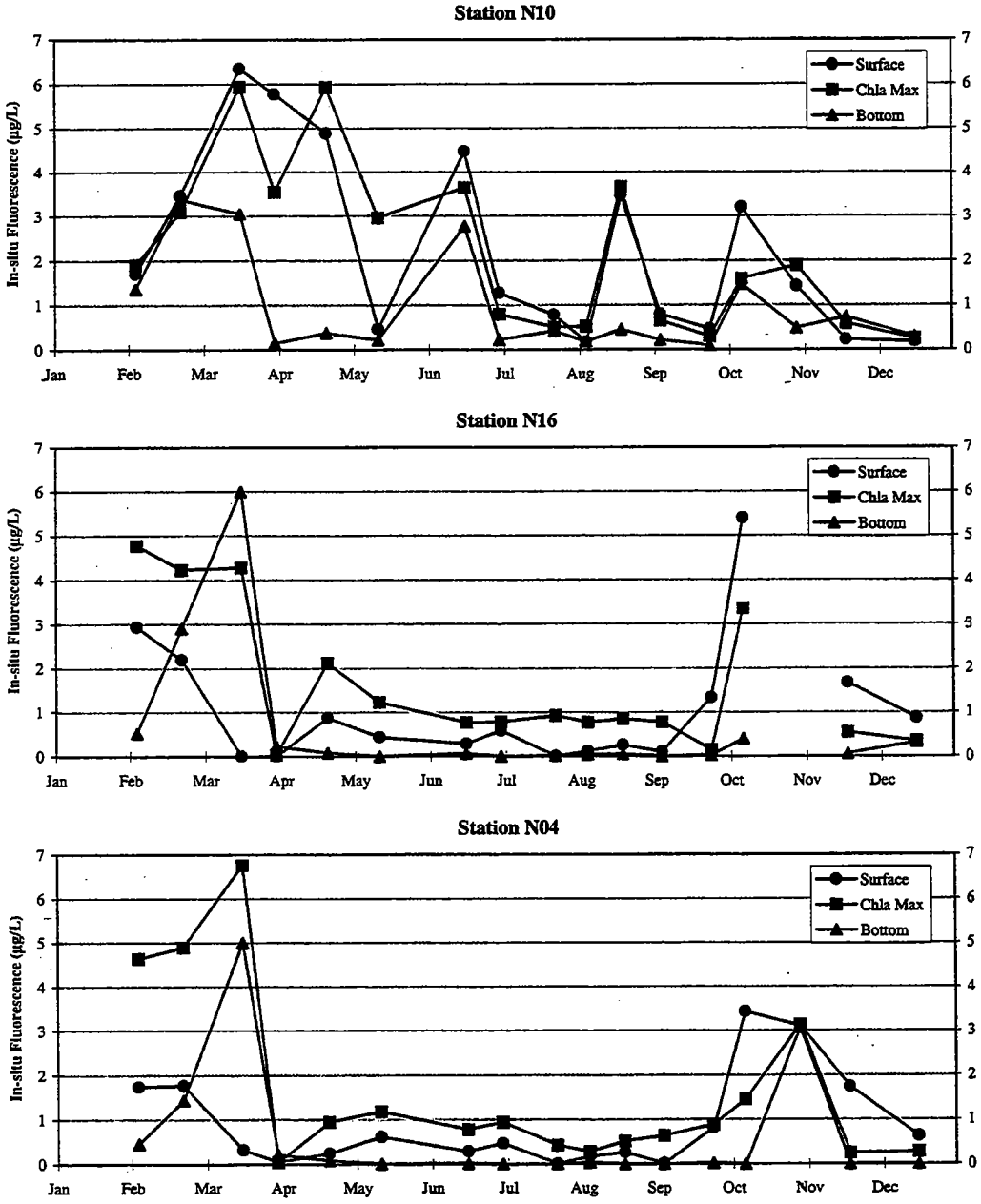

FIGURE 5-2a
1996 In-situ Chlorophyll Fluorescence in the Nearfield

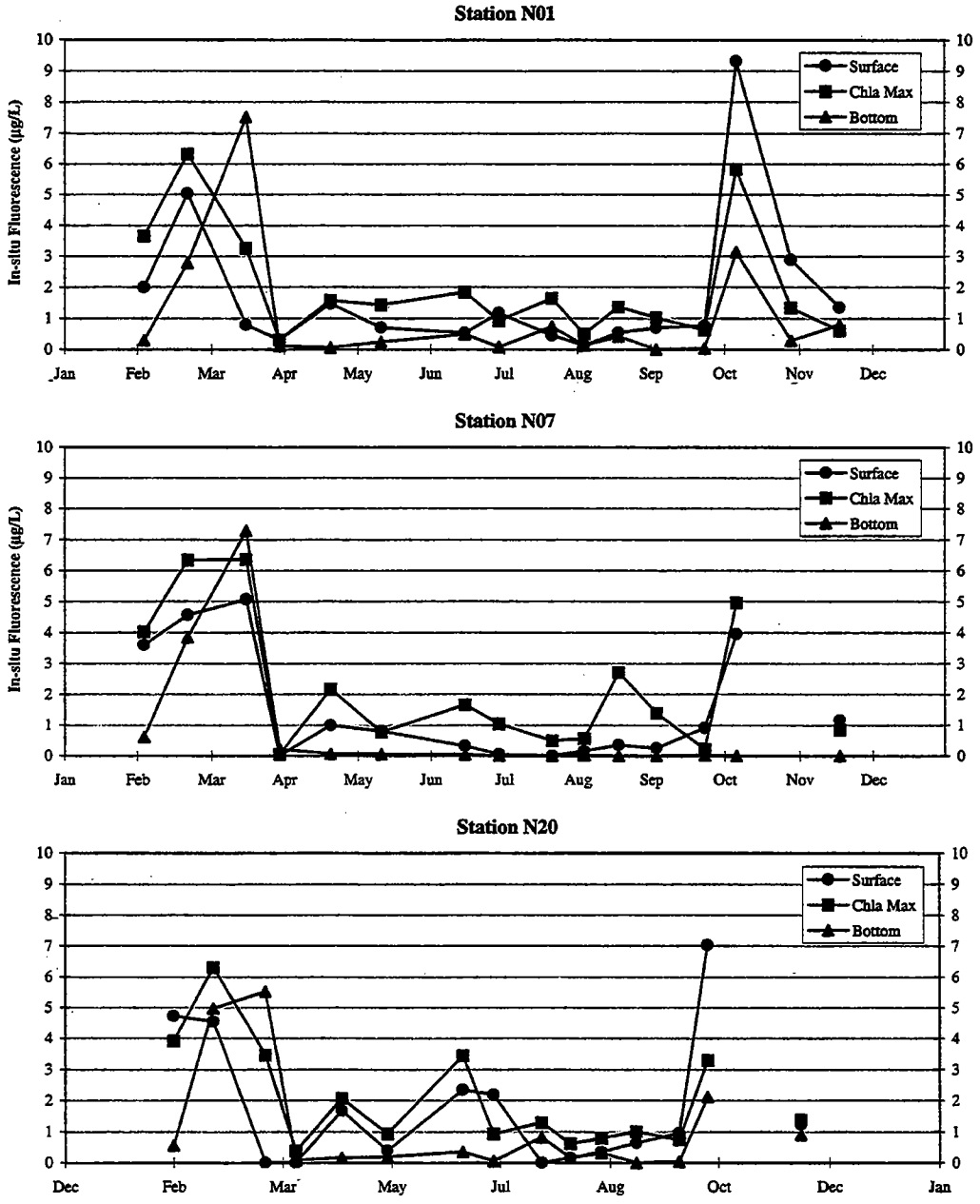

FIGURE 5-2b
1996 In-situ Chlorophyll Fluorescence in the Nearfield

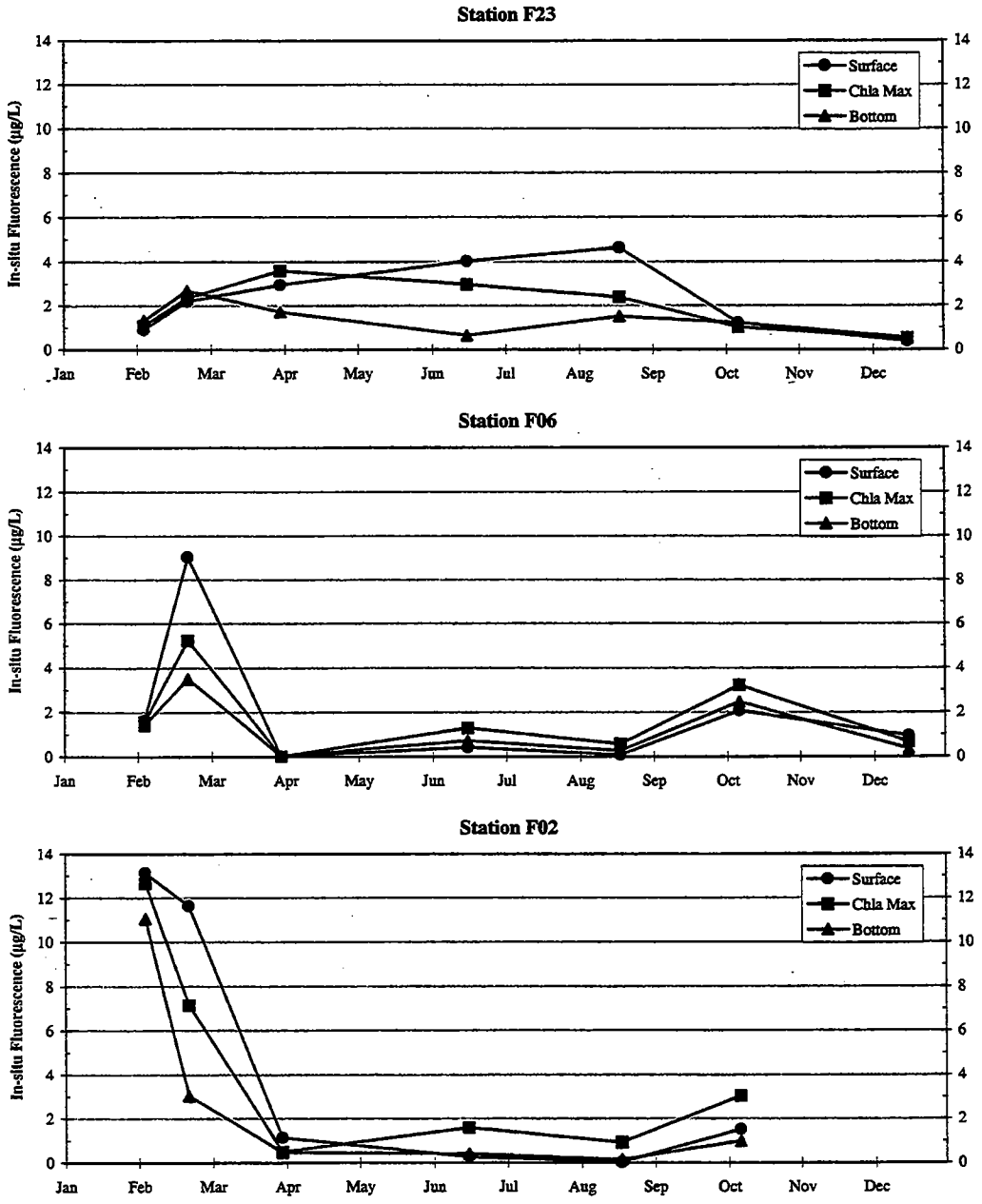

FIGURE 5-2c
1996 In-situ Chlorophyll Fluorescence in the Farfield

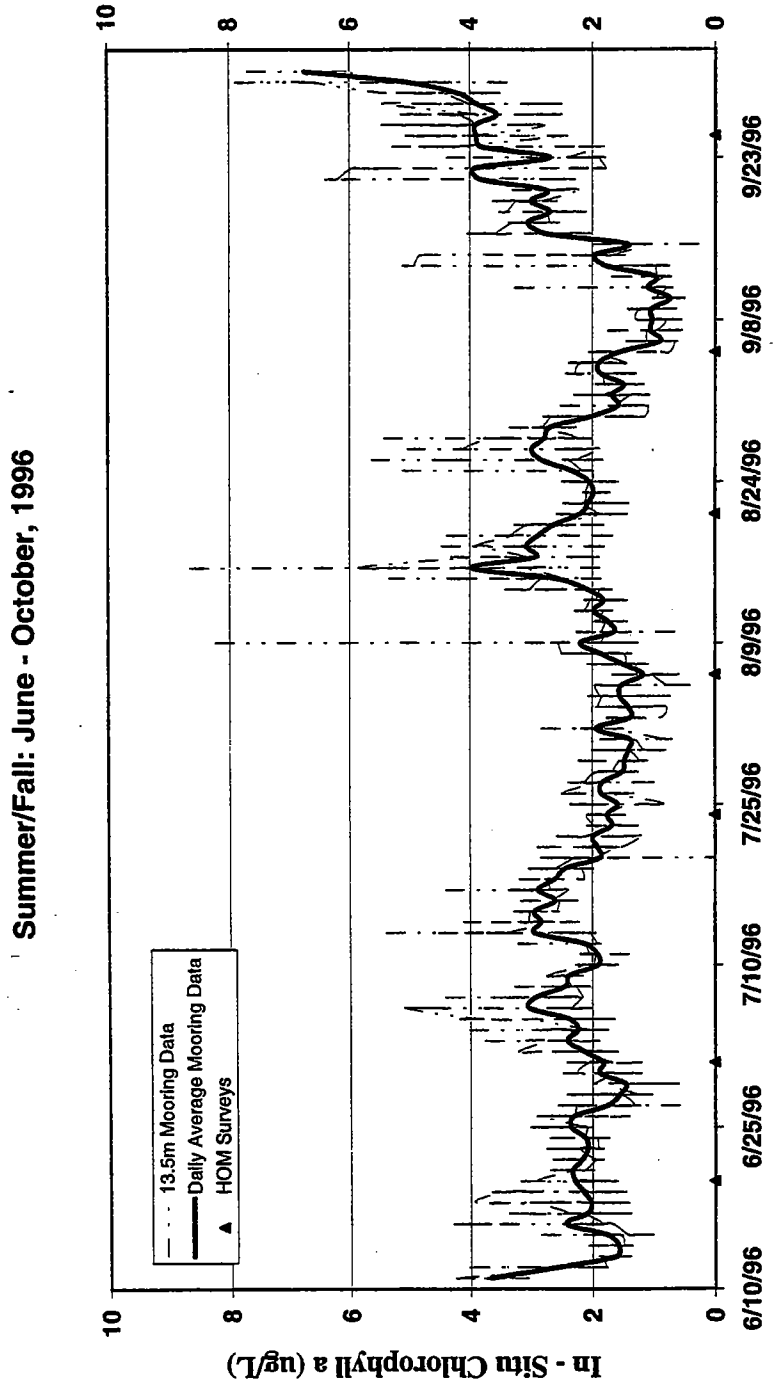

FIGURE 5-3
1996 Moored In-Situ Fluorometric Data
June 10, 1996 - October 1, 1996
Triangles on x-axis mark HOM survey dates

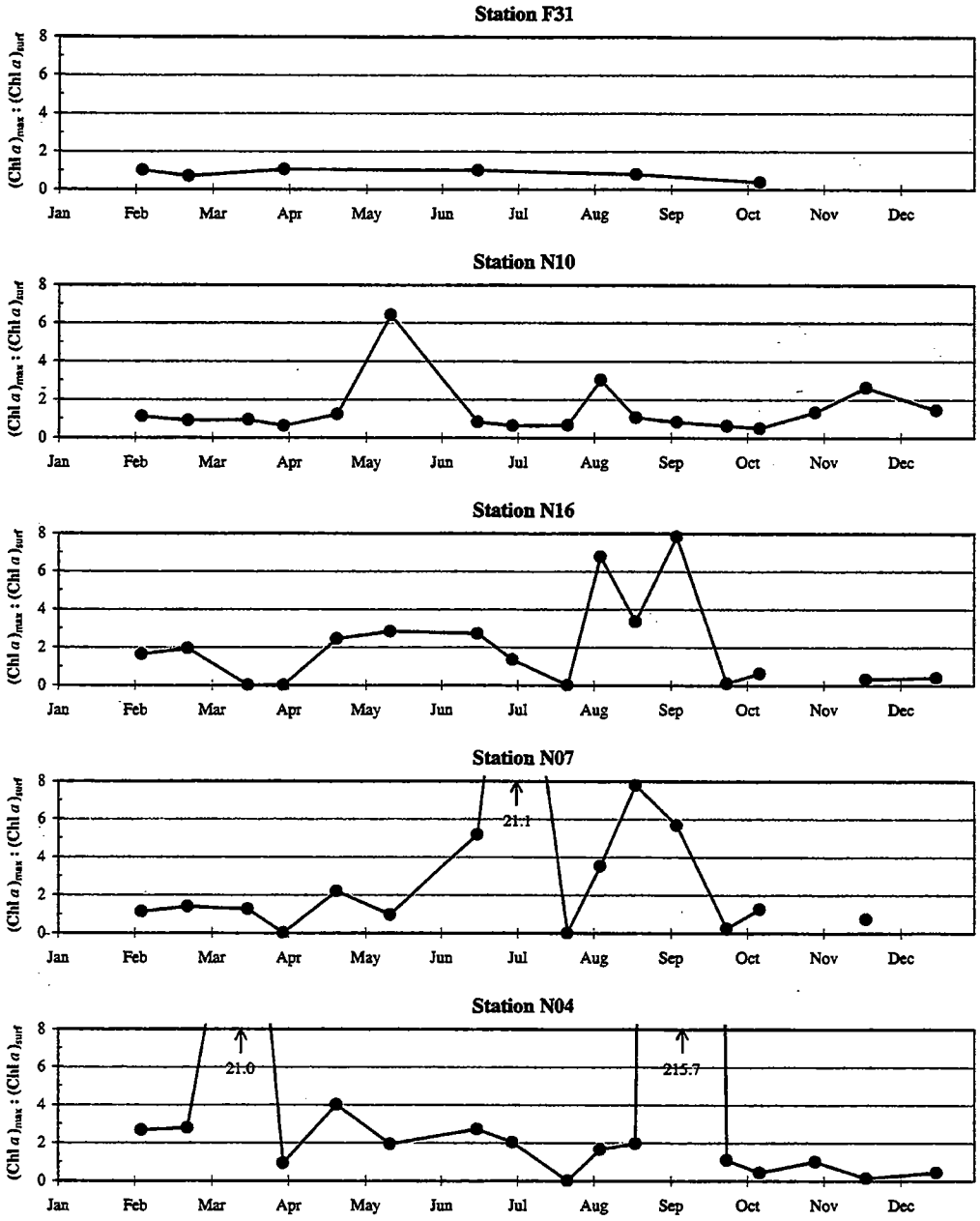

FIGURE 5-4
1996 Ratio of Chlorophyll Maximum : Surface Sample Concentrations
In-situ chlorophyll *a* results.

5-4flu.XLS

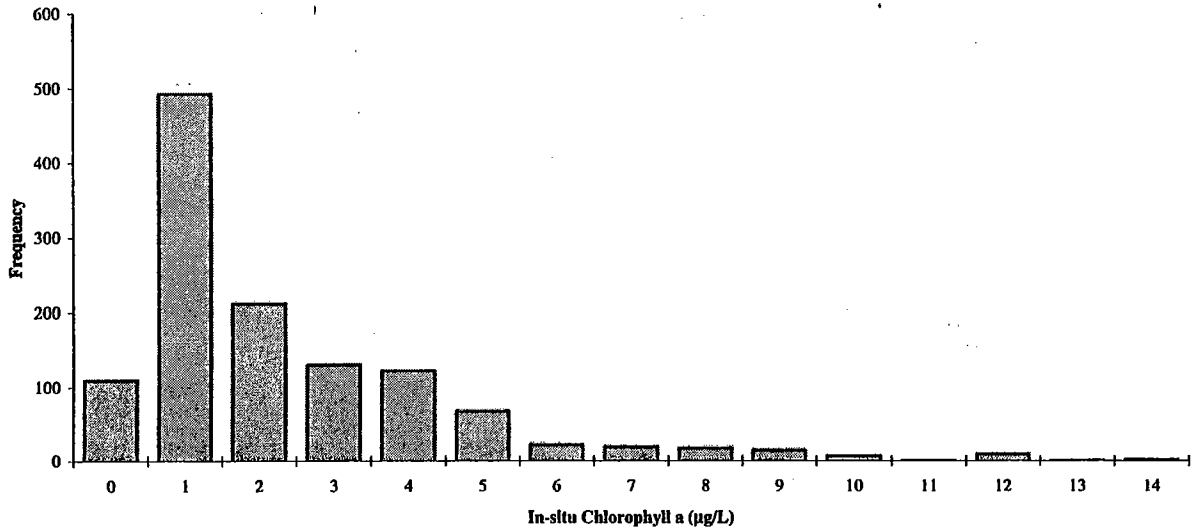

Boundary	30	61	25	12	13	6	0	4	1	0	2	0	1	0	0	155
Cape Cod Bay	1	42	13	8	7	3	0	0	2	4	2	0	5	1	2	90
Coastal	7	38	43	41	36	9	4	0	2	5	0	0	0	0	0	185
Harbor	0	7	16	20	7	10	1	2	3	1	0	1	3	0	0	71
Nearfield	24	255	73	27	44	28	10	10	5	1	2	0	0	0	0	479
Offshore	48	90	42	23	16	11	7	3	4	3	1	0	0	0	0	248
Total Number	110	493	212	131	123	67	22	19	17	14	7	1	9	1	2	1228
Percent	9.0%	40.1%	17.3%	10.7%	10.0%	5.5%	1.8%	1.5%	1.4%	1.1%	0.6%	0.1%	0.7%	0.1%	0.2%	100.0%
Cumulative Number	110	603	815	946	1069	1136	1158	1177	1194	1208	1215[1]	1216	1225	1226	1228	
Cumulative Percent	9.0%	49.1%	66.4%	77.0%	87.1%	92.5%	94.3%	95.8%	97.2%	98.4%	98.9%	99.0%	99.8%	99.8%	100.0%	

Note: Bin number denotes upper limit of bin.

Figure 5-5
Frequency Distribution of 1996 Massachusetts Bay In-situ Chlorophyll *a* Results
All depths, all FF and 6 NF stations, all combined surveys.

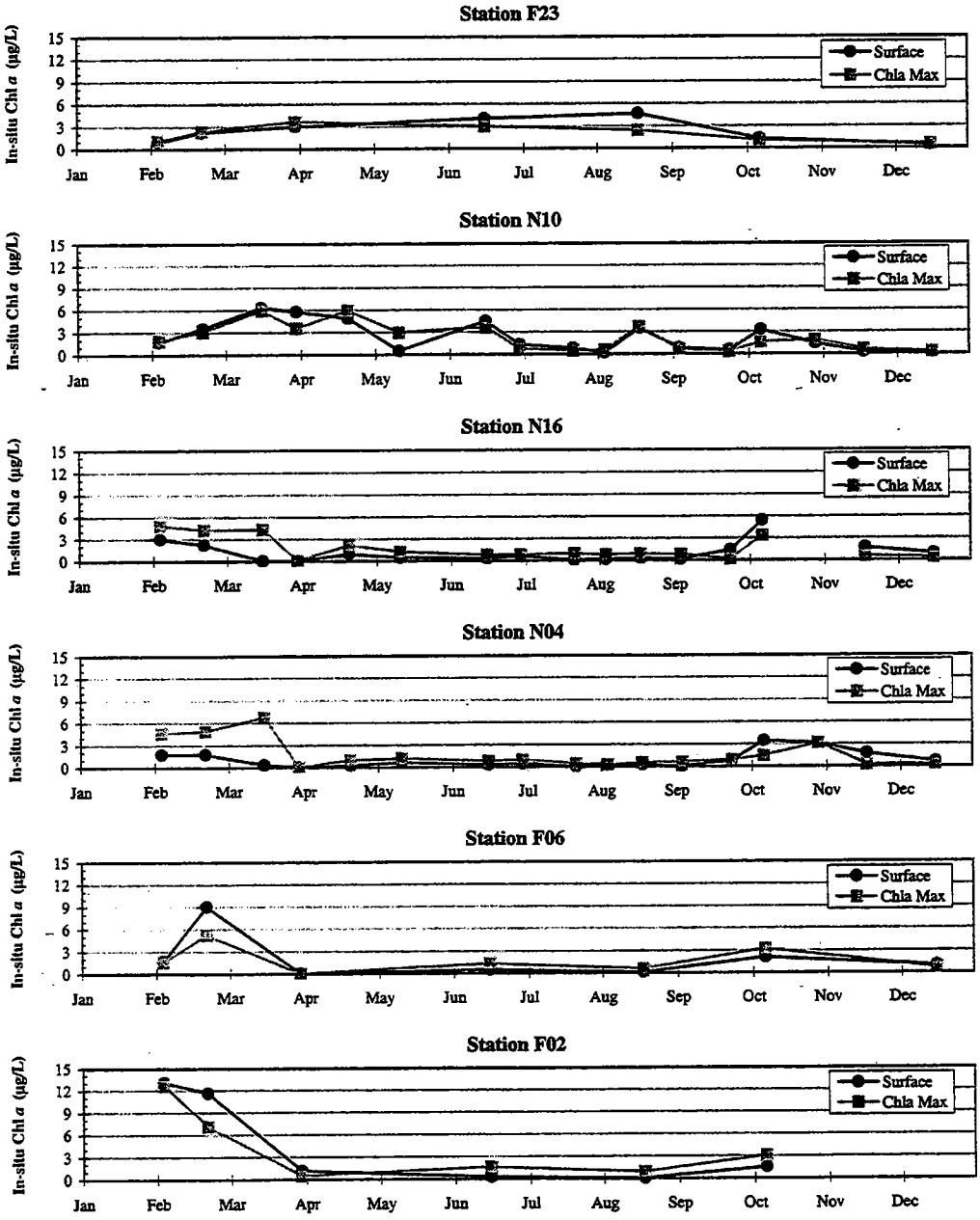

FIGURE 5-6
1996 In-situ Chlorophyll Fluorescence

5-abflu.xls

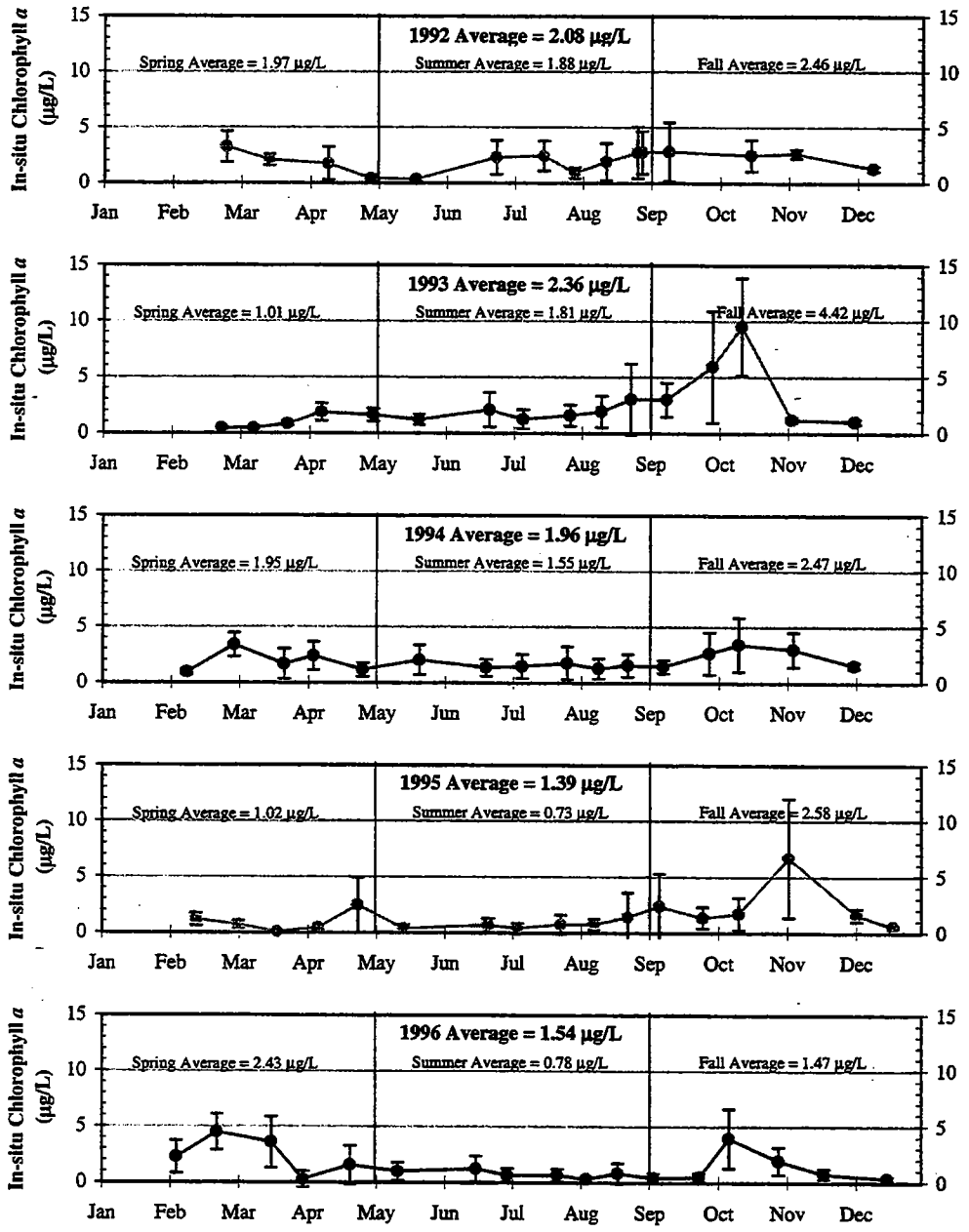

FIGURE 5-7
Nearfield: Interannual In-situ Chlorophyll *a* Survey Averages
All nearfield stations, all depths. 5-10flu.xls

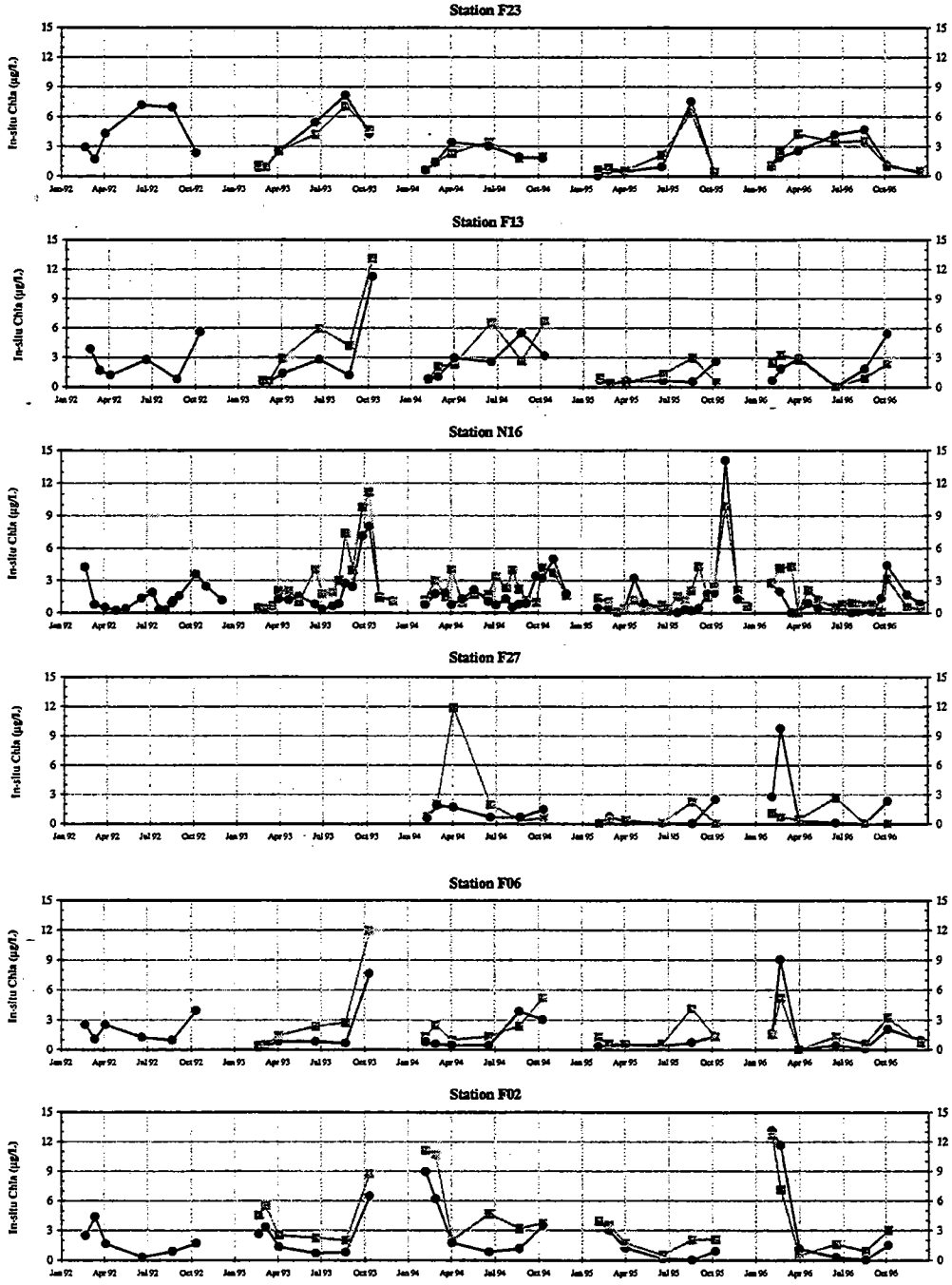

FIGURE 5-8
Interannual In-situ Chlorophyll *a* Fluorescence
Circles = Surface (A); Squares = Mid-Depth (C)

5-8lu.XLS

6.0 DISSOLVED OXYGEN

Dissolved oxygen (DO) concentrations in the water column and the sediments are important from both a regulatory and an ecological perspective. The Commonwealth of Massachusetts has established water quality standards for minimum water column DO concentrations. The state standard for Class SA water, which includes all of the study area outside of Boston Harbor, is 6 mg/L. From an ecological perspective, DO in the water column and sediments is of interest not only because it a requisite for the life of aquatic animals, but because it integrates the biological and physical processes which establish a system's habitat quality.

Accordingly, factors that create or increase the level of DO depletion play key roles in the diversity and productivity of the recipient water. These factors are both natural (stratification, primary production, water depth, temperature, etc.) and anthropogenic (wastewater discharges, cultural eutrophication). Fortunately, it is not the sporadic presence of depressed oxygen concentration but the severity, frequency and duration of low DO that affects aquatic health. The HOM program is designed to provide both adequate spatial and temporal coverage of water column DO throughout the year, and especially during the stratified interval. During stratification, the isolation of the bottom water from atmospheric exchange coupled with *in situ* respiration within both bottom water (Chapter 7.2) and sediments (Howes, 1997; 1998), results in oxygen depletion of the bottom water. This depletion is typically most strongly realized at depth in the water column. Increases in oxygen concentration in deeper water result primarily from periodic ventilation through storm-driven mixing, advection of oxygen rich bottom water (Cibik *et al.*, 1996), and destratification in the fall.

This section reports the results of MWRA's DO monitoring in Massachusetts and Cape Cod Bays. The focus is on the 1996 results and comparisons to the pattern and extent of DO depletion in the previous years of the HOM program. Since the observed DO depletion is fundamentally related to the stratified water column, the focus is on bottom water concentrations in the Nearfield and Stellwagen Basin. The data indicate that over the five years of monitoring, DO depletion and re-aeration in Massachusetts and Cape Cod Bays follows a predictable seasonal pattern that determines the timing, but not the magnitude of the annual DO minimum.

DO results presented in this section consist of calibrated upcast sensor data for the uppermost (surface) and lowest (bottom) sample depths. Downcast vertical profiles of DO and other parameters measured during the 1996 surveys have been reported earlier in periodic nutrient data reports. Additional information on sampling can be found in Section 2, and in the CW/QAPP (Bowen *et al.*, 1997).

6.1 Annual DO Cycle in Nearfield

6.1.1 1996 Results

DO concentration in coastal water is determined by the temperature (and salinity) during atmospheric exchange, inputs through photosynthesis, the level of respiratory uptake, and the time since onset of stratification. It is the interplay of these factors which established the typical seasonal cycle of DO depletion in Massachusetts and Cape Cod Bays and other temperate coastal water in 1996. The highest DO concentrations in the nearfield occurred during winter and early spring (Figure 6-1a), when the water column was well mixed, the water temperature was

at or near the annual minimum (Figure 3-2), and respiration in the water column was low (Section 7.2). DO concentrations peaked in mid-March in both the surface and bottom water, reaching 12.3 mg/L and 11.3 mg/L, respectively. During this time, DO averaged over the nearfield, expressed as a percentage of the saturation concentration, ranged from 91% to 112% (Figure 6-1b). Water column concentrations of DO steadily declined from this peak throughout the summer until the onset of the fall turnover in early October.

Surface and bottom water were frequently different in DO concentration throughout the annual period, with the exception of late spring through mid summer. During this stratified period, surface water was usually oversaturated with DO, although the concentrations were at or lower than those observed for the colder bottom water for this same period (Figure 6-1b). DO in the bottom water then continued to decline in the nearfield, reaching a minimum of 7.55 mg/L in late September, with 87% saturation (Figure 6-1). The minimum reading overall was at station F01 (5.5 mg/L during survey W9614; see Section 6.2.1). With the onset of the fall turnover (late September – early October, see Figure 3-11), the difference in surface and bottom water concentrations began to dissipate and overall concentrations rose. Surface water DO concentrations were at atmospheric equilibrium during the final three surveys of 1996 (Figure 6-1b). Bottom water DO concentrations increased during this period from 8.1 mg/L to 9.2 mg/L (Figure 6-1a).

At several times during 1996 it appeared that the bottom water in the nearfield region was ventilated through mixing with the oxygenated surface water or advection of oxygen-rich water. During late spring (April) and mid-summer (August), the water column DO concentrations remained relatively similar (Figure 6-1a). Small increases in DO concentration, which temporarily reversed the decline of bottom water DO, occurred during the stratified period (e.g., results from mid-June and early August, Figure 6-1a). As discussed in Section 3 and summarized in Table 9-1, these increases coincide with periods of advective transport into the nearfield. Mixing associated with the hurricanes in September may have infused some DO into the bottom water (note increase in saturation in Figure 6-1b). If not for these periodic mitigating events during the interval when bottom water oxygen uptake (water column + sediment respiration) is increasing (Section 7.2), the degree of annual DO depletion would be greater than observed. The prolonged mixing in the fall resulted in the ventilation of bottom water and ended the seasonal decline in bottom water DO during late September (Figure 3-2 and 6-1a).

6.1.2 Interannual Comparison of DO Concentrations

Each year in the baseline record showed similar trends in bottom water DO and timing of DO minima (Figure 6-2). Each year also showed some evidence of periodic increases in bottom water DO concentration during the stratified period. Compared to previous years, nearfield average DO concentrations in 1996 were most similar to 1993. DO concentrations for the first time since 1993 did not fall below 7.0 mg/L during the autumn most likely due to early mixing associated with the three major storms in September 1996. DO concentrations early in 1996 were approximately 0.5 - 1.0 mg/L higher than 1994 or 1995, and similar to the concentrations observed in 1992 and 1993 (Figure 6-2). Note that in 1992 and 1993 the average bottom water concentrations also did not fall below 7.0 mg/L. During the period of density stratification, the surface to bottom differences in DO concentrations were smaller in 1996 than observed for all previous years. Similar to 1993, the top-to-bottom difference in DO had not disappeared by mid-November in 1996.

6.1.3 Interannual Comparison of DO Decline

Declines in nearfield bottom water DO occurred during the summer and early fall in each of the five years of monitoring. The rate of the decline was relatively uniform during each year, ranging from a low of 0.024 mg/L/d in 1992 to a high of 0.031 mg/L/d in 1994 (Figure 6-3). The rates of decline were comparable in each of the five years of baseline monitoring (1992-1996). However, the higher DO concentrations (ca. 1 mg/L) at the onset of the annual decline in 1992 and 1993 appeared to result in proportionally higher minimum concentrations in those years. The DO depletion in 1996 was intermediate to 1992-1993 and 1994-1995, both in initial and final concentrations, and in the rate of decline. Similar relationships were seen in plots of percent saturation (Figure 6-4).

The data indicate that the phenomenon that causes the higher initial mass of oxygen at the onset of stratification does not result in higher rates of oxygen decline, but merely a shift in the final concentration of bottom water oxygen in the fall. While the underlying mechanism is not yet clear, it is likely to be physically, not biologically, linked as the observed temporal shifts in bottom water oxygen concentration can be very rapid and large (Fig 6-2).

6.2 Annual DO Cycle in Stellwagen Basin and Other Areas

6.2.1 1996 Results

DO dynamics in Stellwagen Basin and other parts of Massachusetts and Cape Cod Bays were generally similar to that observed in the nearfield region (Figure 6-5). The average DO concentration in the four Stellwagen Basin stations (F12, F17, F19, and F22) had a maximum value of 11.5 mg/L that occurred early in the year, before the water column became vertically stratified (Figure 6-5a). Although early February survey results indicated that DO concentrations at both the surface and the bottom were slightly undersaturated, oversaturated surface water and undersaturated bottom water occurred from mid-February through November. DO in the bottom water declined steadily through the summer and early fall, reaching a minimum concentration in Stellwagen of 7.7 mg/L (83% saturation) during mid-October (Figure 6-5b). As with the nearfield region, by late November the surface to bottom difference in the mean Stellwagen Basin DO concentration began to disappear. The water column was undersaturated with DO at this time.

Individual measurements of bottom DO concentration within regions often showed a great deal of variability. For example, the minimum bottom water DO for 1996 was 5.5 mg/L, reported during mid-October (W9614) at station F01 in western Cape Cod Bay (Table 6-1). The average bottom water concentration for the Cape Cod Bay region during this survey was 7.9 mg/L (Figure 6-6). More frequent sampling in the nearfield produced lower individual results during W9614, yet the average bottom water result was lower during W9613 (refer to Figure 6-1).

The regions differed slightly in the annual pattern of DO concentration. Maximum bottom water DO concentrations were observed during mid-February for the Boundary, Coastal, Cape Cod Bay and the Offshore regions, ranging from 10.4 to 11.3 mg/L (Figure 6-7). The maximum regional mean bottom water DO

concentration was in the Harbor (11.4mg/L), but this was not observed until early April. Regional differences were also evident in oxygen minima. The minimum observed Coastal region concentration of 8.1 mg/L (88% of saturation) occurred during the mid-August survey (Figure 6-6). DO concentrations reached minimum levels in the offshore and boundary regions in October, and ranged from 7.7 to 7.9 mg/L (Figure 6-6).

6.2.2 Interannual Comparisons

In all five years of sampling, the minimum dissolved oxygen concentration in the bottom water occurred in early October (Figure 6-7). For the five years of sampling, the annual minimum concentration, and the station where the minimum concentration was measured, was as follows:

- 1992 - DO minimum = 7.10 mg/L at nearfield station N10,
- 1993 - DO minimum = 6.68 mg/L at Cape Cod Bay station F02,
- 1994 - DO minimum = 4.82 mg/L at nearfield station N01,
- 1995 - DO minimum = 5.60 mg/L at Cape Cod Bay station F02.
- 1996 - DO minimum = 5.48 mg/L at Cape Cod Bay station F01.

Both nearfield stations N01 and N10 are on the western boundary of the sampling grid, nearest to Boston Harbor and the coastline. Cape Cod Bay station F02 is in eastern half of the Bay, and F01 is in the western half of the bay. The range of bottom water DO concentrations during a survey has been fairly constant over the five years. The range has been occasionally over 3 mg/L, but is generally around 2 mg/L (Figure 6-7).

DO dynamics in Stellwagen Basin appear to be similar over the five years of monitoring. The mean DO concentration of the four stations achieved a maximum in late winter/early spring and declined to a minimum concentration in early October (Figure 6-8). The Stellwagen Basin mean bottom water maximum concentration was approximately 1 mg/L higher in 1992, 1993, and 1996 compared with 1994 and 1995. The mean bottom water DO concentration in Stellwagen Basin stations during the mid-October survey for 1996 was approximately 7.5 mg/L (Figure 6-9).

6.2.3 DO Decline in the Bottom Water of Stellwagen Basin

Oxygen levels within the bottom water of Stellwagen Basin showed a pattern of decline similar to those of the nearfield throughout summer and early fall. Oxygen dynamics within the two systems appear to be responding to similar physical and biological forcing parameters, as the interannual pattern of their oxygen minima show a clear direct relationship (Figure 6-10). The lowest average DO levels in both systems were measured in 1994. However, the extent of the DO decline was generally slightly greater in the more inshore nearfield region of Massachusetts Bay than within the Basin (Figure 6-10). The similarity in DO minima indicates that the effects of a longer interval of bottom water stratification in Stellwagen Basin (due to its greater depth) is offset by the higher rates of oxygen consumption and warmer bottom water temperatures in the nearfield region (Figure 3-4).

The effect of the deeper water on the carbon dynamics of the system can be seen in the lower rates of oxygen decline in the deeper water of the Basins versus the nearfield (1992-1996 average 0.20 versus 0.26 mg/L/day, respectively). The lower rate of decline in the Basin does not manifest itself in less DO depletion as the initial DO concentration is generally lower in the Basin than in the nearfield (lower initial concentration + lower uptake = higher initial concentration + higher uptake; Figures 6-3 & 6-9). In 1996, the rate of DO decline calculated from the bottom water DO timecourse was 0.014 and 0.025 mg/L/d, with parallel values for initial DO concentrations in mid-June of ca. 9.2 mg/L and 9.9 mg/L in the Basin and nearfield, respectively. The result was similar DO minima for the nearfield (7.55 mg/L) and Basin (7.70 mg/L).

Given interest in the bottom water DO minimum in Stellwagen Basin and the limited sampling frequency compared to the Nearfield program, we undertook an additional evaluation based upon integration of all available data collected in 1995 and 1996. This analysis was undertaken, in part, to address concerns that insufficient data were available for the estimation of annual rates of DO decline from the time-course of DO concentration (Figure 6-10). Bottom water DO data from both the water column surveys and the benthic flux program were combined for evaluation. In both 1995 (Figure 6-11) and 1996 (Figure 6-12), the data from each program combine to give a more complete indication of the annual oxygen decline during stratification. Linear regression of these data can be compared to the analysis from the water column sampling data alone (Figure 6-10). It appears that the complete data set yields comparable, though slightly lower rates of decline, compared to the standard analysis (1995: 0.015 vs 0.017 mg/L/d; 1996: 0.012 vs 0.014 mg/L/d). These data support the interannual analysis of Stellwagen Basin DO decline (Cibik *et al.* 1996; Figure 6-13). However, this analysis does not address problems with capturing the DO minimum in the Basin, which occurs later than in the Nearfield, due to its much deeper water depth..

6.3 Discussion

The pattern of DO decline appears to be similar throughout the near and offshore regions covered by the HOM Program. Areas of particular interest, the nearfield region and Stellwagen Basin, have well-correlated annual DO minima. In fact, 1996 annual DO minima were similar region-wide, suggesting common physical and biological processes are controlling DO levels.

Physical factors controlling the extent of the DO depletion are the DO concentration of the bottom water at the onset of stratification, the duration of stratification, and the occurrence of short-term ventilation events. This latter feature was particularly important during the 1996 field season with the onset of Hurricanes Eduardo and Fran, followed by a subsequent northeaster, all during September. This mixing was complemented by what appeared to be an inflow of oxygen rich bottom water between the May and June surveys, and again in early August (Figure 6-1). The progressive vector plots for currents indicate continuing bottom water flow from northeast to southwest through the nearfield during this period (Table 3-1, Appendix A). The effects of the September storms on bottom water DO is more subtle. While the storms clearly caused substantial mixing well into the water column (see Figure 3-2), the effect at the bottom was only to slow the rate of the observed decline through partial reaeration in both the nearfield and Basin. However, the result was a much higher final DO concentration than if the trajectory of DO decline had continued unimpeded until the traditional fall overturn in early October.

Similarities can be seen between the interannual DO concentrations (Figure 6-7) and temperature and salinity profiles (Figures 3-4, 3-9). In 1992, 1993, and 1996 there were two apparent upwelling events between June and August. These physical perturbations coincide with DO increases or decreases in the DO decline rate in the bottom water. Smaller, but similar, events also occurred in 1994 and 1995. The event in 1995 likely prevented the DO levels from reaching the 1994 minimum.

The rates of DO decline have been relatively similar from year to year in both the nearfield (Figure 6-3) and Stellwagen Basin (Figure 6-9). This is consistent with a relatively constant organic matter delivery to the sediments and bottom water during this interval. This is partly the result of the "removal" of the labile organic matter by respiratory consumption as it falls through the water column and that *in situ* production (although variable) is the primary source of organic matter to the system over this interval, and it has been "relatively" constant.

These conditions, coupled with the DO levels at the onset of stratification, can be used to estimate "final" DO concentrations. In its simplest form it is possible to relate DO levels at stratification to DO minima (Figure 6-13). The relationship is consistent with the relative interannual constancy of sub-pycnocline oxygen consumption and the interannual similarity in the timing of the initiation and duration of stratification. It should be noted that in this analysis, the physical events affecting DO in 1996, most likely the storm-related September ventilation, resulted in a much smaller DO decline than would have been expected from the DO level at the onset of stratification. These data indicate that when estimating potential DO minima, one must add to considerations of initial DO concentration at setup, duration of stratification, and sub-pycnocline oxygen uptake, the potential for a year without periodic vertical (mixing or downwelling) or horizontal (deep water oxygen incursions) ventilation events.

Event ID	Survey Minima		Survey Maxima	
	Value (mg/l)	Location	Value (mg/l)	Location
W9601	9.62	F27	11.60	F02
W9602	10.01	F27	11.55	F01
W9603	10.42	N15	11.97	N11
W9604	9.34	N06	12.01	F31
W9605	9.85	N13	10.12	N18
W9606	9.38	N10	9.89	N01
W9607	8.27	F02	10.71	N10
W9608	8.82	N05	10.24	N21
W9609	8.38	N10	9.73	N12
W9610	8.41	N04	9.26	N19
W9611	7.25	F02	9.24	F03
W9612	7.38	N16	8.60	N12
W9613	7.29	N16	7.82	N04
W9614	5.48	F01	8.67	N01
W9615	7.92	N10	8.41	N18
W9616	7.59	N07	9.54	N01
W9617	7.44	F23	9.94	F05

Table 6-1
Magnitude and Location of DO Maxima and Minima in the Bottom Waters

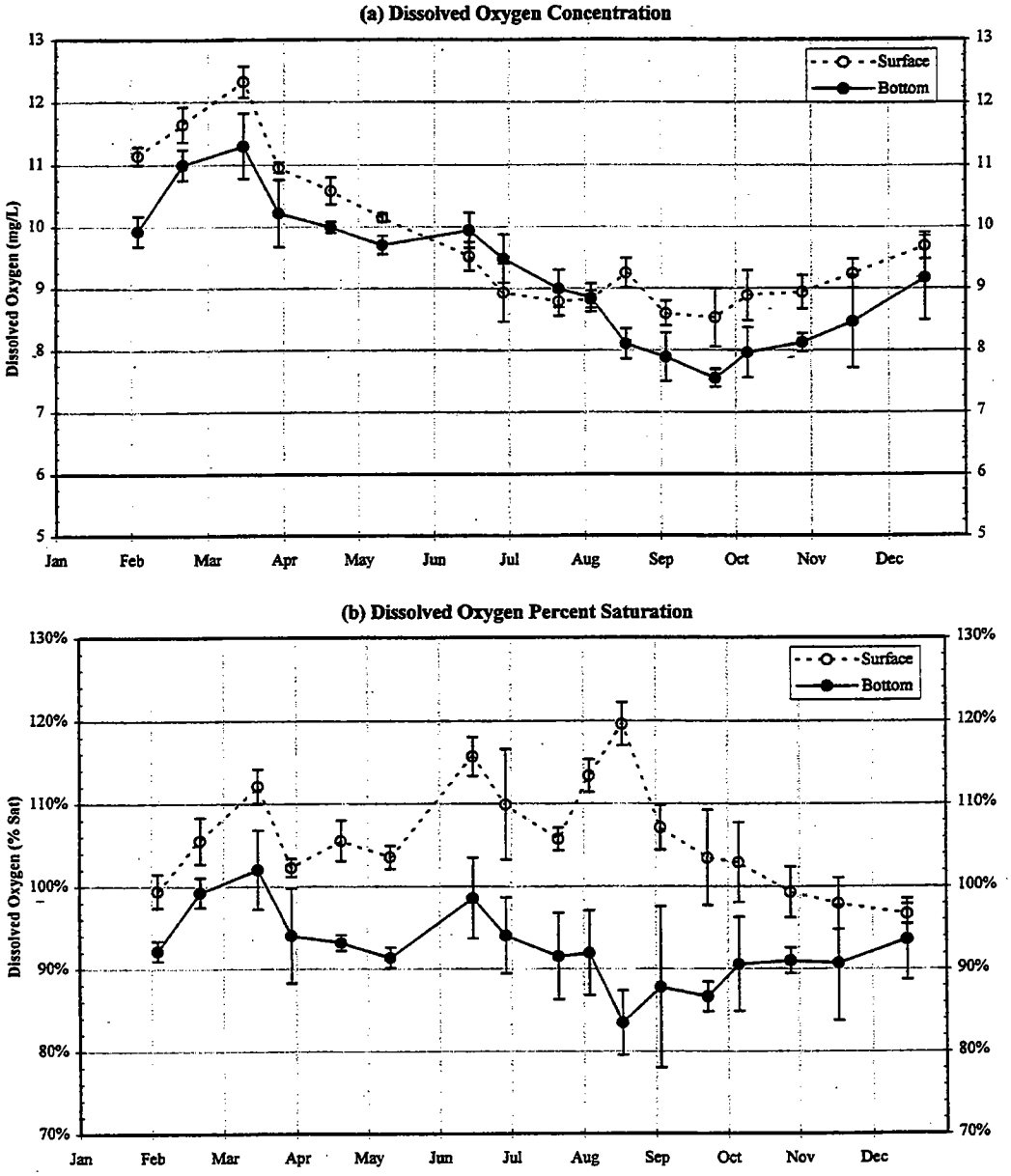

FIGURE 6-1

1996 Nearfield Dissolved Oxygen in Surface and Bottom Waters

Symbols indicate the mean of 17 nearfield stations; error bars represent +/- one standard deviation. 6-1DO.XLS

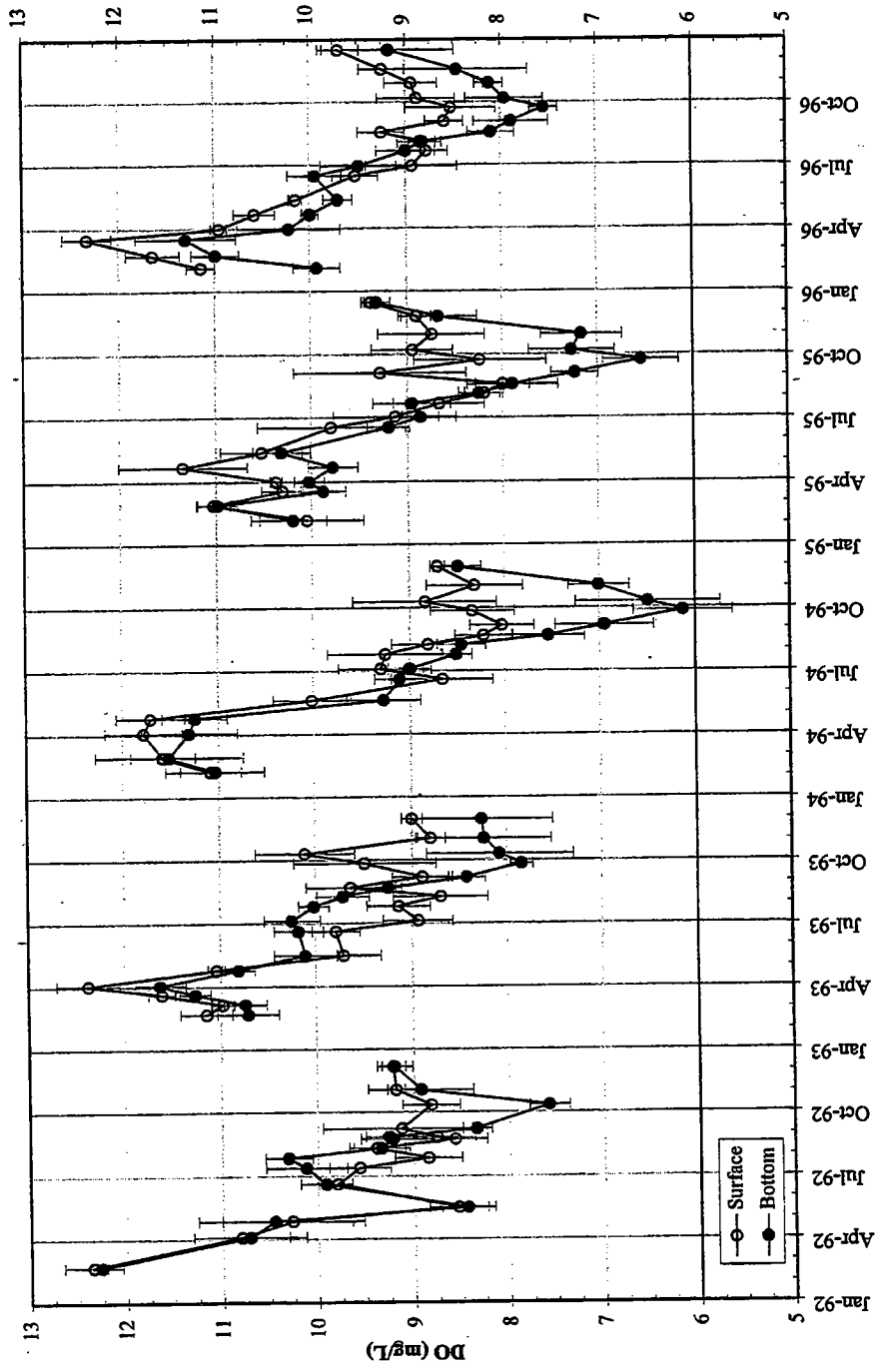

6-2DO.XLS

FIGURE 6-2
Interannual Nearfield Dissolved Oxygen Cycle in Surface and Bottom Waters
Symbols indicate the mean of 17 nearfield stations; error bars represent +/- one standard deviation.

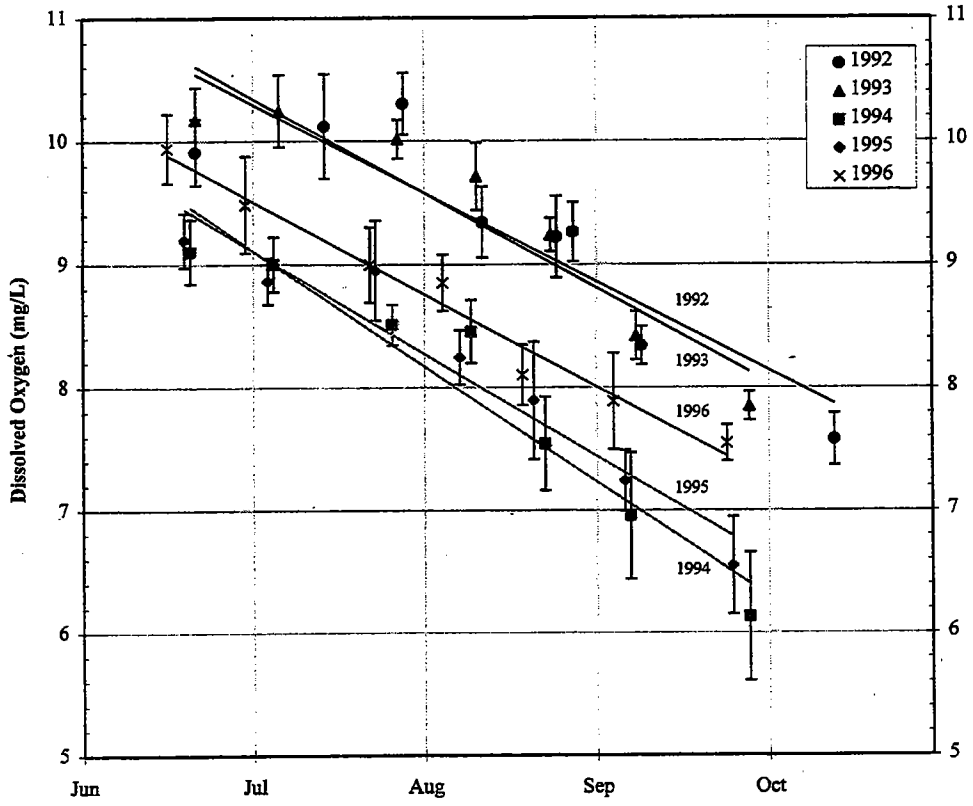

Year	Slope (mg/L/day)	Intercept* (mg/L)	R^2
1992	-0.024	11.0	0.808
1993	-0.025	11.1	0.885
1994	-0.031	10.1	0.929
1995	-0.027	9.9	0.932
1996	-0.025	10.3	0.978

* Predicted DO on June 1st based on:
DO = Slope * Date + Intercept

FIGURE 6-3
Nearfield Dissolved Oxygen Concentrations in Bottom Waters
Symbols indicate the mean of 17 nearfield stations; error bars represent +/- one standard deviation. 6-3DO.XLS

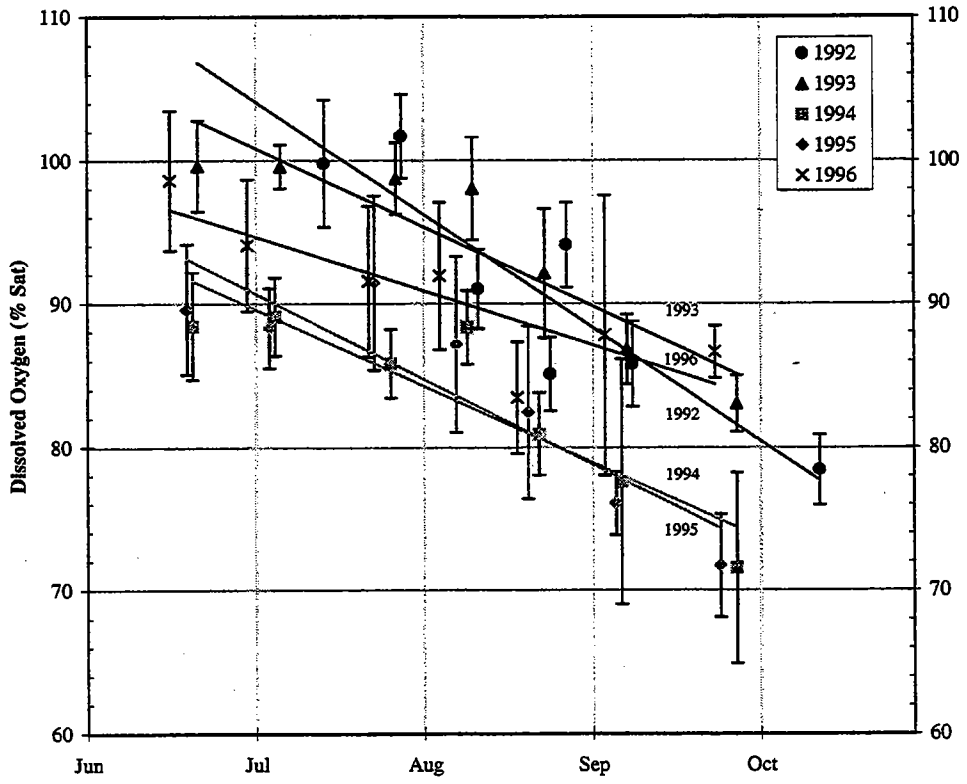

Year	Slope (%/day)	Intercept* (% Sat)	R^2
1992	-0.258	112.0	0.818
1993	-0.181	106.4	0.845
1994	-0.174	94.9	0.821
1995	-0.194	96.6	0.805
1996	-0.123	98.5	0.729

* Predicted DO on June 1st based on:
DO = Slope * Date + Intercept

FIGURE 6-4
Nearfield Dissolved Oxygen Percent Saturation in Bottom Waters
Symbols indicate the mean of 17 nearfield stations; error bars represent +/- one standard deviation.

6-4do.xls

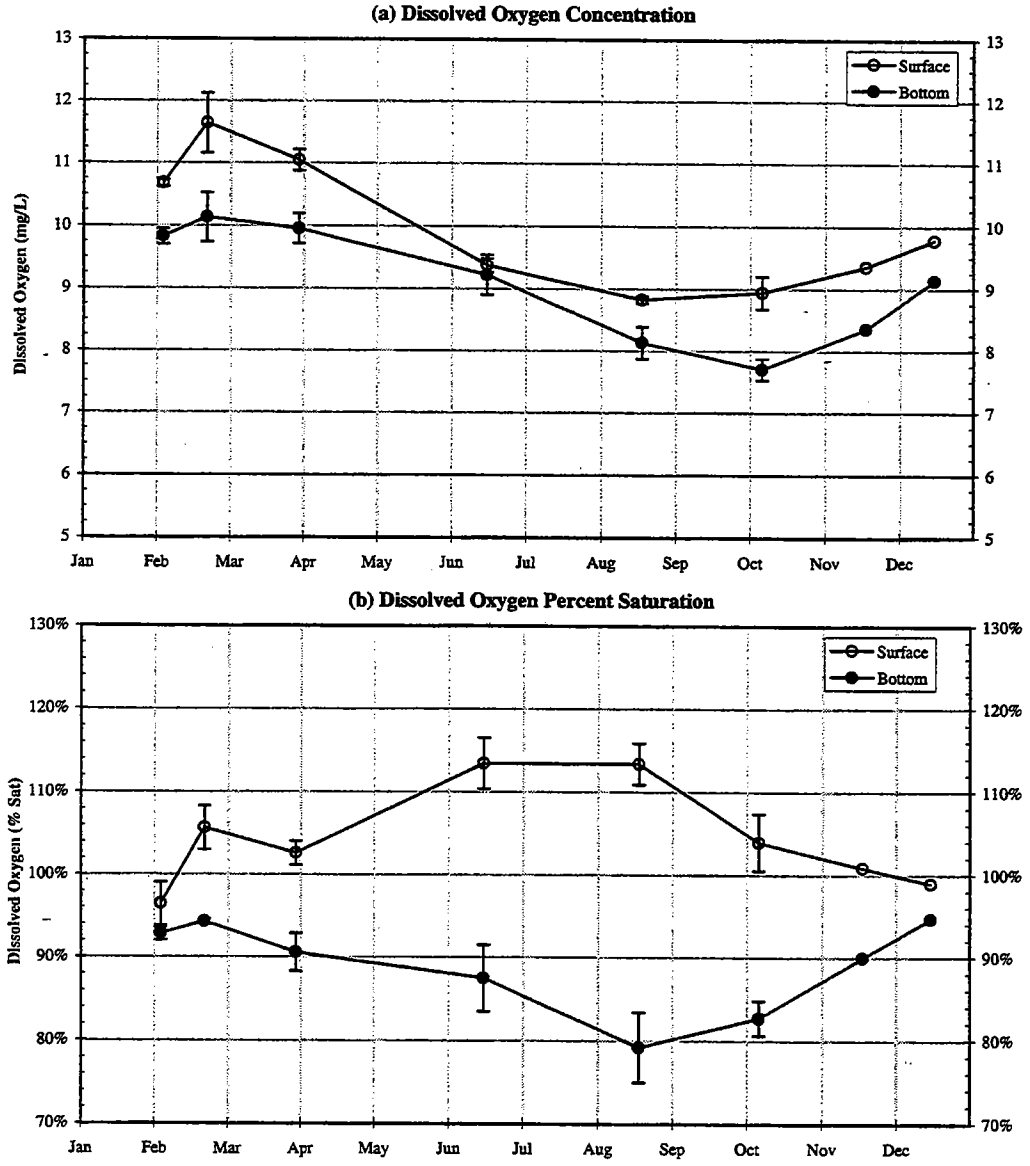

FIGURE 6-5

1996 Stellwagen Basin Dissolved Oxygen in Surface and Bottom Waters

Symbols indicate the mean of 4 Stellwagen Basin stations; error bars represent +/- one standard deviation. 6-5do.xls

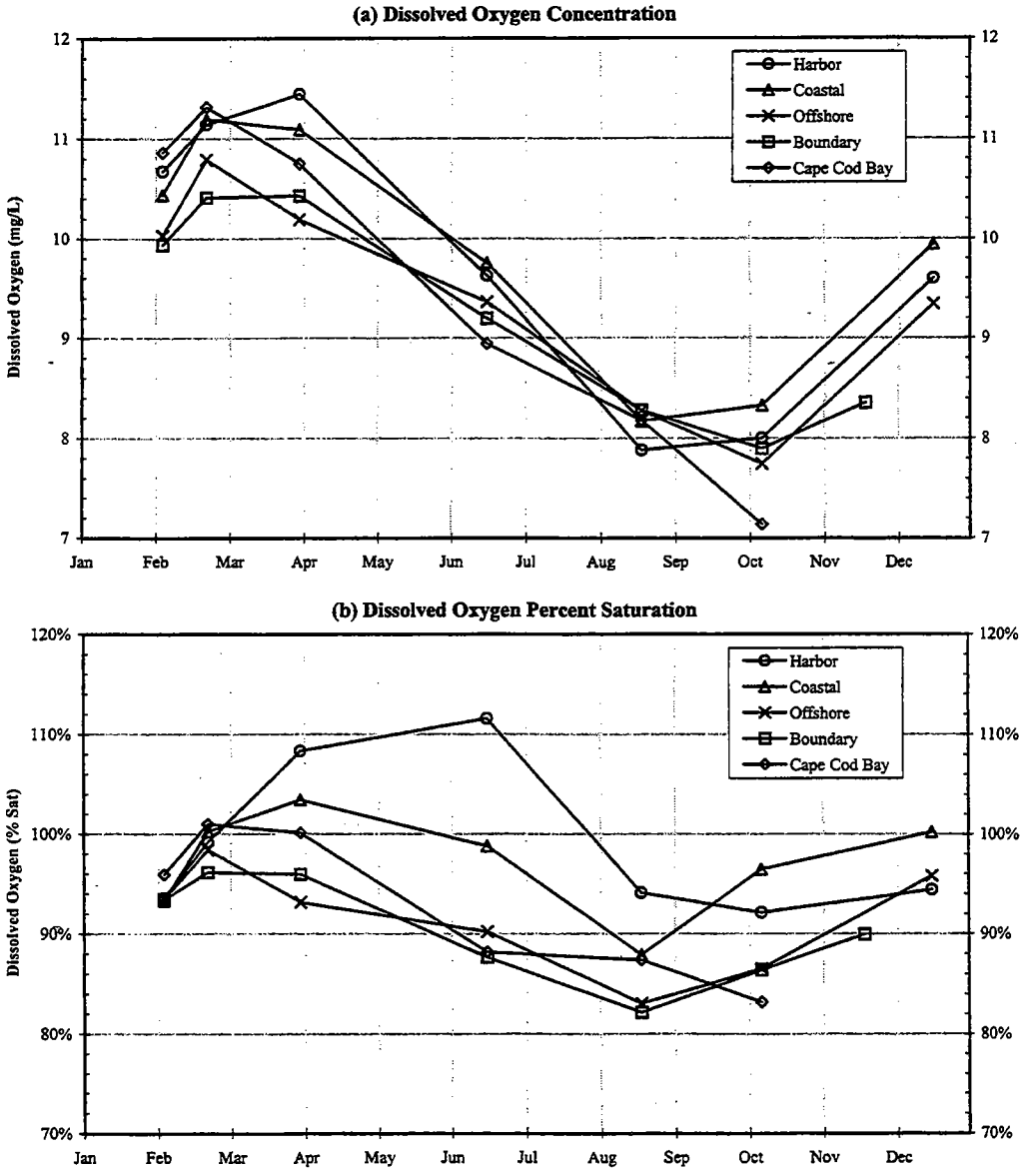

FIGURE 6-6

1996 Spatially Averaged Dissolved Oxygen in the Bottom Waters of Massachusetts and Cape Cod Bays

Symbols represent the average of all stations within each region.

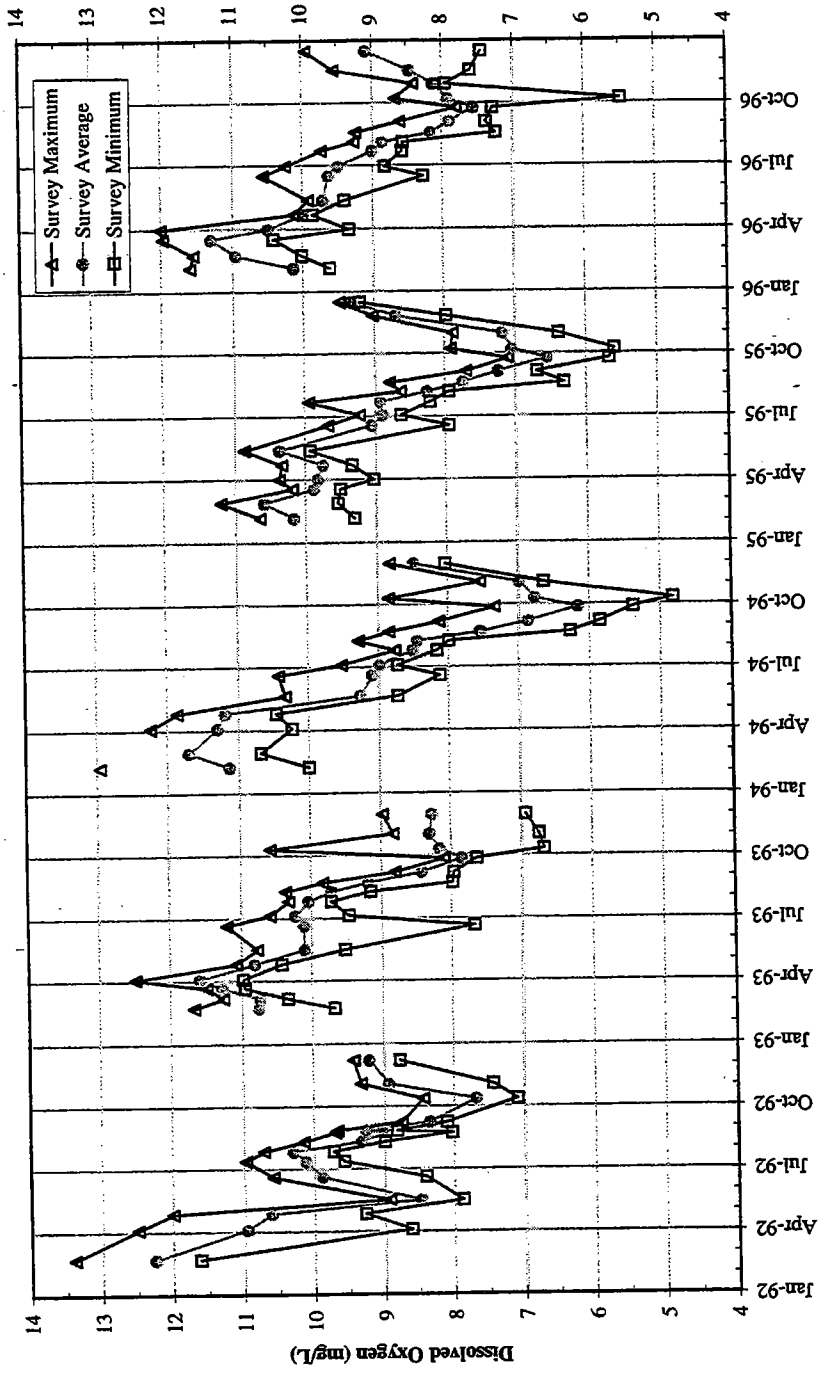

FIGURE 6-7

Interannual Dissolved Oxygen Cycle in Bottom Waters

All nearfield and farfield stations. Symbols indicate maximum, average and minimum value for each survey.

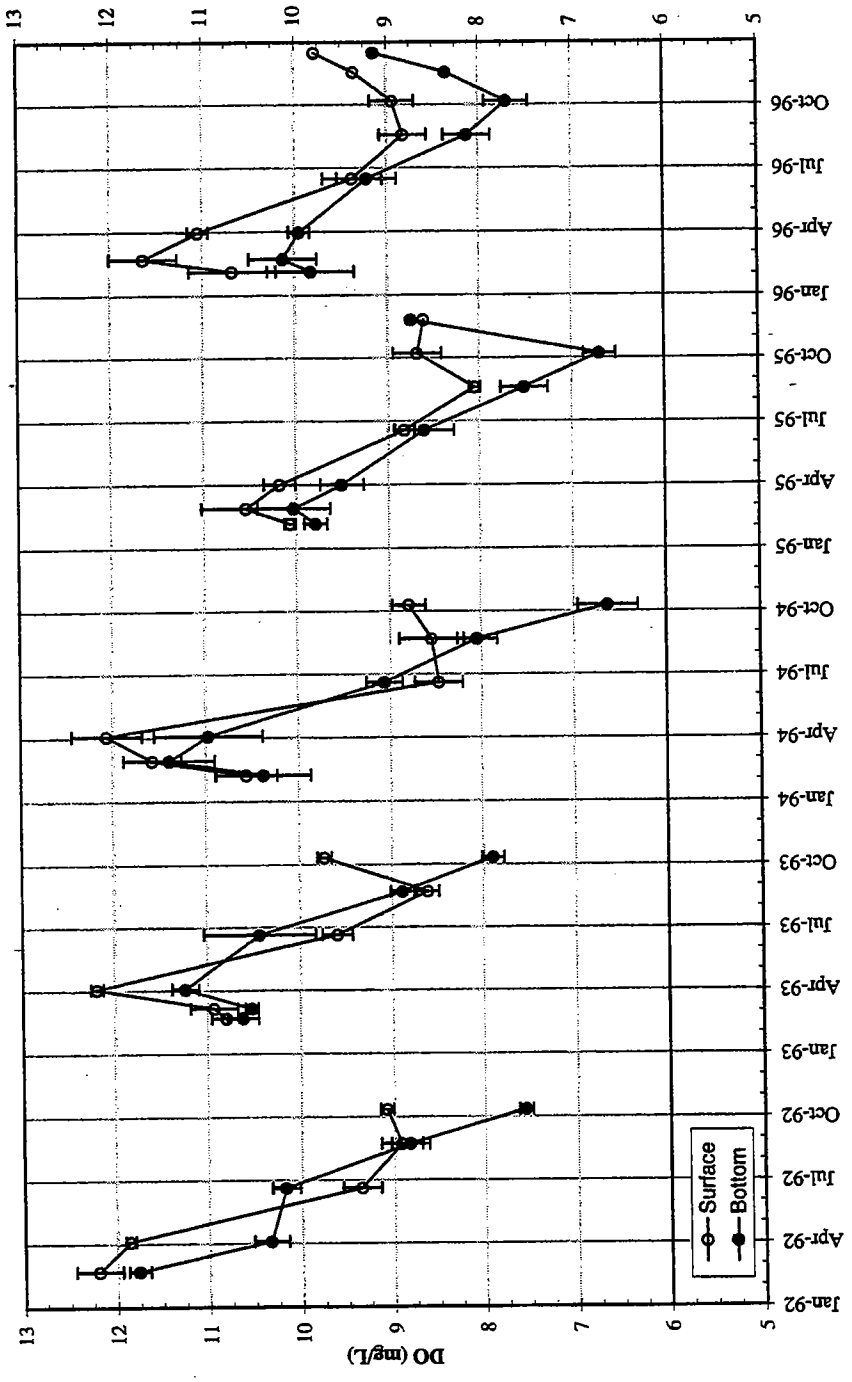

FIGURE 6-8
Interannual Stellwagen Basin Dissolved Oxygen Cycle in Surface and Bottom Waters
Symbols indicate the mean of 4 Stellwagen stations; error bars represent +/- one standard deviation.

6-8do.xls

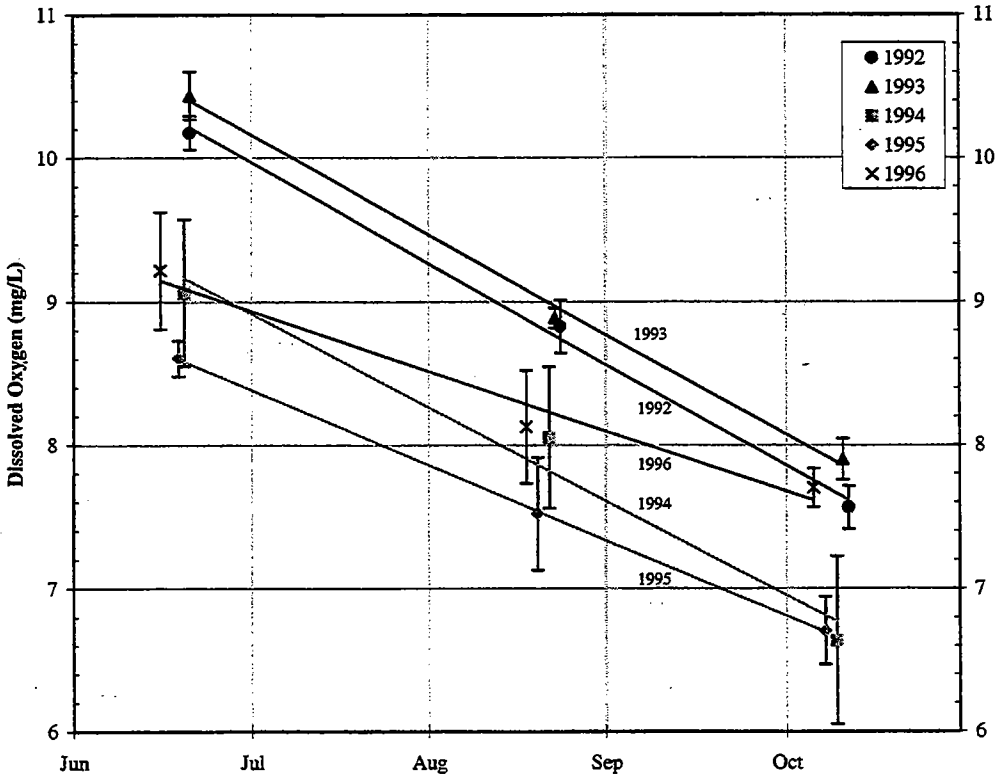

Year	Slope (mg/L/day)	Intercept* (mg/L)
1992	-0.023	10.7
1993	-0.023	10.9
1994	-0.021	9.6
1995	-0.017	8.9
1996	-0.014	9.4
* Predicted DO on June 1st based on: DO = Slope * Date + Intercept		

FIGURE 6-9

Stellwagen Basin Dissolved Oxygen Concentrations in Bottom Waters

Symbols indicate the mean of 4 Stellwagen stations; error bars represent +/- one standard deviation.

6-9do.xls

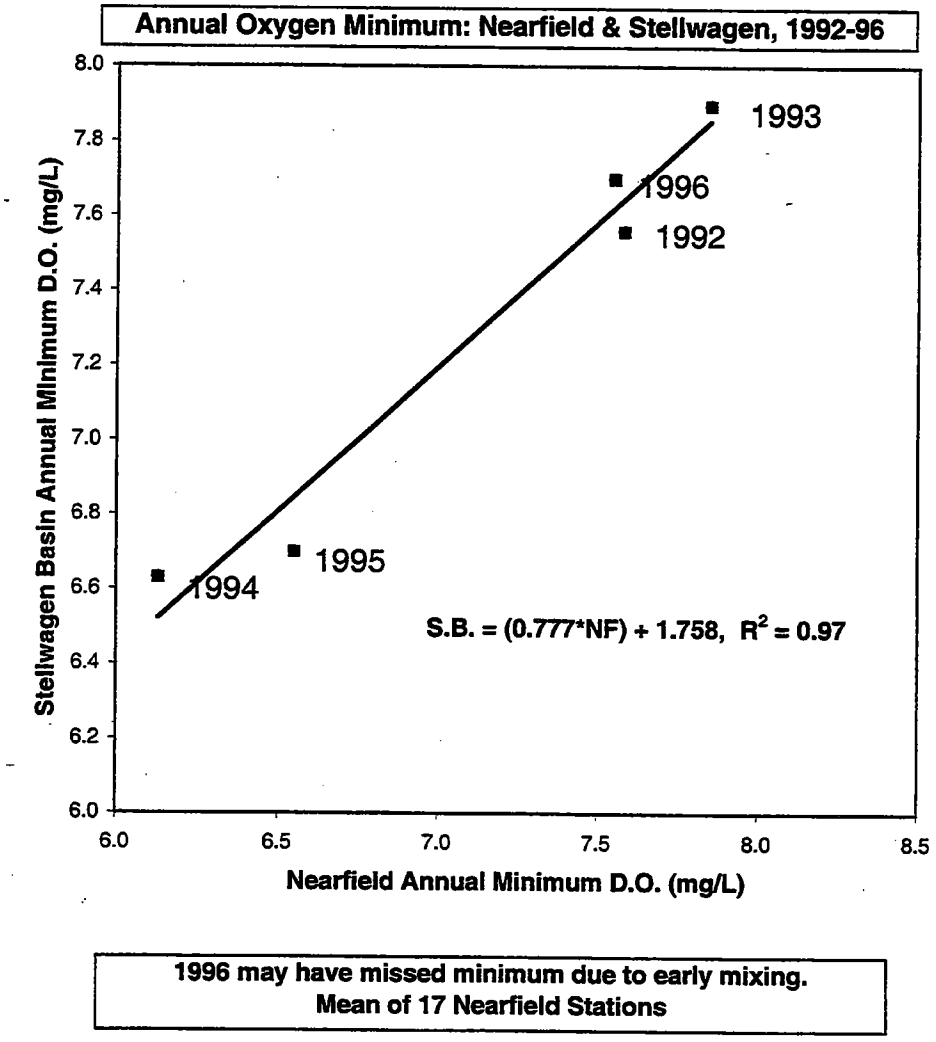

Figure 6-10
Comparison of annual average bottom water D.O. minima in the Nearfield and Stellwagen Basin, 1992-1996.

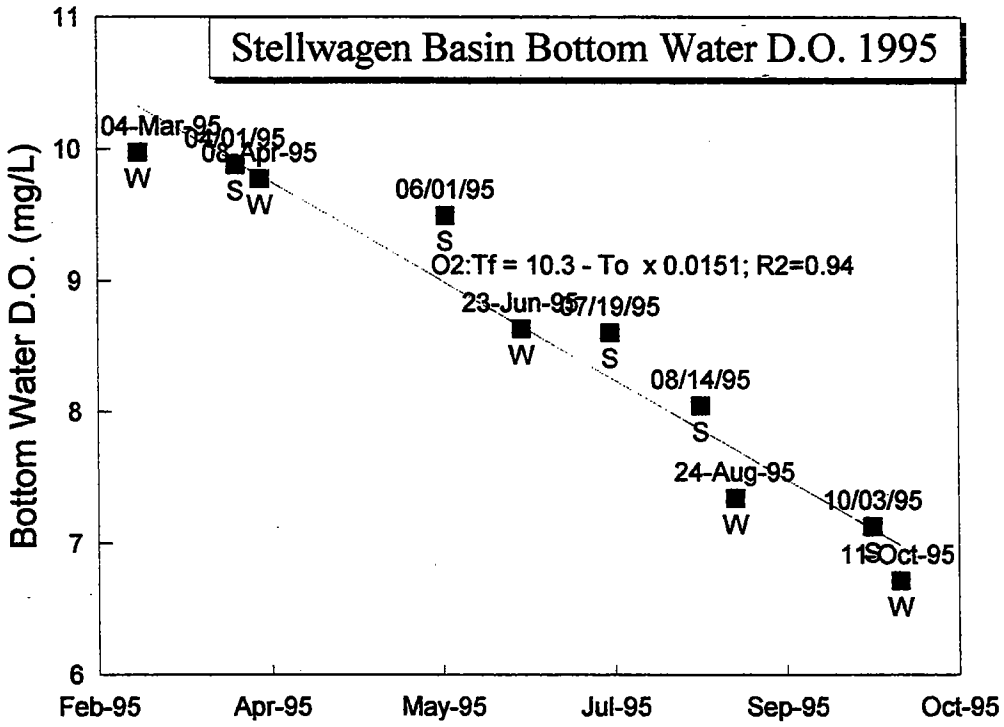

Figure 6-11
Bottom water D.O. concentrations throughout the stratified interval in Stellwagen Basin during 1995. Symbols represent the HOM sub-program (W=watercolumn, S=Benthic Flux). The numbers represent the specific survey day.

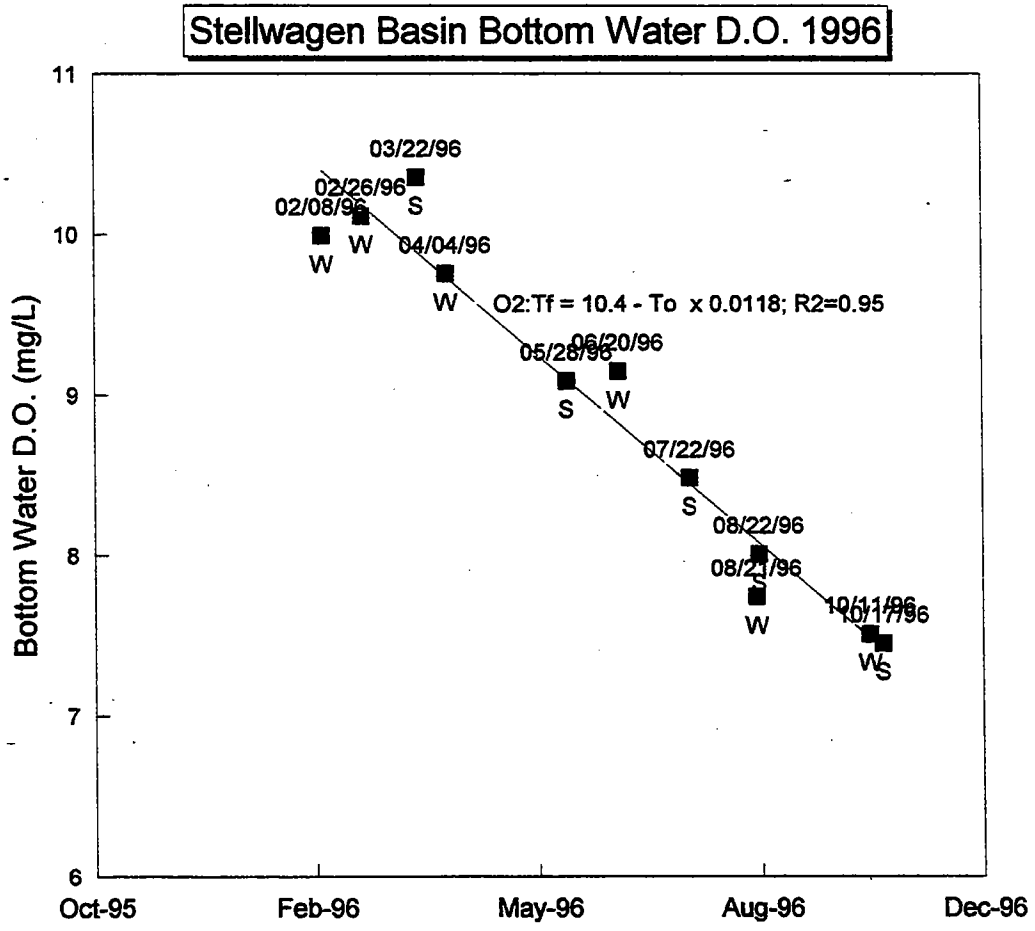

Figure 6-12
Bottom water D.O. concentrations throughout the stratified interval in Stellwagen Basin during 1996. Symbols represent the HOM sub-program (W=watercolumn, S=Benthic Flux). The numbers represent the specific survey day.

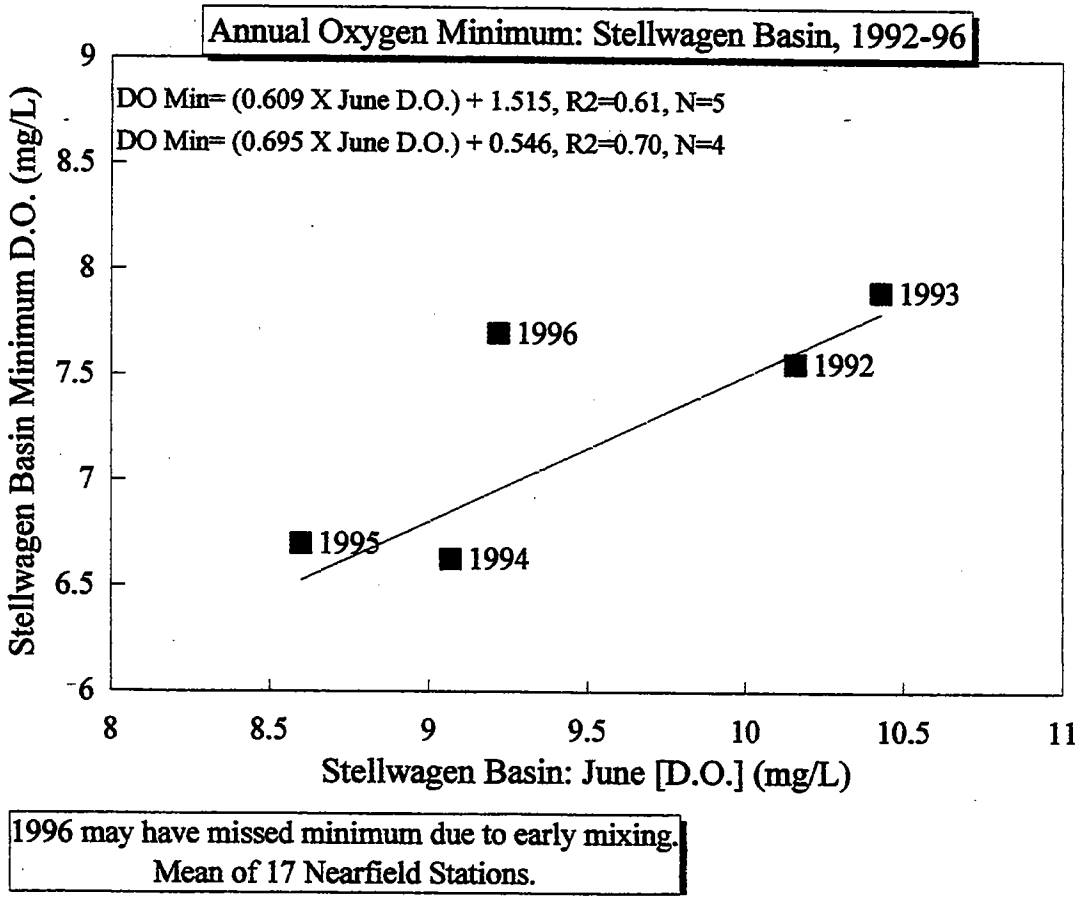

Figure 6-13
Relationship of annual D.O. minima of bottom waters of Stellwagen Basin to D.O. concentration at the onset of stratification, 1992-1996

7.0 PRODUCTIVITY/RESPIRATION

Oxygen depletion in the bottom water of Massachusetts Bay, Stellwagen Basin and Cape Cod Bay results from the decomposition and remineralization of organic matter via respiration within Bay water and sediments. The organic matter comes from external sources (allochthonous) such as rivers and effluent discharges as well as from *in-situ* (autochthonous) production. Oxygen levels are maintained during remineralization of autochthonous carbon within the surface mixed layer because the oxygen produced during photosynthesis is sufficient to support the subsequent respiration of that carbon, and because an atmospheric exchange of oxygen at the surface aids in maintaining oxygen levels near atmospheric equilibrium. Oxygen depletion occurs when there is a physical separation of the oxygen and fixed carbon produced during photosynthesis, isolation of a portion of the water column from atmospheric exchange, or if there are independent outside sources of carbon (e.g., allochthonous inputs). Within the surface mixed layer, differential transport of the fixed carbon (e.g. sinking particles) can cause high oxygen levels despite the decrease in levels that would tend to result from high rates of allochthonous carbon input and physical loss of oxygen to atmosphere during over-saturation. In addition, due to contact with the "infinite" oxygen pool of the overlying atmosphere, oxygen concentrations within the mixed layer are generally at or above saturation (Fig. 6-1b) throughout the year.

In contrast to the mixed layer, the bottom water generally receives additional organic matter beyond that produced from photosynthesis below the pycnocline, typically via sinking of senescent phytoplankton or zooplankton fecal pellets. Such a phenomenon was seen in the nearfield during 1995 as the spring bloom was rapidly consumed by zooplankton grazing (Cibik *et al.* 1996). In addition, inputs of oxygen to bottom water during the stratified period through ventilation is inhibited, so that respiration draws primarily from the initial oxygen pool (the DO "trapped" at stratification). It appears that the physical processes of the timing and duration of stratification and the initial oxygen levels at stratification are the gross proximate controls on the extent of bottom water oxygen depletion (Section 6). The ultimate control, however, is the rate of oxygen consumption related to biological respiratory processes. The observed variation in the interannual oxygen minima in the nearfield (Figure 6-2) is the result of the interplay of the variations in the physical and biological parameters in this quasi-stable system.

Preliminary estimates of oxygen balance within the nearfield (Kelly and Doering, 1995) suggested that allochthonous inputs of organic matter to the nearfield may be significant and that respiration rates during stratification were higher than the observed rates of bottom water oxygen depletion. This latter finding would require significant ventilation of the bottom water during stratification, either through horizontal advection of oxygen-rich deep water or inputs from above the pycnocline via eddy diffusion. It appeared that physical processes may so overwhelm *in situ* biological processes in the determination of the oxygen balance that changes in rates of respiration and productivity might not be good indicators of potential oxygen deficits.

However, more detailed analysis indicates that the oxygen balance of the bottom water is determined primarily through *in situ* processes of phytoplankton production and remineralization (Cibik *et al.* 1996), and that these biological processes can provide essential indicators from which to predict potential future oxygen declines. However, the realization of the full effect of shifts in organic matter inputs through production is infrequent due

to the modification of the oxygen field by short-term stochastic events such as storm driven ventilation of bottom water or periodic inflow of oxygen rich bottom water (Section 6). Measurements of primary production may be useful in detecting nitrogen stimulation that is not manifest in biomass increases (e.g., due to high grazing pressure). Such stimulation of production would result in higher delivery of organic matter to the bottom water, where resultant oxygen reductions may occur.

Clearly, it is critical to determine both the physical and biological processes which control the extent of annual oxygen depletion in bottom water, and particularly the processes which control the delivery and decay of organic matter to the bottom water and sediments at the onset and interval of stratification. The approach taken here to address this problem has been to perform detailed measurements of primary productivity and organic matter respiration within the nearfield study area. Vertical profiles of these biological rates were determined during each of the 17 surveys of 1995 and 1996. Sampling of production and respiration were coupled to allow direct comparisons of the resulting rates. The ultimate goal of this effort is to determine:

- the importance of phytoplankton production to oxygen uptake;
- the role of carbon remineralization within the bottom water and sediments relative to bottom water oxygen depletion;
- the role of the timing of organic matter inputs (spring versus fall bloom versus stratified interval) on the extent of oxygen depletion;
- the role of physical processes in mediating biological effects on oxygen deficits; and
- the coupling of nutrient inputs to carbon fixation and respiration.

Biological rate data are presented within this section, with integration into oxygen and carbon balances in discussed in Section 9.

7.1 Primary Production

7.1.1 Approach to Production Measurement

Phytoplankton production was measured at the edge of Boston Harbor (station F23), and at three increasingly distant stations outside of the Harbor: stations N10 (~ 5 nautical mile); N16 (~10 nm); and N04 (~13 nm). Stations were visited six times (F23, N16) or 17 times (N04, N10) throughout 1996. ^{14}C production was determined as described in the CW/QAPP (Bowen *et al.*, 1997; see also Cibik *et al.*, 1996). Samples were obtained at 5 depths within the euphotic zone down to the ~1-2 % light level, and incubated in the presence of ^{14}C-bicarbonate in a temperature-controlled incubator at light intensities ranging from approximately 5-1200 $\mu Em^{-2}s^{-1}$.

The resulting photosynthesis vs. light intensity (P-I) relationships (Appendix C), measurements of light attenuation with depth (CTD mounted 4π sensor), and incident light time-series measurements (2π scalar

irradiance sensors aboard ship and ashore (see below; Appendix D) were used to determine hourly production ($mgCm^{-3}h^{-1}$) at 15-min intervals throughout the 12 hr day for each sampling depth. Daily depth-dependent production ($mgCm^{-3}d^{-1}$) was determined by integration of hourly production over the course of the photoperiod. Areal production ($mgCm^{-2}d^{-1}$) was determined by integration of measured activity over the depth interval of the measurements. Calibrated chlorophyll-*a* profiles (Appendix E) were used to compute chlorophyll-specific photosynthetic parameters.

An advantage of the above approach is that effects of cloud-mediated fluctuations in light intensity over the course of the day, and gradual variations in light due to changes of season, are automatically incorporated into production computations. Additionally, it is possible to experimentally manipulate the incident light field for the purpose of assessing phytoplankton response to an alternative light field. Cloudless day light fields may be simulated, for example, to assess potential or maximal production even though by chance the actual production measurements were made on an overcast day.

To begin addressing the issue of aliasing of photosynthesis measurements due to a fluctuating light field, a 2π scalar light sensor (Biospherical QSR-240) was installed on the roof of the MWRA lab building at Deer Island for the continuous measurement of incident light, beginning in August 1996. Data were collected every minute, and the average incident light recorded at 15-min intervals. The 15-min interval incident light measurements collected over the photoperiod 0600 - 1800 hrs were used for primary production computations. A Microsoft Quick BASIC 4.5 program was written for computation of the following parameters for Stations N04 and N10: a) daily production ($mgCm^{-3}d^{-1}$) vs. depth (1m intervals) over the season (resolved to the day), b) areal production ($mgCm^{-2}hr^{-1}$) vs. hour of day (resolved to 15 min intervals) over the season (resolved to the day), and c) daily areal production ($mgCm^{-2}d^{-1}$) over the season (resolved to the day). The program also computed areal production in upper 5m and upper 10m of the water column relative to areal P_{max}* (where P_{max}* = $P_{max} \cdot$ [chl*a*]) over the same depth intervals vs. hour of day (resolved to 15 min intervals). This computation yielded areal production expressed as percent saturation vs. hour of day over the above indicated depth intervals. Details of the computations are described in Appendix B.

7.1.2 Seasonal Phytoplankton Production

7.1.2.1 P-I Relationships

P-I curves for deriving α and P_{max} values, used in computation of ^{14}C production, are shown in Appendix C. Of the 230 incubations performed, none showed any obvious indications of photoinhibition.

7.1.2.2 Outer Nearfield Production

Areal production over the 1996 season (Figure 7-1) exhibited substantially different seasonal patterns, generally depending upon distance from shore. In the outer nearfield (stations N04 and N16), areal production was generally characterized by spring and fall blooms, with average productivity around 2-4 times greater than during the summer when stratification limited the supply of nutrients to the euphotic zone (Section 4). The annual

pattern of average photic zone chlorophyll (Figure 7-2) for the outer nearfield (N04, N16) generally followed trends exhibited by areal production. Dominant features were the spring and fall blooms, which exhibited 5 to10-fold increases in chlorophyll biomass relative to other times of year. Biomass maxima typically occurred ~10 days later than areal production maxima, reflecting the time required for the productivity during the blooms to result in observable biomass accumulations.

The spring diatom bloom, beginning in early February and lasting through mid March (Julian days 40-80), increased production from winter values of approximately 100-200 $mgCm^{-2}d^{-1}$ to a peak in late February of approximately 3000 $mgCm^{-2}d^{-1}$. The spring bloom in 1996 was, on average, 3 times more intense in terms of production rate, and produced 4-5 times more chlorophyll biomass, than that which occurred in 1995. Spring production occurred predominantly in the upper 10m of the water column (Figures 7-3 and 7-4) at the peak of bloom activity. This resulted in settling of the chlorophyll maximum (Figure 7-5) over the ~1 ½ month duration of the bloom, from depths of ~15m to a band extending from 20-30m.

Throughout 1996, chlorophyll biomass was greatest during the spring bloom, both in terms of photic zone average (Figure 7-2) and concentration (Figure 7-5). Depletion of nutrients by phytoplankton, particularly silica (Figure 4-6), and possibly grazing by zooplankton, resulted in more than a tenfold reduction in production to the annual low (<100 $mgCm^{-2}d^{-1}$). Zooplankton grazing was apparently responsible for virtually clearing the water of chlorophyll by the beginning of April, just before the onset of summer stratification. The spring bloom in 1996 appeared to extend over the entire outer nearfield, in contrast to 1995 where it appeared to dominate more extensively in the vicinity of station N16. The effects of the increased magnitude of the 1996 spring bloom on water column and sediment respiration are discussed in Section 7.2).

During the stratified summer period, production gradually increased from the post-spring bloom annual minimum to a secondary high of approximately 2000-2200 $mgCm^{-2}d^{-1}$ associated with the onset of the fall bloom. Low summer production was interrupted in the beginning of July (W9608, JD ~183) by an abrupt bloom of the centric diatom *Rhizosolenia* that occurred in the upper 10 m of the euphotic zone (Figures 7-3 and 7-4, Section 8.1). This resulted in a three-fold increase in areal production, from ~600 to 1800 $mgCm^{-2}d^{-1}$. The phenomenon may have been more widespread in the nearfield (e.g., N16), but was missed by the lower resolution sampling program. While its initial activity was captured, the July *Rhizosolenia* bloom was not documented by a large increase in chlorophyll biomass from ship-board measurements (Figure 7-2). However, a three-fold increase in chlorophyll lasting about two weeks was documented in the upper water column (6 m) by the WETLabs sensor on the USGS mooring, located near N16 (Figure 5-3). The bloom may have been a response to an brief excursion of nutrients into the nearfield euphotic zone that also was not resolved by the ship's sampling program.

The fall bloom, beginning at the end of September and lasting until mid November (JD ~270-325) was represented more clearly by "Potential" production (Figure 7-1, open squares; Figure 7-4) estimates where "sunny day" light fields were used exclusively in the computation. The fall bloom lasted for ~2 months, extending from mid-September to mid-November, after which production gradually decreased to winter values. Up to half of total annual production occurred in the spring and fall blooms, though they encompassed only 30% of the annual cycle. This was a pattern similar to observations in 1995 (up to 50% over 16% of annual cycle), though both the

spring and fall blooms in 1996 extended over a longer period. Annual production in the outer nearfield ranged between 340-534 $gCm^{-2}y^{-1}$ and 381-482 $gCm^{-2}y^{-1}$ for outer stations N04 and N16, respectively (day of cruise production - potential production). As mentioned above and discussed in a later section, circumstantial low light on survey days substantially influenced the perceived magnitude of annual production, particularly during the fall bloom.

Compared to 1995, the magnitude of 1996 annual production in the outer reaches of the nearfield (N04 and N07 for 1995, and N04 and N16 for 1996) was ~37% higher (potential production), primarily due to the lack of a well-defined spring bloom and a tempered fall bloom in this region in 1995. Day of survey production was only ~10% higher in this region in 1996, but it is known that the estimate was substantially biased low. It appears, on the other hand, that slightly more inshore (station N16), interannual production was comparable between the two years. Though the sampling frequency for N16 was reduced compared to 1995, it appears from 1996 activity measurements (Figures 7-1, 7-3, and 7-4) and chlorophyll distributions (Figures 7-2 and 7-5) that production at stations N04 and N16 may have been quite similar. Potential production at N16 is probably underestimated due to truncation of the fall bloom during integration of the lower resolution data, and in reality is probably relatively close to the N04 value. Given this to be true, extending the comparison of N16 to include 1996 N04, potential production was essentially the same in this region of the nearfield in 1995 and 1996. Comparison of day of survey activities is more problematic because temporal aliasing due to fluctuating light field (discussed later) has significantly influenced annual production estimates in both years.

7.1.2.3 Inner Nearfield Production

Further inshore at station N10, the pattern of production was very different from the outer nearfield (Figure 7-1). The spring and fall blooms were not as dominant, but rather a complex sequence of activity peaks occurred in mid-March, the end of March, mid-June, late-August and mid-October (W9603, 05, 07, 11, 14). This period produced activities that cycled back and forth between highs of between 4000-5000 $mgCm^{-2}d^{-1}$ and lows ranging near 1000 $mgCm^{-2}d^{-1}$, the approximate average summer stratified production in the nearfield. Because of the proximity of station N10 to the harbor edge, it is within range of the tidally-mediated injections of harbor water into the inner nearfield (Kelly, 1997). These peaks were all associated with blooms in the Harbor and the adjacent coastal water. The magnitude of areal production (Figure 7-1), depth dependent production (Figures 7-3 and 7-4), and photic zone chlorophyll (Figures 7-2 and 7-5; Section 5.0) were similar to that measured at the harbor edge. Correspondence of activity and biomass peaks suggests lateral transport of photosynthetically active water rather than the "growing in" of an *in situ* bloom, which often results in a sequential appearance of activity and biomass peaks.

The strong spring bloom in the outer nearfield may also have occurred in the inner nearfield, but its presence was complicated by contributions from the harbor. The fall bloom, on the other hand, may have developed *in situ* in the inner nearfield as both activity (Figures 7-1 and 7-4) and water column chlorophyll (Figures 7-2 and 7-5) were higher than that at the harbor edge. The perceived magnitude of the fall bloom at N10 was truncated by light field aliasing in a manner similar to that experienced in the outer nearfield. Potential production ranged from 2 - 4 fold higher than when measured using the day of survey light field, though the effect on annual

production estimates was subdued because of the influence from the high activity in harbor water earlier in the year. Annual areal production at N10, ranging between 553-723 $gCm^{-2}y^{-1}$, was intermediate to that observed in the outer nearfield and the harbor edge (Figure 7-1).

7.1.2.4 Harbor Phytoplankton Production

As in 1995, station F23 at the Harbor's edge exhibited the highest daily production rates and annual production of 1996 (Figure 7-1). The majority of production at the harbor edge was restricted to the upper 6-7 m of the water column (Figures 7-3 and 7-4), evident in the large chlorophyll biomass and sharp light attenuation. Maximum seasonal harbor edge areal production was approximately 5500-8000 $mgCm^{-2}d^{-1}$, on average double the highest nearfield bloom production rates (approximately 3000 $mgCm^{-2}d^{-1}$) and nearly three-fold greater than maximum nearfield production during non-bloom periods (about 2000 $mgCm^{-2}d^{-1}$). Total annual production at the harbor edge, ranging between 787-1087 $gCm^{-2}y^{-1}$, was on average between 1.4 and 2 fold higher than annual production measured at the inner and outer nearfield stations, respectively. The shallow harbor station is replete with nutrients throughout the year, and compared with the nearfield, is a less stratified but more tidally active region. Production rates roughly parallel average photic zone biomass (Figures 7-1 and 7-2).

7.1.3 Chlorophyll-Specific Measures of Production

7.1.3.1 Chlorophyll-specific P-I Relationships.

Frequency Distributions. Values for chlorophyll-specific initial slope of light-dependent production, α, expressed in units of $gC(gChla)^{-1}h^{-1}(\mu Em^{-2}s^{-1})^{-1}$ and Pmax, expressed in $gC(gChla)^{-1}h^{-1}$, were determined by dividing α^* and Pmax* by chlorophyll-*a* concentrations determined for each of the 5 depths for stations F23, N10, N16 and N04 and (see Appendix E).

The frequency distributions of these parameters are shown in Figures 7-6 and 7-7. Inspection of the frequency distribution of α among the four stations did not reveal a discernible difference between the outer nearfield stations (N16 or N04), N10 in the inner nearfield, or the harbor edge (F23). When all data were pooled (n=230), a positively skewed distribution (skewness, 1.63) was observed with a median and geometric mean α of 0.0480 and 0.0513 $gC(gChla)^{-1}hr^{-1}(\mu Em^{-2}s^{-1})^{-1}$. There was a cluster of higher values at nearfield stations N10 and N04 and a few at Station F23. Most (86%) of the determined values of α fell below the theoretical maximum of approximately 0.11-0.12 $gC(gChla)^{-1}h^{-1}(\mu Em^{-2}s^{-1})^{-1}$ established by a number of investigators (e.g., Cleveland *et al.*, 1989; Schofield *et al.*, 1991; Lohrenz *et al.*, 1994). 32 values (14%) exceeded an α value of 0.12; 6% were greater than an α value of 0.15. If the high values are omitted, the median and geometric mean for α was determined to be 0.0415 and 0.0425, respectively.

These values are very similar to those obtained in 1995, where the median and geometric mean for α for all data were 0.0432 and 0.0459, respectively. When values exceeding the theoretical maximum (9 values, 4%) were omitted, the median and geometric means were 0.0426 and 0.0436, respectively. However, there were

substantially more values for α that exceeded theoretical limits than occurred in 1995. This is a phenomenon that has been observed by others (e.g., Lohrenz, et. al., 1994), and the causes are unclear. In 1996, the period of these excesses was almost exclusively associated with the sequence of hurricanes that affected the region in the first half of September (Figure 7-7). It is of interest that in 1995 the period where α was driven to (and somewhat beyond) theoretical limits was during a July upwelling event where mixing brought nutrients up into normally stratified water, causing dramatic shifts in phytoplankton physiology. The partial mixing in September of 1996 was more intense than the event in 1995, and was also associated with the initiation of the fall bloom. The intensity and duration of mixing during the 1996 event may have contributed to the greater proportion of high values of α.

As with α in the outer nearfield and harbor edge, P_{max} distributions (Figure 7-8) were not discernibly different from one another, except perhaps for N16 (probably because events that would have resulted in higher P_{max} were not sampled). A discernible drift of the distribution towards higher values of P_{max} was apparent for stations F23, N10 and N04. Pooled data (n=230) revealed a positively skewed distribution (skewness, 2.12), with a median and geometric mean for Pmax of 10.8 and 10.1 $gC(gChla)^{-1}h^{-1}$, respectively. The majority (83%) of the determined values of P_{max} were less than the theoretical maximum of approximately 25 $gC(gChla)^{-1}h^{-1}$ (e.g., Falkowski, 1981; Lohrenz, 1994). Approximately 6% the data were above a value of 40. If these values are omitted, the median and geometric mean for P_{max} was 6.04 and 6.32, respectively. The values for the entire data set (median and geometric mean, 10.8 and 10.1, respectively) were significantly larger than those experienced in 1995 (median and geometric mean, 7.33 and 7.60, respectively) because of the influencing high values of P_{max} during the fall overturn (Figure 7-9).

Seasonal variation in α and P_{max}. Both α and P_{max} exhibited a pattern not unlike that observed during 1995 monitoring (Figures 7-10 and 7-11). These parameters were relatively low, hovering in the range of 0.04-0.06 $gC(gChla)^{-1}h^{-1}(\mu Em^{-2}s^{-1})^{-1}$ and 5 - 15 $gC(gChla)^{-1}h^{-1}$ for α and P_{max}, respectively, over substantial expanses of the water column and year. The general trend is for α and P_{max} to be higher in the upper water column, and for the two parameters to generally co-vary. The most striking feature of the data set was an abrupt 2+-fold increase in both parameters to the theoretical maximum (and beyond in some instances) in the fall. As discussed previously, storms that mixed nutrients into the euphotic zone were a prelude to fall turnover and stimulated an increase in photosynthesis efficiency (increase in α and P_{max}). This resulted in a bloom in photosynthesis (beginning JD ~260) and ultimately an accumulation of chlorophyll biomass (beginning JD ~275) that was second only to the biomass bloom in spring (discussed in section 7.1.6). In addition, an abrupt increase in P-I parameters, particularly P_{max} occurred in July, corresponding to the brief *Rhizosolenia* bloom that was observed in the outer nearfield (Figures 7-1, 7-3, and 7-4), likely in response to mixing of nutrients into the euphotic zone. There were indications of physiological changes in the inner nearfield (N10) but observable enhancements in production were complicated by intrusion of harbor water into the region.

7.1.4 High Temporal Resolution Primary Production Measurements

A large source of uncertainty in the computation of annual production based upon a limited number of surveys (6 to 17 per year) is the effect of light field variability, which can dramatically fluctuate from day to day. As discussed above, we have set an upper limit on annual production by the computation of maximum potential

production based solely upon cloudless day incident light fields throughout the year. True annual production will of course lie somewhere below this upper limit because of periodic cloud cover and fog. Potential for aliasing caused by sampling large amplitude, high frequency phenomena (light) at low temporal resolution precludes production computed from light fields during survey days from being representative of production between surveys. To address these issues, the MWRA began continuous recording of light data during August 1996.

Light field data from August 1st to the end of the year in 1996 are shown in Figure 7-12. The data are presented as integrated incident light (upper panel), which is the total light exposure in $Em^{-2}d^{-1}$ over a 24-hr day, and as a contour plot of light sensor readings ($\mu Em^{-2}s^{-1}$) vs. hour of day and day of year. Two major features are evident. First, there is an approximately two-fold reduction in incident light due to the gradual shortening of day length associated with the onset of winter. In August over half of the photoperiod is exposed to light intensities ≥2000 $\mu Em^{-2}s^{-1}$, which contrasts with December where the light intensities do not exceed much beyond 1500 $\mu Em^{-2}s^{-1}$. Second, the light field is highly variable, with order of magnitude weather-related changes in incident light occurring from one day to the next or persisting for a week or more. These fluctuations can, as will be seen later, result in 2-4 fold changes in areal production. Intra- (e.g., cloud patches) and inter- (e.g., morning/evening fogs) diel fluctuations are seen in the lower panel of Figure 7-12 and emphasize the need for using natural light fields for computation of daily photosynthesis.

Parameters necessary for computation of high temporal resolution primary production are illustrated in Figures 7-13 and 7-14 for stations N04 and N10, respectively. The uppermost panel is the incident light field obtained from Deer Island and the data in the lower four panels were gridded from 1996 survey station data (17 times per year). Depth-dependent light attenuation, expressed as a percent (second panel), coupled with the incident light time series, provided a quantitative measure of the *in situ* light field. High-resolution photosynthesis rates were determined from the temporal and depth-dependent a) *in situ* light field, b) chl*a*_concentration (third panel), and_c) distributions of_α and P_{max} (fourth and fifth panels) using a BASIC program. The availability of incident light data permitted computations for the last five months in 1996, including the periods impacted by the three hurricanes (Eduoard, 2 Sept., JD 246; Fran, 6-9 Sept., JD 250-253; Pacific storm Fausto, 17 Sept., JD 261). These storms initiated the breakdown of summer stratification (flagged by the major increases in α and P_{max} in September, bottom panels), and final turnover and a fall bloom peaking (according to chlorophyll distributions, third panel) in mid- to late-October (JD 280-310).

Results are shown in Figures 7-15 and 7-16. The high-resolution light field is shown in the upper panel and is identical to the light data shown in Figures 7-13 and 7-14. Photosynthesis is expressed on a depth-dependent basis over the season (second panels) and on an areal basis over the course of the photoperiod and season (third panels). The fluctuation in depth-dependent photosynthesis, responding to day to day fluctuations in light field, is clearly evident by the 2-7 fold variations in production contour depth (second panel). This was particularly evident during periods where hurricane-induced mixing spread phytoplankton throughout the water column, as shown for example in the outer nearfield (Figure 7-15, JD ~245-265).

The temporal and seasonal pattern of the light field is also clearly etched into areal production expressed over the day (third panels of Figures 7-15 and 7-16), though underlying changes in photosynthetic capacity of

phytoplankton dominate in controlling the longer term magnitude of production. Activity expressed as percent of total areal production vs. depth is shown in Figures 7-17 and 7-18. For Station N04, 90% of areal production occurred at depths above 19 m during the period mixed by the storms (JD ~245-265), above 5-10 m during the most intense production period (JD ~273-283), and above 3-7 m during the period of greatest biomass accumulation (JD ~283-300). It is of interest to note that the 90% and 99% areal production contours tracked the 5% and 0.5-1% light level contours, respectively, to within 2-3 meters. A similar pattern was observed in the inner nearfield at Station N10, where 90% of areal production occurred above 13-15 m prior to (JD ~220) and during the storm period, above 5-7 m during maximal production rates and ~ 5 m during highest biomass accumulation. The 90% areal production contour tracked the 5% light level as in the outer nearfield, except after the late fall decline in biomass where it penetrated nearly to the 1% light horizon. The 99% areal production contour approximately tracked the 0.5-1% light level contour, though with somewhat less fidelity than in the outer nearfield, reflecting a more deeply penetrating population of low light-adapted phytoplankton in late fall.

Shown in Figure 7-19 is a surface plot of the incident light field and resultant areal production. In comparison with the incident light field (left panel), hourly areal production (center and right panels) have a "flattened" appearance, indicating that a significant fraction of water column production was in some state of light saturation. Between 80-90% of the photoperiod was in fact greater than 80% of light saturation on sunny days for a significant portion of the late summer and early fall in the outer nearfield (N04) upper water column (0-5m) (panels 4 and 5 of Figures 7-15 and 7-16; Figure 7-20). Even in late fall when incident light was significantly reduced, 50-60% of the photoperiod exceeded 80% of light saturation. A similar overall pattern was observed in the inner nearfield (N10) with between 70-80% and 40-50% of the photoperiod being greater than 80% of light saturation. As would be expected, the relative presence of light scattering particles in the water column influence the depth at which significant levels of light-saturated photosynthesis occurred (e.g., 0-10, 0-15 m). It is only during periods of relatively low chlorophyll content in the water column that light saturated photosynthesis penetrated deeply into the water column. At both the inner and outer nearfield stations, dramatic reductions in light saturated photosynthesis occurred primarily when fall bloom biomass was at a peak (Figure 7-17 and 7-18).

Using the high resolution light field for stations N04 and N10, daily areal production (Figure 7-21) is compared with survey results for actual and potential production (determined using both survey-day light fields and sunny day light fields). Potential for temporal aliasing of areal production is clearly evident in this figure, as essentially every survey throughout the fall bloom period (W9612 – W9617) occurred by chance on a cloudy day. As shown in Figure 7-22, the degree to which fluctuating light influences the day to day magnitude of areal production spans a range of 2-5 fold. In 1996, the magnitude of fall production in the nearfield based on integrated survey data was underestimated by 60-70% compared with production estimated by integration of the high resolution data (Table 7-1). As was the case in 1995 (Cibik *et al.*, 1996), potential production estimates were necessary to understand the true magnitude of the fall bloom. In 1996, calculations of potential production showed that the fall bloom occurred from mid-September through November, and provided an upper estimate on production (N10, 180-219 gCm^{-2}; N04, 257-265 gCm^{-2}, Table 7-1). The higher estimates were derived from the upper envelope shown in Figure 7-22, which is more highly resolved than potential production estimates based on survey data.

Station N04. In the outer nearfield, the dominant feature during the period that daily light levels were recorded was the fall bloom (Figures 7-15, third panel; 7-16, second panel; composite Figure 7-23, panel D). The response to nutrient intrusions appeared to occur in two stages (Figure 7-24, upper panel; Figure 7-23, panel B). The first (late August, JD ~230-245) appeared to be associated with advection of water into the nearfield from the Gulf of Maine (Section 3, Table 9-1). It appeared that there was a similar response throughout the outer nearfield, as the temporal pattern of the nutrient time series for data averaged from stations N04, N07, N16, and N20 (Figures 4-17, 4-18) were similar to that shown in Figures 7-24 and 7-23 for station N04 alone. This event was followed in early September (JD ~245-250 to ~270-275) by more significant region-wide mixing of the water column by the sequence of hurricanes (Figure 7-23, arrows). Response to this second influx of nutrients appeared to continue into early October (JD ~270-280), at which point the fall turnover occurred (Table 9-1) and the entire water column was replete with nutrients.

During the fall turnover, two distinctive periods of activity were evident, separated by approximately 20 day interval in mid-October (JD ~282-305) of significantly lower production. The initial increase in production began just after the sequence of storms in September, and lasted through the beginning of October (JD ~258-283). Photosynthetic capacity was dramatically enhanced as evidenced by patterns of α and P_{max} (JD ~240-270in Figure 7-13, bottom two panels; Figure 7-23, panels E and F; Figures 7-10 and 7-11). This was followed by more deeply distributed production as phytoplankton were mixed deeper into the water column (JD ~250-275). The most intense activity occurred over a 10-day period beginning with the end of September (JD ~273-283). Though biomass was high throughout most of October (JD ~275-305), greatest accumulations occurred just after the 10 day burst of high surface production (upper 7 m of the water column; compare dashed lines in Figure 7-24, lower panel

The activity during the fall bloom may have been interrupted by more than one week of overcast weather (JD ~263-273). The average incident light during this period was 37 $\pm$15 $Em^{-2}d^{-1}$, compared to relatively sunny periods prior to and afterwards (avg. incident light = 58 $\pm$14 $Em^{-2}d^{-1}$, Figures 7-15 and 7-21, upper panels; Figure 7-23, panels A and D). The second peak in activity began around the beginning of November (JD ~305) and lasted approximately two weeks (JD ~318). Activity thereafter gradually dissipated to winter production rates over a 30-day period.

The decline in photosynthesis between blooms was not the result of dramatic changes in incident light, but rather to a changing physiological state of the phytoplankton as bloom biomass accumulated in the upper half of the water column. Figure 7-13 (lower two panels) and Figure 7-23 (panels E and F) show that α and P_{max}, hence photosynthetic efficiency, were both high during the 2-3 week period of storm-induced mixing and onset of fall turnover when nutrient-limited phytoplankton were responding to increased nutrient. These parameters diminished to summer values as increased bloom biomass (third panel) reduced available light to the upper 5-7 meters of the water column (5% light level, 90% areal production; Figure 7-13, 7-17) and placed the majority of the water column in a state of light limitation sufficient to affect physiological state. Another indication of this is evident in Figure 7-25, which illustrates the depth and time dependent distributions of α^* and P_{max}^*. These incorporate water column chlorophyll content, and in effect demonstrate the photosynthetic capacity of the water

column (i.e.,_α*, P_{max}*, *in situ* light and the P-I equation are used to compute production), which is clearly reduced between the observed blooms.

When fall mixing intensified in early November, accumulated biomass began to dissipate and nutrients penetrated higher into the euphotic zone, apparently stimulating a new period of enhanced photosynthetic competence (note increases in α and P_{max}, Figures 7-13, 4th and 5th panels; Figure 7-23, panels E and F). The result was a second month-long period of photosynthetic activity (Figures 7-15 and 7-23) that constituted 42% of the total organic carbon produced in the fall (Figure 7-21). The second bloom did not result in a distinct biomass peak, as it occurred during a period of substantial mixing.

Station N10. A similar scenario in production was evident for the inner nearfield. The fall bloom (JD ~272-292) is a dominant feature in addition to an earlier production maximum (JD ~227-245) resulting from harbor influences (Figures 7-21, W9611; 7-26, middle panel; Figure 7-27, panels 2 and 4). As in the outer nearfield, substantial mixing resulted from the hurricane activity in September. The mixing dissipated the mid- to late-August activity bloom and associated chlorophyll biomass, and introduced deep nutrients into the euphotic zone (Figures 7-26, panel 1; 7-27, panel 2). This resulted in dramatic increases in both α and P_{max} (Figures 7-14, lower panels; 7-27, lower panels) that resulted 7-10 days later in an intense surface activity bloom (JD ~273-285, 292), followed in an additional 7-10 days by a substantial accumulation of chlorophyll biomass (JD ~280-293, Figures 7-26 and 7-27). This late September-early October bloom extended throughout the nearfield as it occurred at the same time at both stations N10 and N04 (Figures 7-23 and 7-27). The secondary activity bloom observed in November at station N04 in the outer nearfield was not discernible closer to shore (N10). Though evidence for an enhanced physiological state (increased α and P_{max}, Figures 7-14 and 7-27) was evident in the inner nearfield, water column photosynthetic potential (α* and P_{max}*, Figures 7-25 and 7-28) was reduced because of a lower chlorophyll biomass in this region in November (compare Figures 7-23, 7-24, 7-26, and 7-27).

7.1.5 Modeling of Phytoplankton Production

Development of a proxy measure of photosynthetic activity based upon routinely determined environmental variables has been an important goal of the HOM program. To date, the model that has been the most thoroughly investigated is based upon correlating a composite parameter, BZ_pI_o, with measured ^{14}C-phytoplankton production (Kelly and Turner, 1995; Kelly,1997), where B is the average photic zone chlorophyll *a* concentration, Z_p is the photic zone depth (BZ_p = chlorophyll *a* content of photic zone) and I_o is the daily incident light. The model is calibrated by linear regression to yield the equation:

$$\mathbf{P(^{14}C) = m \cdot BZ_pI_o + C} \qquad \text{Equation 1}$$

where:

$P(^{14}C)$ = ^{14}C-primary production, [$mgCm^{-2}d^{-1}$]

m = slope; (P - C)/BZpIo, [$mgCm^2(mgChla)^{-1}E^{-1}$]

BZ_pI_o = composite parameter, $[(mgChl\textit{a})m^{-3} \bullet m \bullet Em^{-2}d^{-1} = (mgChl\textit{a})m^{-2}Em^{-2}d^{-1}]$

C = intercept (ideally = 0), $[mgCm^{-2}d^{-1}]$

Significant linear regressions were obtained when P and BZ_pI_o were derived from data collected over the annual cycle (Kelly and Doering, 1995; Kelly, 1997; Cibik *et al.*, 1996; present report), though there was substantial variability about the regression line. When modeled estimates of production in 1994 were compared with ^{14}C production measured in 1992-94, the general trend of the annual cycle was followed (Kelly and Doering, 1995; Kelly, 1997). In 1994, the regression for the nearfield (N16 and other nearfield stations) did not appear to be significantly different from the harbor edge (F23), which lead to a proposal that a region-wide formulation of the model was appropriate (Kelly and Doering, 1995; Kelly, 1997). However, there was potential for rather large error in estimating production at any particular point in time (Cibik *et al.*, 1996).

Regressions obtained in 1995 and 1996 from a station at the harbor edge (F23) and at stations of varying distance from shore in the nearfield (N04, N07, N16 and N10), are shown graphically in Figures 7-29 and 7-30, and determined values for slope and intercept shown in Table 7-2. Quality of fit varied broadly (r^2, 0.25-0.96), as did error on the estimates of the slope (m, 10-74 %) and intercept (C, 75-254 %). Unlike the findings in 1994 (Kelly and Doering, 1995; Kelly, 1997), data for 1995 and 1996 showed a clear trend of decreasing slope with distance from shore (Figure 3). Though in 1995 the slope terms obtained at the outer nearfield stations (N04 and N07) did not significantly differ (two tailed t-test; $p>>0.05$), all remaining stations significantly differed from one another in slope as one approached the coast (two tailed t-test; N04 ≠ N16, N07 ≠ N16, N16 ≠ F23; $p<0.05$). A similar pattern was observed in 1996 (two tailed t-test; N04 ≠ N16, N16 ≠ N10; $p<0.05$).

Because of the large error in determination of the slope for station F23, it was not possible to discern a significant difference between stations N10 and F23 (two tailed t-test; $p>>0.05$). In addition to spatial differences in slope, there is potential for interannual differences. Both stations N04 and F23 exhibited significantly different slopes when compared with its counterpart in 1995 and 1996 (two tailed t-test; $p<0.05$). Station N16, on the other hand exhibited insignificantly different slopes over a three year period (1995-1996; $p>0.05$). The harbor edge station F23 clearly exhibited the greatest potential for variation in slope. It was strongly influenced by the high activity periods in late June and late August (surveys 7, 11) which possessed ≥ 10 fold (1995) or 2-3 fold (1996) greater activity than the average that occurred during the remainder of the year. It is interesting to note that if the high summer values (surveys 7, 11) are omitted from the regression, the resultant slopes (Figure 3) are substantially reduced and relatively consistent from year to year (see F23; 1994, 1995 low and 1996 low). Hence, inshore there appears to be potential for a seasonal biasing of the BZ_pI_o regression that may vary from year to year (slopes; 1994, 0.63; 1995, 1.87; 1996, 0.88).

Suitability of a proxy measure of primary production requires sufficient fidelity to accurately quantify integral production for the year or various subintervals of the year. For example, the proxy must be suitable for both production during the stratified period as well as when the water column is mixed. It should also allow the investigator to accurately detect the occurrence and duration of bloom events. A head-to-head comparison of BZ_pI_o modeled vs. measured ^{14}C-production is shown in Figures 7-31 and 7-32 for 1995 and 1996, respectively.

Calibrating BZ_pI_o regressions were conducted in the nearfield (N16) and harbor edge (F23) in 1994 (Kelly and Doering, 1995; Kelly, 1997) and at various stations by us in 1995 and 1996. In our opinion, the BZ_pI_o model did not hold up well with respect to the desired properties mentioned above.

The model generally reflected trends in photosynthesis (for example, periods of relatively low production vs. periods of high production were generally tracked). However, when viewed quantitatively and in more detail, the fidelity of the model deteriorated. First, calibration of the model changed from year to year. Compare, for example, 1994 & 1995 calibrations for 1995 (Figure 7-31), and 1995 and 1996 calibrations for 1996 (Figure 7-32). When the data were viewed collectively there was an incremental improvement in the match between modeled and measured production, typically occurring when the calibration was performed in the same year. The fidelity of representation of major seasonal events seemed to vary by year and by station. For example, during the early and late spring bloom events in 1995, station N16 estimates were over and underestimated by ~2-fold and ~1/3, respectively. Further, the timing of the spring bloom at station N04 in 1996 was represented by the model to occur approximately one month later in the year than actually occurred, and the magnitude of this displaced bloom was misrepresented by 25-30%. The fall bloom was significantly underestimated at station N16 in 1995, and especially station N04 in 1996. Finally, production during the summer stratified period was often misrepresented by 2 or more fold (e.g., 1995-N16, N04; 1996-N04).

In a minority of instances, the model agreed reasonably with measured production (e.g., Station N16 in 1996). When modeled production is plotted against measured production (Figures 7-33 and 7-34) the magnitude of deviation of individual data points from a 1:1 relationship can often exceed several fold. Given that bloom and other (e.g., grazing) events occur abruptly, single outlying points can result in significant qualitative and quantitative misrepresentation of seasonal or stochastic events. Shown in Figure 7-35, modeling errors can result in 3-fold (F23) to 1/3 (N16, N10, N04) errors in estimates of annual production, and model calibration does not appear to be stable from year to year. Apparent agreement of modeled annual production with measured production can result from the fact that the model does adequately represent true production (1996, N16) or from circumstantial compensation resulting from dramatic over- and underestimation of true production at different periods in the annual cycle (1996, N04).

Incorporated within the linear BZ_pI_o model are two inherent assumptions: a) photosynthesis is on average light limited so that a fluctuation in I_o will result in a linearly proportional change in production, and b) water column chlorophyll *a* is equally efficient at organic carbon production over the spatial and temporal scale that the regression is computed (i.e., quantum efficiency is constant). High-temporal resolution production measurements discussed earlier (see Figures 7-15, 7-16, and 7-20) showed that on sunny days, much of the photoperiod can be at > 80% of light saturation in the upper 5-15 m of the water column, where ~50-90% of areal production is occurring (see Figures 7-17 and 7-18). That light saturation may be influencing the BZ_pI_o regression was first discussed by Cibik *et al.* (1996), where BZ_pI_o and measured areal production were computed in slices throughout the water column. At all stations, data from surface samples were biased low in the BZ_pI_o vs. ^{14}C-areal production plots, indicating that effects of light saturation resulted in lower production than would be predicted from average chlorophyll *a* content and incident light. The depth-resolved BZ_pI_o regressions did not dramatically improve over the regressions computed for the entire water column, suggesting that other effects influencing photosynthetic efficiency were also occurring.

By implementing identical procedures used to compute areal production under the ambient daily light field vs. the maximum theoretical daily light field, it was possible to assess the effects of incident light (I_o) on the BZ_pI_o vs. ^{14}C-areal production regressions for all stations at various times of the year. To do this a typical sunny late June light field (see theoretical light time series in Figure 9607B of Appendix D) was attenuated by a multiplier to provide daily incident light which ranged from a maximum of approximately 85 $Em^{-2}d^{-1}$ down to approximately 5 $Em^{-2}d^{-1}$. ^{14}C-areal production was computed normally using P-I terms α^* and P_{max}^*, light attenuation properties of the water column for given stations and time of year, and various daily incident light field time series modified as described above. Plots for a given station and time of year will by definition be at a constant photosynthetic efficiency defined by α^* and P_{max}^* and will reflect only the effects of varying light field. If the model $P(^{14}C) = m \cdot BZ_pI_o + C$ (C ideally = 0) is by and large obeyed, the resultant plots for each survey should be linear and fall along the same line.

^{14}C-areal production and attendant composite BZ_pI_o parameters, determined as described above are plotted in Figures 7-36 to 7-39 for several surveys at stations N04, N16, N10 and F23 (open circles, survey number indicated on symbol). Data illustrated by the shaded squares represent BZ_pI_o and ^{14}C-areal production under the actual light field during the days of the surveys and is also represented in the regressions shown in Figure 7-30 for these stations[1]. Immediately evident is the fact that the curves are nonlinear. The empirical equation $P(^{14}C) = m \cdot BZ_pI_o + C$ does not inherently describe the true BZ_pI_o vs. ^{14}C-areal production relationship. A more appropriate empirical equation would be mathematically analogous to that which describes the P-I relationship in Massachusetts Bay such as:

$$\mathbf{P(^{14}C) = Ps(1-exp(-k \cdot BZ_pI_o))} \qquad \text{Equation 2}$$

where:

$P(^{14}C)$ = ^{14}C-primary production, $[mgCm^{-2}d^{-1}]$

Ps = limit ^{14}C-primary production at high BZ_pI_o, $[mgCm^{-2}d^{-1}]$

BZ_pI_o = composite parameter, $[(mgChl\textit{a})m^{-3} \cdot m \cdot Em^{-2}d^{-1} = (mgChl\textit{a})m^{-2}Em^{-2}d^{-1}]$

k = constant, $[(mgChl\textit{a})^{-1}m^2E^{-1}m^2d]$

The quality of fit to this model of survey data obtained over the annual cycle (i.e., shaded squares) will depend upon the extent to which the efficiency of photosynthesis and other factors are consistent over this time period. If efficiency is relatively invariant over the season (survey to survey) the various curves will overlap and the fit will be good. If, on the other hand, the efficiency significantly varies or fluctuates over the season, overlap will be poor and the fidelity of the fit affected. As can be seen in Figures 7-36 to 7-39, several of the curves overlapped well and several varied widely. In widely divergent cases (Figures 7-36 and 7-39, stations N04 and F23), placement of given data points used for the composite regression will very much depend upon the light field of

[1]The displacement of the datum points from the curves presented results from effects of qualitative differences in the shape of the daily light field time series which will be discussed later.

the day. If survey 14 for station N04, for example, were to have been a sunny day (shaded square, 14*) rather than the strongly overcast day that it was (shaded square, 14; see Figure 9614A, Appendix D), the datum point would have diverged from the photosynthesis pattern of other cruises (e.g., 3, 4 and 6) or a composite regression line (dashed line, fit to all N04 data) by 2 fold.

Similar arguments can be made for station F23 in which there is a broad spectrum of curves over the season. In this case, one can readily see the potential for a very different distribution of production vs. BZpIo relationships (i.e., shaded squares) had there been a different array of daily light fields. Data for station N16, on the other hand, are more tightly grouped and differences in light field intensity less influential on the pattern of photosynthesis. Note the reduced scatter of individual datum points about the linear (Figure 7-30) and exponential (Figure 7-40) regression lines for this station.

An additional potential source of variability relates to effects of the shape of the daily light field on production. The I_o term of the BZ_pI_o model incorporates only light integrated over the course of the day. It is possible to have generally overcast conditions, characterized by reduced light intensity throughout the day (e.g., Figures 9604B or 9614A, Appendix D), or a sunny day punctuated by varying periods of cloudiness (e.g., Figures 9613, 9614B of Appendix D). It is possible for these qualitatively different light fields to possess similar values for I_o and, hence, BZ_pI_o. Production, on the other hand, will be influenced by this qualitative difference, in particular the relative fraction of the day that the light is significantly near saturating levels. The potential magnitude of this effect is illustrated in Figure 7-41. In this example, phytoplankton production at station N16 was computed under a number of mid-October (W9614) light field scenarios, beginning with a completely sunny day (curve A, $I_o = 62.2$ $Em^{-2}d^{-1}$). Areal production and BZ_pI_o was computed for the sunny day and for increasingly overcast days (curves B-E, $I_o = 55.5\text{-}25.5$ $Em^{-2}d^{-1}$) and compared with sunny days truncated by periods of increasing cloudiness (I_o of curves F-I are identical to those of curves B-E, respectively). Shown in the lower panel, the effect of a punctuated cloudy light field (open squares, light curve identified within symbol) is to incrementally reduce production, relative to overcast conditions possessing the same magnitude daily incident light (open circles). The effect is maximal (approximately 12%) when the day is about equally divided between sunny and cloudy periods. The effect of the true W9614 light field is shown by the shaded square (see also Figure 9614B, Appendix D). Displacement of production under the natural light field shown in Figures 7-36 to 7-39 (shaded squares) is largely due to these effects (the attenuated light fields used to generate the curves were similar to B-E in Figure B13).

It is evident that the major source of error in the BZ_pI_o model is related to seasonal and spatial variations in photosynthesis efficiency. Use of the above-described exponential model (Equation 2), for example, does improve the composite fit to the data, but only incrementally (Figures 7-40 and 7-42). Effects of the non-zero intercept in the linear model (C, in Equation 1) are removed when the exponential model (Equation 2) is used. Compare, for example, Station N04 when modeled with linear Equation 1 (1996 model, Figure 7-32) and with exponential Equation 2 (Figure 7-42). Station N16 is modeled quite well using the exponential fit. However, more often than not (e.g., stations F23, N10, N04), production is not modeled well quantitatively (Figure 7-42).

As mentioned earlier, one of the assumptions incorporated into the BZ_pI_o model is that the water column is equally efficient at organic carbon production over the spatial and temporal scale of the regression. The fact that

readjustment of the BZ_pI_o regression to incorporate effects of light saturation only incrementally improved the ability of the model to predict seasonal production suggests the above assumption is not true. A hint of this was illustrated earlier in plots of chlorophyll-specific production vs. depth vs. time and also in Figures 7-43 and 7-44 where euphotic zone chlorophyll-specific production is shown over the 1995 and 1996 annual cycle. Chlorophyll-specific production is clearly not constant over time and in fact can vary by more than an order of magnitude. Variability on a similar scale was also evident in seasonal plots of depth-integrated expressions of α (Figures 7-45 and 7-46 for 1995 and 1996, respectively) and P_{max} (Figures 7-47 and 7-48, for 1995 and 1996, respectively) where by definition effects of light saturation are incorporated into the parameter. There is not a consistent pattern in any of the variables from station to station or from year to year at the same station. Most of the large increases of all parameters relate to stochastic or seasonal intrusions of nutrients into the nutrient-limited euphotic zone as was discussed earlier.

It is of interest to note the one instance where the BZ_pI_o model did model seasonal areal production reasonably well was Station N16 in 1996 (Figure 7-32), particularly when effects of light saturation were incorporated into the model (Equation 2; Figure 7-42). Since the regressions were derived over the annual cycle, goodness of fit at Station N16 would imply that water column photosynthetic efficiency must have been relatively consistent in 1996. Inspection of the data for N16 in Figures 7-44, 7-46, and 7-48 indicates this to be the case, relative to all other stations. Because N16 was sampled only 6 times during 1996 it is possible that this consistency may have resulted from the fact that times where α and P_{max} may have dramatically changed were not sampled.

This exercise suggests that if means were available to normalize the effects of variability in photosynthetic efficiency, the simple BZ_pI_o model might be made applicable to real world photosynthesis. An example would be incorporation of an empirically derived or easily measured factor into the equation in much the same way that the empirically determined fugacity coefficient is introduced into the ideal gas law to allow its application in the real world (i.e., at pressures greater than near vacuum). Re-inspection of the idealized BZ_pI_o regression equation (Equation 1) provides a possible suggestion:

$$\mathbf{P(^{14}C) = m \cdot BZ_pI_o} \qquad \text{Equation 3}$$

When ordinarily implemented, the slope term (m) is defined to be a constant. The above discussion indicates that m is really a variable that can change quite dramatically in magnitude. Inspection of the units of m, $[mgCm^2(mgChl\textit{a})^{-1}E^{-1}]$, indicates that they are the same as those for depth-integrated α (note axis legends in Figures 7-45 and 7-46). If a proxy measure of depth integrated α were easily obtainable for each station at various times of the year without the necessity of conducting ^{14}C-P-I incubations, equation 3 might be applicable as a proxy measure of primary production. Evidence in the literature suggests that a bio-optical measure of the desired parameter may be possible.

Over the past decade much has been gained in the understanding of the optical properties of photosynthesis. As illustrated in Figure 7-49, sub-cellular physiological and biophysical events during photosynthesis can be sensed fluorometrically and expressed mathematically. The initial slope of a chlorophyll-specific P-I curve_α, for example, is the product of two parameters that can be measured optically, the maximum quantum yield of

photosynthesis (Φ_{max}; [mol CO_2 fixed (mol Photons)$^{-1}$ and a^* the chlorophyll-specific spectrally averaged *in vivo* absorption cross-section [m^2 (molChla)$^{-1}$] (e.g., Cleveland *et al.*, 1989). As discussed in the legend of Figure 7-49, a proxy index for Φ_{max}, ($\Delta\Phi_{max}$), is theoretically attainable from DCMU fluorescence measurements and a^* can be obtained via specialized spectrophotometric absorption measurements made on phytoplankton samples impinged upon glass fiber filters. The bio-optical techniques are somewhat involved and must be conducted carefully, but they are dramatically less involved than the process of conducting ^{14}C-P-I incubation studies.

The factor α may also be expressed as the product $\sigma_{PSII}\eta$, where σ_{PSII} is the functional absorption cross-section of photosystem II (PSII, discussion below) [m^2 quanta^{-1}] and η is the concentration of functional PSII reaction centers [mol O_2 or C (mol Chla)$^{-1}$] (e.g., Falkowski, 1992). Chlorophyll-specific light saturated production P_{max} = η/τ, where τ is the turnover time [h^{-1}] for electron flow through the photosynthetic electron transport chain. Several of the parameters composing α and P_{max} (e.g., Φ_{max}, η and σ_{PSII}) vary with phytoplankton nutrient status and underlie the observed seasonal and stochastic changes in α and P_{max} in the above ^{14}C studies. By use of specialized fluorometers based on the principles discussed in the legend of Figure 7-49, it may be possible to acquire a proxy measure of α from a single flurometric measurement. If this is verified it may be possible to provide all of the parameters on the right hand side of equation 3 from straight forward CTD / fluorometric measurements. An inexpensive Pulse During Probe fluorometer (based on concepts described in Olson, *et al.*, 1996) is presently in development in the laboratory of C. Taylor.

This topic will be discussed further in the upcoming 1997 Annual report where DCMU fluorescence studies were conduced in concert with ^{14}C incubation studies.

7.2 Water Column and Sediment Respiration

Water column and sediment respiration are the dominant sinks of oxygen within the Massachusetts Bay water column. In systems like Massachusetts and Cape Cod Bays, water column respiration typically accounts for the majority of carbon mineralization (on an areal basis, m-2). However, during stratification when oxygen depletion is a concern, oxygen uptake in bottom waters is more equally distributed between water column and sediments (Cibik et al., 1996). The increased relative importance of sediment oxygen uptake during stratification results from 1) a major reduction in the vertical transport rate of labile organic matter to support bottom water respiration compared to the intervals of vertical mixing; and 2) the differential "holding" times of organic matter in the water column versus sediments (i.e., particles fall through the water but are held in the sediments).

Particle retention by sediments allows periodic organic matter deposition events (usually following blooms) to result in oxygen demand on bottom waters for extended periods (months compared to days). In order to understand the carbon and oxygen dynamics of Massachusetts Bay and the factors which control bottom water oxygen depletion, detailed water column respiration measurements were conducted within both the nearfield and Stellwagen Basin. Sediment respiration measurements (Benthic Flux Program) focused on depositional environments to determine the dynamics and upper limits of sediment oxygen uptake through this pathway. Measurements focused on the vertical distribution of water column uptake rates, as well as sediment uptake, during the mixed and stratified water column periods, to relate the fate of photosynthetically-derived organic

matter to the draw-down of bottom water oxygen levels (Section 6). The measurements also supported development of a carbon balance (see Section 9) to ascertain the potential importance of allochthonous carbon inputs; and development of an oxygen balance from which to assess the potential for increases in oxygen deficits under changing organic matter inputs.

Both water column and sediment respiration are controlled by the availability of labile organic matter and the environmental temperature. These two regions of oxygen uptake differ primarily in their ability to "store" organic matter while it is being re-mineralized. Organic particles typically have a relatively short life span (days-weeks) within the water column, as they are freely advected or sink to the bottom sediments. In contrast, organic particles reaching the sediments remain available for decomposition for months to years, with refractory compounds often permanently accumulating in depositional areas. The result is that water column rates of respiration at fixed locations typically show larger and more frequent temporal variations compared to sediment rates, which are buffered by the more constant nature of their organic matter pool. The following sections detail the major results of the water column (7.2.1) and sediment (7.2.2) respiration measurements within Massachusetts Bay through 1996).

7.2.1 Water Column Respiration

Water column oxygen uptake is dominated by the respiration of phytoplankton, zooplankton, and heterotrophic microorganisms. Within the bottom waters of Massachusetts Bay, heterotrophic activity predominates. Our measurements represent the combined oxygen uptake by all of these forms, whereas oxygen inputs from all sources, including photosynthesis, are excluded by the incubation methodology.

Rates of water column respiration were determined in the same time series and locations in the nearfield (stations N04, N10 and N16) and Harbor (station F23) as the primary production measurements (Section 7.1, Figure 1-2). In addition, profiles of respiration and associated water column parameters were collected in Stellwagen Basin (station F19). Measurements were made at three depths (surface, mid and bottom). During stratification, the upper two depths were generally within the surface mixed layer (at the surface and near the pycnocline) except in Stellwagen Basin, where the mid-depth sample was typically below the pycnocline. Since oxygen depletion in Stellwagen Basin is one of the main focus points of the oxygen program, but only sampled 6-7 times throughout the year by the Water Column Program, additional bottom water sampling was collected in concert with the 5 benthic flux surveys and included in this analysis.

Water column respiration was assayed using triplicate samples collected to determine initial conditions, and parallel triplicate bottles for incubation to determine oxygen uptake at each depth. Samples were kept at in situ temperatures in the dark. Since open water rates of oxygen consumption are typically low due to carbon availability, care was taken to maintain "clean" incubation bottles. Bottles were acid- washed (HCl) between surveys, and periodically "digested" with potassium persulfate to remove organic films. As a result, triplicate incubations typically had a C.V. of ca. 10%. Analysis of DO concentration was by Winkler reaction and potentiometric titration (Oudot et al., 1988). Both respiration (in units of uMO2 hr-1) and carbon-specific

respiration (uMO2 uMC hr-1) rates at each of the sampling depths are presented below. Carbon-specific respiration was calculated by normalizing respiration rates to the total particulate organic carbon concentration (POC) measured in parallel with respiration in each sample. Carbon-specific respiration provides an indicator of how biologically available (labile) the POC substrate material is for microbial breakdown.

7.2.1.1 Vertical Distribution of Water Column Respiration

Respiration ranged from showing a weak (ca. two-fold) vertical gradient within the water column to a very strong gradient (>10 fold) from surface to bottom waters in both the nearfield (Figure 7-50, 7-51) and Stellwagen Basin (Figure 7-52). Not surprisingly, the magnitude of the vertical gradient appeared to be controlled primarily by the degree of vertical mixing of the water column (see Figures 3-10, 3-11).

Water column respiration was not always uniform between stations within the nearfield (Figure 7-51). Differences were not consistent, but rather followed the patterns of primary production at the various stations (see Sect. 7.1 above). In general, the westernmost station (N10) showed slightly higher rates of oxygen uptake. This effect was most evident within the surface water, and most dramatic during the August Rhizosolenia bloom at that station (Figure 8-3). Overall, there were no sustained inter-station differences throughout 1996, which is consistent with the general pattern in productivity (Figure 7-1). The surveys where N10 showed significantly higher rates compared with the rest of the nearfield (e.g., survey W9604, W9607, and W9611) occurred during periods of high activity in the Harbor, which can influence this station (Kelly, 1997). In contrast, the nearfield did typically show higher rates of respiration than the waters of Stellwagen Basin. These differences were particularly pronounced in the bottom waters during the stratified interval. The differences likely relate to differences in the spatial sources of organic substrate and to the greater depth of Stellwagen Basin, which allows for greater decay of organic particles before they reach the bottom waters.

During winter and early spring when the water column was unstratified, vertical structure in respiration rates depends primarily upon the ability of mixing to create a vertically homogeneous distribution of organic matter. Although the water column is relatively isothermal during the mixed intervals (Figure 3-1, 3-2, 3-3), it is clear that significant vertical heterogeneity exists in the particulate field. This vertical structure is evident in both the nearfield and Stellwagen Basin in key respiration-related parameters such as photosynthesis, chlorophyll a and POC (Figures 7-3, 7-5, 7-53). It also appears that vertical differences in these organic matter source parameters are generally proportional to the observed vertical differences in oxygen uptake (Figures 7-50, 7-52).

In the outer nearfield stations (N04, N16), the difference between surface and bottom water respiration rates was not found during the March survey (W9603) due to increased respiration rates in bottom waters from the sinking of the late winter bloom. By April, vertical differences in respiration were beginning to be controlled by differential water temperature as some locations. These results indicate that even during the mixed interval, the substrate and biological processes controlling oxygen uptake within the water column are not uniformly distributed, but tend to be concentrated in the surface waters. Surface water respiration rates showed higher rates of oxygen uptake throughout the year.

It is notable that even during the mixed period, particulate organic matter levels, most likely photosynthetically derived, remain significantly higher within the surface than bottom waters. It is clear that during the mixed interval, the POC distribution is the predominant factor generating the vertical gradient in water column respiration. However, the generally low absolute rate of respiration is likely the result of the low environmental temperatures during this interval. It also appears that "biological stratification" within the study area generally persists throughout both the (physically) stratified and mixed intervals.

While vertical differences were evident in both the mixed and stratified intervals, water column respiration rates during stratification were much more strongly depth-dependent, with mixed layer rates more than an order of magnitude higher than bottom waters. The higher rates within the upper layer appear to be the result of the higher POC levels and more than 10°C higher temperatures. In addition to the quantity of POC, the quality of the organic matter also favors higher respiration within the surface waters. By correcting the in situ rates for the variable POC levels (i.e., the carbon-specific respiration rate), it is possible to gain insight into variations in organic matter quality (i.e., liability) with depth (Figures 7-54a, b). During the mixed period, the water column is generally isothermal so that similarity in carbon specific rates over depth can only be the result of similar substrate quality. At these times it appears that accelerated delivery of POC to bottom waters results in similar substrate quality (though not quantity) throughout the water column. However, during the stratified period, differences in substrate quality, in addition to substrate quantity and temperature, appear to be a primary factor supporting higher surface versus bottom water rates. In fact, the surface to bottom difference in carbon-specific respiration during the stratified interval is a factor of 2-3 higher than is typically due to temperature effects alone.

Additional support for the importance of organic matter quality/delivery is demonstrated by the spike in bottom water carbon-specific respiration during the August "advection" event (Figures 3-2, Section 7.2 above). The August (and subsequent) samplings of the nearfield showed elevated carbon-specific respiration at depth. It appears that the late summer increase in production, combined with the August physical event, resulted in a shift in the organic matter field in the bottom waters. This shift can be seen as a step increase between Surveys W9611 and W9612 in the total respiration rate (Figure 7-50) and surveys W9607 and W9608 versus W9610 and W9611 in the carbon-specific rates of the bottom water. These results indicate both an increase in the delivery of available substrate and an increase in its liability, which is consistent with both accelerated particle delivery (through zooplankton grazing or mixing) and increased euphotic zone production.

It is possible to determine the relative importance of temperature versus organic matter quantity and quality effects on water column respiration by evaluating the relationship of carbon specific respiration to environmental temperature. Nearfield and Stellwagen Basin stations exhibited a direct relationship between the rate of oxygen uptake per unit carbon and the environmental temperature (Figure 7-55, 7-56), although the relationship is not equally apparent within each of the two regions. In the nearfield, a positive relationship appears only at the higher temperatures (ca. 8-18°C), which predominate the data from the stratified interval and early fall. The reasons for this is currently unclear, but is likely related to the wide variation in carbon quality from the winter and early spring blooms, which obscures the effect of temperature at the lower range. In contrast, during the stratified interval, carbon quality may be relatively more constant and temperature effects, therefore more apparent.

The results from Stellwagen Basin show a much clearer picture of the temperature effects. When the mixed layer data are analyzed, a clear linear relationship with temperature is seen with a calculated Q10 of 2.9 (compared to 2.5 for the 1995 data alone). The lack of a relationship in the bottom water respiration is almost certainly due to large seasonal differences in organic matter quality (high during mixed period versus low during stratification), which again obscures the temperature effect. The results indicate that both temperature and substrate quality are responsible for the vertical structure in oxygen uptake in this system. The 10-fold differences in carbon-specific respiration in the bottom water within the same temperature regime (compared to the ca. 3-fold temperature effect) is testament to the limitation of respiration by the quality of organic substrate. Therefore, during the interval when input of oxygen from surface waters is restricted, factors that increase either the delivery of labile organic matter to bottom water, or bottom water temperature, should serve to increase respiratory oxygen demands.

7.2.1.2 1992 - 1996 Interannual Comparison

Water column respiration rates were not a focus of study during the 1992-1994 monitoring effort. As a result interannual comparisons are limited. In addition, since respiration was measured on only six surveys, seasonal comparisons between years are not supported. Sufficient data do exist from 1994 (Kelly and Doering, 1995) from which to make some general observations. However, no bottom water respiration data were collected during 1994. The first year of comprehensive water column respiration measurements was 1995, so that most of the discussion will involve only 1995 and 1996 results.

Water column respiration within both the nearfield (N04, N16) and Stellwagen Basin (F19) showed similar patterns and rates in 1995 and 1996 (Figures 7-58, 7-59). While the rates in the nearfield varied throughout the year, respiration rates during the spring bloom were generally similar throughout the water column. During the stratified period, distinctly higher rates occur in surface and mid-water versus bottom water as discussed previously. Similarly, Stellwagen Basin respiration rates were consistent between years.

While the data vary, surface water respiration rates within the nearfield in 1994, 1995 and 1996 were generally higher than offshore, consistent with the lower levels of chlorophyll a at the offshore stations (Figure 5-11, 5-12). In addition, the general trend of significantly higher respiration rates in surface versus deeper waters was observed in all years. However, the vertical distribution of respiration rates was not as obvious in 1994 between nearfield and offshore stations (e.g., Figure 19 in Kelly and Doering, 1995). Unfortunately, the limited sampling does not allow a rigorous comparison of rates in mixed versus stratified water column. However, the magnitude of the Kelly and Doering's model-projected bottom water respiration in 1994 (Kelly and Doering, 1995) was higher than that measured in 1995 or 1996. The lowest nearfield projected rate in 1994 was ca. 0.05 mg O2/L/d, while the average bottom water measured rate during stratification in 1995 (Mean (SE)) was at N04 (0.016 (0.003) mg O2/L/d) and N16 (0.018 (0.001) mg O2/L/d), and in 1996 at N04 (0.019 (0.003) mg O2/L/d) and N16 (0.015 (.003) mg O2/L/d). Only at the eastern most, shallowest, Harbor influenced station (N10) did the bottom water respiration approach the earlier modeled rates, 0.046 (.012) mg O2/L/d.

At this point it appears that the model, as parameterized, does not yield realistic rates. The probable causes of this result are: (1) the model is based upon 1994 surface and mid water respiration rates, which include the large seasonal influences of both carbon quality, quantity, and temperature. In both 1995 and 1996 there was a lack of correlation between surface and bottom water respiration rates at all stations (particularly during stratification, Figure 7-57); (2) the model employs data collected throughout the year, while 1995 and 1996 results document seasonal differences in carbon quality (Figure 7-54, Cibik et al. 1996); and (3) the model combines inshore and offshore rates, ignoring the horizontal gradient in respiration.

If the projected bottom water respiration rates in 1994 were accurate, the cause for the higher rates is unknown. It does not appear to be related to concentrations of POC (Figures 7-45) which were higher in 1995 when measured respiration rates were lower. Nor does the difference in respiration relate to differences in temperature during sampling (Figure 3-4). It is most likely that the differences in rate result from limited data in 1994, which did not capture the sharp decrease in respiration from surface to bottom waters, and the fact that consideration was not given to seasonal differences (all data were pooled). Modeling vertical changes in rates requires that the temperature and organic matter quality and quantity show constant differences year-round. It is now clear that these factors controlling respiration rates show significant differences between stratified versus vertically-mixed periods.

7.2.2 Sediment Respiration

Annual oxygen uptake by benthic sediments is a measure of total community metabolism which controls organic matter turnover within the benthos. Total community metabolism includes the respiration of benthic animals and plants, as well as carbon remineralization by heterotrophic microorganisms. Sediment respiration is similar to water column respiration in that it is controlled primarily by the availability of decomposable organic matter and in situ temperature. However, it differs in three major aspects. First, sediments can accumulate organic matter inputs over relatively long periods and therefore allow cumulative increases in oxygen uptake as organic matter is deposited over periods of weeks to months. Organic particles within the water column typically have relatively short residence times, especially in the non-turbulent waters below the pycnocline. Therefore, deposition into sediments represents the mechanism for potential carryover of Fall or Spring bloom material into the stratified period.

Second, the water column throughout the nearfield and Stellwagen Basin appears to be fully oxygenated, whereas, oxygen penetration into the sediments of these systems is relatively shallow (centimeters). The result is that in the sediments, unlike the water column, a fraction of the organic matter decay is through anaerobic microbial processes, such as denitrification and sulfate reduction. Denitrification, although at present not a major pathway for carbon mineralization, represents an important potential sink for fixed nitrogen, particularly if concentrations of nitrate in the overlying water increase (Section 4). Within deeper sediments, sulfate reduction produces sulfide as an end-product, some of which is permanently stored within the sediments as metal sulfides, but most of which is re-oxidized to sulfate on an annual basis. However, due to the time-lag between sulfide formation in the deeper anoxic layer and oxidation of sulfide by surface exchanged oxygen, single time-point estimates of the rate of surface oxygen uptake can either over- or underestimate the rate of carbon mineralization

taking place. In most systems, an amount equivalent to the mass of sulfide produced over the course of a year is oxidized each year (except for that permanently buried), thus the annual oxygen uptake rate reflects the annual carbon remineralization rate.

Furthermore, in systems like Massachusetts Bay, carbon flow through sulfate reduction is almost certainly small relative to aerobic processes and therefore errors due to the sulfide oxidation time-lag are likely very small even on single time-point samples. Increases in the mass of total reduced sulfur and/or non-pyritic reduced sulfur over several years has been suggested as an indicator of an increase in the rate of organic matter loading to sediments. While reduced sulfur pools can reflect loading rates, they represent the residue of the much larger reduction-oxidation cycle. In contrast, annual sediment oxygen uptake rates represent the total carbon remineralization rate, which should be a direct indicator of the annual loading of decomposable organic matter to the benthos.

Third, while both water column and sediment oxygen uptake affect bottom water oxygen levels, water column uptake is distributed throughout the hypolimnion, whereas sediment uptake is concentrated at the sediment-water interface. Only through mixing, diffusion, etc. does sediment oxygen uptake interact with the full hypolimnion. The result is that the deepest waters of a system typically contain the lowest concentrations of oxygen on an annual basis (see Section 5). The increased distance from the oxygen "source" in the overlying mixed layer further influences this phenomenon. In addition, sediment oxygen dynamics are important on an ecological basis in that where low oxygen or high sulfide levels occur, infaunal populations, hence food chain dynamics, are affected.

For these reasons, and the fact that sediments can be reliably re-sampled over a prolonged interval, sediment oxygen and nutrient dynamics have been measured over several years in the monitoring program. In 1995 and 1996, in concert with the detailed water column respiration and photosynthesis measurements, sediment respiration was assayed at 4 stations during 5 events each year. Issues to be addressed involve the role of sediments (along with water column respiration) in system carbon/nutrient mineralization and bottom water oxygen depletion, and their sensitivity as an indicator of organic matter loading rates.

Sediment oxygen uptake within the sediments of the western nearfield and Stellwagen Basin show a seasonal cycle linked to temperature and organic matter availability. All sites showed increasing oxygen uptake with initially increasing bottom temperatures. However, the overall pattern of respiration differed in some major respects between the years. Although in the nearfield the rates of oxygen uptake during the stratified interval compared well between 1995 and 1996, different rates were evident during the mixed interval. In 1996, during winter and early spring the sediments were about two times as active as during 1995. In contrast, during the late fall mixed interval, all of the stations showed a decline in rates not seen in 1995, even under steadily increasing temperatures. The temperature cycle was very different from that of the surface waters (see Section 3). Temperature was highest on the last survey in early October near the time of overturn (Figure 3-1C).

It is the interplay of organic matter delivery and temperature that generates the seasonality in sediment respiration. The effect of the temperature cycle is to produce the highest rates of respiration during the stratified period and fall and lower rates during the winter and early spring prior to stratification. The effect of the colder

pre-stratification waters should be to help to "preserve" freshly deposited spring bloom material until waters warm. This warming occurs post-stratification. The effect of the warmer sediments during the fall bloom should be to promote the degradation of freshly deposited bloom material. Given the temporal sequence, much of the fall bloom is likely degraded prior to the onset of stratification during the following spring and summer.

Since water column mixing occurs at the fall bloom (and is intricately associated with it, Sections 4 and 7.1), the effect of the fall bloom on the bottom water oxygen deficit is unclear. The data suggest that the significantly larger spring bloom in 1996 may have been responsible for the higher rates of sediment remineralization during the first half of the year, compared to the same period in 1995. These high rates of decay appear to have consumed much of the deposited labile pool from the spring bloom by the end of the stratified period. This consumption, coupled with the lower summer time production in 1996 versus 1995, may underlay the drop off in rates by the late September-early October survey. The decline in sediment remineralization rates by the final survey, which was during the fall bloom and at high environmental temperatures, is consistent with the temporal lag between the organic matter production and delivery to the sediments. The maximum effects of the 1996 fall bloom on sediment respiration most likely occurred after the final sediment survey.

Given the significance of benthic respiration to the overall bottom water oxygen balance during stratification, as well as the seasonal distribution of rates, it appears likely that the spring bloom plays a more important role in oxygen deficits than the fall bloom. As stated for water column respiration (section 7.2.1.2), factors that increase delivery of organic matter through the pycnocline during stratification should result in increased levels of annual oxygen depletion in bottom water in both the nearfield and Stellwagen Basin. Before it is possible to determine the proportional increase in oxygen deficit per unit carbon deposited, an evaluation of the potential lability of the organic matter delivered must be evaluated.

7.2.3 Cycles of Carbon Fixation, Remineralization and Oxygen

While water column mixing and stratification play the major role in mediating the vertical distribution of respiration rates through temperature and organic matter delivery, the ultimate factors controlling respiration is the timing and mass delivery of labile organic matter input from both photosynthesis and allochthonous sources. While the role of allochthonous sources requires further examination, it is clear that respiration within the euphotic zone generally parallels the measured rate of carbon fixation (Figure 7-59, 7-61). Departures from this trend typically are related to bloom events where production typically exceeds respiration (and sinking), which allows biomass to increase (Figure 7-61). However, major photosynthetic events do show increases in respiration rates due to increased biomass. This bloom effect is typically strongest in the fall bloom, possibly due to its longer duration and warmer water temperatures. But it is during the summer stratified interval, when organic matter pools are lowest, (Figure 7-53) that the closest coupling is seen between respiration and photosynthesis (Figure 7-59).

It also appears that there frequently is a temporal lag during the stratified interval between major production or delivery events and increases in bottom water respiration. This lag can be seen in the 1995 data, where a mid-summer bloom peaked during W9512 (with a parallel peak in mixed layer respiration), but the bottom water

response was not seen until the following survey (W9513). Similarly, the bottom water respiration maximum during the spring bloom and fall bloom intervals in 1996 did not occur until the survey following the production maxima (W9602 vs. W9603, W9613 vs. W9614). Given the variability in daily photosynthesis with light field (cf. Sect. 7.1) relative to the greater temporal averaging which occurs in the factors controlling respiration rates, the photosynthesis/respiration relationship observed within the euphotic zone is reasonable. Although variable, it appears that carbon fixation exceeds respiration within the euphotic zone throughout the year, but also that in situ respiration remineralizes an amount nearly equivalent to fixation. As noted in the previous section, since almost all of the carbon fixed by photosynthesis occurs within the mixed layer, both organic matter quantity and quality are always highest within this zone (Section 7.1).

The near equivalence in organic matter production and remineralization within the euphotic zone (predominantly within the mixed layer), serves as a "biofilter", reducing organic matter transport to bottom waters during stratification. The lower bottom water respiration rates found throughout the nearfield and offshore stations during stratification are consistent with a low delivery of organic matter (Figure 7-50, 7-52, 7-57). However, as stated above, factors that increase organic matter delivery can increase oxygen uptake from bottom waters. One such event may have been associated with the centric diatom bloom during September 1995, surveys W9512 and W9513. The spike in bottom water respiration during survey W9513 may have been related to delivery of bloom material to bottom waters as the bloom underwent senescence. The die-off of the centric diatom bloom coincided with the initial breakdown of stratification, which provides a mechanism for increased vertical transport. However, it is also possible that the high zooplankton populations during this bloom also facilitated vertical transport through fecal pellet formation (Cibik et al., 1996).

The importance of this process to bottom water respiration and DO was seen in a series of similar events during the stratified interval in 1996. The first event followed a of the water column in mid-July. The result was a large increase in production (W9609) and an approximate two-fold increase in bottom water respiration rates by the following survey. However, rather than a spike in respiration, rates remained high, most likely due to the continued disturbances to the water column (presumably with enhanced particle transport) by the major storms which occurred in rapid succession during September (Figure 3-2).

Under existing conditions, seasonal variations in bottom water oxygen uptake appear to be dominated by the availability of organic matter (with secondary temperature effects). High rates of bottom water respiration occur during the unstratified intervals, when vertical transport of POC is uninhibited and carbon fixation from the high productivity periods (i.e., late winter and fall blooms) is greatest. In contrast, during the stratified period, bottom water respiration remains low, consistent with the generally small pool of chlorophyll a and low rates of photosynthesis within the mixed layer (see Section 7.1). During stratification, the vertical transport of organic matter to deeper water is restricted both by the strong pycnocline and by the significantly increased respiratory capacity of the surface waters due to the warmer summer temperatures (Q10=2-3). However, it is becoming clear that during the stratified interval, there is a highly labile organic matter pool within the surficial mixed layer and that large increases in bottom water respiration result when physical processes enhance the vertical transport of this pool. This conclusion is supported by the observed stimulation of bottom water respiration associated with short-term mixing and advection events, and the onset of fall destratification. This response is consistent with strong vertical gradients in both the quality (Figure 7-54) and quantity (7-62) of organic matter within the water

column. It appears that oxygen dynamics within the nearfield during stratification, while controlled in part by the onset and duration of stratification, are also strongly influenced by the timing and extent of organic matter delivery to the bottom waters and sediments.

While the major site of organic matter decay throughout the year is in the water column, particularly in the mixed layer, the sediments become relatively more important during stratification due to the "starvation" of bottom water by reduced organic matter transport through the pycnocline (Figure 7-62). The importance of the sediments to the stratified interval DO decline varies inversely with the depth of the water column. In the nearfield, sediments account for more than half of the oxygen uptake compared to only about one-third in Stellwagen Basin (Table 7-3).

The relative roles of water depth and sediment versus bottom water respiration on the DO pool can be evaluated from the high resolution DO profiles (Figure 7-63). During the stratified interval, the gradient in DO below the pycnocline is relatively small in spite of the relative importance of sediment respiration. This is consistent with some degree of vertical "mixing' below the pycnocline, which prevents significant oxygen minima just above the sediment-water interface, although the rate is likely low as a DO gradient remains apparent at most sites. Further evaluation of the vertical time-series indicates that the onset of destratification in the fall (Figure 7-64) occurs earlier at the shallow water inshore stations. This provides a mechanism to reduce the annual extent of DO depletion at these sites where respiration is highest. It is clear that the bottom waters of the deeper water sites have a longer interval of stratification than inshore. The impact of this longer interval is currently offset by the lower respiration rates in the sediments and water column with increasing distance from shore. This longer interval for oxygen decline provides a mechanism for increased sensitivity of the offshore areas to oxygen declines due to increased organic matter delivery during the stratified interval or possibly during the spring bloom.

While we will continue to evaluate the relative importance of the spring and fall bloom versus production during the stratified interval to sediment respiration and annual DO depletion, we can make some preliminary findings. From the available 1995 and 1996 results it is clear that water column respiration is important in intercepting labile carbon before deposition. During stratification, interception by respiration is complemented by decreased rate of delivery due to the presence of the pycnocline, resulting in decreased bottom water respiration even as temperatures warm. However, since the spring bloom occurs during the mixed interval, the delivery of bloom material to the sediments is unimpeded. In addition, unlike the fall bloom when water temperatures and respiration rates are high, spring bloom material is formed and transported during an interval of low temperature and relatively low respiration.

The approximately two-fold higher sediment respiration rates during the spring and early stratification periods in 1996 relative to 1995 is consistent with the much larger spring bloom in 1996 (largest of the baseline period, see Section 5). However, the lower summer production during 1996 versus 1995, the short-term ventilation events, and the early onset of mixing all combined to prevent significantly low oxygen minima for 1996. We can only conclude that annual oxygen mimina within Massachusetts Bay are controlled by both fine-scale physical features and large-scale physical–biological processes. The fine-scale physical features control short-term

organic matter delivery to the sediments, either through direct transport or by stimulating bloomlets by altering nutrient regimes. The large scale physical-biological processes structure the magnitude of the spring bloom and the timing of its deposition relative to stratification. Large-scale physical processes control the onset and duration of stratification and de-stratification within Massachusetts Bay. The data indicate that factors which increase organic matter delivery to the bottom waters in spring and summer are likely to result in enhanced DO depletion.

Measurement	Station N10	Station N04
Production on Day of Cruise	107	118
Potential Production	180	257
Potential Production Envelope	219	265
High Resolution Production	168	202

TABLE 7-1
Areal Production (gCm^{-2}) between August 8, 1996 - December 31, 1996

Station	1994, 1995					
	Slope	Error (%)*	Intercept	Error (%)*	r^2	n
F23	1.87	± 0.18 (9.6)	-574	± 641 (112)	0.96	6
N16	0.64	± 0.11 (17)	317	± 578 (182)	0.68	17
N07	0.43	± 0.23 (54)	322	± 377 (117)	0.48	6
N04	0.39	± 0.084 (22)	440	± 330 (75)	0.58	17
Kelly, et al.;1994**	0.61	--	-94	--	0.53	22
Kelly, et al.;1994**	0.56	--	20	--	0.73	12

Station	1996					
	Slope	Error (%)*	Intercept	Error (%)*	r^2	n
F23	0.88	±0.65 (74)	700	±1780 (254)	0.31	6
N10	0.85	±0.15 (18)	480	±851 (177)	0.68	17
N16	0.56	±0.10 (18)	422	±425 (101)	0.88	6
N04	0.23	±0.10 (43)	728	±652 (90)	0.25	17

* Standard error of estimate.

** Kelly and Turner, 1995; Kelly and Doering, 1997.

TABLE 7-2
Coefficients for Linear Regression of ^{14}C- production vs. BZ_pI_o

Source of O_2 Uptake	Year	Rate (mg/L/d)	% Observed Decline
Nearfield: D.O. Depletion	1995 1996	-0.027 -0.025	100 100
Watercolumn Respiration	1995 1996	-0.016 -0.015	61 60
Sediment Respiration	1995 1996	-0.021 -0.023	78 92
Total Respiration	1995 1996	-0.037 -0.038	139 152
Stellwagen Basin: D.O. Depletion	1995 1996	-0.015 -0.014	100 100
Watercolumn Respiration	1995 1996	-0.011 -0.013	73 92
Sediment Respiration	1995 1996	-0.004 -0.005	29 35
Total Respiration	1995 1996	-0.015 -0.018	101 128

TABLE 7-3

Contribution of Watercolumn and Sediment Respiration to Bottomwater Oxygen Decline in the Nearfield and Stellwagen Basin, 1995 and 1996

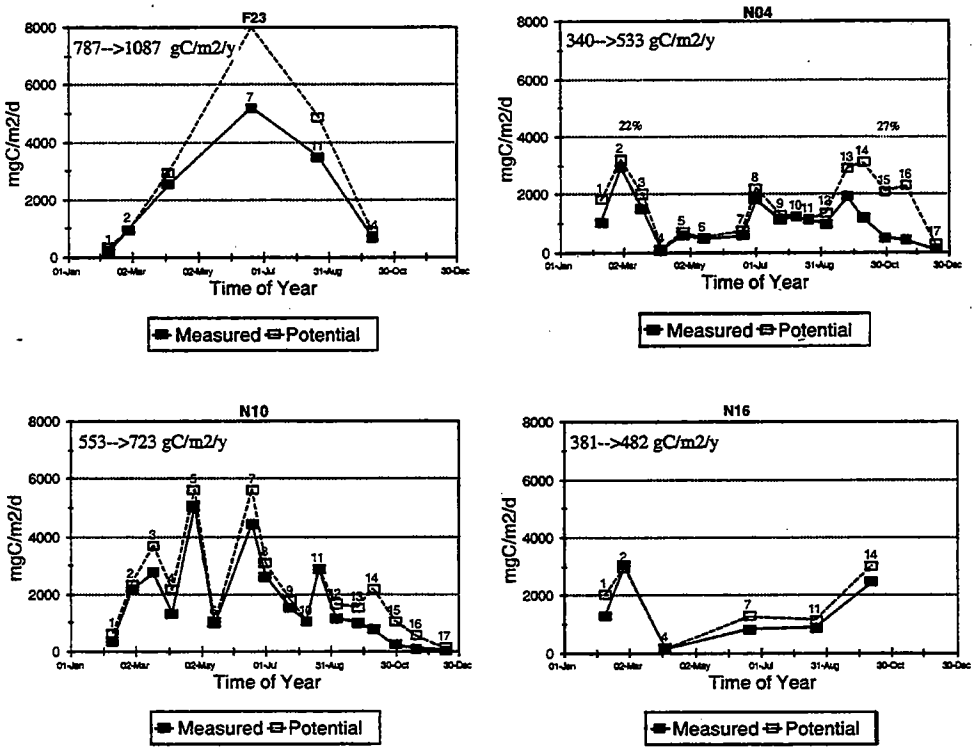

Figure 7-1

Areal production and potential areal production for the 1996 season. Areal production was determined using the incident light regime on the day of the cruise. Potential areal production was determined using a theoretical incident light regime that is equivalent to a cloudless day at the indicated time of year. Annual production and potential annual production is indicated by the range respectively depicted in the inset of each panel. Survey numbers indicated by the numbers above each datum point.

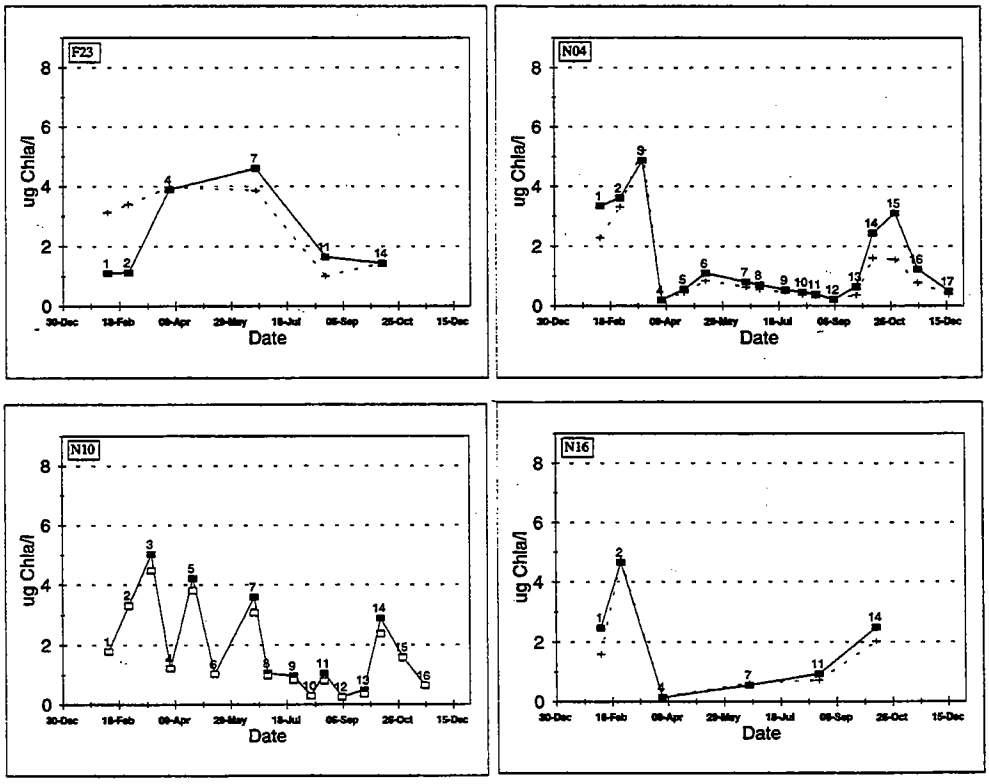

Chlorophyll Distribution in 1996

FIGURE 7-2

Chlorophyll-*a* distribution at the harbor edge and nearfield in 1996. Open and closed squares, average chlorophyll-*a* concentration in the photic zone above the 0.5% light level. Crosses, average chlorophyll-*a* concentration in the entire water column.

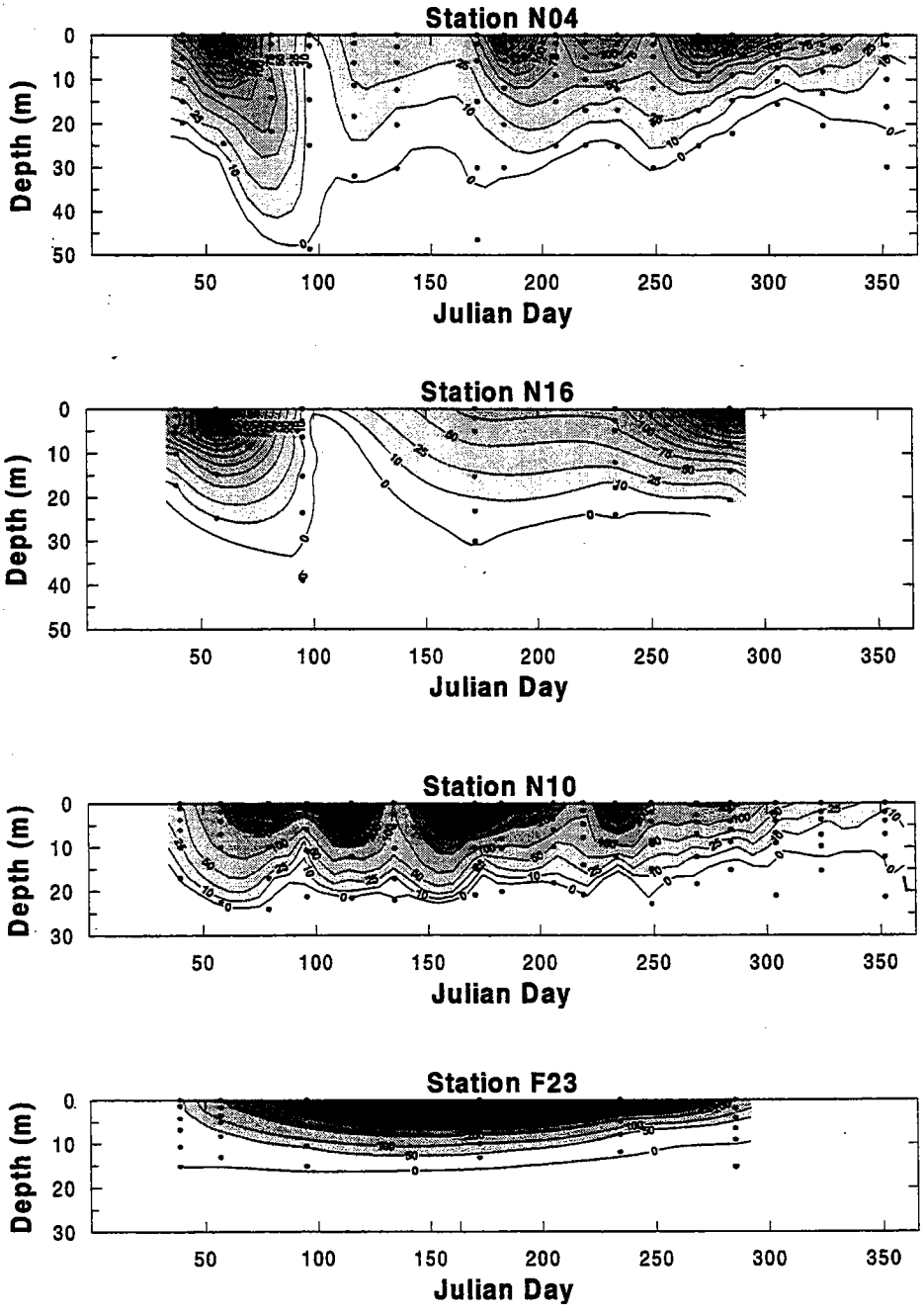

FIGURE 7-3
Daily production. Contour values expressed in $mgCm^{-3}d^{-1}$.

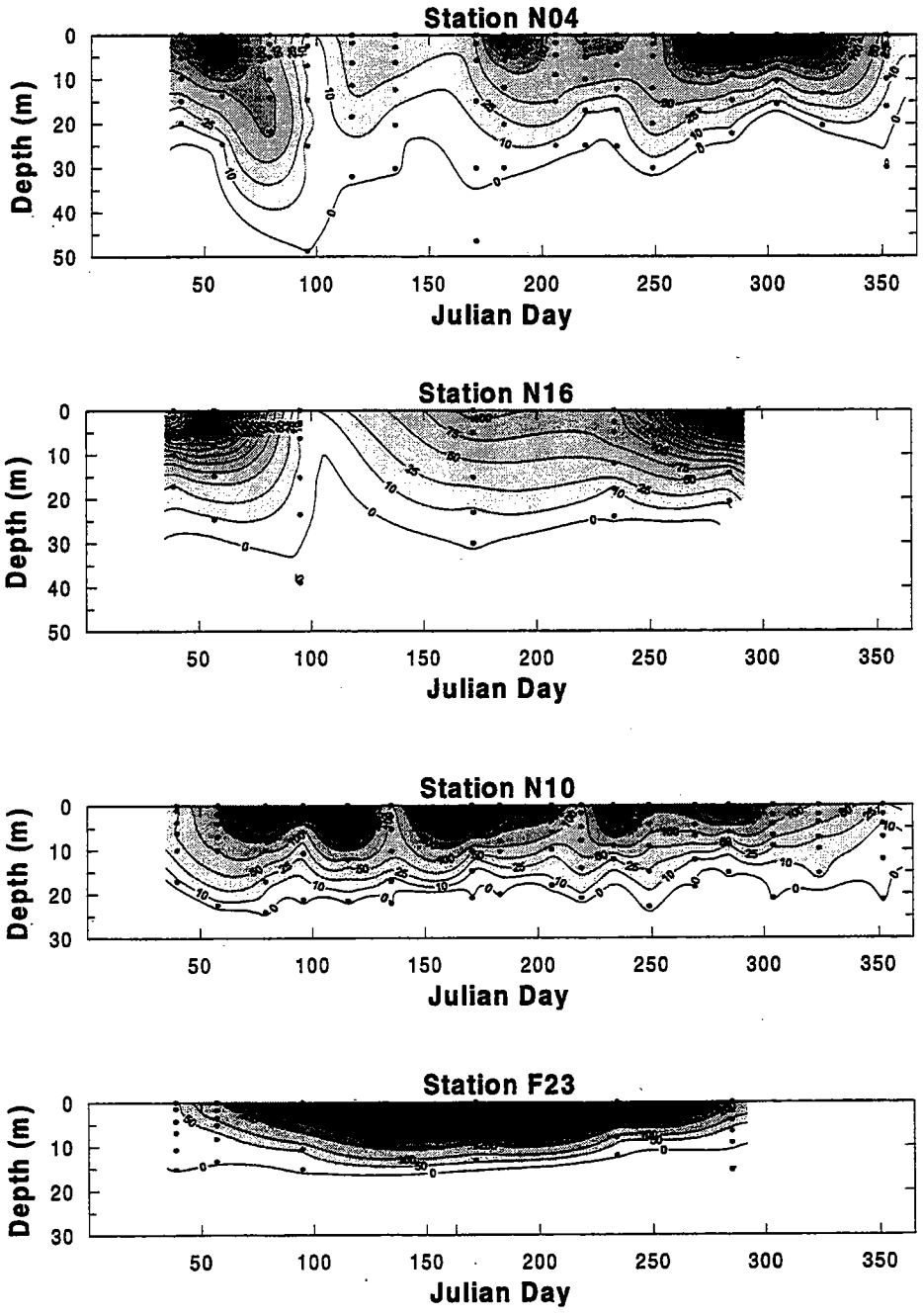

FIGURE 7-4
Potential daily production. Contour values expressed in $mgCm^{-3}d^{-1}$.

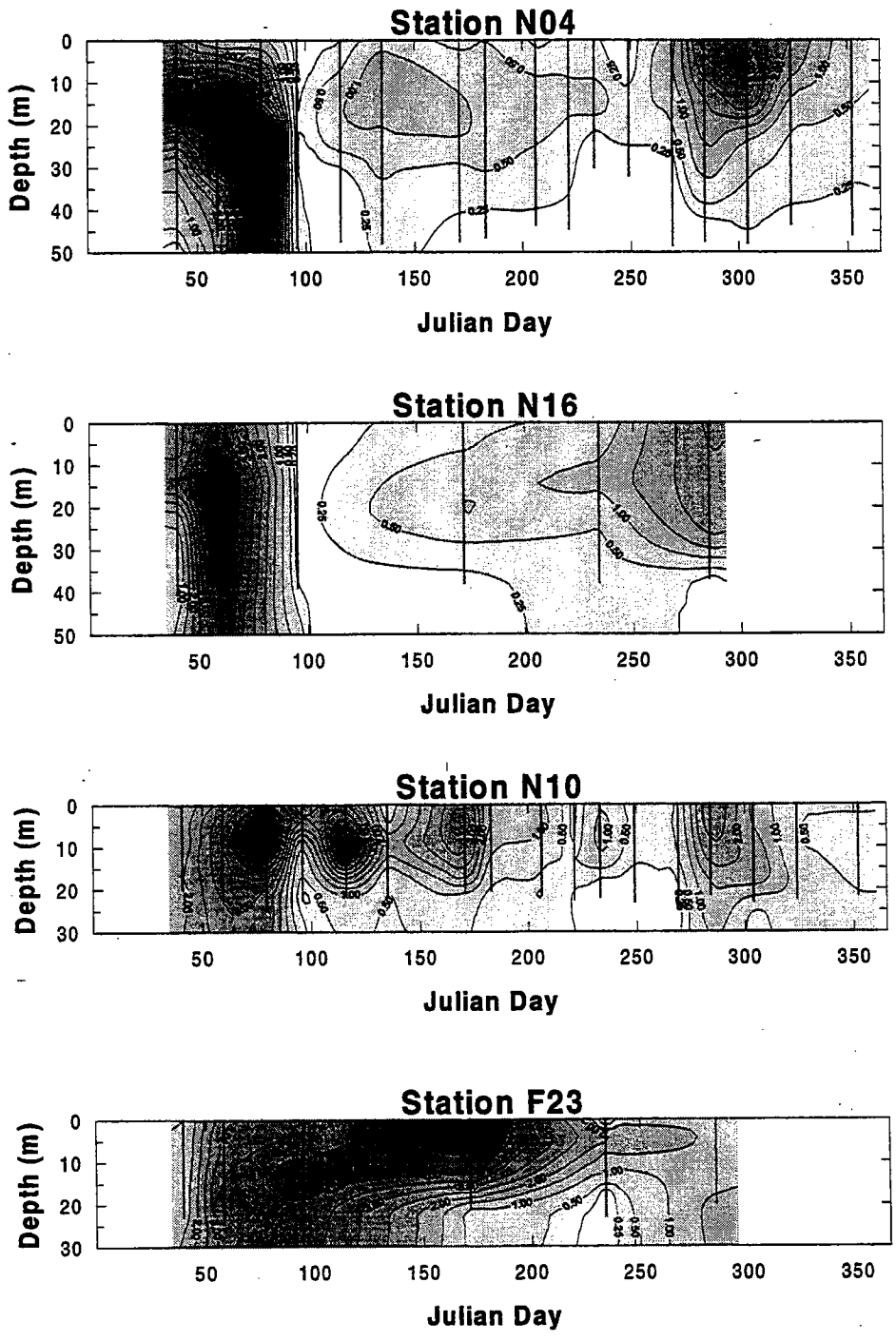

FIGURE 7-5

Chlorophyll-*a* distribution in the water column of the harbor edge and nearfield region in 1996. Dotted vertical lines represent date and depth of fluorescence measurement.

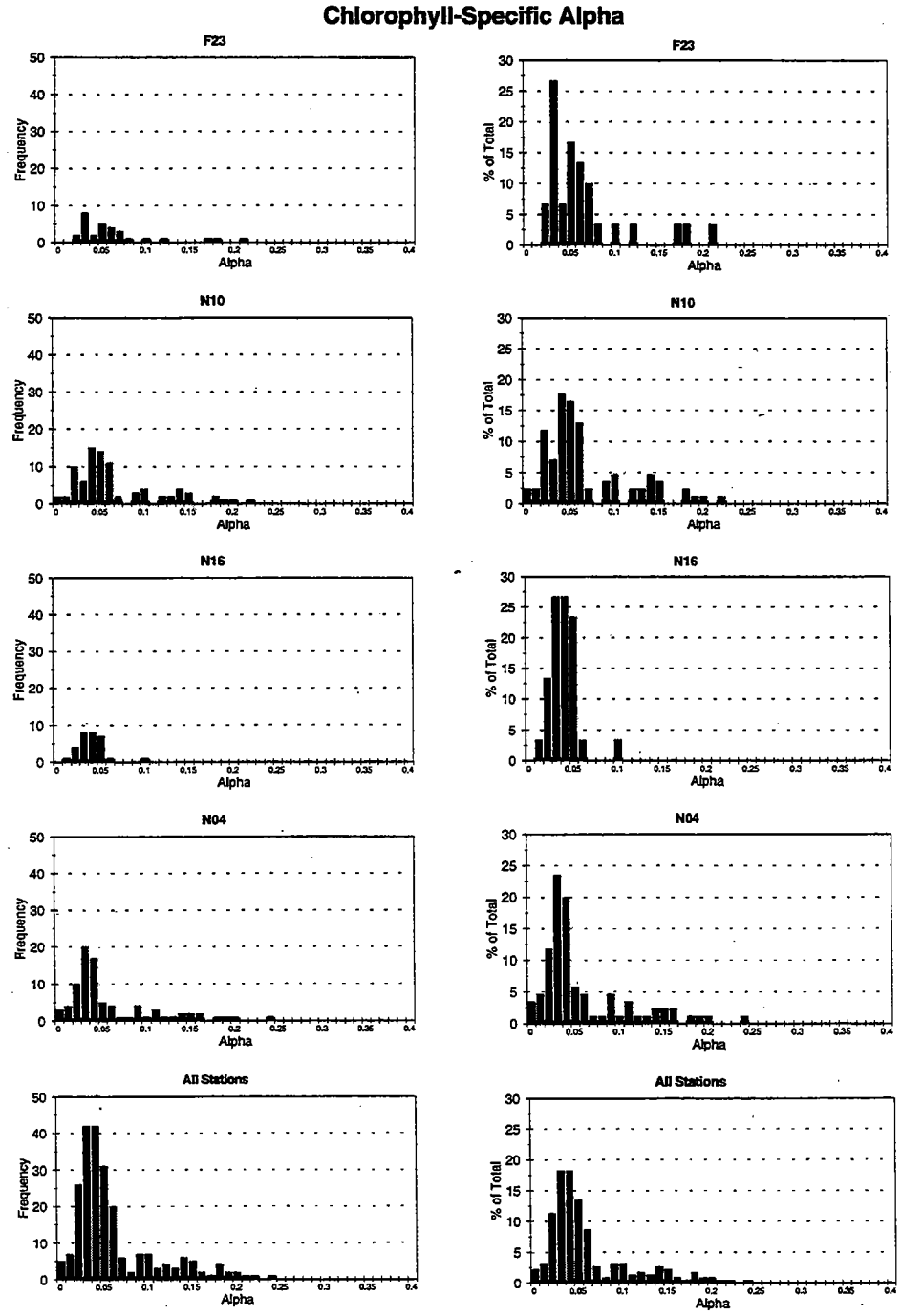

FIGURE 7-6
Frequency distribution for chlorophyll-specific alpha for Stations F23, N10, N16 and N04 in 1996.

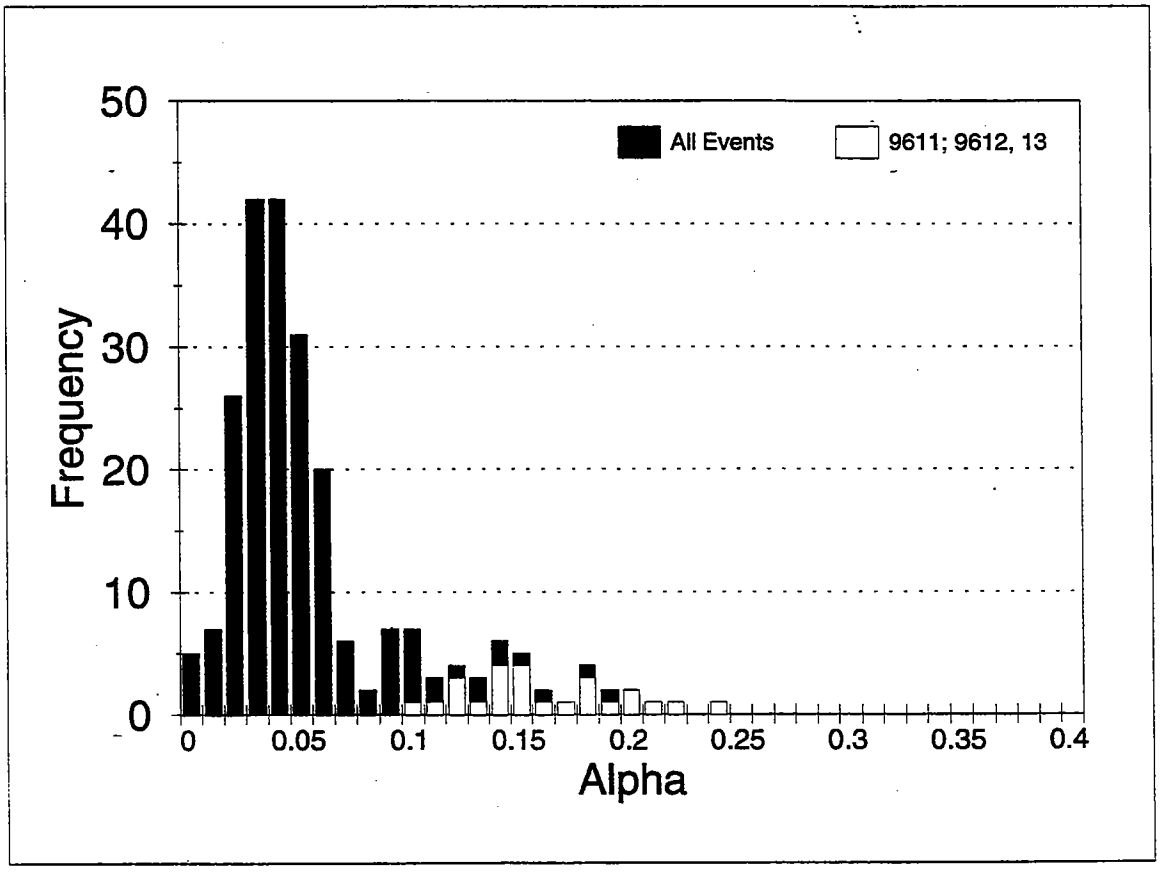

FIGURE 7-7

Frequency distribution for chlorophyll-specific alpha for Stations F23, N10, N16 and N04 for select surveys in 1996. White bars represent frequency distribution of data from surveys W9611, W9612, W9613.

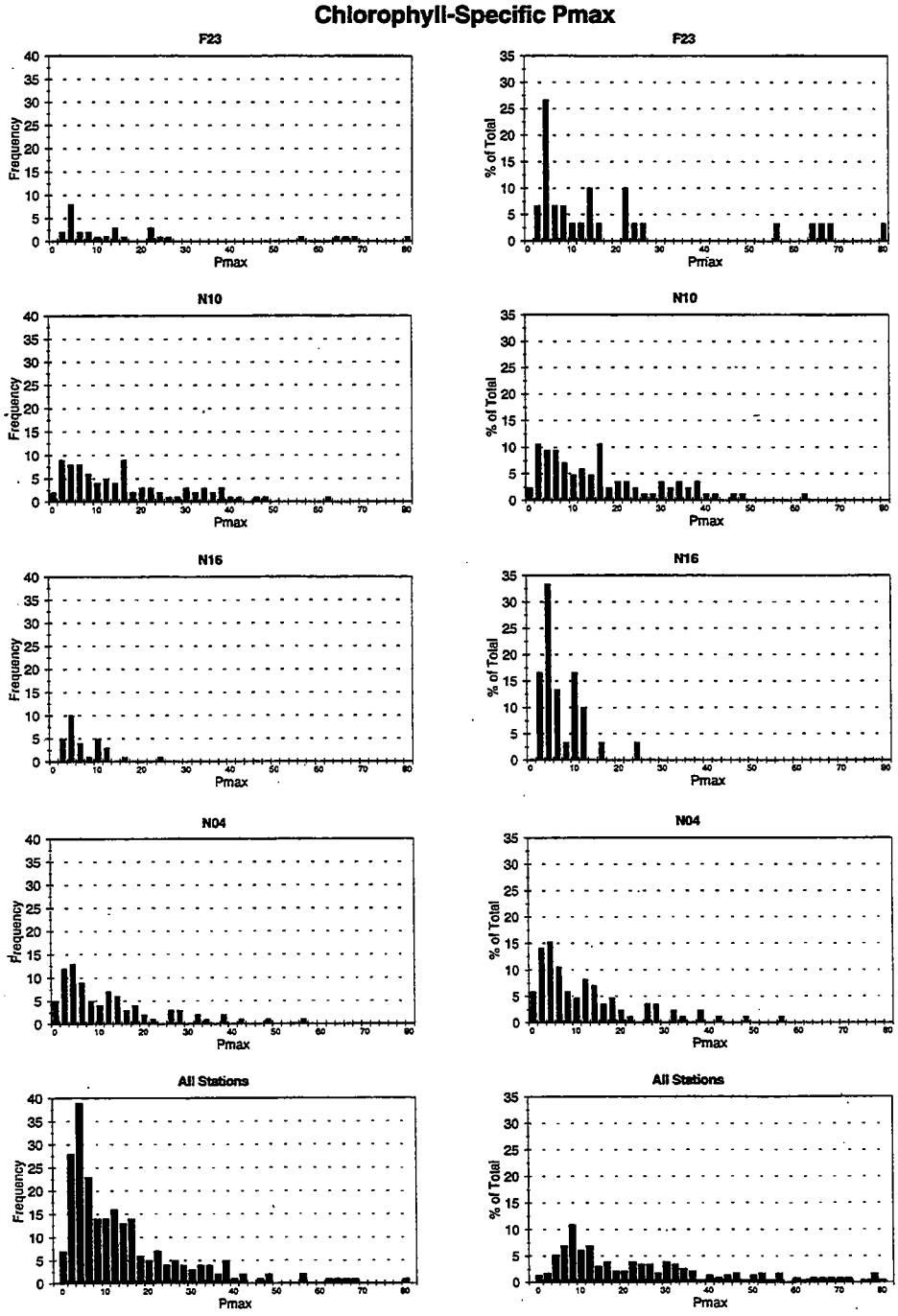

FIGURE 7-8
Frequency distribution for chlorophyll-specific P_{max} for Stations F23, N10, N16 and N04 in 1996.

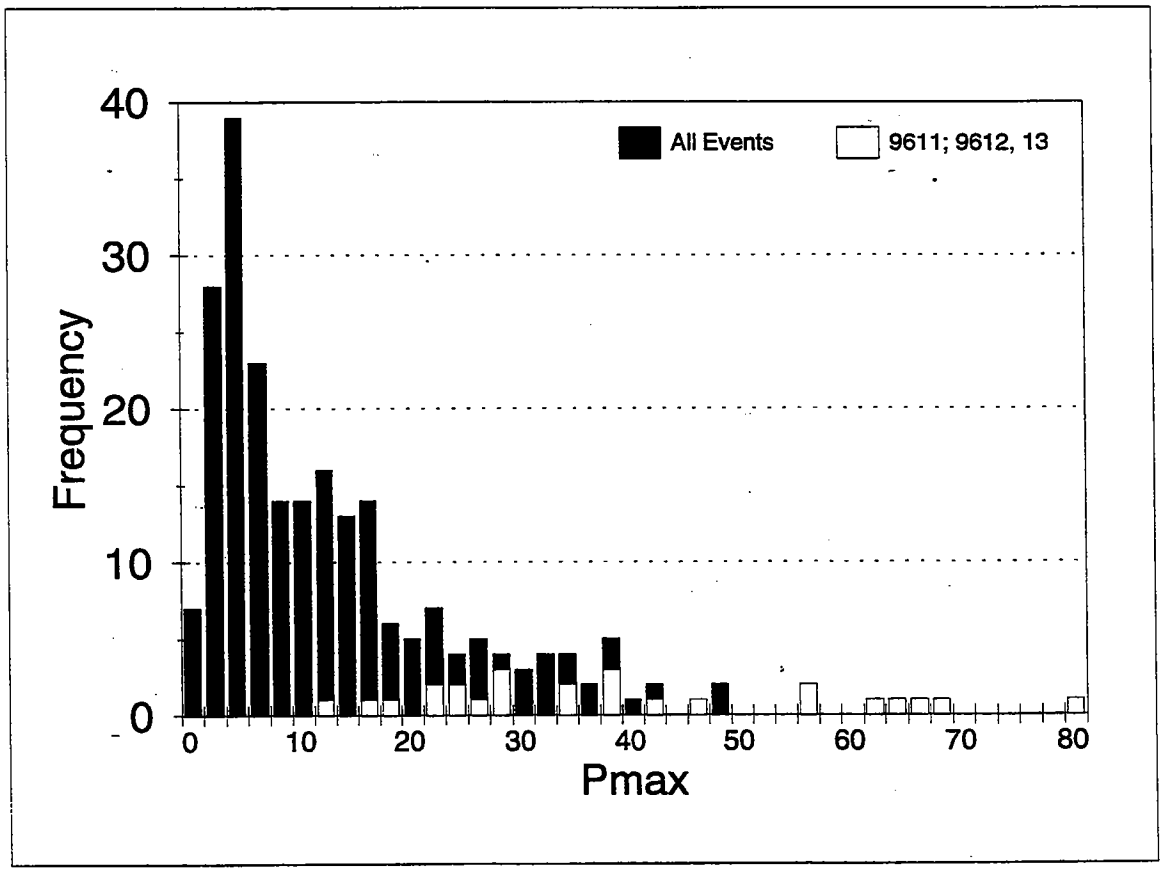

FIGURE 7-9

Frequency distribution for chlorophyll-specific P_{max} for Stations F23, N10, N16 and N04 for select surveys in 1996. White bars represent frequency distribution of data from surveys W9611, W9612, W9613.

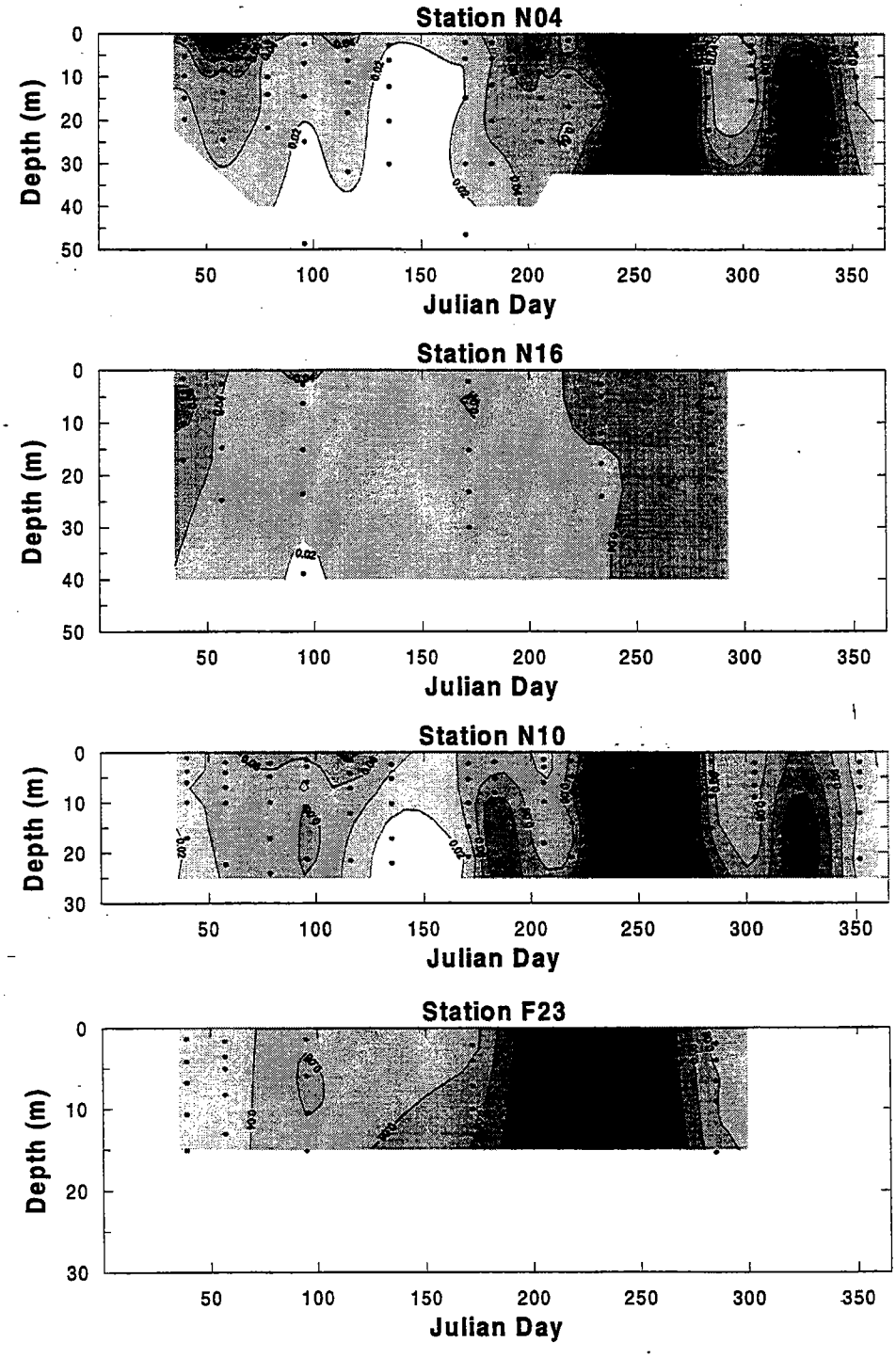

FIGURE 7-10
Contour plot of chlorophyll-specific alpha for 1996

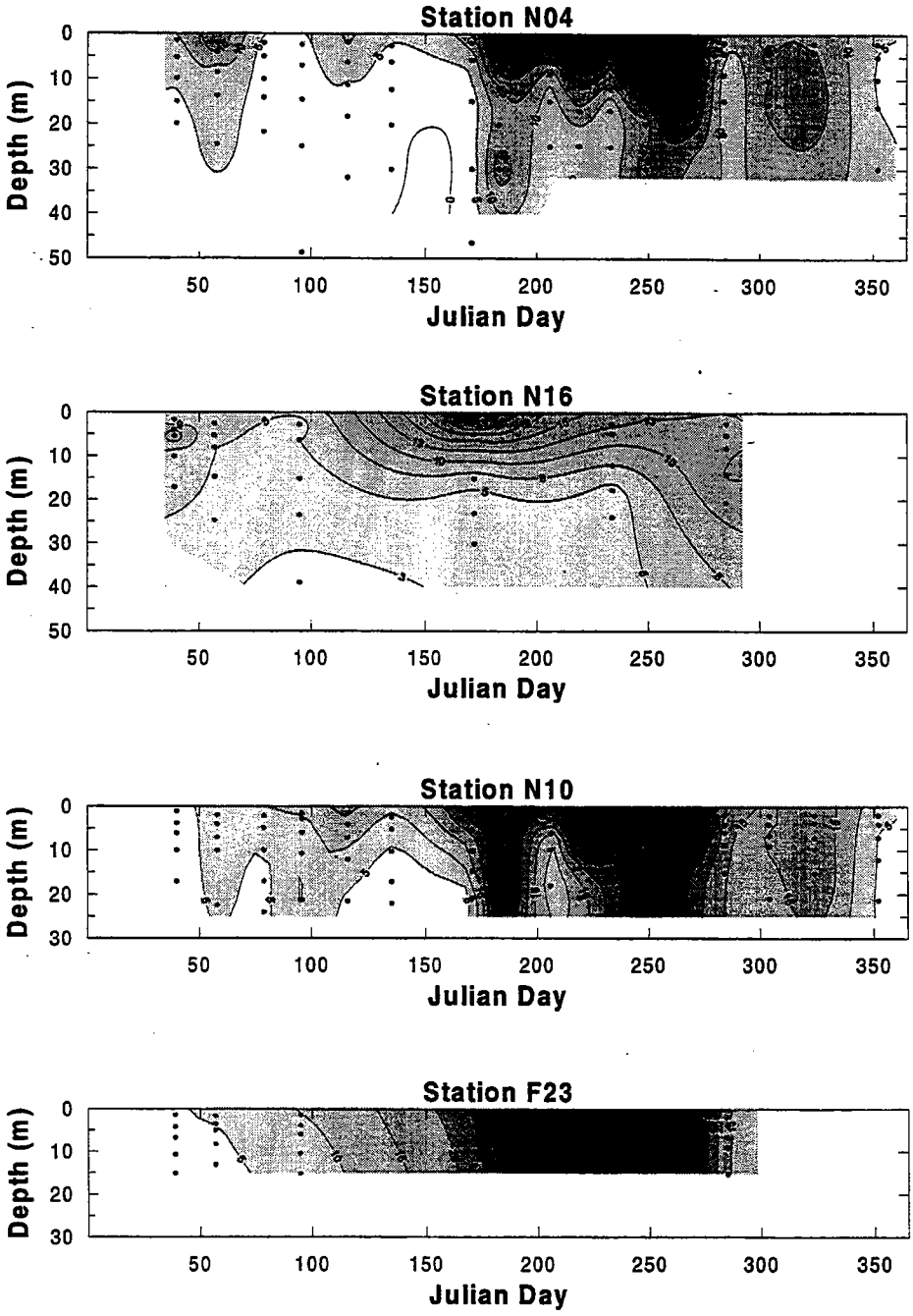

FIGURE 7-11
Contour plot of chlorophyll-specific P_{max} for 1996

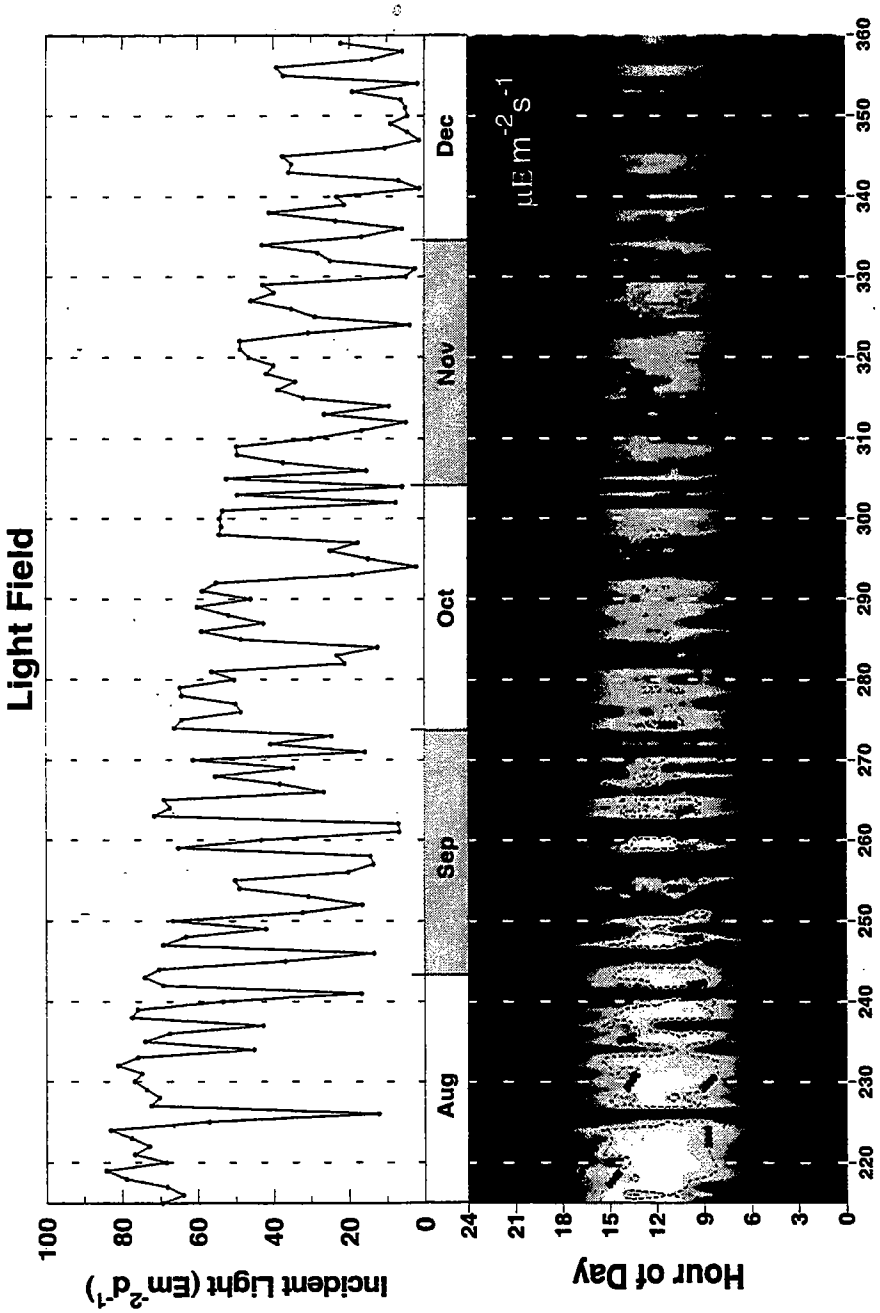

Figure 7-12
Incident light field in the fall of 1996. Upper panel, integrated incident light obtained by summation (BASIC program) of the 15 min sensor readings (uEm-2s-1) multiplied by 900 sec (sample)-1 and by 10-6 E mE-1 to yield total incident light exposure over the 24 hr diel cycle (Em-2d-1). Lower panel, contour plot of light sensor readings vs. hour of the day (resolved to 15 min intervals) and daily time interval during the year.

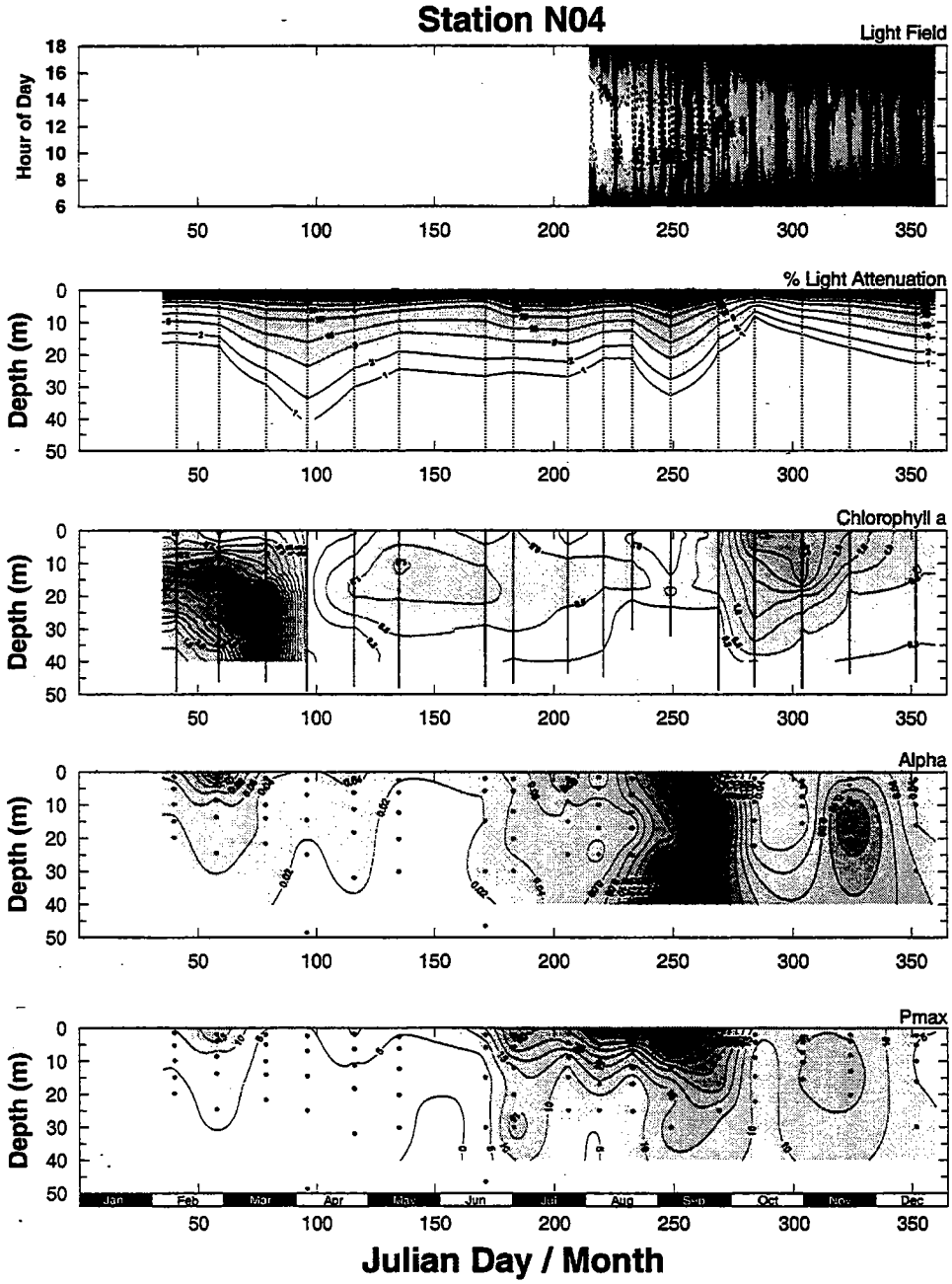

Figure 7-13
Parameters used for computation of high temporal resolution primary production at Station N04. Panel 1, Deer Island incident light measurements at 15 min intervals from 0600 to 1800 hrs, standard time. Panel 2, percent subsurface light (Iz/Iz=0 x100) vs. depth over the season, where Iz is the 4pi light field at depth z recorded by the CTD, Iz=0 is the 4pi light field just under the sea surface at depth zero. Panel 3, Chlorophyll a concentration, [chla], vs. depth over the season. Panel 4, chlorophyll-specific a vs. depth over the season. Panel 5, chlorophyll-specific Pmax vs. depth over the season.

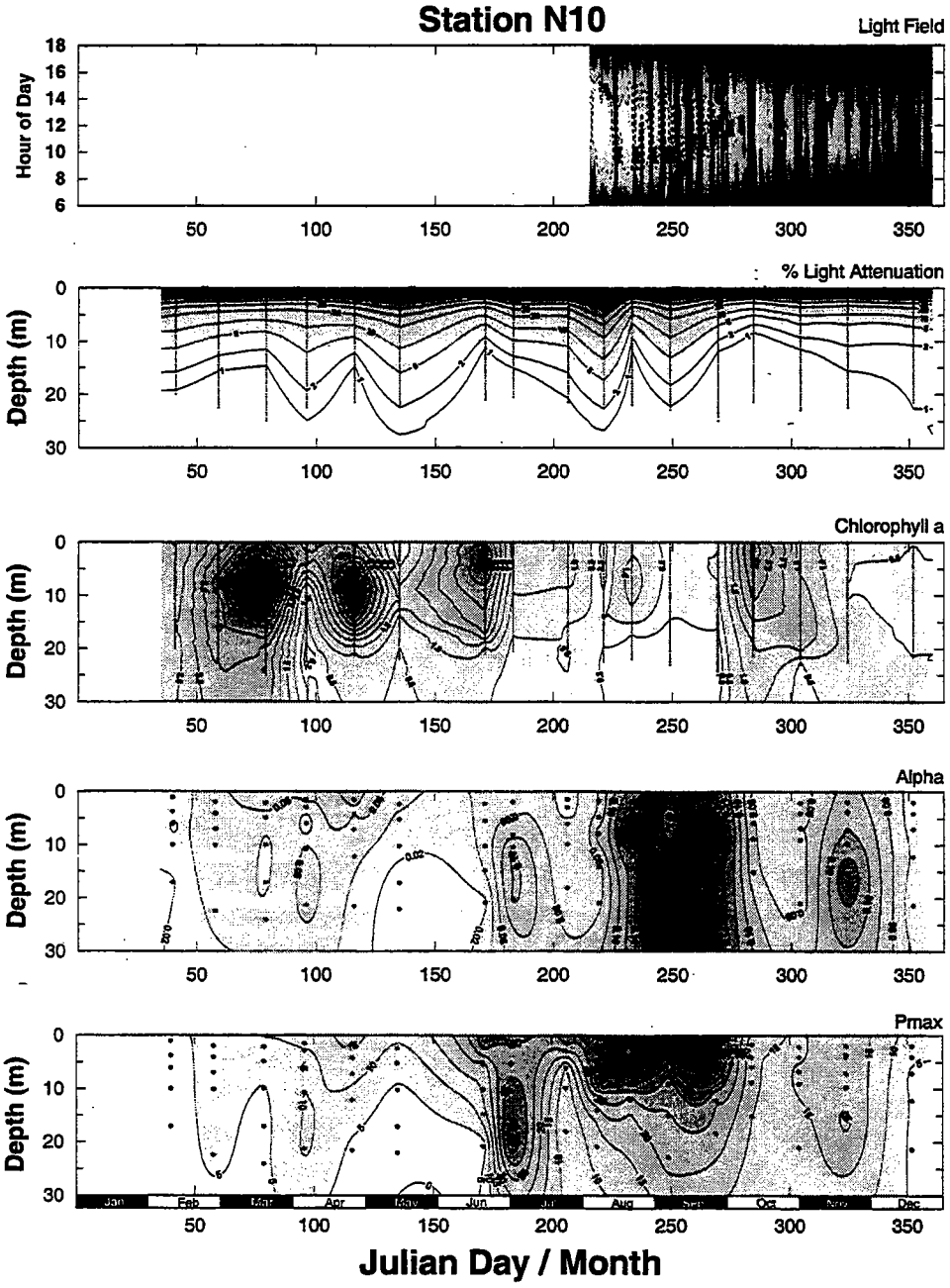

Figure 7-14
Parameters used for computation of high temporal resolution primary production at Station N10. Identification of panel contents are as described in the legend of Figure 7-13.

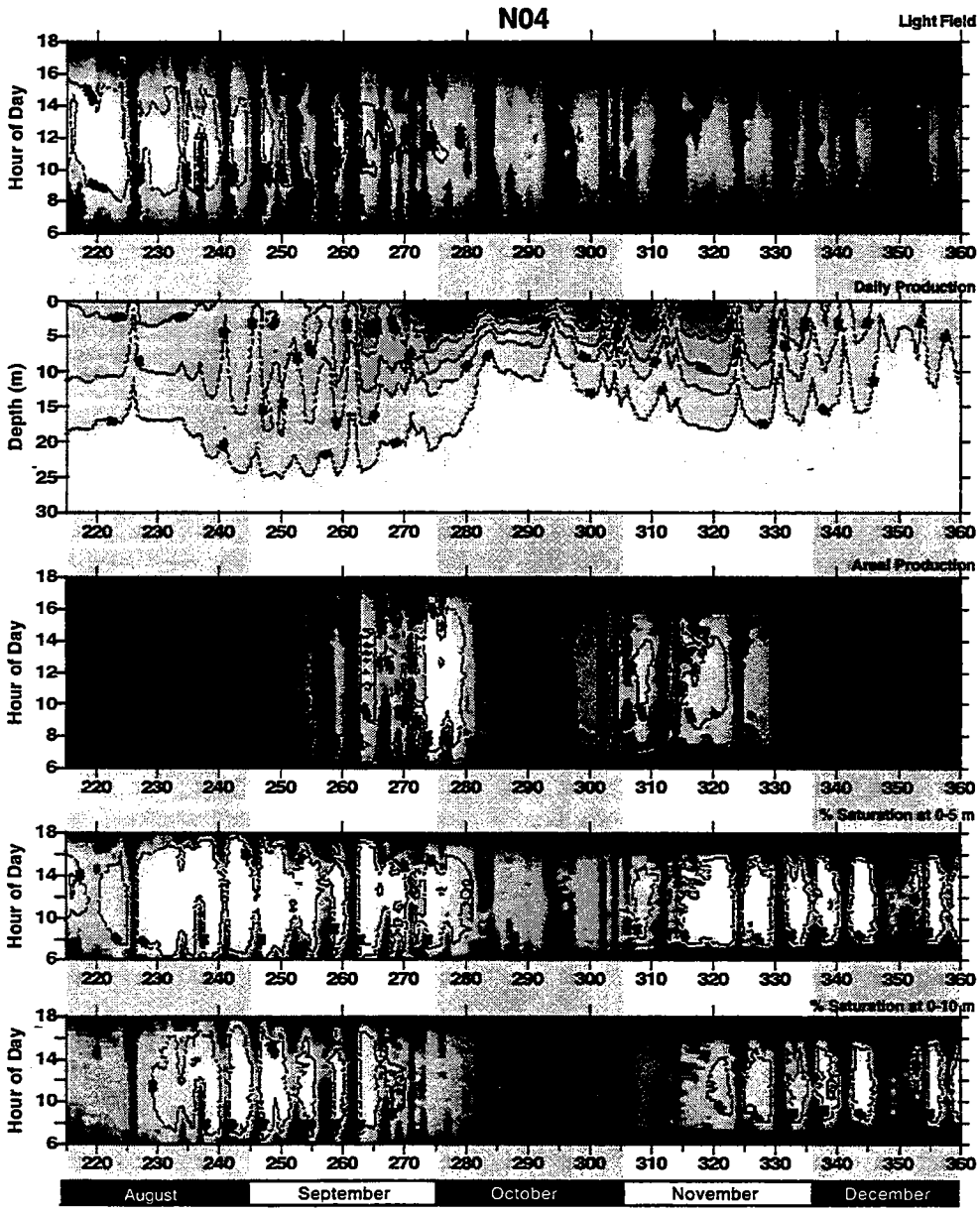

Figure 7-15

High temporal resolution production at Station N04 during the fall of 1996. Data in Figure 7-13 from Julian day 215 - 360 were used for computations using a BASIC program as described in Methods. Panel 1, fall light field expressed in uEm-2s-1. Panel 2, daily production (mgC m-3d-1) vs. depth (1 m intervals) over the season (resolved to the day). Panel 3, areal production down to 40m (mgCm-2hr-1; note production goes to zero before 40m) vs. hour of day (resolved to 15 min intervals) over the season (resolved to the day). Panels 4 and 5, areal photosynthesis percent saturation from 0-5 m and 0-10 m depth vs. hour of day (resolved to 15 min intervals) over the season (resolved to the day), respectively. Percent saturation was computed as areal production in upper 5 m and upper 10 m of the water column relative to areal Pmax* over the same depth intervals vs. hour of day. Pmax* was computed as the product Pmax x [chla] from the data in Figure 7-13.

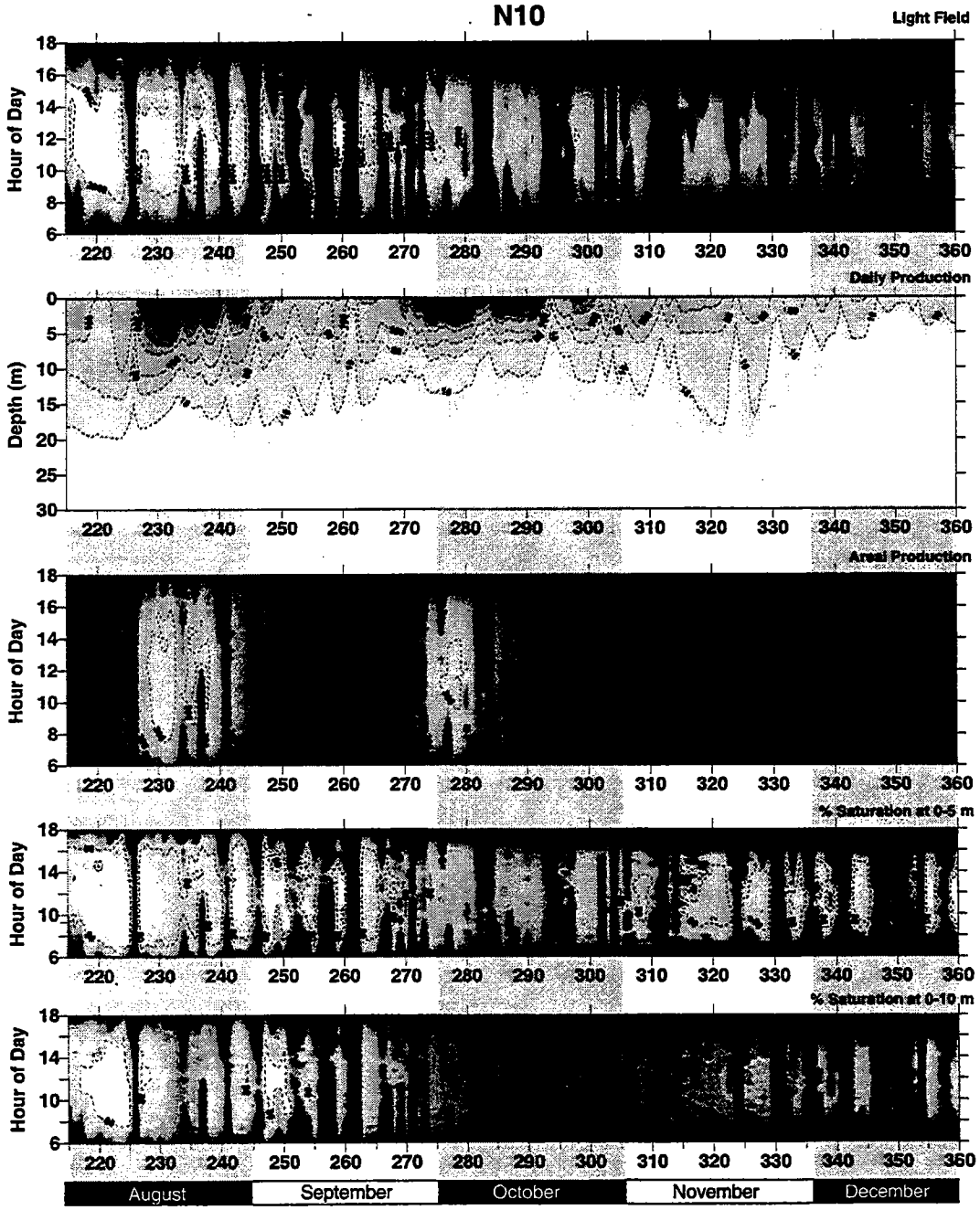

Figure 7-16
High temporal resolution production at Station N10 during the fall of 1996. Panel contents are as described in the legend of Figure 7-15 except that production is determined to a depth of 30 m (production goes to zero before 30 m).

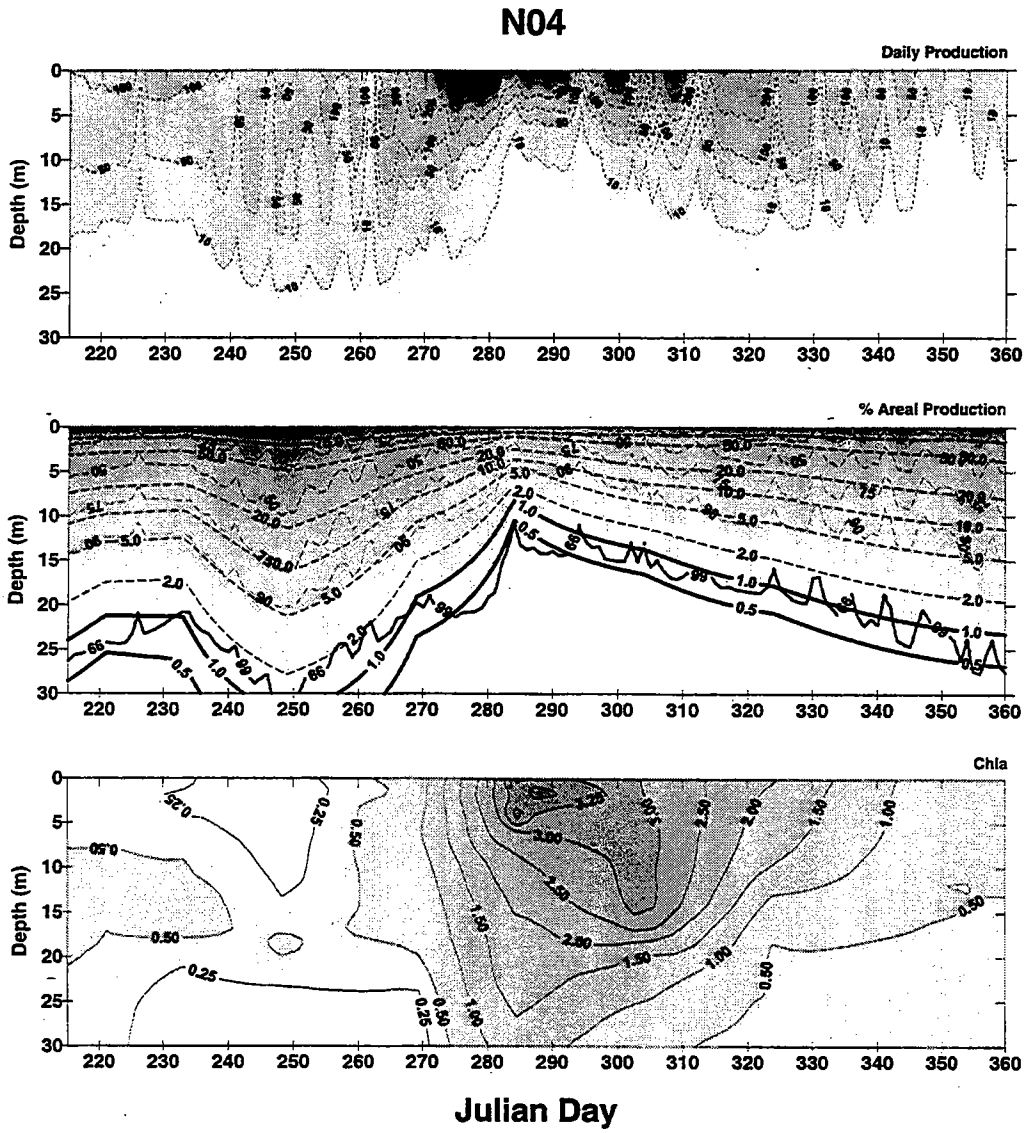

Figure 7-17
Percent of total areal production vs. depth in water column for Station N04 in 1996. Panel 1, daily production (mgCm-3d-1). Panel 2, percent total areal production (Pd / P0.5 x 100); where Pd = areal production integrated to depth d, P0.5 = areal production down to the 0.5% light level) vs. depth in water column (shading, wavy dashed lines). Percent subsurface incident light (Iz/Iz=0 x 100) vs. depth in water column (smooth dashed lines), where Iz is the 4pi light field at depth z recorded by the CTD, Iz=0 is the 4pi light field just under the sea surface at depth zero. Heavy dashed and solid lines are the 99% areal production contour and 0.5 - 1 % light levels, respectively. Panel 3, chlorophyll a concentration contours.

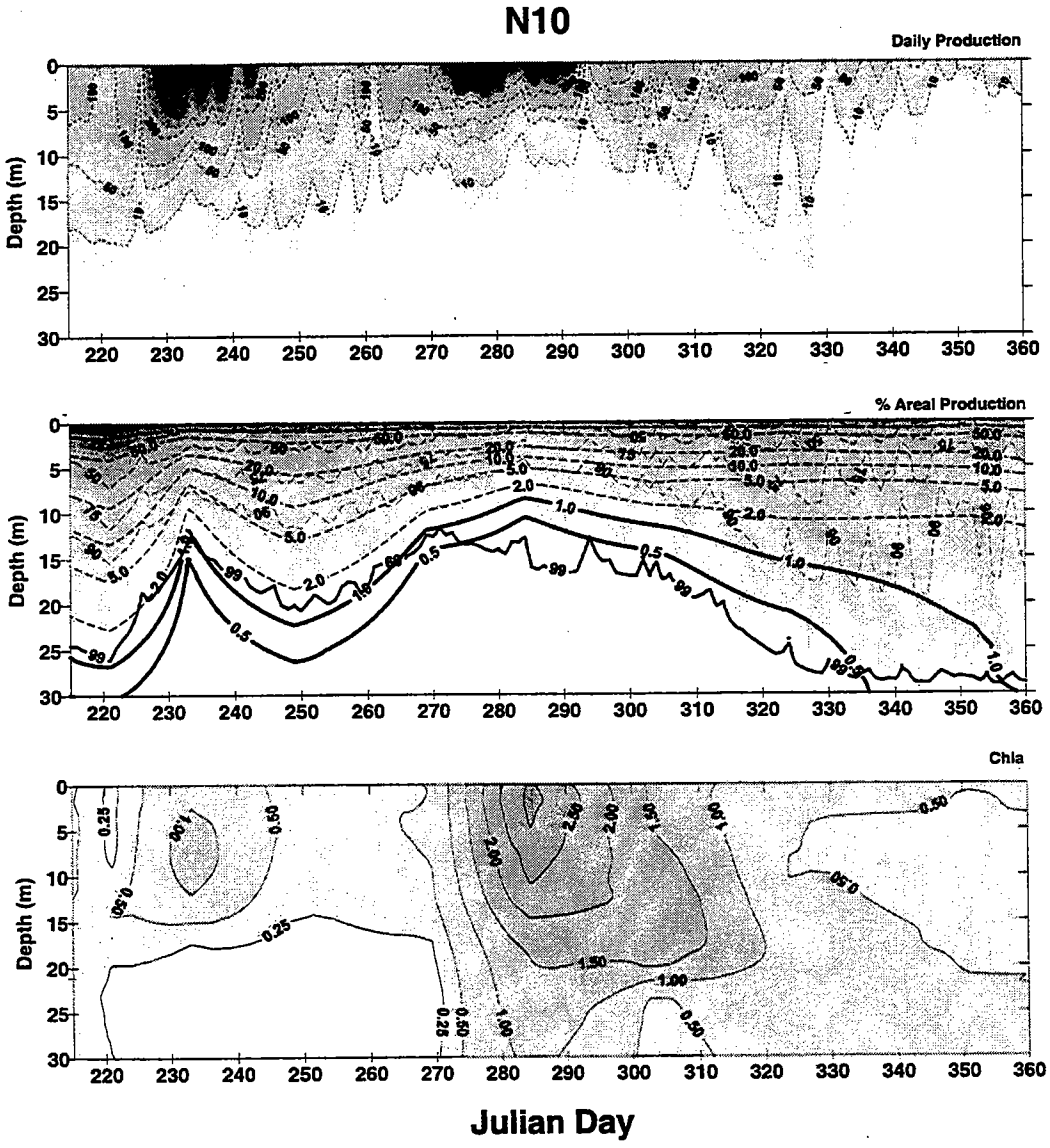

Figure 7-18
Percent of total areal production vs. depth in water column for Station N10 in fall 1996. Panels are as described in the legend of Figure 7-17.

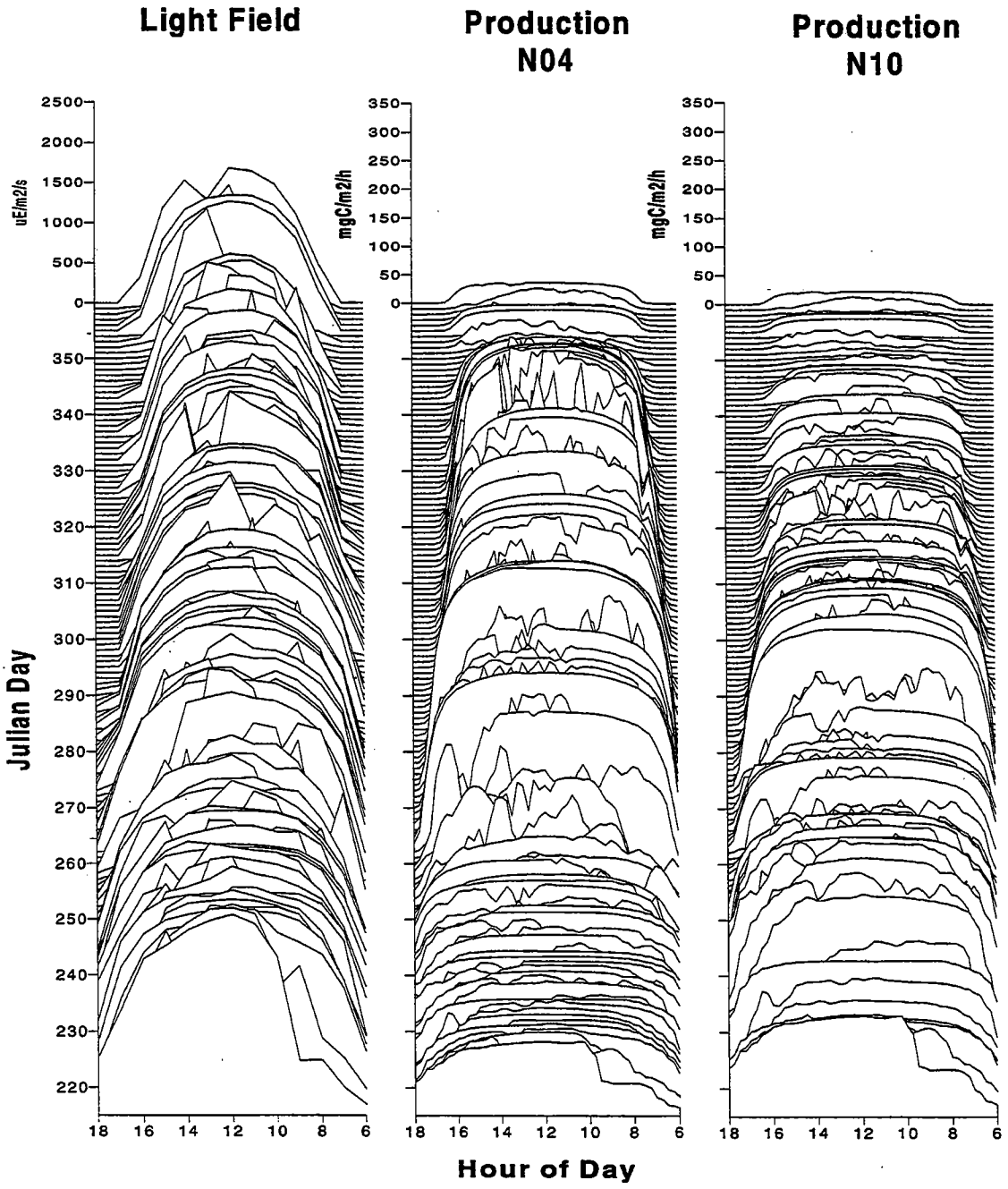

FIGURE 7-19

Surface plot of daily light field and resultant areal hourly production at Stations N04 and N10 during fall of 1996. Left panel, Deer Island light sensor readings as described in the legend of Figure 7-12. Middle and right panels, areal production down to the 0.5% light level ($mgCm^{-2}h^{-1}$). Compare with data in Figures 7-15 and 7-16, third panels.

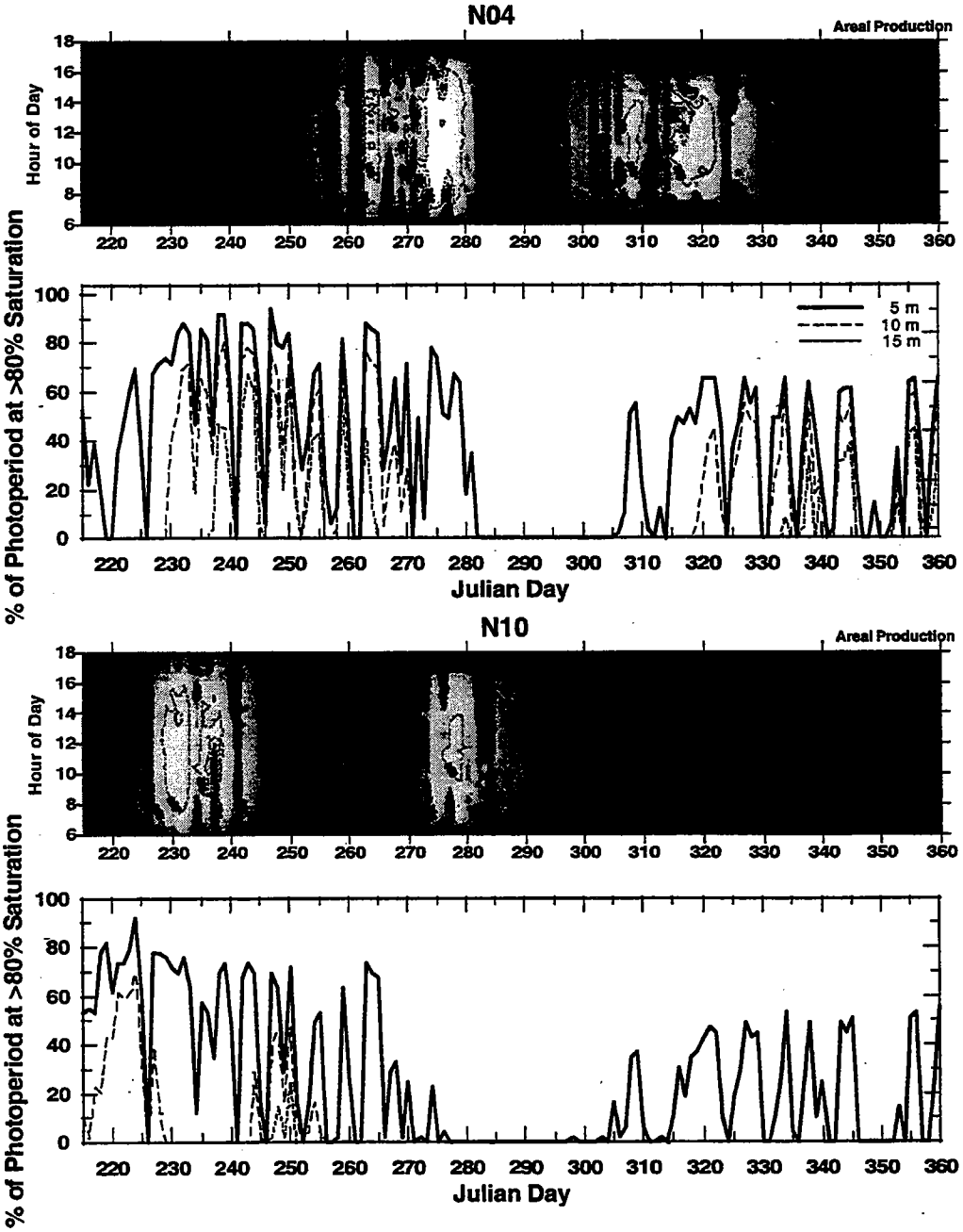

Figure 7-20
Percent of photoperiod in which areal photosynthesis is greater than 80% of saturation for Stations N04 and N10 in fall of 1996. Determinations made over depth intervals 0-5 m (black lines), 0-10 m (dashed lines) or 0-15 m (fine dashed lines).

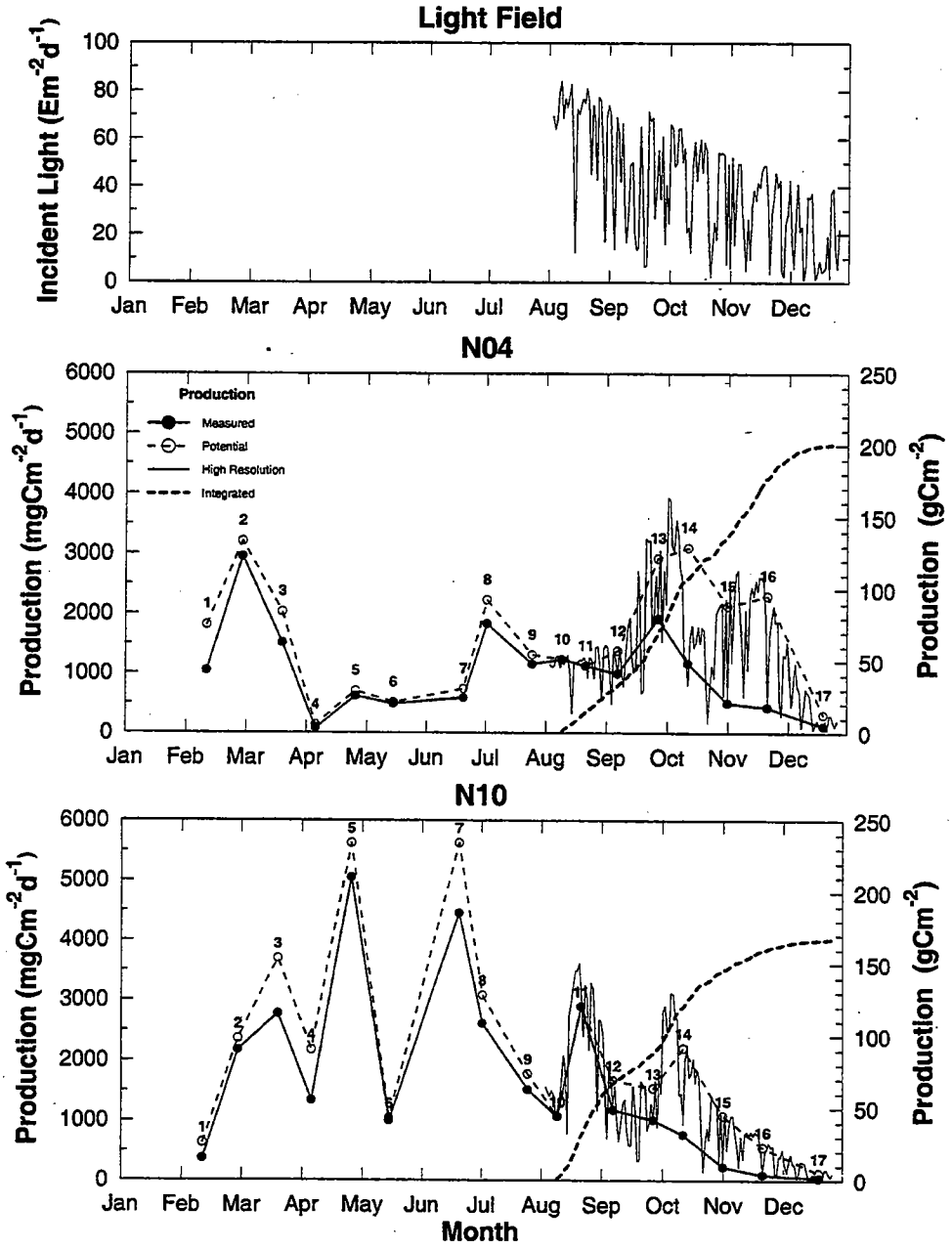

Figure 7-21. High temporal resolution areal production at Stations N04 and N10 during the fall of 1996. Panel 1, incident light field as described in the legend of Figure 7-12. Panels 2 and 3, areal production for Stations N04 and N10, respectively. Closed circles-solid line, areal production (mgCm-2d-1) determined on the survey day indicated by the number using the incident light field that occurred on that day. Open circles-dashed line, potential areal production determined on the survey day using a cloudless day incident light field that would occur at the time of year of the survey. Thin solid line, high resolution areal production computed using the Deer Island incident light time series and gridded photosynthesis parameters as described in Methods. Thick dashed line, integrated seasonal production (gCm-2) obtained by summation of daily areal production.

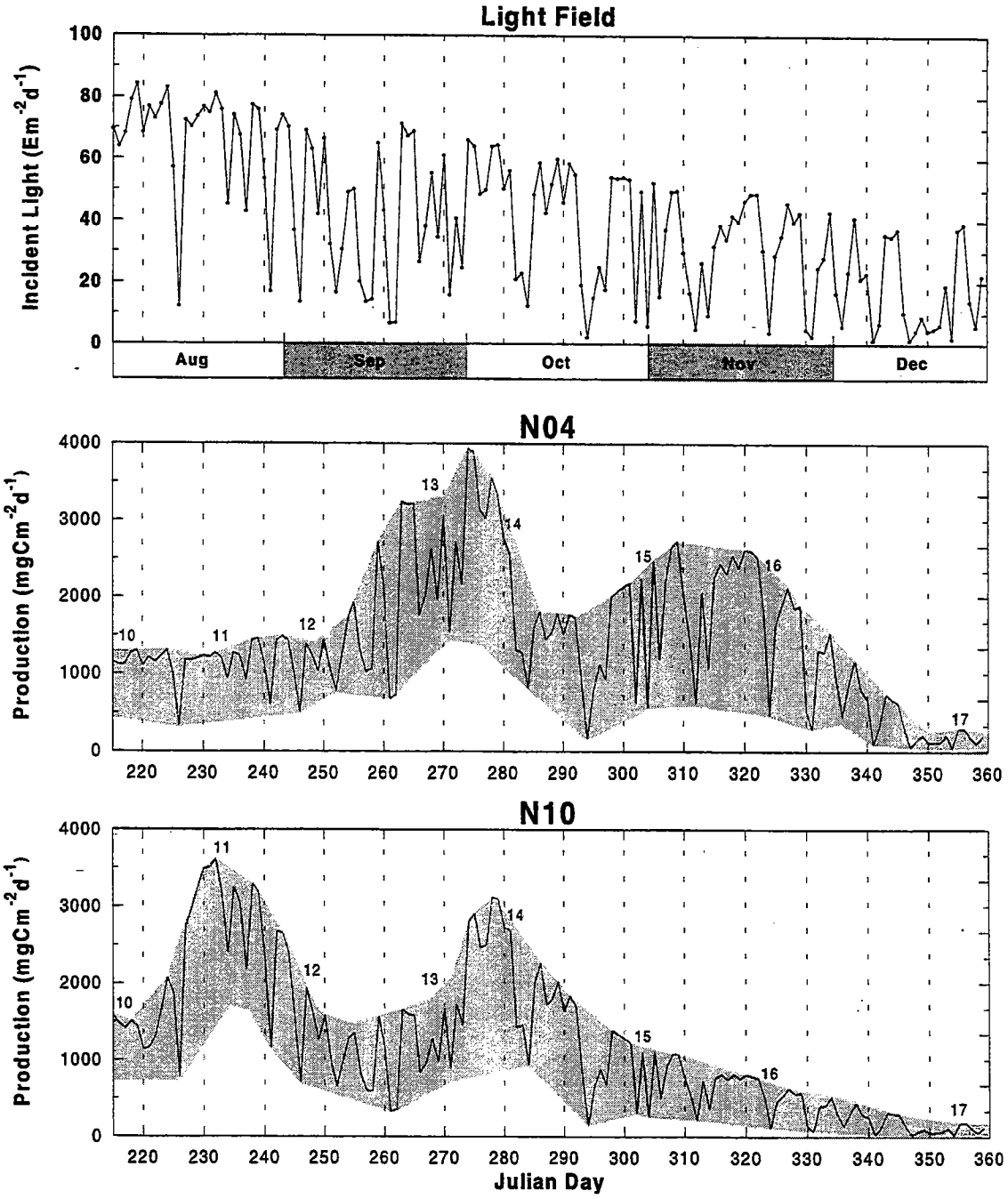

FIGURE 7-22

Envelopes of areal production at Stations N04 and N10 occurring on sunny and maximally cloudy days during the fall 1996. Panel 1, incident light field. Panels 2 and 3, areal production as shown in Figure 7-21.

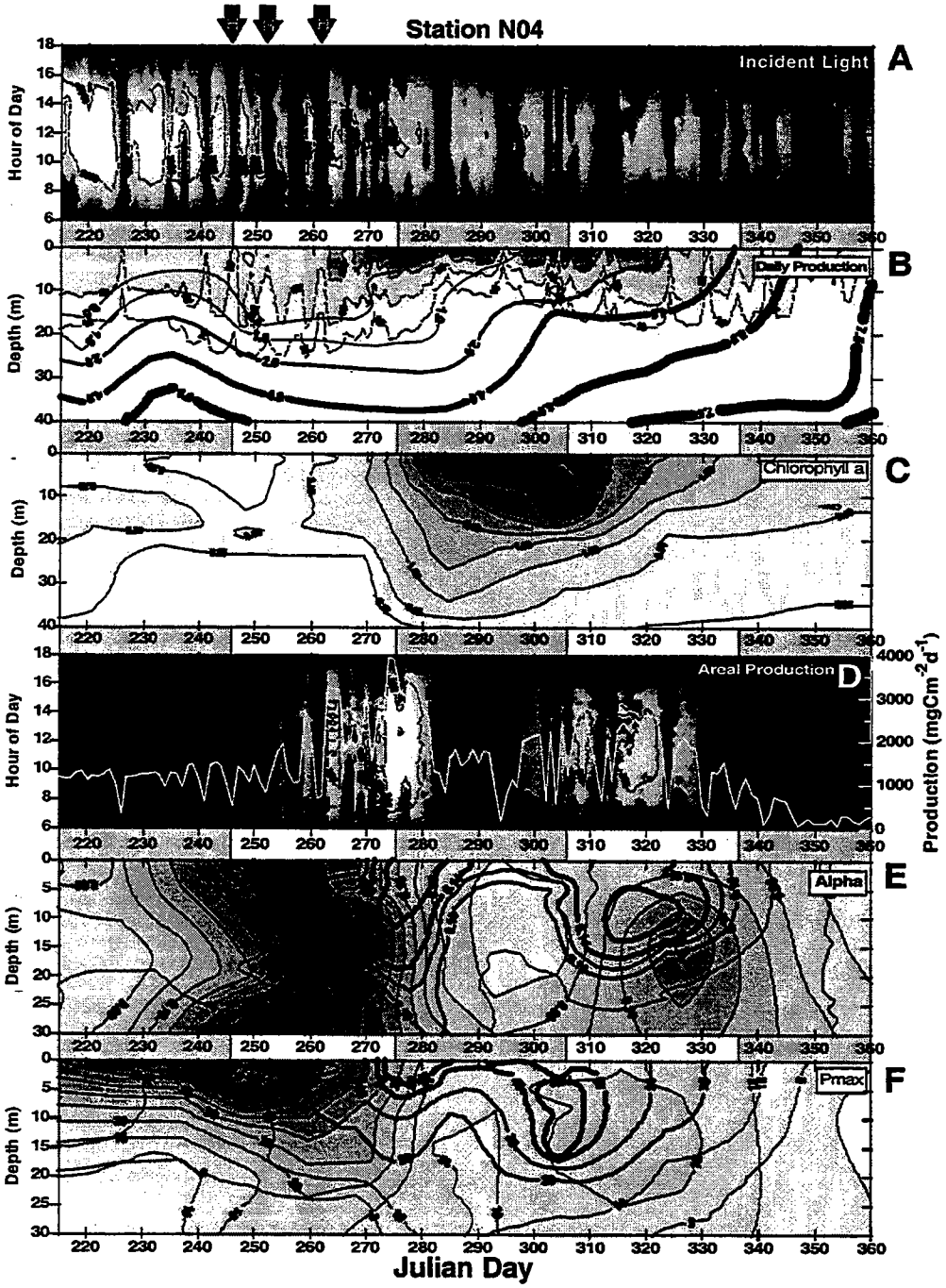

Figure 7-23

Comparison of major variables influencing primary production for Station N04 in fall 1996. Panel A, incident light field (yellow, uEm-2s-1). Panel B, daily production (mgCm-3d-2) and DIN nutrient field (red, thickness of line proportional to concentration in uM). Panel C, water column chlorophyll a content (ugl-1). Panel D, areal production (shading, mgCm-2h-1; white line, mgCm-2d-1). Panel E, chlorophyll-specific Alpha (gC(gchla)-1h-1(uEm-2s-1)-1) and alpha* (black line, gCl-1h-1(mEm-2s-1)-1, alpha* = alpha x [chla]). Panel F, chlorophyll-specific Pmax (gC(gchla)-1h-1) and Pmax* (black line, gCl-1h-1) Pmax* = Pmax x [chla]).

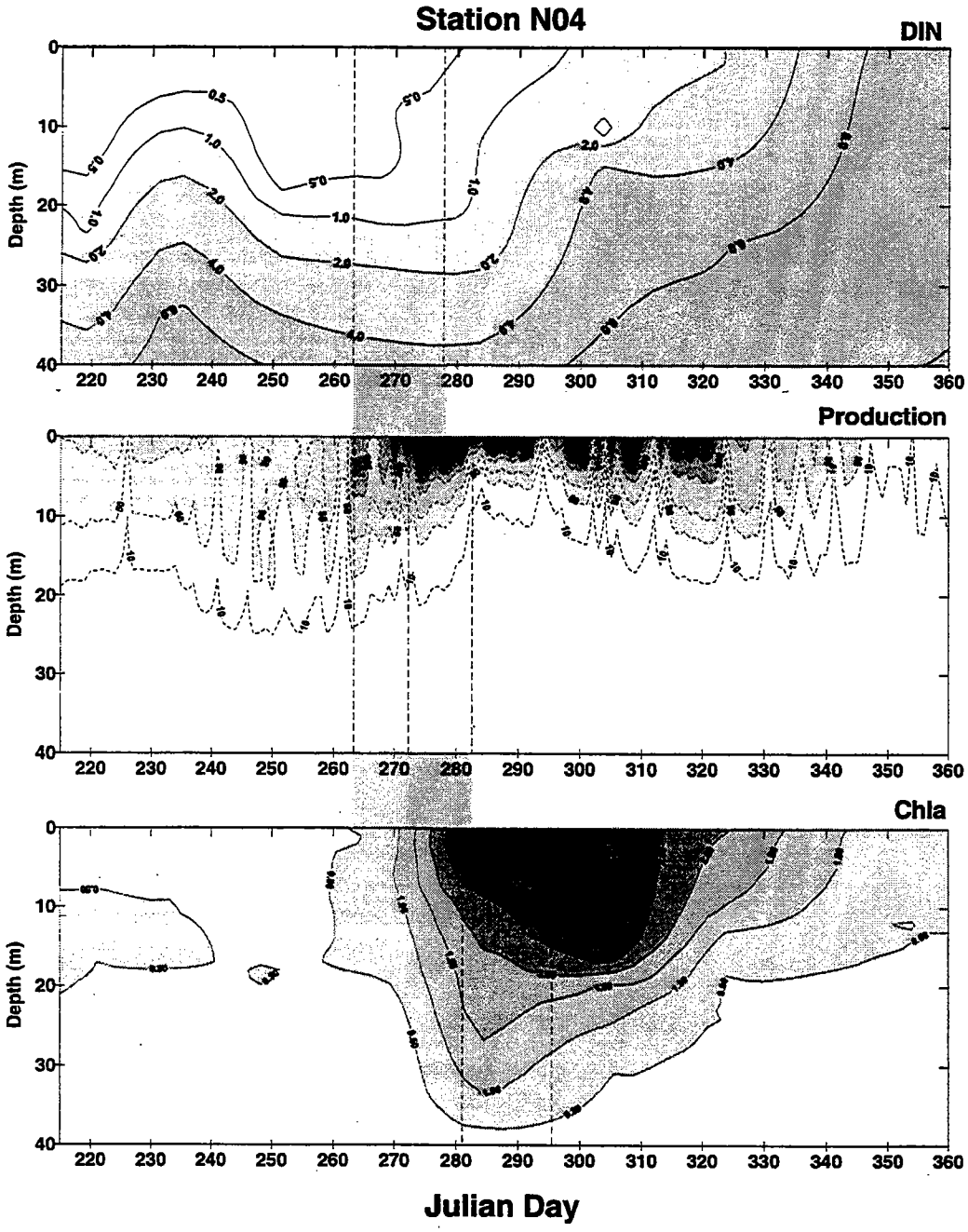

Figure 7-24
Comparison of DIN nutrient field, daily production and water column chlorophyll at Station N04 in fall 1996. Dashed vertical lines illustrate approxmate displacement in time of DIN nutrient intrusion (uM), resultant production (mgCm-3d-2) and chlorophyll a accumulation (ugl-1).

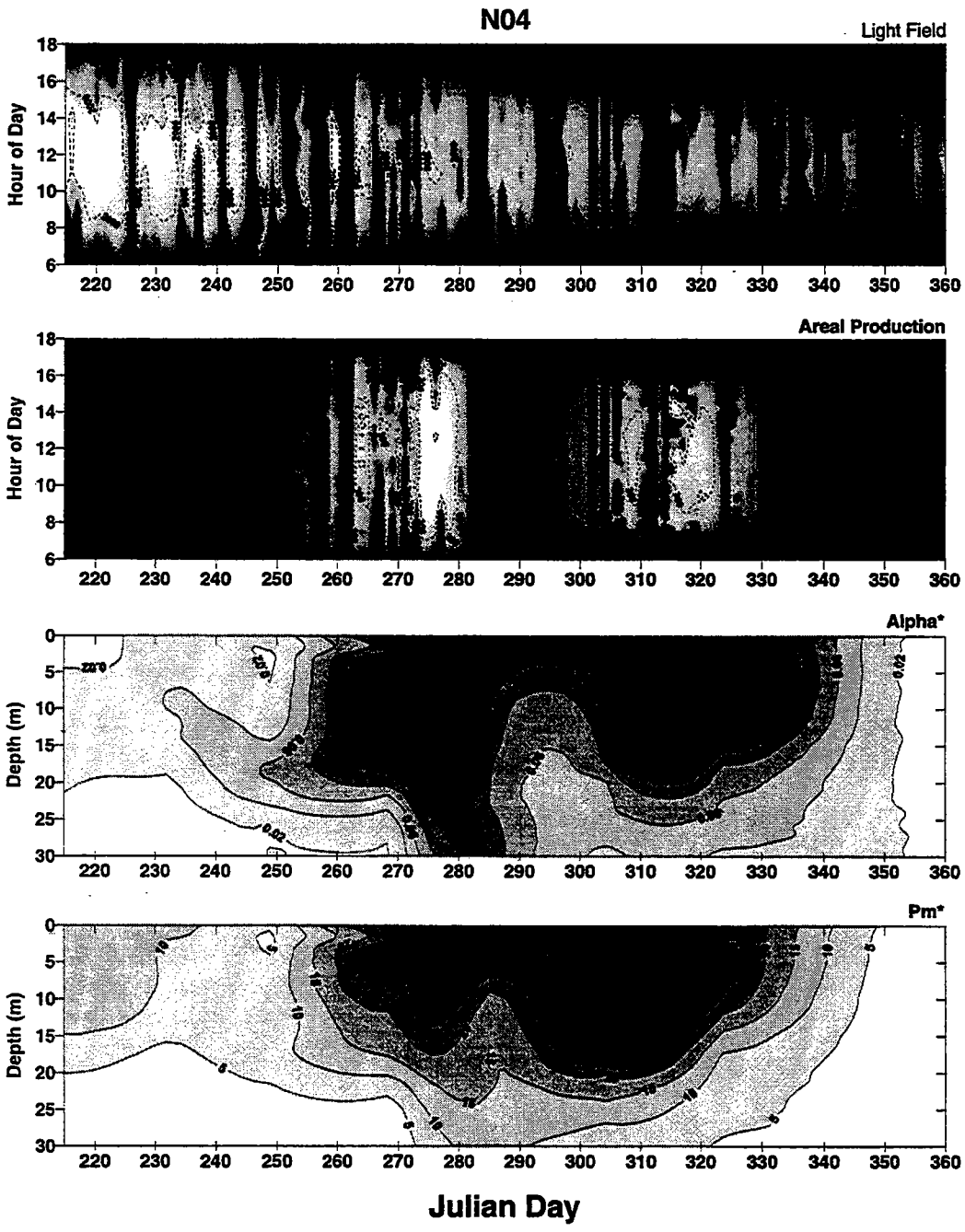

Figure 7-25
Comparison of Station N04 areal production with alpha* and Pmax* in fall 1996. Panel 1, incident light field (uEm-2s-1). Panel 2, Areal production (mgCm-2h-1). Panels 3 and 4, alpha* and Pmax*, respectively (see legend of Figure 7-23 for units).

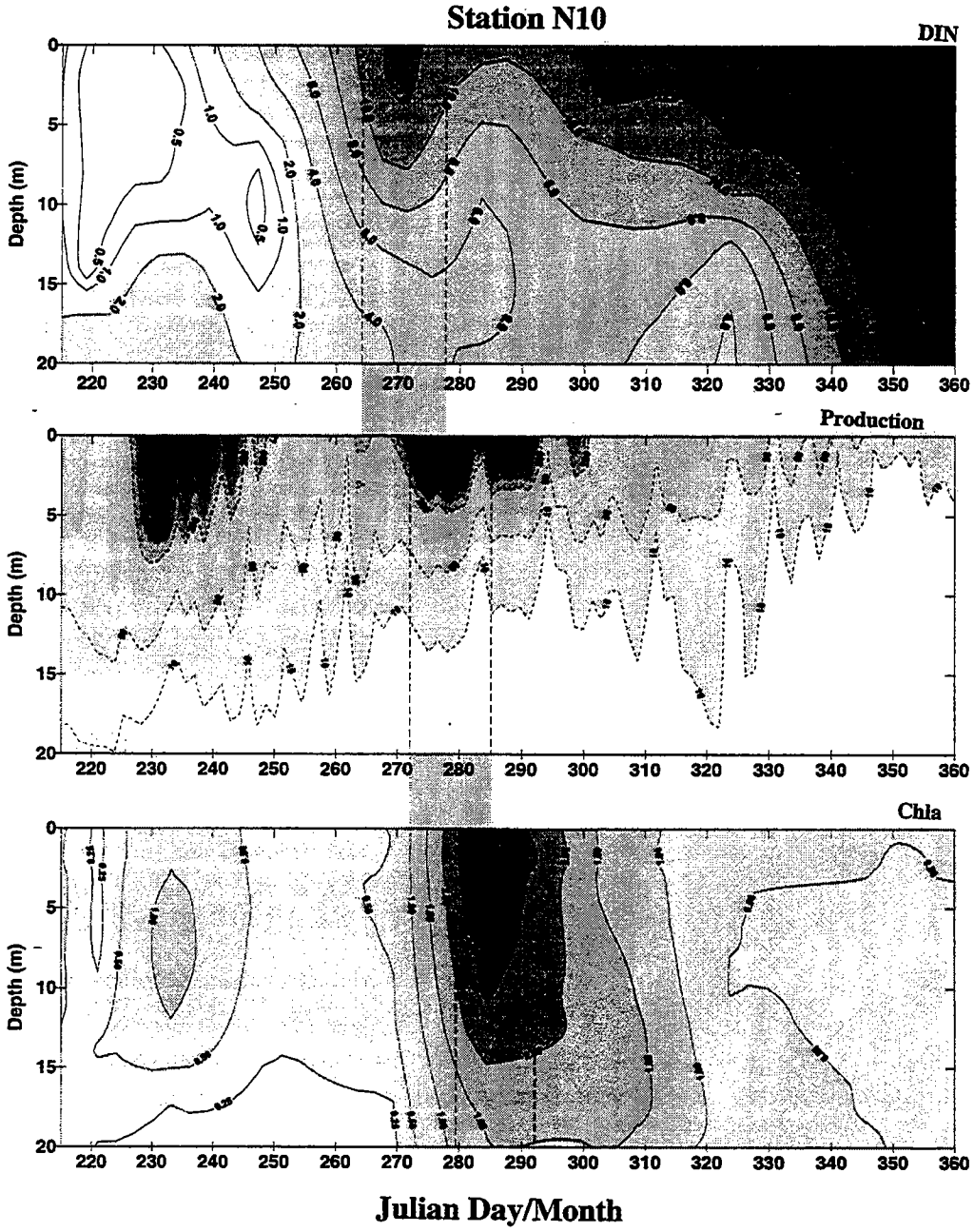

Figure 7-26
Comparison of DIN nutrient field, daily production and water column chlorophyll at Station N10 in fall 1996. Dashed vertical lines illustrate approxmate displacement in time of DIN nutrient intrusion (uM), resultant production (mgCm-3d-2) and chlorophyll a accumulation (ugl-1).

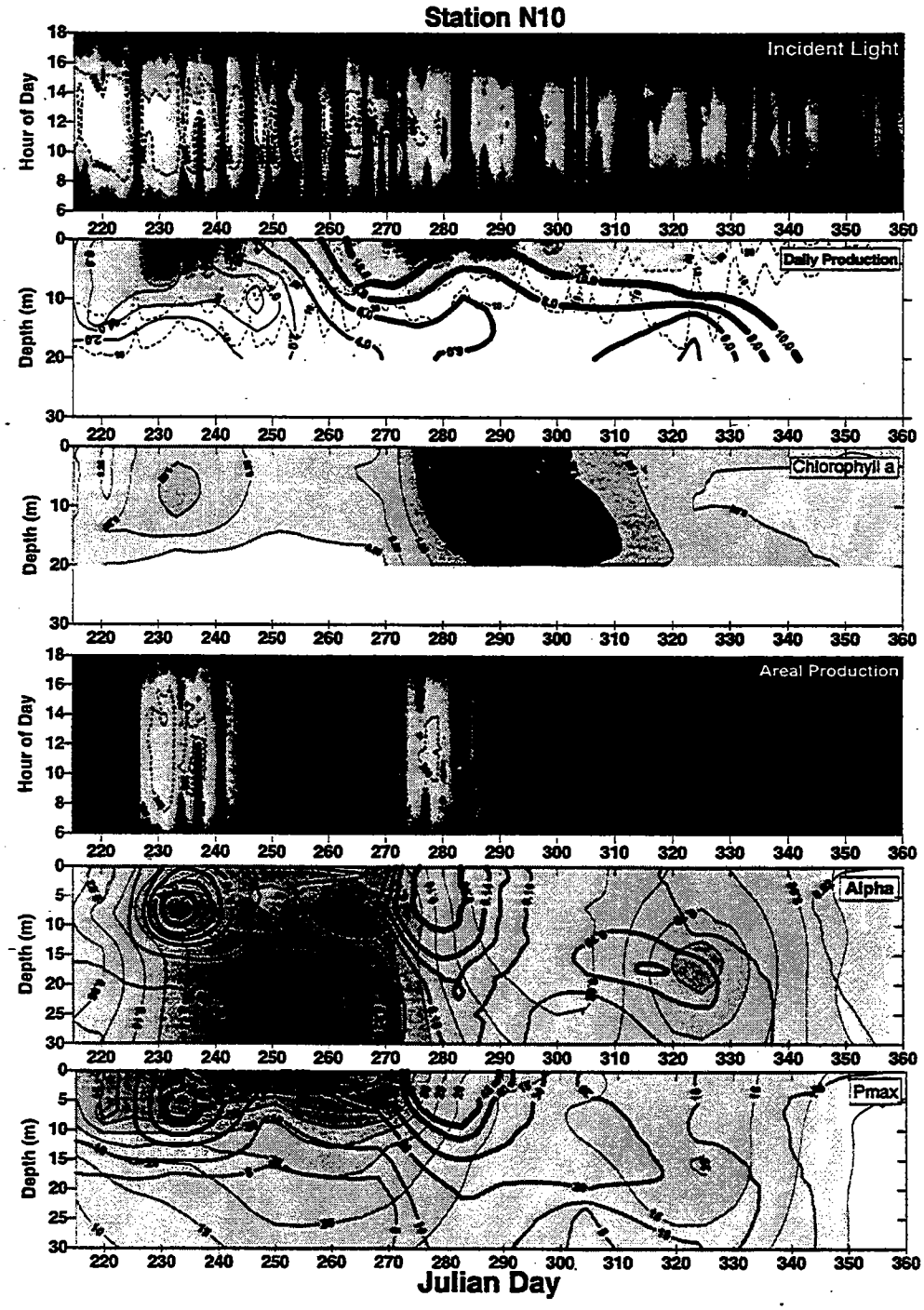

Figure 7-27
Comparison of major variables influencing primary production for Station N10 in fall 1996. See legend of Figure 7-23 for description of variables.

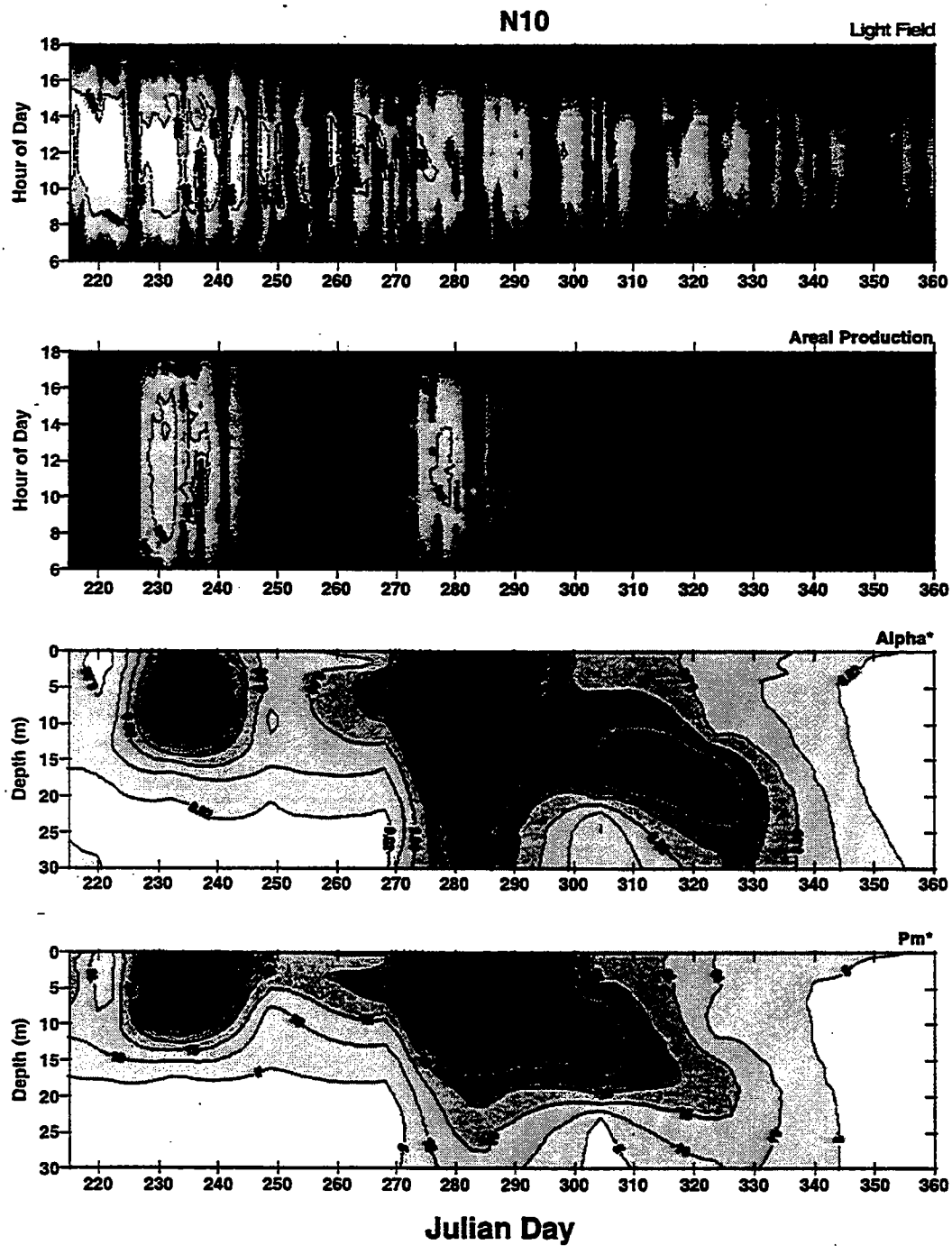

Figure 7-28
Comparison of Station N10 areal production with alpha* and Pmax* in fall 1996. See legend of Figure 7-25 for description of variables.

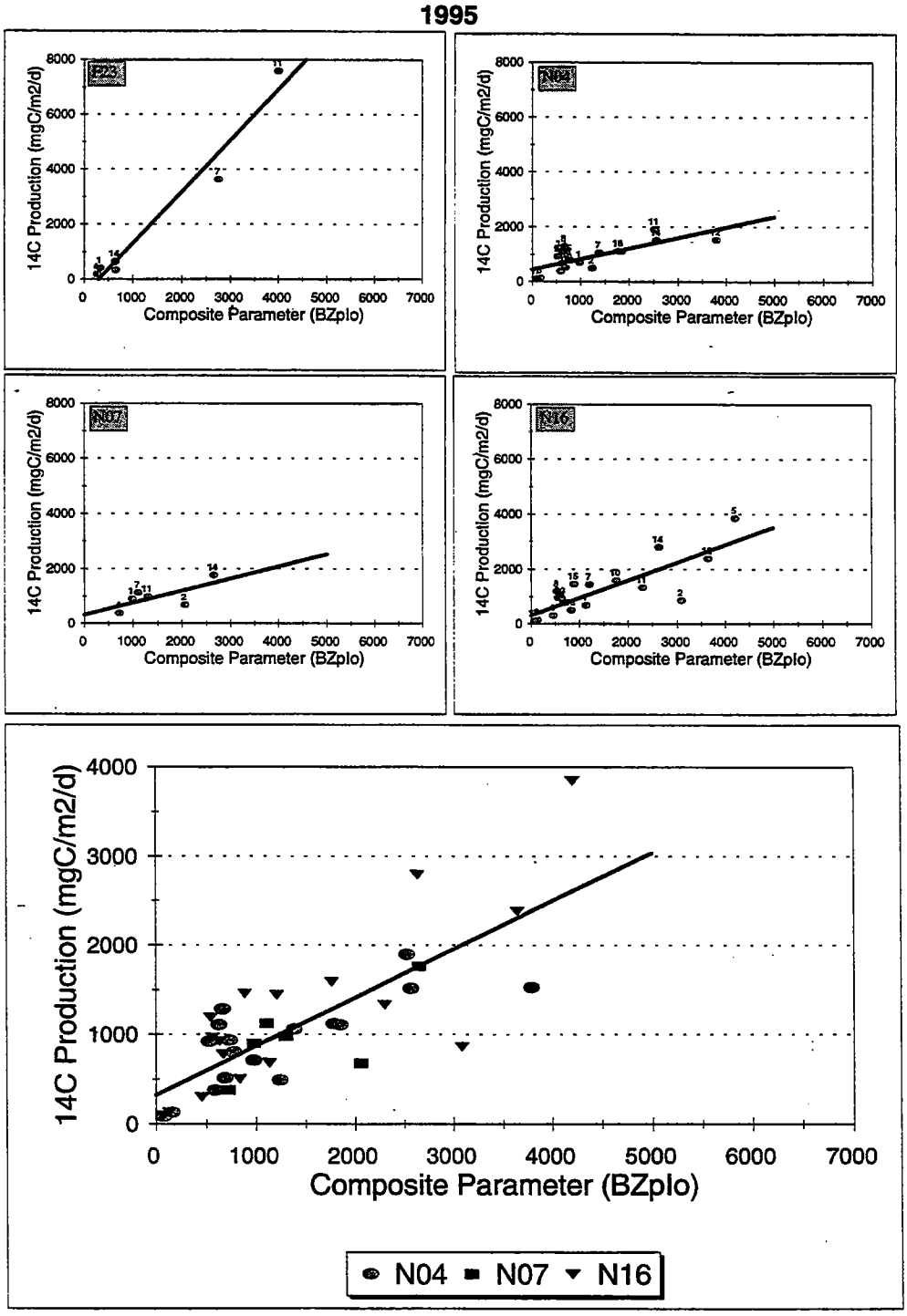

FIGURE 7-29
Linear regressions of ^{14}C-production vs. composite parameter BZ_pI_o for Stations F23, N16, N07 and N04 in 1995.

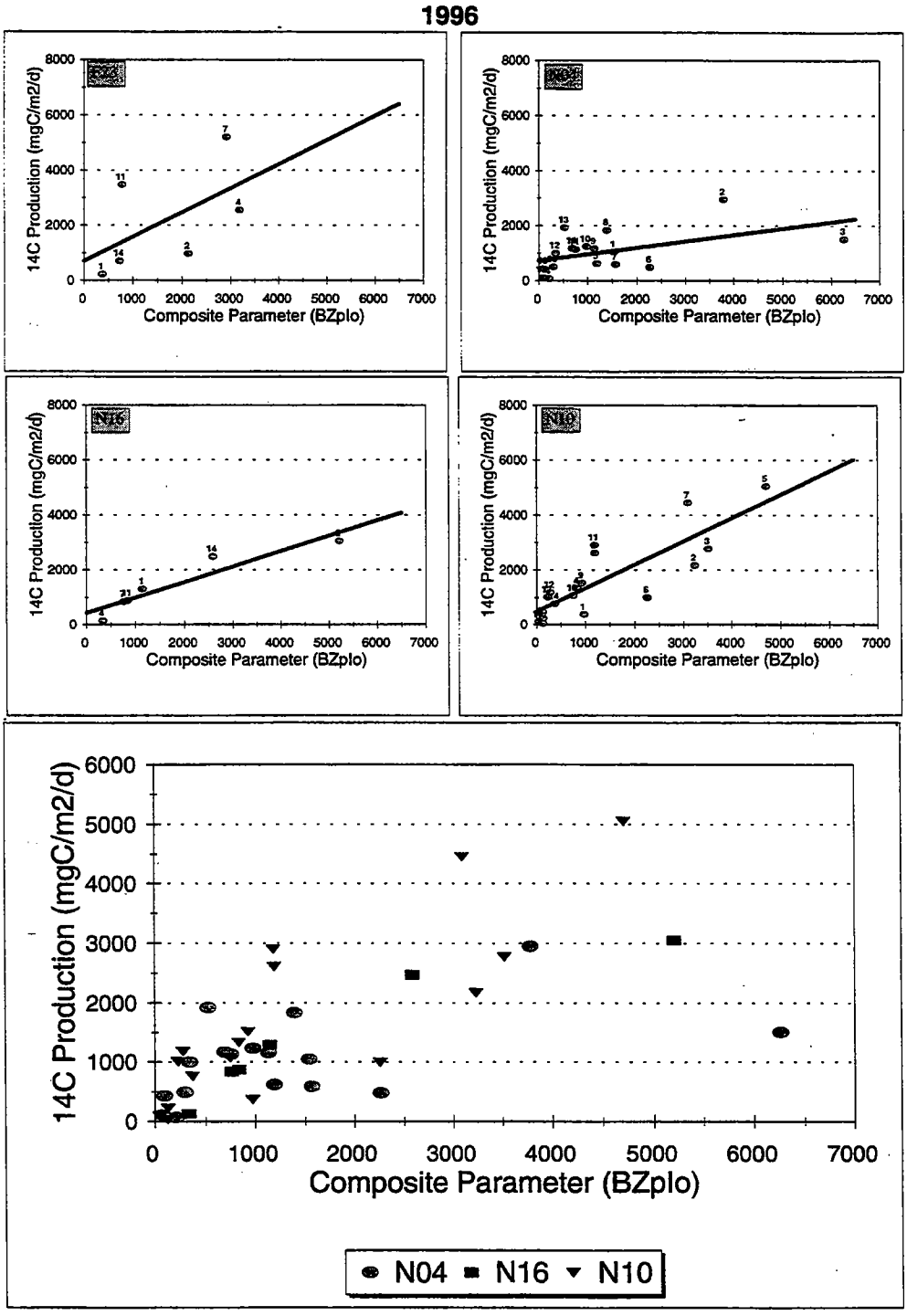

FIGURE 7-30
Linear regressions of ^{14}C-production vs. composite parameter BZ_pI_o for Stations F23, N10, N16 and N04 in 1996.

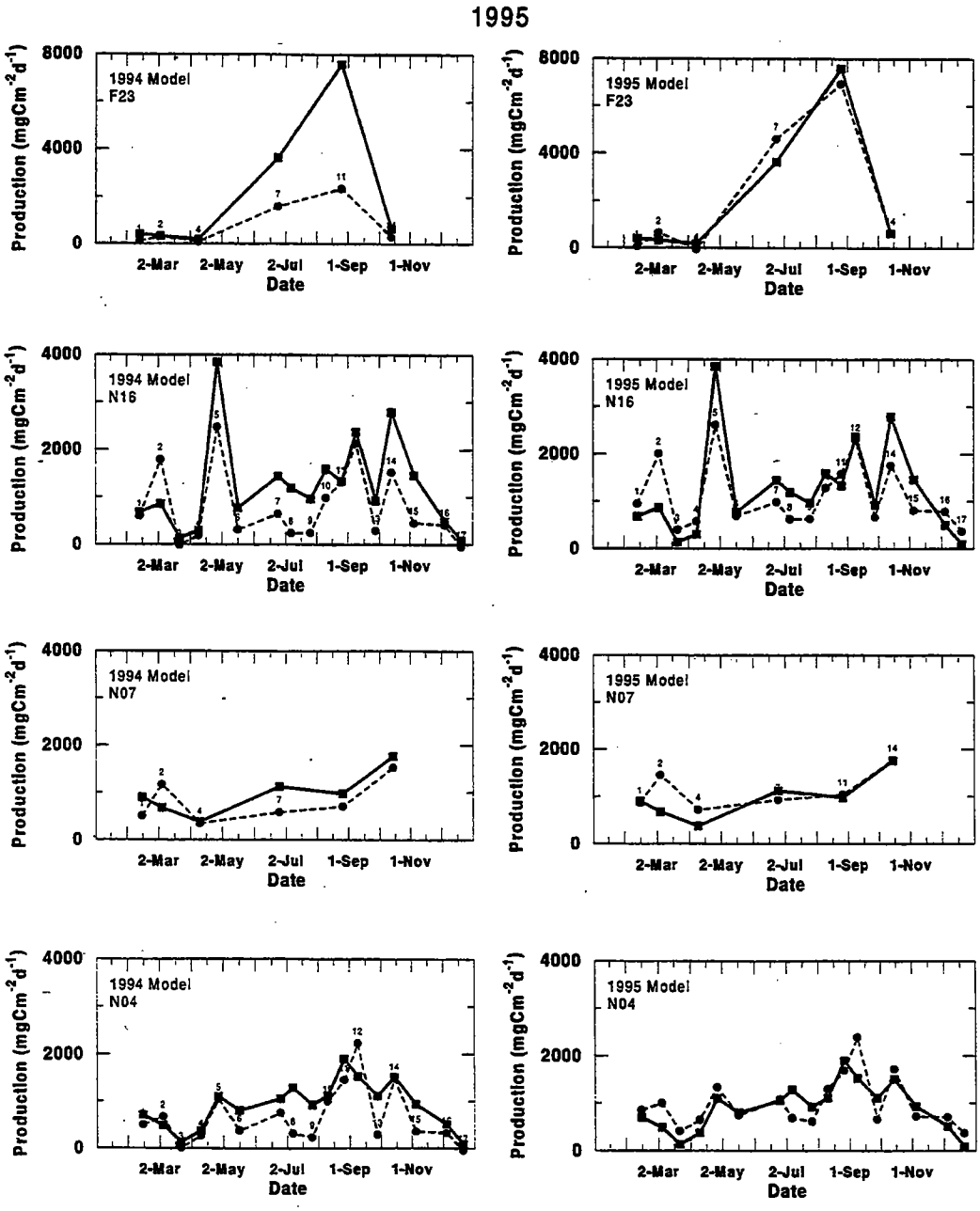

FIGURE 7-31

Comparison of measured 1995 seasonal ^{14}C-production with production estimated using BZ_pI_o regression parameters. Solid lines, measured ^{14}C-production; dashed lines, model estimated production. Left hand series of panels, estimates of 1995 production using 1994 regression parameters. Right hand series of panels, estimates of 1995 production using 1995 regression parameters.

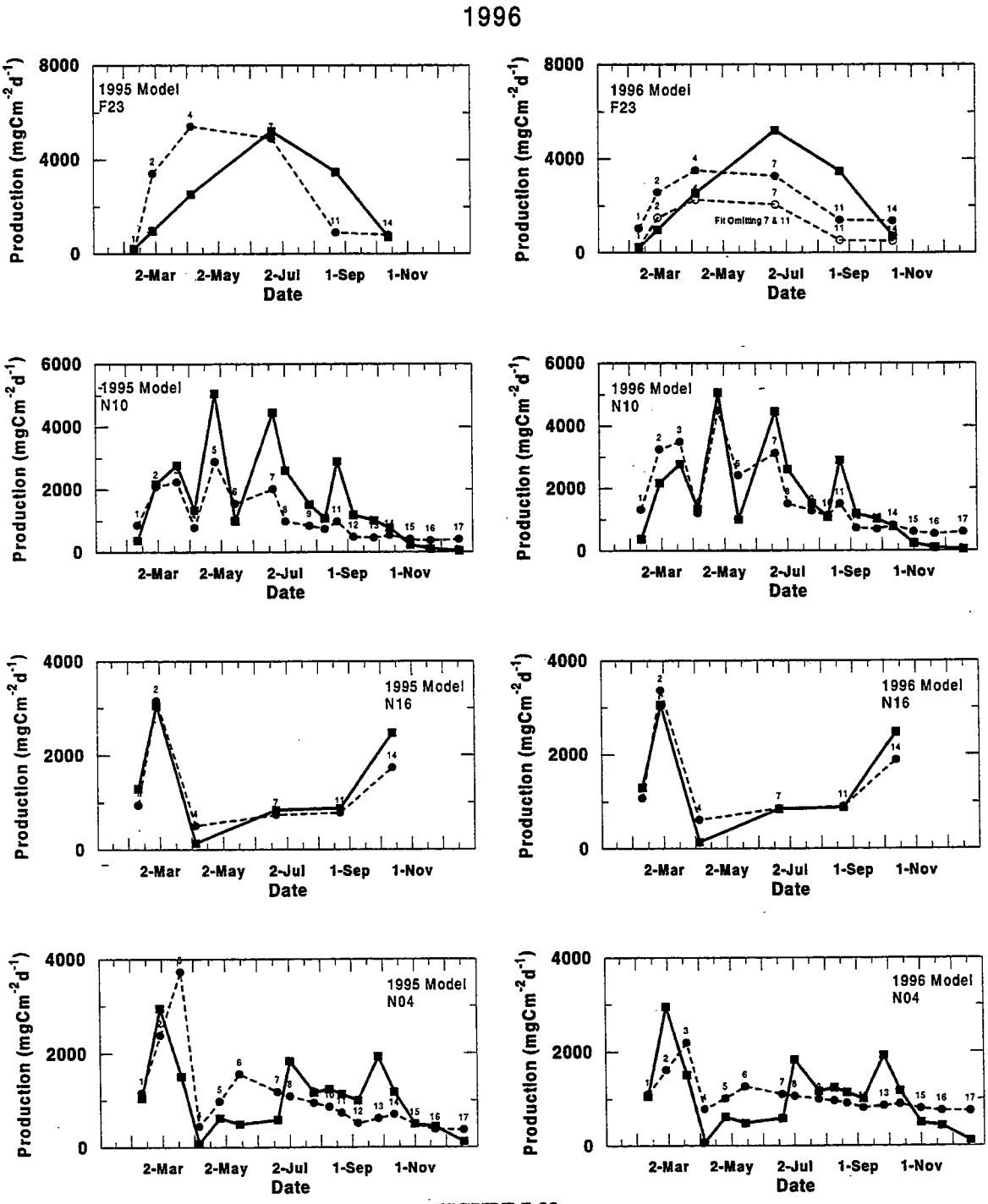

FIGURE 7-32

Comparison of measured 1996 seasonal ^{14}C-production with production estimated using BZ_pI_o regression parameters. Solid lines, measured ^{14}C-production; dashed lines, model estimated production. Left hand series of panels, estimates of 1996 production using 1995 regression

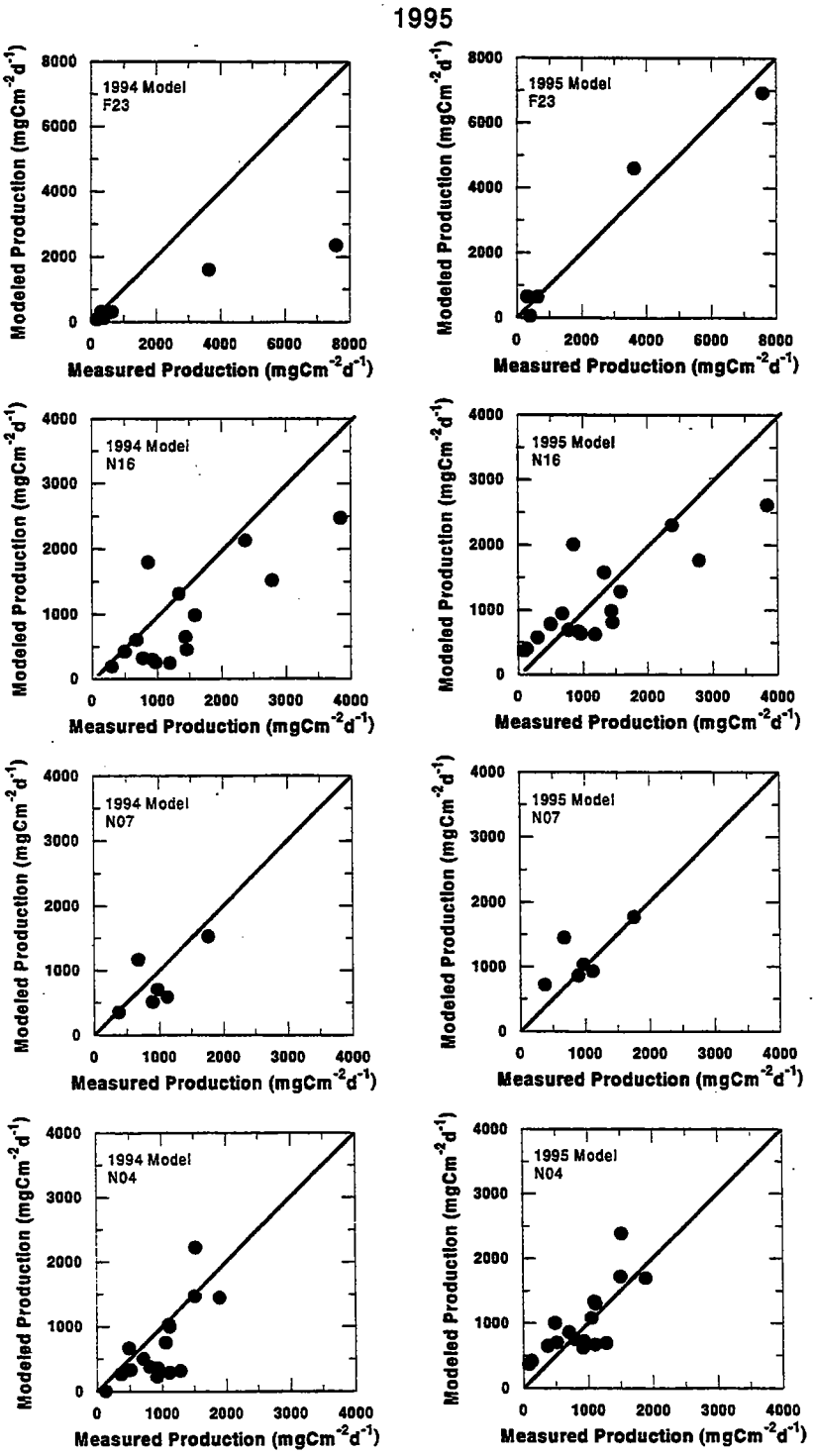

FIGURE 7-33
Plots of BZ_pI_o modeled production vs. measured ^{14}C-production for 1995 data. Solid line, 1:1 line.

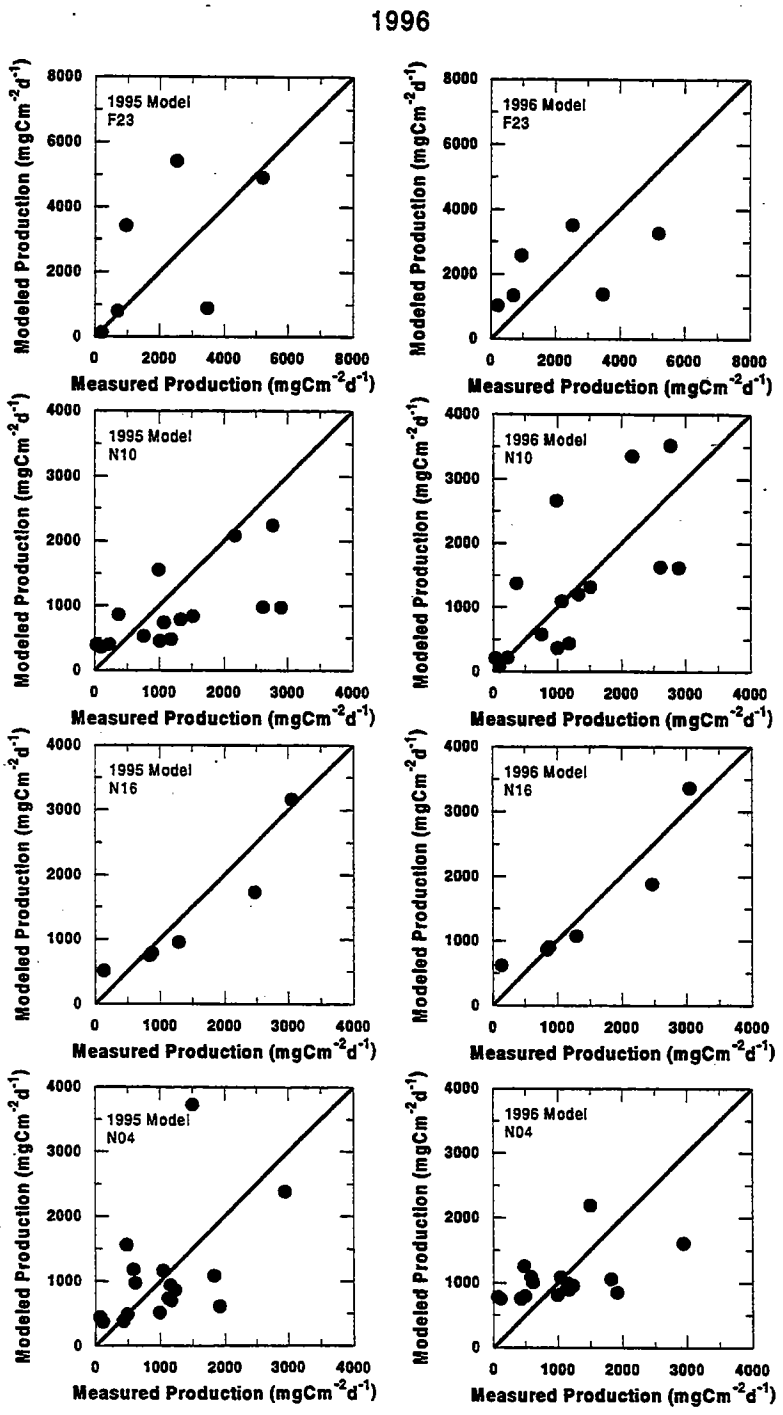

FIGURE 7-34
Plots of BZ_pI_o modeled production vs. measured ^{14}C-production for 1996 data. Solid line, 1:1 line.

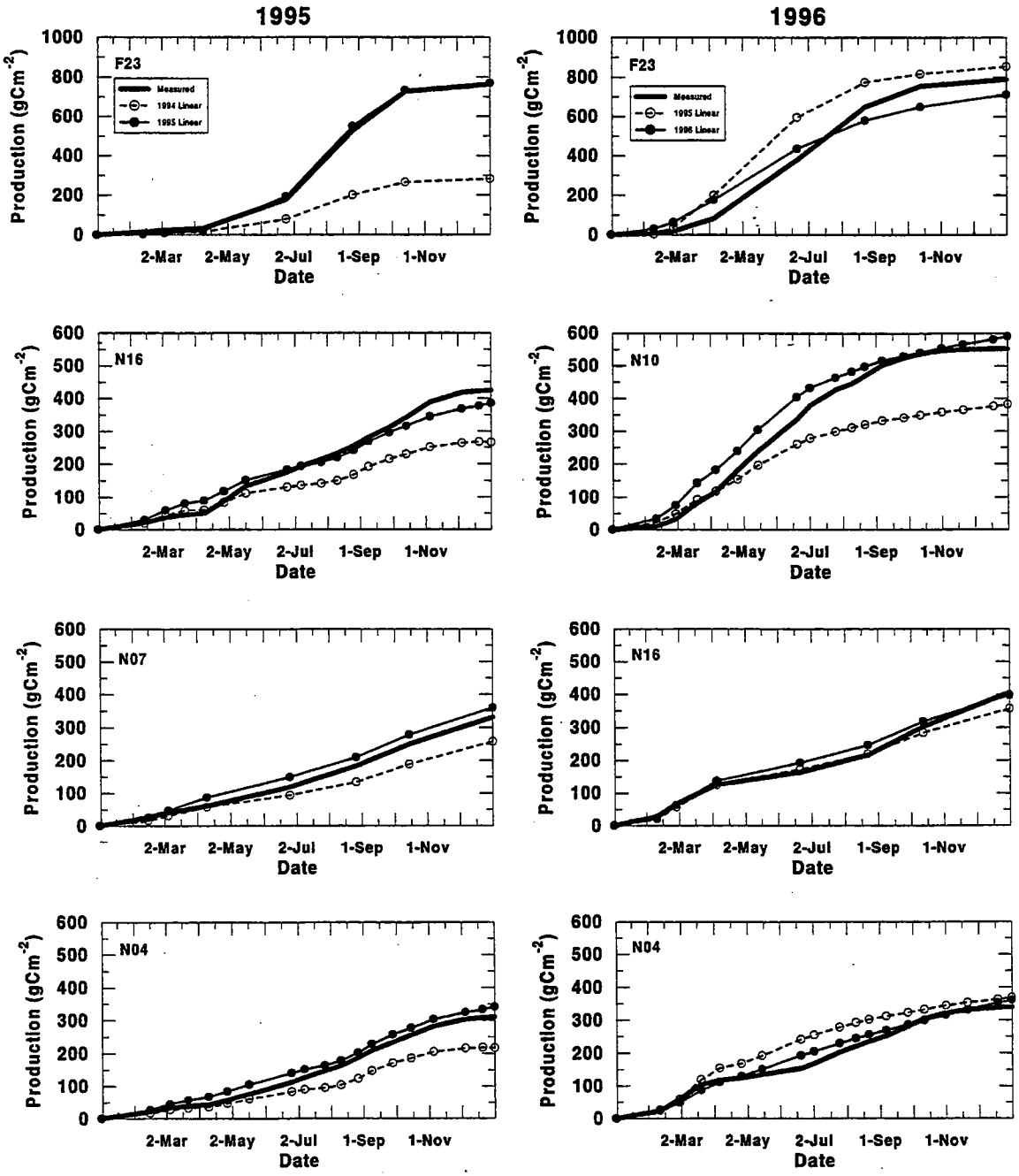

FIGURE 7-35

Comparison of the effects of modeling error on determination of annual or seasonal production. Heavy solid line, integrated production determined from measured ^{14}C-production. Dashed line, integrated production from the BZ_pI_o model calibrated from previous year's data. Thin solid line, integrated production from the BZ_pI_o model calibrated from present year's data.

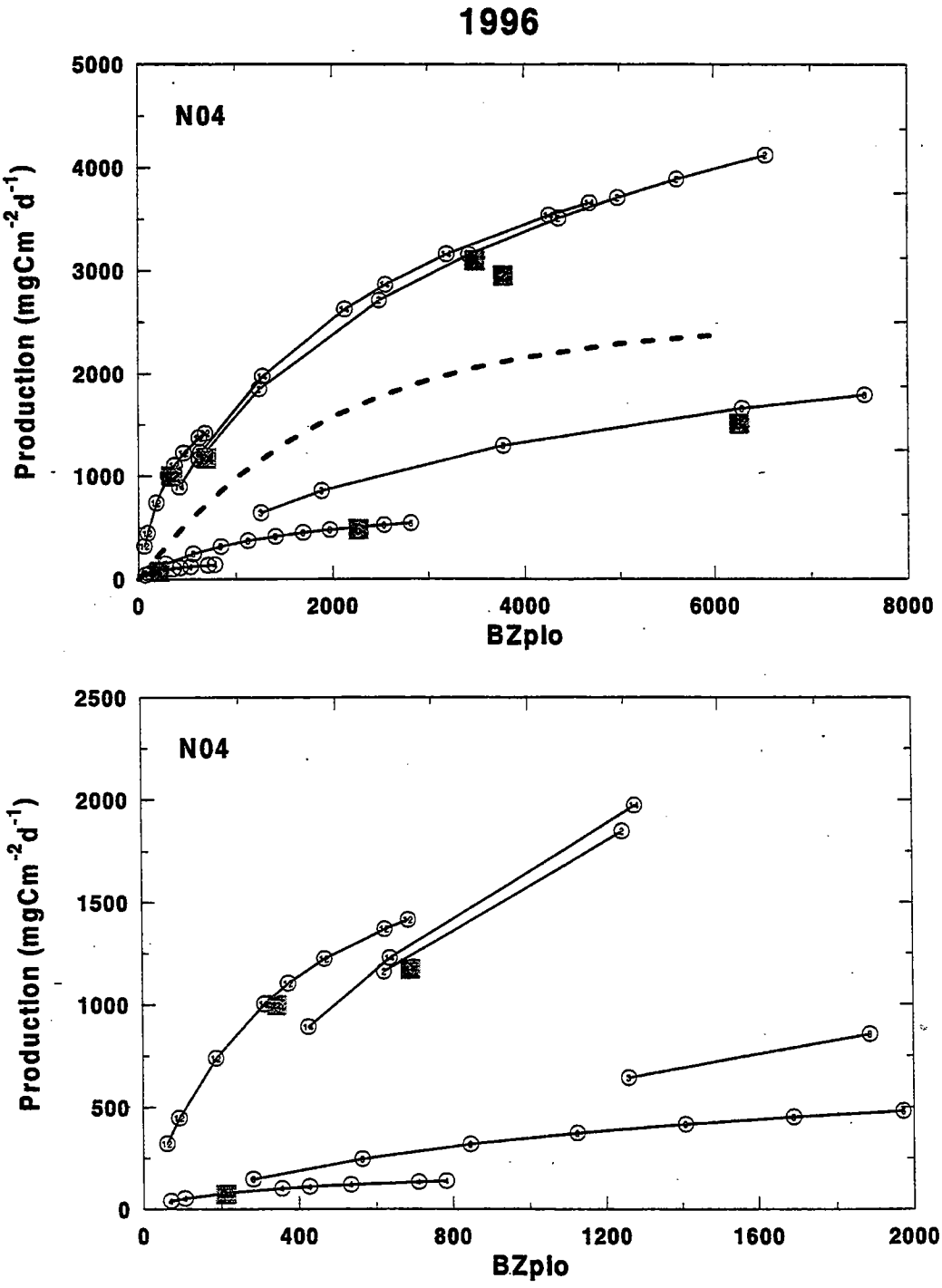

FIGURE 7-36

Relationship of water column areal production vs. the composite parameter BZ_pI_o for Station N04. The only component varied in the composite parameter was I_o as described in the text. Resultant areal production was computed in the normal fashion (Cibik, et. al., 1997, Methods). Open circles, areal production obtained at I_o ranging from 5 to ~80 $Em^{-2}d^{-1}$. Shaded squares, production occurring under the natural incident light field on the date of the survey.

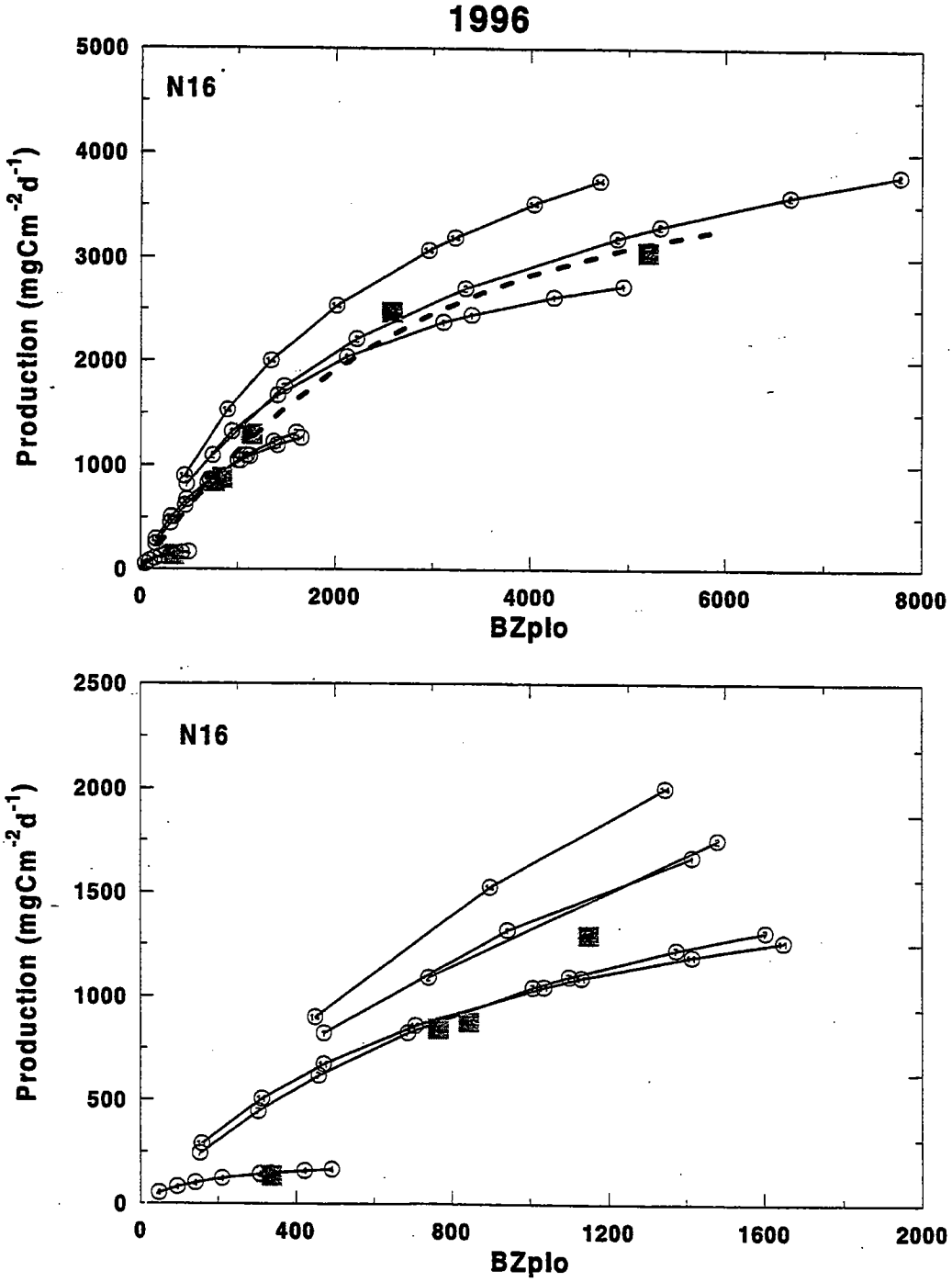

FIGURE 7-37
Relationship of water column areal production vs. the composite parameter BZ_pI_o for Station N16. Legend as in Figure 7-36.

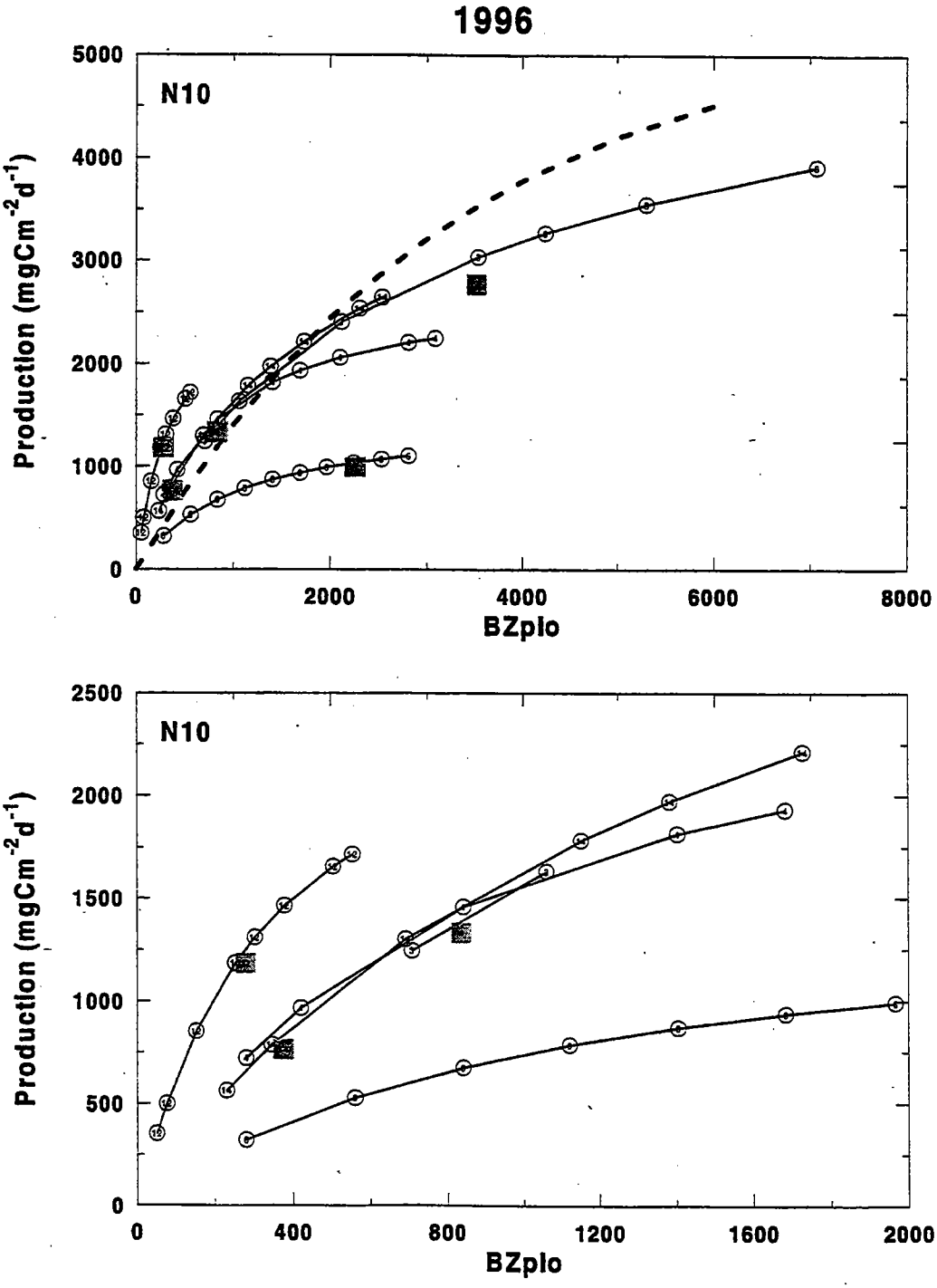

FIGURE 7-38
Relationship of water column areal production vs. the composite parameter BZ_pI_o for Station N10. Legend as in Figure 7-36.

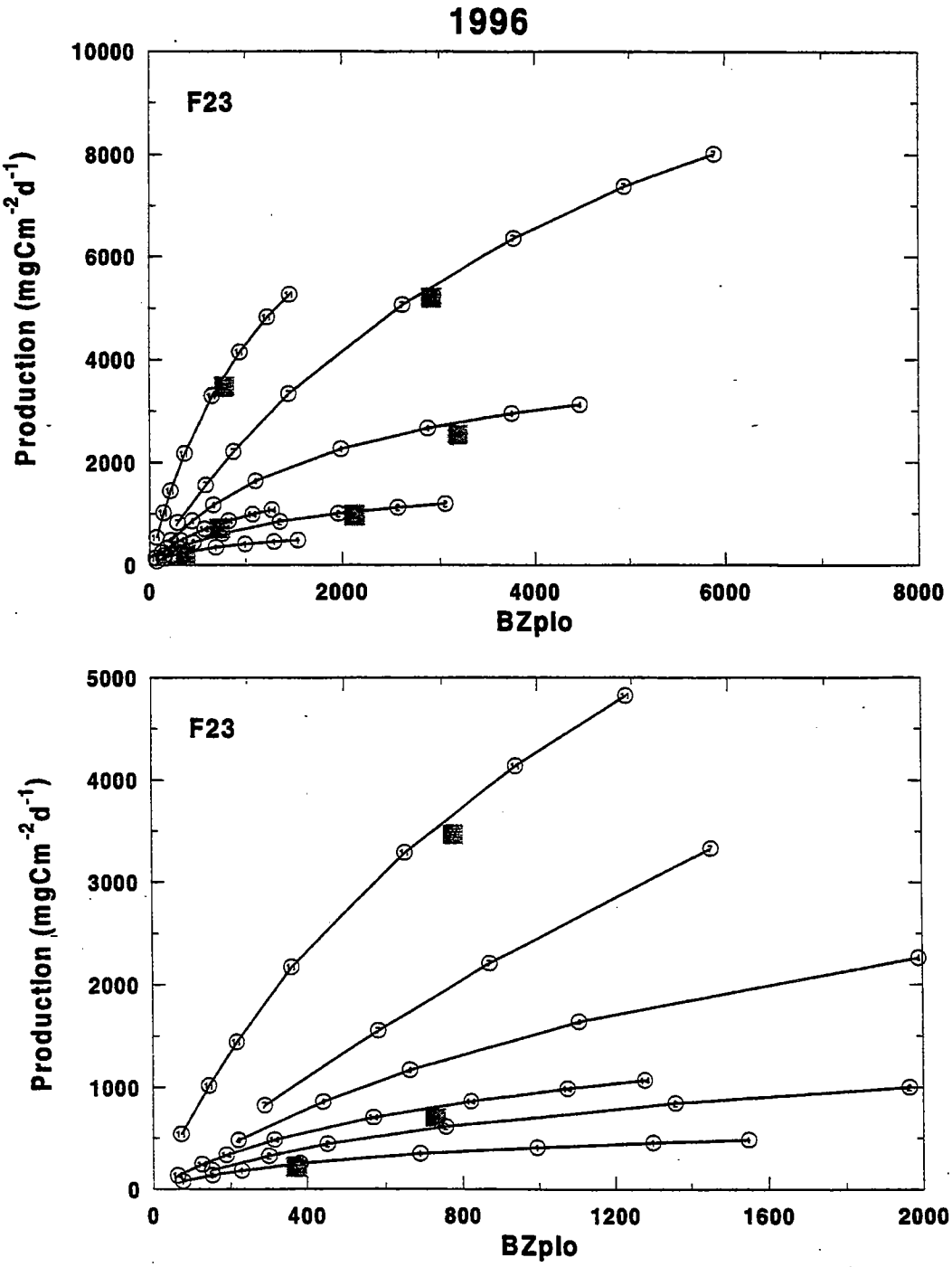

FIGURE 7-39
Relationship of water column areal production vs. the composite parameter BZ_pI_o for Station F23. Legend as in Figure 7-36.

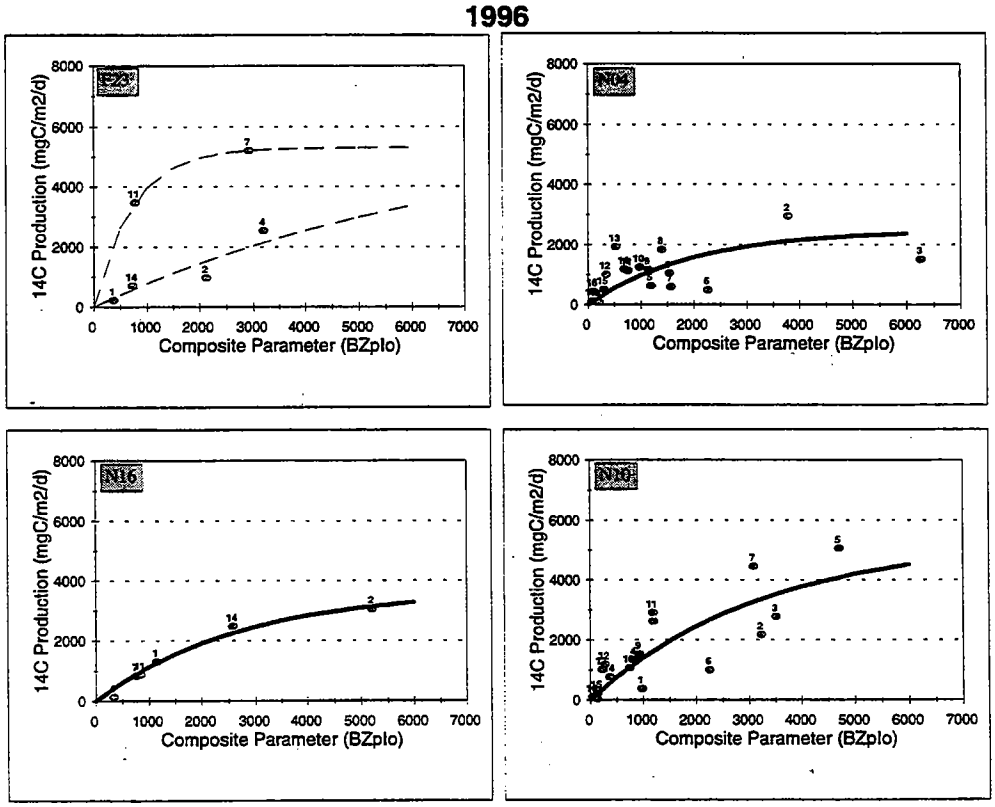

FIGURE 7-40
Nonlinear regressions of ^{14}C-production vs. composite parameter BZ_pI_o for Stations F23, N10, N16 and N04 in 1996

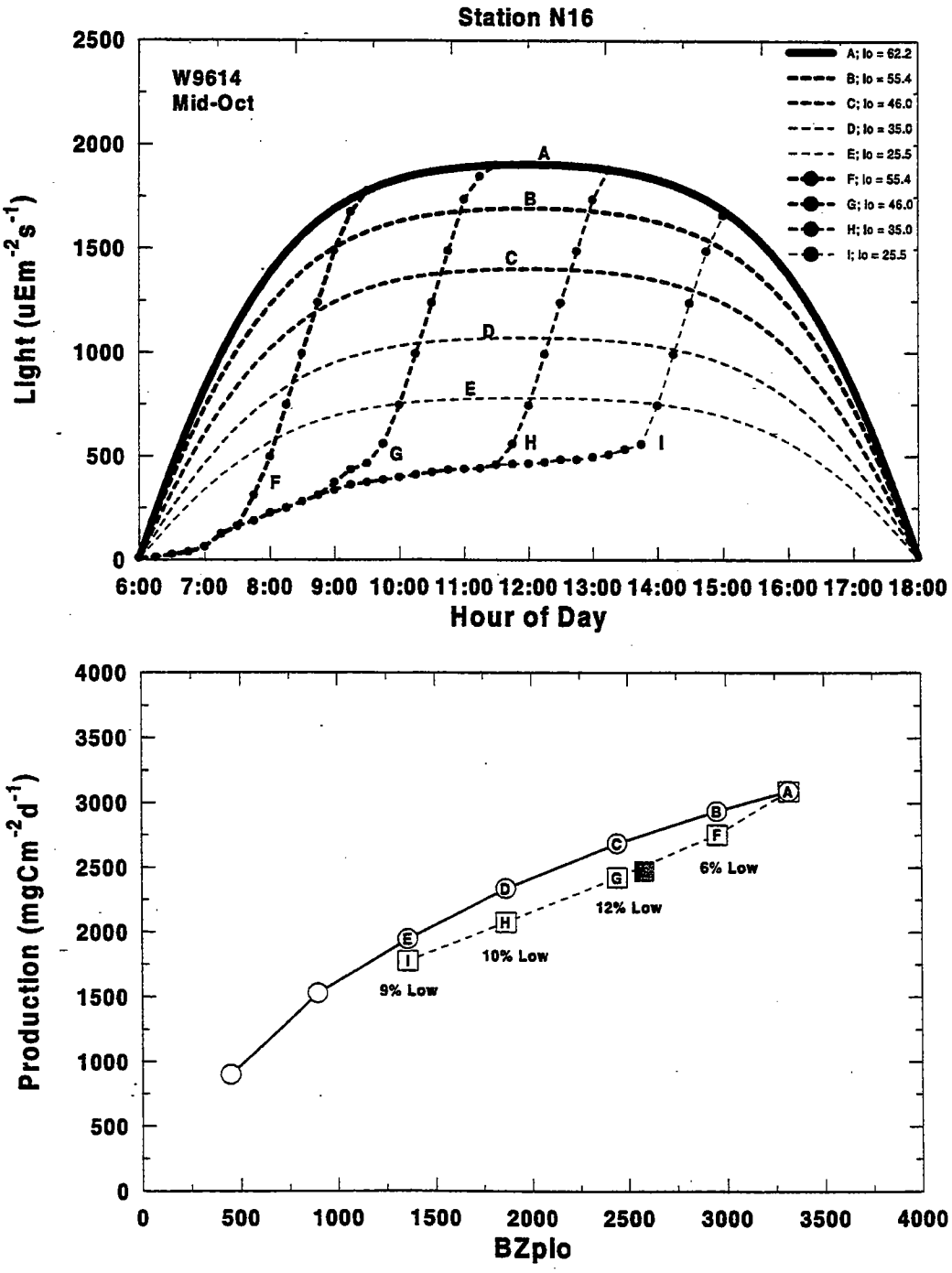

FIGURE 7-41

Effect of the shape of the incident daily light field upon areal production. Upper panel, hypothetical light field on overcast days (B-E) or sunny days (A) truncated by varying periods of cloudiness (F-I). Note that the total incident daily light ($Em^{-2}d^{-1}$) is the same for curves B & F, C & G, D & H, E & I. Lower panel, effect of indicated light field on areal production. Shaded square, production under the natural light field experienced during the W9614 survey.

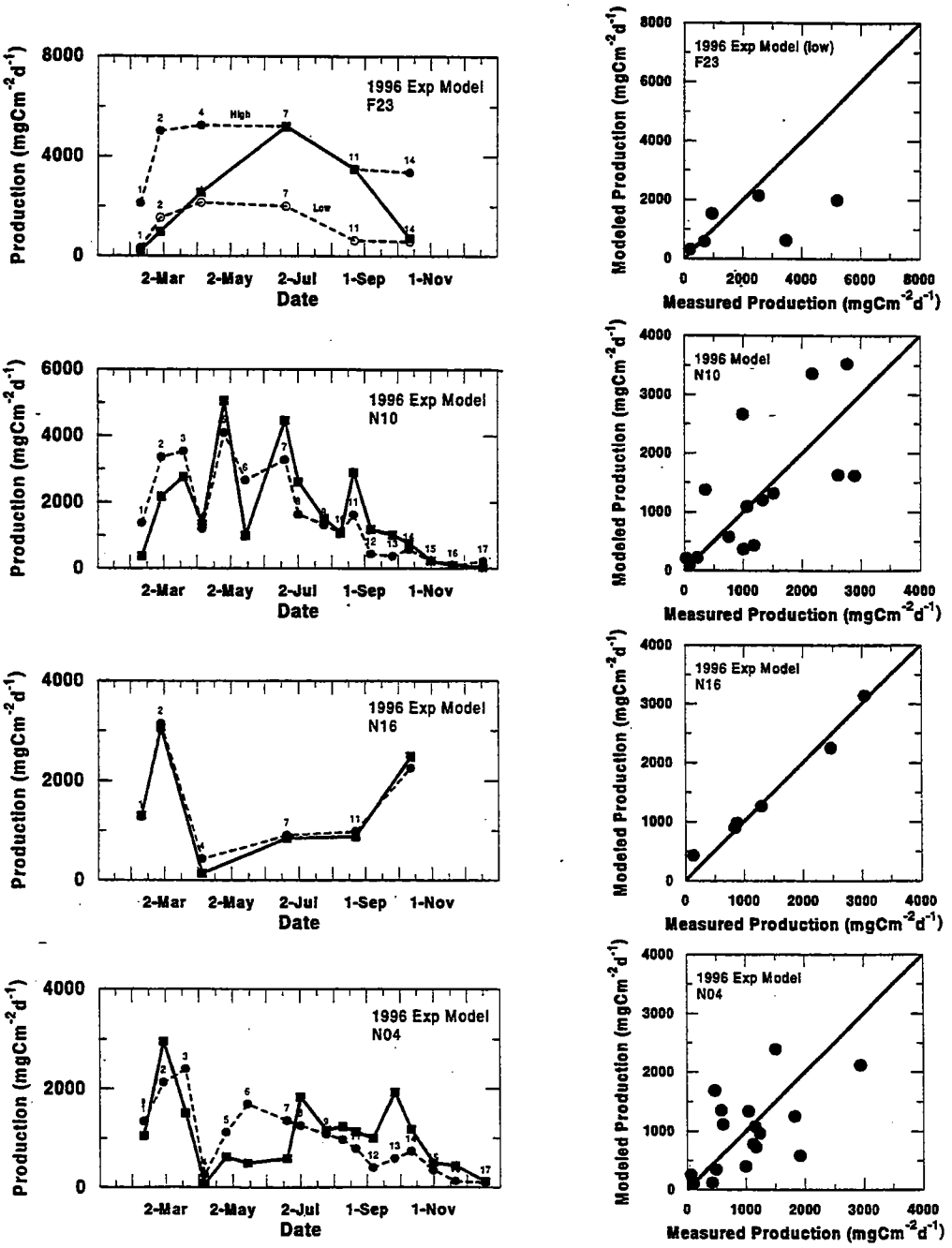

FIGURE 7-42

Comparison of measured 1995 seasonal ^{14}C-production with production estimated using nonlinear BZ_pI_o regression parameters. Left panels, Solid lines, measured ^{14}C-production; dashed lines, model estimated production. Right panels, Plots of BZ_pI_o modeled production vs. measured ^{14}C-production for 1996 data. Solid line, 1:1 line.

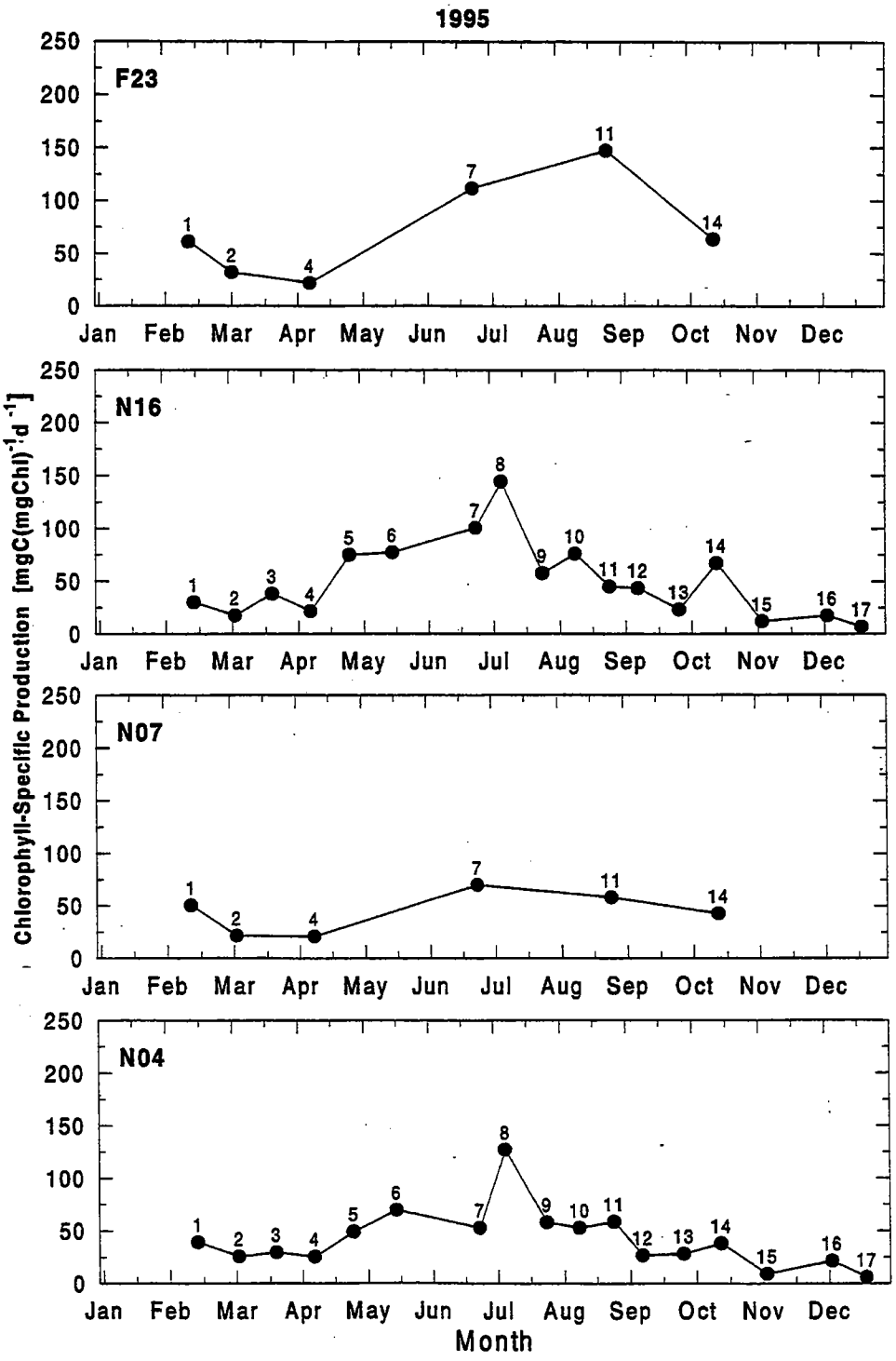

FIGURE 7-43
Water column chlorophyll-specific production over the 1995 season

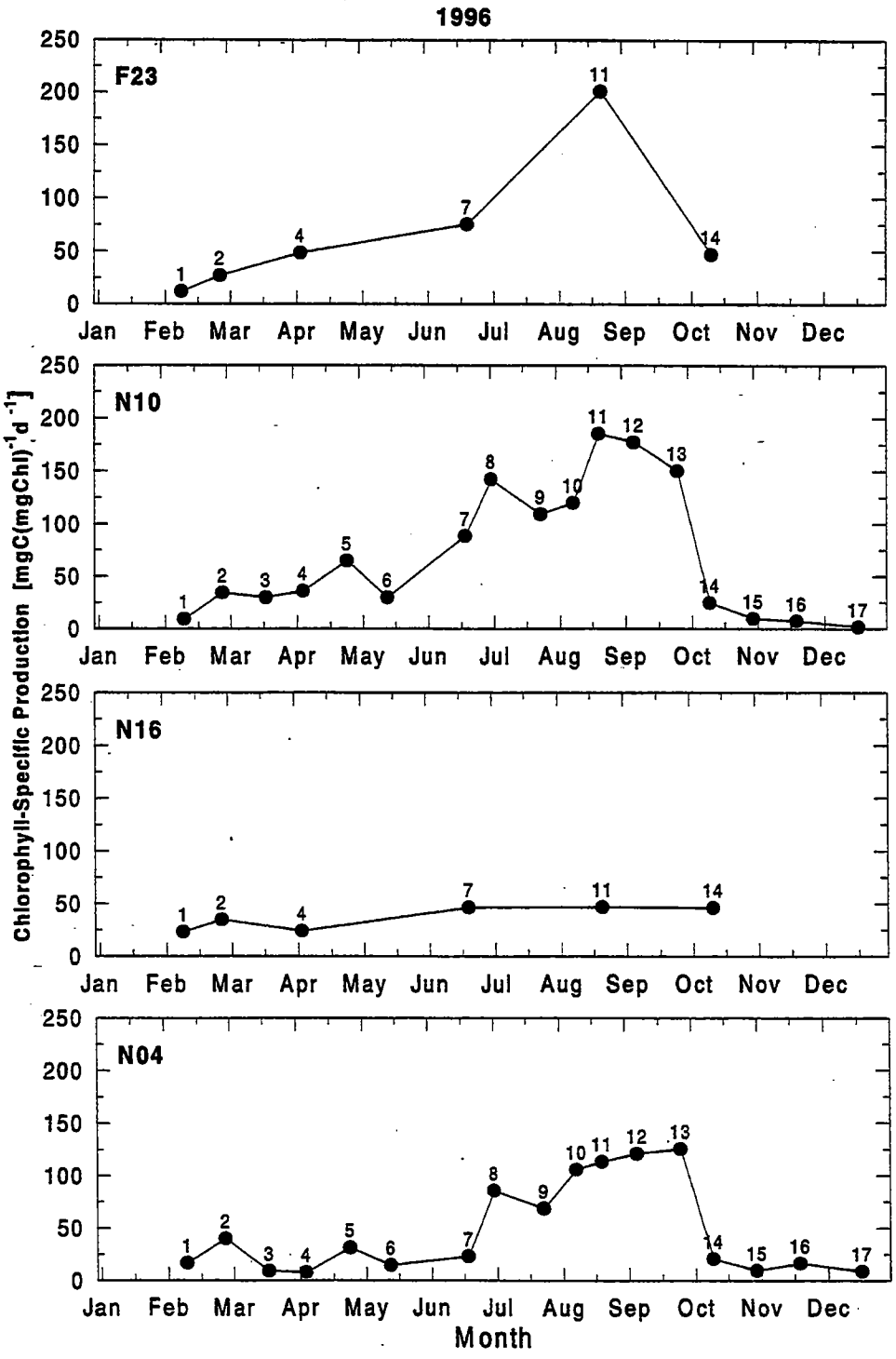

FIGURE 7-44
Water column chlorophyll-specific production over the 1996 season

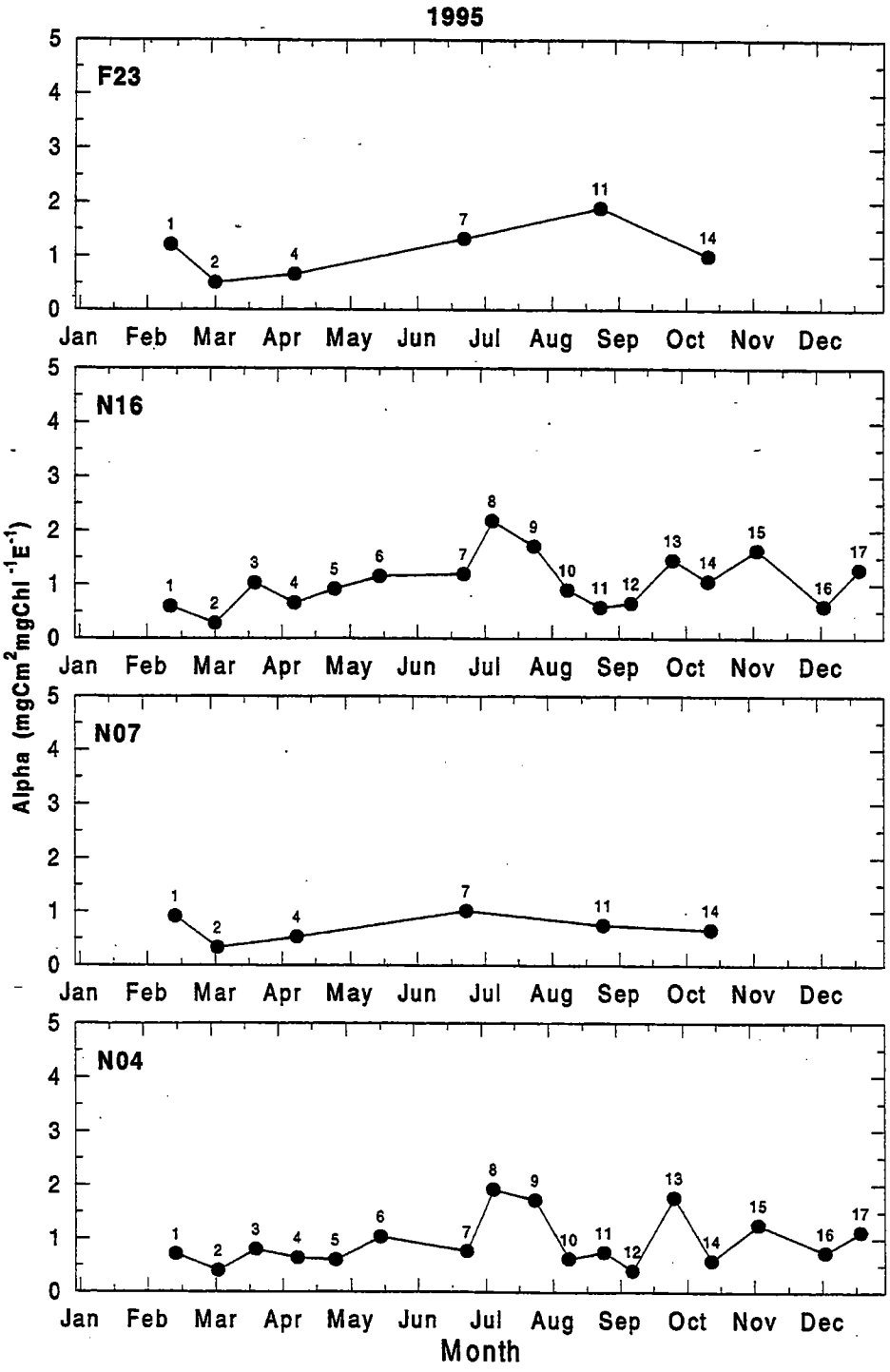

FIGURE 7-45
Depth integrated Alpha over the 1995 season

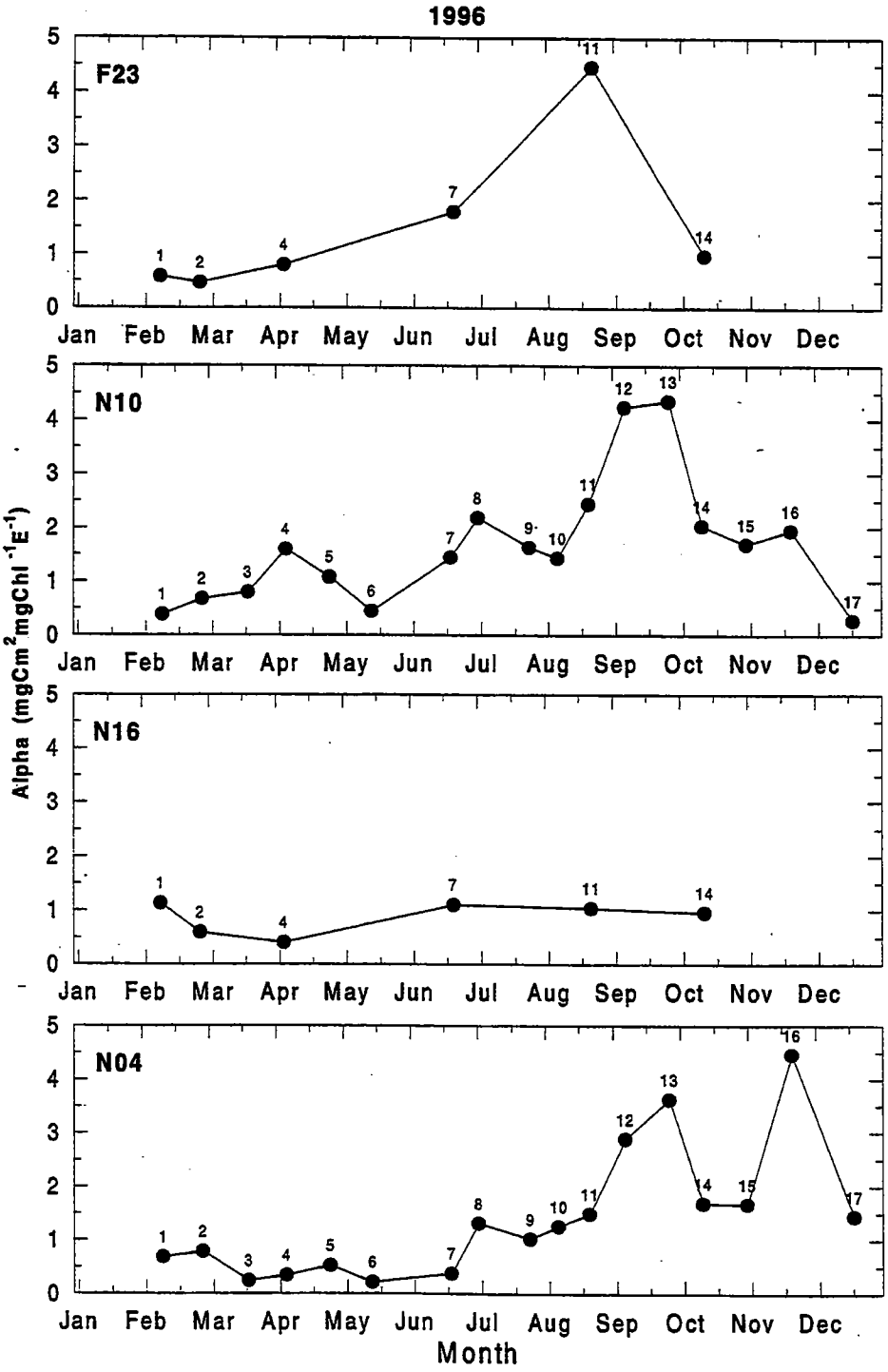

FIGURE 7-46
Depth integrated Alpha over the 1996 season

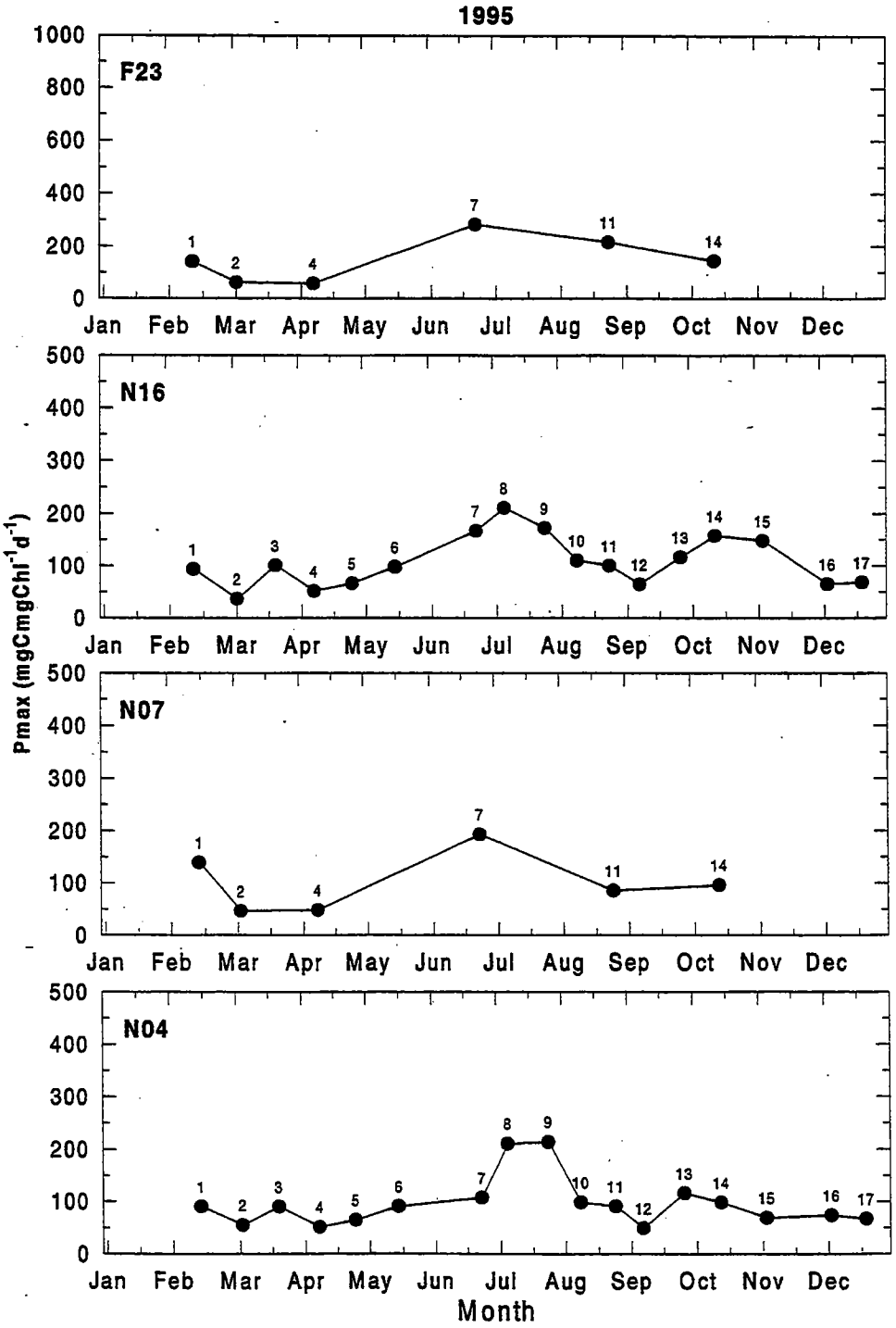

FIGURE 7-47
Depth integrated Pmax over the 1995 season

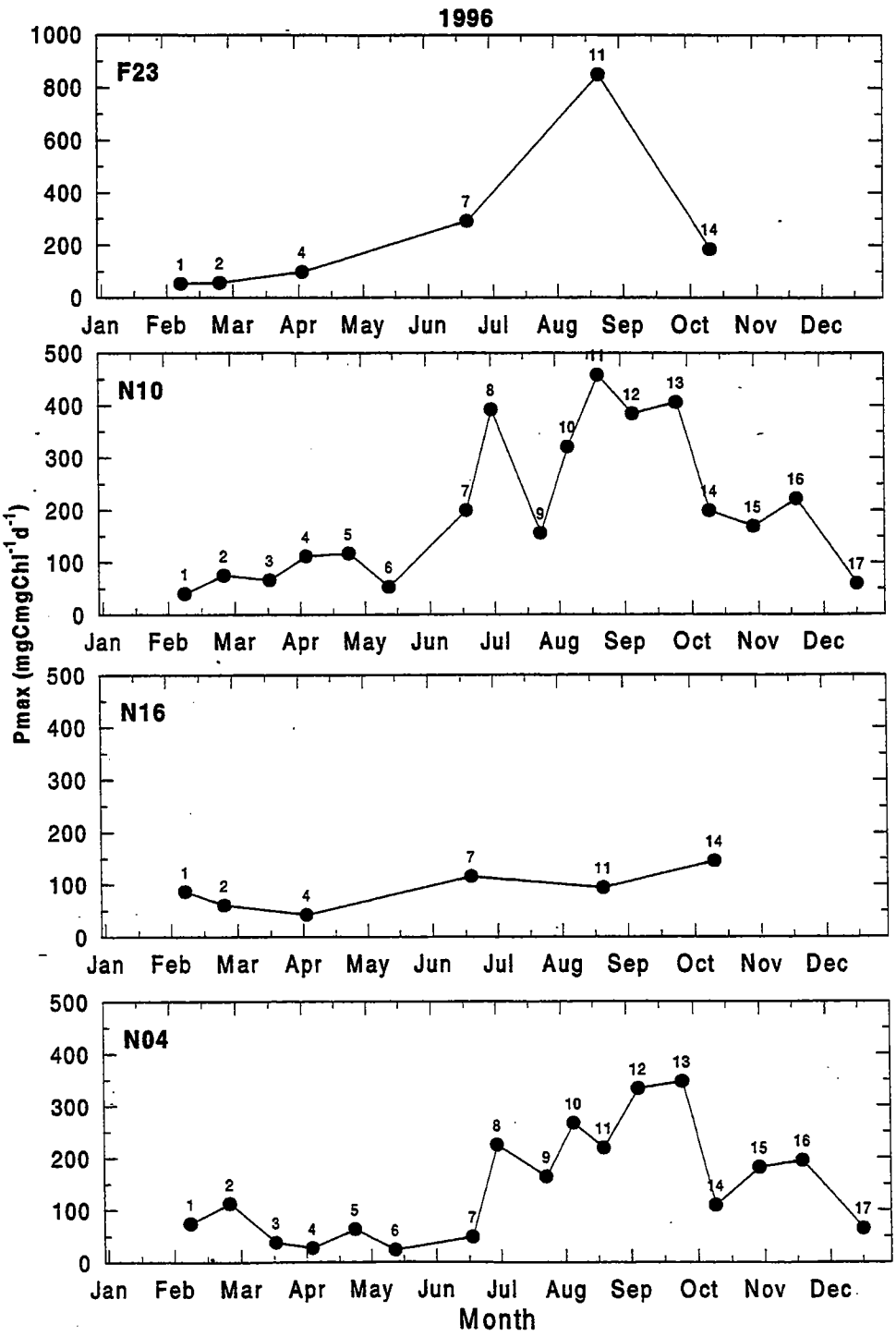

FIGURE 7-48
Depth integrated Pmax over the 1996 season

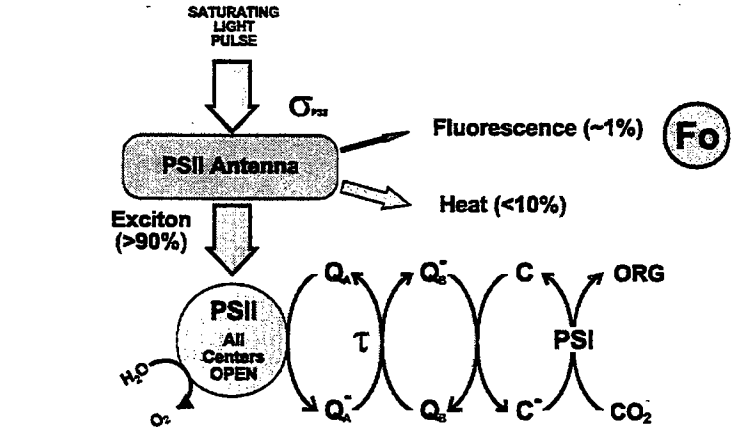

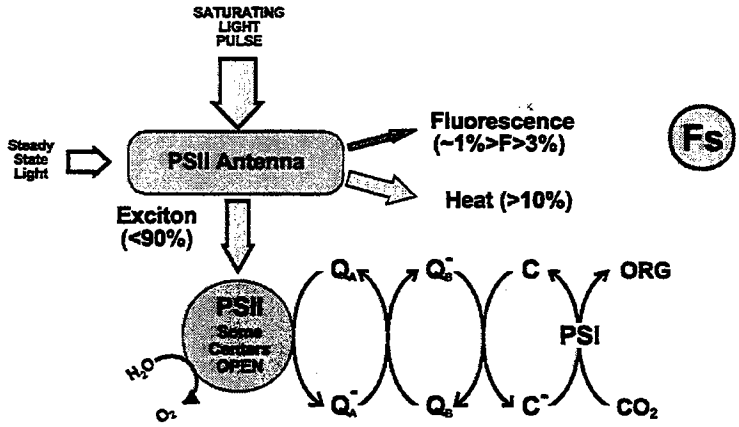

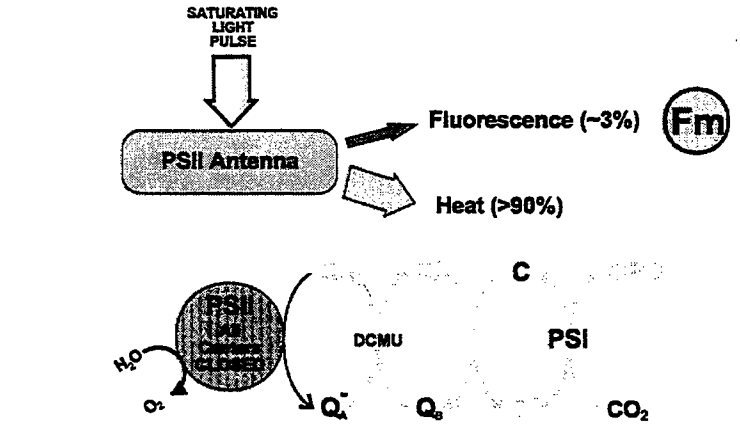

$$\Delta\Phi = \frac{F_m - F_o}{F_m} = \frac{F_{DCMU} - F_o}{F_{DCMU}}$$

FIGURE 7-49

Simplified schematic of the functioning of the light producing components of the phytoplankton photosystem. Photosynthesis light reactions are executed by photosystem II (PSII) which is composed of a pigment "antenna" (shown in green) that is the primary absorber of light and PSII reaction centers that are associated with a primary electron acceptor Q_A (shown in pink). When light strikes the antenna a chlorophyll molecule is ultimately transformed into an excited state. This energy is either passed on to a PSII reaction center (blue arrows) or dissipated as heat and fluorescence (red and pink arrows, respectively). When an "exciton" is passed to a PSII reaction center Q_A accepts an electron derived from the oxidation of water. When Q_A is reduced (Q_A^-) the reaction center will not accept another exciton and is said to be "closed." Energy from the absorption of another photon by the antenna will be dissipated as heat and fluorescence. The reaction center is returned to the "open" energy accepting state by the reoxidation of Q_A by transfer of an electron to a secondary electron acceptor Q_B and ultimately, via a complex electron transport chain, to photosystem I (PSI) where CO_2 is reduced to organic carbon. During steady state photosynthesis at a given light intensity a steady state fraction of the large population of PSII reaction centers of the photosynthetic apparatus will be in either the "open" and "closed" state and a proportional amount of "stimulated" or "active" fluorescence emitted (Fs, middle panel). If phytoplankton cells are sequestered in the dark for a period of time, continued electron transport to PSI ultimately results in the oxidation of Q_A and PSII in a state where all reaction centers are open (upper panel). If the cells are subjected to a saturating pulse of visible light there is a initial maximal transfer of energy to the entirely open population of PSII reaction centers and a resultant minimal fluorescent emission (Fo), which can be sensed by an appropriate detector. Soon, however, the saturating flood of energy passed to PSII results in the complete reduction of Q_A, closure of all reaction centers and resultant approximately 2-3 fold increase in fluorescence. Measurement of maximal fluorescence (Fm) should be made before electron transport results in significant reopening of the reaction centers. The ratio (Fm - Fo)/Fm is the maximum change in the quantum yield of fluorescence ($\Delta\Phi_{max}$), and can be used as a surrogate index of Φ_{max} (Falkowski, 1992). It is possible to use the photosynthesis inhibitor DCMU and a standard fluorometer to acquire an estimate of $\Delta\Phi_{max}$. Fo is determined by the measurement of in vivo fluorescence as quickly as possible after introduction of dark adapted samples (30 min in dark) into the fluorometer. After the reading is made DCMU is introduced into the sample, followed by exposure for ~ 1 min to white light to close all reaction centers by prevention of the reoxidation of the electron carrier Q_A.

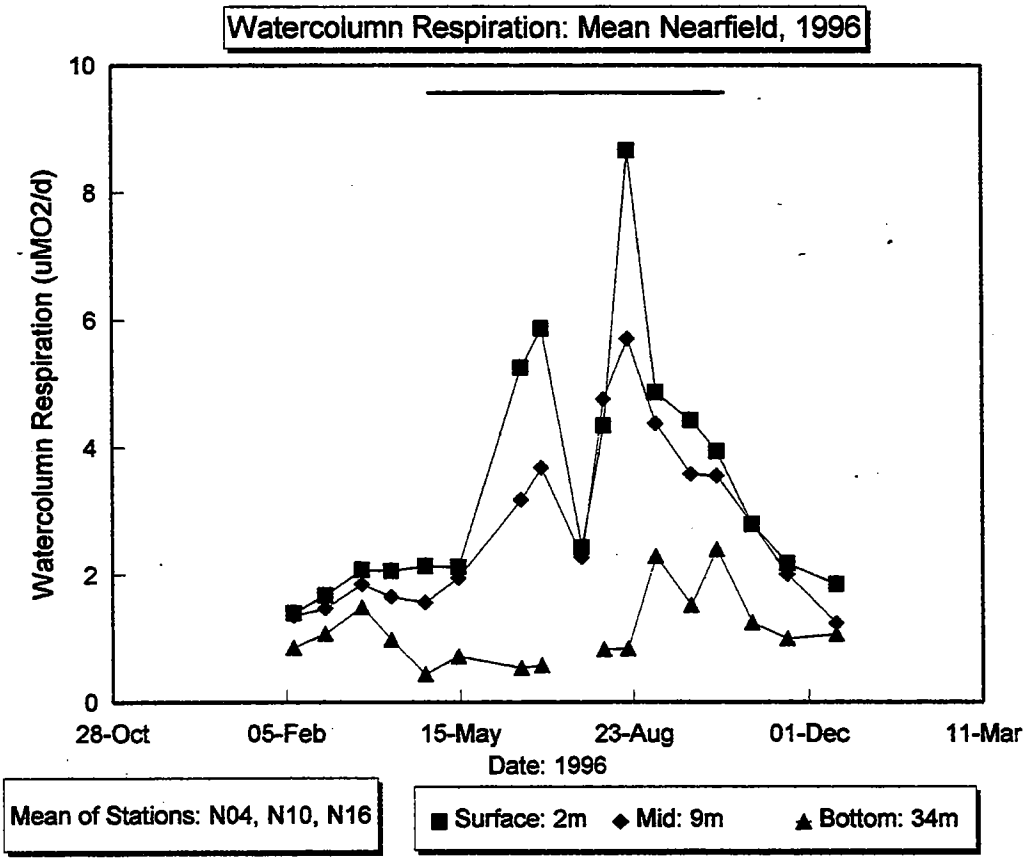

FIGURE 7-50

Vertical distribution of average water column respiration in the Nearfield region of Massachusetts Bay throughout 1996. Bar represents interval of stratification.

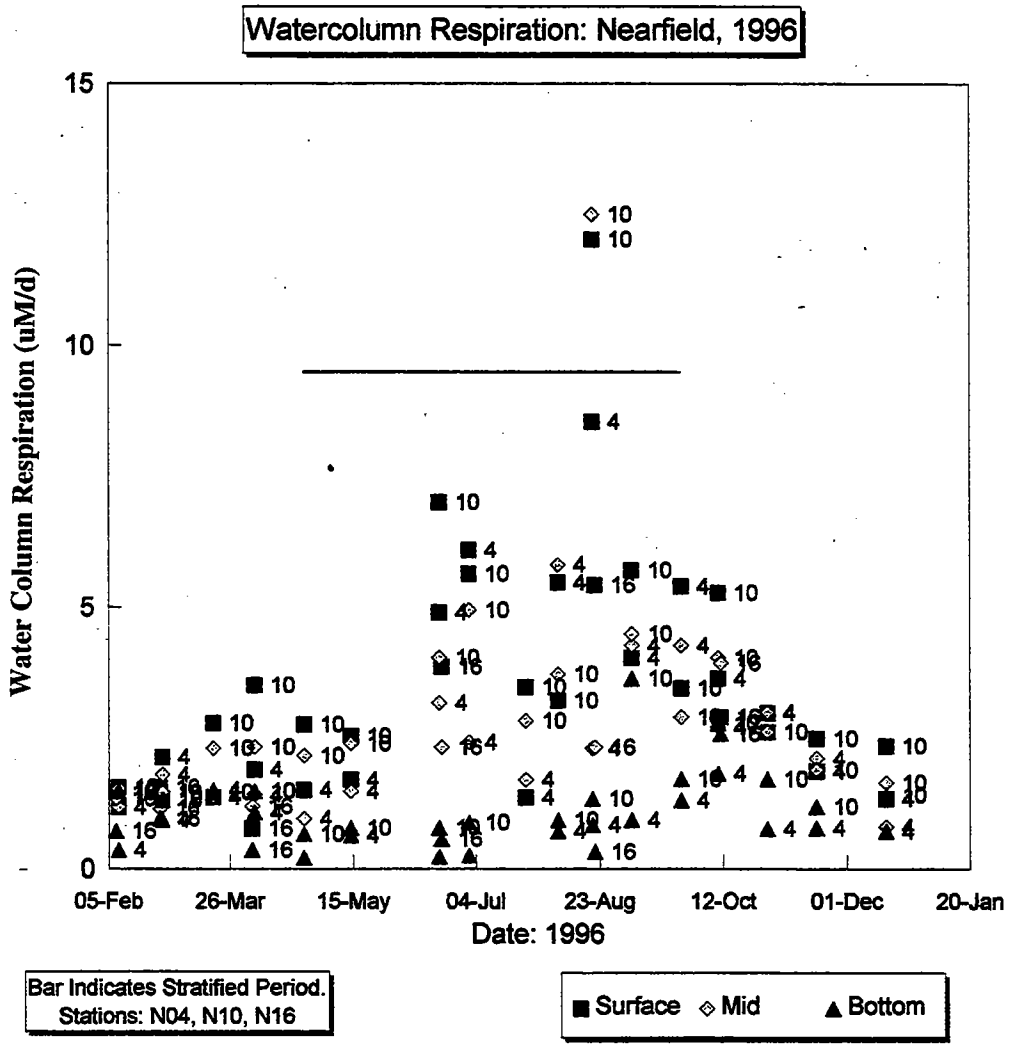

FIGURE 7-51

Vertical distribution of water column respiration at stations N04, N10 and N16 within the Nearfield region of Massachusetts Bay throughout 1996. Bar represents interval of stratification.

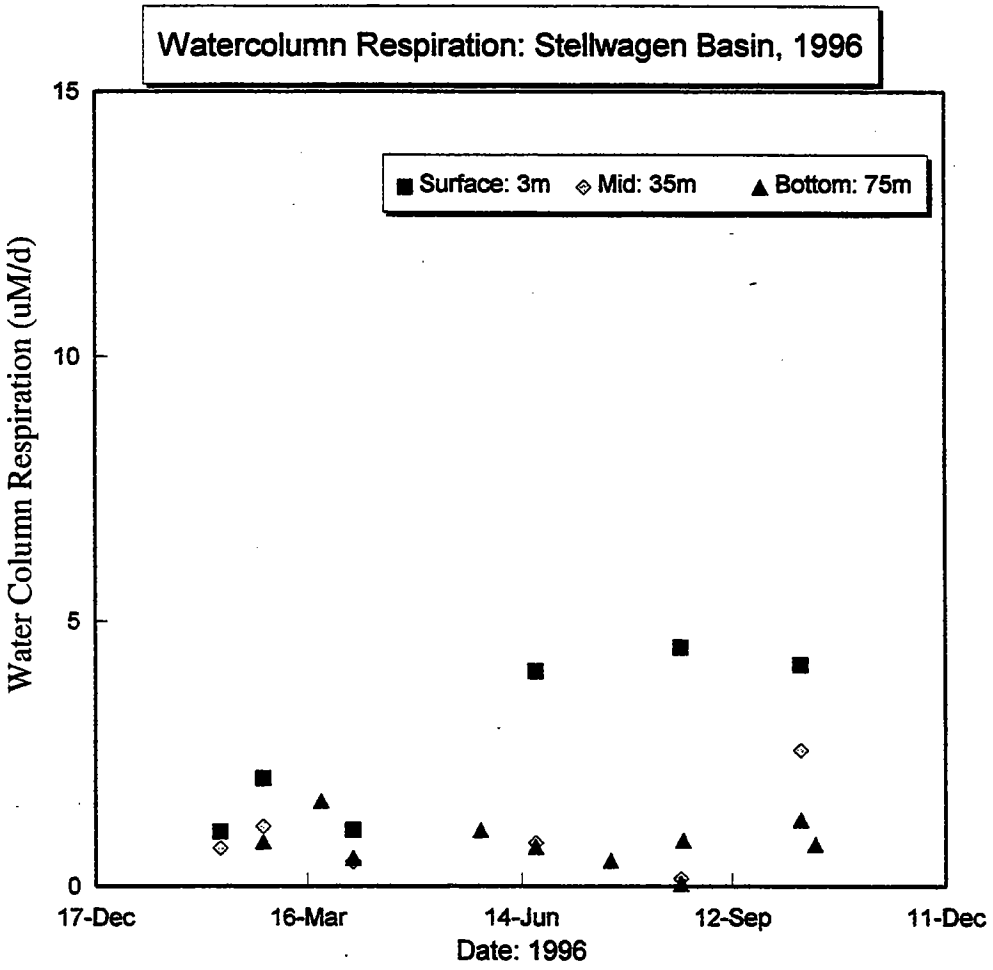

FIGURE 7-52

Vertical distribution of water column respiration at station F19 in Stellwagen Basin throughout 1996.

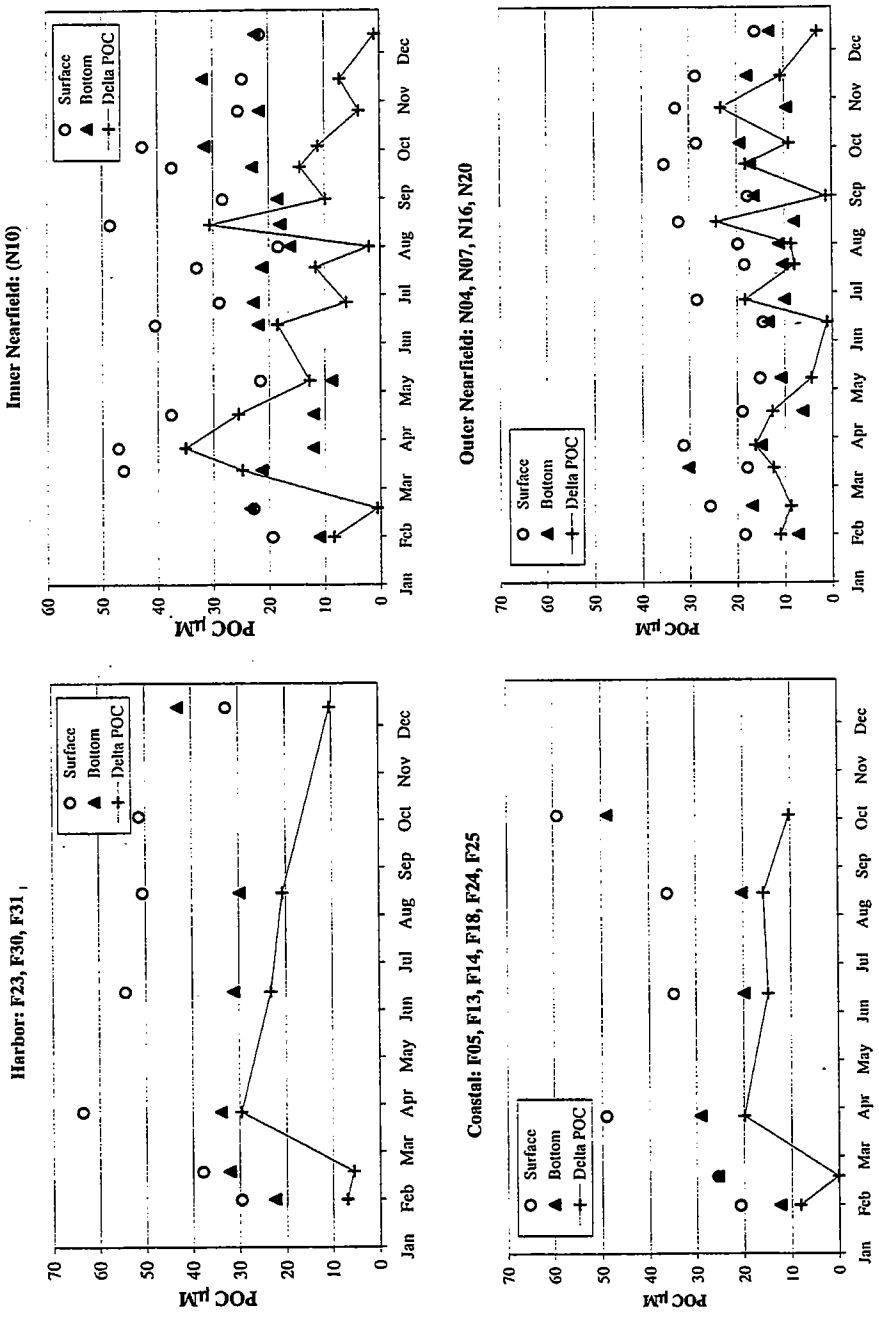

FIGURE 7-53a
1996 Regional Particulate Organic Carbon (POC) Concentration Averages
Surface, Bottom, and Delta (Surface-Bottom) Survey Averages

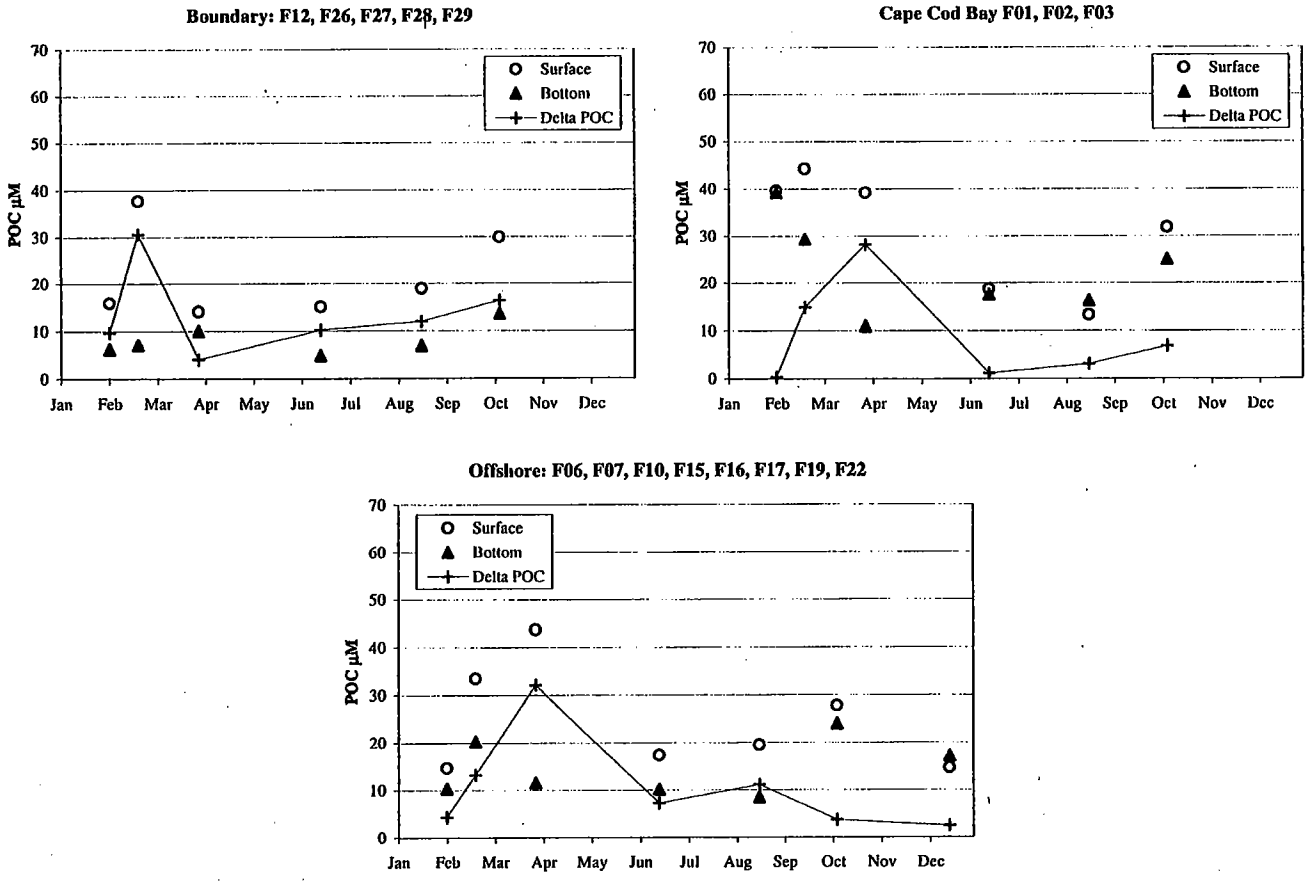

FIGURE 7-53b

1996 Regional Particulate Organic Carbon (POC) Concentration Averages

Surface, Bottom, and Delta (surface-Bottom) Survey Averages

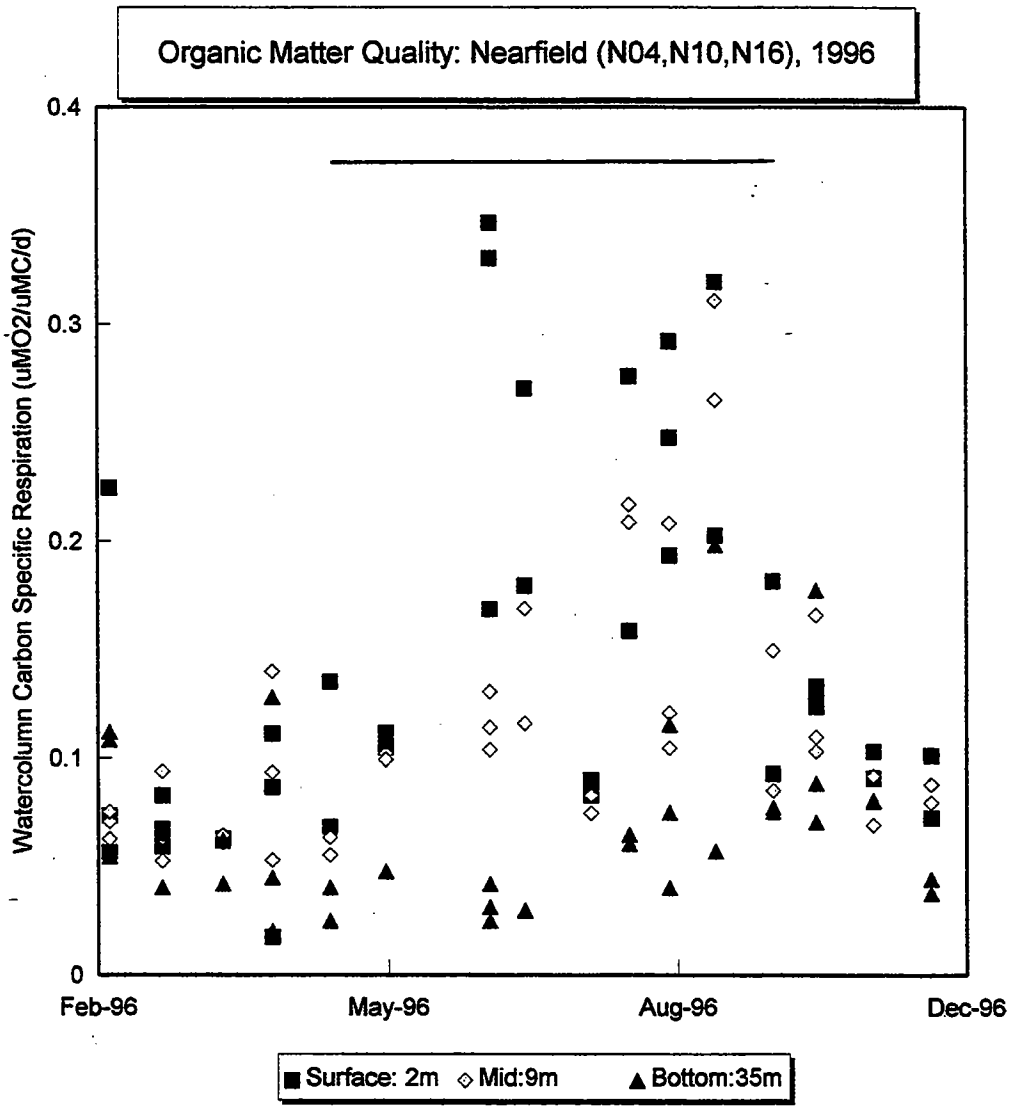

FIGURE 7-54

Vertical distribution of carbon-specific water column respiration in the Nearfield region of Massachusetts Bay throughout 1996. Bar represents interval of stratification.

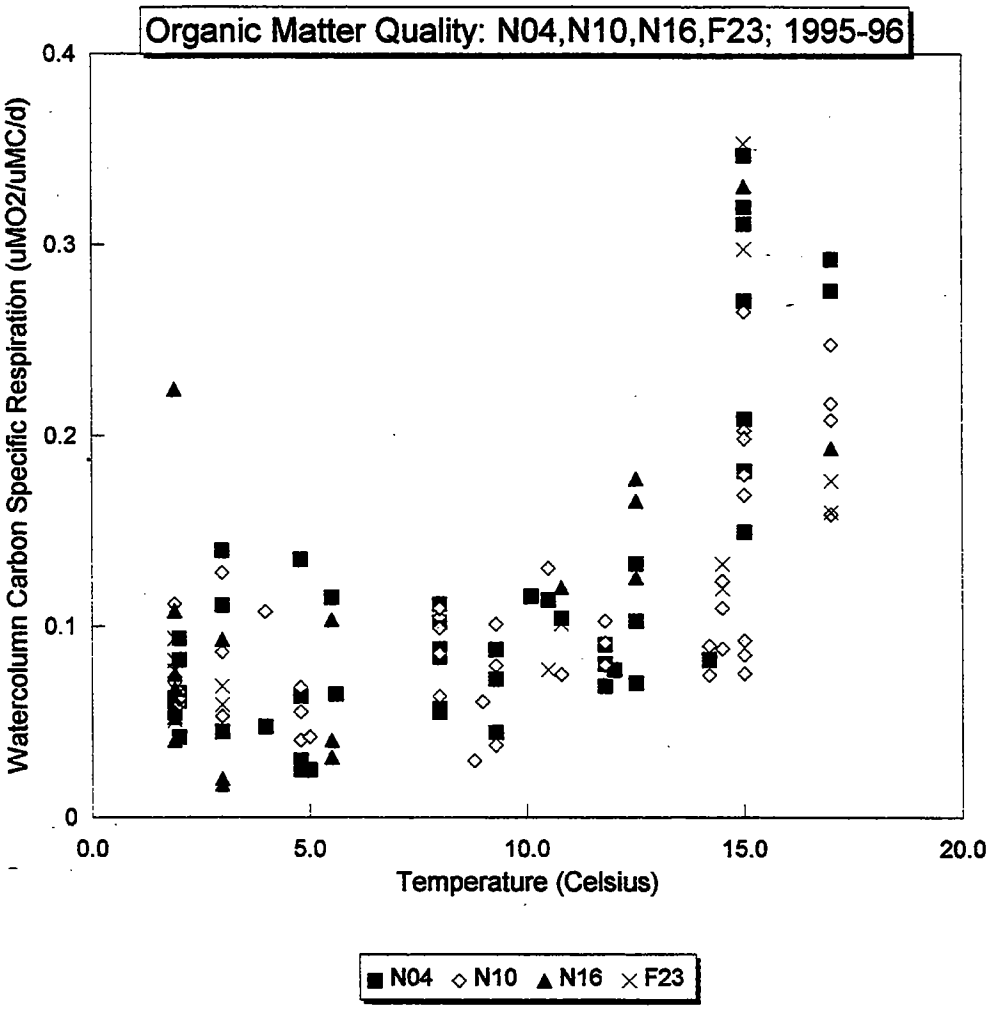

FIGURE 7-55

Relationship of carbon-specific water column respiration versus temperature in the surface, mid and bottom water of the Nearfield region of Massachusetts Bay in 1995 and 1996.

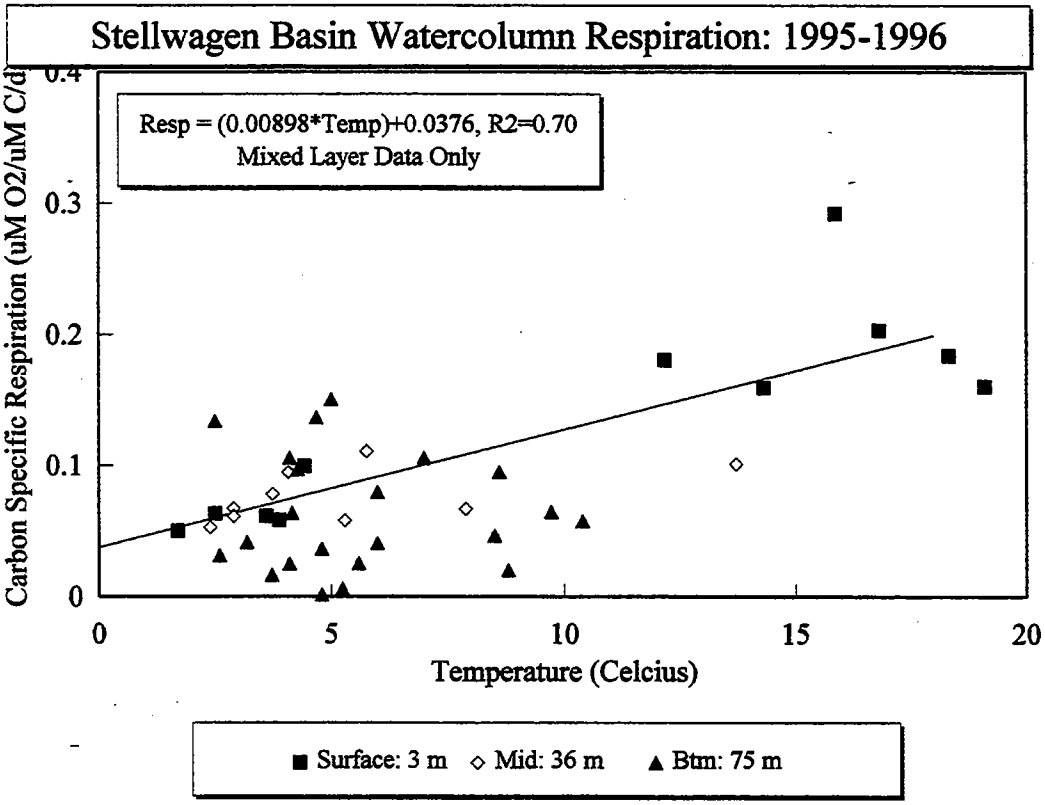

FIGURE 7-56

Relationship of carbon-specific water column respiration versus temperature in the surface, mid and bottom water of Stellwagen Basin 1995 and 1996.

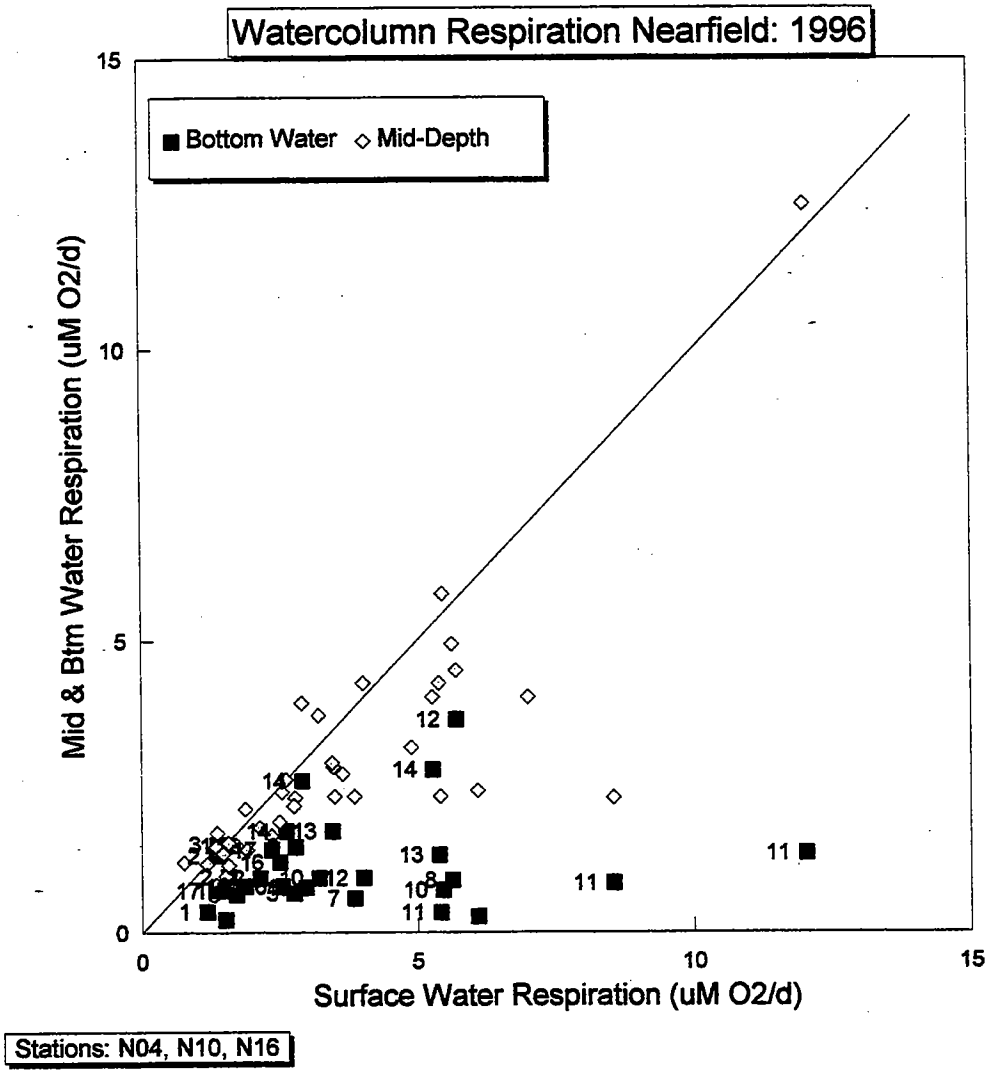

FIGURE 7-57

Comparison of respiration rates at mid and bottom depths versus surface waters in the Nearfield region of Massachusetts Bay throughout 1996. Numbers indicate survey.

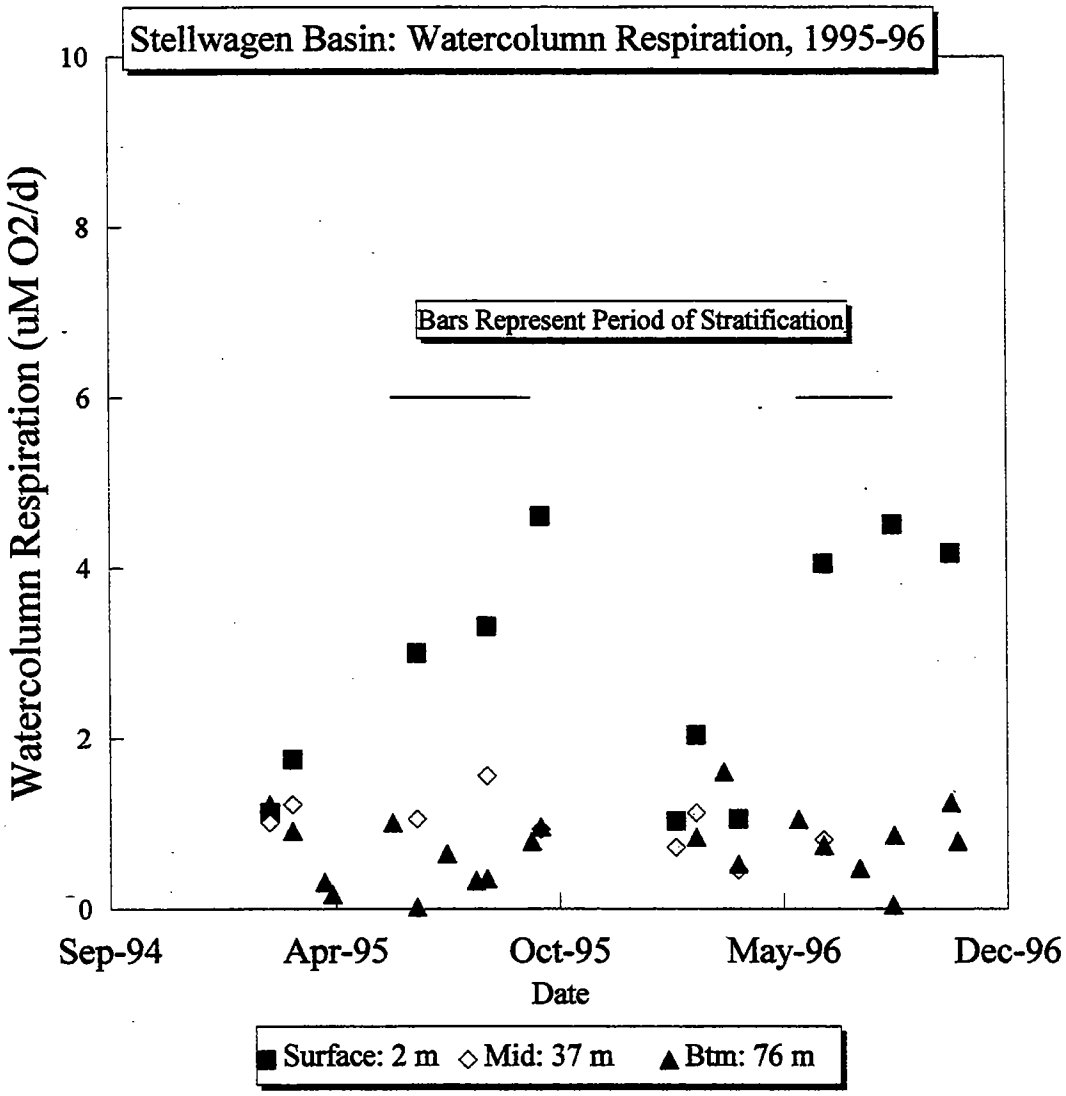

FIGURE 7-58

Depth distribution of water column respiration in 1995 and 1996 in Stellwagen Basin. Data are the compilation of measurements on both water colum and benthic flux surveys.

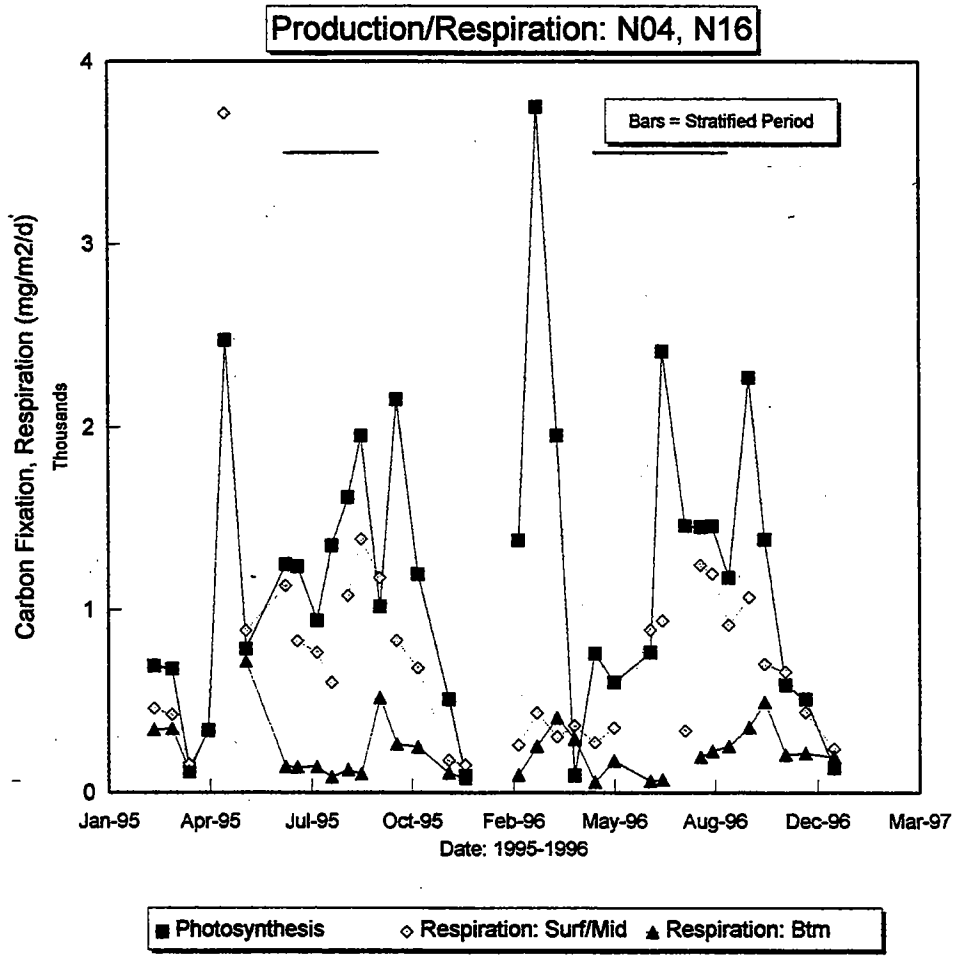

FIGURE 7-59

Mixed and bottom layer water column respiration compared to measured carbon fixation in the Nearfield region of Massachusetts Bay in 1995 and 1996.

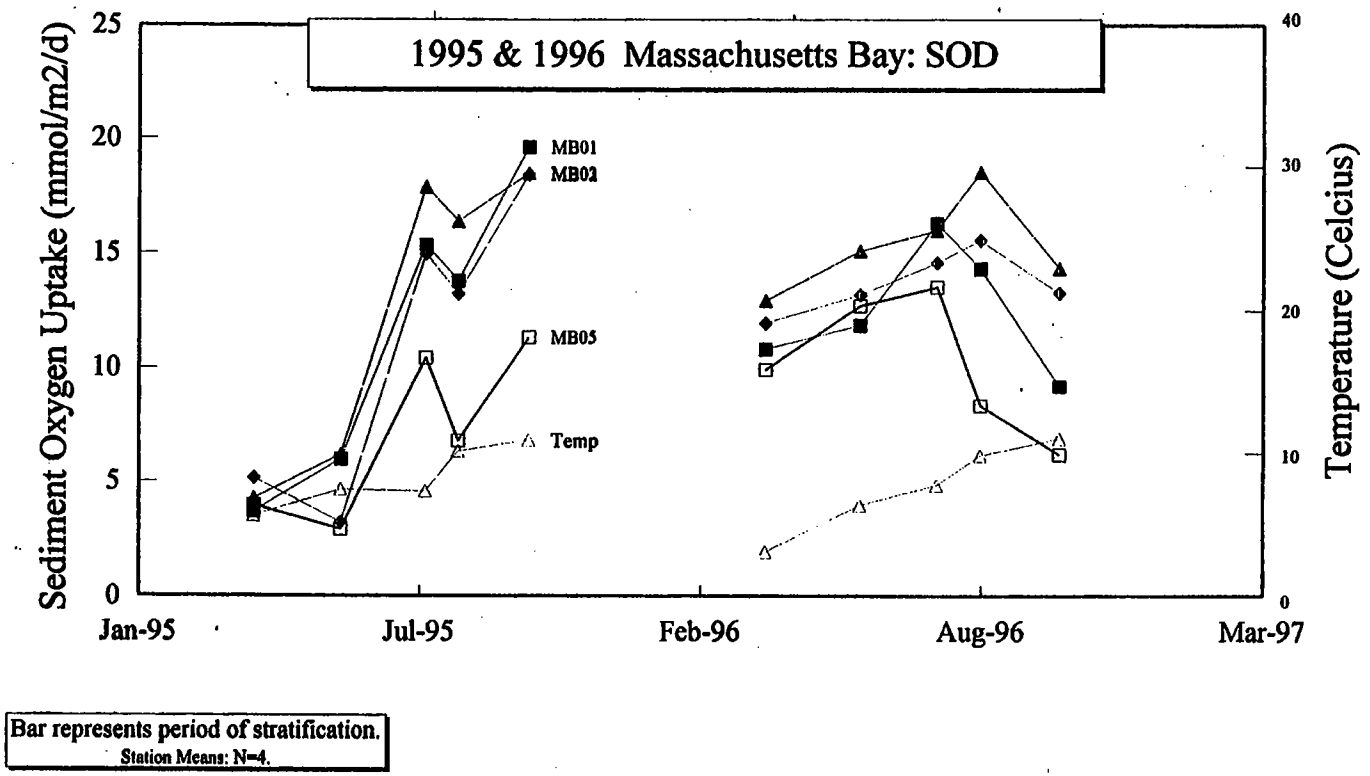

FIGURE 7-60

Sediment respiration within the Nearfield (MB01,02,03) and Stellwagen Basin (MB05) in 1995 and 1996. Temperature represents system average.

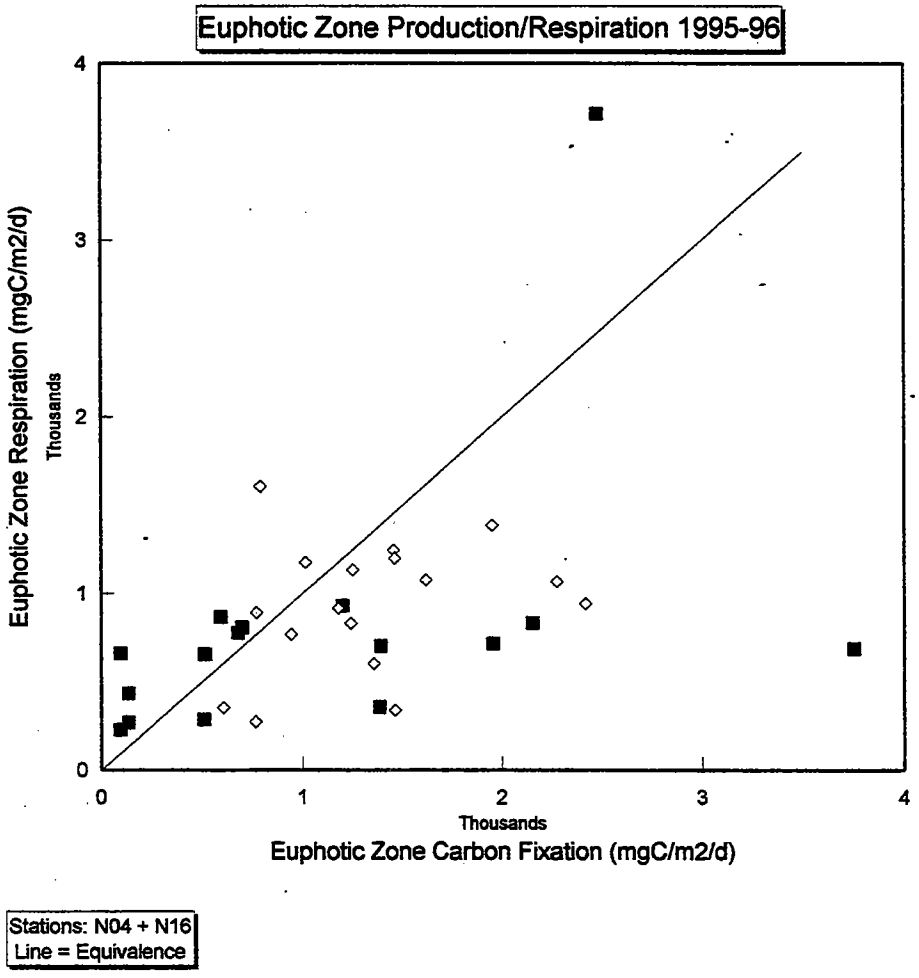

FIGURE 7-61

Respiration versus carbon fixation within the euphotic zone of the Nearfield in 1995 (diamonds) and 1996 (boxes).

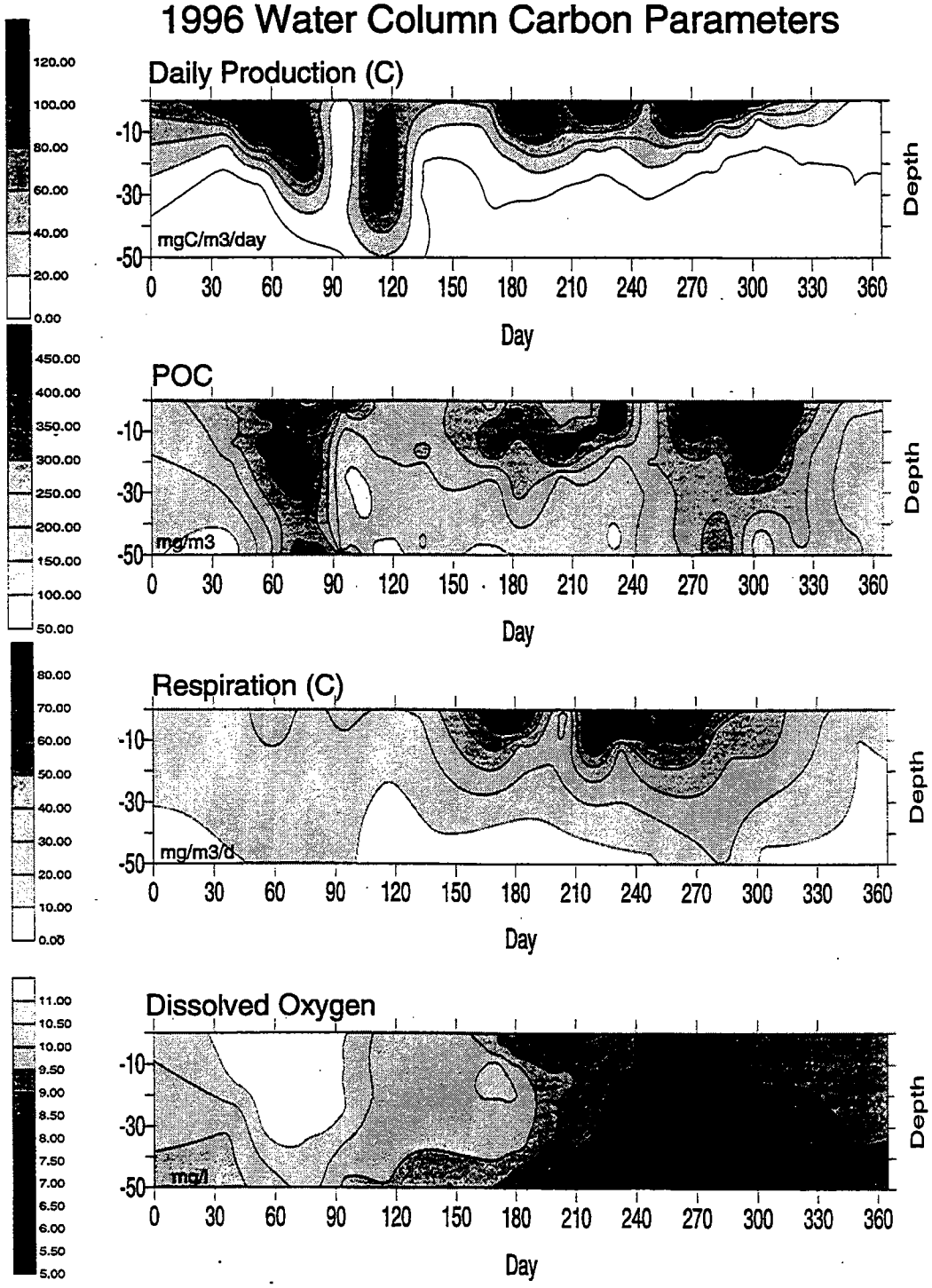

FIGURE 7-62

Contour plots of production and water column respiration rates and pools of particulate organic carbon (POC) and oxygen within the Nearfield of Massachusetts Bay during 1996.

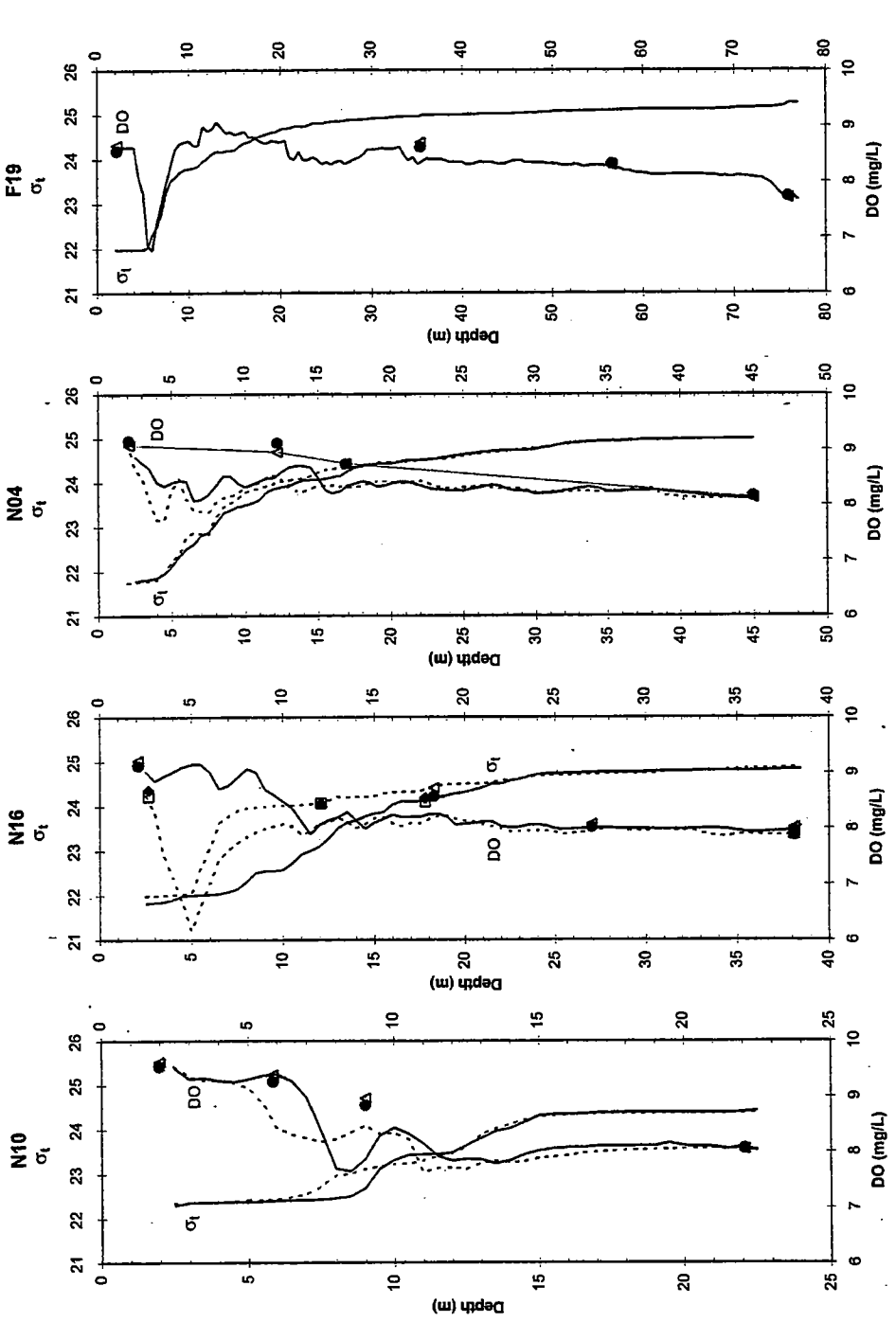

FIGURE 7-63

Distribution of Water Column DO Relative to Density During W9611
Open Symbols = Upcast Sensor Data; Closed Symbols = Lab Data

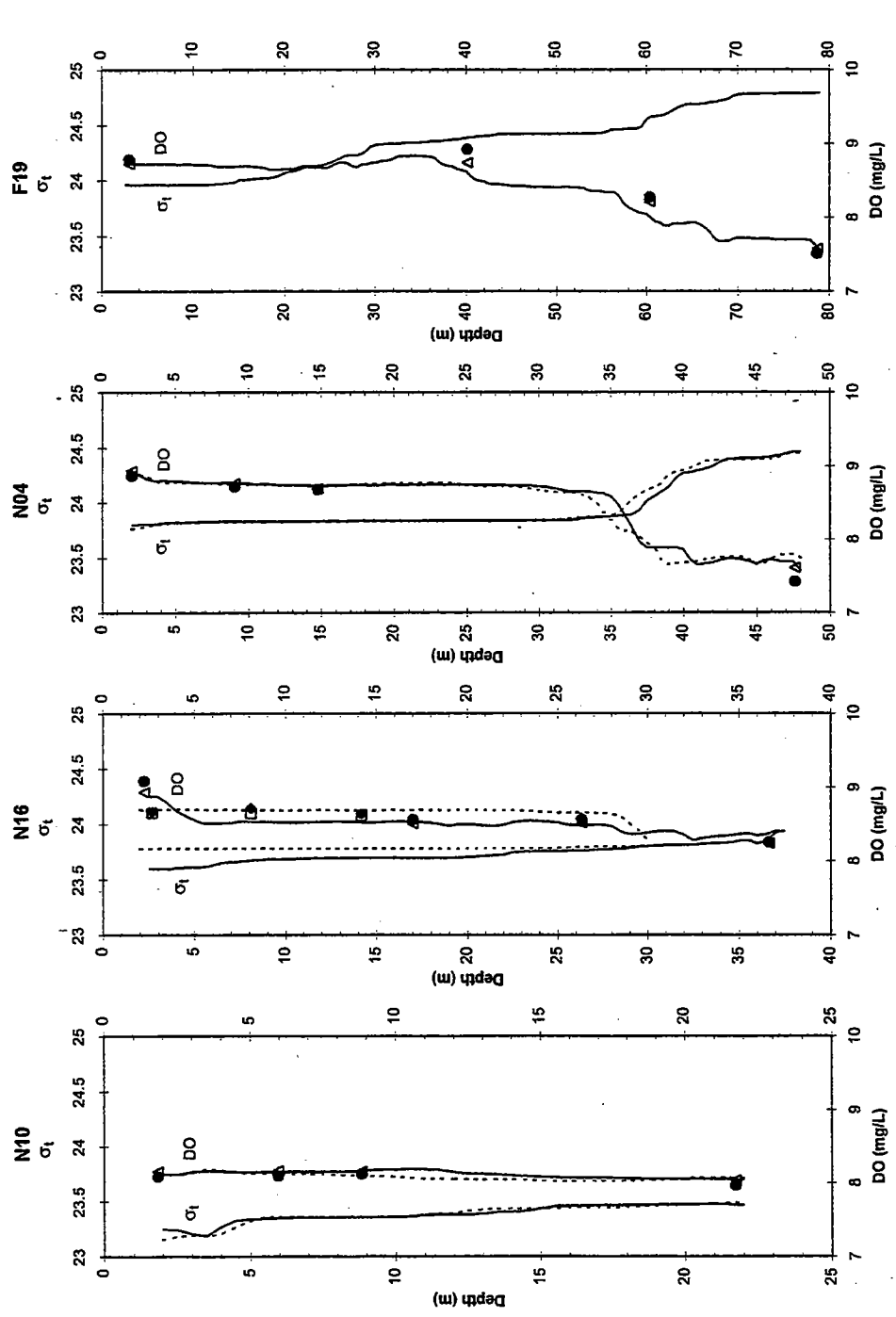

FIGURE 7-64

Distribution of Water Column DO Relative to Density During W9614
Open Symbols = Upcast Sensor Data; Closed Symbols = Lab Data

8.0 PLANKTON

The 1996 HOM Program included analysis of the plankton community in Boston Harbor, Massachusetts Bay, and Cape Cod Bay during 11 nearfield and six combined nearfield/farfield surveys conducted from February to December. Two stations were occupied in the nearfield surveys, with an additional ten locations sampled during the combined events (Figure 8-1). Sampling included whole-water phytoplankton collections at the surface (<2.5m) and at the water column mid-depth, which we operationally refer to in this report as the chlorophyll maximum (chl_{max}), as determined from in-situ fluorescence hydrocasts. Additional samples were taken at these two depths and screened through 20μm Nitex mesh to retain and concentrate larger dinoflagellate species. Oblique zooplankton tows were performed at each of the stations. Details regarding sampling and analysis can be found in the Combined Work Plan/QAPP for water column monitoring (Bowen *et al.*, 1997).

Quantitative taxonomic analyses were performed during 1996, continuing the monitoring record begun in 1992. For 1996, carbon equivalence estimates were made for both phytoplankton and zooplankton communities using species-specific carbon data from the literature. The objective of these analyses is to provide the baseline from which to evaluate the potential effects of the relocation of the Deer Island discharge to its 1999 discharge site in Massachusetts Bay. This evaluation focuses on the potential alteration in biomass or community structure that may result from the stimulatory effects of nutrient enrichment, or alternatively from inhibitory effects due to effluent toxicity. Additionally, these data can support assessments of the phytoplankton community's effect on water clarity or color.

In this section, the 1996 plankton record is presented with a discussion of spatial and temporal trends. Comparisons are made with previous baseline data collected from 1992 to 1995.

8.1 Phytoplankton

8.1.1 Abundance and Species Succession in the Nearfield

Whole-water phytoplankton results from the more frequently sampled stations in 1996 (inner nearfield station N10 and outer nearfield station N04) showed an annual cycle that varied with location (Figure 8-2). Total abundance at N10 consistently increased through April, while abundance at N04 fell during late March, followed by a slight rebound. The less frequently sampled N16, in the center of the nearfield, seemed to track results from N04. Station N10 showed subsequent peaks in August, prior to fall mixing, and in late-September/October. Station N04 showed an additional peak during June. Cell densities were highest in August at N10, and during the fall bloom at N04.

During most surveys (particularly in summer months), the phytoplankton assemblage was numerically dominated by small (<10 μm) flagellated species. Exceptions were during March and April, when samples were dominated by centric diatoms (Figures 8-3 a and b). However, carbon equivalence estimates for the individual taxa present during the surveys indicated diatom species were often dominant in terms of biomass, particularly during bloom events (e.g., March, mid-August and October, Figures 8-4 a and b). Dominant diatom taxa during these peaks

included *Chaetoceros* and *Thalassiosira* spp. (spring); *Rhizosolenia fragilissima* and *Rhizosolenia delicatula* (summer periods), and *Skeletonema costatum, Rhizosolenia fragilissima*, and *Guinardia flaccida* (fall).

Other groups occasionally contributed to the overall biomass during some periods. For example, during late winter/spring, and again during the fall, dinoflagellate species occasionally comprised from 40 to 60 percent of estimated biomass, particularly at nearfield station N16 (Figures 8-4 a and b). An unidentified species of *Gonyaulax* was the dominant dinoflagellate in the early spring period, while *Ceratium longipes* contributed to the dinoflagellate biomass in late spring. The late summer dinoflagellate responsible for the relatively high biomass contribution was *Ceratium longipes*, with additional contribution by *Ceratium tripos, Ceratium fusus,* and *Protoperidinium.*

8.1.2 Regional Comparisons for 1996

8.1.2.1 Whole-Water Samples

Phytoplankton data from the six combined nearfield-farfield sampling events in 1996 were reviewed to examine spatial and temporal trends in other regions relative to the three nearfield stations. To facilitate this review, individual survey results were averaged for the regions depicted in Figure 2-1. Survey results were then plotted for total densities and for major taxonomic groups (Figures 8-5 through 8-10). Note that only one station was sampled within the each of the offshore and boundary regions (Figure 8 -1).

Highest overall total phytoplankton and microflagellate densities were evident in the harbor and coastal water (Figures 8-5 and 8-6). Based on total abundance results from the six farfield surveys, annual maxima in the harbor, coastal, and nearfield water occurred in the summer and early fall. Cape Cod Bay had the highest relative total cell densities in late winter/early spring, but had low densities during the summer.

Chlorophyll data indicated that the spring bloom in Cape Cod Bay occurred earlier than other regions (Figure 5-2b). Densities of centric and pennate diatoms were higher in Cape Cod Bay relative to the other regions throughout this period (Figures 8-7 and 8-8). The nearfield reached its spring maximum three weeks later (documented during a nearfield-only sampling event). Peak abundances of centric diatoms were reached in April in the inshore water and nearfield, whereas Cape Cod Bay and the Boundary water had much lower densities, similar to the offshore region. Microflagellates and centric diatoms appeared to contribute to the fall bloom event around the end of October.

Pennate diatoms appeared to decrease gradually from February to June and increase gradually from June throughout the remainder of the year at most stations, although the more intensive sampling at the nearfield stations gave some indication of the substantial variability which can occur. Cryptophyte abundances (Figure 8-9) were consistent with the other groups, with summer maxima and higher densities in the harbor. However, dinoflagellates (Figure 8-10) had the greatest densities in the offshore areas during the fall months. These regional averaging schemes will not reveal localized blooms of individual species or genera, however.

These blooms are currently being investigated for a number of dinoflagellate species, and will be reported elsewhere.

8.1.2.2 Toxic and Nuisance Species

The HOM program includes monitoring for toxic and nuisance species, particularly *Alexandrium tamarense*, *Phaeocystis pouchetii*, and *Pseudo-nitzschia multiseries*. *Alexandrium tamarense* is a dinoflagellate which can cause paralytic shellfish poisoning (PSP) when shellfish which have concentrated the toxin are consumed. *Alexandrium* in the Massachusetts Bay region may arise from two sources: locally from benthic cysts and from advective transport of cells arising from riverine discharges in southern Maine, usually during the period April to June (Anderson and Keafer, 1992; Franks and Anderson, 1992). Once established, abundance and distribution are governed by nutrient availability, wind patterns and coastal currents. These physical controlling factors may alternatively disperse the population offshore or lead to conditions of increased residence time which allow localized blooms (Anderson and Keafer, 1995).

During 1996 there were four surveys in the nearfield during the period when *Alexandrium* is most likely to be encountered, and only two (mid-June) in the farfield. There was no evidence of *Alexandrium* in the nearfield or other Massachusetts Bay regions in the 1996 HOM plankton data (Figure 8-11). However, separate surveys by D.M. Anderson under a joint Sea Grant/MWRA contract did document the distribution and abundance of toxic *Alexandrium tamarense* cells in the bay in the late-spring/early summer period of 1996 in very low densities (D. Anderson, personal communication). There were no instances of shellfish toxicity in Massachusetts Bay coastal water during the reporting period.

Phaeocystis may occur as individual flagellated cells which are typically in the 5μm to 8 μm diameter range (thus capable of passing through the 20μm Nitex screen used to concentrate the larger, rarer taxa). It may also form gelatinous colonies which can range from 500μm to 2,000μm in diameter, which would be retained on the Nitex screening. Similarly, the diameter (< 8μm) of the rod-shaped *Pseudo-nitzschia* cells could permit their passage through the screen, although their longitudinal colony formation and long length (70-160μm) would likely result in retention of most cells. Both whole-water analyses and screened samples were therefore examined for the presence of these two species.

Phaeocystis was reported in the late winter and spring 1996 HOM plankton monitoring (Figure 8-12a,b), typical of its annual distribution cycle. The maximum density reported for this taxon was 179,000 cells/L in a surface screened water sample (station F27) during W9604 (Murray *et al.*, 1998).

The toxin-producing strains of *Pseudo-nitzschia* cannot be differentiated from non-toxic species under the light microscope. The potential distribution of *Pseudo-nitzschia multiseries* in the nearfield was examined by plotting

all reported results for the morphologically similar species *Pseudo-nitzschia pungens* (Figure 8-13a). This approach should be viewed as a conservative indicator of whether a toxic species may be present. The 1996 record indicated that *P. pungens* occurred primarily in the summer and fall, with maximum densities at station N10 during W9611 (14,000 cells/L). Concentrations never exceeded 100,000 cells/L, a density threshold above which the toxic form can cause accumulations of toxin in shellfish (Bates, 1997).

8.1.3 1992-1996 Interannual Comparisons

While the previous (1992 to 1994) HOM sampling included six sampling stations in the nearfield, sampling was reduced in 1996 to three stations (N10, N16, N04) within the nearfield. The addition of station N04 serves as an additional source of data on every nearfield survey during 1996, as N16 was only sampled during farfield surveys. This approach also allowed examination of the gradient across the nearfield represented by these two stations.

The general trend toward multiple peaks and increasing densities in whole-water samples through the summer evident in the 1996 record was also seen in previous years, both in total cell densities (Figure 8-14) and the seasonal succession of taxa within major groups (Figures 8-15 through 8-19). The seasonal increase is typically attributable to increases in microflagellate abundance (Figure 8-15).

Also evident in all years of the interannual record is the elevated abundance of phytoplankton at the inshore station N10, which is true for most of the major groups (Figures 8-15 through 8-19). This is largely a function of the higher nutrient availability inshore.

The plankton data demonstrate the considerable interannual variability that characterizes the nearfield. As was seen in the nearfield chlorophyll data (Figure 5-7), the 1996 spring diatom maximum (Figure 8-16) was stronger than previous years, both with respect to density and duration. Summertime diatom densities appeared to be somewhat lower than previous years, but periodic blooms during the stratified period were still evident.

The distributions of *Alexandrium*, *Phaeocystis*, and *Pseudo-nitzschia* also show a high degree of interannual variability (Figures 8-11, 8-12, and 8-13). *Alexandrium* was detected by the HOM program in 1992, 1993, and 1994, but not in 1995 or 1996 (Figure 8-11). Concentrations were low (<100 cells/L in all but one sample) in all three years according to these data.

Phaeocystis colonies were detected in 1992, 1993, 1994, and 1996 but not in 1995 (Figure 8-12). Concentrations of this species varied by four orders of magnitude in these years, with 1992 and 1994 having the highest concentrations. *Pseudo-nitzschia pungens* and *Pseudo-nitzschia seriata* were generally observed in the fall, with densities relatively constant from year to year (Figure 8-13a, b).

8.2 Zooplankton

8.2.1 Annual Cycle of Total Zooplankton and Major Groups

As in previous years, total zooplankton abundance in 1996 was highest during the latter half of the year. Peak abundance occurred in August at station N10 and in June at stations N04 and N16 (Figure 8-20). Abundance was usually below 40 animals/liter prior to June and above this value later in the year. Highest abundance was observed at station N04 in June with a value of over 180 animals/liter. After the summer/fall peak, abundances fell to low levels in November and December and remained low through the spring.

Zooplankton abundance was dominated by copepods, which constituted about 90% of the total zooplankton (Figure 8-21). Barnacle nauplii were observed during the spring in the inner nearfield, but their abundance was small relative to that of the copepods (<10%). All other groups of zooplankton combined typically constituted only a small fraction of the total zooplankton abundance.

About half of the copepods collected were naupliar stages, the other half being copepodite stages, which includes the adults. There appeared to be a relatively greater proportion of naupliar stages during the first half of the year (Figure 8-21). Naupliar stages made up over half of the copepods collected during the late winter and spring but less than half during the summer and fall. Given the higher abundance of total copepods during the latter half of the year, this relative shift in life stage composition then reflects the relatively larger seasonal increase in copepodite versus naupliar life stages.

The lower abundance of nauplii relative to copepodites is largely a result of extrusion of the smaller naupliar stages through the meshes of the net, though the somewhat shorter duration of the nauplier life stages is a factor. But the higher mortality of the later life stages should make those stages even less abundant relative to nauplii.

8.2.2 Regional Patterns of Dominant Taxa

The dominant zooplankton taxa were observed to have particular geographic affinities, as was observed in prior years. Taxa usually had either nearshore or offshore affinities, although a few dominant taxa were equally abundant everywhere.

Typical taxa having an offshore affinity are shown in Figures 8-22 to 8-25 and include: *Calanus finmarchicus, Centropages typicus, Oikopleura dioica,* and echinoderm larvae. Abundance of these species is highest at the boundary stations and decreases markedly at the inshore stations especially near Boston Harbor. These species maintain large populations in the Gulf of Maine, and their presence in the bay is in large part due to advective input from that region. Also shown in these plots are the seasonal cycle of each taxon in each region. It can be seen that *Oikopleura, Calanus*, and echinoderm larvae are primarily abundant during spring, while *Centropages typicus* is a dominant fall species. The larvaceans also are abundant during fall at the nearfield and Cape Cod Bay stations.

Two dominant taxa are known to be abundant offshore but are also plentiful near shore: *Oithona similis* and *Pseudocalanus* sp (Figures 8-26 and 8-27). Peak *Oithona* abundance occurred during the latter half of the year while *Pseudocalanus* were most abundant during late spring/early summer. *Pseudocalanus* abundance was lower at the boundary station near the Gulf of Maine than at the other stations, reflecting its affinity for regions where the bottom depth is shallower than 100m.

Several taxa have affinities for nearshore regions (Figure 8-28 to 8-37). These taxa include copepods that lay bottom resting eggs (*Centropages hamatus* and *Temora longicornis*), the copepods *Acartia tonsa* and *Acartia hudsonica*, the estuarine copepods *Eurytemora herdmani* and *Pseudodiaptomus coronatus*, meroplanktonic larvae (polychaete and barnacle), the cladoceran *Podon* sp. and harpacticoid copepods. Several of these taxa have ties to the sea floor either through production of benthic resting eggs, parental adult populations, or through epibenthic/planktonic migration behavior. The *Acartia* spp are thought to be restricted to nearshore environments due to some combination of food limitation and possibly salinity intolerance of their nauplii (Cibik *et al.*, 1998a). *Centropages hamatus* and *Temora longicornis* are restricted to shallow regions where tidally induced resuspension of bottom sediment prevents their bottom resting eggs from becoming buried. Thus, these dominant zooplankton taxa can be grouped according to their nearshore or offshore affinities Table 8-1)

8.2.3 Annual Cycles of Dominant Copepod Species by Region

The dominant copepod (and zooplankton) species in terms of abundance is *Oithona similis*, while *Calanus finmarchicus* was the dominant species in terms of biomass. *Oithona similis* was numerically dominant in all regions except in the harbor. *Calanus* reached peak abundance during the spring/summer period. [note: the contribution of each species to total zooplankton biomass was approximated by multiplying numerical abundance by literature values for body carbon weight of adults. While this method overestimates total biomass, it does provide a reasonable weighting for examining the relative proportion of biomass among species. Body weights used for the 10 species plotted (*Oithona* to *Centropages hamatus*) were 1, 10, 10, 10, 15, 10, 125, 1, 1, 10, respectively. For species where body weights were unknown, weights of similar sized species were used.]

In the nearfield region (Stations N04, N10, and N16), numerically dominant species during spring were Oithona, Pseudocalanus, and Calanus (Figure 8-38). During the second half of the year, Oithona, Centropages typicus, and Temora were numerically dominant, with Centropages typicus dominating the fall biomass. Peak abundance values were between 20-30/liter for Oithona, and between 5-10/liter for each of the other species. Due to its large body size, Calanus overwhelmingly dominated the spring zooplankton biomass. Beginning in 1996, station N04 was sampled instead of station N16 during the nearfield surveys. In comparing the seasonal patterns of stations N04 and N16, we found no apparent difference in species abundance and biomass cycles (Figures 8-39 and 8-40).

In Cape Cod Bay (stations F01 and F02) (Figure 8-41), abundance was highest during mid summer and was dominated by variety of species including *Oithona, Pseudocalanus, Temora, Centropages typicus, Centropages hamatus, Microsetella norvegica*, and *Acartia tonsa*. Spring dominants included *Oithona, Pseudocalanus*, and *Calanus*. Peak *Oithona* abundance was near 25/liter, while maximum abundance of the other species was less than 5/liter. In terms of biomass, *Calanus* again was overwhelmingly dominant during spring. Summer/fall biomass was dominated by *Pseudocalanus, Temora*, and *Centropages hamatus*.

At the boundary station F27 (Figure 8-42), *Oithona* and *Calanus* were the numerical dominants during spring and *Oithona* and *Centropages typicus* dominated during summer/fall. *Calanus* dominated the biomass completely during the first half of the year while *Centropages typicus* was the biomass dominant during fall.

At station F06 (so-called "offshore" station, but really nearshore in character) (Figure 8-43), species composition is much more equitable among the ten species. *Oithona* again is the clear dominant in terms of abundance with a peak value during fall between 15-20 / liter, and *Calanus* dominates the spring biomass. Spring abundance is dominated by *Oithona, Pseudocalanus*, and *Calanus*, while fall abundance, not including *Oithona*, comprises all the species (except *Acartia hudsonica*) in approximately equal numbers. This station then, like the nearfield, represents a transition zone between the nearshore and offshore zooplankton communities.

In the "coastal" region (stations F24, F25, F13) (Figure 8-44), spring abundance is again dominated by *Oithona, Pseudocalanus,* and *Calanus*, while summer/fall abundance is dominated by *Oithona, Pseudocalanus, Acartia tonsa, Temora,* and lesser numbers of *Centropages typicus, Acartia hudsonica, Microsetella,* and *Centropages hamatus*. Spring biomass was dominated by *Pseudocalanus* and *Calanus*. At these more inshore stations, the overwhelming dominance of *Calanus* in terms of biomass no longer occurs and the smaller *Pseudocalanus* becomes equally important.

In Boston Harbor (stations F23, F30, and F31) (Figure 8-45), *Acartia tonsa* and *Acartia hudsonica* are dominant in terms of abundance and overwhelmingly dominant in terms of biomass. *Oithona* and *Pseudocalanus* are also abundant in the harbor. Peak *Acartia* abundance is 15-25/liter. *Calanus finmarchicus* still dominates the spring biomass even though its abundance is low relative to other regions.

8.2.4 Interannual Observations of Dominant Taxa

Annual cycles in abundance of zooplankton were compared for the MWRA survey years 1992- 1996 at the six stations that were sampled in all years. In terms of total zooplankton abundance (Figure 8-46), no apparent difference was seen between years, except at station N16 which had higher values during the spring. The 1996 values at the other stations fell within the scatter of the 1992-1995 data.

Abundance of copepod nauplii in 1996 appeared to be higher than most other years at stations F13, N16, F01, and F02 (Figure 8-47). Abundance at these stations was near the upper edge of the 5-year range in the data throughout the year. It is not clear what caused higher abundance at these stations, but 1996 was characterized by lower than normal winter temperatures and a generally lower seawater density in the outer nearfield. It is also not possible to attribute the high abundance to a particular species since the nauplii were not classified to species.

Unlike copepod nauplii, *Oithona* abundance in 1996 was similar to the previous years (Figure 8-48). Abundance of this species was lower in the harbor (F23) in all years. Highest abundance of *Oithona* occurred in 1992 during fall at stations F02, F13, and N16. Abundance of *Pseudocalanus* and *Paracalanus* (combined for analysis due to taxonomic discrepancies between years) also had no apparent differences with prior survey years (Figure 8-49). The first half of the year is typically dominated by *Pseudocalanus* which is a boreal animal, while *Paracalanus* is dominant during the second half of the year. Unlike previous years, no *Paracalanus parvus* were observed in the

1996 samples. This species is subtropical, and its abundance can vary significantly from year to year. Its complete absence from the region in 1996 is curious however and requires further investigation.

Comparing March of 1992 and 1996 in Cape Cod Bay (F01, F02), it can be seen that the abundance of *Pseudocalanus* was similar in both years even though 1992 was characterized by a massive bloom of *Phaeocystis pouchetti* and 1996 had no such bloom. It appears then that the high concentration of these algae does not affect *Pseudocalanus* abundance.

Acartia spp. (tonsa and *hudsonica* combined due to taxonomic discrepancies between years) abundance in 1996 was similar to past years (Figure 8-50). The highest abundance of this genus occurred in the harbor stations in the fall of all years. Its abundance decreases markedly away from shore, and, in comparing inner and outer nearfield stations (N10 vs N04), it can be seen that a strong gradient in its abundance exists across this region (Figure 8-51).

Calanus finmarchicus abundance in 1996 also was similar to prior survey years (Fig. 8-52). Some of the highest results for *Calanus finmarchicus* were seen during 1996, particularly at Stations N10 and N16.

8.3 Plankton Discussion

The nearfield currently represents a transition between coastal and offshore assemblages, which is particularly evident in the zooplankton data. The existing nutrient gradient from the harbor to offshore water likely dictates much of this transitional nature, although other physical and chemical factors also exert controls that vary temporally and spatially.

The change in the loading and distribution of nutrients associated with the outfall relocation may result in changes in plankton abundance and community composition. The phytoplankton may respond with increased biomass and/or altered community structure. Potential changes in zooplankton may be attributable to these changes in phytoplankton community structure (bottom-up effects) due to the close relationship between the two communities (Figure 8-53). These general changes will be subject to seasonal differences, and in particular, to the differences in water column physics and chemistry under non-stratified and stratified conditions.

One possible manifestation of a eutrophic response by the zooplankton community is that the assemblage in the nearfield may lose its transitional character and become more similar to the inshore assemblage. The nearshore species would become dominant in the nearfield region, potentially displacing the offshore species assemblage. Since most of the dominant inshore zooplankton species are warm-water species, this displacement would likely be most pronounced in summer and fall.

Another scenario which has been postulated is a decrease in the surface loading of nutrients to the nearfield due to the elimination of the surface loading from the harbor (Kelly, 1993). While increased flux across the pycnocline was predicted during stratified periods, it was calculated to be less than 20 percent of the existing horizontal surface flux. Based on such mass loading calculations and water quality model projections (Hunt and

Steinhauer, 1994), a net reduction in chlorophyll biomass in nearfield surface water was predicted. Given the seasonal stratification pattern in the nearfield, this scenario would have the most pronounced effect during the summer.

These two scenarios suggest the possibility that the nearfield zooplankton assemblage may shift in either direction (toward a coastal or offshore assemblage) depending on the degree of eutrophication. Further, the physical dynamics of the system will undoubtedly influence the basic seasonal trends. Most influential among these will be large-scale upwelling or mixing events during stratified periods, advection of large nutrient-rich or nutrient-poor water masses into the nearfield, and interannual variability in temperature and salinity.

Coastal Assemblage	Offshore Assemblage
Centropages hamatus	*Centropages typicus*
Temora longicornis	*Calanus finmarchicus*
Acartia tonsa	*Pseudocalanus sp.*
Acartia hudsonica	*Oithona similis*
Eurytemora herdmani	*Larvaecans*
Pseudodiaptomus coronatus	*Echinoderm larvae*
Harpacticoid copepods	
Cladocera	
Barnacle nauplii	
Polychaete larvae	

TABLE 8-1
Geographical Affinity of Zooplankton Taxa

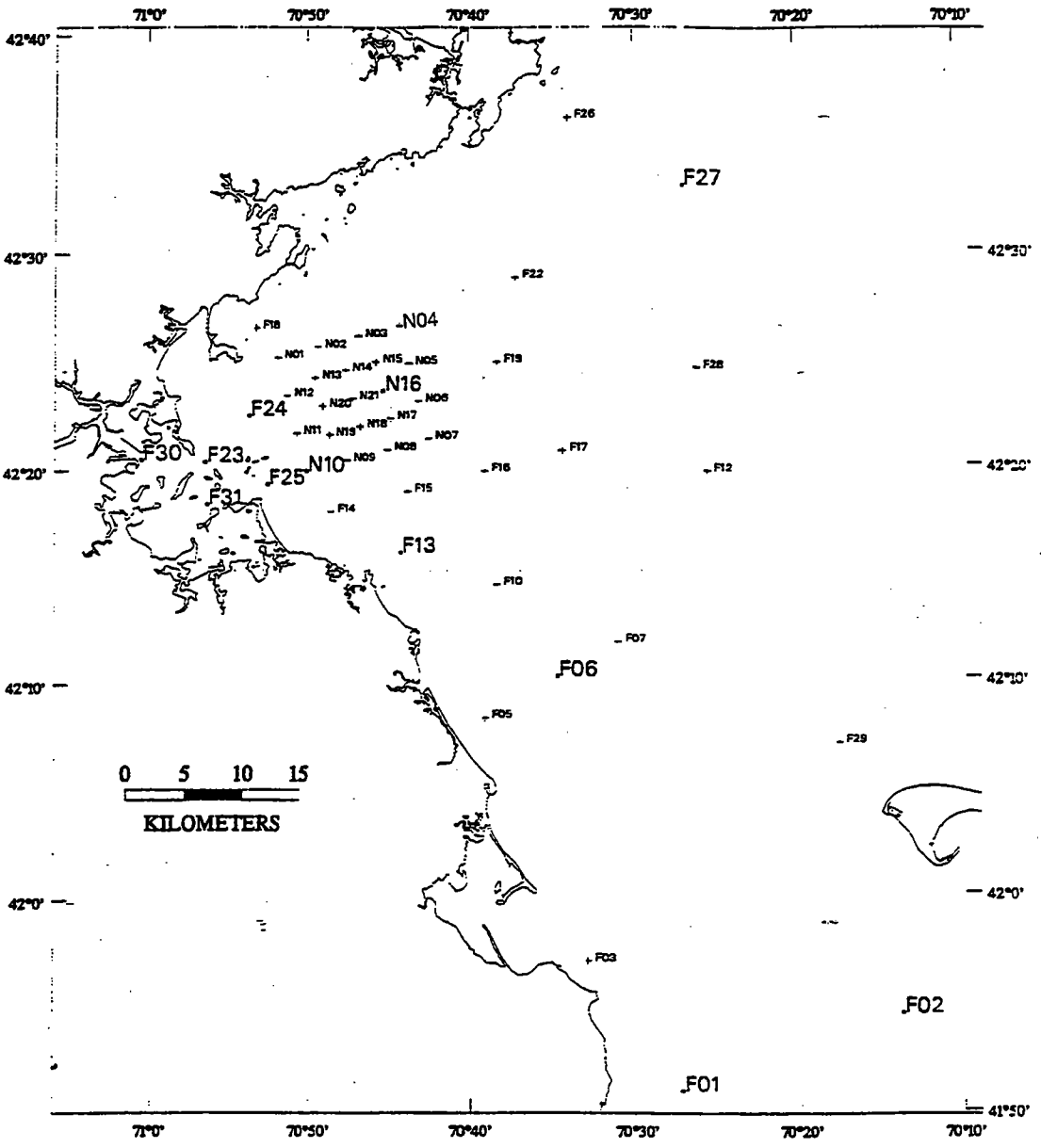

FIGURE 8-1
HOM Plankton Station Locations
(shown in enlarged text)

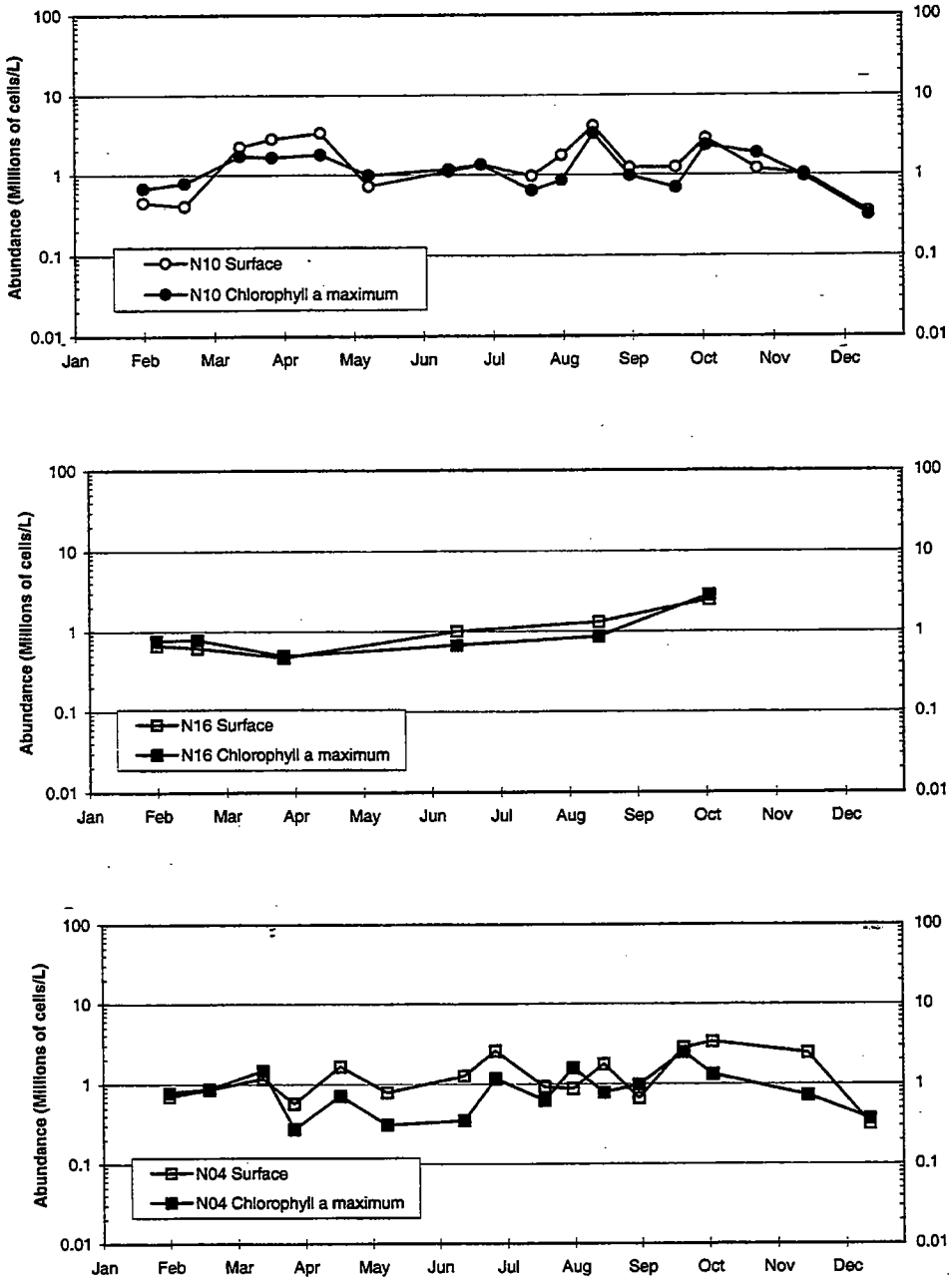

FIGURE 8-2
1996 Total Phytoplankton Abundance in Nearfield at Surface and Chlorophyll a maximum depths
Top: N10, Middle: N16, Bottom: N04

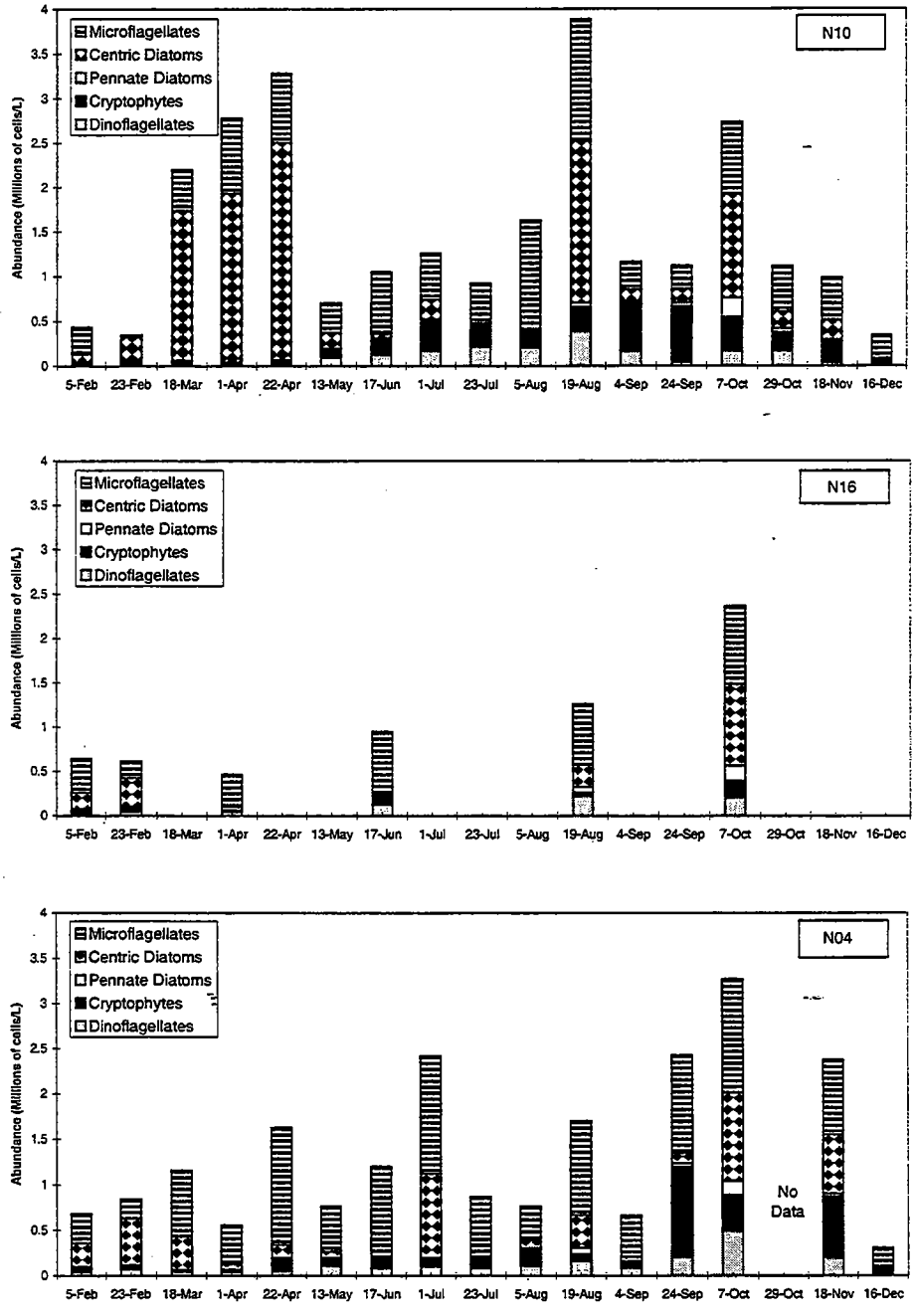

FIGURE 8-3a
Distribution of Major Taxonomic Groups in 1996 Surface Samples
Nearfield Stations
Top:N10, Middle: N16, Bottom: N04

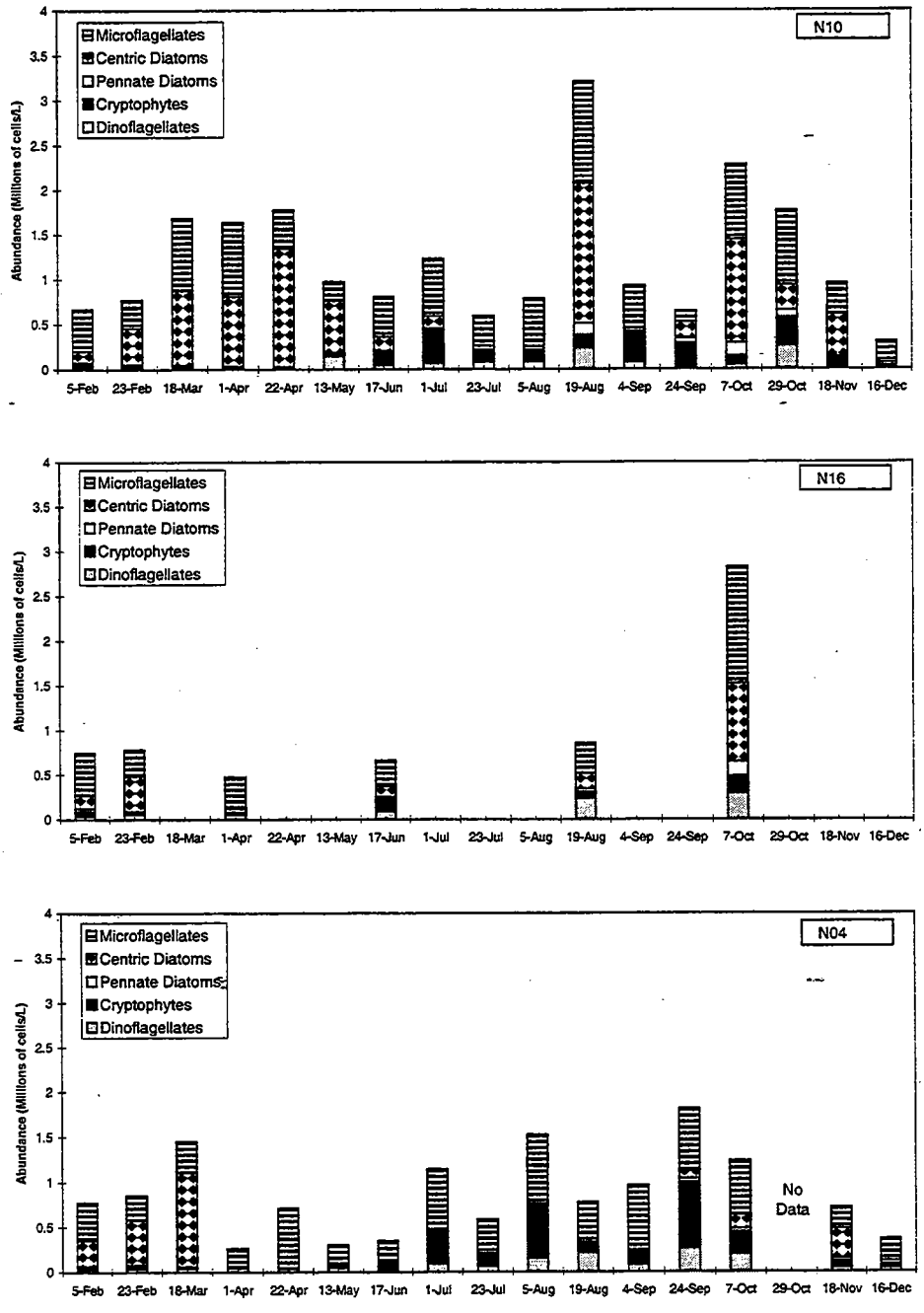

FIGURE 8-3b
Distribution of Major Taxonomic Groups in 1996 Chlorophyll *a* Maximum Samples
Nearfield Stations
Top:N10, Middle: N16, Bottom: N04

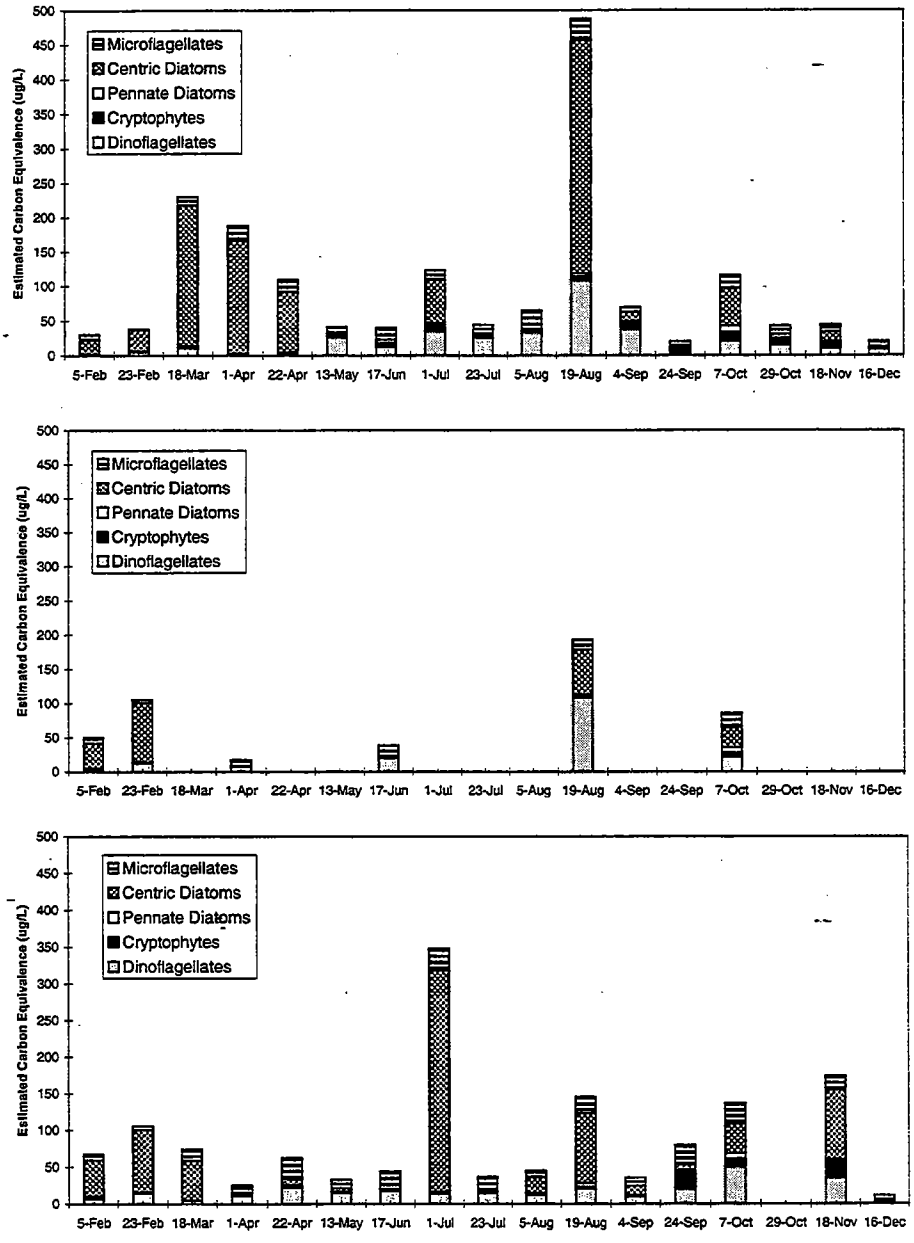

FIGURE 8-4a
Distribution of Carbon by Major Taxonomic Groups in 1996 Surface Samples
Nearfield Stations
Top: N10, Middle: N16, Bottom: N04

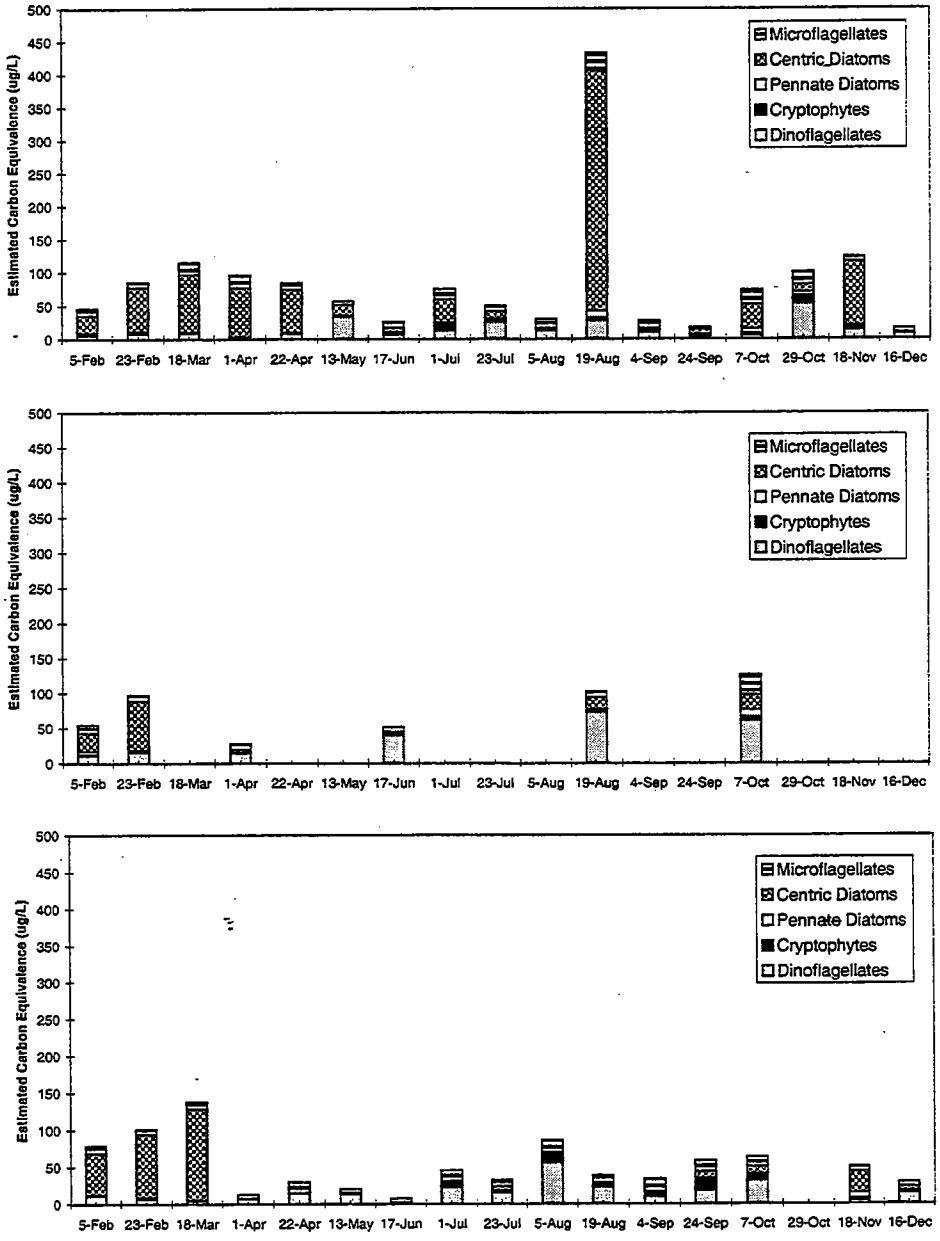

FIGURE 8-4b
Distribution of Carbon by Major Taxonomic Groups in 1996 Chlorophyll a Maximum Samples
Nearfield Stations
Top: N10, Middle: N16, Bottom: N04

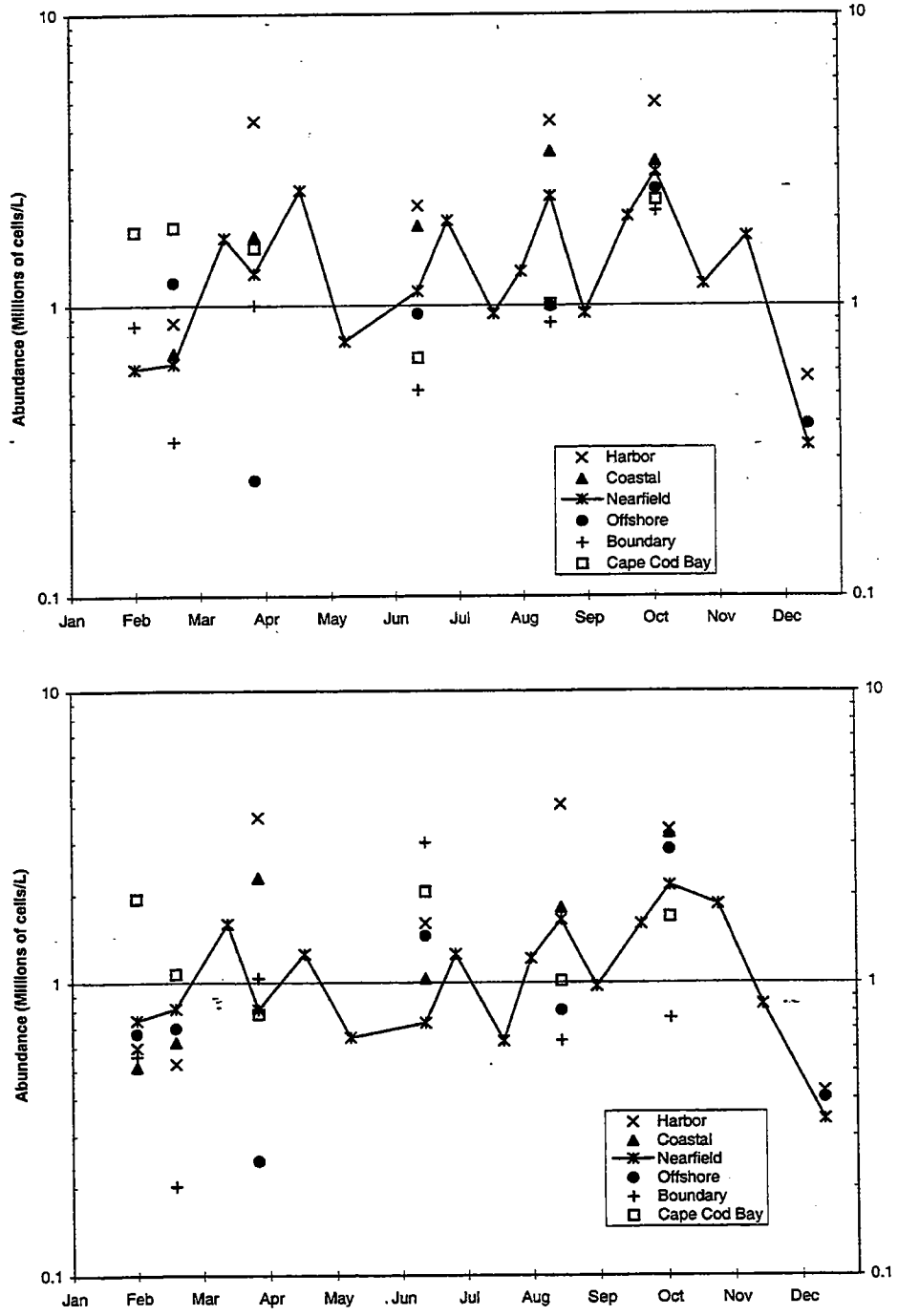

FIGURE 8-5
1996 Regional Total Phytoplankton Abundance
Top: Surface Data, Bottom: Chlorophyll *a* Maximum Data

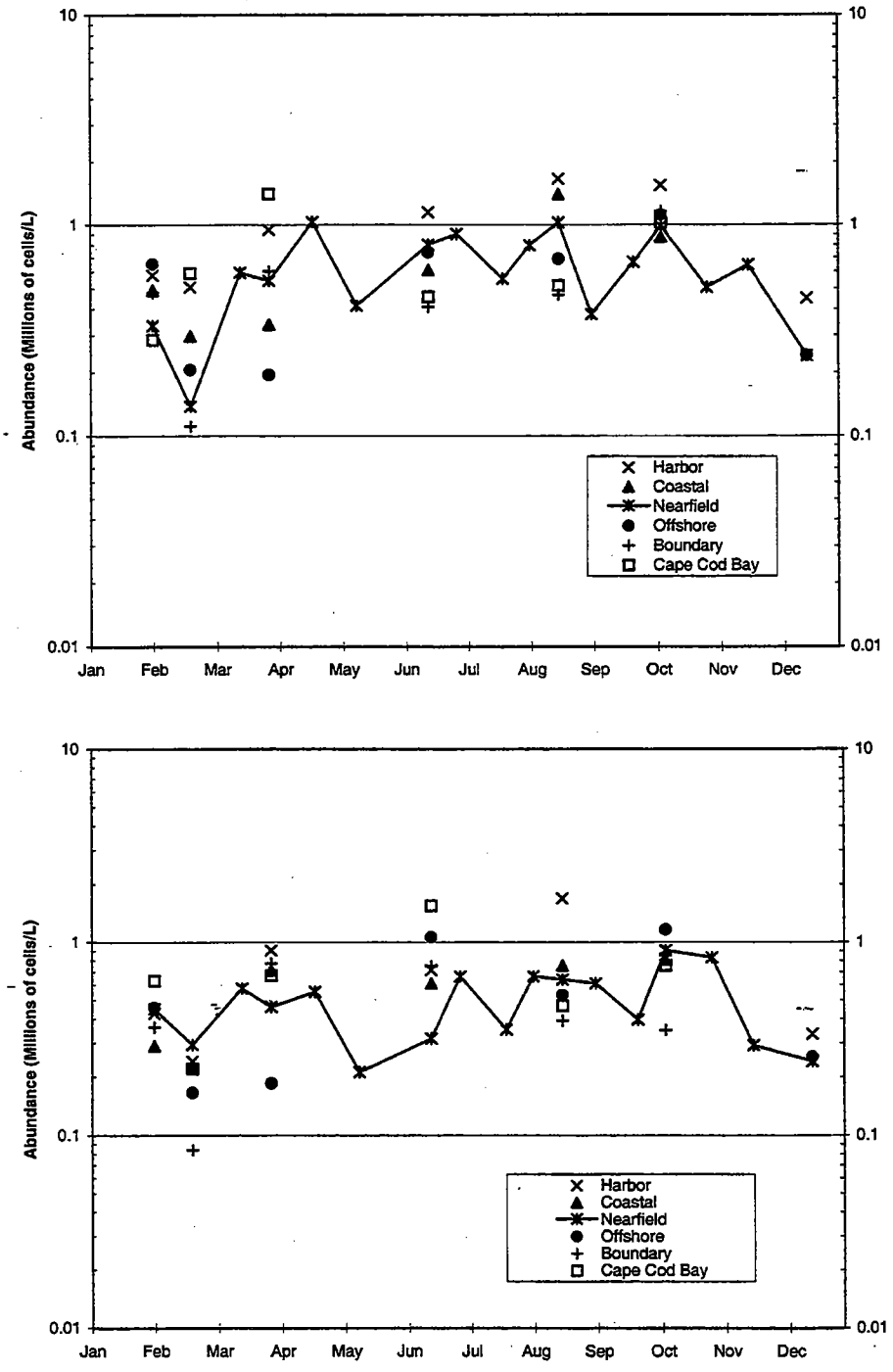

FIGURE 8-6
1996 Regional Abundances for Microflagellates
Top: Surface Data, Bottom: Chlorophyll *a* Maximum Data

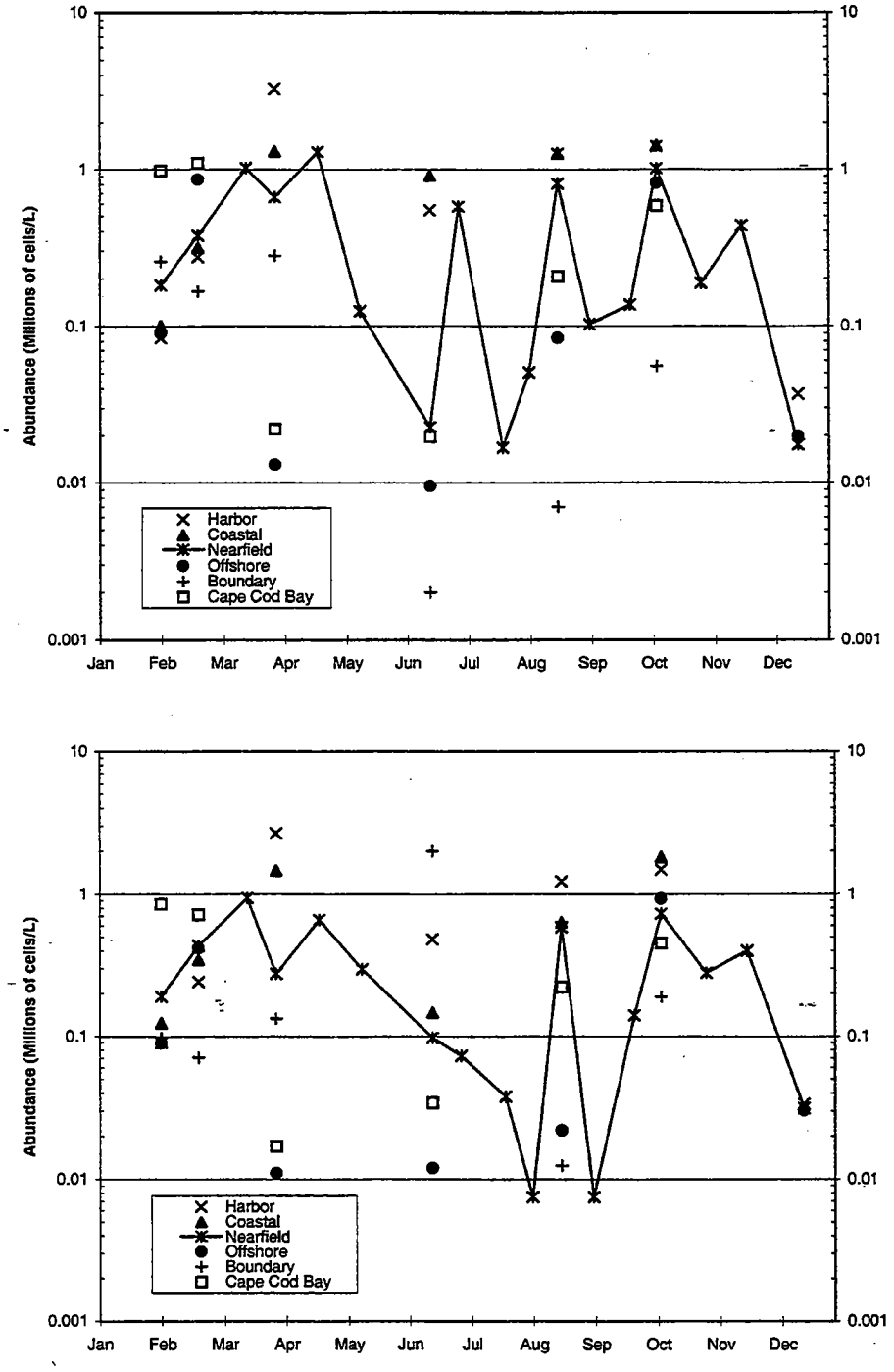

FIGURE 8-7
1996 Regional Abundances for Centric Diatoms
Top: Surface Data, Bottom: Chlorophyll *a* Maximum Data

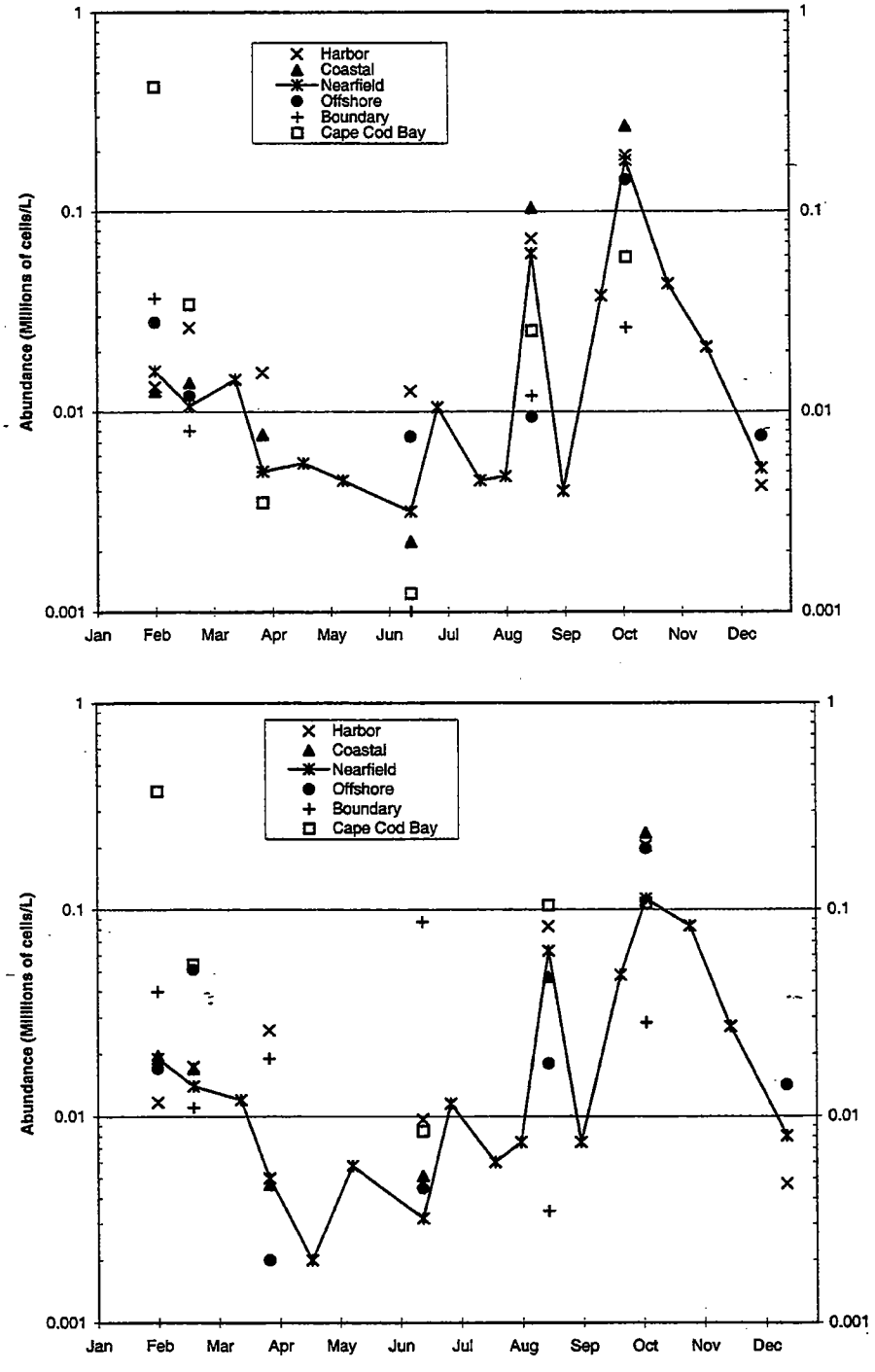

FIGURE 8-8
1996 Regional Abundances for Pennate Diatoms
Top: Surface Data, Bottom: Chlorophyll *a* Maximum Data

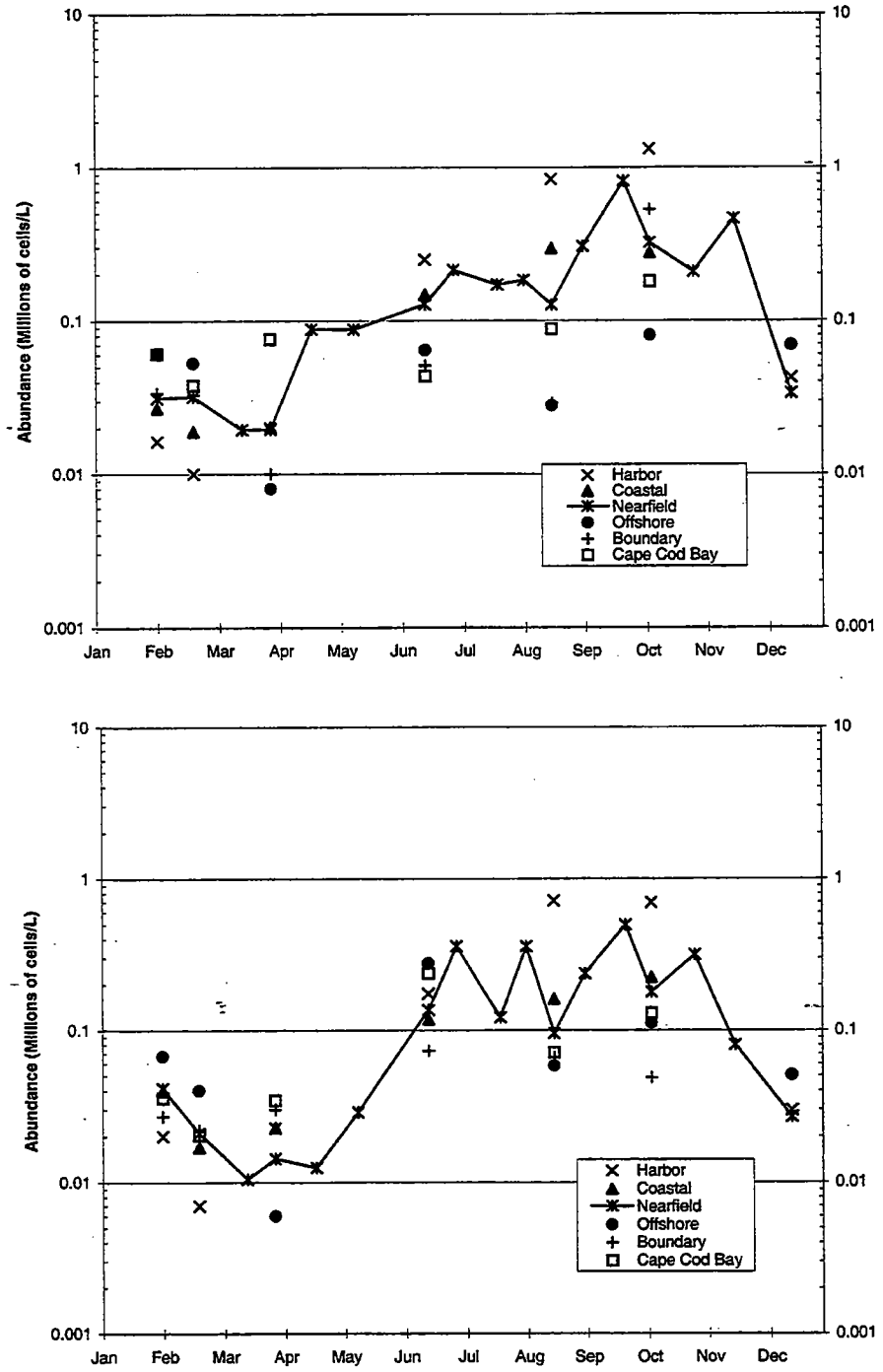

FIGURE 8-9
1996 Regional Abundances for Cryptophytes
Top: Surface Data, Bottom: Chlorophyll *a* Maximum Data

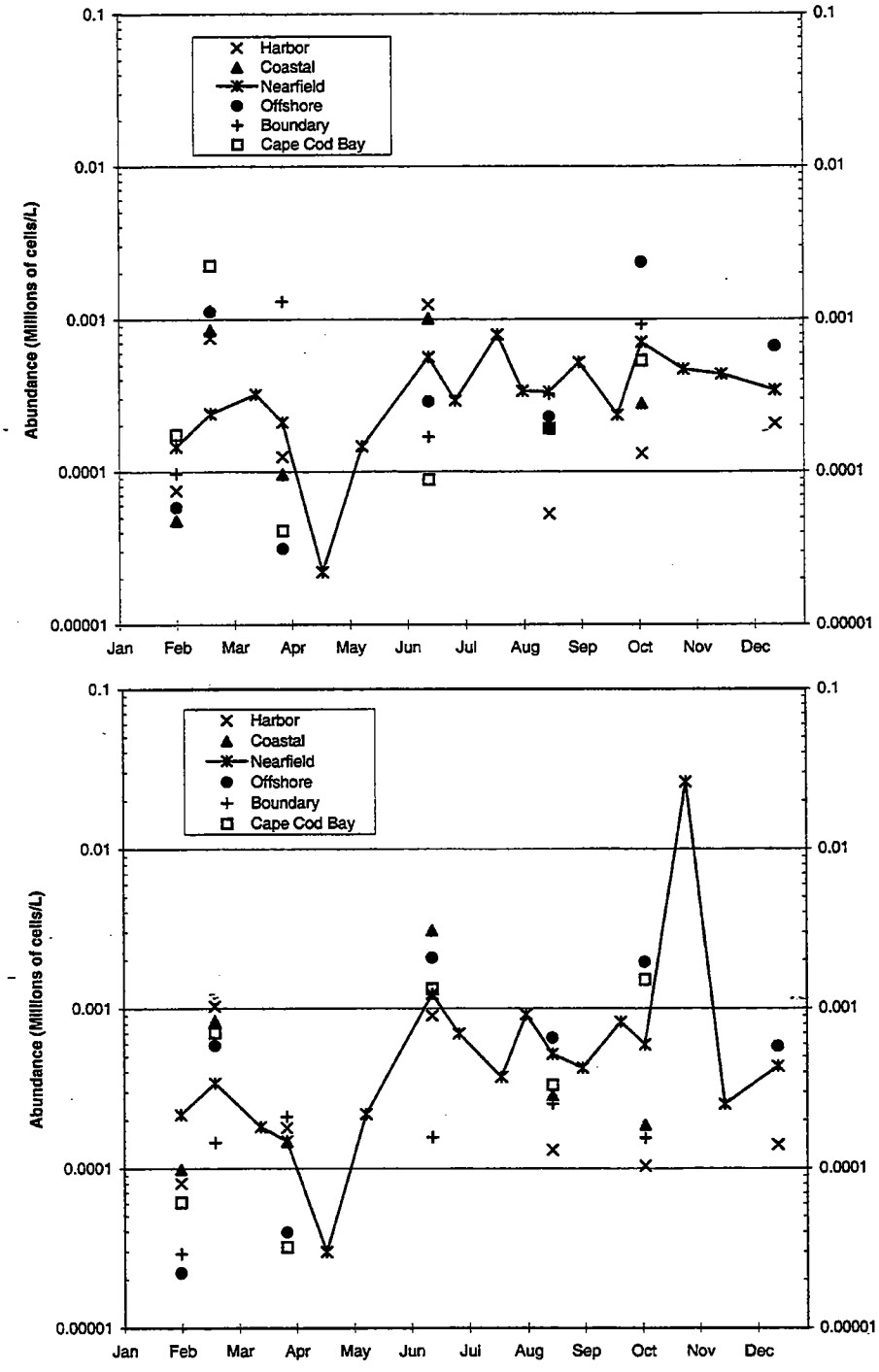

FIGURE 8-10
1996 Regional Abundances for Dinoflagellates
Top: Surface Data, Bottom: Chlorophyll *a* Maximum Data

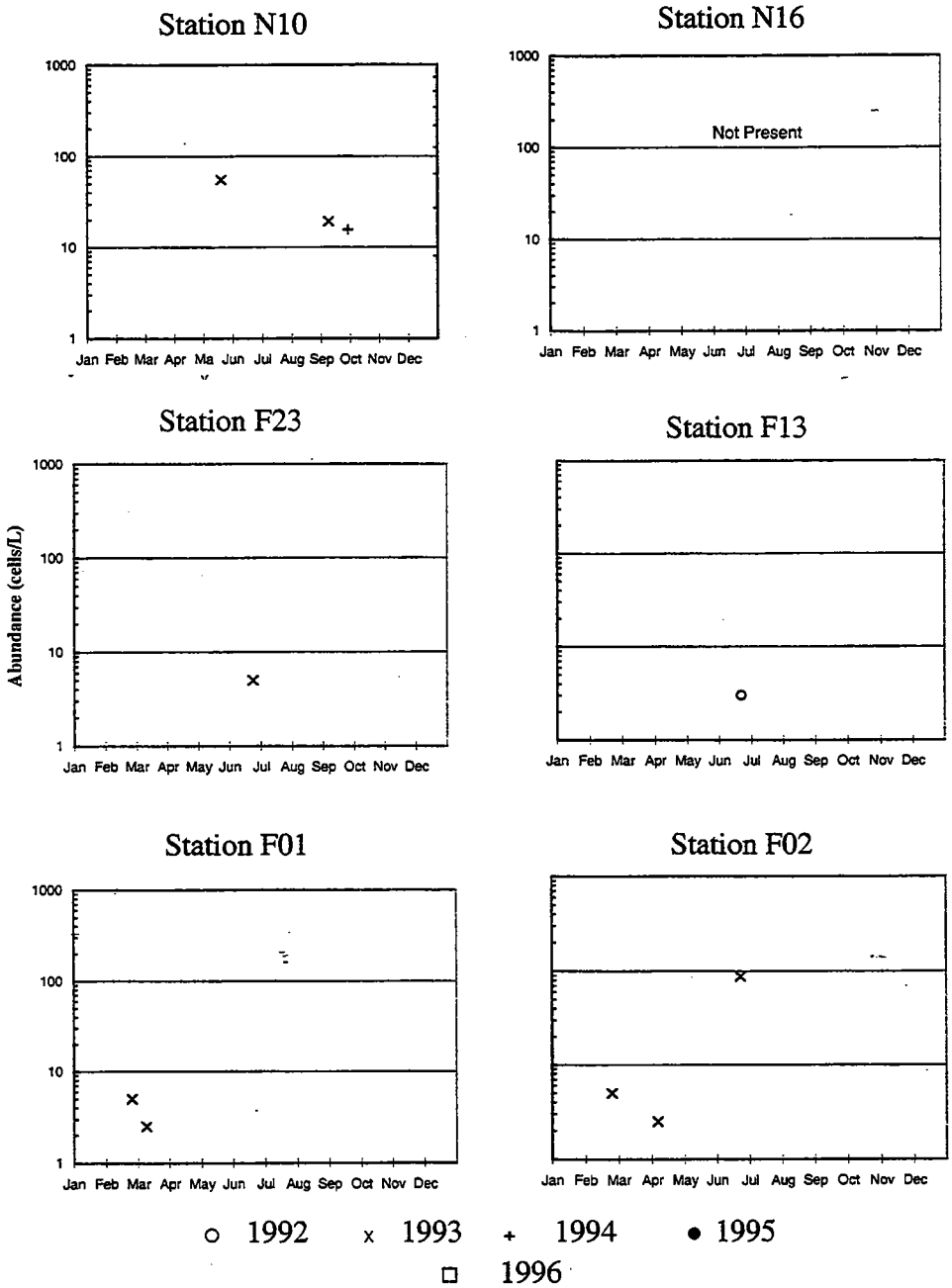

FIGURE 8-11
Interannual Distribution of *Alexandrium tamarense* by Region
(Screened Samples, Depth Averaged)

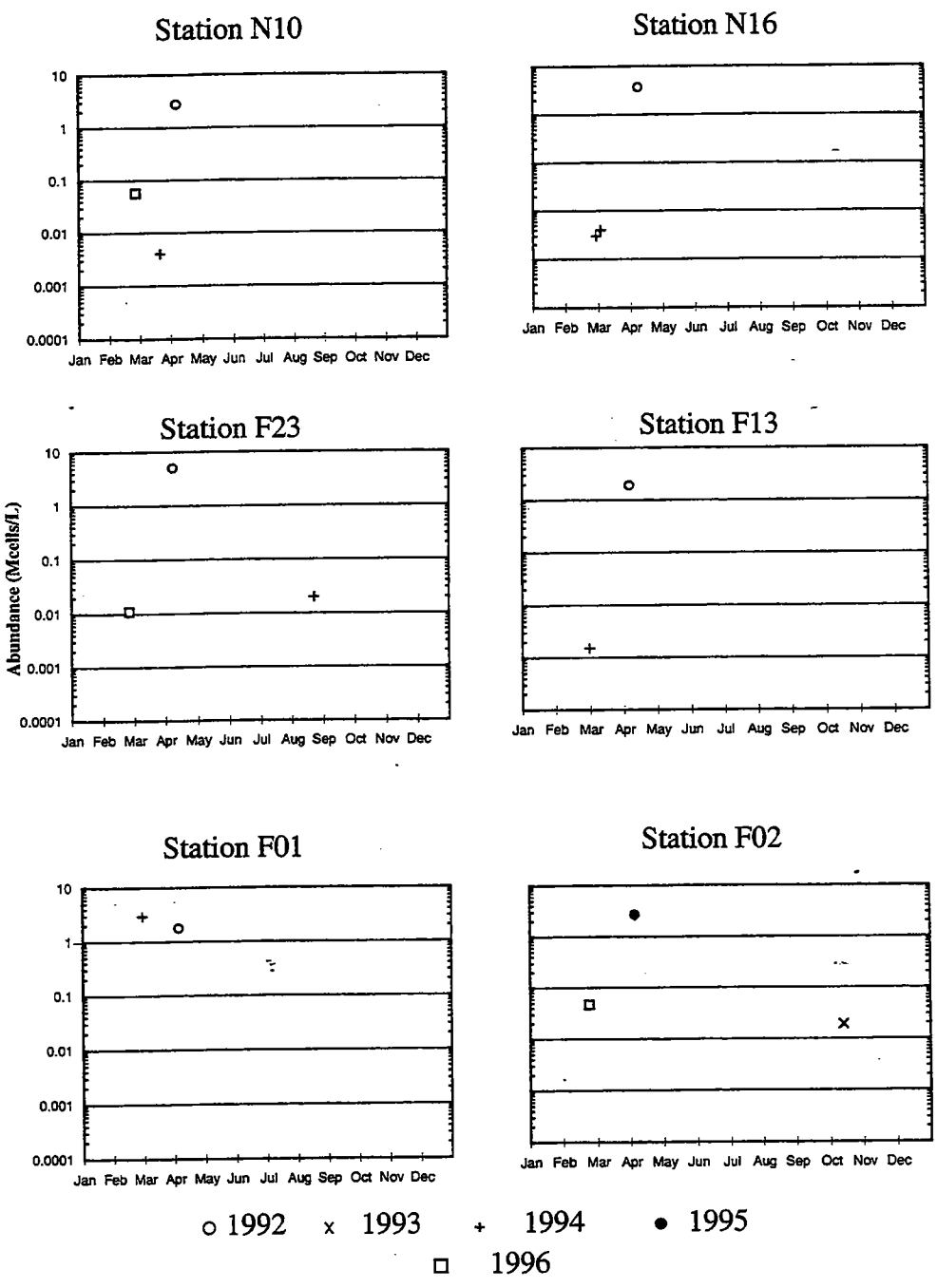

FIGURE 8-12a
Interannual Distribution of *Phaeocystis pouchetii* by Region
(whole-water samples)

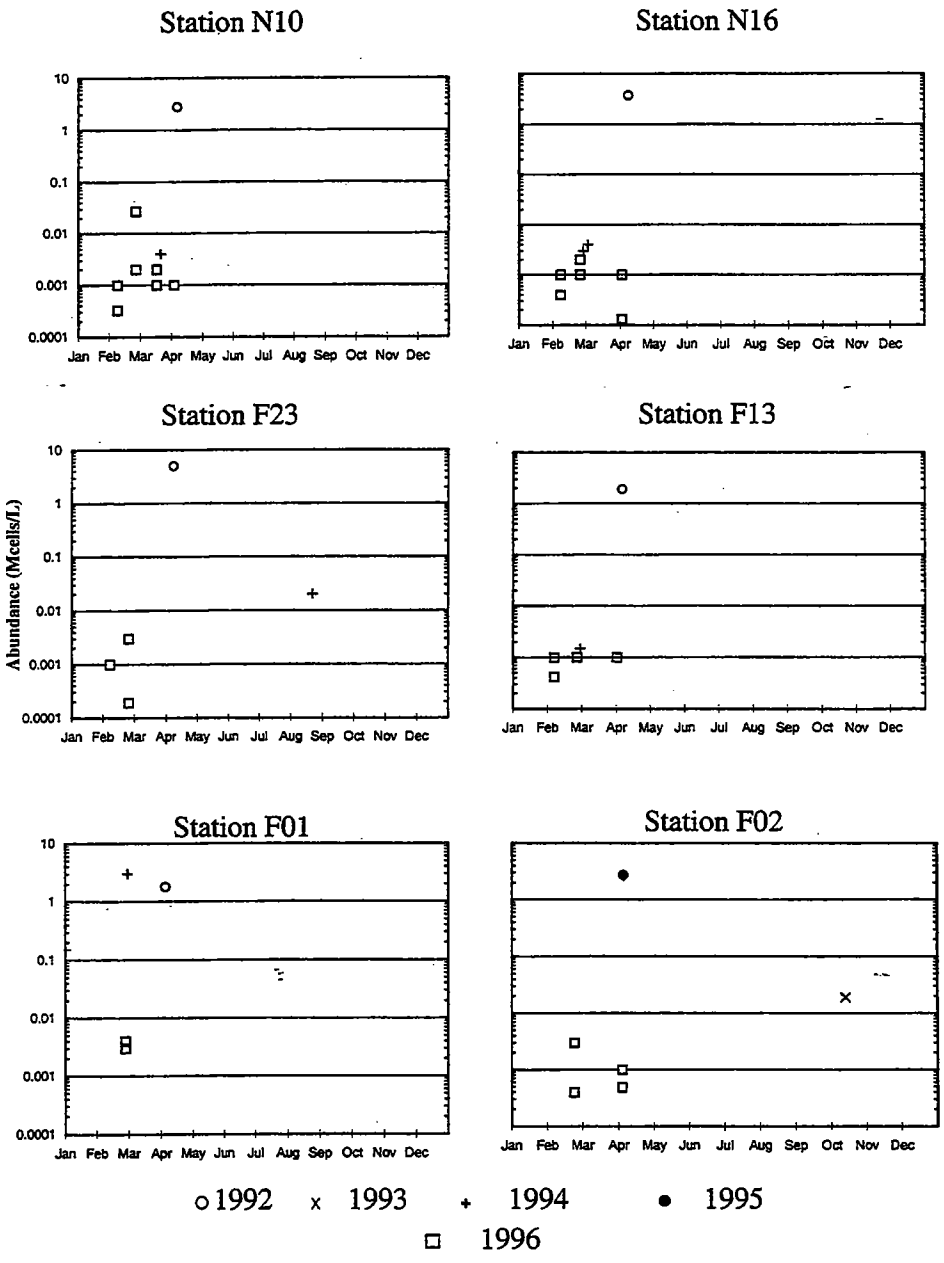

FIGURE 8-12b
Interannual Distribution of *Phaeocystis pouchetii* by Region
(screened samples)

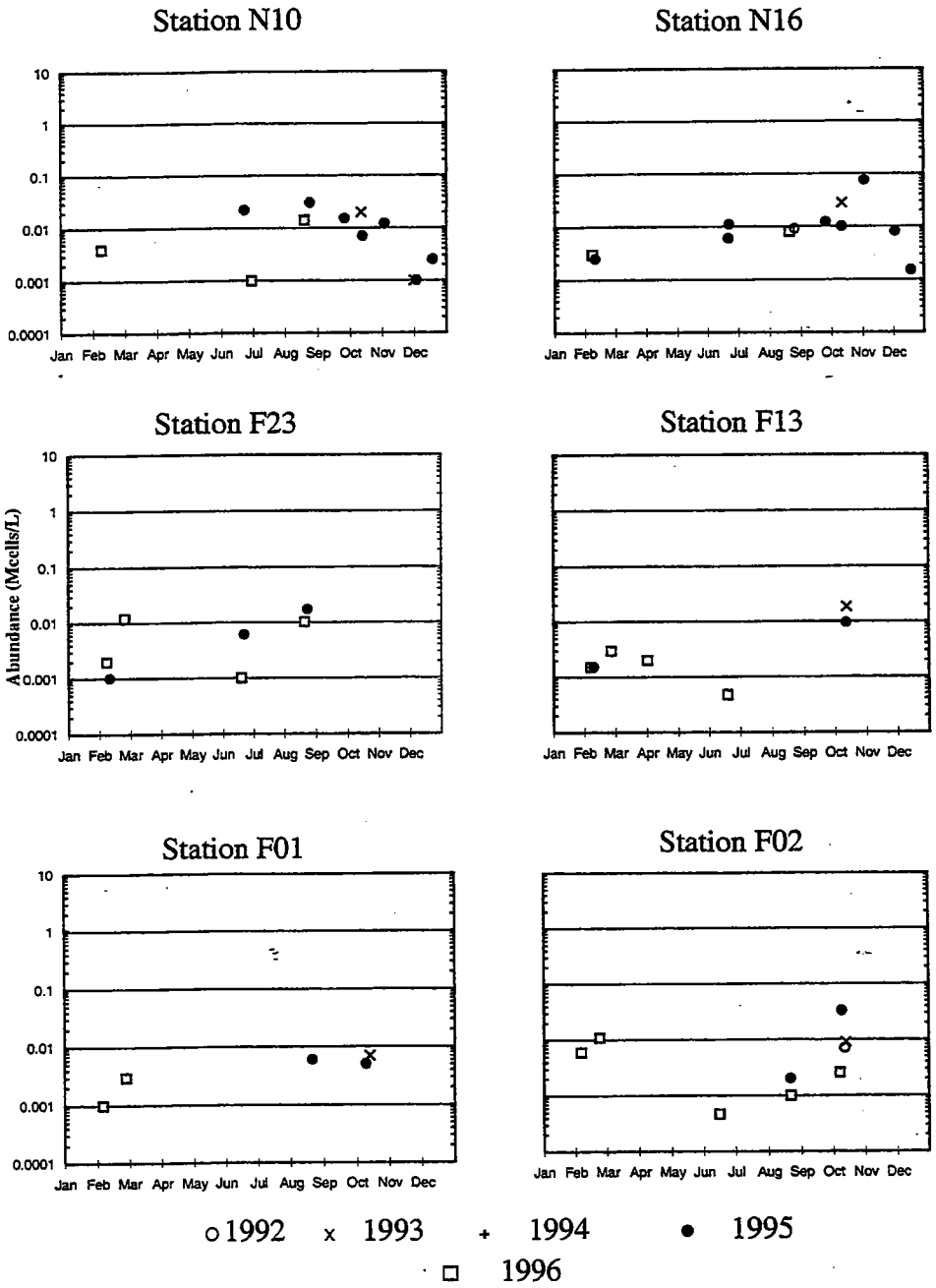

FIGURE 8-13a
Interannual Distribution of *Pseudo-nitzschia pungens* by Region
(whole-water samples)

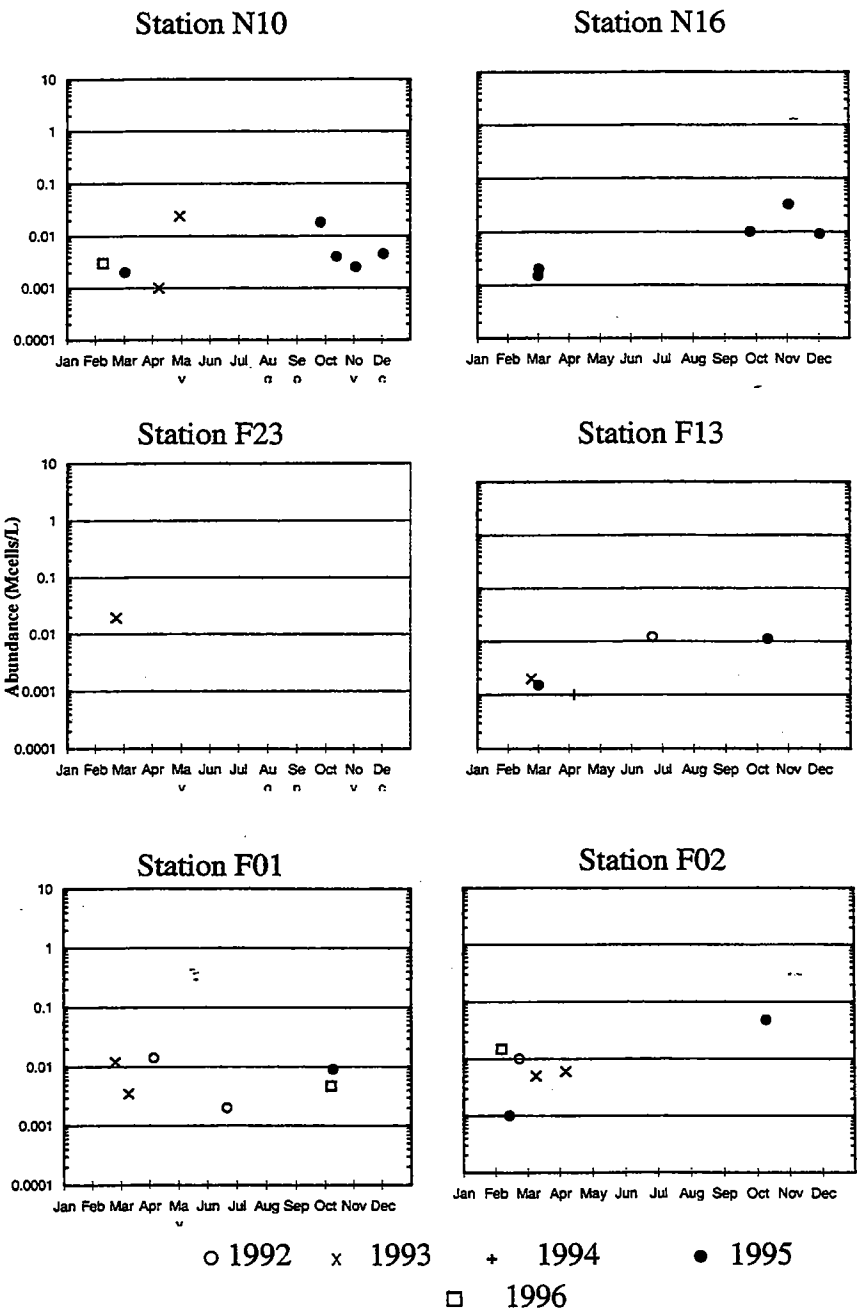

FIGURE 8-13b
Interannual Distribution of *Pseudo-nitzschia seriata* by Region
(whole-water samples)

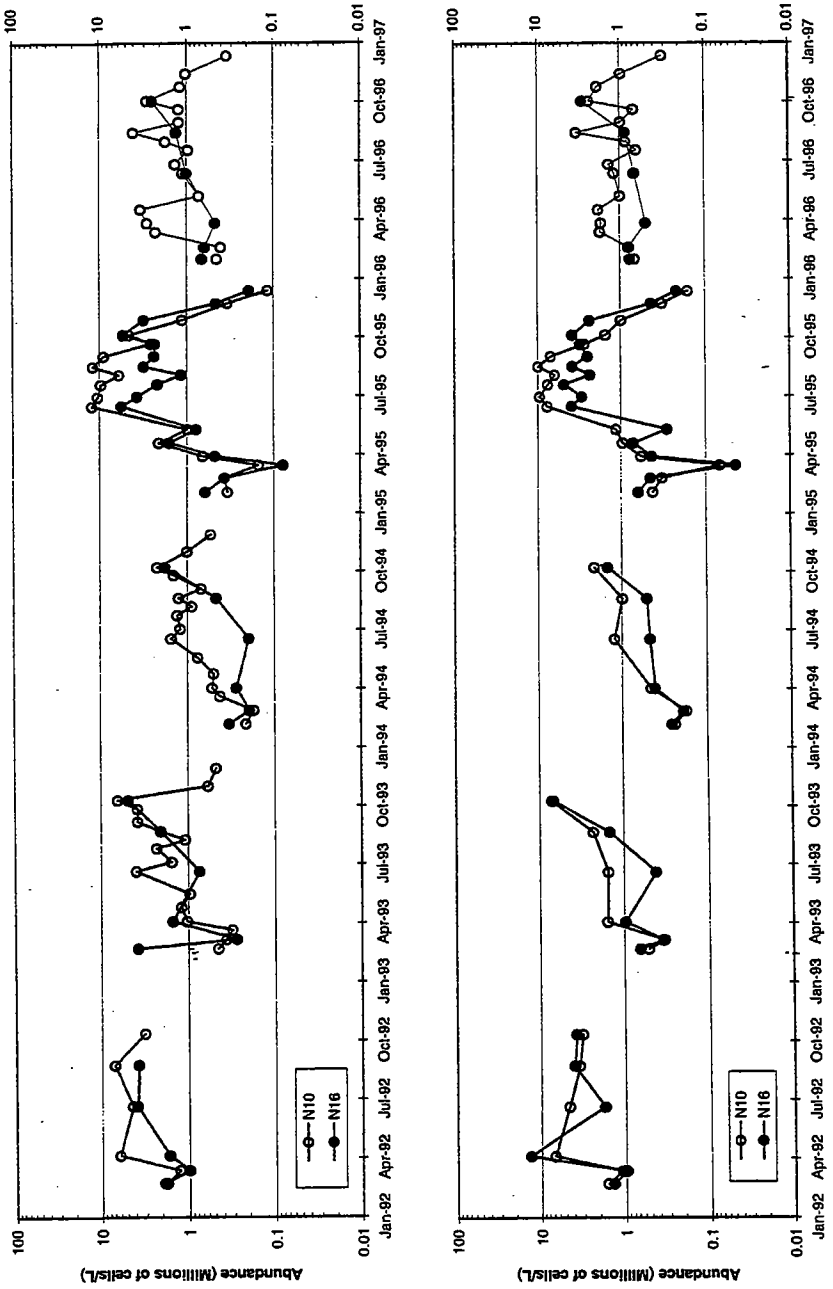

FIGURE 8-14
1992 - 1996 Total Phytoplankton Abundance in Nearfield Stations N10 and N16
Top: Surface Data, Bottom: Chlorophyll *a* Maximum Data

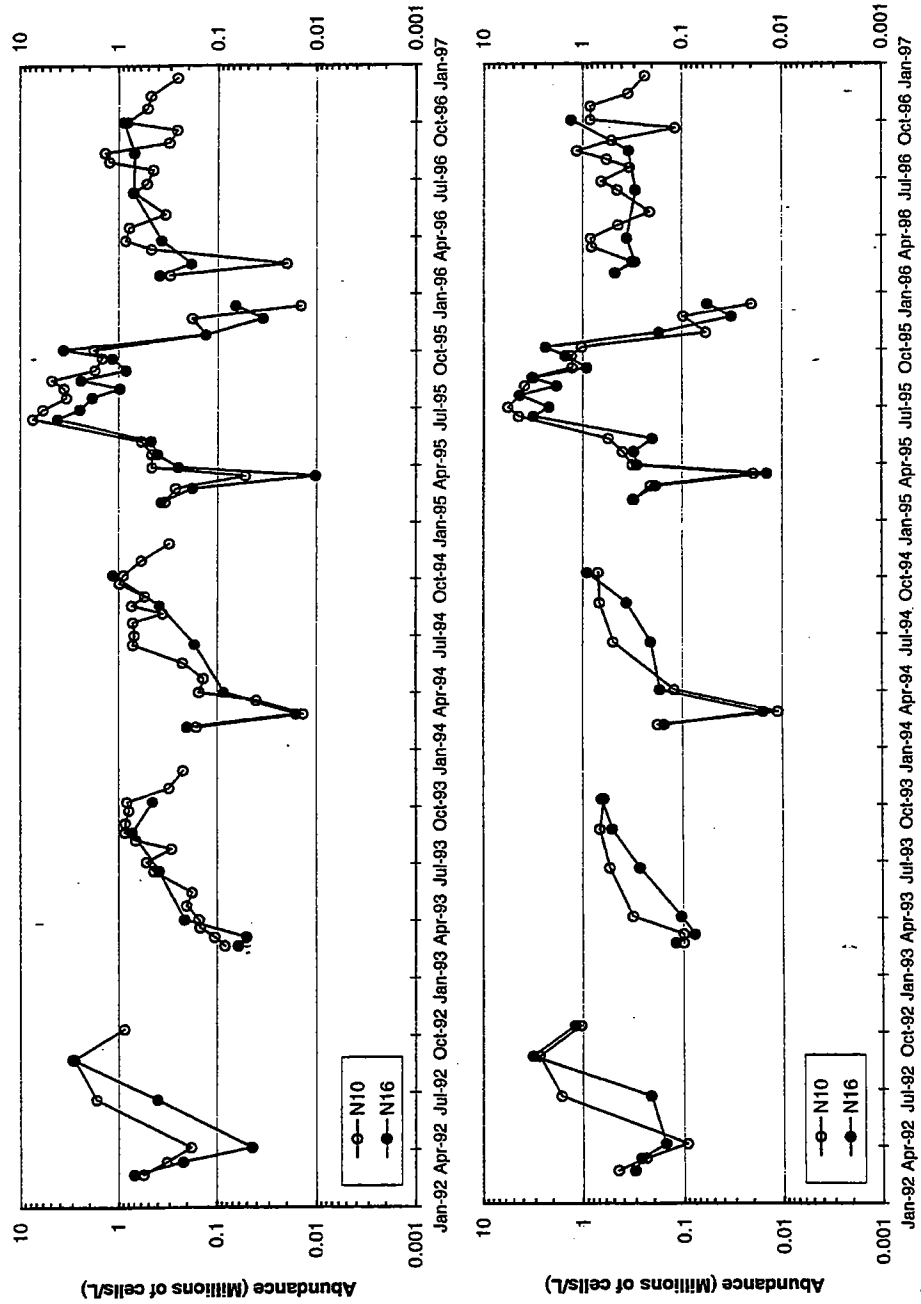

FIGURE 8-15
1992-1996 Seasonal Nearfield Pattern for Microflagellates in Nearfield Stations N10 and N16
Top: Surface Data, Bottom: Chlorophyll a Maximum Data

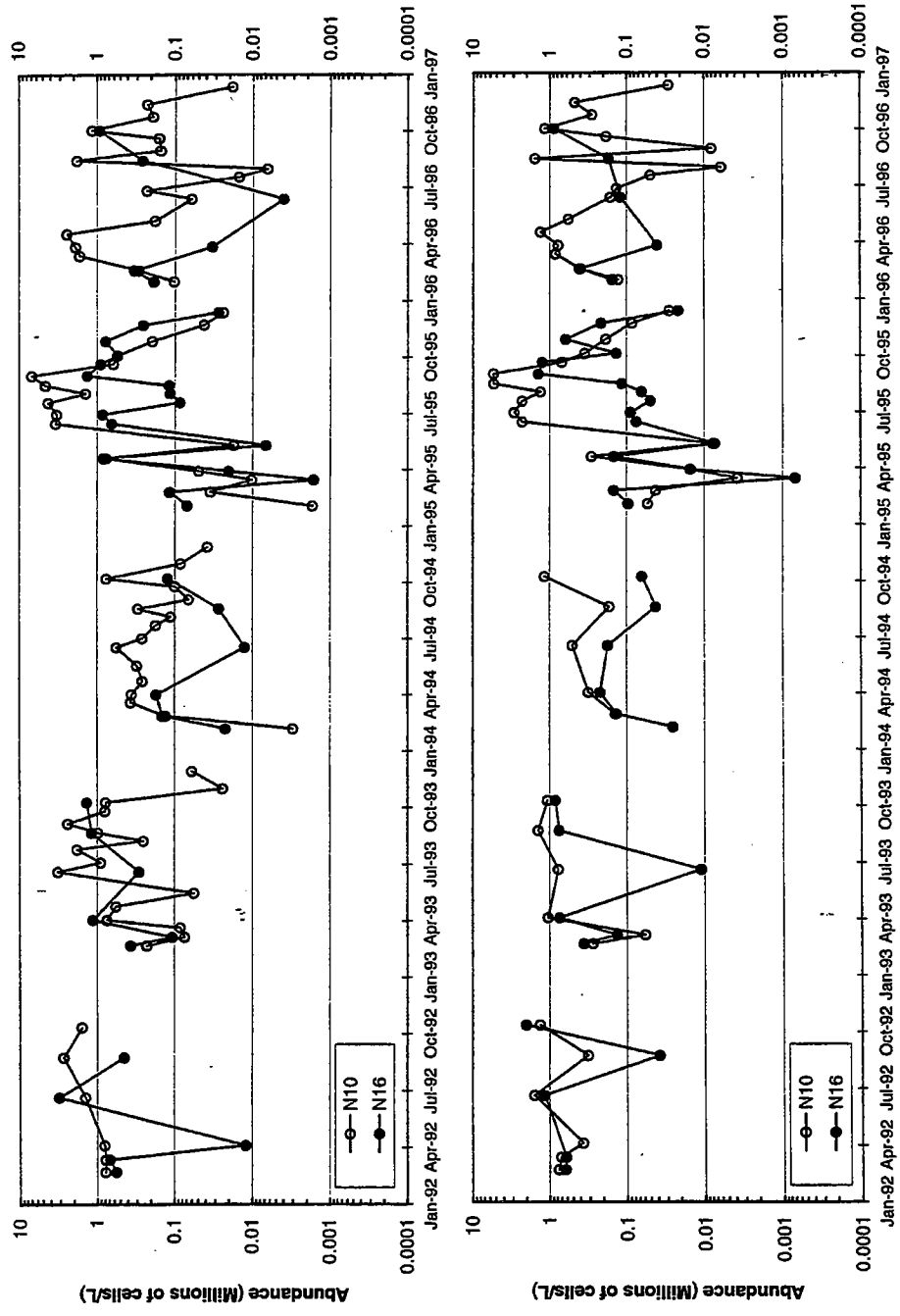

FIGURE 8-16
1992-1996 Seasonal Nearfield Pattern for Centric Diatoms in Nearfield Stations N10 and N16
Top: Surface Data, Bottom: Chlorophyll a Maximum Data

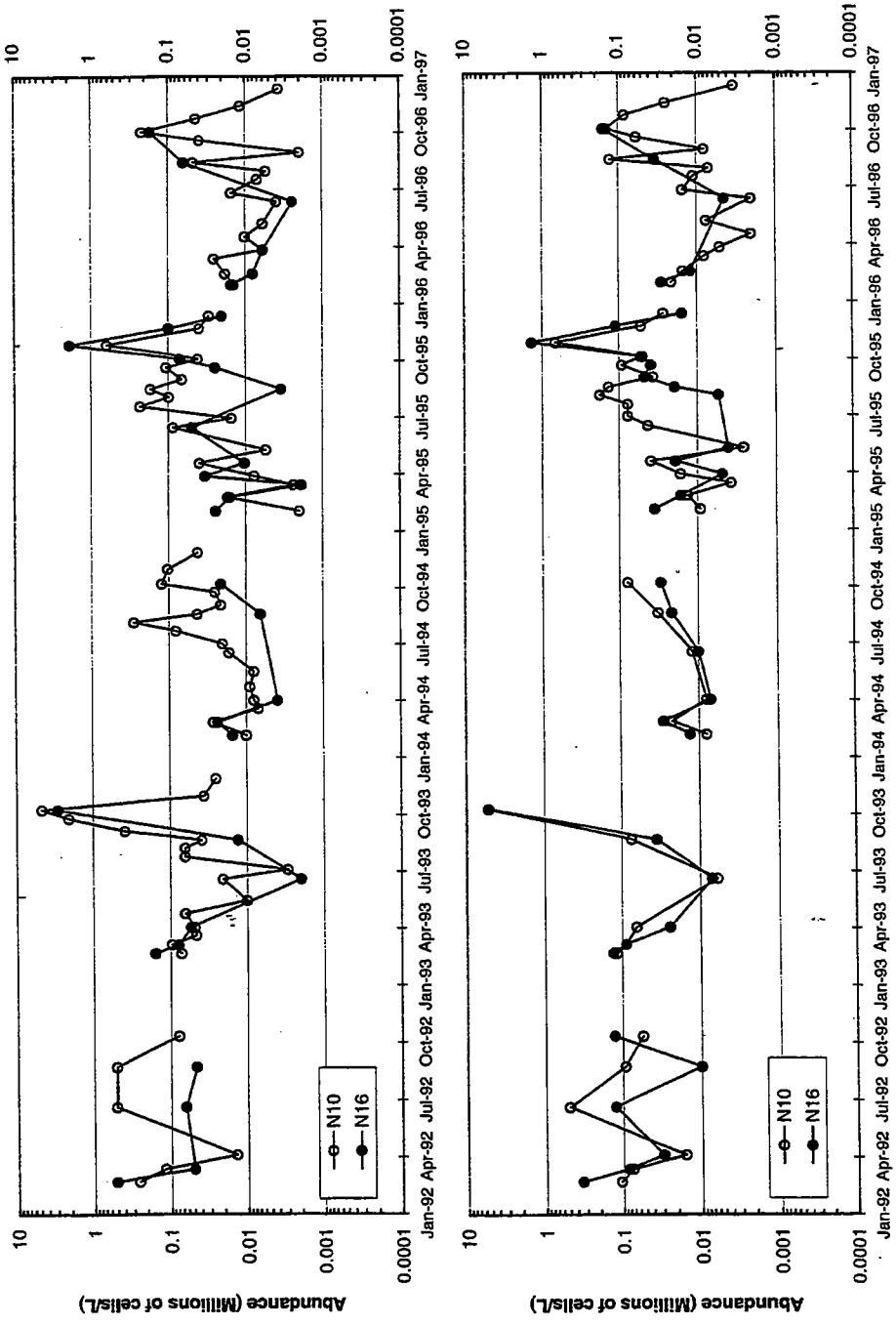

FIGURE 8-17
1992-1996 Seasonal Nearfield Pattern for Pennate Diatoms in Nearfield Stations N10 and N16
Top: Surface Data, Bottom: Chlorophyll a Maximum Data

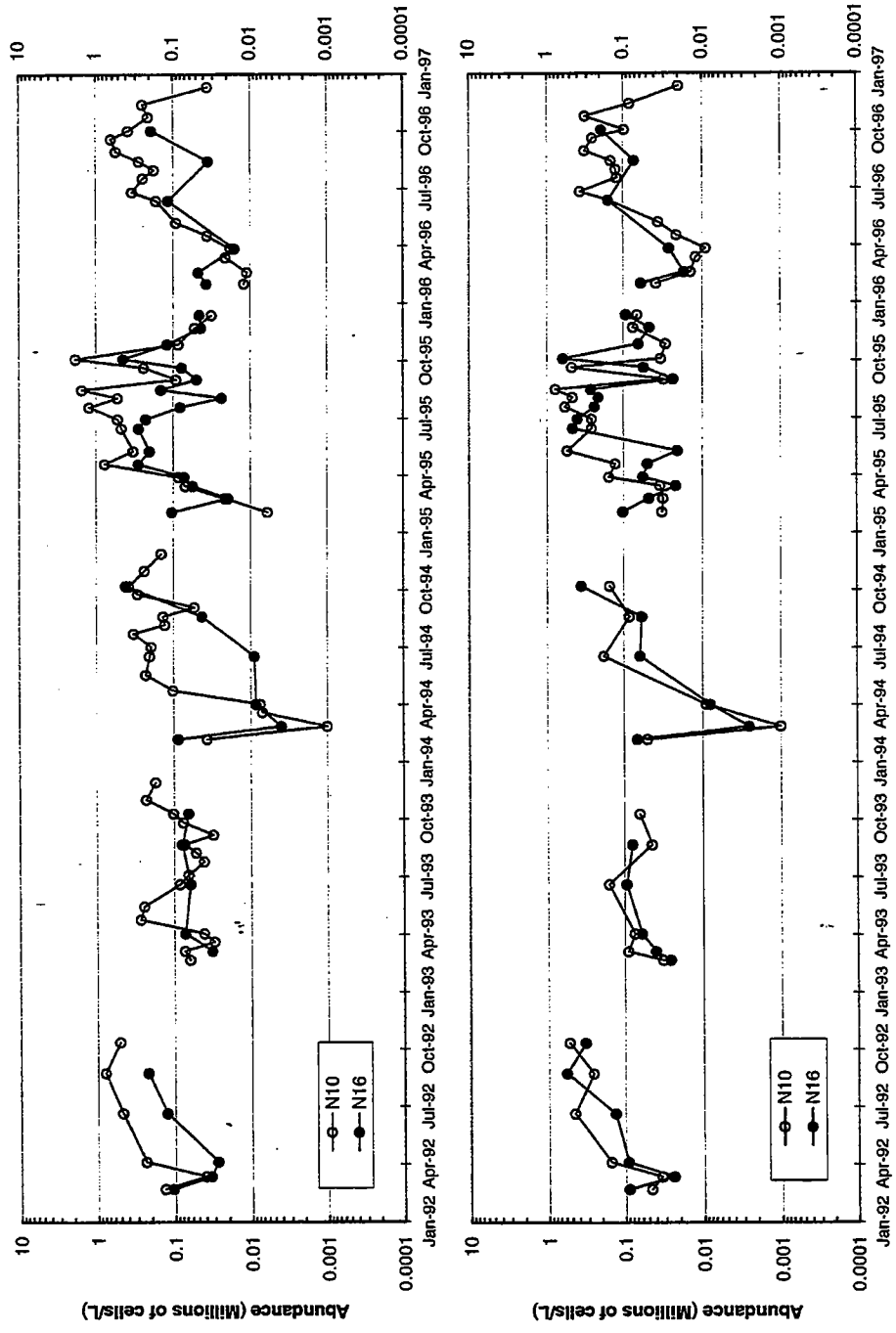

FIGURE 8-18
1992-1996 Seasonal Nearfield Pattern for Cryptophytes in Nearfield Stations N10 and N16
Top: Surface Data, Bottom: Chlorophyll a Maximum Data

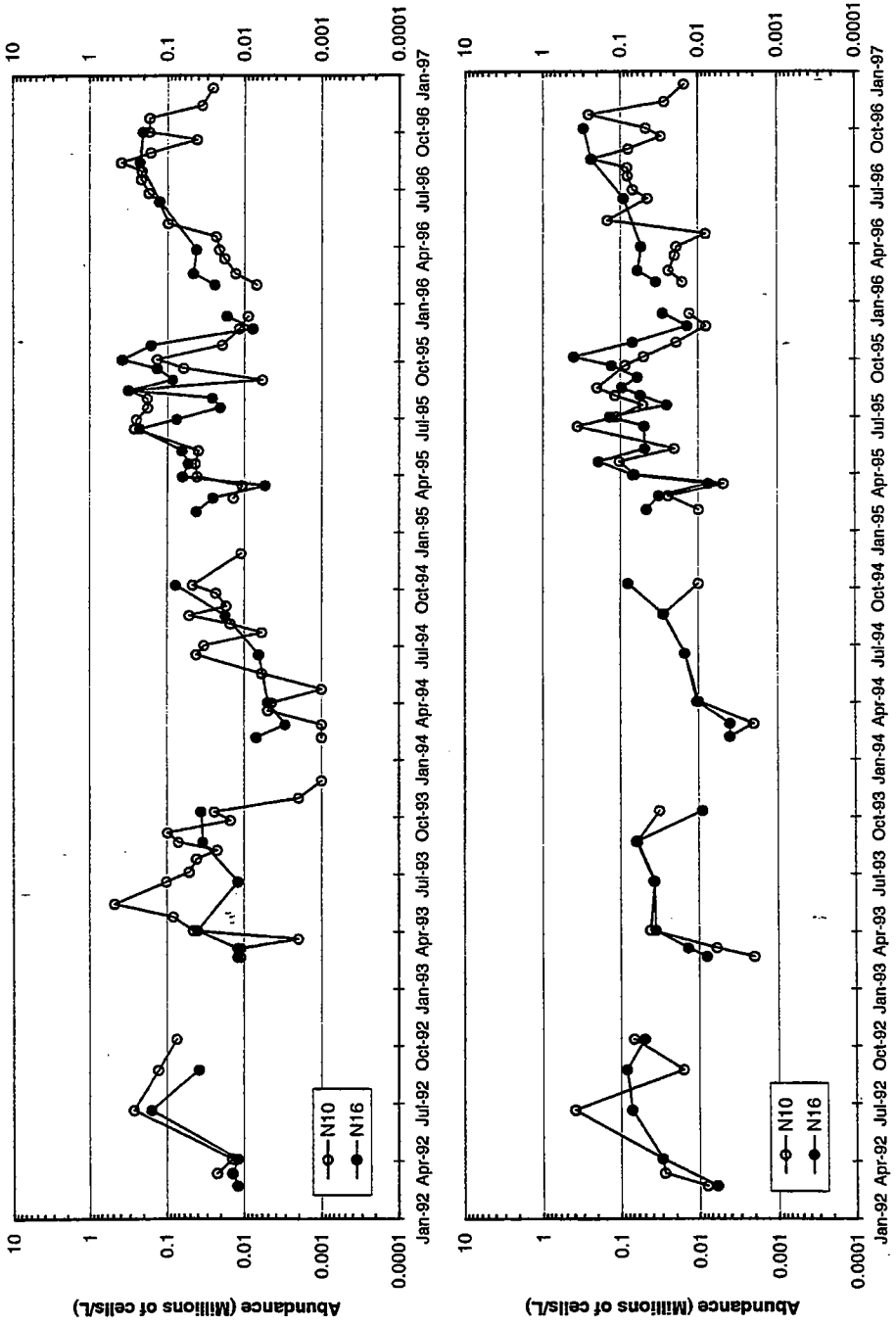

FIGURE 8-19
1992-1996 Seasonal Nearfield Pattern for Dinoflagellates in Nearfield Stations N10 and N16
Top: Surface Data, Bottom: Chlorophyll a Maximum Data

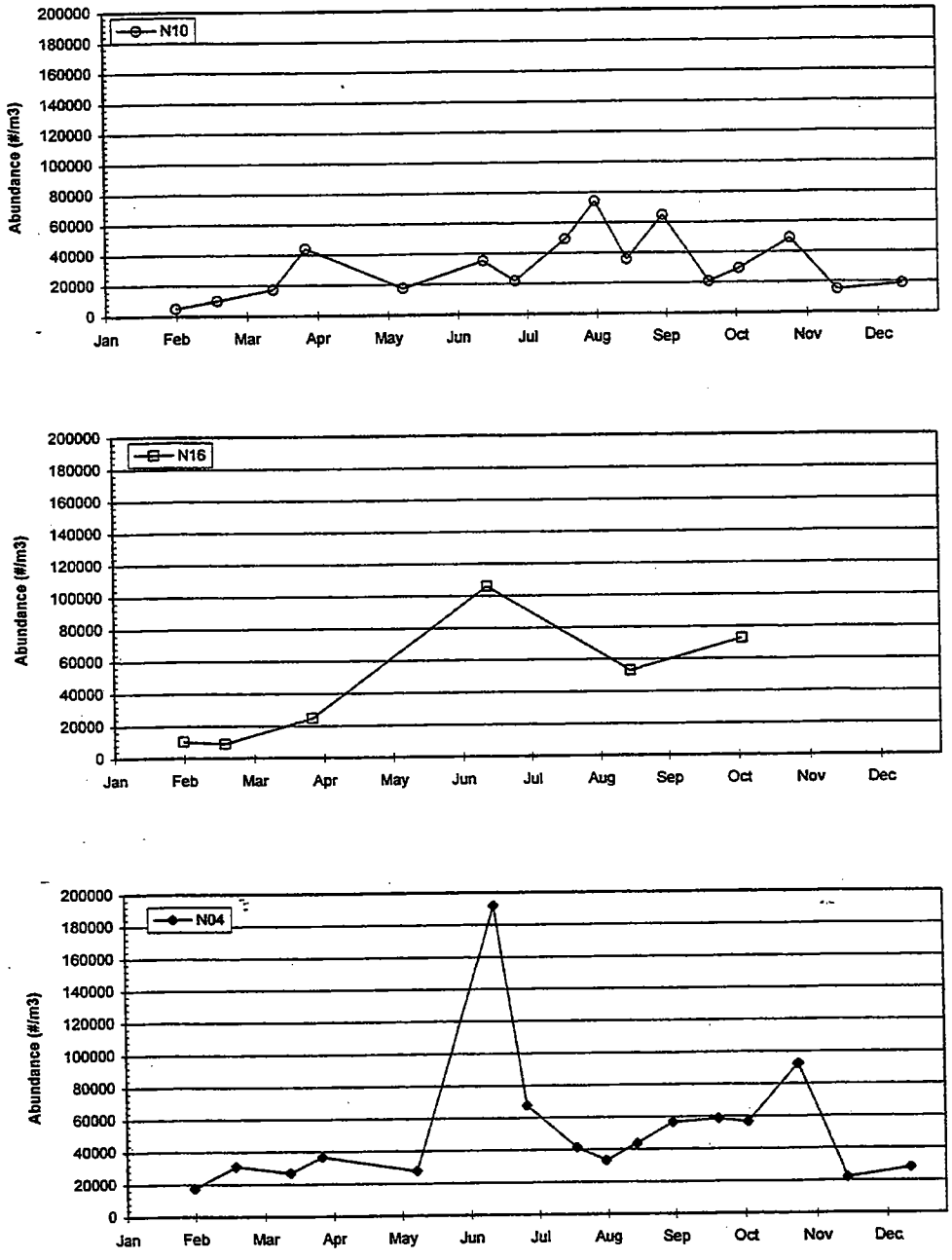

FIGURE 8-20
1996 Total Zooplankton Abundance
Nearfield Stations Top: N10, Middle: N16, Bottom: N04

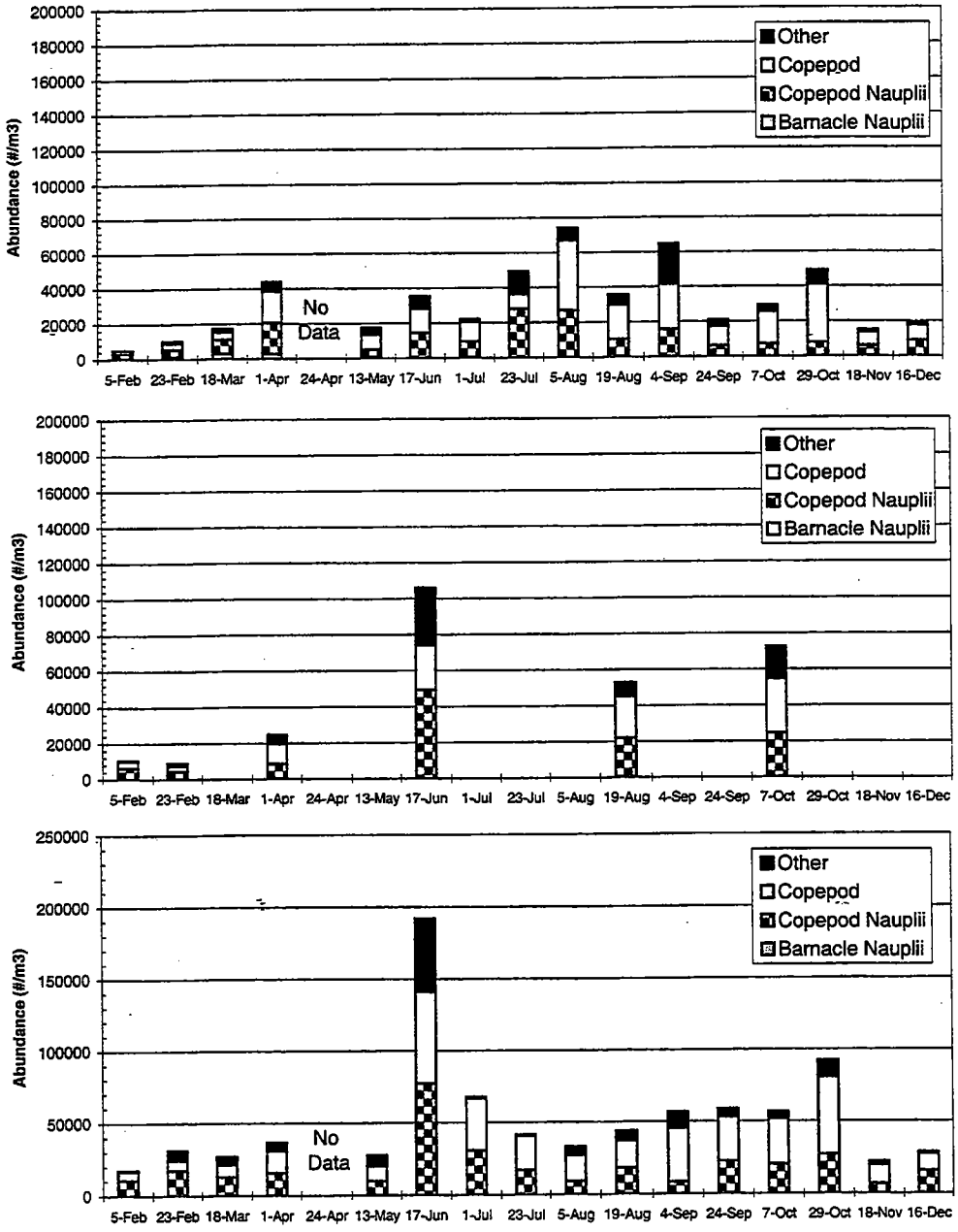

FIGURE 8-21
1996 Total Zooplankton Abundance by Group
Nearfield Stations Top: N10, Middle: N16, Bottom: N04

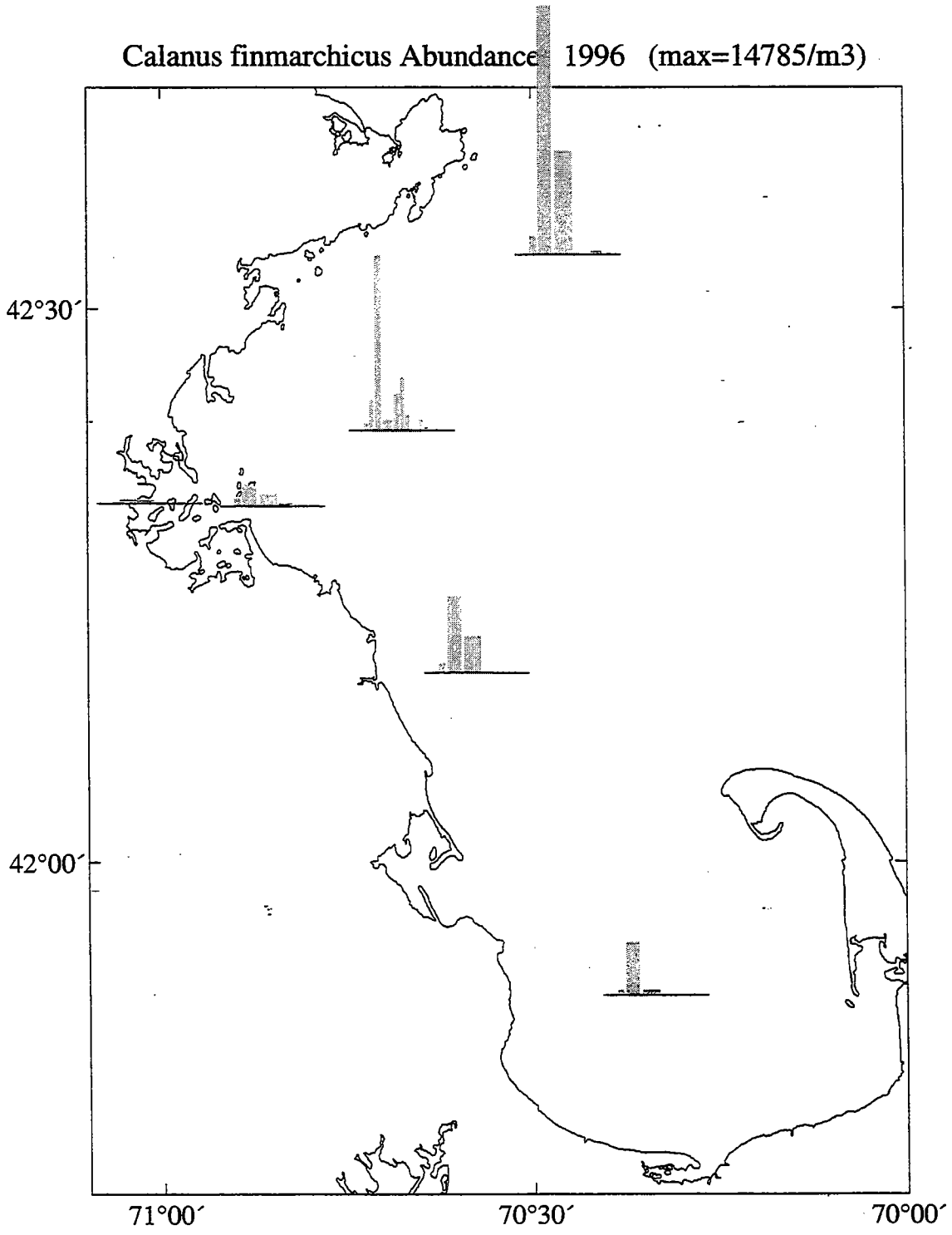

FIGURE 8-22
1996 *Calanus finmarchicus* Abundance (Maxima = 14785/m^3)

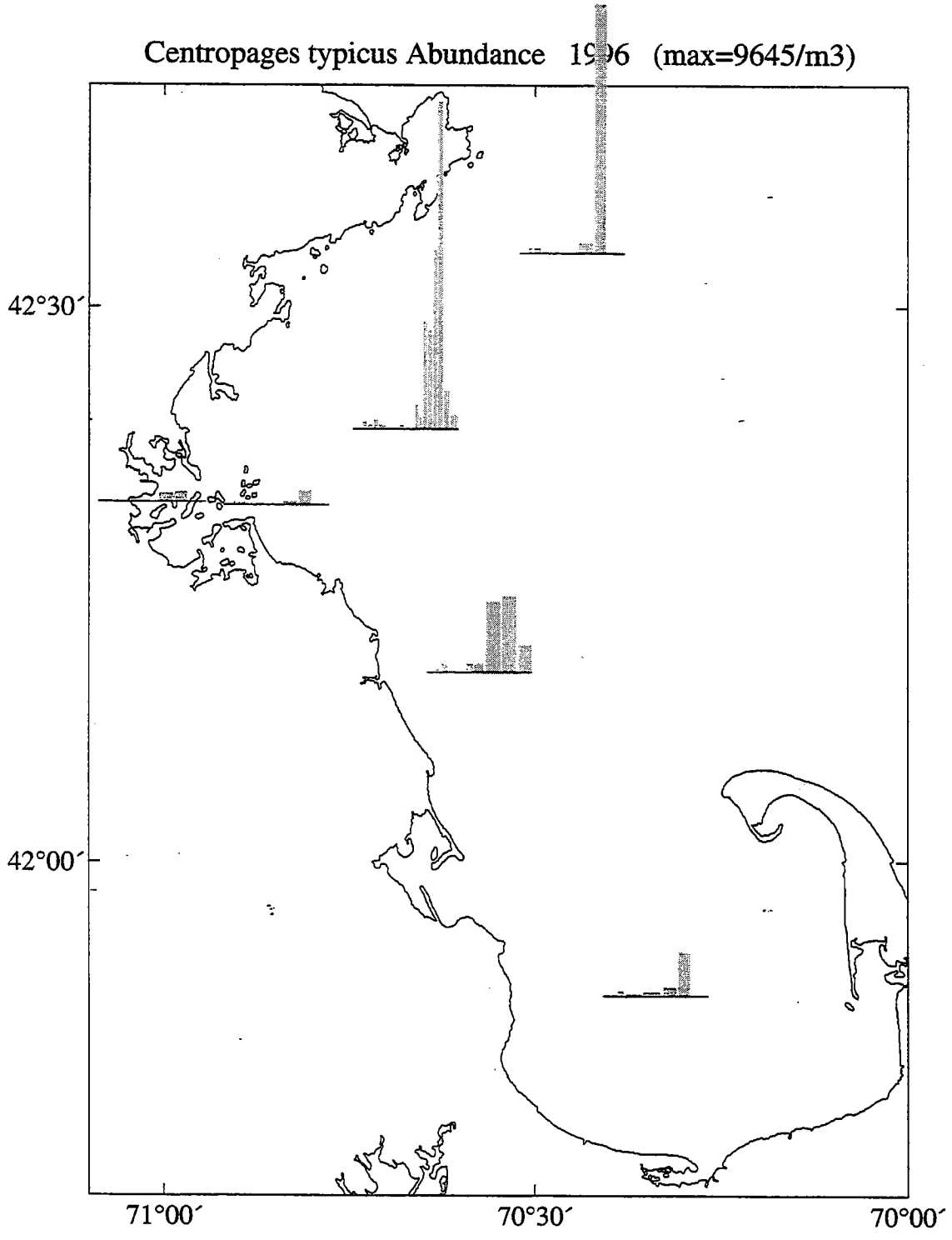

FIGURE 8-23
1996 *Centropages typicus* Abundance (Maxima = 9645/m^3)

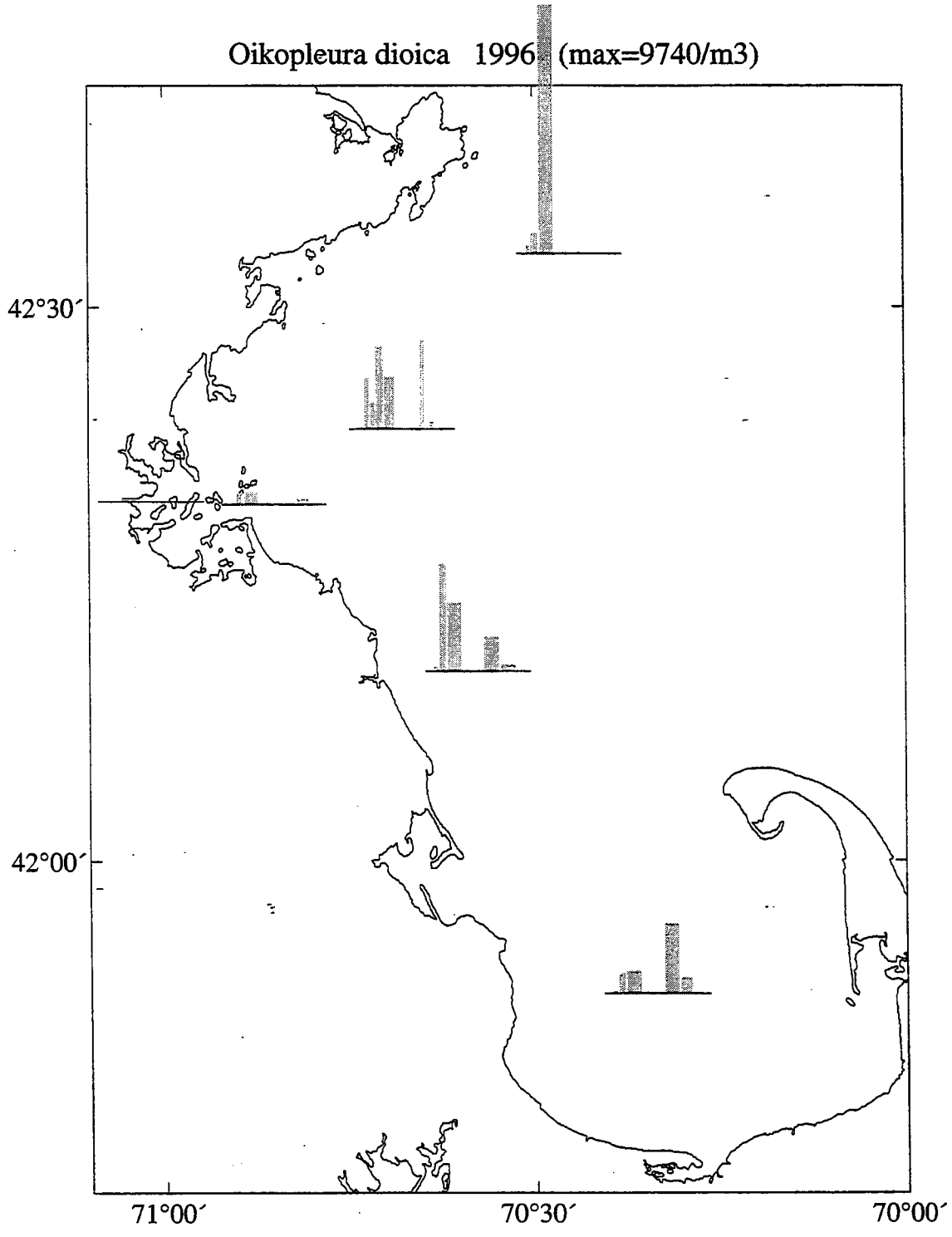

FIGURE 8-24
1996 *Oikopleura dioica* Abundance (Maxima = 9740/m^3)

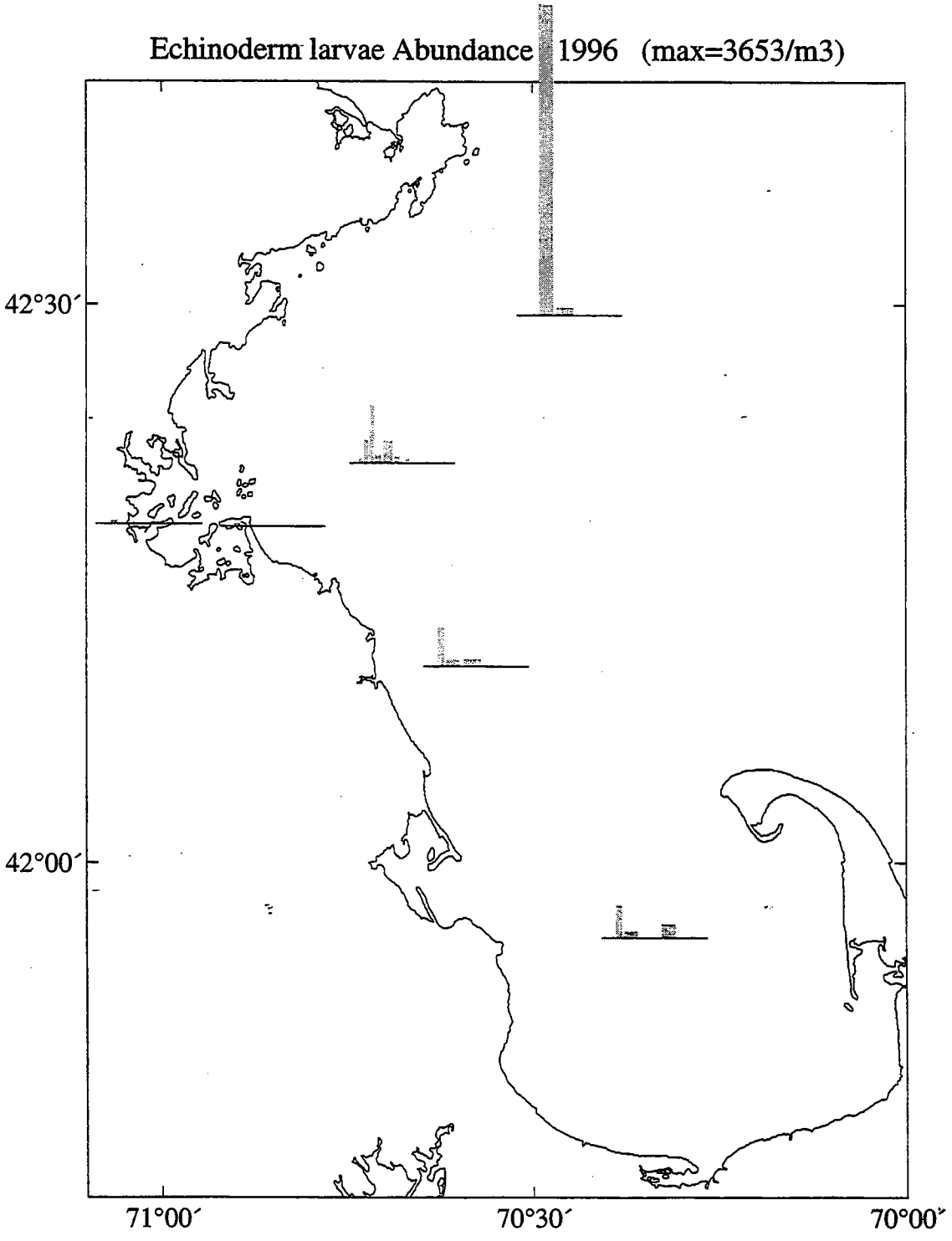

FIGURE 8-25
1996 Echinoderm larvae Abundance (Maxima = 3653/m^3)

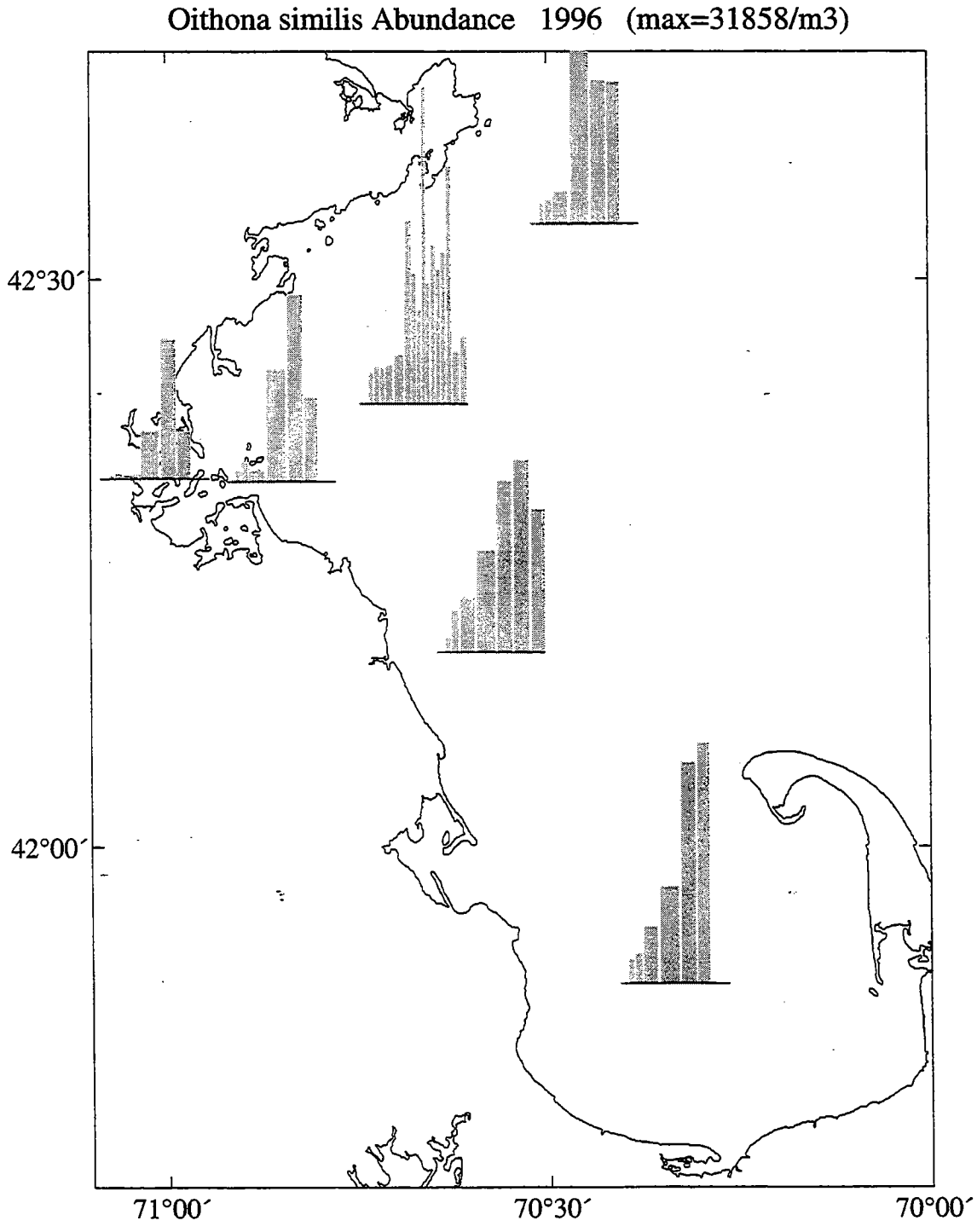

FIGURE 8-26
1996 *Oithona similis* Abundance (Maxima = 31858/m^3)

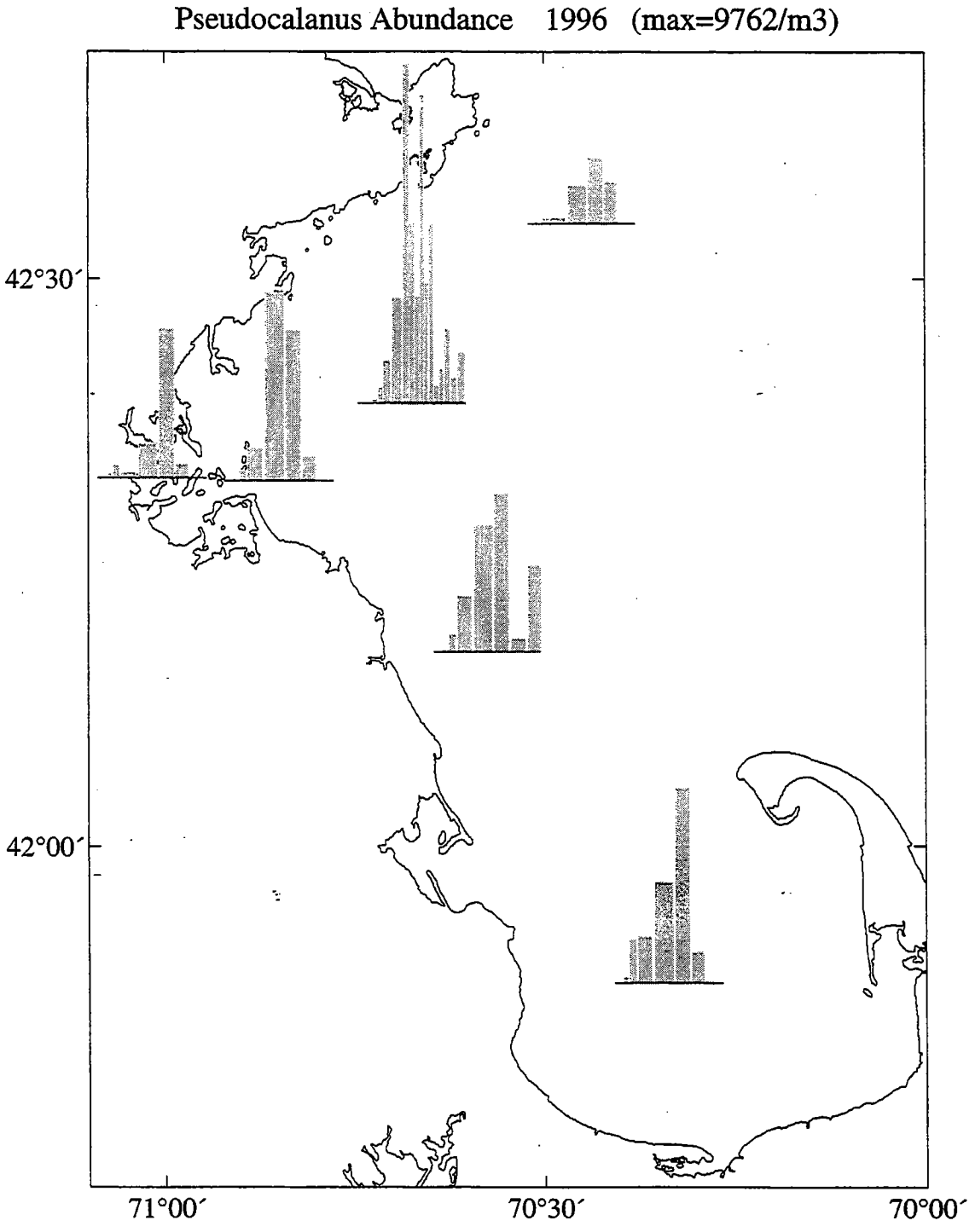

FIGURE 8-27
1996 *Pseudocalanus* spp. Abundance (Maxima = 9762/m^3)

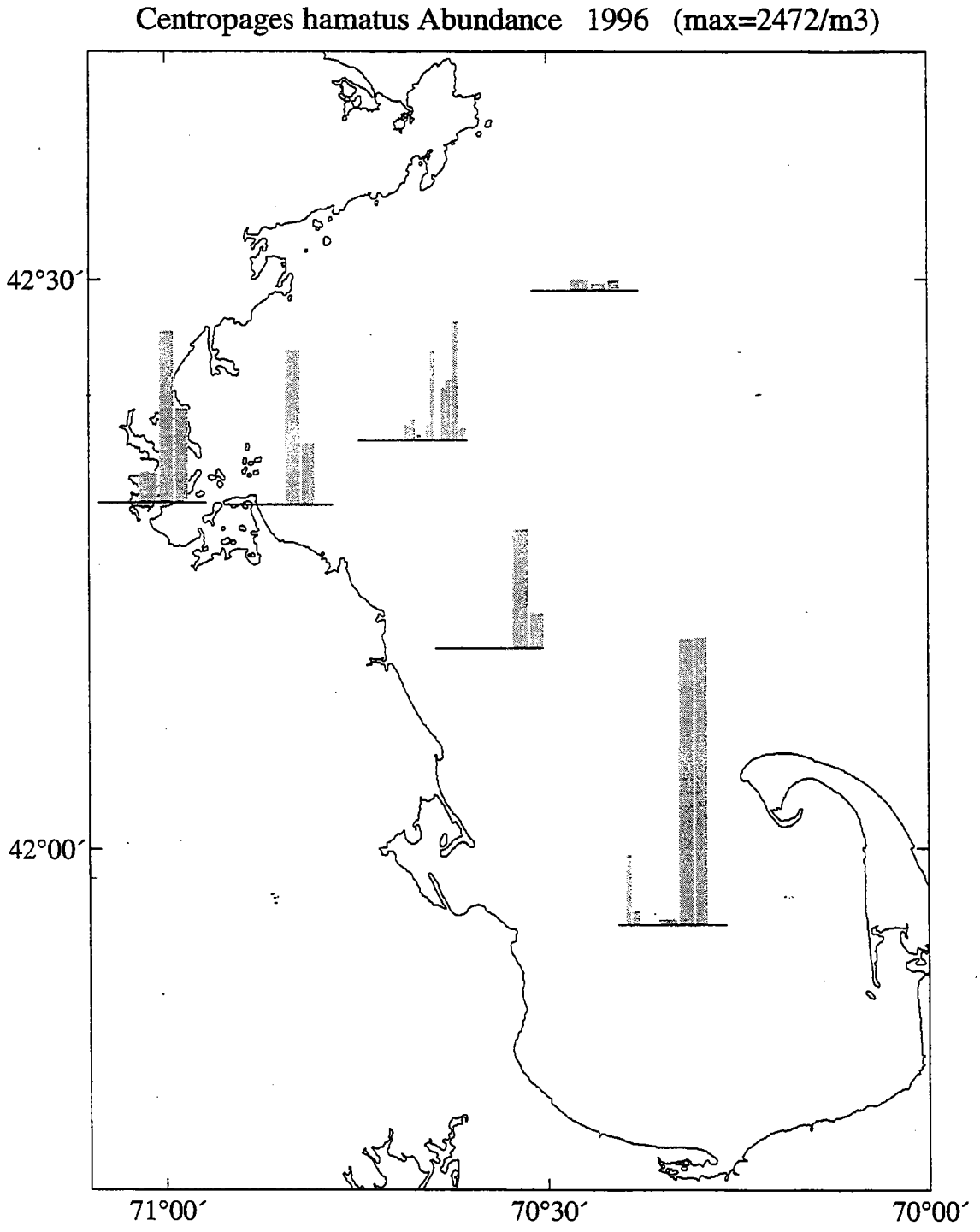

FIGURE 8-28
1996 *Centropages hamatus* Abundance (Maxima = 2472/m^3)

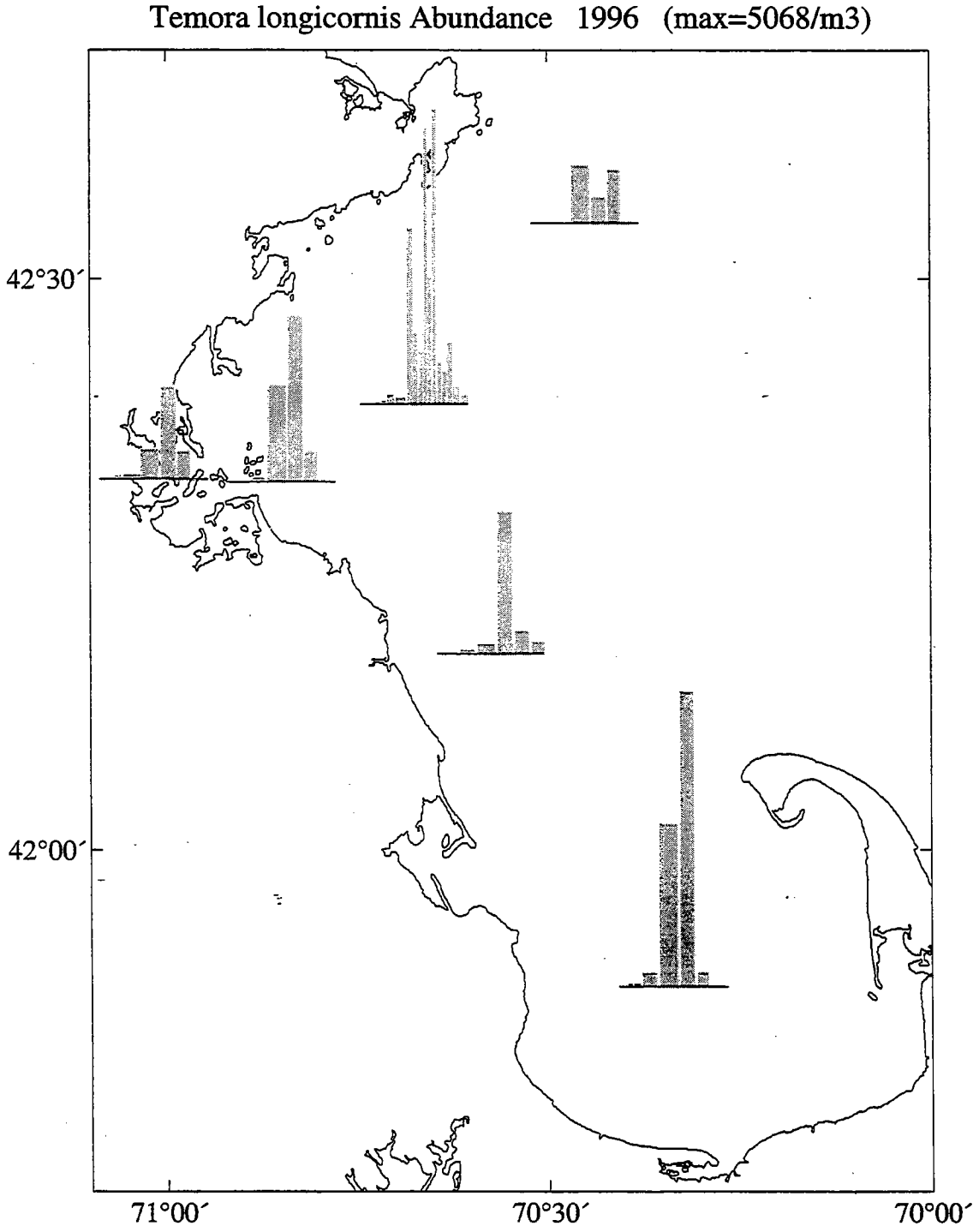

FIGURE 8-29
1996 *Temora longicornis* Abundance (Maxima = 5068/m^3)

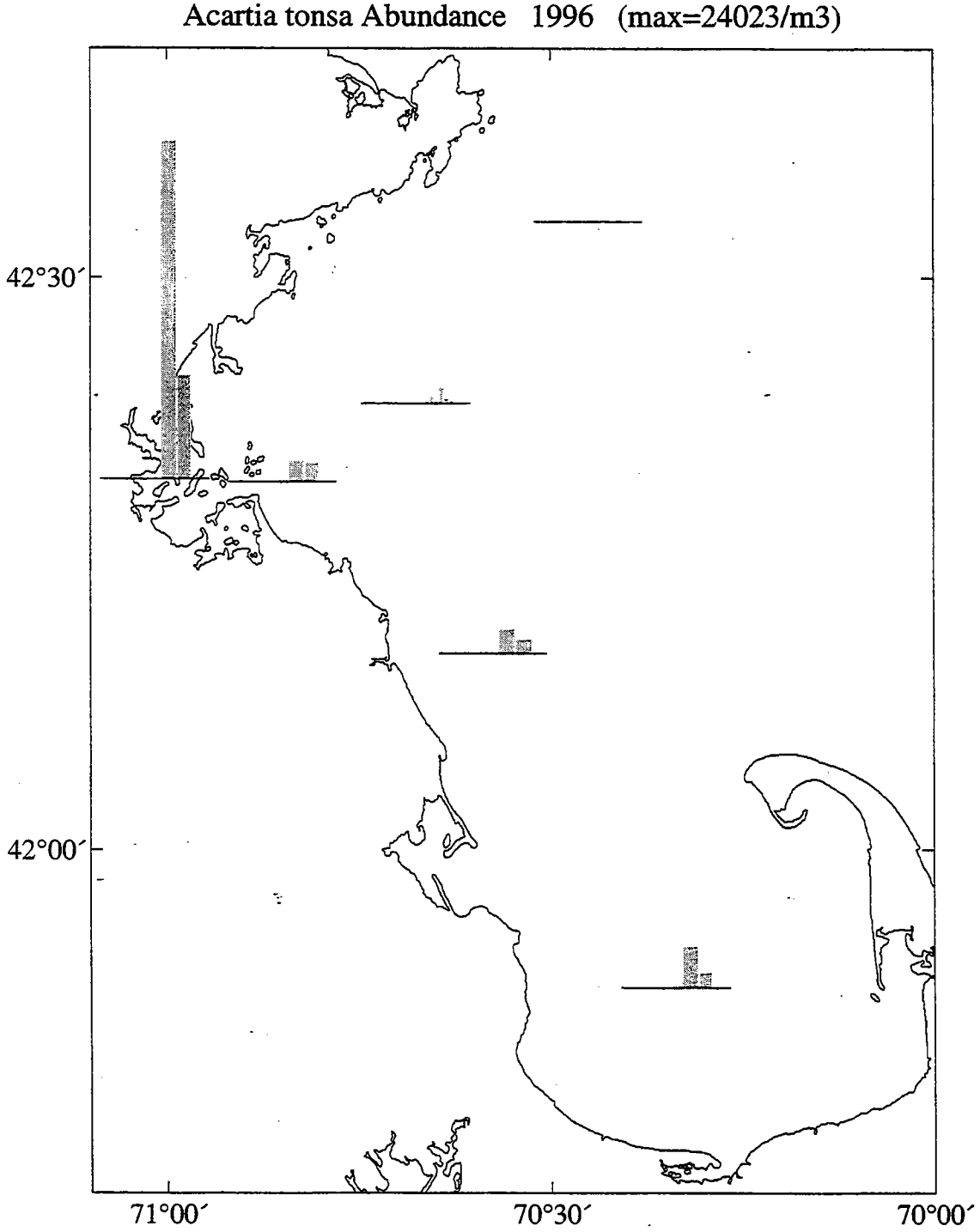

FIGURE 8-30
1996 *Acartia tonsa* Abundance (Maxima = 24023/m^3)

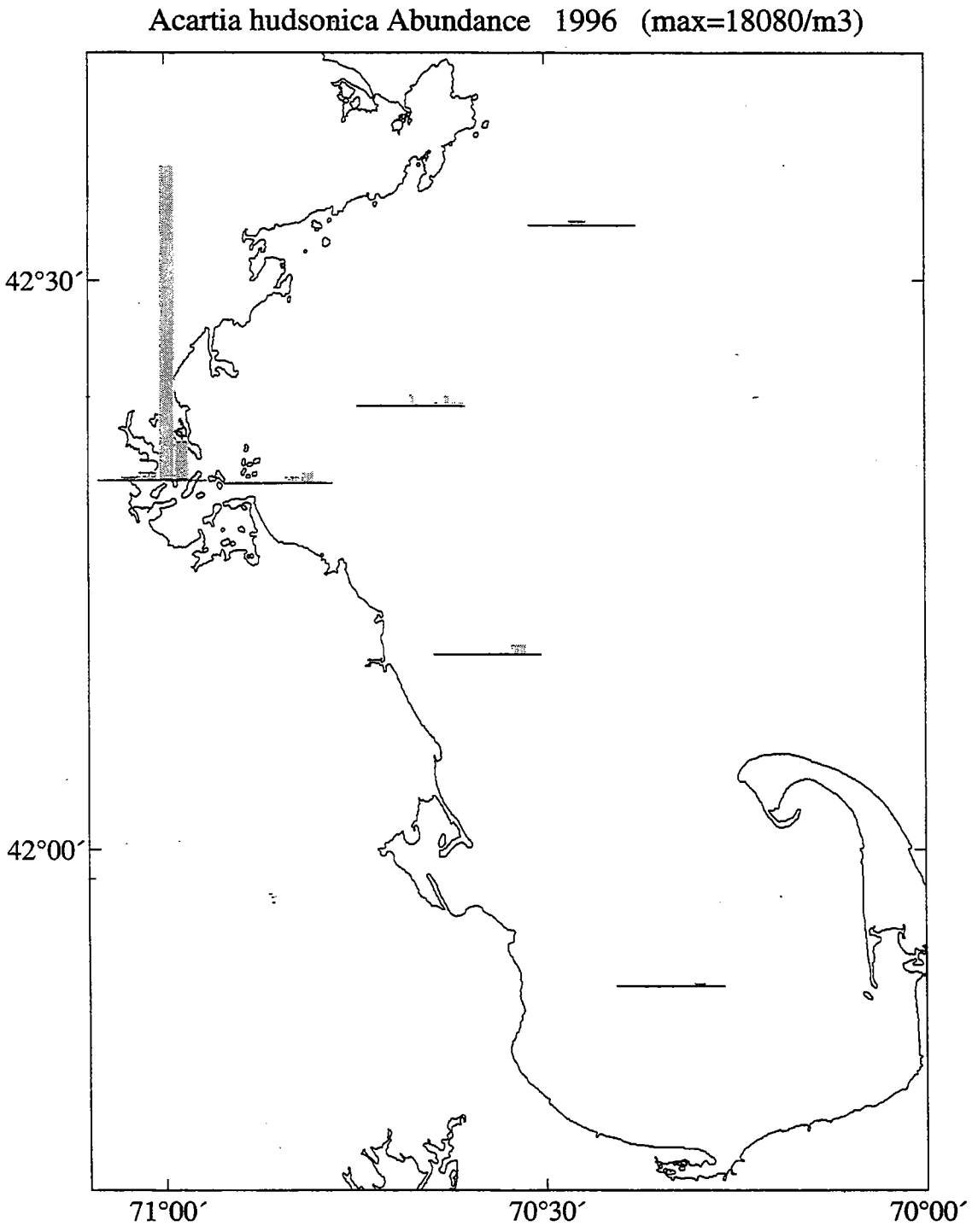

FIGURE 8-31
1996 *Acartia hudsonica* Abundance (Maxima = 18080/m^3)

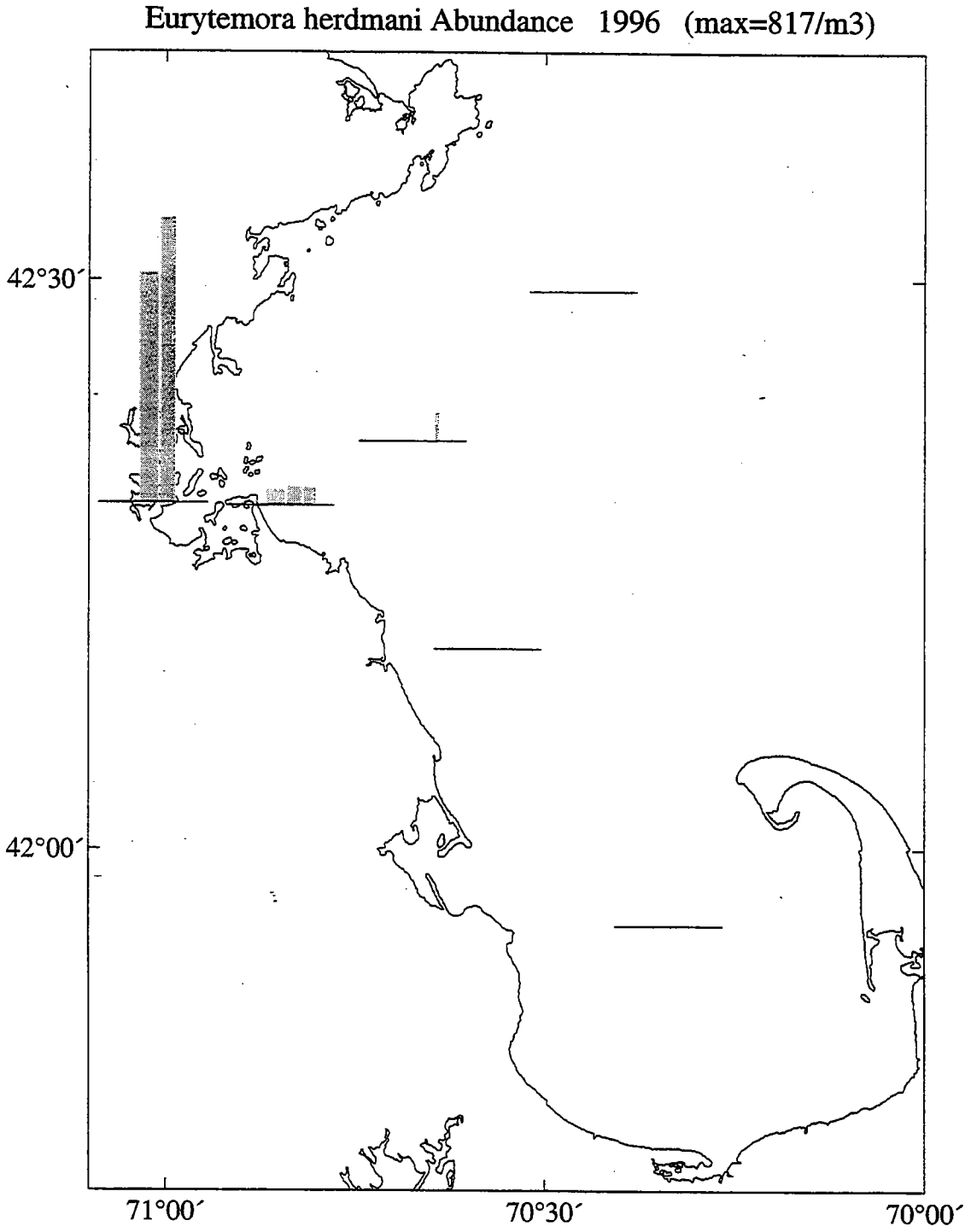

FIGURE 8-32
1996 *Eurytemora herdmani* Abundance (Maxima = 817/m^3)

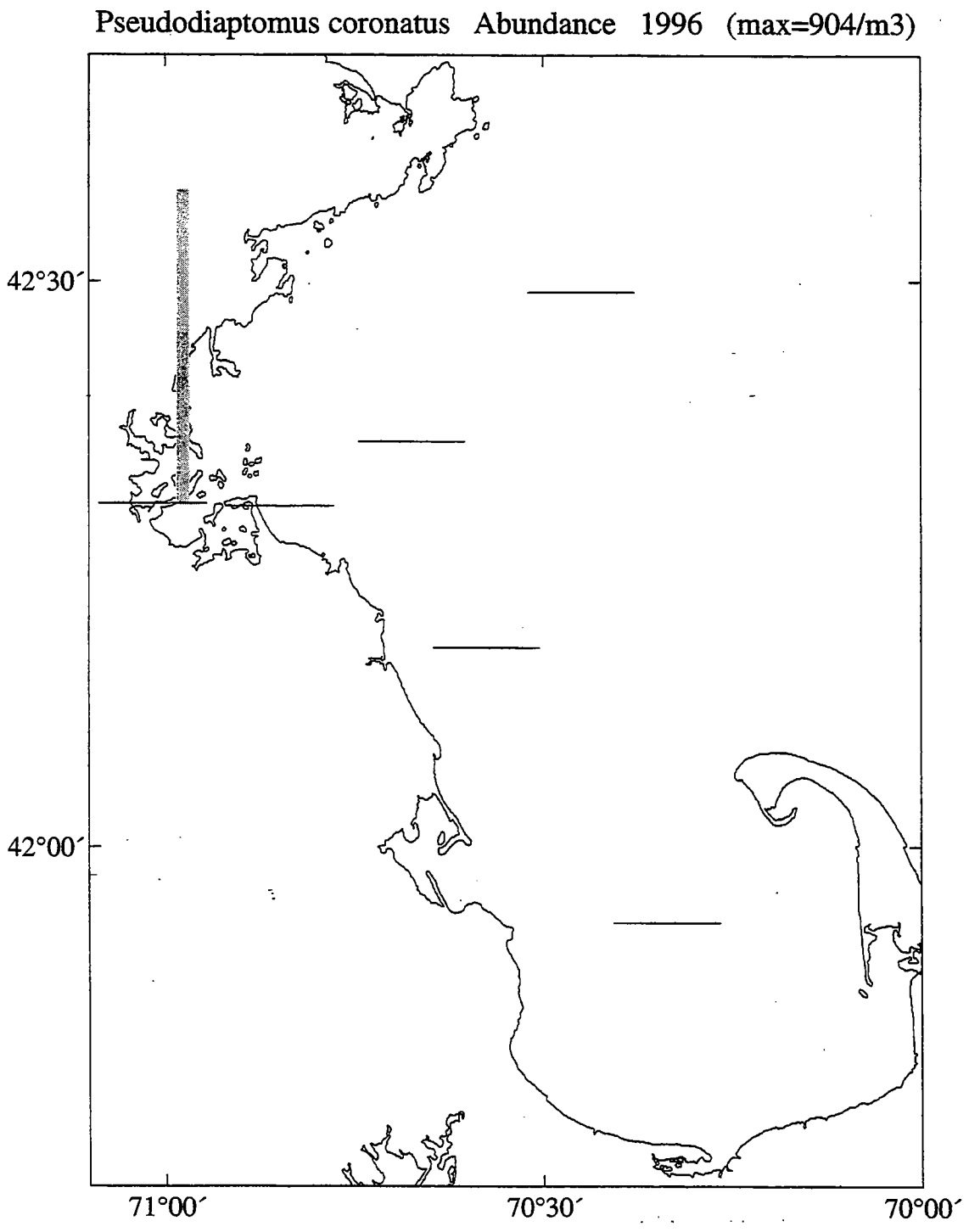

FIGURE 8-33
1996 *Pseudodiaptomus coronatus* Abundance (Maxima = 904/m^3)

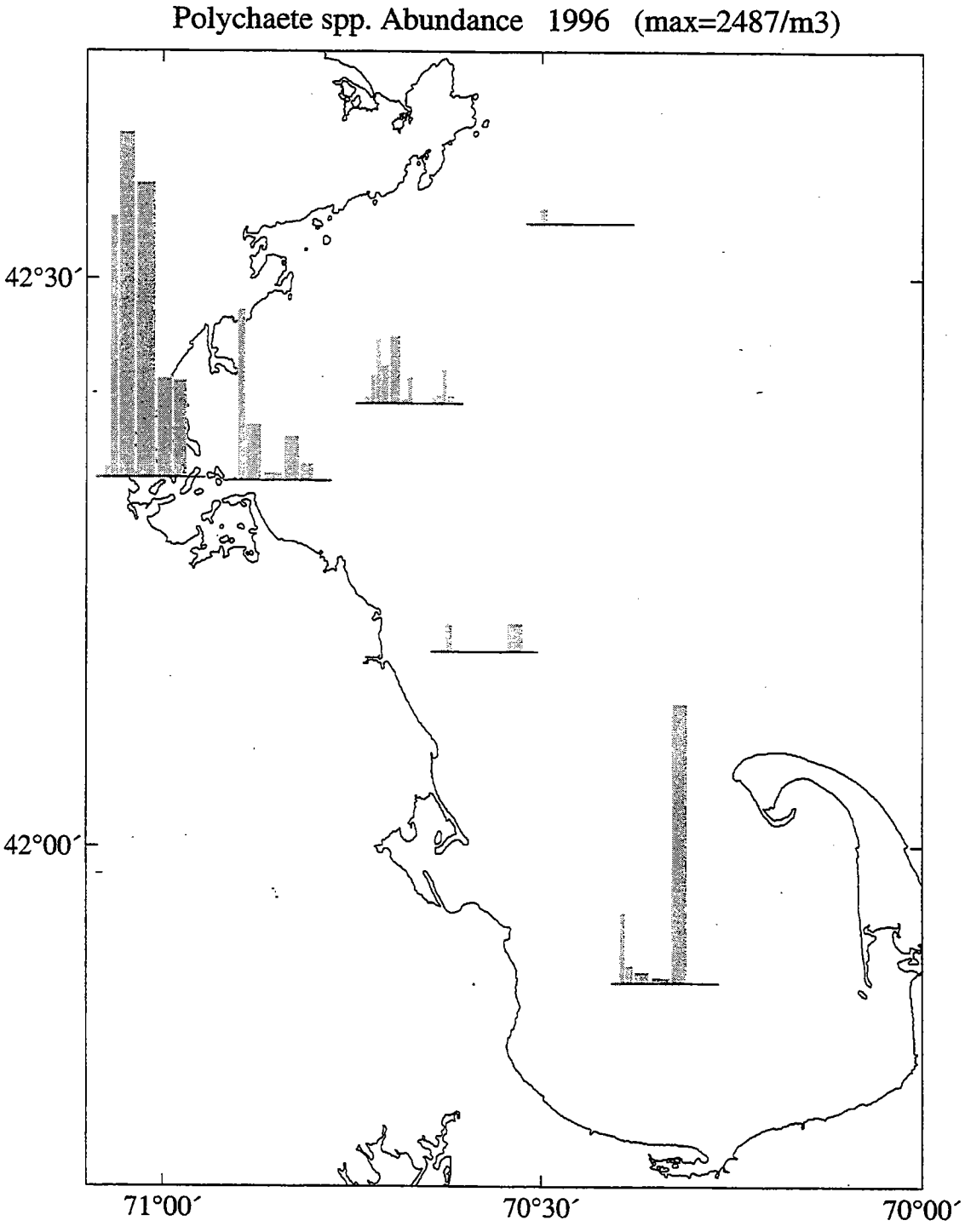

FIGURE 8-34
1996 Polychaete spp. Abundance (Maxima = 2487/m^3)

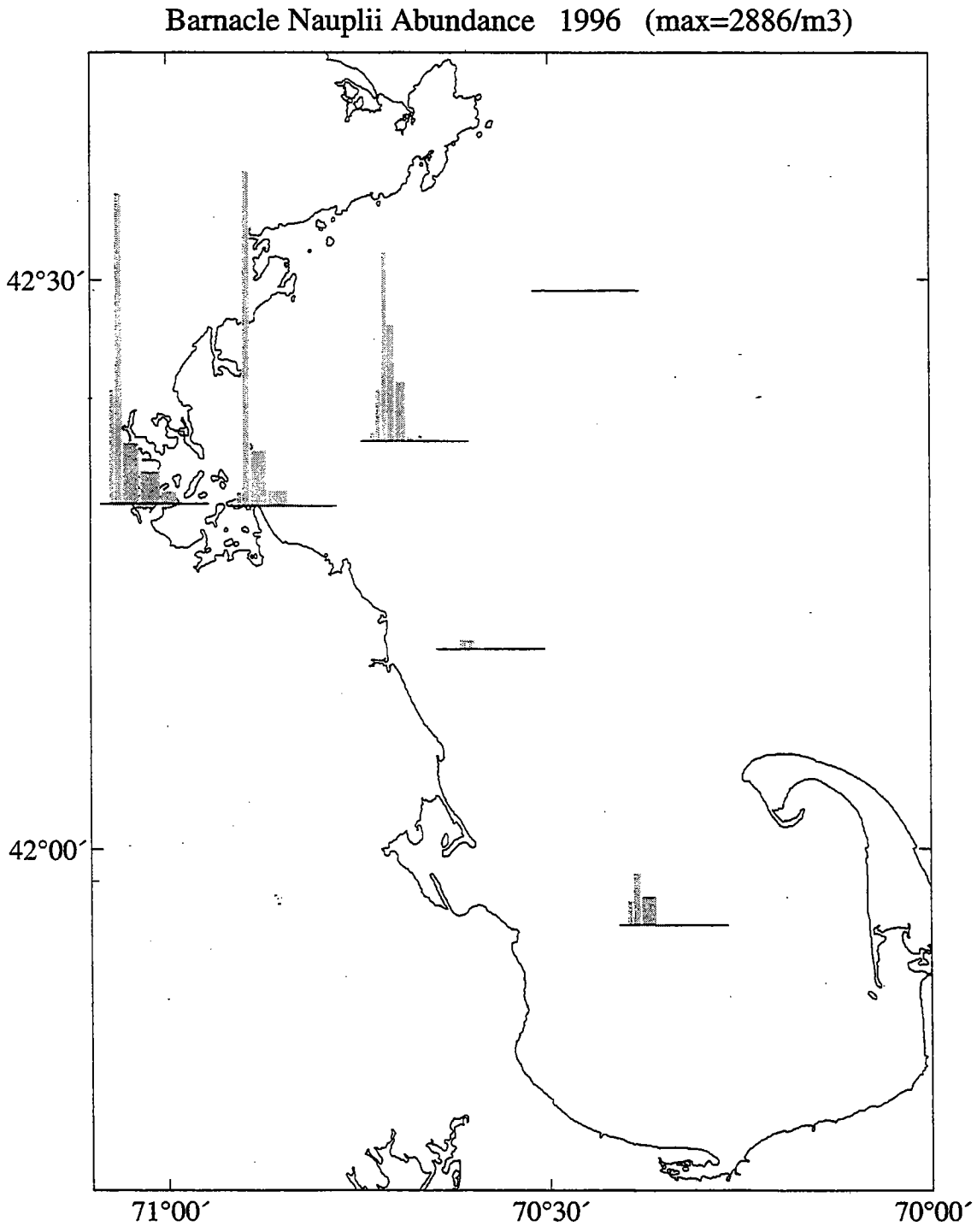

FIGURE 8-35
1996 Barnacle Nauplii Abundance (Maxima = 2886/m^3)

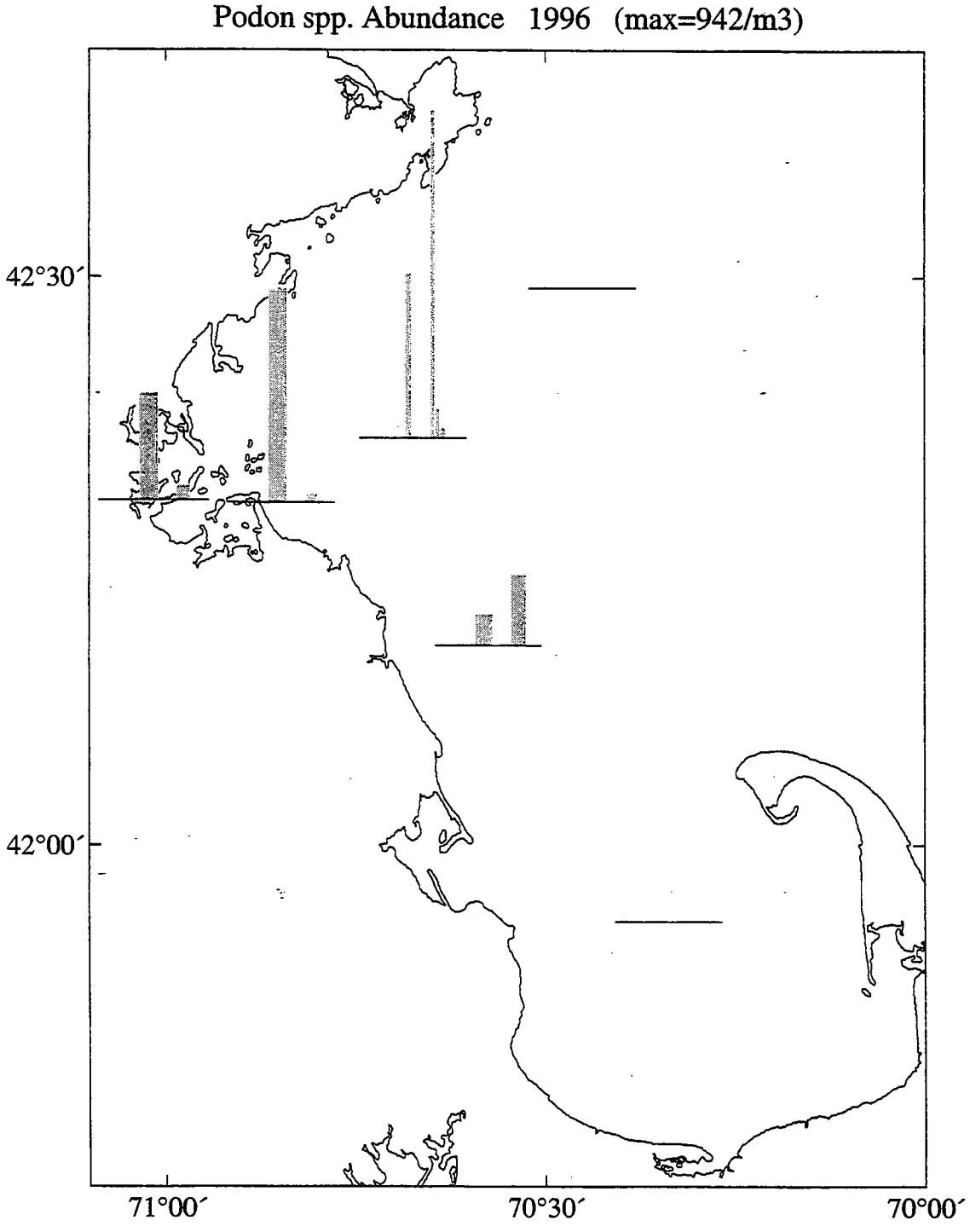

FIGURE 8-36
1996 Podon spp. Abundance (Maxima = 942/m^3)

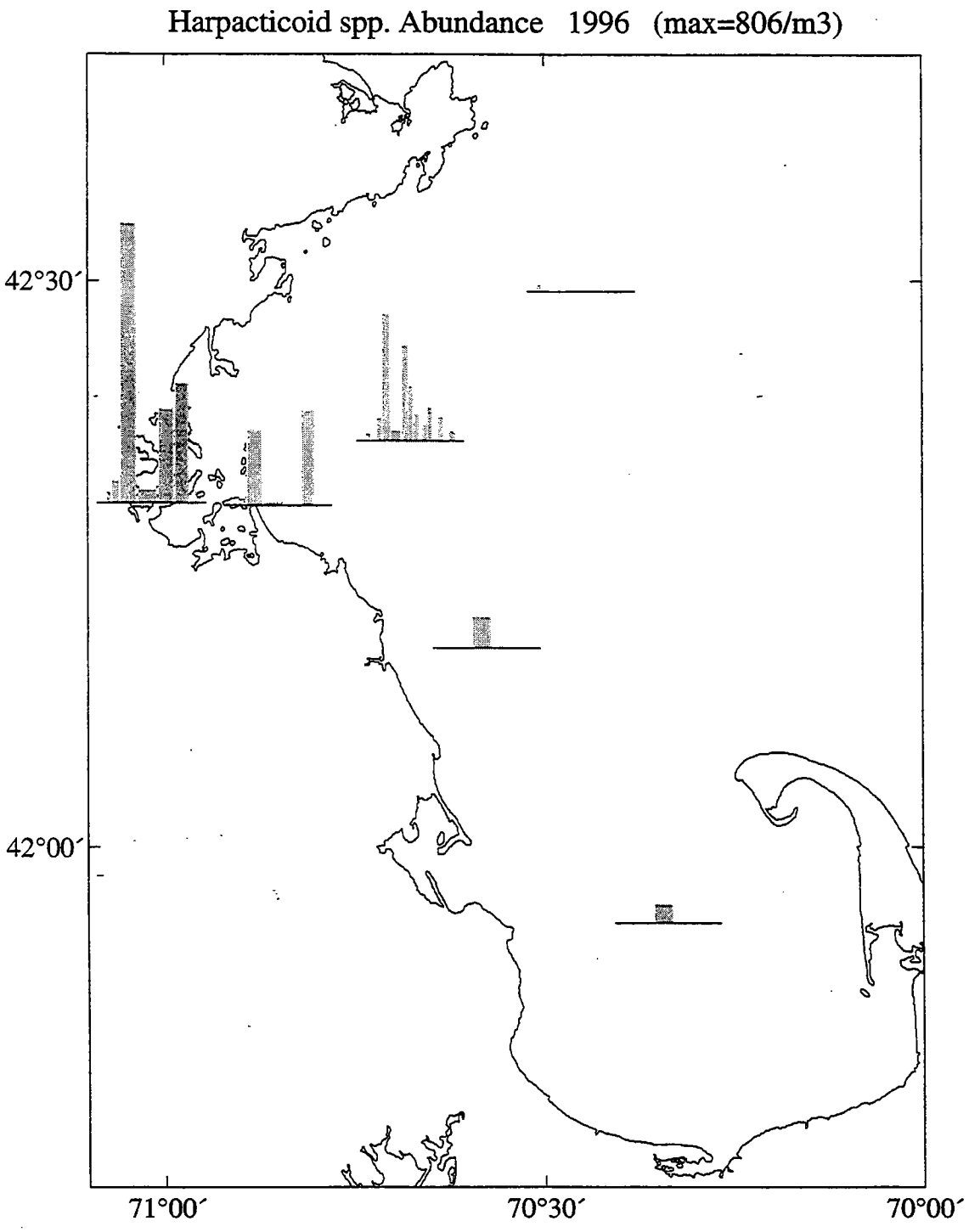

FIGURE 8-37
1996 Harpacticoid spp. Abundance (Maxima = 806/m^3)

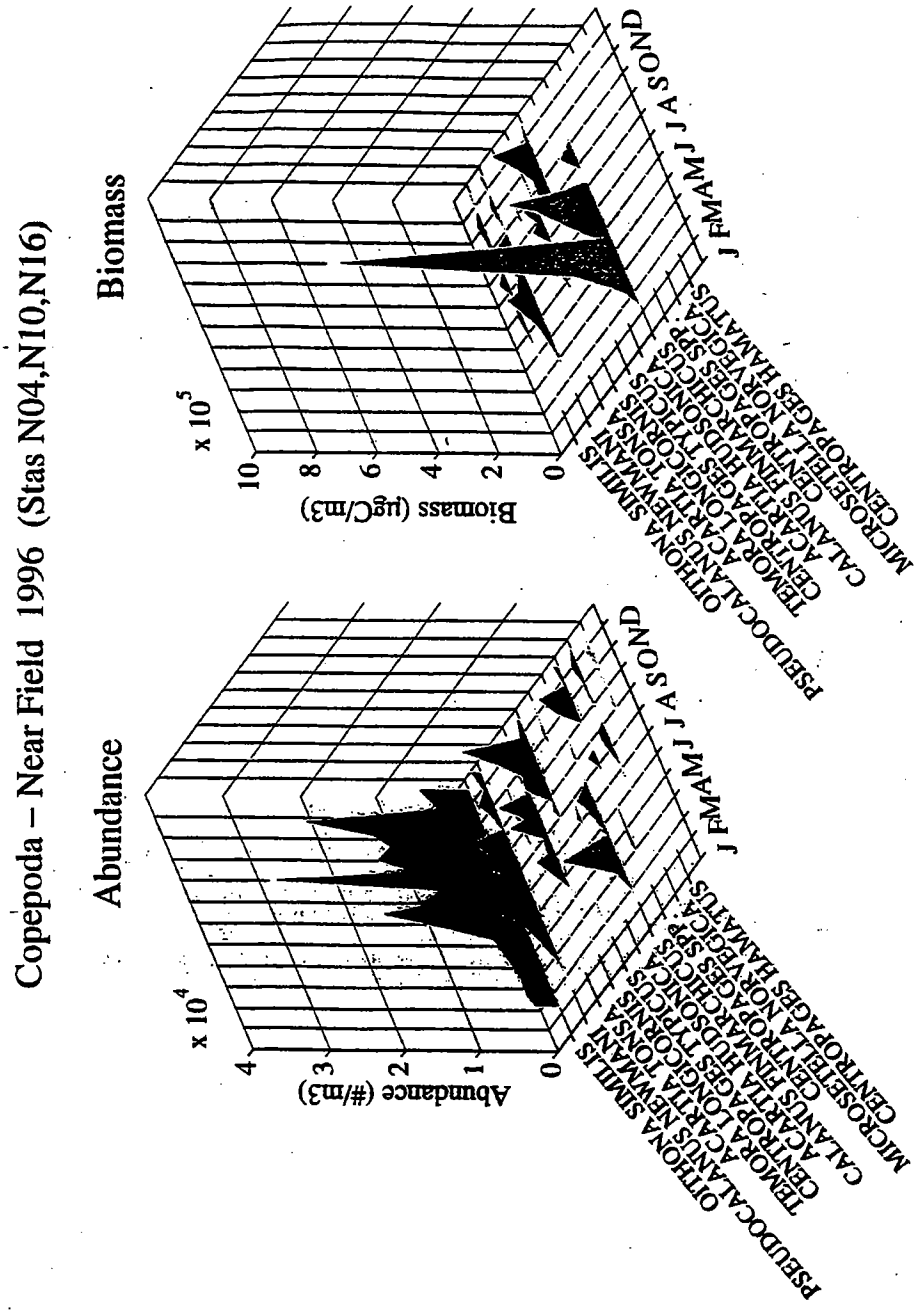

FIGURE 8-38
1996 Seasonal Abundance and Biomass of Dominant Copepod Species in the Nearfield (Stations N04, N10, N16)

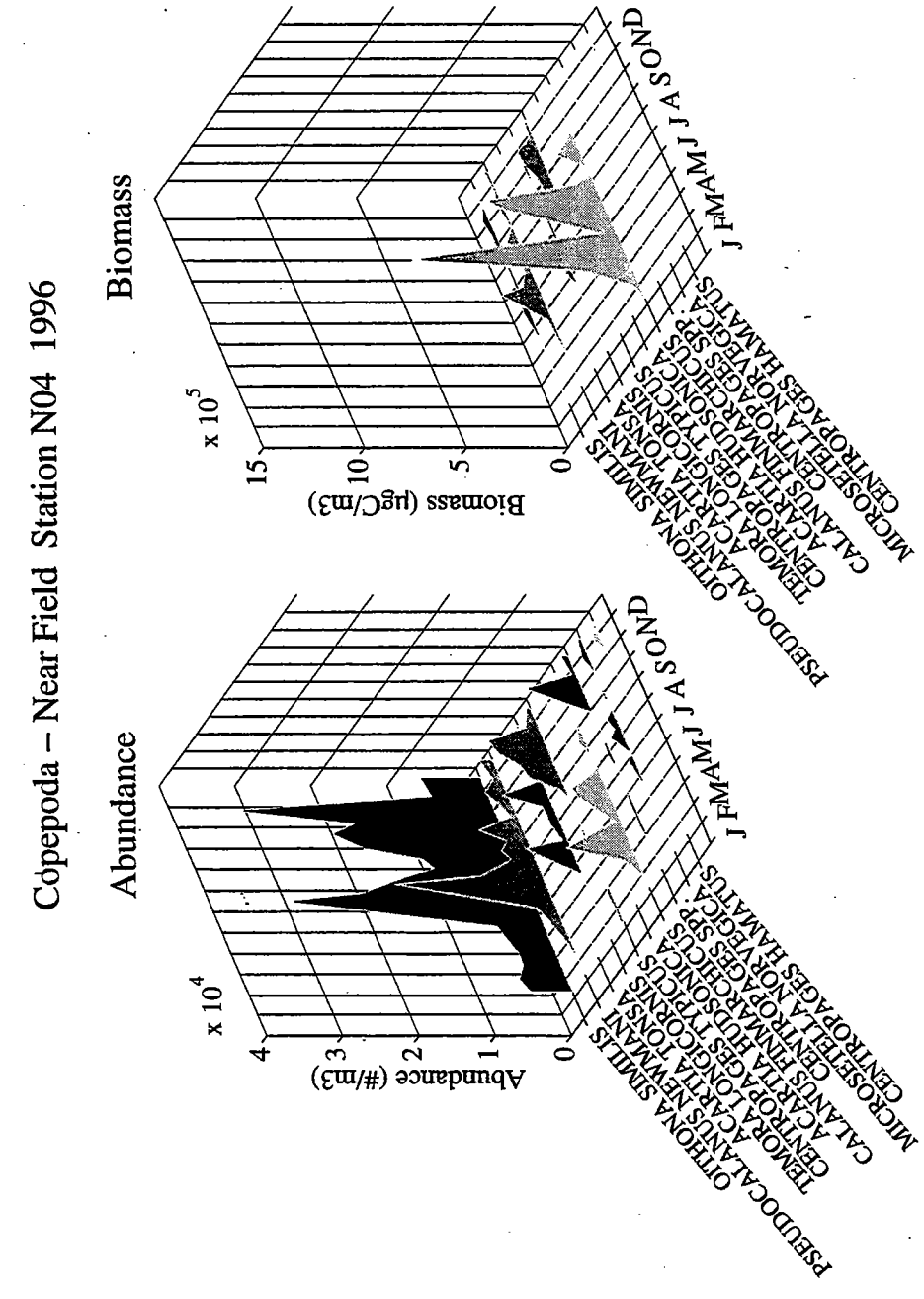

FIGURE 8-39
1996 Seasonal Abundance and Biomass of Dominant Copepod Species at Nearfield Station N04

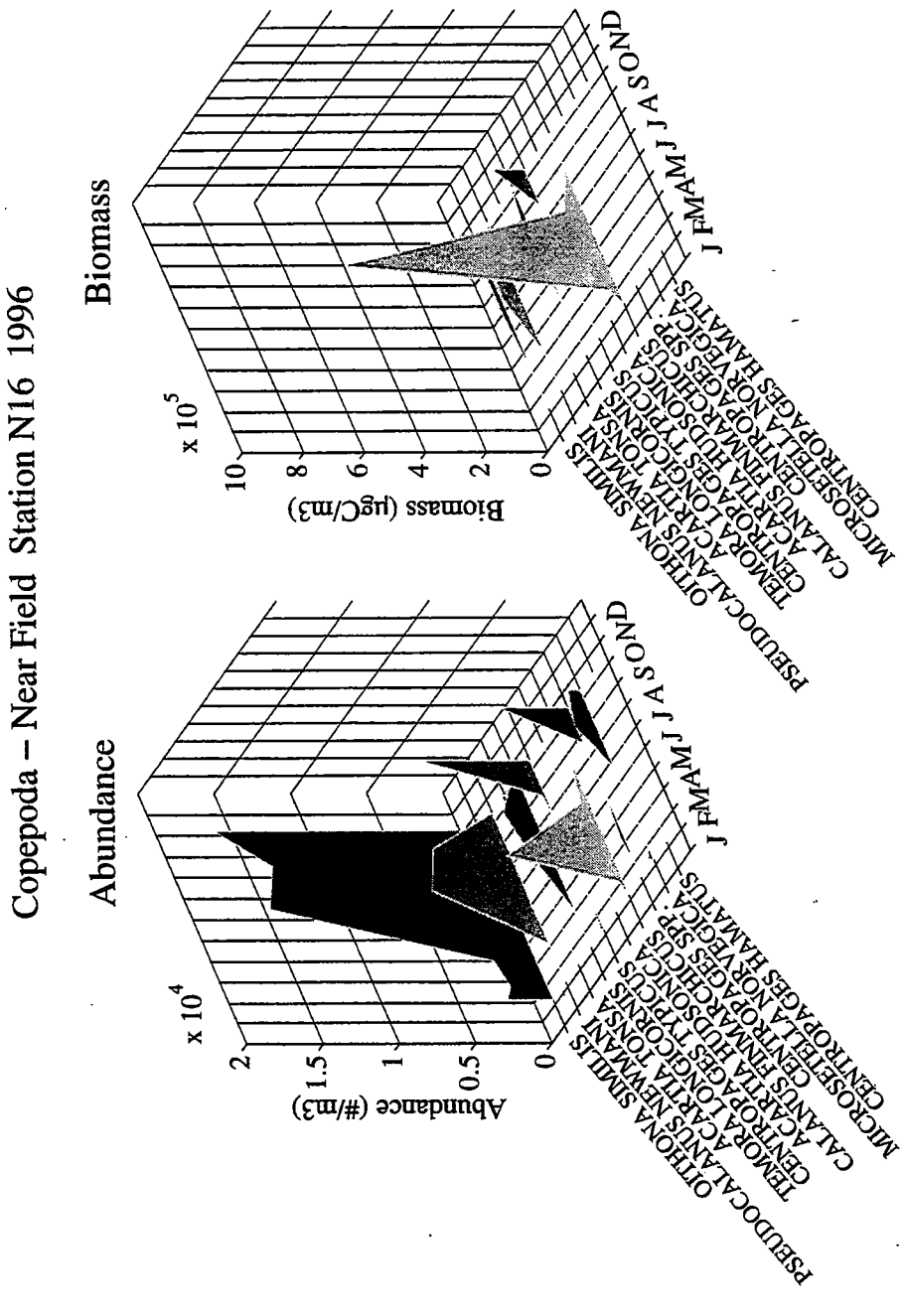

FIGURE 8-40
1996 Seasonal Abundance and Biomass of Dominant Copepod Species at Nearfield Station N16

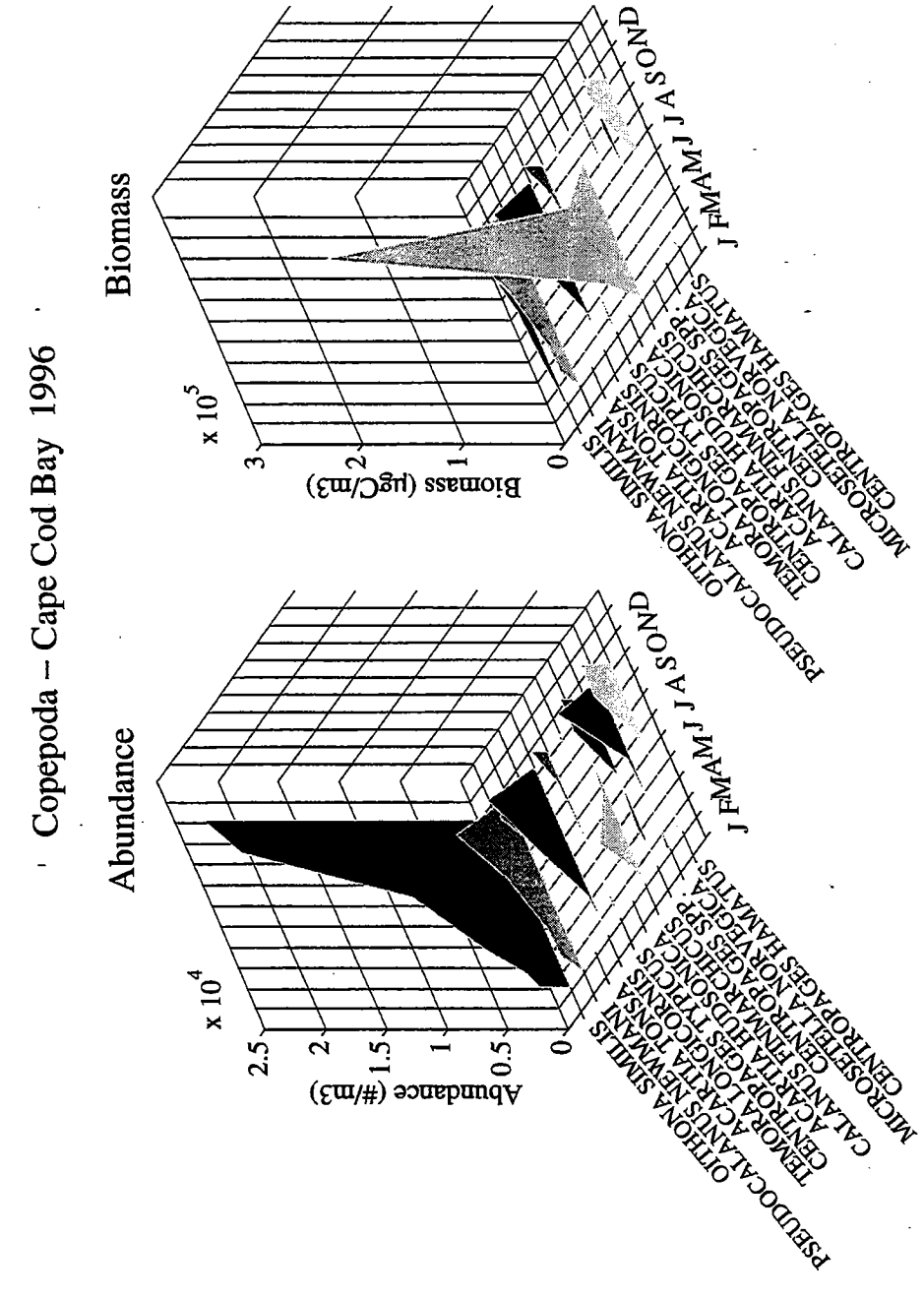

FIGURE 8-41
1996 Seasonal Abundance and Biomass of Dominant Copepod Species at Cape Cod Bay Stations

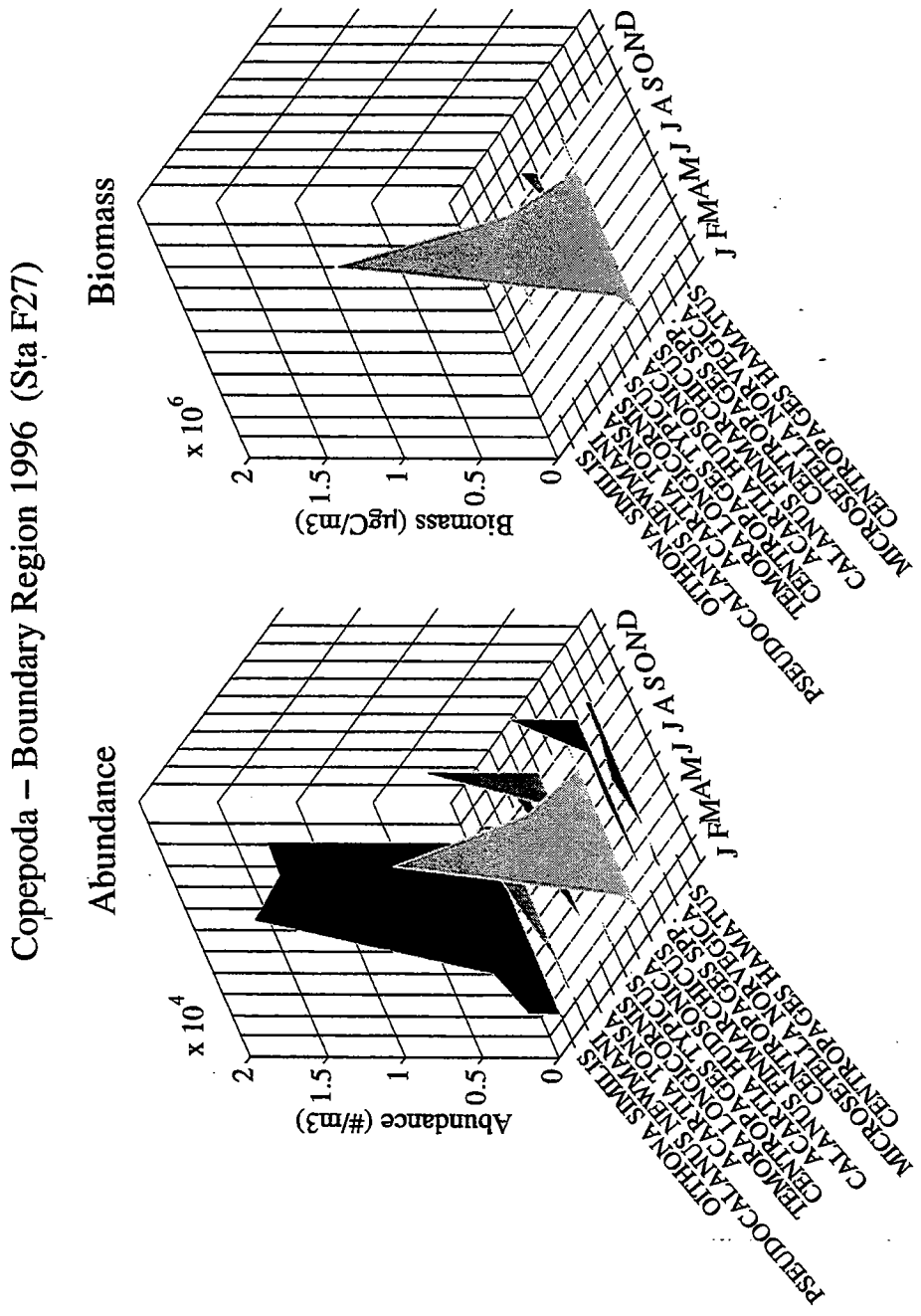

FIGURE 8-42
1996 Seasonal Abundance and Biomass of Dominant Copepod Species at Boundary Stations

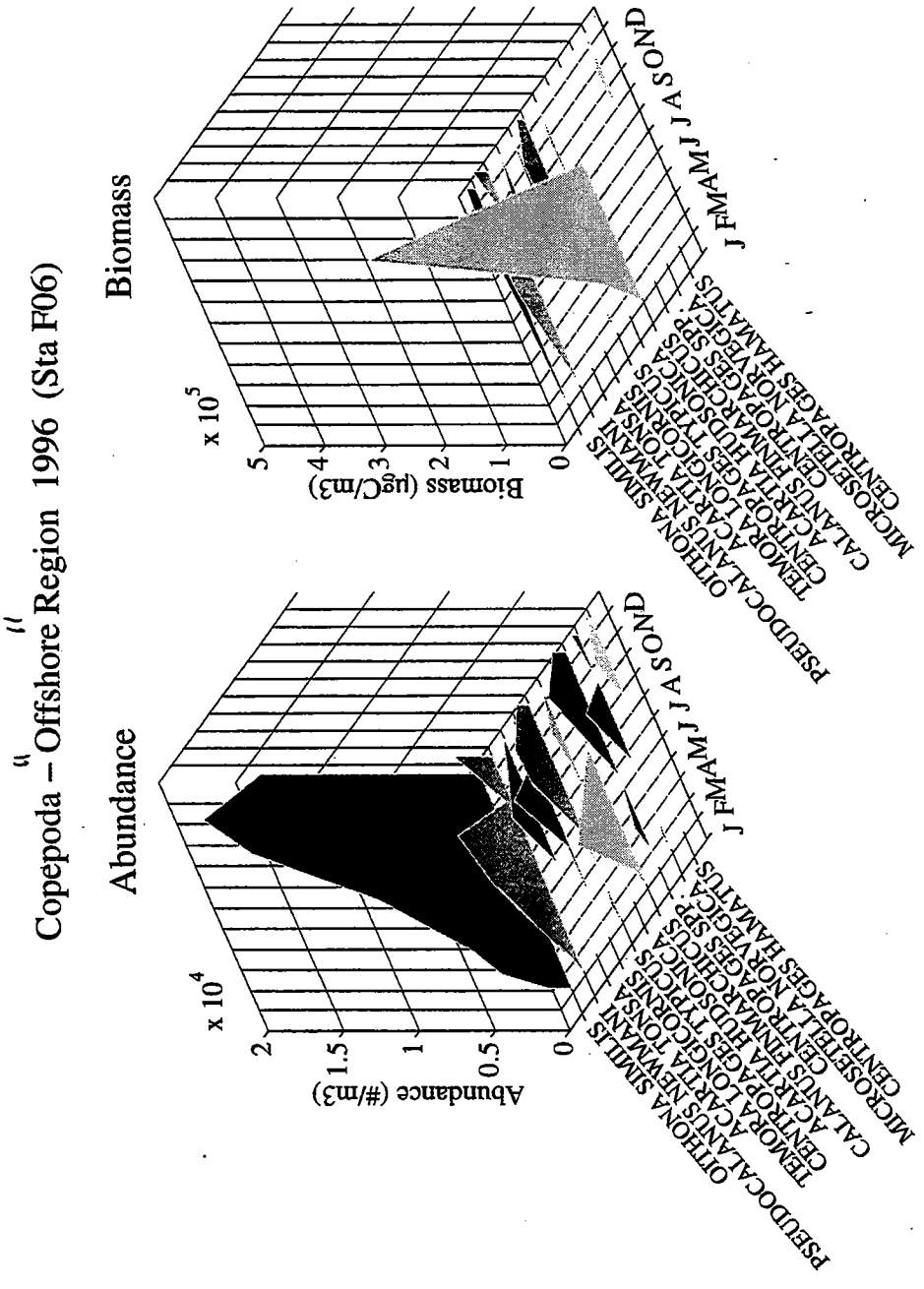

FIGURE 8-43
1996 Seasonal Abundance and Biomass of Dominant Copepod Species at Offshore Stations

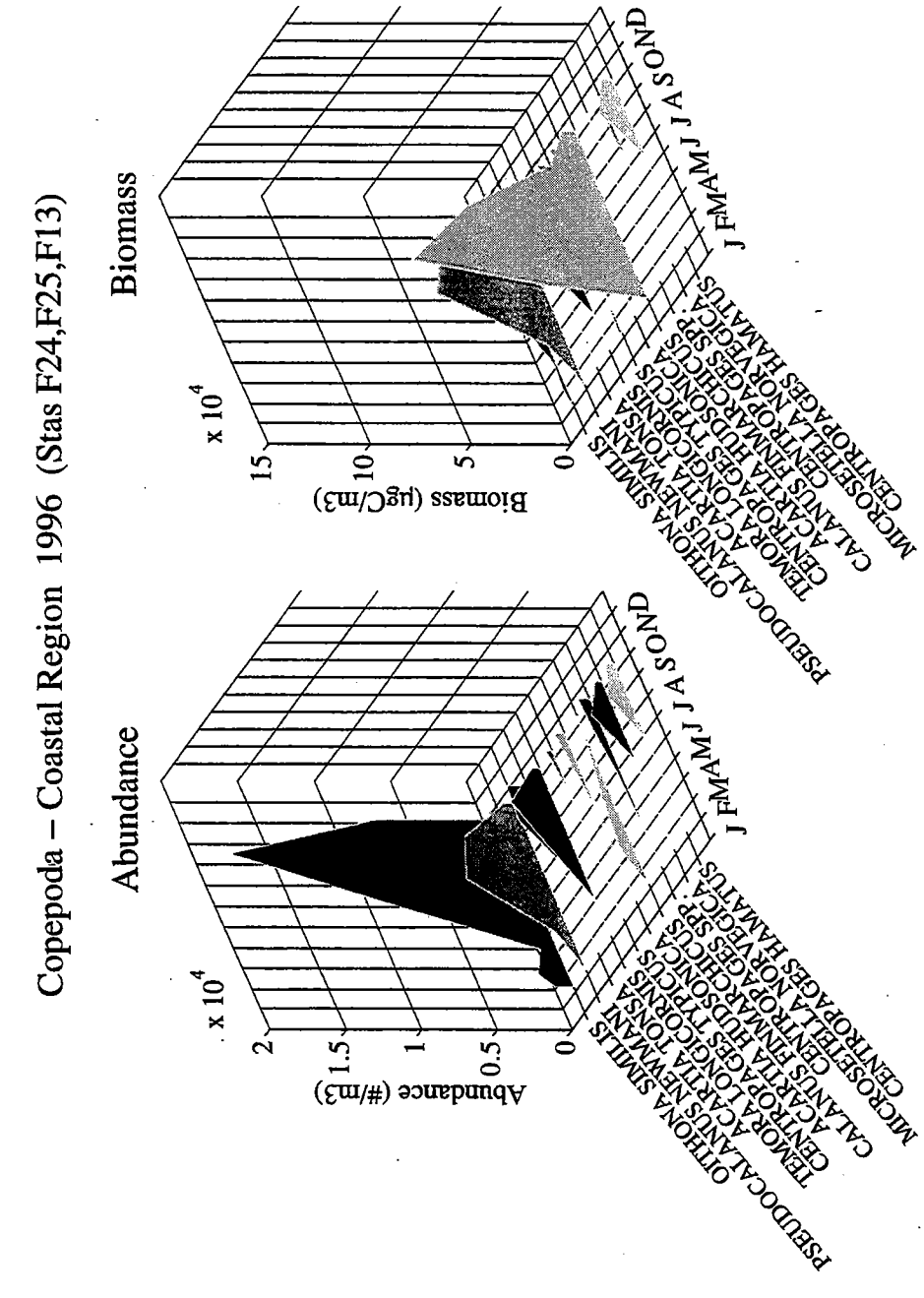

FIGURE 8-44
1996 Seasonal Abundance and Biomass of Dominant Copepod Species at Coastal Stations

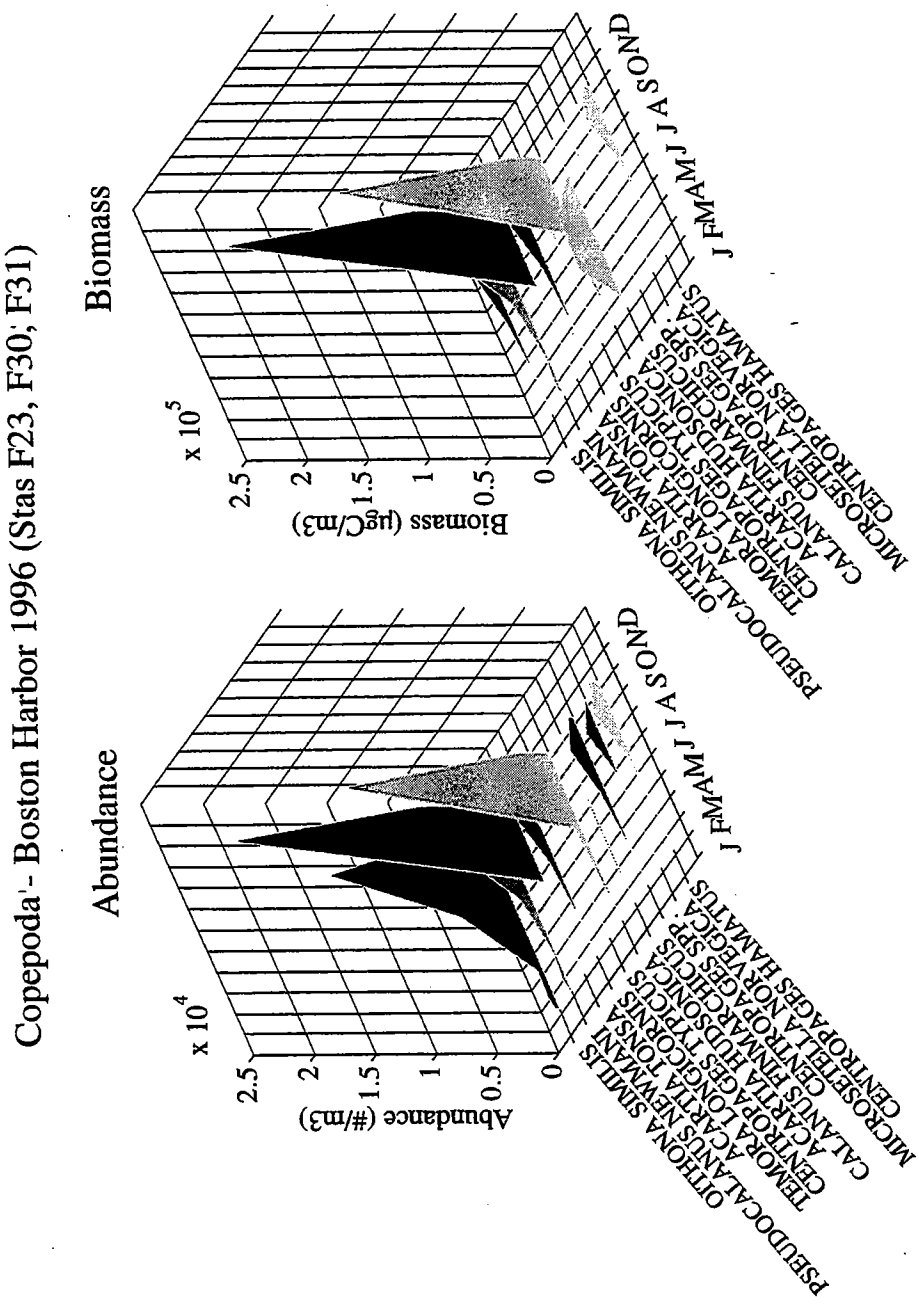

FIGURE 8-45
1996 Seasonal Abundance and Biomass of Dominant Copepod Species at Boston Harbor Stations

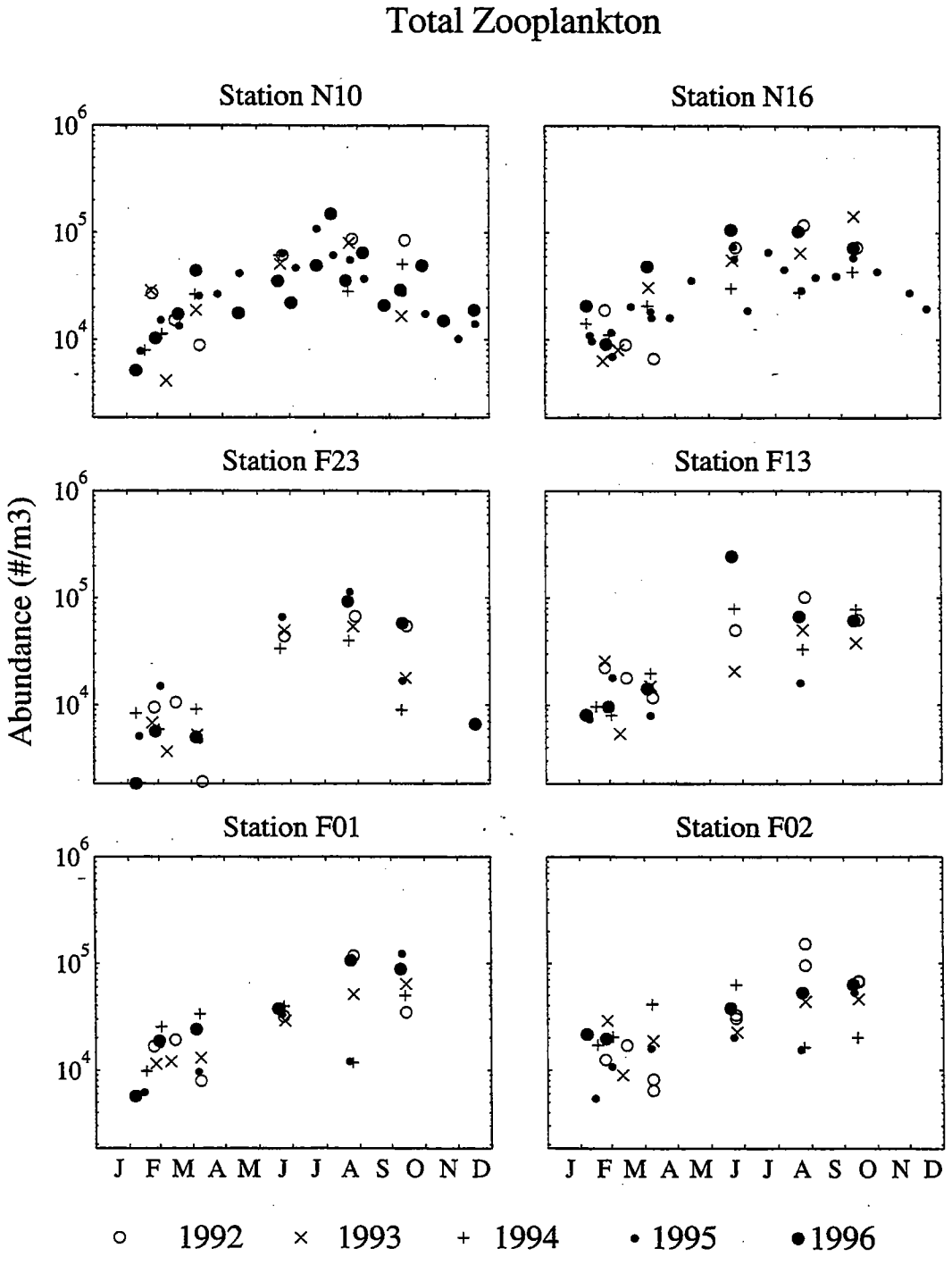

FIGURE 8-46
Interannual Distribution of Total Zooplankton by Region

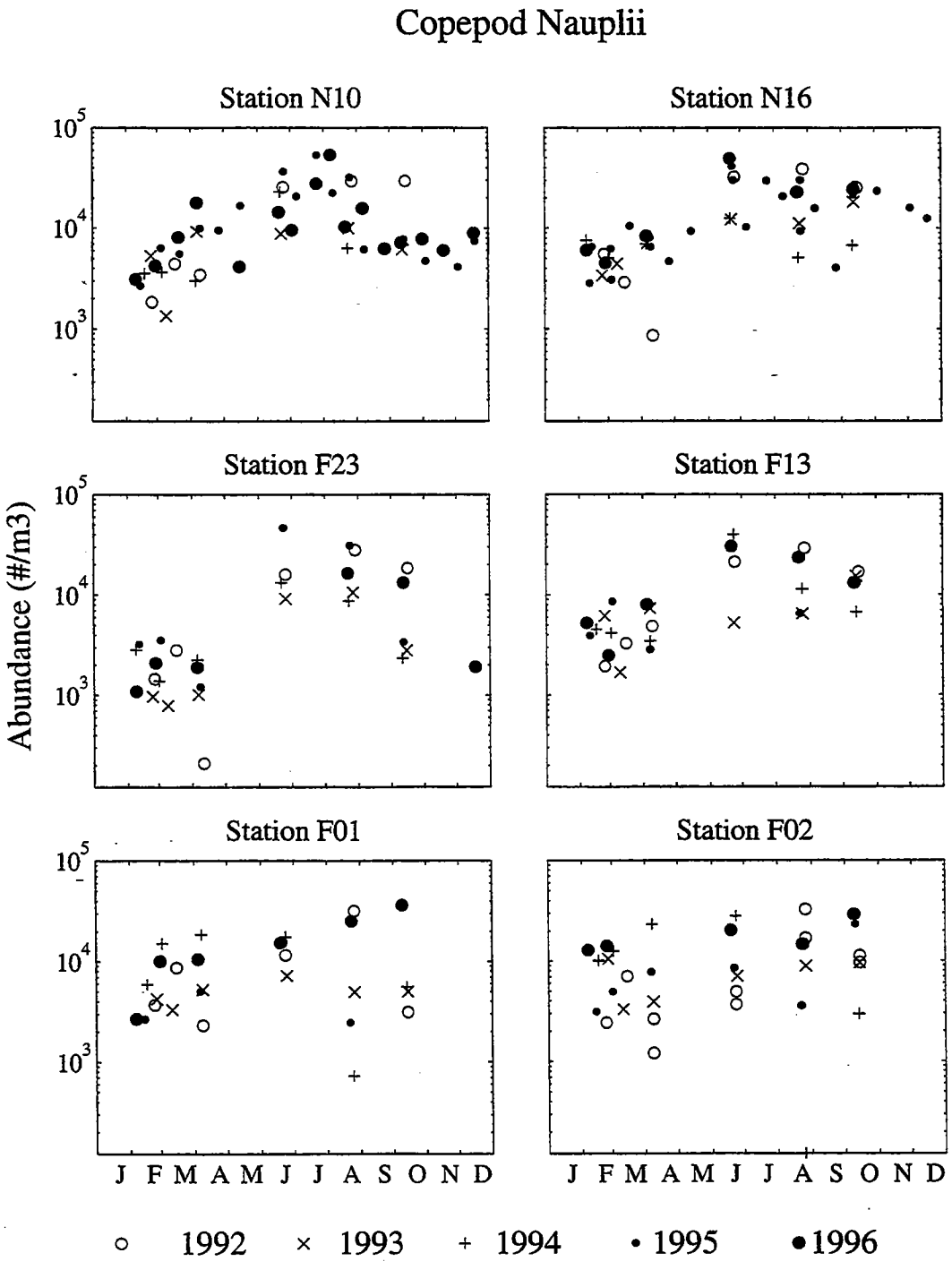

FIGURE 8-47
Interannual Distribution of Copepod Nauplii by Region

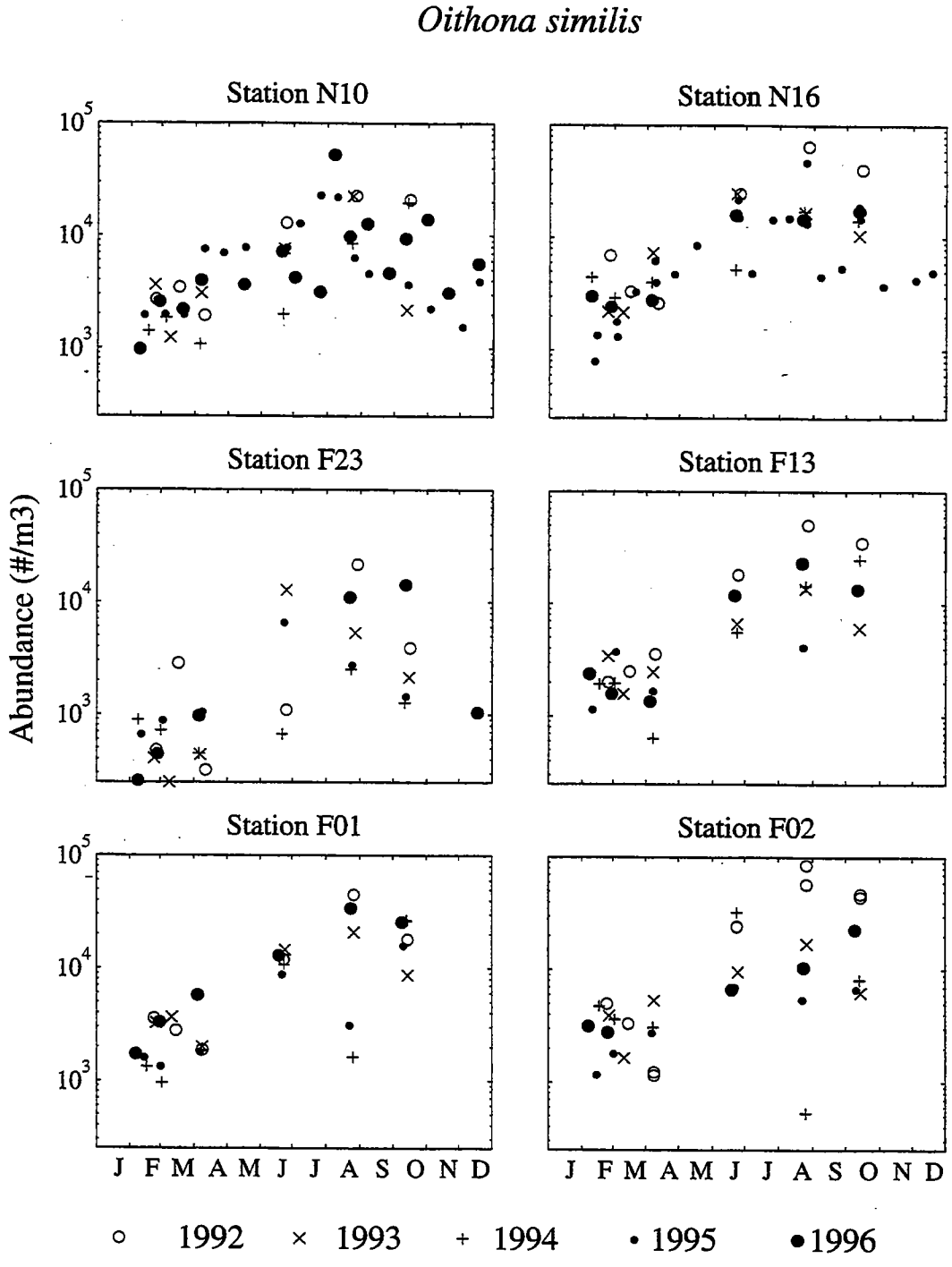

FIGURE 8-48
Interannual Distribution of *Oithona similis* by Region

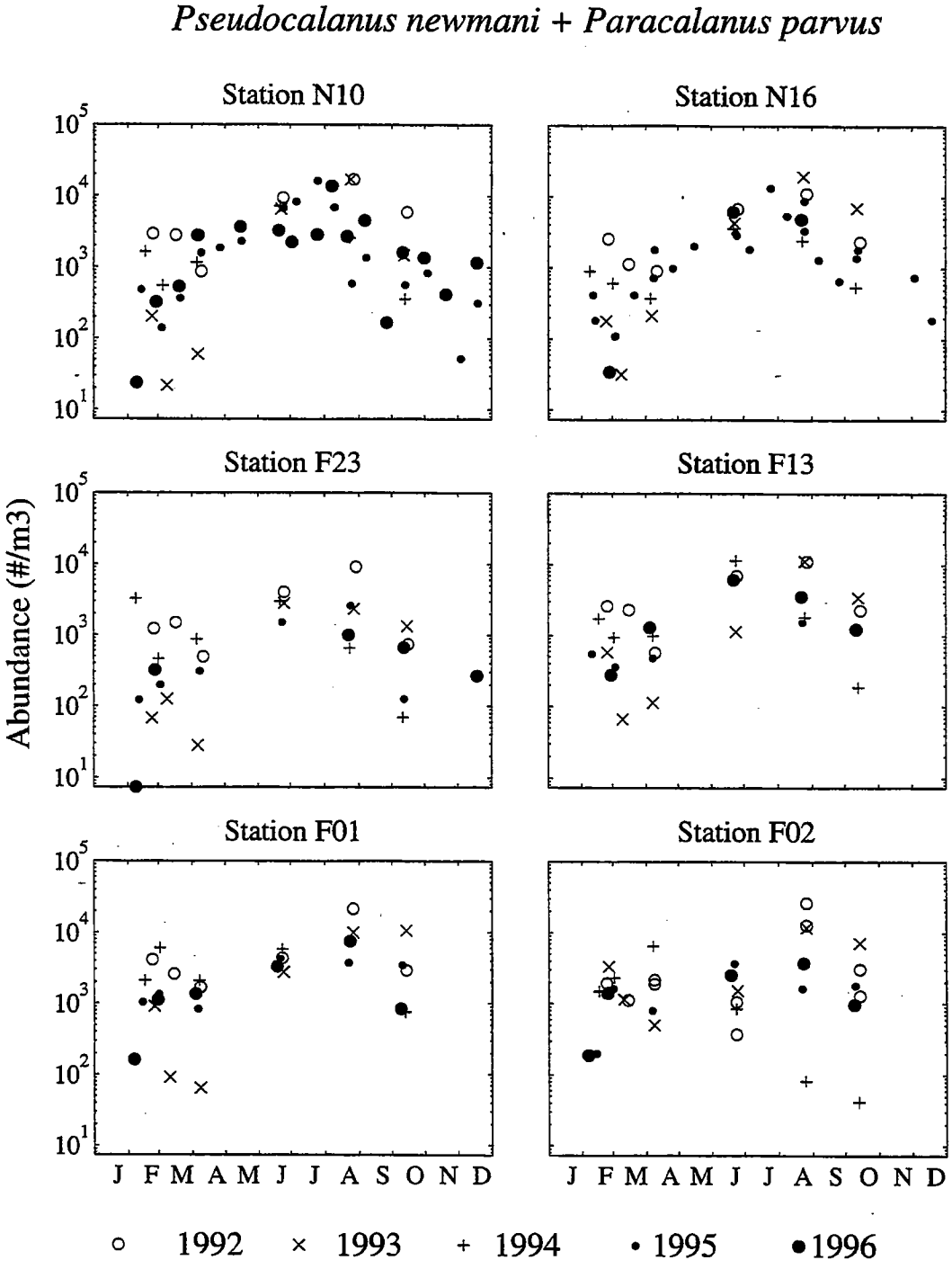

FIGURE 8-49
Interannual Distribution of *Pseudocalanus newmani* and *Paracalanus parvus* by Region

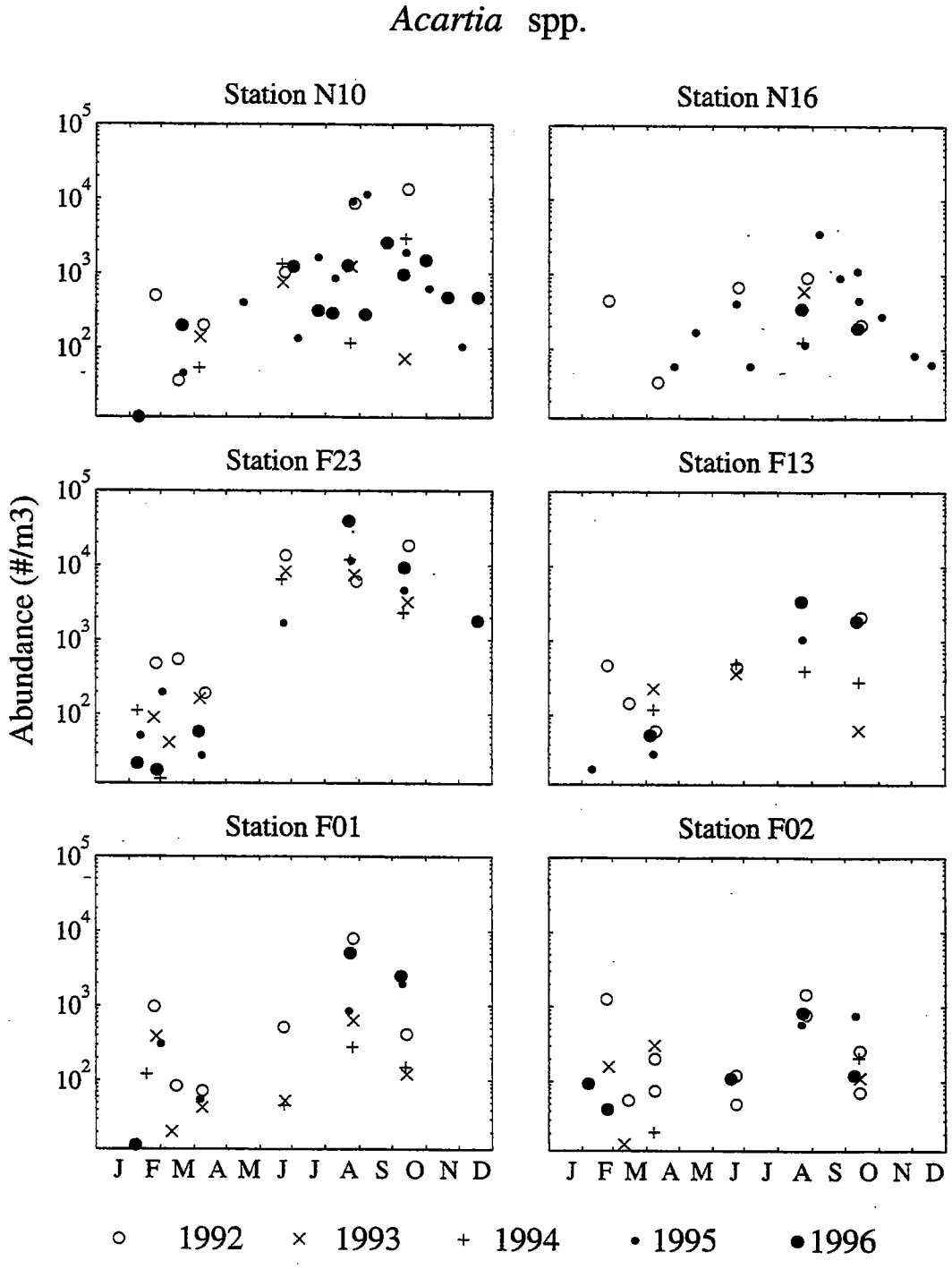

FIGURE 8-50
Interannual Distribution of *Acartia* spp. by Region

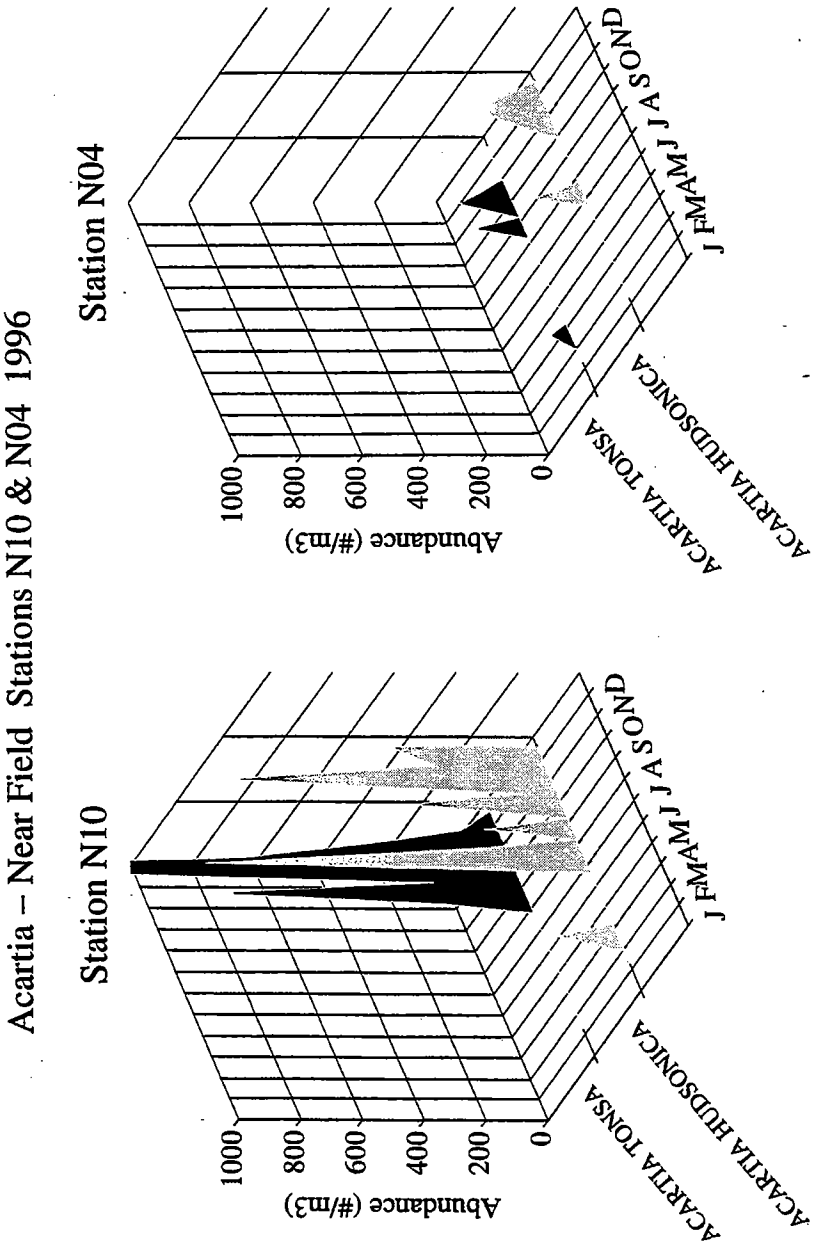

FIGURE 8-51
1996 Seasonal Abundance of *Acartia tonsa* and *Acartia hudsonica* at Nearfield Stations N10 and N04

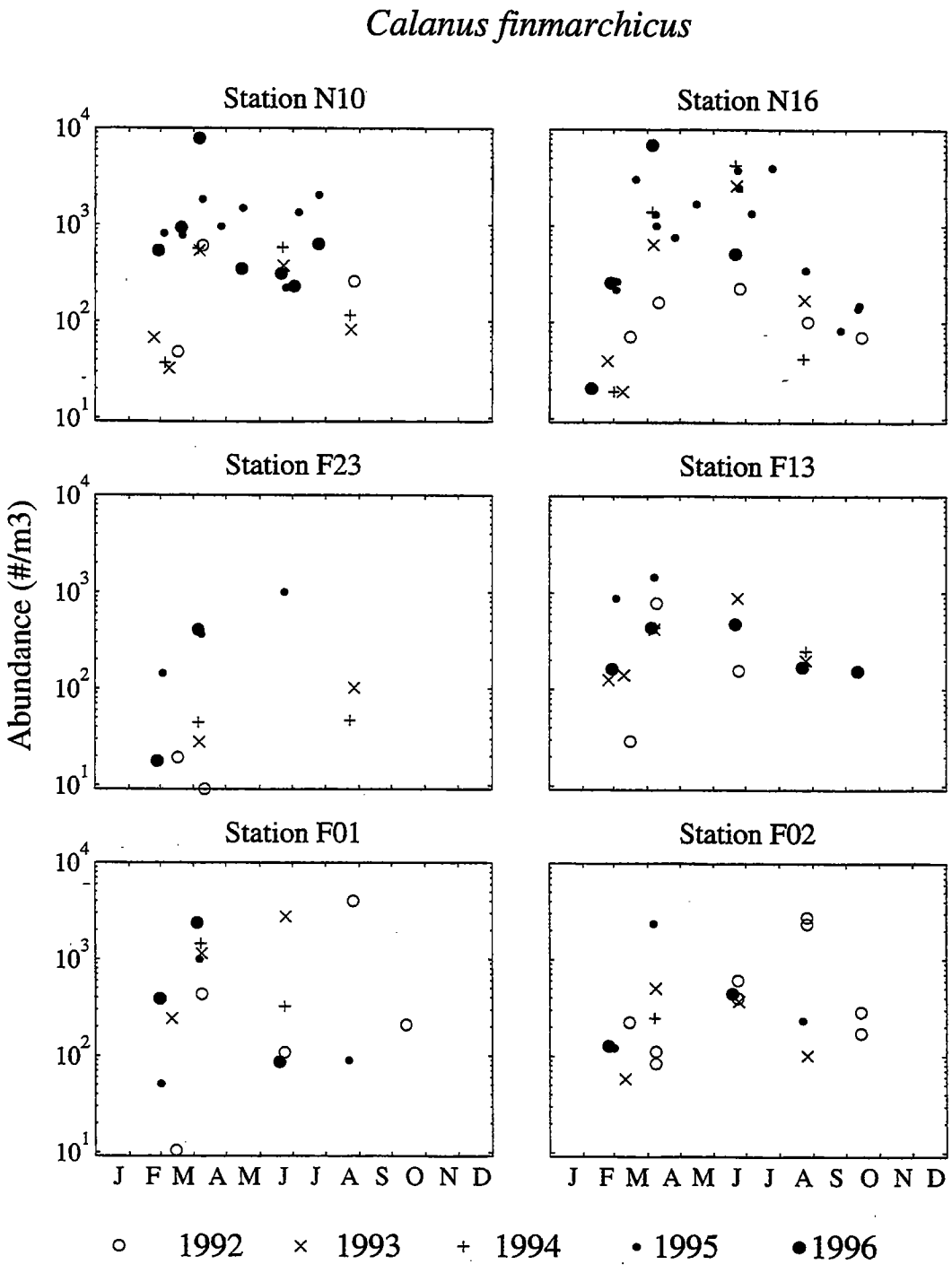

FIGURE 8-52
Interannual Distribution of *Calanus finmarchicus*. by Region

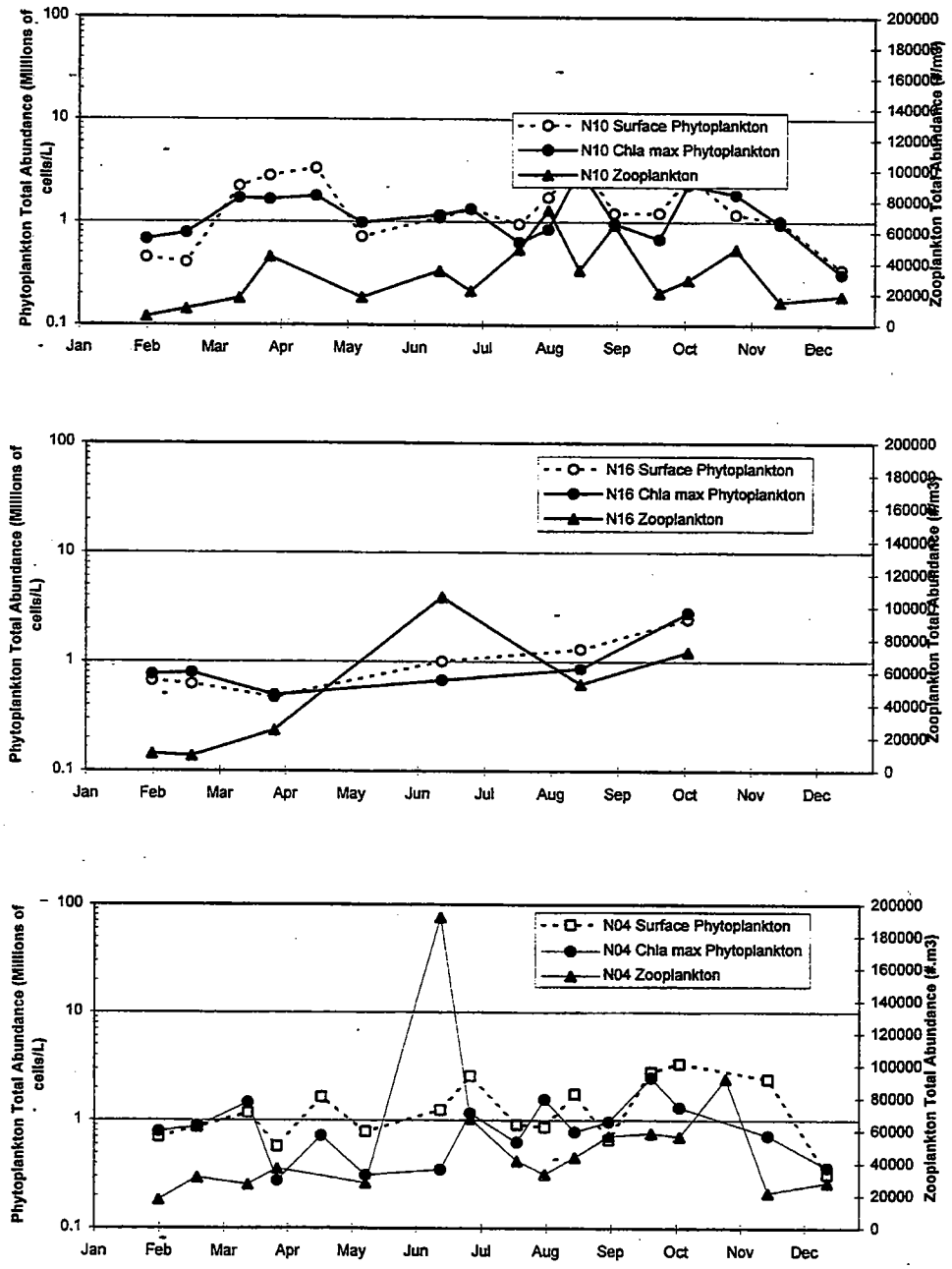

FIGURE 8-53

1996 Phytoplankton and Zooplankton Annual Cycles for Nearfield Stations
Top: N10, Middle: N16, and Bottom: N04

9.0 DISCUSSION

This section provides an overview of the major water column events that occurred during the 1996 monitoring program. These results are discussed relative to data from previous years of monitoring and our current understanding of the Massachusetts Bay system. Table 9-1 provides a summary of results presented in previous sections of this report. For each area of the water column program, significant events in terms of the structure and biotic activity in the nearfield are identified, facilitating integration of the various monitoring results.

Water column stratification began in the inner nearfield by late April, and by mid-May in the outer region of the nearfield. Warm, calm weather during early May, and a large intrusion of low-salinity water from riverine discharge to the north of the region augmented development of stratification. Despite its early setup, 1996 was earmarked by a series of storms which periodically eroded the pycnocline. Tropical storm Bertha caused partial mixing of the water column during July, while more thorough mixing resulted from Hurricanes Eduoard, Fran, and Josephine during early to mid-September. The September mixing resulted in an early breakdown in stratification, followed by complete de-stratification in early October. Additional heavy rainfall during October was associated with Hurricanes Josephine and Lili, making 1996 the wettest year on record.

The largest late winter/spring bloom of the baseline monitoring period was documented in 1996, with the average seasonal chlorophyll concentration around 40 percent higher than the previous maximum. The bloom, dominated by centric diatoms, developed across Massachusetts Bay by the end of February, and persisted in the inner nearfield through April. Ambient nutrients were stripped from the water column by mid-March, terminating the spring bloom. However, the advection of water from the north during early April appeared to re-supply nutrients to surface waters, particularly silicate. This re-supply may have caused the continued bloom in the harbor and adjacent coastal regions. Subsequent increases in water column nutrients during May/June, July, and August due to advective transport and mixing also resulted in increased productivity and chlorophyll biomass.

The early release of bottom water nutrients into the euphotic zone during the September and October storm-driven mixing set the stage for an early fall bloom. Estimates of potential productivity based on continuous irradiance monitoring indicated the fall bloom exceeded the spring bloom in magnitude. The magnitude of the bloom was also a function of its long duration as well, with high productivity lasting through November. The early turnover also terminated the annual DO decline by late September.

A worst-case scenario for annual bottom water DO minima would be comprised of a large spring bloom, early onset of stratification, low DO at the onset of stratification, an absence of summer ventilation events, and a delayed fall turnover. During 1996, the initial components of this scenario were in place. Had the large spring bloom, early stratification, and low initial bottom water DO concentrations been followed by a late turnover and no significant bottom water ventilation events, 1996 could well have produced the lowest DO concentrations of the baseline period.

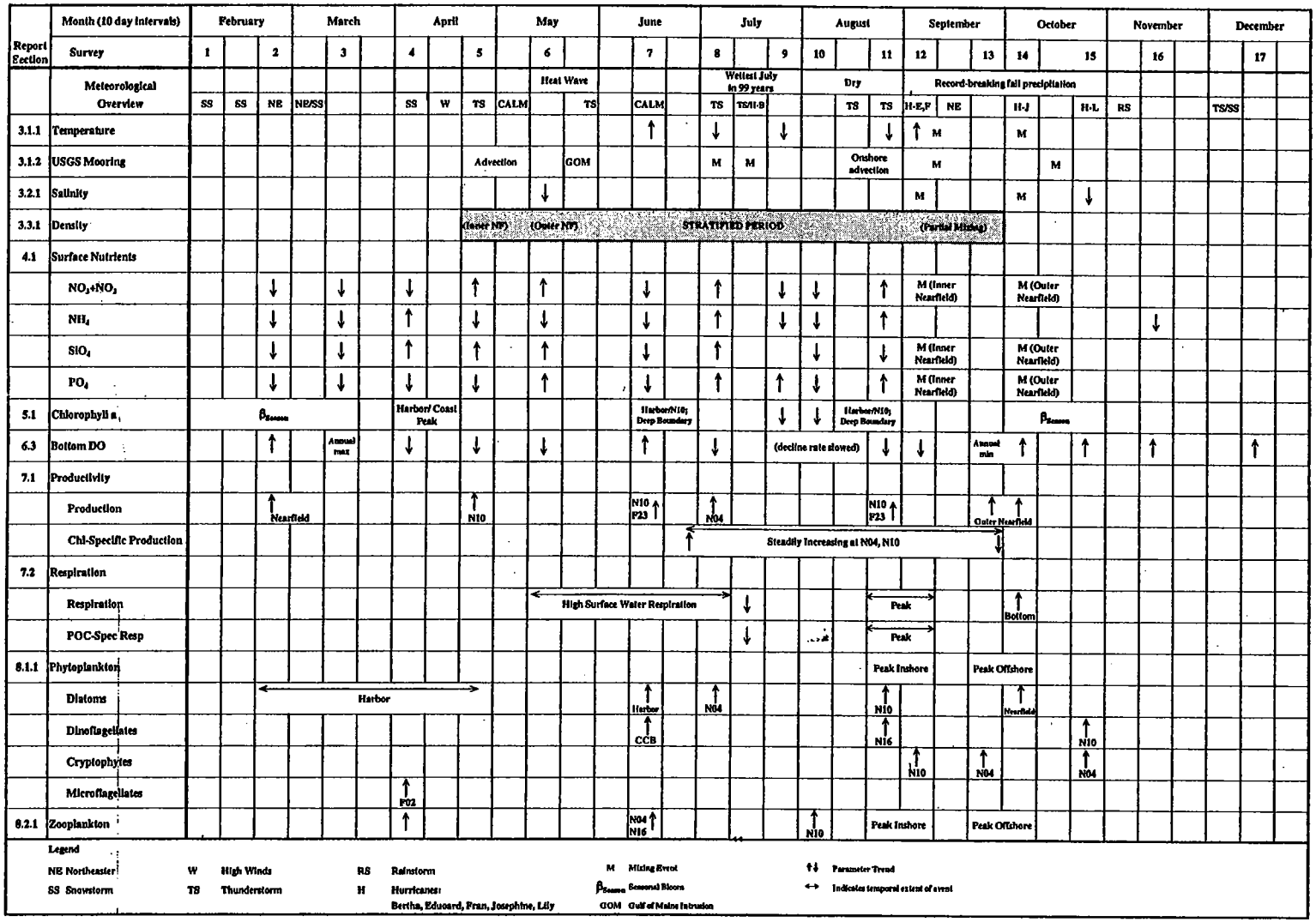

TABLE 9-1
MWRA 1996 Water Column Monitoring Integrated Results

10.0 REFERENCES

Anderson, D.M. and B.A. Keafer. 1992. Paralytic Shellfish Poisoning on Georges Bank: In-situ Growth or Advection of Established *Dinoflagellate* Populations. In: J. Wiggen, et al., (eds.), Gulf of Maine Workshop Report.

Anderson, D.M. and B.A. Keafer. 1995. Toxic Red Tides in Massachusetts and Cape Cod Bays. Final Report to the Massachusetts Water Resources Authority, January 31, 1995.

Anderson, D.M. 1997. Personal Communication with Steve Cibik.

Bates, S.S. 1997. Personal communication with Steve Cibik, March 5, 1997. Also see: http://www.maritimes.dfo.ca/science/mesd/he/science/toxins/index.html

Becker, S.M. 1992. The seasonal distribution of nutrients in Massachusetts Bay and Cape Cod Bays (Master of Science). Durham, NH: University of New Hampshire. 127p.

Bowen, J., K. Hickey, B. Zavistoski, T. Loder, B. Howes, C. Taylor, E. Butler, and S. Cibik. 1997. Draft Combined Work/Quality Assurance Project Plan for Water Quality Monitoring: 1995-1997. Prepared for the Massachusetts Water Resources Authority, Boston, MA, under Contract S186. 73pp.

Cibik, S. J., B. L. Howes, C. D. Taylor, D. M. Anderson, C. S. Davis and T. C. Loder III, R.D. Boudrow, J.D. Bowen. 1996. 1995 Annual Water Column Monitoring Report. Prepared for the Massachusetts Water Resources Authority, Environmental Quality Department, Boston, MA, Report ENQUAD 96-07. 254pp.

Cibik, S.J., P.M. Murray, K. B. Lemieux, R. A. Zavistoski, B. L. Howes, C. D. Taylor, D. M. Anderson, C. S. Davis and T. C. Loder. 1998. Second Semi-Annual Water Column Monitoring Project: August - December, 1996. Boston: Massachusetts Water Resources Authority. Report ENQUAD 98-07. 354pp.

Cibik, S.J., K.B. Lemieux, C.D. Davis, D.M. Anderson. 1998a. Massachusetts Bay Plankton Communities: Characterization and Discussion of Issues Relative to MWRA's Outfall Relocation. Massachusetts Water Resources Authority.

Cleveland, J.S., M.J. Perry, D.A. Kiefer and M.C. Talbot. 1989. Maximal Quantum Yield of Photosynthesis in the Northwestern Sargasso Sea. J. Mar. Res. 47, 869-886.

Falkowski, P.G. 1992. Molecular ecology of phytoplankton photosynthesis. p. 47-67. In P.G. Falkowski and A. Woodhead (eds.), Primary Productivity and Biogeochemical Cycles in the Sea. Plenum Press, New York.

Falkowski, P.G. 1981. Light-shade adaptation and assimilation numbers. J. Plankton Res. 3, 203-216.

Franks, P.J.S. and D.M. Anderson. 1992. Along shore Transport of a Toxic Phytoplankton Bloom in a Buoyancy Current: *Alexandrium tamarense* in the Gulf of Maine. Mar. Biol. 112:153-164.

Geyer, W.R., G.B. Gardner, W.S. Brown, J. Irish, B. Butman, T.C. Loder, and R.P. Signell. 1992. Final report: Physical Oceanographic Investigation of Massachusetts and Cape Cod Bays. August 1, 1992. 497 pp.

Howes, B.L. 1997. Sediment metabolism within Massachusetts Bay and Boston Harbor: Relating to sediment-water column exchanges of nutrients and oxygen in 1995. Massachusetts Water Resources Authority Environmental Quality Technical Report

Howes, B.L. 1998. Sediment metabolism within Massachusetts Bay and Boston Harbor: relating to system stability and sediment-water column exchanges of nutrients and oxygen in 1996. Massachusetts Water Resources Authority Environmental Quality Technical Report

Hunt, C.D. and M. Steinhauer. 1994. MWRA Nutrient Indicator Workshop, held on January 20, 1994. Proceedings prepared for the Boston: Massachusetts Water Resources Authority. Report ENQUAD ms-20. 180pp.

Kelly, J. 1993. Nutrients and Massachusetts Bay: An Update of Eutrophication Issues. Boston: Massachusetts Water Resources Authority. Report ENQUAD 93-17. 119 pp.

Kelly, J.R and J. Turner. 1995. Water Column Monitoring in Massachusetts and Cape Cod Bays: Annual Report for 1994. Boston: Massachusetts Water Resources Authority. Report ENQUAD 95-17. 163 pp.

Kelly, J.R. and P.H. Doering. 1995. Nutrient Issues Update 1995: Metabolism in Boston Harbor, Massachusetts and Cape Cod Bays, MA (USA) during 1992-1994. Boston: Massachusetts Water Resources Authority Report ENQUAD 95-19. 38 pp.

Kelly J.R. 1997. Nitrogen flow and the interaction of Boston Harbor with Massachusetts Bay throughout 1996. Estuaries, 20:365-380.

Loder, T. C. III and R. Boudrow. 1997. Nutrients in Massachusetts Bay - A decade's view. Invited Talk Presented at Coastal Zone97 Workshop: Ten-year Review of Management Issues and Scientific Studies in Massachusetts Bay and Boston Harbor. Boston, July 24, 1997.

Lohrenz, S.E., G.L. Fahnenstiel and D.G. Redalje. 1994. Spatial and Temporal Variations of Photosynthetic Parameters in Relation to Environmental Conditions in Coastal Waters of the Northern Gulf of Mexico. Estuaries. 17, 779-795.

Murray, P. M., S. J. Cibik, K. B. Lemieux, R. A. Zavistoski, B. L. Howes, C. D. Taylor, D. M. Anderson, C. S. Davis and T. C. Loder. 1998. First Semi-Annual Water Column Monitoring Project: February-July, 1996. Boston: Massachusetts Water Resources Authority. Report ENQUAD 98-01. 434pp.

NRCC. 1997. Climate Impacts January –December 1996. Northeast Regional Climate Center. Cornell University, New York: http://met-www.cit.cornell.edu/.

Olson, R.J., A.M. Chekalyuk and H.M. Sosik. 1996. Phytoplankton photosynthetic characteristics from fluorescence induction assays of individual cells. Limnol. Oceanogr. 41, 1253-1263.

Oudot, C., R. Gerard, and P. Morin. 1988. Precise shipboard determination of dissolved oxygen (Winkler procedure) for productivity studies with a commercial system. Limnology and Oceanography 33:146-150.

Schofield, O., B.B. Prezelin, R.C. Smith, P.M. Stegmann, N.B. Nelson, M.R. Lewis and K.S. Baker. 1991. Variability in Spectral and Nonspectral Measurements of Photosynthetic Light Utilization Efficiencies. Mar. Ecol. Prog. Ser. 78, 253-271.

Taylor, D. 1998. Personal Communication with Steve Cibik

Townsend, D.W., L.M. Cammen, J.P. Christensen, S.G. Ackelson, M.D. Keller, E.M. Haugen, S. Corwin, W.K. Bellows, J.F. Brown. 1991. Seasonality of Oceanographic Conditions in Massachusetts Bay. 114 pp. Bigelow Laboratory for Ocean Sciences Technical Report No. 83, October 1991. West Boothbay Harbor, ME 04575. Boston: Massachusetts Water Resources Authority. Report ENQUAD MS-01. 114pp.

USGS. 1997a. Online current meter data. http://crusty.er.usgs.gov/epic/.

USGS. 1997b. Data plot index for USGS mooring. http://woodshole.er.usgs.gov/~fhotchki/plitindex.html.

Massachusetts Water Resources Authority
Charlestown Navy Yard
100 First Avenue
Boston, MA 02129
(617) 242-6000